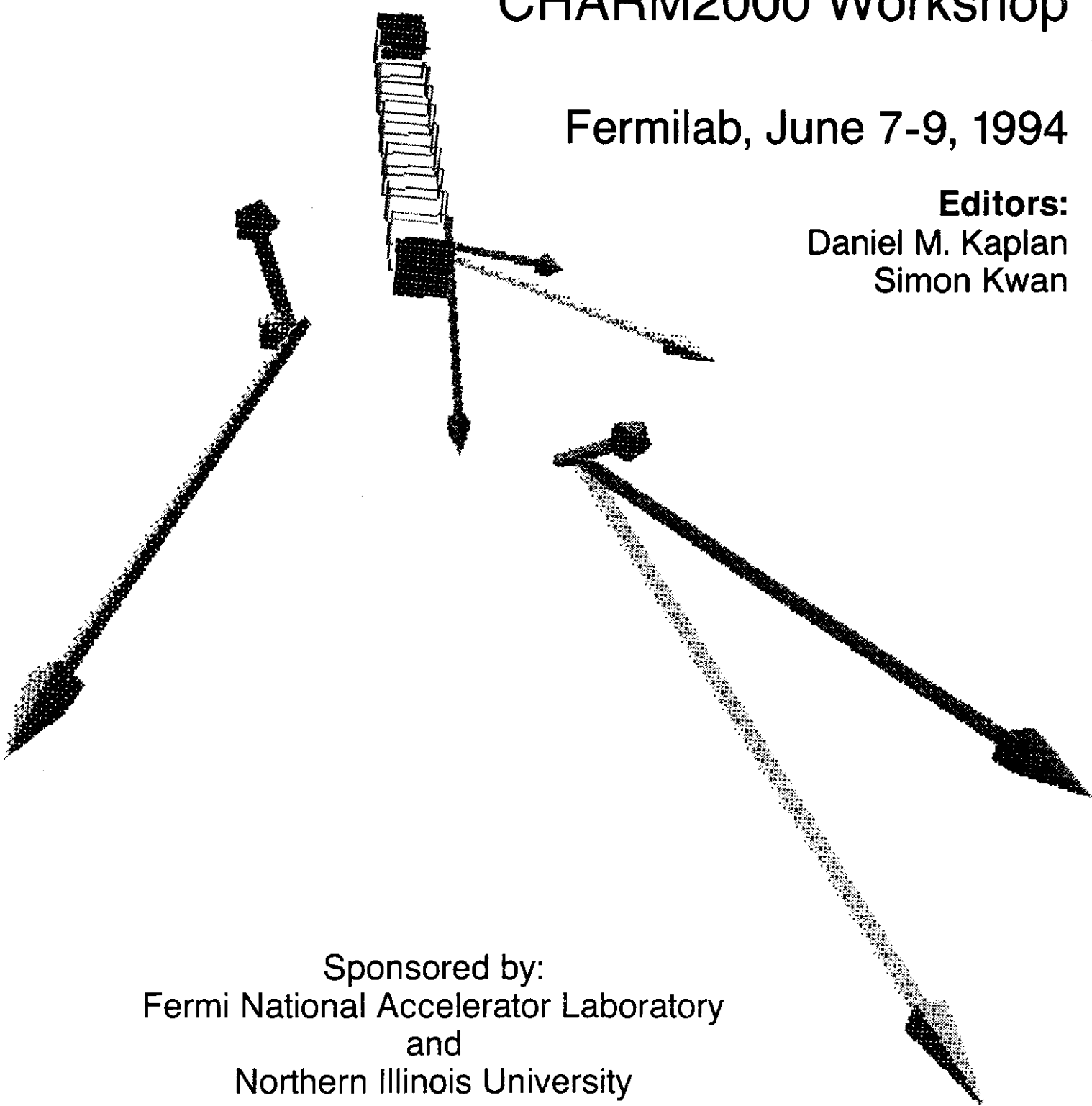


The Future of High-Sensitivity Charm Experiments: Proceedings of the CHARM2000 Workshop

Fermilab, June 7-9, 1994

Editors:
Daniel M. Kaplan
Simon Kwan



Sponsored by:
Fermi National Accelerator Laboratory
and
Northern Illinois University

The Future of High-Sensitivity Charm Experiments:

Proceedings of the CHARM2000 Workshop



Fermilab, June 7-9, 1994

Editors:

Daniel M. Kaplan, Northern Illinois University
Simon Kwan, Fermilab

Sponsored by:

**Fermi National Accelerator Laboratory
Northern Illinois University**

Epitome

On June 7-9, 1994, over 100 attendees heard 35 plenary talks on the Future of High-Sensitivity Charm Experiments. Twelve working groups focused on the physics opportunities and technical challenges facing this field. Speakers representing the CLEO, BES, SLAC B-Factor, Fermilab E653, E687/831, E769/791, E781, and CERN WA82/92 and WA89 collaborations reviewed the current status and future prospects. Exponential growth in charm sensitivity during the past decade, along with the rapid pace of advance in technology and computing, suggests the goal of 10^8 reconstructed decays (three orders of magnitude beyond current samples) for an experiment to run in the Year ≈ 2000 . This served as a unifying theme for the diverse areas of charm physics surveyed: spectroscopy, semileptonic decays, QCD tests, baryons, rare and forbidden decays, charm mixing and CP violation.

In contrast with beauty, for which the most exciting prospects are detailed tests of CP violation in the Standard Model, the grail for charm is physics Beyond the Standard Model, for which the rates of flavor-changing neutral currents, mixing, and CP violation expected in the Standard Model present negligible backgrounds. Observable effects in one or more of these areas are expected in theories which make useful predictions about the fermion masses and mixings, such as supersymmetry, technicolor and left-right-symmetric, grand-unified, and multiple-Higgs theories.

Also discussed were progress in pixel and diamond detectors, scintillating-fiber tracking, vertex triggers, and other new techniques which make the promise of a 10^8 -charm experiment realistic. Organizers and attendees were enthusiastic about the prospects for advancing the "programmatic" production, spectroscopy and decay physics by three orders of magnitude and essaying sensitivities of order 10^{-5} for mixing, 10^{-7} for rare decays, and 10^{-3} for CP asymmetries.

CONTENTS

Epitome	iii
Introduction	ix
Advisory and Organizing Committees, Working Group Convenors, and Workshop Staff	xi
Workshop Program	xiii
List of Participants	xvi

1 Invited Talks

Experimental Issues in High-Sensitivity Charm Physics	1
Jeffrey A. Appel	
Semileptonic Decays, Absolute Branching Ratios, and Charm Mixing.....	11
Jim Wiss	
Searching for CP Violation, Flavor Changing Neutral Currents, and Lepton Number Violation in Charm Decay.....	25
Paul D. Sheldon	
Future Experimental Charm Physics at $\sqrt{s} = 10$ GeV	35
Dave Z. Besson and Arne P. Freyberger	
BES Program and Tau/Charm Factory Prospects	57
Walter Toki	
Inclusive Charm Decays from QCD	67
Mike Luke	
Charm Mixing and CP Violation in the Standard Model	75
Gustavo Burdman	
Charm as a Probe of New Physics	85
Sandip Pakvasa	
Hadrons with Two Heavy Quarks	95
Jean-Marc Richard	
Future of Charm Photoproduction at Fermilab in the Next 3 Years and Beyond	103
John P. Cumalat	

CONTENTS

Charm Baryon Physics – Present and Future.....	111
Jim Russ	
Channeling Spin Precession as a Technique for Measuring Charm Baryon Magnetic Moments	123
Richard A. Carrigan, Jr. and Vincent J. Smith	
A Tau-Charm Factory at Argonne	135
Jim Norem and José Repond	
Charm Yields in a Dedicated B Experiment at RHIC	143
M. Atiya, S. White, and M. Marx	
Perspectives on Vertex Detectors.....	153
Luigi Moroni	
Diamond Detectors	163
Richard J. Tesarek	
Low-Pressure MSGC and a Search for a High-Efficiency Secondary-Electron Emitter .	171
David F. Anderson and Simon Kwan	
Fiber tracking	173
Randy Ruchti	
Particle Identification Issues for CHARM2000	193
Eli I. Rosenberg	
Transition Radiation Detectors	201
Marleigh Sheaff	
A Secondary-Vertex Trigger for Beauty Search	213
Dario Barberis <i>et al.</i>	
Triggers for High-Sensitivity Charm Experiments	221
David C. Christian	
A High-Rate Fixed-Target Charm Experiment	229
Daniel M. Kaplan	
Testing QCD in Charm Production	237
Giovanni Ridolfi <i>et al.</i>	
Anomalous Charm Production at Large x_F	251
Wai-Keung Tang	

CONTENTS

Direct Measurements of V_{cd} and V_{cs}	267
Tim Bolton	
Pentaquark Search with Energetic Hadron Beams	275
Murray A. Moinester <i>et al.</i>	
Reducing Systematic Effects in High-sensitivity Charm Experiments	287
Krishnaswamy Gounder and Donald Summers	
What Charm Can Tell Us About Beauty	297
Jonathan L. Rosner	
CHARM2000 Workshop Summary	313
Rollin J. Morrison	
 2 Contributed Papers	
Open Questions in Charm Decays Deserving an Answer	323
Ikaros Bigi	
Perturbative QCD Fragmentation Functions as a Phenomenological Model	335
Kingman Cheung	
Spectra of Heavy-Light Mesons	345
Estia J. Eichten, Christopher T. Hill, and Chris Quigg	
Orbitally Excited Heavy-Light Mesons Revisited	355
Estia J. Eichten, Christopher T. Hill, and Chris Quigg	
The E781 Trigger and Data-Acquisition System	371
Jürgen Engelfried	
The $D^0 - \bar{D}^0$ Mixing Search – Current Status and Future Prospects	375
Tiehui Liu	
Upper Limits for Charm Hadron Decays to Two Muons Plus a Hadron	395
Etsuko Niu	
W -Emission for $\Delta S = 1$ and $\Delta C = 1$ Weak Decays	407
Michael D. Scadron	
Charmonium Hadroproduction and CHARM2000	411
Leonard Spiegel	

CONTENTS

Polarization as a Probe to the Production Mechanisms of Charmonium in πN Collisions.....	415
Wai-Keung Tang <i>et al.</i>	
Warm Liquid Calorimetry Using TMP:An Update	423
WALIC Collaboration	
 3 Working-Group Summaries	
Charm Baryon Working Group Report	427
Harry W. K. Cheung and Peter Cooper	
CP Violation in the Charm Sector	433
K. Gounder <i>et al.</i>	
Report by the Charmed Mesons Working Group	435
Donald Isenhower <i>et al.</i>	
Summary Report of the Mixing Working Group	441
Tiehui Liu	
QCD Tests Working Group Summary	443
Vassili Papavassiliou	
Summary of the Rare Decay Working Group	451
Ai Nguyen and Paul Sheldon	
Semi- and Fully-Leptonic Decays of Charm	453
Dario Barberis <i>et al.</i>	
Architecture Working Group Summary	459
Charles N. Brown, Daniel M. Kaplan, and Donald J. Summers	
Triggering, Data Acquisition, and Computing Working Group Summary	463
Catherine C. James and Mike Halling	
Vertexing Working Group Summary	465
Charles Ray Newsom	
 4 Author Index	 469

Introduction

The past decade has seen an exponential rise in the sensitivities of charm experiments. The number of reconstructed decays is expected to reach 10^6 at CLEO and in the next round of fixed-target experiments (E781 and E831) at Fermilab; $> 10^8$ appears a feasible goal for the next generation of experiments. With this capability comes the potential to make charm decays an increasingly incisive probe into the Standard Model and to search beyond it.

The Workshop on the Future of High-Sensitivity Charm Experiments brought together theorists and experimentalists to explore both the motivation for and the technical challenges of achieving such sensitivity. Among the topics covered were expectations for charm mixing, CP violation, and flavor-changing neutral currents in the Standard Model and its possible extensions, testing perturbative and nonperturbative QCD and the Heavy-Quark Effective Theory, and advances in vertex detection, track reconstruction, particle identification, triggering, and data acquisition and analysis. Such key questions as

- what will be done and what left to do after current experiments
- which measurements will be the most incisive
- comparison of fixed-target vs. e^+e^- vs. hadron collider
- the importance for charm physics of possible accelerator upgrades

were discussed in invited talks and working-group sessions.

It is difficult at the inception of planning for a workshop to anticipate the level of interest. We organized CHARM2000 on rather short notice (about two months), publicizing it and receiving registrations mostly by electronic mail; posters were sent out a mere three weeks before the workshop. Based on the number of preregistrants we reserved Fermilab's Curia II meeting room (capacity 100). During Ken Stanfield's introductory talk it became apparent that we were bursting at the seams, so we negotiated a move to 1 West.

We attribute this enthusiastic response to the breadth and depth of charm physics, which stems from a number of circumstances:

- 1) The charm quark is the only charge-2/3 quark able to form bound states which can be perturbatively treated, yet it is light enough that higher-order and nonperturbative corrections can be tested.
- 2) Charmed particles can be produced in sufficient numbers for precision studies and high-sensitivity searches.
- 3) The Standard Model effects which give beauty its allure are suppressed in charm, making it a suitable venue to search for TeV-scale physics beyond the Standard Model.

At the workshop it became clear that current and upcoming experiments are far from exhausting the potential of charm physics to elucidate these issues. Charm will continue to be exciting as new levels of sensitivity are reached, and the ingenuity of experimenters will continue to be rewarded.

International Advisory Committee

J. A. Appel, *Fermilab*
E. L. Berger, *Argonne National Laboratory*
J. D. Bjorken, *SLAC*
C. N. Brown, *Fermilab*
J. Butler, *Fermilab*
G. Charpak, *CERN*
H. W. K. Cheung, *Fermilab*
D. C. Christian, *Fermilab*
P. Cooper, *Fermilab*
S. Csorna, *Vanderbilt University*
P. H. Garbincius, *Fermilab*
D. Hitlin, *California Institute of Technology*
R. Kass, *Ohio State University*
K. Kinoshita, *Virginia Institute of Technology*
J. Lach, *Fermilab*
L. M. Lederman, *Illinois Institute of Technology*
C. Quigg, *Fermilab*
L. Rossi, *University of Genova*
E. Shibata, *Purdue University*
M. Sokoloff, *University of Cincinnati*
M. Witherell, *University of California at Santa Barbara*

Organizing Committee

John P. Cumalat, *University of Colorado*
Daniel M. Kaplan, *Northern Illinois University*
Simon Kwan, *Fermilab*

Working Group Convenors

Charmed Baryons

Harry W. K. Cheung, *Fermilab*
Peter Cooper, *Fermilab*

Charm CP Violation

Sandip Pakvasa, *University of Hawaii*
Michael Sokoloff, *University of Cincinnati*

Charmed Mesons

Scott Radeztsky, *University of Wisconsin*
Shekhar Shukla, *Fermilab*

Charm Mixing

Tiehui Liu, *Harvard University*

QCD Tests

Tom Carter, *Fermilab*

Vassili Papavassiliou, *Argonne National Laboratory*

Rare Decays

Ai Nguyen, *Fermilab*

Paul D. Sheldon, *Vanderbilt University*

Semi- and Fully-Leptonic Decays

Arne Freyberger, *University of Florida*

Peter H. Garbincius, *Fermilab*

Architecture/Beam Options

Charles N. Brown, *Fermilab*

Donald J. Summers, *University of Mississippi*

Particle Identification

Eli I. Rosenberg, *Iowa State University*

Marleigh Sheaff, *University of Wisconsin*

Tracking

Seog Oh, *Duke University*

Randy Ruchti, *Notre Dame University*

Triggering, Data Acquisition, and Analysis

Mike Halling, *Fermilab*

Catherine James, *Fermilab*

Vertex Detection

Charles Ray Newsom, *University of Iowa*

Workshop Staff

William Luebke, *Northern Illinois University*

Olivia Vizcarra, *Fermilab*

CHARM2000 Workshop program
=====

MONDAY, 6/6

6:00-9:00 pm Registration/reception WH2 crossover

TUESDAY, 6/7

8:00 am Registration WH2 crossover

Session I: Review of current experiments Curia II D. Kaplan, chair

8:30 Stanfield Welcome, fixed-target prospects

***** too many people for Curia II --> move to 1-West! *****

8:45 Appel Experimental issues in high-sensitivity charm physics

9:15 Wiss Semileptonic decays and absolute branching ratios,
and charm mixing

10:15 Coffee break (15 min)

10:30 Sheldon CP violation, FCNC, and other rare decays

11:00 Freyberger Charm results from CLEO

Session II: Future experiments D. Christian, chair

11:40 Besson Future of charm physics at CLEO

12:00 Toki BES, PEP-II, and tau/charm prospects

12:30 Lunch (1 hr 15 min)

Session III: Issues in charm theory D. Christian, chair

1:45 Luke HQET and inclusive semileptonic charm decays

2:15 Burdman Charm mixing and CP violation in the Standard Model

2:45 Pakvasa Rare decays, CP violation, and mixing beyond the Standard
Model

3:15 Richard Baryons with more than one charm quark

3:45 Coffee break (15 min)

4:00 - 7:00 Working groups I: Physics topics

WEDNESDAY, 6/8

Session II (cont'd)

C. Brown, chair

8:30 Cumalat Future of photoproduction
8:55 Russ Charmed baryons
9:20 Carrigan Charmed-baryon magnetic moments
9:35 Dunietz An idea about charmed-baryon factories
10:05 Repond Possible tau/charm factory at Argonne

10:20 Coffee break (15 min)

10:35 White Charm production at RHIC
10:50 Butler Comparing fixed-target and collider

Session IV: Experimental techniques

J. Cumalat, chair

11:05 Moroni Perspectives on vertex detectors
11:30 Tesarek Diamond detectors
11:45 Parker Monolithic pixel detectors
12:00 Anderson Gas microstrip detectors
12:15 Ruchti Fiber tracking

12:30 Lunch (1 hr 15 min)

1:45 Rosenberg/Sheaff Particle ID
2:15 Barberis WA82/92 vertex trigger
2:40 Christian Triggers for a high-sensitivity charm experiment
3:05 Kaplan A possible high-rate experiment

3:30 Coffee break (15 min)

3:45 - 6:45 Working groups II: Experimental techniques and issues

7:00 pm Workshop Banquet at Chez Leon

THURSDAY, 6/9

Session V: Theory, experiment, and summary

D. Kaplan, chair

List of Participants

Akchurin, Nural, University of Iowa	Luke, Michael, University of Toronto
Appel, Jeffrey A., Fermilab	Moinester, Murray, Tel Aviv University
Barberis, Dario, University and INFN/Genova, Italy	Moroni, Luigi, INFN Milano (Italy)
Besson, Dave, University of Kansas	Morrison, Rollin, University of California at Santa Barbara
Bolton, Tim, Columbia University	
Brown, Chuck, Fermilab	Newsom, Charles Ray, University of Iowa
Burdman, Gustavo, Fermilab	Nguyen, Ai, Kansas State University
Butler, Joel N., Fermilab	Niu, Etsuko, CERN
Carrigan, Richard, Fermilab	Niu, Kiyoshi, CERN/Nagoya University
Cason, Neal, University of Notre Dame	Norem, Jim, Argonne National Laboratory
Cheung, Harry, Fermilab	Oh, Seog, Duke University
Cheung, Kingman, Northwestern University	Onel, Yasar, University of Iowa
Christian, David, Fermilab	Pakvasa, Sandip, University of Hawaii
Chung, Yeon Sei, Korea University	Papavassiliou, Vassili, Argonne National Laboratory
Cooper, Peter, Fermilab	Parker, Sherwood, University of Hawaii
Cooper, W. E., Fermilab	Peng, K. C., Illinois Institute of Technology
Cumulat, John, University of Colorado	Perasso, Laura, INFN Milano (Italy)
de Oliveira, Edgar C., CBPF/CNP, Brazil	Priestein, Dave, University of California at Berkeley
di Corato, Maria, Milano University and INFN	Procario, Michael, Carnegie Mellon University
Dunietz, Isi, Fermilab	Quigg, Chris, Fermilab
Durandet, Casey, University of Wisconsin	Reidy, James J., University of Mississippi
Eichten, Estia, Fermilab	Repond, Jose, Argonne National Laboratory
Engelfried, Jürgen, Fermilab	Richard, Jean-Marc, Inst. des Sciences Nucleaires, Univ. Joseph Fourier
Fernandez, Arturo, Univ. Autonoma de Puebla, Mexico	Ridolfi, Giovanni, CERN
Freyberger, Arne, University of Florida	Rosenberg, Eli I., Iowa State University
Garbincius, Peter H., Fermilab	Rosner, Jonathan L., University of Chicago
Gardner, Robert W., University of Illinois	Ruchti, Randy, University of Notre Dame
Garren, Lynn, Fermilab	Russ, Jim, Carnegie Mellon University
Gounder, K., University of Mississippi	Rust, David R., Indiana University
Grim, Gary, University of California at Davis	Scadron, Michael D., University of Arizona
Hahn, Alan, Fermilab	Schwartz, Alan, Princeton University
Halling, Mike, Fermilab	Selove, Walter, University of Pennsylvania
Herrera, Gerardo, CINVESTAV/Fermilab	Sheaff, Marleigh, University of Wisconsin
Horvath, John F., Purdue University	Sheldon, Paul, Vanderbilt University
Isenhower, Donald, Abilene Christian University	Shukla, Shekhar, Fermilab
James, Catherine, Fermilab	Sokoloff, Michael D., University of Cincinnati
Kaplan, Daniel M., Northern Illinois University	Spiegel, Lenny, Fermilab
Karchin, Paul, Yale University	Stanfield, Kenneth C., Fermilab
Kennedy, Chris, Yale University	Summers, Don, University of Mississippi
Kinoshita, Kay, Virginia Tech	Tang, Wai-Keung, SLAC
Kopeliovich, Boris, JINR	Tesarek, Richard, Rutgers University
Kreymer, Arthur, Fermilab	Toki, Walter, Colorado State University
Kwan, Simon, Fermilab	Torretta, Donatella, Fermilab
Lach, Joe, Fermilab	Watanabe, Shoji, University Wisconsin - Madison
Lau, Kwong, University of Houston	White, Sebastian, Brookhaven National Laboratory
LeBrun, Paul, Fermilab	Wiss, Jim, University of Illinois, Urbana-Champaign
Liu, Ted (Tiehui), Harvard University	Yager, Philip M., University of California at Davis
Lopez, Angel M., University of Puerto Rico	Zhang, Chong, Kansas State University

1 Invited Talks

EXPERIMENTAL ISSUES IN HIGH-SENSITIVITY CHARM EXPERIMENTS

Jeffrey A. Appel
Fermi National Accelerator Laboratory*

CHARM2000 Workshop

June 7, 1994

Abstract

Progress in the exploration of charm physics at fixed target experiments has been prodigious over the last 15 years. The issue before the CHARM2000 Workshop is whether and how this progress can be continued beyond the next fixed target run. An equivalent of 10^8 fully reconstructed charm decays has been selected as a worthy goal. Underlying all this is the list of physics questions which can be answered by pursuing charm in this way. This paper reviews the experimental issues associated with making this next step. It draws heavily on the experience gathered over the period of rapid progress and, at the end, poses the questions of what is needed and what choices may need to be made.

*Work supported by the U.S. Department of Energy under contract No. DE-ACO2-76CHO3000.

1. Progress and Projections

One measure of the progress in charm physics over the last 15 years is the number of charm decays fully reconstructed by a single experiment. In 1980, a fixed target experiment was lucky to observe one hundred such decays. Many experiments before had actually failed to produce significant signals at all. However the real progress has come since that time. Figure 1 demonstrates the exponential growth in Fermilab fixed target charm samples since 1980.^[1] The rate of growth has averaged 1.7 per year, a factor of 5 per running period. This growth is projected to continue at about the same rate into the next running period also.

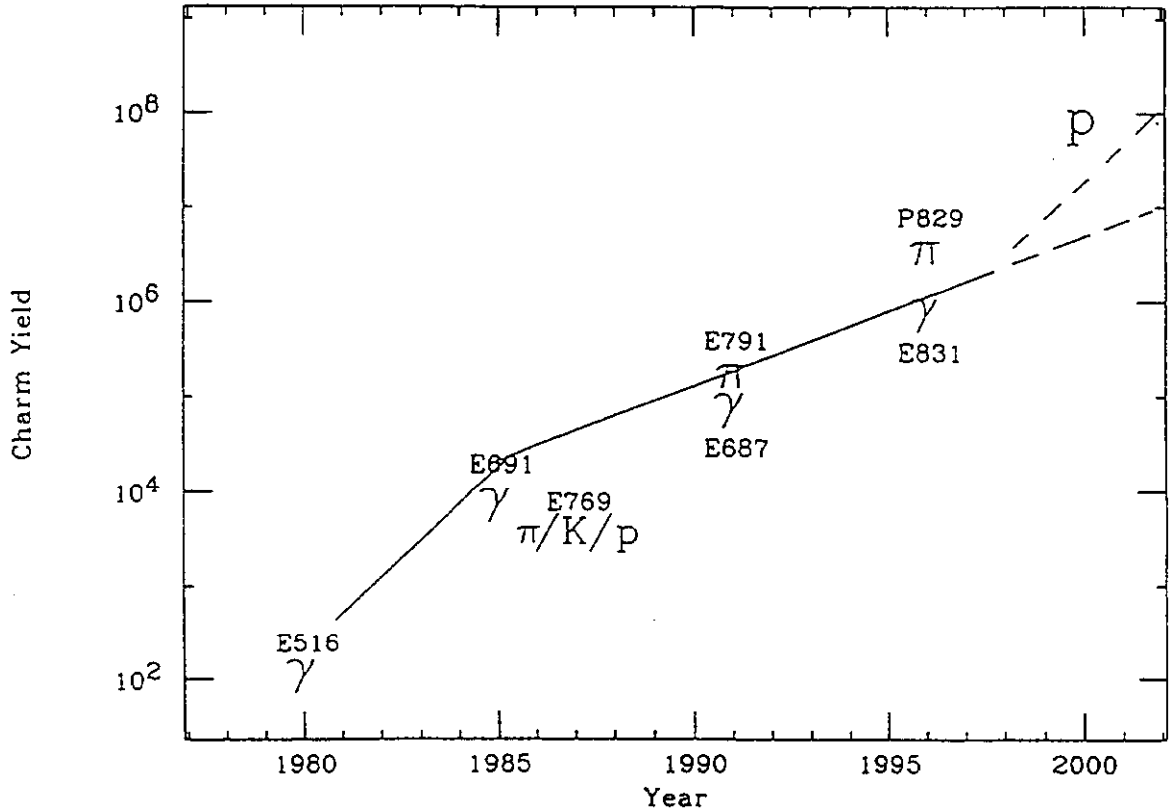


Fig. 1. Progression of the number of reconstructed charm decays in Fermilab fixed-target experiments.

The announced goal of the CHARM2000 Workshop is 10^8 fully reconstructed charm decays. As can be seen in Fig. 1, this requires a step as great as the most aggressive single step achieved in the history of the last 15 years.

2. New Techniques Along the Way So Far - Critical Issue

The single biggest step in the progress shown in Fig. 1 appeared with the ability to do precision vertex determination combined with the ability to handle vastly increased amounts of data.^[2] These advances were made possible by the introduction of silicon microstrip detectors (SMDs) and parallel processing farms of inexpensive computers. These, in turn, allowed the

experimenters to take advantage of the good duty factor and high intensity, high energy beams of the Tevatron accelerator. The rather open on-line event selection is what resulted in an impressive range of physics capability, and is why the CHARM2000 goal is stated in terms of fully reconstructed charm decays.

The size of the biggest step in increased charm capability came mostly because of the silicon microstrip detectors. These have been widely recognized as *the* important technological innovation making high statistics charm experiments possible in a fixed target environment. The precision tracking of particles with the SMDs is used in the separate identification of the primary interaction vertex and the charm particle decay vertex. This, in turn, has two features which are both essential in improving capability: first, the selection of events which have a high probability of charm in them and second, the identification of that subset of tracks coming from a charm decay. Both features assist in improving the signal over background. The latter feature is specially critical in hadroproduction where the total number of tracks in a charm event is quite high.

In spite of the importance of the SMDs, additional technological innovation has been needed. This additional innovation was primarily associated with handling ever increasing amounts of data. Off-line computer power increased about as fast as the increase in charm samples. However, it has also been necessary to speed up the front end signal processing, to increase data readout rates, to add on-line data storage, as well as to increase long term data storage density and cost effectiveness. These features have been the primary engines of increased physics capability since the introduction of the SMDs.

The list of technological advances has been quite long. All of the advances have been necessary in order to maintain the exponential growth of the number of reconstructed charm decays. The reach of the next fixed target run depends on applying these same set of improvements. However, aside from the anticipated reduction in the per-calculation-cost of off-line computing, no new technology has yet been identified for the next run. What can one say about the period beyond the next fixed target run? Some new technology will need to be applied to continue the current rate of improvement. Some extra ordinary improvement will be needed to reach 10^8 reconstructed charm decays.

3. Other Relevant Experimental Issues

Beyond the critical issue of technological innovation, there exists a rather long list of choices to be made in preparing an experiment. These choices may be influenced, even driven, by any technological innovation planned. Failing to have identified an obvious such innovation, it is still possible to review the issues which have been important so far. These had best be considered when an experiment is conceptualized.

It is important to remember that an experiment is always a compromise among divergent pulls. Yet, one often hears that a particular factor is enough to justify proposing a new effort. In fact, it is the combination of choices which must work together to achieve an experimental goal. Thus, no one of the following set of issues can be viewed independently of the others. They each play a role in determining how well an experiment can do in reaching toward a particular goal. And, the particularity of the goal matters. Different goals (at a minimum, different final decay modes of a particular charm particle) will have different benefits from any experiment configuration choice. There is no choice which is best for everything.

3.1. Cross Sections and Rate Projections

By now, cross sections for the common charm particles as seen in particular decay modes are well measured by multiple experiments. In photoproduction, the cross section is forward peaked (typically reaching a maximum at Feynman x of 0.2) and the cross section is slowly saturating at the energies achievable with today's Tevatron.[3] In hadroproduction, the cross section is still rising at Tevatron energies, growing by a factor of two for each factor of two in available beam energy.[4] The mesons are produced more centrally and, for protons, are symmetric about Feynman x of 0.0. The falloff with Feynman x is quite steep, although leading particle effects may be useful for restricted classes of charm studies (e.g., baryon physics as proposed for E781). The total cross section for photoproduction reaches about 1 microbarn, while for forward hadroproduction (Feynman $x > 0.0$) the cross section is more like 20 microbarns.

3.2. Incident Particles

While the cross section for charm production is essential for reaching the 10^8 level of reconstructed charm decays, the cross section is not the only feature of importance related to the incident particle type. The track multiplicity in events, for example, and the resulting signal to background are important. After all, the reason to seek 10^8 decays is to reach more rare occurrences, and backgrounds must be reduced to make the signals useful for physics.

Photoproduction and hadroproduction track multiplicities are shown in Fig. 2. The most likely number of tracks in photoproduction E691 was 10, while in hadroproduction E791 the value is about 14. Even among the hadroproduction beam options, there are differences. Signal to background is somewhat worse for protons than for pions and kaons, even after selecting optimal cuts. Of course, the event selection for proton induced events is more demanding and the efficiency is lower - just as was the case in going from photoproduction to hadroproduction and achieving the same signal to background levels. There is about a factor two lower acceptance in hadroproduction relative to photoproduction when the same signal to background is required.

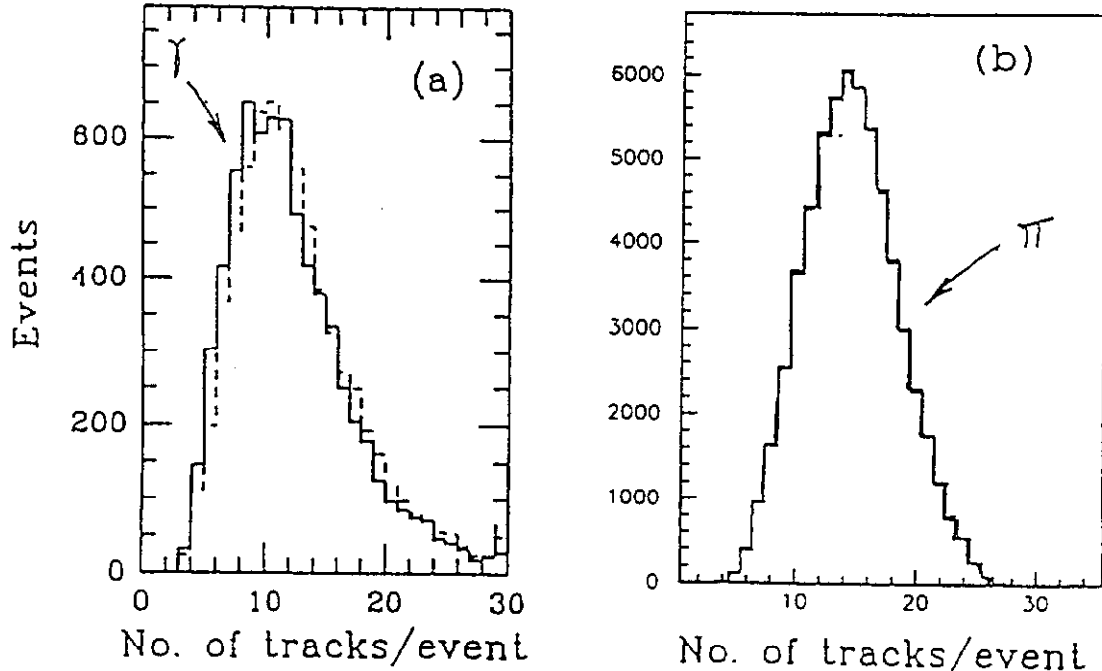


Fig. 2. Charged track multiplicity in (a) photoproduced charm events and (b) hadroproduced charm candidate events.

3.3. Event Topologies

The cloud of particles produced in the violent interactions which produce charm may be a problem in terms of event reconstruction complexity and backgrounds. However, there is a silver lining to that cloud. In particular, the higher average track multiplicity is useful in identifying the primary interaction point. The precision with which that vertex can be specified is also improved. Having an incident high momentum track is also useful in specifying the transverse location of the primary interaction.

3.4. A Dependence and Other Target Material Issues

Heavy nuclear targets appear beneficial in rate calculations since the charm production rate is roughly proportional to the atomic weight of the target, A . On the other hand, heavy targets are ruled out for photoproduction (due to pair conversions of the beam). In hadroproduction, there are a number of penalties paid for a heavy target. These include (1) higher track multiplicity with the concomitant worse signal to background for a given set of cuts, (2) lower efficiencies for most signals at the optimal cuts, (3) possibly worse mass resolution (certainly when decays are allowed in the target or when multiple target foils are used).

3.5. Decays in Free Space

The importance of secondary interactions as a source of backgrounds for charm signals has become increasingly apparent to experimenters. Candidate charm decays appear at downstream locations where there is material. E687 is showing generic charm generated Monte Carlo events which model the wings of mass distributions only when the decays are selected as appearing in free space.^[5] Otherwise (i.e., when vertices are allowed to appear in matter), the backgrounds are significantly worse.

3.6. Acceptance Issues

In designing an experiment, a kinematic region for accepted events is selected consciously or unconsciously. This selection has implications for (1) the rates of reconstructed decays, (2) the resolutions of mass and other parameters and (3) the signal to background ratios. Typically, where the rates are smaller, the signals are cleaner. Thus, less background is generally evident in plots at higher Feynman x and at higher transverse momentum. On the other hand, since higher Feynman x corresponds to higher decay particle momenta, the mass resolution is surprisingly worse at high Feynman x . In E791, for example, the mass resolution at Feynman x of 0.8 is three times worse than at the optimal 0.1. Multiple scattering dominates only below this value of Feynman x . This may come as a surprise to people used to e^+e^- environments.

There is a little noticed implication of acceptance for mixing searches in D^0 hadronic decays. The acceptance as a function of proper lifetime is a function of the selection criteria used. The more selective one becomes, as required to push mixing limits further, typically the more reduced is the efficiency for short lifetimes. On the one hand, this helps in getting away from the background posed by doubly Cabibbo suppressed decays which have an exponential dependence on proper lifetime. The mixing signal is expected to be maximal at two proper lifetimes. On the other hand, once one allows for interference between the doubly Cabibbo suppressed decay amplitude and the mixing amplitude, one needs acceptance in the short lifetime regime as well, in

order to separate the two possible sources of decay. Doubly Cabibbo suppressed decays are background to the much more interesting possibility of D^0 mixing.

In the same way that inefficiency at shorter lifetimes affects the D^0 mixing capability of an experiment, it also influences the capability of observing one charm particle relative to another. Since tighter cuts are required in charm hadroproduction than in photoproduction, the capability of hadroproduction for charm mesons will be optimal relative to photoproduction. For the shorter-lived charm baryons, on the other hand, hadroproduction experiments will have reduced efficiency.

4. Trigger, Data Acquisition, and Off-Line Computing Issues

While trigger, data acquisition and off-line computing has been made a separate section of this review, it is really a continuation of the previous section on experimental issues. Choices of experimental configuration have a direct effect on triggering, data acquisition and off-line computing. It would be better to think of the whole configuration together. Restricting acceptance of the detector to particular regions of phase space or particle types directly affects triggering and is a part of it. The choice of very wide acceptance and the selection of more complicated events directly influence the computing load of the experiment, both on-line and off-line.

4.1. Triggers - Event Selection Issues

The main goal of the experiment trigger is to enrich the charm fraction of the sample of events which enter the data acquisition stream and pass along it. This enrichment, E , is the product of the rejection of unwanted events, R , and the efficiency of the trigger for the events of interest, eff .

$$E = R * eff \quad (1)$$

The goal is to optimize E , not R or eff alone. The associated issues include the level of sophistication required and the level of complexity needed. Somewhere among these words should be read cost and difficulty.

Recent fixed target triggers for charm have been notable for their directness, simplicity, and openness. This is in distinction to the first charm experiment at the Tagged Photon Laboratory, E516. In that case, a very fast and sophisticated system (the ECL-CAMAC Trigger Processor^[6]) was designed and built to select events with large forward going effective mass, based on measurements of recoiling protons alone. The system worked very well technically. However, it failed to enrich the sample of recorded events. The measurement was indirect and the efficiency for the average charm particle was low. The more open triggers in use now either accept almost all hadronic interaction events or select those events with high forward effective mass (approximated by transverse energy) measured directly by observing the relevant particles themselves.

The options for selecting charm events at the trigger level comprise a reasonably long list. A version of the list presented in 1981 at Erice is shown in Table I. As far as I am aware, this was the first time that transverse energy was suggested as a trigger for charm in fixed target experiments.^[7] Missing from the Erice trigger list is direct observation of evidence for secondary charm decay vertices. Many have proposed, and recently experiments at CERN and E789 at Fermilab have used sophisticated triggers looking for such evidence on-line. These triggers are the most direct charm cuts one can use on-line. They are similar to the important off-line analysis selection cuts for charm events used by all. However, two things should be noted. Even having

the full reconstruction of events with final calibrations of the detector, early-selection subsets of data have only been reduced by typical factors of 5-10 using this kind of information. The smallness of this factor may be due, in part, to the ability to handle large data sets and to a natural conservatism.

Table I.

Trigger Possibilities	
A. Target Recoil	
1. High Forward Mass	
*a. Missing Mass à la TPL	
b. $T > T_{MIN}$ or Recoil $KE > KE_{MIN}$	
2. Coherence of Scattering From Nucleus	
a. For later reconstruction	
b. Primakoff trigger for η	$c, b...$
B. Decay Product	
1. High p_T	
*a. Leptons	
b. Charged particles	
2. Decay Chain	
a. K^\pm in Cerenkov/momentum correlation	
b. K^0, Λ^0 - Downstream V^0 or ΔQ	
c. π^\pm from $D^* \rightarrow D \pi$	
$B^{**} \rightarrow B \pi$	
d. ΔQ 's near target	
e. ν - missing energy	
C. Event Topology	
1. Multiplicity	
2. $\Sigma p_T , \Sigma p_T^2, \Sigma w^2$ from calorimeters	
(*Triggers which had been used by 1981)	

However, it will take courage to reject larger factors on-line than experiments have been willing to reject off-line. The largest rejection which can be obtained reasonably with a transverse energy requirement on-line is about 5. In conjunction with such a transverse energy cut, the extra rejection of a secondary vertex trigger will be worse. The larger factors of rejection sometimes cited also fail to maintain efficiency for final charm samples. The factors of enrichment which one reads in the literature are usually for the longest-lived charm particles only.

4.2. Data Acquisition Issues

Most recently at Fermilab, experiments have taken to increasingly powerful data acquisition systems and recording increasingly large data sets. This has been made possible by improvements in electronic circuits, to be sure, but mostly by the growth of parallelism and the cost effectiveness of writing data to 8mm magnetic tape. Table II demonstrates this pattern from the experiments at the Tagged Photon Laboratory. The data set sizes have grown by a factor of 700 in the decade of the 80's, the number of events by 1000. The number of reconstructed charm decays in final data sets has grown by even more, a factor of about 2000. A continuation of this trend requires technology beyond what is presently foreseeable. Thus, there is great interest in improving triggers and/or moving more computing on-line in the future.

Table II.

Growth of DA Parallelism							
Time Frame	Exp.	# Data Streams	# CPUs	# Output Streams	# Events	Data Set Size	# Reconstruct Charm
1980 - 2	E-516	1	1	1	20 M	70 GBytes	100
1984 - 5	E-691	2	1	1	100 M	400 GBytes	10,000
1987 - 8	E-769	7	17	3	400 M	1,500 GBytes	4,000
1991 - 2	E-791	8	54	42	20,000 M	50,000 GBytes	200,000

4.3. Off-Line Computing Issues

The trend toward more cost effective computing seems to be continuing at the same phenomenal rate as over the last decade. This implies that continuation of the general slope seen in Fig. 1 is possible from this point of view. However, even with these expected gains, additional improvements will be required to reach 10^8 reconstructed charm decays. Again, the trigger is usually hoped to provide the answer.

5. Summary and Conclusions

It is necessary to put all the above considerations together in proposing an experiment to achieve the goal of 10^8 reconstructed charm decays. Using the example of a hadron beam experiment proves instructive. What happens if one tries to reach the goal? The flow is shown in Table III. A first pass through the conceptual design steps requires a return to the first step in an iterative procedure. It is not clear that one can reach the goal by simple extension of current concepts.

Table III.

REACHING FOR 10^8 RECONSTRUCTED CHARM DECAYS - SIMPLE HADRONIC EXTENSION?		
1. Reconstructed charm = $0.005 \times$ number of charm events	→	2×10^{10} charm events
2. Charm events = 0.002 of hadron induced interactions	→	10^{13} interactions
3. 2-10% interaction length target hadrons	→	1.5×10^{14} inc.
4. 3×10^6 seconds of beam spill	→	30-160 Mhz beam
5. Suppose 100 MBytes/second into DA pipeline		
6. and 3 KBytes/event	→	30 K events/second
7. Given the above lines 2 and 4	→	3 Mhz interaction rate
8. Given above lines 6 and 7	→	Trigger $R = 100$
9. But, as trigger rejection must go from today's factor of 5	→	Return to line 1
<i>(Remember to reduce efficiency in line 1 when R increases)</i>		

The basic question in my mind is whether a 10^8 reconstructed charm decay experiment can be achieved by this simple extension of current techniques. A new technological breakthrough (akin to that provided by SMDs) is required. Furthermore, even with 10^8 reconstructed decays, do we know how to extrapolate current precision and upper limits into the future? What would be the equivalent number of decays needed in terms of physics reach? Narrowing the physics goals to the most important ones will allow more incisive choices and better matched compromises.

For these reasons, I prefer to think about 10^8 equivalent charm decays. That is, without a new breakthrough, I don't expect a generic, open geometry experiment whose physics reach is represented by extrapolation to 10^8 . We will need to narrow our focus, our experiment design, to

particular physics goals. Then, it may be possible to achieve the desired physics sensitivity for those particular goals. Otherwise, we need something that breaks with recent tradition. Hopefully, the CHARM2000 workshop will point the way to the best choices of physics and experiment setup.

Acknowledgements

I am specially indebted to my colleagues on the series of charm experiments performed over the last 15 plus years at the Tagged Photon Laboratory. I want to mention specifically Gilvan Alves, Steve Bracker, Tom Carter, Catherine James, Paul Karchin, Simon Kwan, Lalith Perera, Milind Purohit, Marleigh Sheaff, Don Summers, Keith Thorne, Andrew Wallace, and Zhongxin Wu whose works I have specifically consulted in preparing this review. I also thank David Christian for use of his plot in Fig. 1.

References

- ¹ D.C. Christian, *private communication*.
- ² (E691 Collaboration) J. R. Raab et al.; *Phys. Rev. D* **37**, 2391 (1988).
- ³ E687, NA14 and E691 data summarized by A. Ali, *DESY 93-105*, Lectures given at the *XXI International Meeting on Fundamental Physics*, Miraflores de la Sierra, Madrid, 9-15 May, 1993; to appear in the *Proceedings* (Eds. F. Barreiro et al.).
- ⁴ NA27, NA32, E653 and E769 data on pions and NA27, E653, E743 and E769 data on protons summarized by A. Wallace et al., *FERMILAB-Conf-94/184*.
- ⁵ (E687 Collaboration), J. Cumalat and L. Moroni, in *Proceedings of the CHARM2000 Workshop*.
- ⁶ J. Martin et al, *FERMILAB-CONF-81/40-EXP* and *CERN Microproc.1981:164* (QCD201:T6:1981).
- ⁷ J. A. Appel, *Europhysics Study Conf. on Search for Charm, Beauty and Truth*, Erice, Sicily, Nov 15-22, 1981. Published in *Erice EPS: Charm 1981:555* (QCD161:E86:1981).

Semileptonic Decays, Absolute Branching Ratios and Charm Mixing

Jim Wiss

University of Illinois at Urbana-Champaign

413 Loomis Lab

1110 W. Green

Urbana, IL. 61801

Abstract

We review recent results on charm semileptonic decays, make some guesses at the future of charm semileptonic physics, outline a method for measuring charm absolute branching fractions in fixed target experiments, and review recent progress in obtaining limits for $D^0 - \bar{D}^0$ mixing.

1 Charm Semileptonic Decay

I will fail in my attempt to do adequate justice to the huge number of new, interesting experimental results which have been made available in the last few years given space limitations. Below is a highly schematic table which summarizes the states which have been studied, how they have been studied, and either the realized or future () physics potential of such measurements.

Exp	decay	physics	tricks	Cabibbo allowed?
e^\pm , ft	$D^0 \rightarrow K^- \ell \nu$	$f_+(q^2)$	D^* WS	✓
ft	$D^+ \rightarrow K^* \ell \nu$	$A_1(0), V_1(0), V_2(0)$	WS	✓
e^\pm , ft	$D_s^+ \rightarrow \phi \ell \nu$	Abs Bf ff		✓
e^\pm	$D^+ \rightarrow \pi \ell \nu$	V_{cd}/V_{cs} ($f_+(q^2)$)	D^* , $\gamma\gamma$	X
e^\pm	$\Lambda_c^+ \rightarrow \Lambda \ell \nu$	Abs Bf , HQET	WS	✓
ft, e^\pm	$D_s^+ \rightarrow (\eta + \eta') \mu \nu$	(Vec/PS)		✓
ft	$D^+ \rightarrow \rho \mu \nu$	$(V_{cd}/V_{cs} \rightarrow V_{bu})$	6 evt	X

Results from fixed target experiments (ft) continue to complement those from e^+e^- annihilation (e^\pm). Charm semileptonic studies provide a wealth of information including:

important probes of quark dynamics through measurements of form factors ($f_+(q^2)$) and ($A_1(0), V_1(0), V_2(0)$), model dependent information on the absolute branching ratios (Abs BF) for the D_s^+ and Λ_c^+ , information on CKM matrix elements (V_{cd}/V_{cs}), and tests of HQET. Determination of CKM matrix elements (V_{bu}) and more stringent tests of HQET will be possible through the interplay of studies of both charm and beauty semileptonic decay results. At present there is a long standing theoretical problem with the observed ratio of vector to pseudoscalar decay widths for $D^+ \rightarrow K^* \ell \nu$ relative to $D^+ \rightarrow K \ell \nu$ [1] which may be clarified through comparisons of the width for $D_s^+ \rightarrow \phi \mu \nu$ to $D_s^+ \rightarrow (\eta + \eta') \mu \nu$ (Vec/PS). Because of the undetected ν , one only partially reconstructs the final state leaving the important experimental challenge of proving exclusivity of the final state; ie one must establish that one is observing the claimed final state without additional, undetected neutrals. A variety of experimental techniques can be brought to bear on the problem of isolating semileptonic decays from both non-charm and charm backgrounds. Frequent use is made of D^* tagging (D^*). One often has the ability to exploit the charge correlations between leptons and kaons or D^* decay pions and thus eliminate backgrounds through a wrong sign subtraction (WS). Often, in fixed target experiments, Cabibbo forbidden decays (X) are subject to particle mis-identification backgrounds from the much more copious Cabibbo allowed (\checkmark) decays.

1.1 $D^0 \rightarrow K^- \ell^+ \nu$ and $D \rightarrow \pi \ell \nu$

These decays are particularly interesting to study since they can provide information on the q^2 dependence of the charm semileptonic form factors, $f_+(q^2)$. The decay rate expression for $K \ell \nu$ is:

$$\frac{d\Gamma}{dq^2} = \frac{G_F^2 |V_{cs}|^2 P_K^3}{24\pi^3} \{ |f_+(q^2)|^2 + m_\ell^2 |f_-(q^2)|^2 \dots \} \quad (1)$$

where P_K is the momentum of the kaon in the D^0 rest frame and one of the two allowed form factors $f_-(q^2)$ becomes unimportant in the limit of zero lepton mass. Two parameterizations are used for $f_+(q^2)$:

$$f_+(q^2) = \frac{f_+(0)}{(1 - q^2/m_{pole}^2)} \quad \text{or} \quad f_+(q^2) = f_+(0)e^{\alpha q^2}$$

The first form is motivated by the belief that the coupling of the cs quarks to the virtual W^\pm should be dominated by bound states¹ of the $c\bar{s}$ system; the second form is motivated [2] by the ISGW model. Figure 1(a) illustrates the difference between $f_+^2(q^2)$ for a pole form, an exponential form and a linear form. Over the restricted q^2 range available for the presently studied $D^0 \rightarrow K^- \ell^+ \nu$ decay, one is primarily measuring just the slope ratio, $(df_+/dq^2(0))/f_+(0)$. To go further, we will probably have to wait for the future for measurements of $D^0 \rightarrow \pi^- e^+ \nu$ so that the q^2 domain can extend much closer to location of the anticipated D^{*+} (rather than D_s^{*+}) pole. Figure 1(b) illustrates that $f_+^2(q^2)$ has a rather subtle, asymmetric, and difficult to measure influence on $d\Gamma/dq^2$. Most of one's ability to measure beyond $f_+(0)$ and $df_+/dq^2(0)$ occurs at large q^2 where the rate is low.

¹Hence one expects that m_{pole} should be set to the mass of the vector $D_s^*(2110)$ since it has the same spin-parity as the current described by the form factor.

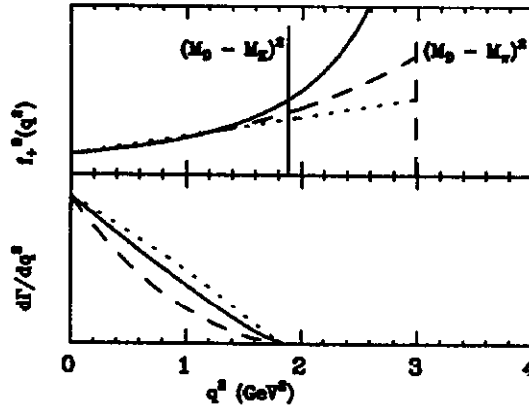


Figure 1: (a) Various parameterizations of $F_+^2(q^2)$ over the kinematic range for $D^0 \rightarrow K^- e^+ \nu$ (vertical solid) and $D^0 \rightarrow \pi^- e^+ \nu$ (vertical dashed). The pole form (solid), exponential form (dashed) and a linear form (dotted) are displayed. (b) $d\Gamma/dq^2$ for $m_{pole} = 2.1 \text{ GeV}$ (solid), $m_{pole} = \infty$ (dashed), $m_{pole} = 1.8 \text{ GeV}$ (dotted)

Much of the information on the detailed decay shapes originally came from fixed target experiments which exploit their generally excellent vertexing capability in order to “close” the decay kinematics and measure q^2 . The momentum of the unobserved neutrino can be measured to within a two fold ambiguity by balancing p_t about the line between the primary and secondary vertex. The CLEO Collaboration [2] recently devised a way of obtaining q^2 information without using information about the D^0 line of flight which is illustrated in Figure 2.

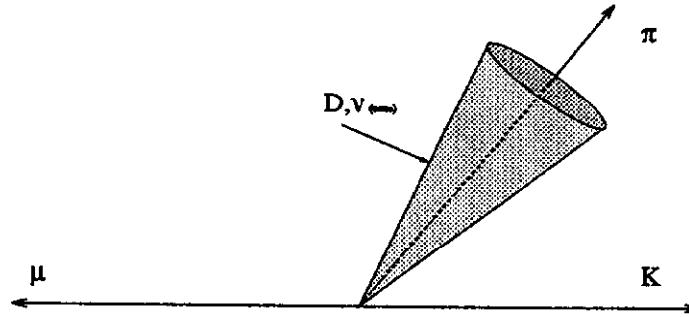


Figure 2: Boost the π from the $D^{*+} \rightarrow \pi^+(K^- \ell^+ \nu)$ decay to the $K^- \ell^+$ rest frame. The ν momentum can be computed from the D^0 mass; and the angle θ between the π and the ν can then be computed from the D^{*0} mass. q^2 is bounded by minimum q^2 on the neutrino cone closest to ℓ and a maximum q^2 furthest from ℓ .

Figure 3 shows the fits to the $d\Gamma/dq^2$ distribution obtained by CLEO and preliminary results obtained by the E687 collaboration. One can measure $f_+^2(0)$ by integrating the $d\Gamma/dq^2$ expression given by Eqn. (1) using the measured $f_+(q^2)/f_+(0)$ shape and setting the integrated width to the measured total width for $\Gamma(K^- \ell^+ \nu)$. In some experiments, $\Gamma(K^- \ell^+ \nu)$ is obtained by measuring the ratio of $K^- \ell^+ \nu / K^- \pi^+$ yields which can be converted to a width using the $D^0 \rightarrow K^- \pi^+$ absolute branching ratio and the known D^0 lifetime. The below table summarizes information on the $f_+(q^2)$ form factor which describes $D^0 \rightarrow K^- \ell^+ \nu$ decay.

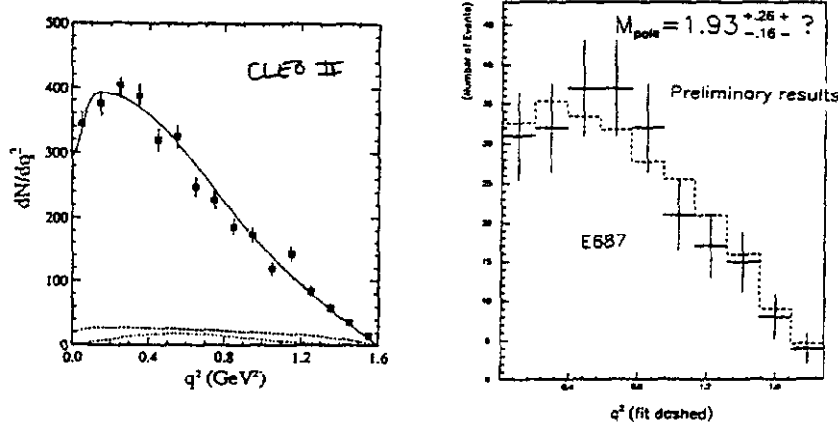


Figure 3: The uncorrected $d\Gamma/dq^2$ distribution obtained in a ≈ 2700 sample of $D^0 \rightarrow K^- \ell^+ \nu$ decays from CLEO and a preliminary, uncorrected $d\Gamma/dq^2$ distribution from a ≈ 500 event sample obtained by E687.

Exp.	Mode	m_{pole}	$ f_+(0) $
E691[3]	$K^- e^+ \nu_e$	$2.1^{+0.4}_{-0.2} \pm 0.2$	$0.79 \pm 0.05 \pm 0.06$
CLEO(91)[4]	$K^- e^+ \nu_e$	$2.1^{+0.4+0.3}_{-0.2-0.2}$	$0.81 \pm 0.03 \pm 0.06$
CLEO(93)[2]	$K^- l^+ \nu_l$	$2.00 \pm 0.12 \pm 0.18$	$0.77 \pm 0.01 \pm 0.04$
MKIII[5]	$K^- e^+ \nu_e$	$1.8^{+0.5+0.3}_{-0.2-0.2}$	$ V_{cs} (0.72 \pm 0.05 \pm 0.04)$
E687 (prelim)	$K^- \mu^+ \nu_\mu$	$1.93^{+0.26+?}_{-0.16-?}$	$0.70 \pm 0.04 \pm ?$

All results appear consistent with the expected D_s^{*+} pole mass of 2.1 GeV. The $f_+(0)$ values are also consistent with theoretical estimates: $f_+(0) \approx 0.7 - 0.9$. CLEO obtains an exponential fit to the alternative form: $f_+(q^2) \propto \exp(0.29 \pm 0.04 \pm 0.06) q^2$ which as illustrated in Figure 1 (a) is nearly indistinguishable from the pole form (but has more symmetrical error bars).

CLEO [6] has recently made a measurement of $D^+ \rightarrow \pi^0 \ell \nu / K^0 \ell \nu$ which is substantially free of the usual misidentification background expected for a π^\pm . Their signal is brought out through tagging via $D^{*+} \rightarrow \pi^0 D^+$ decay. They summarize their measurement as: $|f_\pi/f_K|^2 |V_{cd}/V_{cs}|^2 = .085 \pm .027 \pm 0.014$ since present theoretical uncertainties in the form factors exceed uncertainties in the CKM matrix ratio. Using $|V_{cd}/V_{cs}|^2 = 0.051 \pm .002$ obtained from neutrino produced charm data [7], CLEO obtains a form factor ratio consistent with unity as expected theoretically.

1.2 $D \rightarrow \bar{K}^* \ell^+ \nu$ and $D_s^+ \rightarrow \phi \ell^+ \nu$

The vector $\ell \nu$ decay process involves a hadronic current describing the overlap of the D and vector meson wave functions which (in the limit of zero lepton mass) can be described by two axial and one vector form factor: $A_1(q^2)$, $A_2(q^2)$, and $V(q^2)$. A variety of theoretical methods including QCD sum rules, quark models, and lattice gauge theory have been brought

to bear on the prediction of the three form factors.

Although the full expression for the decay width is rather lengthy, a clear exposition can be found in the seminal reference [8]. It has become customary to assume that q^2 dependence of the form factors is dominated by the $D_s^{(*)}$ spectrum of poles (2.1 GeV for the vector and 2.5 GeV for the axial). Given the narrow q^2 domain, this is tantamount to assuming values for the form factor q^2 slope ratios near 0. This leaves one with three measurements $A_1(0)$, $A_2(0)$, and $V(0)$. It has become traditional to factor out $A_1^2(0)$ from the decay width, leaving two ratios: $R_V = V(0)/A_1(0)$ and $R_2 = A_2(0)/A_1(0)$ which serve to describe the *shape* of the decay distribution. The value of $A_1(0)$ then follows from the decay width which is generally estimated by measuring the branching ratio of the semileptonic decay with respect to a reference state and then using the absolute branching fraction of the reference state and D lifetime to compute a total decay width. The decay width shape depends on q^2 and three decay angles: the polar angle describing the vector \rightarrow two pseudo-scalar, the polar angle describing the decay of the virtual $W \rightarrow \ell \nu$, and the azimuthal acoplanarity angle between the vector meson and virtual W decay planes. At present, information on the form factors comes primarily from: E691 [8], E653 [9], and E687 [10]. These fixed target experiments use vertexing methods to estimate the ν momentum and thus measure considerably smeared values of q^2 and the three decay angles. Figure 4 compares the R_2 and R_V measurements obtained by E691, E653, and E687 with the preliminary results from E791 based on an analysis of 15 % of their data. The most striking aspect of Figure 4 is that the earlier,

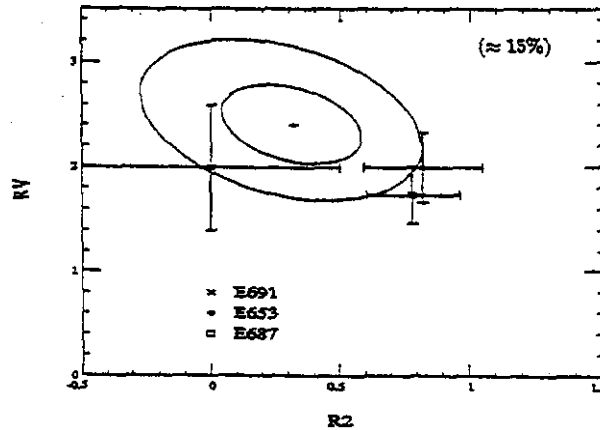


Figure 4: Comparison of the R_2 and R_V form factors. Shown are the 1 and 2 σ contours describing the E791 preliminary measurement with the earlier measurements (shown by error bars) of E691, E653, and E687.

E691 data are consistent with an R_2 form factor ratio consistent with zero; while the E653 and E687 prefer R_2 values near ≈ 0.74 . However, our fit for a combined average of the published E691, E653, and E687 $\{R_V, R_2\}$ values gives a 60 % confidence level for the hypothesis that all three experiments are consistent with average values of $R_V = 1.86 \pm 0.20$, $R_2 = 0.72 \pm 0.14$, and an implied virtual W spin polarization of $\Gamma_L/\Gamma_T = 1.21 \pm 0.1$. The preliminary E791 result tends to split the difference on R_2 .

Several of the many theoretical estimates come very close to predicting E691/E653/E687 averages for R_V and R_2 . As just one example, one recent estimate from lattice gauge theory [11] obtains values of $R_V = 1.99 \pm 0.22^{+0.31}_{-0.35}$, and $R_2 = 0.70 \pm 0.16^{+0.20}_{-0.15}$ which agrees with

our experimental average with a CL of 95 %.

When these shape parameters are fed back into the decay rate expression to obtain values for $A_1(0)$, the agreement with theory is not good. E691 obtains $A_1(0) = 0.46 \pm 0.05 \pm 0.05$, while E687 obtains $0.56 \pm 0.04 \pm 0.03$, for a combined average of about 0.5. Theoretical estimates for $A_1(0)$ tend to cluster around 0.8. For example, Reference [11] predicts $A_1(0) = 0.84 \pm 0.14 \pm 0.28$. This indication of a $K^*\ell\nu$ shortfall is borne out by directly comparing the ratio of $K^*\ell\nu/K\ell\nu$ which experimentally ranges from 0.4 – 0.6 where it is expected to be much closer to ≈ 1 . Recall that there is fair agreement between theory and experiment for the value of the $f_+(0)$ form factor which controls the rate for $D \rightarrow K\ell\nu$ decay.

The rate for decay $D_s^+ \rightarrow \phi\ell^+\nu$ decay is frequently used to obtain estimates of the D_s^+ absolute branching fractions. The absolute branching fraction into a given final state f is related to the lifetime of the given charm particle (C) and the decay width via: $\Gamma(f) = \hbar B(f)/\tau$. In the spectator model, one generally assumes equality of each inclusive semileptonic width, $\Gamma(C \rightarrow X\ell\nu)$, however an explicit model is required to relate the semileptonic widths between decays into two exclusive final states. One obtains D_s^+ absolute branching fractions by relating $\Gamma(D_s^+ \rightarrow \phi\ell^+\nu)$ to the width of a reference state with a well measured absolute branching fraction.

The 1992 Particle Data Group [7] average for $B(D_s^+ \rightarrow \phi\pi^+) = (2.8 \pm 0.5)\%$. E687 [16] references their $\phi\ell\nu$ width to $\Gamma(D^+ \rightarrow \bar{K}^{*0}\mu^+\nu)$ and measures $B(D_s^+ \rightarrow \phi\pi^+) = (3.1 \pm 0.9 \pm 0.5 \pm 0.4)\%$ using a fit where contamination from various suppressed backgrounds such as $D^+ \rightarrow \phi\mu^+\nu$ are measured from a fit to the decay kinematics rather than being stipulated as zero. When such backgrounds are assumed to be negligible, E687 gets $(2.9 \pm 0.5 \pm 0.45 \pm 0.39)\%$. CLEO [13] references their $\phi\mu\nu$ width to $\Gamma(D^0 \rightarrow K^{*-}\ell^+\nu)$ and obtains $B(D_s^+ \rightarrow \phi\pi^+) = (5.1 \pm 0.4 \pm 0.4 \pm 0.7)\%$ assuming a negligible level for OZI suppressed backgrounds. The difference between these numbers reflect both the choice of reference state as well as differences in the assumptions for the semileptonic width ratios ².

A recent, unresolved experimental controversy has arisen concerning the relationship between the form factors for $D_s^+ \rightarrow \phi\mu^+\nu$ and $D^+ \rightarrow \bar{K}^{*0}\mu^+\nu$ decay which are expected [11] [14] to be very close. E653 [15] measures $R_V = 2.3^{+1.1}_{-0.9} \pm 0.4$ and $R_2 = 2.1^{+0.6}_{-0.5} \pm 0.4$ based on a sample of 19 events for $D_s^+ \rightarrow \phi\mu^+\nu$. E653 measures an R_2 value which is about 2.5σ from the E691/E653/E687 average of $R_2 = 0.74 \pm 0.14$ for $\bar{K}^{*0}\mu^+\nu$ decay. E687 [16] measures $R_V = 1.8 \pm 0.9 \pm 0.2$ and $R_2 = 1.1 \pm 0.8 \pm 0.1$ on their sample of 90 $D_s^+ \rightarrow \phi\mu^+\nu$ decays. The E687 $\phi\mu\nu$ form factor measurements are consistent with the measured $\bar{K}^{*0}\mu^+\nu$ factors as expected; but are not inconsistent with the E653 measurements either.

1.3 $\Lambda_c \rightarrow \Lambda\ell^+\nu$

Both CLEO [19] and ARGUS [20] see evidence for this decay by looking for an excess of $\Lambda\ell^+$ compared to $\Lambda\ell^-$ events and by placing kinematic cuts (such as cuts on $M(\Lambda\ell^+)$)

²E687 uses 0.9 ± 0.12 as a composite [7] of theoretical estimates of the $\phi\mu^+\nu/\bar{K}^{*0}\mu^+\nu$ ratio. CLEO uses a $\phi\mu^+\nu/K^{*-}\mu^+\nu$ ratio of 1.0 which is the prediction of the modified ISGW model.

to control possible backgrounds with additional neutrals. In analogy with the previous discussion on the D_s^+ , the relative $\Lambda\ell\nu$ yield can be used to infer absolute Λ_c branching fractions using an assumption of a universal charm semileptonic width, $\Gamma(C \rightarrow X\ell\nu)$, which can be estimated as the average of the (consistent) inclusive widths for the D^+ and D^0 . CLEO measures $B(\Lambda_c \rightarrow \Lambda\ell^+\nu) = (6.67 \pm .35 \pm 1.35)\% \times \mathcal{F}$, where $\mathcal{F} = \Gamma(\Lambda\ell\nu)/\Gamma(X\ell\nu)$, ie the unknown fraction of inclusive $X\ell\nu$ which are exclusively $\Lambda\ell^+\nu$.³

An even more interesting result concerns the polarization of the final state Λ which is predicted [18] to be large in HQET. Both CLEO and ARGUS measure the decay asymmetry for $\Lambda\ell\nu$ by fitting their data to the form: $d\Gamma/d\cos\theta \propto 1 + \alpha \alpha_\Lambda \cos\theta$ where θ is the angle between \vec{p} (the Λ decay proton) and $-(\vec{\ell} + \vec{\nu})$ evaluated in the Λ rest frame; and $\alpha_\Lambda = .64$ is the well known self-analyzing asymmetry of the Λ . The Λ_c momentum can be estimated both from the thrust axis and visible decay products. CLEO obtains $\alpha = -0.89^{+0.17+0.09}_{-0.11-0.05}$; while ARGUS obtains -0.91 ± 0.49 . Use of HQET for the heavy charmed quark reduces the four possible helicity form factors to just two, and allows one to predict α as a function of q^2 in terms of the unknown ratio of the remaining form factors $R = f_2/f_1$. As $q^2 \rightarrow 0$ the longitudinal helicity dominates and $\alpha \rightarrow -1$ irrespective of the value of R as shown in Figure 5. In the limit of infinite product baryon mass $f_2(q^2) \rightarrow 0$, while $f_1(q^2)$ remains finite and thus one expects $|R| < 1$. At the average probed q^2 range of $\approx .7 \text{ GeV}^2$, one would expect $\alpha \approx -0.9$ in agreement with the measurements.

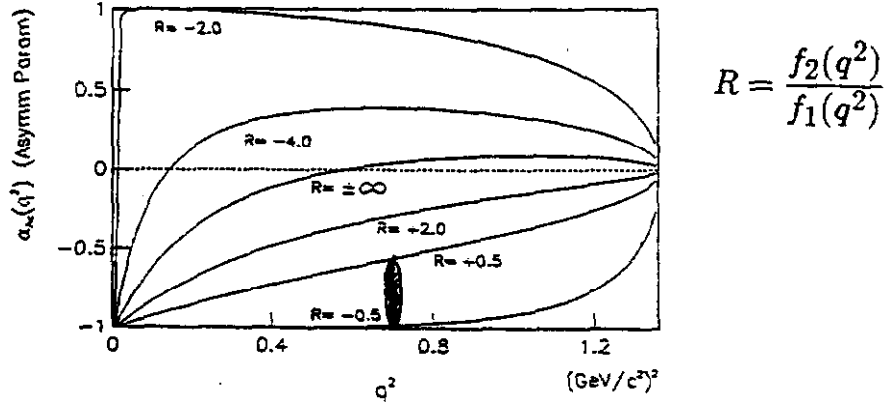


Figure 5: Predicted asymmetry parameter α as a function of q^2 for various form factor ratios, R .

2 Future prospects

Certainly it will be of interest to further study the q^2 dependence of charm semileptonic decay. As discussed earlier, the process $D \rightarrow \pi\ell\nu$ will allow one to probe much closer to the possible D^* poles in $f_+(q^2)$. However particle identification in a fixed target environment, or high efficiency $\pi^0 \rightarrow \gamma\gamma$ reconstruction is likely to be challenging.

One can estimate the anticipated statistical errors in vector $\ell\nu$ physics using the *a priori*

³As a guide, $(K + K^*)\ell\nu/X\ell\nu \approx 0.9$ in $D^{0/+}$ decays

error matrix formula [17]:

$$E_{\alpha\beta}^{-1} = N \int \frac{d\vec{x}}{I(\vec{x})} \frac{\partial I(\vec{x})}{\partial t_\alpha} \frac{\partial I(\vec{x})}{\partial t_\beta} \quad (2)$$

For an experiment with perfect resolution on the q^2 and the decay angles, employing the standard likelihood fit which uses all four decay quantities, this formula predicts statistical errors of $\sigma(R_V) = 4.7/\sqrt{N}$ and $\sigma(R_2) = 4.1/\sqrt{N}$ for form factors near the E691/E653/E687 average. My experience is given the substantial resolution smearing, $\sigma(R_V) = 7/\sqrt{N}$ and $\sigma(R_2) = 5/\sqrt{N}$ are probably more realistic error estimates.⁴ If the vector and axial pole masses are included as fit parameters as opposed to being assumed, the error on the vector pole mass is expected to be $24/\sqrt{N}$; while the error on the axial pole mass is expected to be $56/\sqrt{N}$. The statistical error in R_V essentially doubles when the pole mass is unconstrained.

Experiment E831 expects to collect a fully reconstructed, clean sample of 20000 $\overline{K}^{*0}\mu\nu$ decays, 2250 $\phi\mu\nu$ decays, and 500 $\rho\mu\nu$ decays. In pole constrained fits, these yields suggest that in the absence of systematic errors R_2 could be measured to 5 %, 14%, and 29 % for the K^* , ϕ , and ρ decay respectively. These calculations show that statistical errors on the vector pole mass in $\overline{K}^{*0}\ell\nu$ decays would be 160 MeV which is roughly the present precision of the vector pole for the $f_+(0)$ form factor as determined from $K\ell\nu$ decay.

Systematic uncertainties are, of course, much harder to predict. I believe instrumental systematics for $\overline{K}^{*0}\mu\nu$ decay are likely to be very small. As a way of illustrating this, consider the 18 bin fit employed by E687 [10] where one fits for R_V and R_2 by measuring the fractions of decays which are observed in 18 bins of $\cos\theta_\nu \times \cos\theta_\ell \times q^2$ where 3 bins span each angle, and two bins span q^2 . Consider possible systematics problems that arise from a scenario where the center 10 mrad of a muon detector system has suffered a loss in efficiency. Lack of knowledge of this efficiency will create a systematic error to the extent that the fraction of events with a muon produced in the central 10 mrad varies from bin to bin. Figure 6(a) however shows this fraction is remarkably constant over the 18 bins. Often, as in E687, one triggers events on an hadronic energy threshold. The exact threshold is often difficult to properly model and correct for. Figure 6(b) shows that the fraction of photoproduced events with a hadronic energy deposition exceeding 70 GeV is very uniform over the 18 bins as well. The final instrumental study concerns shower clustering in the reconstruction of $\overline{K}^{*0}e\nu$ decay. We plot the closest transverse distance between the e and $\overline{K}^{*0} \rightarrow K^-\pi^+$ secondary on a shower counter located about 25 meters downstream of the target. Here we see that clustering distance varies considerably from bin to bin. To me this suggests that understanding inefficiencies in electron identification due to shower clustering may set a systematic error when one uses e^\pm rather μ^\pm leptons.

Although instrumental systematics may be relatively easy to control, backgrounds are likely to continue to be serious sources of systematic error. I believe it is possible to remove nearly all sources of non-charm background in a vertex-based fixed target charm experiment by demanding that the secondary vertex lies outside of the target. Figure 7 illustrates this

⁴These are the errors expected in the 18 bin likelihood fit used by E687 [10] where the $\cos\theta_\nu \times \cos\theta_\ell \times q^2$ space is divided into 3 bins, 3 bins, and 2 bins respectively.

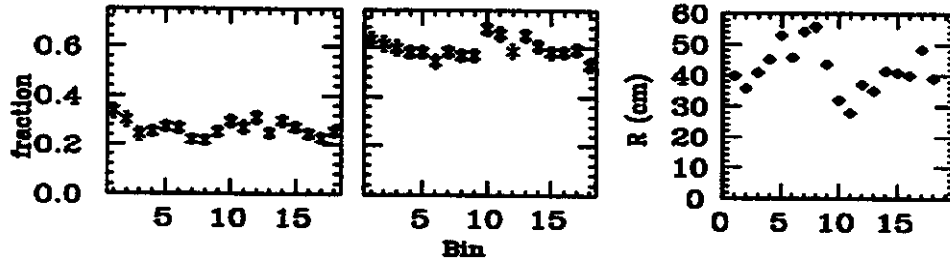


Figure 6: (a) The fraction of $\overline{K}^{*0}\mu\nu$ decays with a muon detected in the central 10 mrad as a function of the $\cos\theta_\ell \times \cos\theta_\ell \times q^2$ bin number. (b) The fraction of decays with more than 70 GeV of energy deposited in a hadron calorimeter. (c) The minimum distance between the e^+ either the daughter K^- or π^+ .

for E687 data by comparing the observed $M(K^-\pi^+\pi^+)$ distribution to the distribution of a pure $c\bar{c}$ Monte Carlo based on JETSET/PHYTHIA. The agreement in both level and shape is quite striking, suggesting that nearly all background is of a charm origin. However Figure

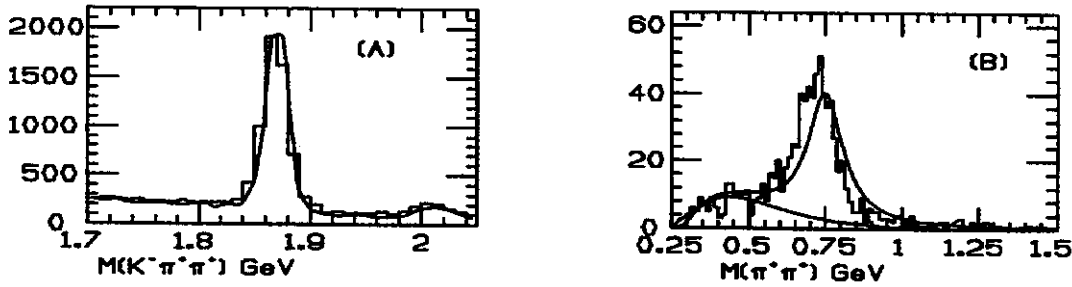


Figure 7: (A) $M(K^-\pi^+\pi^+)$ for D^+ candidates observed in E687 downstream of the target. The overlaid curve is a pure $c\bar{c}$ Monte Carlo with no non-charmed backgrounds. (B) $M(\pi^+\pi^+)$ for simulated events of the form $D^+ \rightarrow \overline{K}^{*0}\mu^+\nu$ where the kaon has been misidentified as a pion. The line shape is that expected for $D^+ \rightarrow \rho\mu^+\nu$ decays over a background.

7(b) shows that charm backgrounds can be particularly pernicious by showing how much a $D^+ \rightarrow \overline{K}^{*0}\mu^+\nu$ decay looks like the Cabibbo suppressed $D^+ \rightarrow \rho\mu^+\nu$ decay when the kaon is Cerenkov misidentified as a pion. Our experience has suggested that for Cabibbo allowed states uncertainty about the background contamination can easily contribute a 10 % systematic error. Of course as mammoth charm samples are obtained, these backgrounds may become better understood and the systematic error associated with them might fall. Beyond the next round of charm experiments one may well reach the place where experimental errors become smaller than theoretical uncertainties which in Lattice Gauge Theory[11] are expected to diminish to less than 10 %.

3 Measuring charm absolute branching fractions in fixed target experiments

Many of the semileptonic physics topics not related to form factor shape are tied to semileptonic widths and thus ultimately to knowledge of the absolute branching fraction. At present, these are known with a fractional error of about $\pm 2\%$ and a systematic error of about double that with nearly all information coming from e^+e^- annihilation experiments.

The most recent measurements come from CLEO collaboration[21] who measure absolute branching ratios by tagging $\tilde{\pi}$ from $D^* \rightarrow \tilde{\pi} D$. If one can reliably tag $\tilde{\pi}$'s without reconstructing the accompanying D , an absolute branching fraction can be obtained, say for $B(D^0 \rightarrow K\pi)$, by dividing the efficiency corrected yield of reconstructed $D^{*+} \rightarrow (K^-\pi^+)\tilde{\pi}^+$ decays by the yield of $\tilde{\pi}^+$ tags:

$$B(D^0 \rightarrow K\pi) = \frac{1}{\epsilon} \frac{(K\pi)\tilde{\pi}^+}{(\tilde{\pi}^+)} \quad (3)$$

Because we find that the primary vertex multiplicity detected in the E687 forward spectrometer is very low (≈ 2.2 tracks), we believe that it is fairly easy to cleanly tag $\tilde{\pi}$'s in photoproduction and thus measure absolute branching fractions in fixed target experiments as well. Because of the limited energy release in D^* decay, scaling the $\tilde{\pi}$ momentum by the ratio of the D^* to pion mass serves as a good estimate of the momentum of the parent D^* . Hence $\Delta_t^2 = (\vec{D}_t^{(r)} + m_*/m_\pi \vec{\tilde{\pi}}_t)^2$ where $\vec{D}_t^{(r)}$ is the \vec{p}_t carried by the recoil D produced against the $D^* \rightarrow \tilde{\pi} D^0$ is essentially a slightly smeared version of the p_t^2 carried by the photoproduced $D\bar{D}$ pair. Figure 8 (b) illustrates a large excess of right sign $\tilde{\pi}$ events at low Δ_t^2 indicating a copious number of tagged $\tilde{\pi}$'s equal to roughly 1/10 of the number of inclusive $K\pi$, $K2\pi$, and $K3\pi$ D 's reconstructed by E687. These tagged $\tilde{\pi}$'s found against a recoil $D^{(r)}$

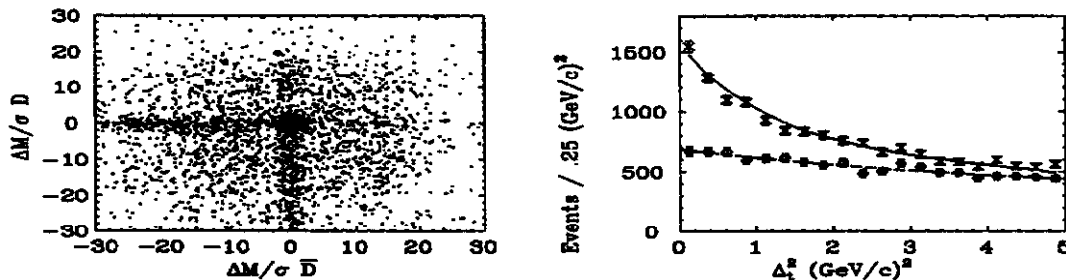


Figure 8: (a) Scatter plot of the normalized mass $(m - m_{nom})/\sigma$ of D versus \bar{D} showing an ≈ 320 event excess of events where E687 fully reconstructs both members of a photoproduced $D - \bar{D}$ pair into the $K\pi$, $K2\pi$ and $K3\pi$ decay modes. (b) Search for $\tilde{\pi}$ from the decay $D^{*+} \rightarrow \tilde{\pi} D$. The distribution for the p_t balance variable, Δ_t^2 for $\tilde{\pi}$'s produced against a reconstructed recoil D . The upper, solid curve is for right sign combinations and is a smeared version of the p_t^2 distribution obtained for fully reconstructed $D\bar{D}$ events. The lower, dashed curve is for wrong sign combinations.

form the denominator sample for Eqn. (3); the numerator sample are from events where both a D and recoil $D^{(r)}$ are fully reconstructed. Figure 8(a) taken from Reference [22] shows the yield of these events obtained in E687. Scaling up this yield appropriately for E831, we anticipate fractional statistical errors on $B(D^0)$ of $(2.5 \rightarrow 4.5)\%$ with considerably different systematics from those in e^+e^- annihilation. Reference [23] describes how one can bootstrap the $B(D^0)$ measurements to get estimates of $B(D^+)$ and more speculatively, $B(\Lambda_c^+)$.

4 $D^0\bar{D}^0$ Mixing

In analogy with the $K^0 - \bar{K}^0$ system, it should be possible for a D^0 produced in $D^{*+} \rightarrow \pi^+ D^0$ decay to mix into a \bar{D}^0 (with a probability r_{mix}) and then decay as a \bar{D}^0 (eg via $\bar{D}^0 \rightarrow K^+ \pi^-$). Mixing is observed to be nearly complete ($r_{mix} \approx 1$) in the $K^0 - \bar{K}^0$ system, very large in the $B^0\bar{B}^0$ system, and is expected to be very, very small for the $D^0\bar{D}^0$ system with Standard Model estimates ranging from $r_{mix} \approx 10^{-10}$ to 10^{-7} . The smallness of D mixing relative to say B mixing can be understood in terms of the ratios of CKM elements and masses of quarks that run around the virtual loops, which appear in the “box” diagrams responsible for generating the ΔM between the mass eigenstates[24]. To the experimentalist, a very low Standard Model expectation for r_{mix} is both bad news (probably won’t see mixing!) and good news (a signal implies physics beyond the Standard Model[25] such as 4th Quark, left-right supersymmetry, and/or Higgs multi-doublets). The possibility that long-range interaction contributions (such as $D^0 \rightarrow K^+ K^- \rightarrow \bar{D}^0$) could significantly boost r_{mix} to the $10^{-4} \rightarrow 10^{-3}$ level has been frequently discussed in the theoretical literature [26] but the prevailing conclusion within the Standard Model seems to be that $r_{mix} < 10^{-7}$ which is likely to be inaccessible to experiment for quite a while.

At present, the best experimental upper limit ($r_{mix} < 3.7 \times 10^{-3}$) comes from E691[27] who searched for $D^{*+} \rightarrow \pi^+(K^+\pi^- \text{ \& } K^+\pi^-\pi^+\pi^-)$ decays as a mixing signature as described above. It should be possible to observe a false $D^{*+} \rightarrow \pi^+(K^+\pi^-)$ mixing signal from doubly Cabibbo suppressed decays (DCSD) which have been observed at the $\approx 1\%$ level by CLEO [28]. Mixing can be distinguished from DCSD and other backgrounds by measuring the time evolution of the decay vertices: $dN(DCSD)/dt \propto \exp -t/\tau$ whereas $dN(mixing)/dt \propto t^2 \exp -t/\tau$. The maximum yield of $D^{*+} \rightarrow \pi^+(K^+\pi^-)$ from mixing occurs at a secondary proper time of $2 \times \tau$ (τ is the D^0 lifetime) since one must “wait for the D^0 to mix into the \bar{D}^0 ”. Comparable (model dependent) limits for mixing, which are free from the complication of DCSD, have been obtained previous to E691 by searching for same-sign μ ’s (presumably from charm semileptonic decays) produced in fixed target muon[29] ($r_{mix} < 0.012$) and pion[30] ($r_{mix} < .0056$) experiments.

The logical successors to E691 in establishing a mixing limit through $D^* \rightarrow \pi^+(K^+\pi^-)$ decay are Fermilab E791 and E687. E791 has recently set a preliminary limit of $r_{mix} < .0047$ based on 1/3 of their data set and using the $K\pi$ decay mode alone. Figure 9 illustrates the cleanliness of the E791 signal by comparing the D mass and $D^* - D$ mass difference lego plots for right sign $D^* \rightarrow \pi^+(K^-\pi^+)$ and wrong sign $D^* \rightarrow \pi^+(K^+\pi^-)$ candidates. In order to achieve this remarkable signal to noise, E791 unleashed a wide assortment of powerful tricks to reject backgrounds from random pions – most notably the use of neural networks and Fisher discriminants. Their limit is extracted by making a fit to lifetime evolution including the mixing evolution, the exponential evolution expected for WS D band events, and random backgrounds whose lifetime evolution is parameterized as a sum of two exponentials. The background lifetimes and yields, the rate of DCSD, and the mixing parameter are among the 16 fit parameters used in their likelihood fit. Special care is taken in the process of extracting the errors from MINUIT in order to convert to a limit. They obtain a preliminary value for

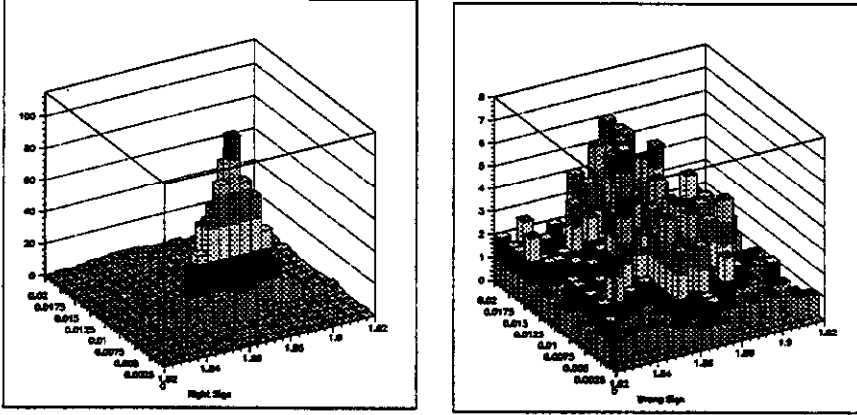


Figure 9: Right sign and wrong sign mass versus $Q (= M(K\pi\pi) - M(K\pi) - M(\pi))$ lego plots obtained by E791 on 1/3 of their data.

$r_{DCSD} = 1.9^{+0.6}_{-0.8} \times 10^{-2}$ from their fit.

We turn last to a progress report on mixing limits from E687 where we use both the $K\pi$ and $K3\pi$ decays of the D^0 . Based on an analysis of our 87/88 data ($\approx 10\%$ of the full E687 sample), we [31] reported a limit of $r_{mix} < 6 \times 10^{-3}$. We then doubled the sample by including about 1/10 of the 90/91 data sample and quoted [32] an encouragingly improved value of $r_{mix} < 3.4 \times 10^{-3}$. Perhaps the limit would continue to improve as $1/N$? When this same analysis was applied to our full data sample, we obtained a rather discouraging upper limit of $r_{mix} < 4 \times 10^{-3}$ indicating the onset of non-zero backgrounds which implies rather sluggish $1/\sqrt{N}$ future improvement. The right sign and wrong sign D versus $D^* - D$ scatterplot of the full E687 data sample is shown in Figure 10.

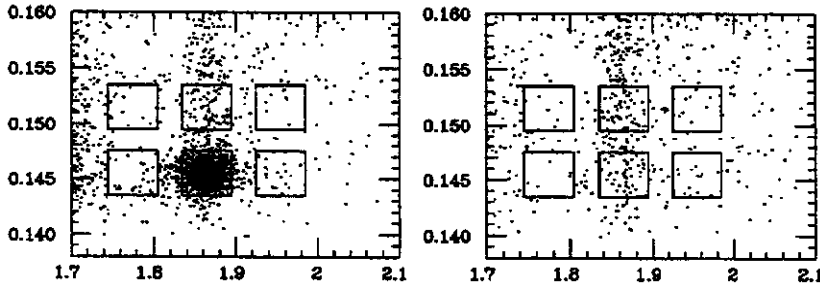


Figure 10: Right sign and wrong sign $K\pi$ mass versus $D^* - D$ mass difference scatter plots obtained by E687. The wrong sign D^0 band is due to real D^0 combined with a random wrong sign π from the primary vertex. The boxes indicate signal regions and regions used in finding the time evolution of the random backgrounds.

The full, E687 sample with the presently explored cuts is indeed clean, but clearly not

clean enough! We are actively pursuing new cuts to eliminate random backgrounds. Hence we are not even reporting a new preliminary mixing limit, but rather just giving a progress report with a possibly long journey ahead. Although it is tempting to assess the quality of an experiment on the smallness of its upper limits, Figure 11 suggests that such temptations should be resisted! Figure 11 shows ten simulated histories of how a mixing limit will improve as one accumulates more and more statistics. We note that the final limit fluctuates wildly once $1/\sqrt{N}$ sets in.

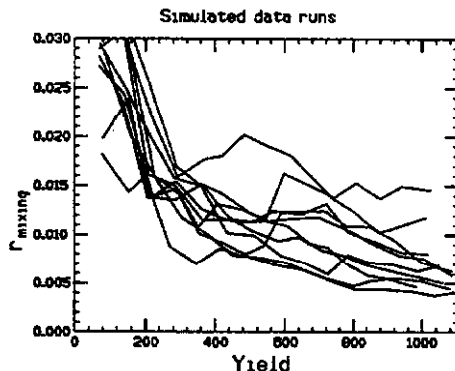


Figure 11: A simulated mixing limit history as a function of yield of $K3\pi$ events collected in 10 independent runs of an experiment like E687.

Milind V. Purohit has recently noted [33] that the CLEO observation of DCSD [28] implies that all mixing limits based on non-observation of a $D^* \rightarrow (K^+\pi^-)\tilde{\pi}^+$ signal must ultimately hit the dreaded $1/\sqrt{N}$ limit even if the time evolution is employed in the fit. Purohit estimates that the inclusion of time should reduce limits by $\approx 1/\sqrt{5}$ over limits based on simple counting of wrong sign events. To improve limits as $1/N$ one must base limits on semileptonic decays which is likely to be a daunting challenge for CHARM2000.

5 Acknowledgements

I would like to acknowledge the efforts of my many E687 colleagues including Ray Culbertson, Rob Gardner, John Cumalat, and Will Johns. I would also like to acknowledge help from Kathy O'Shaughnessy for providing me the preliminary E791 $K^{*+}\mu\nu$ analysis, Milind Purohit of the E791 Collaboration for providing me an extensive excellent report on $D^0 - \bar{D}^0$ mixing including the latest E791 result, and Aida El-Khadra for help in dealing with the phenomenology of charm semileptonic decays.

References

- [1] J.P. Cumalat, in **The Fermilab Meeting DPF92**, 10-14 November 1992, published by World Scientific Publishing Co, edited by Carl H. Albright, Peter H. Kasper, Rajendran Raja, John Yoh.
- [2] CLEO Collab., Phys. Lett. B317 (1993) 647.
- [3] E691 Collab., J.C. Anjos, et al., Phys. Rev. Lett. 62 (1989) 1587.

- [4] CLEO Collab., Phys. Rev. D 44 (1991) 3394.
- [5] Mark III Collab., Phys. Rev. Lett. 66 (1991) 1011.
- [6] CLEO Collab., Phys. Rev. Lett. 71 (1993) 1311.
- [7] Particle Data Group, K. Hikasa *et al.*, Phys. Rev. D 45 S1 (1993)
- [8] E691 Collab., J.C. Anjos *et al.*, Phys. Rev. Lett. 65 (1990) 2630.
- [9] E653 Collab., K. Kodama *et al.*, Phys. Lett. B 274 (1992) 246.
- [10] E687 Collab., P.L. Frabetti *et al.*, Phys. Lett. B 307 (1993) 262.
- [11] C.W. Bernard, A.X. El-Khadra, and A. Soni, Phys. Rev. D 45 (1992) 869.
- [12] E687 Collab., P.L. Frabetti *et al.*, Phys. Lett. B 313 (1993) 253.
- [13] CLEO Collab., F. Butler *et al.*, Phys. Lett. B 324 (1994) 255
- [14] V. Lubicz, G. Martinelli, M.S. McCarthy, and C.T. Sachrajda, Phys. Lett. B 274 (1992) 415
- [15] E653 Collab., K. Kodama *et al.*, Phys. Lett. B 309 (1993) 483.
- [16] E687 Collab., P.L. Frabetti, *et al.*, Physics Letters B 328 (1994) 187
- [17] See W.T. Eadie *et al.*, Statistical Methods in Experimental Physics, Elsevier, New York, 1988.
- [18] J.C. Korner and M. Kramer, Phys. Lett. B 275 (1992) 495
- [19] CLEO Collab., T. Bergfeld *et al.*, Phys. Lett. B 323 (1994) 219.
- [20] ARGUS Collab., H. Albrecht *et al.*, Phys. Lett. B 326 (1994) 320.
- [21] CLEO Collab., D.S. Akerib *et al.*, Phys. Rev. Lett. 71 (1993) 3070
- [22] E687 Collab., P.L. Frabetti, *et al.*, Phys. Lett. B 308 (1993) 193
- [23] J. Wiss, in **Heavy Quarks at Fixed Target (HQ93)**, Frascati Physics Series, edited by S. Bianco and F.L. Fabbri (1993) 189.
- [24] See for example, E.D. Cummins and P.H. Bucksbaum, **Weak interactions of leptons and quarks**, Cambridge University Press, New York, 1983.
- [25] See for example, K.S. Babu *et al.*, Phys. Lett. B 205, (1988) 531; E. Ma, Mod. Phys. Lett. A 3 (1988) 319; A. Datta, Phys. Lett. B 154 (1985) 287.
- [26] See for example, L. Wolfenstein, Phys. Lett. B 164 (1985) 170; J.F. Donahue *et al.*, Phys. Rev. D 33 (1986) 179; P. Colangelo, G. Nardulli, and N. Paver, Phys. Lett. B 242 (1990) 71; H. Georgi, Phys. Lett. B 297 (1992) 353; L. Hall and S. Weinberg, Phys. Rev. D 48 (1993) 979.
- [27] E691 Collab., J.C. Anjos *et al.*, Phys. Rev. Lett. 62 (1989) 513.
- [28] CLEO Collab., D. Cinabro *et al.*, CLNS-93-1262 (Dec 1993).
- [29] BCDMS Collab., A. Benvenuti *et al.*, Phys. Lett. B 158 (1985) 531.
- [30] E615 Collab., W.C. Louis *et al.*, Phys. Rev. Lett. 56 (1986) 1027.
- [31] R. Culbertson for the E687 Collaboration, **The Vancouver Meeting, Particle & Fields '91**, Edited by David Axen and Douglas Bryman, & Martin Comyn, World Scientific (1991) 423.
- [32] J. Wiss for the E687 Collaboration, Invited talk at the 1992 Joint April Meeting of the American Physical Society and the American Association of Physics Teachers, April 1992, Washington, D.C. (unpublished).
- [33] M. V. Purohit, in **Heavy Quarks at Fixed Target (HQ93)**, Frascati Physics Series, edited by S. Bianco and F.L. Fabbri (1993).

Searching for CP Violation, Flavor Changing Neutral Currents, and Lepton Number Violation in Charm Decay

Paul D. Sheldon
Vanderbilt University, Nashville, TN 37235

Abstract

In the standard model, CP violation and Flavor Changing Neutral Currents (FCNC) are expected to be small in charm decay, while Lepton Family Number Violation (LFNV) and Lepton Number Violation (LNV) are forbidden. This, combined with the distinctive signature of these effects, make them ideal for searches for physics beyond the standard model. Charm decay may be the only window on this new physics, since it is possible that the mechanism responsible will only couple to u -type quarks. Currently, many experimental groups are presenting new (and mostly preliminary) results on searches for FCNC, LFNV, LNV and CP violation in charm decay. In almost all cases, these new limits represent a substantial improvement over previous results or are the first reported. After reviewing the current status of the field, the potential of an experiment with 10^8 reconstructed charm decays is discussed.

The common thread tying searches for rare/forbidden charm decay and searches for CP violation in charm decay is new physics – physics beyond the standard model. Flavor changing neutral currents (FCNC) in charm decay are expected to be extremely rare in the standard model, while lepton number violating (LNV) and lepton family number violating (LFNV) decays are forbidden. CP violation is expected to be very small. An anomalously large rate for any of the above would be a strong signal for new physics; the anticipated rarity of each means there is a large window of sensitivity. Most importantly, this window may be unique to charm: it is possible that the new physics will couple only to u -type quarks.

Currently, many experimental groups are presenting new (and mostly preliminary) results on searches for FCNC, LFNV, and LNV in charm decay, with sensitivities to branching ratios in the range $10^{-5} - 10^{-4}$. For some modes the resulting limits are the first reported. For the rest of the modes, the limits typically represent an improvement of 1–2 orders of magnitude over previously published limits [1].

There are also recent results [2] from a search for direct CP violation in charm decay. The experimenters set limits of roughly 10–20% on the CP decay-rate asymmetry for some Cabibbo suppressed D^0 and D^+ decay modes. The limits are the first reported for D^+ modes, and represent a significant improvement in the old limit for the D^0 mode [3].

In the following, searches for rare and forbidden decay (FCNC, LFNV, LNV) are discussed separately from searches for CP violation. In each case, the current status of searches is discussed, followed by a discussion of the challenges and potential of a hypothetical experiment (“Charm 2000”) with a sample of 10^8 reconstructed charm decays.

1 Searches for Rare and Forbidden Charm Decay

In the standard model, FCNC decays such as $D^0 \rightarrow e^+ e^-$ and $D^+ \rightarrow \pi^+ \mu^+ \mu^-$ are second-order electroweak and are expected to be extremely rare. Schwartz [4] calculates a D^+ inclusive branching ratio of 1.8×10^{-8} . Calculations [5] of exclusive branching ratios vary from 10^{-17} to 10^{-8} . Anomalously large rates would imply non-standard model tree-level FCNC diagrams or non-standard model contributions to higher-order loop diagrams. Either way, to quote from Schwartz, “...rare decays probe particle states and mass scales which cannot be accessed directly.”

LFNV and LNV decays such as $D^+ \rightarrow \pi^+ \mu^- e^+$ or $D^+ \rightarrow \pi^- e^+ e^+$ are forbidden in the standard model. However, unlike charge conservation (which is required by gauge invariance), there is no fundamental principle which requires lepton number conservation. It therefore seems reasonable that at some level lepton number conservation should be violated.

1.1 Methods

In determining the branching ratio for a decay mode (or setting a limit on one), the relative branching ratio (*RBR*) method has two advantages. The method is relatively simple:

$$RBR = \frac{BR(D \rightarrow X_{\text{FCNC}})}{BR(D \rightarrow X_{\text{Norm}})} = \frac{N_{\text{obs}}(X_{\text{FCNC}})}{\epsilon(X_{\text{FCNC}})} \frac{\epsilon(X_{\text{Norm}})}{N_{\text{obs}}(X_{\text{Norm}})} \quad (1)$$

where ϵ is the acceptance times efficiency for each mode, and N_{obs} is the number of observed decays (or the upper limit on that number). Secondly, because it is the ratio of ϵ for each mode that is important, many sources of systematic error cancel. To determine the absolute branching ratio, one then multiplies *RBR* by the absolute branching ratio for the normalizing mode (using the world average from the particle data book [1], for example.) Uncertainties in the absolute branching ratio for the normalizing mode will therefore contribute to the errors in this method.

An alternative to the above approach is to use knowledge of the production cross-section and beam flux (or luminosity) to calculate the number of produced charm mesons, so that:

$$BR(D \rightarrow X_{\text{FCNC}}) = \frac{N_{\text{obs}}(D \rightarrow X_{\text{FCNC}})}{\epsilon(D \rightarrow X_{\text{FCNC}})} \frac{1}{N_{\text{produced}}(D)}. \quad (2)$$

Uncertainties in ϵ (due to triggering, acceptance, reconstruction efficiency, ...) are important in this method. In addition, cross-section and flux measurements are difficult to make, and this is often reflected in large errors in $N_{\text{produced}}(D)$.

1.2 Current Limits

Until very recently, the best limits on FCNC, LFNV, and LNV charm decays were all a few years old. With the possible exception of $BR(D^0 \rightarrow \mu^+ \mu^-)$, this is about to change significantly.

1.2.1 E653 (Topological Search)

Fermilab experiment E653 has preliminary limits on several dimuon modes, including the first limits for D_s^+ and Λ_c^+ decay modes. E653 employed a hybrid emulsion detector with emulsion/silicon vertexing. Their results are based on data taken in a 600-GeV π^- beam during the 1990–91 fixed target run. An initial skim of their data resulted in 950 dimuon events in their fiducial volume. In 49 events, both muons were consistent with coming from a common vertex and were unmatched with tracks in the primary vertex. Of these 49, 33 were judged to be events in which both charm particles decayed semimuonically (which was consistent with their Monte Carlo prediction of this background). There was strong evidence that at least one of the muons in 13 other events was from a secondary interaction or kaon decay. This left 3 candidate events: two 2-prong secondaries, no 3-prong, and one 4-prong.

This topological approach has a tremendous advantage: in principle it can be used to set limits on any dimuon decay mode, as long as the relevant charm particle production cross section is known and the efficiency/acceptance of the decay can be calculated. E653 uses their measured charm meson production cross-sections, and uses the Λ_c^+ cross-section measured by other experiments. Their efficiencies for each mode range from 4.6 – 15.9%. Table 1 shows their 90% CL limits.

1.2.2 E789 ($D^0 \rightarrow \mu^+ \mu^-$ Search)

Fermilab experiment E789 has recently reported [6] a limit on $BR(D^0 \rightarrow \mu^+ \mu^-)$, based on a partial sample of their data taken in the 800-GeV primary proton beam during the 1990–91 fixed-target run. The E789 apparatus is a limited aperture spectrometer, optimized for 2-body heavy flavor decays. Four stations of 50 micron pitch silicon microstrip detectors are used to reconstruct secondary vertices.

E789 uses a hybrid of the relative branching ratio and cross-section approaches, using their observation of $J/\psi \rightarrow \mu^+ \mu^-$ to normalize their result. As a result, their uncertainties in triggering and reconstruction efficiency largely cancel out:

$$BR(D^0 \rightarrow \mu^+ \mu^-) = A^{-0.10} BR(J/\psi \rightarrow \mu^+ \mu^-) \frac{\Delta y \cdot d\sigma_{J/\psi}/dy|_{y=0}}{\sigma(D^0) + \sigma(\bar{D}^0)} \frac{\epsilon_{J/\psi}}{\epsilon_D} \frac{N_{\text{limit}}(D^0 \rightarrow \mu^+ \mu^-)}{N_{\text{obs}}(J/\psi \rightarrow \mu^+ \mu^-)}. \quad (3)$$

For the J/ψ , the differential cross-section was used since the cross-section at 800-GeV had not yet been published. It is relatively flat over the rapidity range (Δy) of their acceptance. The “ $A^{-0.10}$ ” factor accounts for the differing A dependence of the J/ψ and D^0 cross-sections.

Table 1: 90% CL Upper Limits ($\times 10^5$) on FCNC, LFNV, and LNV Charm Decay Modes.

Type	Mode	E653	E687	E771	E789	E791	PDG (expt.)
FCNC	$D^0 \rightarrow e^+ e^-$						13 MK3
	$D^0 \rightarrow \mu^+ \mu^-$		2.7	1.2	3.1		1.1 E615
	$D^0 \rightarrow \rho^0 e^+ e^-$						45 CLEO
	$D^0 \rightarrow \rho^0 \mu^+ \mu^-$	24					81 CLEO
	$D^0 \rightarrow \pi^0 \mu^+ \mu^-$	17					
	$D^0 \rightarrow \bar{K}^0 e^+ e^-$						170 MK3
	$D^0 \rightarrow \bar{K}^0 \mu^+ \mu^-$	25					
	$D^+ \rightarrow \pi^+ e^+ e^-$						250 MK2
	$D^+ \rightarrow \pi^+ \mu^+ \mu^-$	22	9.7			4.6	290 CLEO
	$D^+ \rightarrow K^+ e^+ e^-$						480 MK2
	$D^+ \rightarrow K^+ \mu^+ \mu^-$	33	8.5				920 MK2
	$D^+ \rightarrow \rho^+ \mu^+ \mu^-$	58					
	$D_s^+ \rightarrow K^+ \mu^+ \mu^-$	60					
	$\Lambda_c^+ \rightarrow p \mu^+ \mu^-$	33					
LFNV	$D^0 \rightarrow \mu^\pm e^\mp$						10 ARGUS
	$D^+ \rightarrow \pi^+ \mu^+ e^-$						330 MK2
	$D^+ \rightarrow \pi^+ e^+ \mu^-$						330 MK2
	$D^+ \rightarrow \pi^+ \mu^\pm e^\mp$						380 CLEO
	$D^+ \rightarrow K^+ \mu^+ e^-$						340 MK2
	$D^+ \rightarrow K^+ e^+ \mu^-$						340 MK2
LNV	$D^+ \rightarrow \pi^- e^+ e^+$						480 MK2
	$D^+ \rightarrow \pi^- \mu^+ e^+$						370 MK2
	$D^+ \rightarrow \pi^- \mu^+ \mu^+$	20	17				680 MK2
	$D^+ \rightarrow K^- e^+ e^+$						910 MK2
	$D^+ \rightarrow K^- \mu^+ e^+$						400 MK2
	$D^+ \rightarrow K^- \mu^+ \mu^+$	33	20				430 MK2
	$D^+ \rightarrow \rho^- \mu^+ \mu^+$	60					
	$D_s^+ \rightarrow K^- \mu^+ \mu^+$	60					
	$\Lambda_c^+ \rightarrow \Sigma^- \mu^+ \mu^+$	72					

Using sidebands in the dimuon invariant mass spectrum to estimate the background in the D^0 mass region, they find -4.1 ± 4.8 candidate events, and set a limit of $BR(D^0 \rightarrow \mu^+ \mu^-) < 3.1 \times 10^{-5}$ (90% CL). They believe it is possible that their limit will drop below 1.0×10^{-5} when they include all of their data.

1.2.3 E771 ($D^0 \rightarrow \mu^+ \mu^-$ Search)

Fermilab E771 also has a preliminary limit on $BR(D^0 \rightarrow \mu^+ \mu^-)$, from data collected during the 1990-91 fixed-target run with the 800-GeV primary proton beam (interacting in

their silicon target). Like E789, they use their J/ψ signal to normalize their result. (They use their measurement of the J/ψ production cross section.) Based on 40% of their data sample, and without using their silicon vertex detector, they obtain a limit of $BR(D^0 \rightarrow \mu^+ \mu^-) < 1.2 \times 10^{-5}$ (90% CL). Due to their lack of vertexing information, E771 has substantial background in the signal region (roughly 1000 events per 20 MeV bin). The upper limit (90% CL) on the number of signal events in their sample is 108.7.

When they add information from their silicon microstrip detector, and analyze their full data set, they anticipate reducing their limit by a factor of 2.

1.2.4 E791 ($D^+ \rightarrow \pi^+ \mu^+ \mu^-$ Search)

Fermilab E791 is currently reporting a limit on $BR(D^+ \rightarrow \pi^+ \mu^+ \mu^-)$, based on 1/3 of their full data sample. E791 used an open-geometry spectrometer with 23 planes of silicon microstrip detectors to collect events in a 500-GeV π^- beam during the 1990–91 fixed-target run.

E791 uses the relative branching ratio approach, normalizing to the decay $D^+ \rightarrow K^- \pi^+ \pi^+$. After a series of vertexing and muon ID cuts, they are left with 5 fully reconstructed $\pi^+ \mu^+ \mu^-$ candidate events in the D^+ mass region. They expect 4.6 events from false muon tags, which they estimate from data by finding the number of times two tracks are identified as muons in $D^+ \rightarrow K^- \pi^+ \pi^+$ decays. If they take the product of this double-misidentification probability and the number of $\pi^+ \mu^+ \mu^-$ candidates they have before muon ID cuts, they get 4.6 events. With 9692 events in their normalizing mode, E791 finds $BR(D^+ \rightarrow \pi^+ \mu^+ \mu^-) < 4.6 \times 10^{-5}$ (90% CL).

1.2.5 E687 (Dimuon Searches)

Fermilab E687 has preliminary results on several dimuon modes (see Table 1). E687 is an open-geometry photoproduction experiment with 12 planes of silicon microstrips for vertexing. They collected their data in the wide-band photon beam during the 1990–91 fixed target run.

E687 uses the relative BR method ($D^0 \rightarrow K^- \pi^+$ for 2-body modes and $D^+ \rightarrow K^- \pi^+ \pi^+$ for 3-body modes). Their hadronic misidentification probability in charm events is typically 1% for muons (and electrons). After vertexing and muon ID cuts, they typically have no events in the signal regions of their invariant mass plots.

The limits quoted in Table 1 used only the inner muon ID system. The outer muon system performed poorly during the 1990–91 run. Electron ID information is available; limits on dielectron and electron-muon modes are in progress.

E687 will run again (as E831) in the next fixed target run, and will increase their data sample by a factor of 10. They also will upgrade their muon and electron ID systems. With improved muon systems, their acceptance*efficiency for dimuon modes should increase by a

factor of six to eight.

1.2.6 Summary

Essentially all of the new results on FCNC, LFNV, and LNV charm decays are preliminary or based on partial data sets. The current status of searches is summarized in Table 1. The new results typically represent an improvement of 1–2 orders of magnitude over old limits (if old limits existed). For many modes there are no new results yet, but this situation should change within the next year (the list should also get longer).

1.3 Charm 2000 — Potential and Challenges

A “back of the envelope” estimate of the potential sensitivity of a 10^8 reconstructed charm experiment can be made using eq. 1. In making this estimate I am assuming an open-geometry, general purpose experiment such as E791, E687, or the straw-man experiment suggested by Dan Kaplan during the conference. The ratio of ϵ for the rare and normalizing mode should be approximately one. The number of observed events in normalizing modes such as $D^0 \rightarrow K^- \pi^+$ or $D^+ \rightarrow K^- \pi^+ \pi^+$ is roughly 25% of the total reconstructed sample. If no candidate events are observed (a big if) then the upper limit on the number of observed rare decays is 2.3. Finally, to get a limit on an absolute BR , one needs to multiply by the absolute BR for the normalizing mode, which is typically 3–10%. Assuming 10%, one finds that the potential limit is roughly $1/N_{\text{recon}}$, or 10^{-8} .

It has been suggested that Charm 2000 should not be a general purpose experiment, but should be one or more “dedicated” experiments. Estimating the sensitivity of a dedicated rare decay experiment is much more difficult, since it would probably not be a “scaling up” of a current experiment. In this case, the estimate above represents a lower limit on the expected sensitivity (otherwise the motivation for a dedicated experiment is greatly diminished).

One of the advantages of searching for charm decays into final states containing two charged leptons is the tools one has for background rejection. Lepton ID tends to be efficient and clean (hadronic misidentification rates of 1% can easily be obtained). A strength of fixed-target experiments is excellent vertexing, which can be used to require that the daughter tracks of a candidate (especially the two leptons) form a good vertex, well isolated from the primary and from other tracks in the event.

Efficient background rejection is very important because limits decrease as $1/N$ only as long as there are no backgrounds. Once backgrounds kick in, limits decrease with increasing statistics only as $1/\sqrt{N}$. Charm 2000 is an extrapolation of three orders of magnitude, and it is impossible to anticipate all sources of background. Sources that must certainly be considered are discussed below.

1.3.1 Misidentified Charm Decay

Backgrounds from charm decays are a problem because vertexing doesn't help reject them. As an example, consider the decay $D^+ \rightarrow \pi^+ \pi^- \pi^+$. If two of the pions are misidentified as muons, this decay will look like $D^+ \rightarrow \pi^+ \mu^- \mu^+$ and should pass any vertexing cuts applied. The resulting invariant mass will be close to the D^+ mass: E687 finds that the mass peak of such events is shifted by roughly $20 \text{ MeV}/c^2$, whereas their mass resolution is approximately $10 \text{ MeV}/c^2$. If the muon fake probability is 0.1%, then the double fake probability is roughly 10^{-6} . The branching ratio for $D^+ \rightarrow \pi^+ \pi^- \pi^+$ is about 10^{-3} , so this background would then occur at the 10^{-9} level. If the fake probability is 1% (more typically of current experiments), this background is important at the 10^{-7} level, which is too high.

1.3.2 Random Combinatorics

The principle function of vertexing cuts is to eliminate random combinations of fake and/or real leptons. For the purposes of this discussion, "fake" leptons are hadrons ($\pi/K/p$) which are either misidentified or which decay in flight, and "real" leptons come from charm semileptonic decay. The resolution of the vertexing system and the fake ID probability determine the level at which the combinatoric background becomes significant.

To estimate the random combinatoric background for Charm 2000, and provide feedback for the design of the experiment, detailed studies will be required. However, a rough guesstimate can be illustrative. If this background is just below the sensitivity of current experiments, then it will have to be reduced by three orders of magnitude for Charm 2000. A factor of 100 would come from reducing the lepton fake probability to 0.1% (ignoring for now the contribution of real leptons, *i.e.* those from semileptonic charm decay). The required increase in rejection due to improved vertexing would then be a factor of 10 (which sounds hard).

1.3.3 Other Physics Processes

It is possible for other physics processes to contribute to the decay modes of interest in FCNC searches. For example, $BR(D^+ \rightarrow \rho \pi^+) < 1.2 \times 10^{-3}$, and $BR(\rho \rightarrow \mu^+ \mu^-) = 4.6 \times 10^{-5}$. If $D^+ \rightarrow \rho \pi^+$ occurs just below the limit on its BR , then $BR(D^+ \rightarrow \rho \pi^+ \rightarrow (\mu^+ \mu^-) \pi^+)$ will be about 5×10^{-8} .

1.3.4 Summary

Efficient rejection of fake leptons is crucial to searches for rare and forbidden charm decay. Fake probabilities of 0.1% will probably need to be obtained by Charm 2000. Vertex resolution is also very important, although it will take some work to quantify the required improvement over the current generation of experiments. If backgrounds can be efficiently

eliminated (a big if), a general purpose Charm 2000 experiment has the potential to set limits on rare decays at the level of $10^{-7} - 10^{-8}$.

2 Searches for CP Violation in Charm Decay

CP violation can occur in charm decays via the interference of two weak decay amplitudes to the same final state. *Indirect* CP violation is mediated by $D^0 - \bar{D}^0$ mixing. For example, the two amplitudes might be $D^0 \rightarrow K^+ K^-$ and $D^0 \rightarrow \bar{D}^0 \rightarrow K^+ K^-$. However, the interference is largest if the two amplitudes are roughly equal. Since mixing is expected to be extremely small, indirect CP violation is not expected to be a big effect.

Even in the absence of mixing, a decay mode (*e.g.* Cabibbo-suppressed mode) that has two weak amplitudes contributing to the same final state can exhibit *direct* CP violation. Final state interactions (FSI) induce a phase shift between the two weak amplitudes, leading to a decay-rate asymmetry between a charm meson decay and its CP conjugate: $\Gamma(D \rightarrow f) \neq \Gamma(\bar{D} \rightarrow \bar{f})$. FSI are substantial in charm decay, and the two weak amplitudes can be similar in size. Asymmetries as large as 0.1-1.0% are possible in the standard model [7], especially in D^+ decay.

2.1 Recent Results

A few years ago, E691 set an upper limit of 45% on the CP asymmetry for the Cabibbo suppressed mode $D^0 \rightarrow K^+ K^-$ [3]. Recently, E687 has presented results [2] for $D^0 \rightarrow K^+ K^-$ (with a D^{*+} tag) and $D^+ \rightarrow K^+ K^- \pi^+$. The $D^+ \rightarrow K^+ K^- \pi^+$ mode is complicated by the possibility of intermediate resonant states ($\bar{K}^{*0} K^+$ and $\phi \pi^+$). The CP asymmetry could be different for each decay mode, since the strong phase shift and relative size of the two weak decay amplitudes varies. They therefore look separately for an asymmetry in the resonant decay modes as well as the $K^+ K^- \pi^+$ mode. For the $\phi \pi^+$ ($\bar{K}^{*0} K^+$) mode, non-resonant events are removed by subtracting sideband events in the ϕ (\bar{K}^{*0}) mass plot.

Equal numbers of D and \bar{D} mesons are not produced in photoproduction, so they use Cabibbo favored modes ($D^0 \rightarrow K^- \pi^+$, $D^+ \rightarrow K^- \pi^+ \pi^+$) to determine the production ratio. Their raw, uncorrected production asymmetry is roughly 5%. Using Cabibbo allowed modes to normalize the production asymmetry has the advantage of mitigating many sources of potential systematic error (for example, a charge dependent acceptance). Because there are about 20 times more events in the normalization modes, there is little effect on the statistical error.

E687's measurements of the CP asymmetry in each of the above modes are given in Table 2, along with 90% CL upper limits.

Table 2: CP Asymmetry: $(\Gamma_D - \Gamma_{\bar{D}})/(\Gamma_D + \Gamma_{\bar{D}})$

Decay Mode	Measured Asymmetry	90% C.L. limit
$D^0 \rightarrow K^+ K^-$	0.024 ± 0.084	$-11\% < A_{CP} < 16\%$
$D^+ \rightarrow K^- K^+ \pi^+$	-0.031 ± 0.068	$-14\% < A_{CP} < 8.1\%$
$D^+ \rightarrow \bar{K}^{*0} K^+$	-0.12 ± 0.13	$-33\% < A_{CP} < 9.4\%$
$D^+ \rightarrow \phi \pi^+$	0.066 ± 0.086	$-7.5\% < A_{CP} < 21\%$

2.2 Charm 2000

Errors in the above asymmetries will decrease as \sqrt{N} . Extrapolating from E687 (10^5 reconstructed charm, $\sigma(A_{CP}) = 7\text{--}14\%$), Charm 2000 should be sensitive to asymmetries of 0.2–0.5%. This is in the range of standard model expectations, and if new physics produces a larger asymmetry it will almost certainly be observable.

Charm 2000 will have to worry about a production asymmetry. One search strategy might be to ignore this complication and use a “shotgun” approach: measure asymmetries for several modes, and look for statistically significant differences. (Essentially this is what E687 did.) This method will work unless nature conspires to make the CP asymmetry the same for all modes (which seems highly unlikely).

Another search strategy which may prove fruitful at Charm 2000 is one suggested by Bigi [8]. One looks for a “triple correlation” in the decay planes of vector–vector charm meson decays such as $D^+ \rightarrow \bar{K}^{*0} K^{*+}$. If the polarization and momentum of the \bar{K}^{*0} are $\vec{\epsilon}_0$ and \vec{p}_0 , and $\vec{\epsilon}_+$ is the polarization of the K^{*+} , then the triple correlation for D^+ decay is $C_+ = \langle \vec{p}_0 \cdot (\vec{\epsilon}_0 \times \vec{\epsilon}_+) \rangle$. CP is violated if $C_+ + C_- \neq 0$.

Acknowledgments

The author is grateful to the Vanderbilt University Research Council and the National Science Foundation for their generous support, and would like to thank Dan Kaplan, Bob Panvini, and Alan Schwartz for sharing their ideas and insights on this topic.

References

- [1] Particle Data Group, K. Hikasa et al., Phys. Rev. D45 (1993) S1.
- [2] E687 Collab., P. L. Frabetti et al., FERMILAB-Pub-94/071-E, accepted for publication in Phys. Rev. D Rapid Comm.
- [3] E691 Collab., J. C. Anjos et al., Phys. Rev. D Rapid Comm. 44 (1991) R3371.
- [4] A. J. Schwartz, Modern Phys. Lett. A, Vol. 8, No. 11 (1993) 967.
- [5] See, for example, the contribution of S. Pakvasa to this conference.
- [6] E789 Collab., C. S. Mishra et al., FERMILAB-Pub-94/083-E.
- [7] M. Golden and B. Grinstein, Phys. Lett. B222 (1989) 501; F. Buccella et al., Phys. Lett. B302 (1993) 319.
- [8] I. Bigi, SLAC-Report-343 (1989) 169.

Future Experimental Charm Physics at $\sqrt{s}=10$ GeV

Dave Z. Besson,
University of Kansas
Lawrence, KS 66045
and Arne P. Freyberger
University of Florida
Gainesville, FL 32611

(on behalf of the CLEO collaboration)

Abstract

The future of charm physics at $\sqrt{s}=10$ GeV is considered, using the present CLEO experiment as a starting point. Detector design, event yields, and limiting experimental systematics are considered. The projections are general and applicable to the B-factories presently planned for both SLAC and KEK, as well as the upgraded CLEO-III experiment.

1 Introduction

Sometime in the late 1970's, when Johnny Rotten and the Pistols were deciphering basic 4/4 for a prog-rock ridden pop establishment which had drifted into overproduction, multiple Moogs, and Louie L'Amour - laced lyrics, there was a band of four Rockaway Beach - bred longhairs in leathers and ripped dungarees that were habitually blowing out the woofers on the house PA at CBGB's in New York City. They were called the Ramones[1]. Roger Daltrey, who had by that time drifted away from his anti-establishment roots and was playing movie roles opposite Bridget Bardot, offered the following advice to Johnny Ramone: "You look like, but you don't play like leather-clad rockers. Noone will ever take your music seriously".

The CLEO experiment at $\sqrt{s} \sim 10.55$ GeV, although to the outside world leather-clad in B-physics, has maintained a strong charm physics program. Judged by sheer numbers of publications, this charm program has actually been more prolific than its bottom physics program. Present charm physics at CLEO has been covered by Arne Freyberger [2]. I will discuss future charm physics that will be done at the upgraded CLEO experiment (1995-2000), and at high-luminosity 10 GeV machines in general (including the SLAC or KEK B-factories).

2 Inclusive charm production rates at ECM=10 GeV

The cross-section for the production of charm-anticharm events in e^+e^- collisions at $\sqrt{s}=10$ GeV is approximately 1.1 nb; this is, of course, simply the $e^+e^- \rightarrow \mu\mu$ point charge cross-section multiplied by the ratio of $(q_c/q_\mu)^2$ multiplied by the color factor of approximately 3. Typical cross-sections for production of charmed particles at CESR are given in Table 1. We note the following:

- There is a canonical factor of 1/3 expressing the relative likelihood of popping an $s\bar{s}$ pair out of the vacuum compared to either a $u\bar{u}$ or a $d\bar{d}$ pair at $\sqrt{s}=10$ GeV. Correspondingly, the production rate of D_s relative to $(D^0 + D^+)$ is approximately 1/6 - we are three times as likely to produce a primary $c\bar{u}$ or a $c\bar{d}$ state compared to a $c\bar{s}$ state.
- The production of J=1 vectors relative to J=0 pseudoscalars ($D^* : D$) has been measured to be approximately 3:1 for D-mesons, as expected by simple 2J+1 spin counting arguments; this ratio has not yet been quantified for $D_s^* : D_s$. Breakdown of 2J+1 spin counting occurs for L=1 mesons — production of L=1, J=2 orbitally excited charmed mesons occurs at ~5-10% of the inclusive rate of the ground state meson rather than being a factor of 5 times larger; a similar pattern holds for Λ_c^* 's relative to Λ_c 's as well. This is presumably a consequence of the penalty incurred by having a unit of orbital angular momentum between the c quark and the other quarks in the hadron.
- The production of charmed baryons relative to charmed hadrons is roughly equal to the production rate for protons to pions in electron-positron collisions, i.e. smaller by approximately an order of magnitude.
- The smallness of the cross-section for ψ production on the continuum indicates that $c\bar{c}$ pairs are popped from the vacuum extraordinarily rarely, if at all, at $\sqrt{s}=10$ GeV. This makes the observation of the doubly-charmed baryon[3] at a 10-GeV machine unlikely to antedate an appearance in the World Cup Finals by a team from the United States[4].

A typical e^+e^- B-factory experiment will take two thirds of its data at the $\Upsilon(4S)$ resonance ($E_{beam}=5.29$ GeV) for B-decay studies ($\Upsilon(4S) \rightarrow B\bar{B}$), and one-third of its data on the continuum at center-of-mass energies 60 MeV below the $\Upsilon(4S)$ resonance ($E_{beam}=5.26$ GeV). Since the resonant $\Upsilon(4S)$ cross-section of 1nb is a factor of 3 smaller than the continuum $e^+e^- \rightarrow \text{hadrons}$ cross-section, the data at energies off the resonance peak are useful for evaluating the continuum backgrounds to the $\Upsilon(4S)$ data. The hadronic cross-section as it depends on center of mass energy is shown in Figure 1, showing the narrow ($\Upsilon(1S)$, (2S), and (3S)) $b\bar{b}$ bound state resonances, and the $\Upsilon(4S)$. The $\Upsilon(4S)$ is the lowest-lying state massive enough to decay into $B\bar{B}$, and is therefore broader than the lower resonances below threshold. Since $b \rightarrow c$, also included in Table 1 is the production cross-section for charmed hadrons from B-decays; this is a source of charm which has not yet been fully exploited. As discussed by Isi Dunietz[5] at this conference, B-decays to baryons may be very useful for determining absolute branching ratios for charmed baryons.

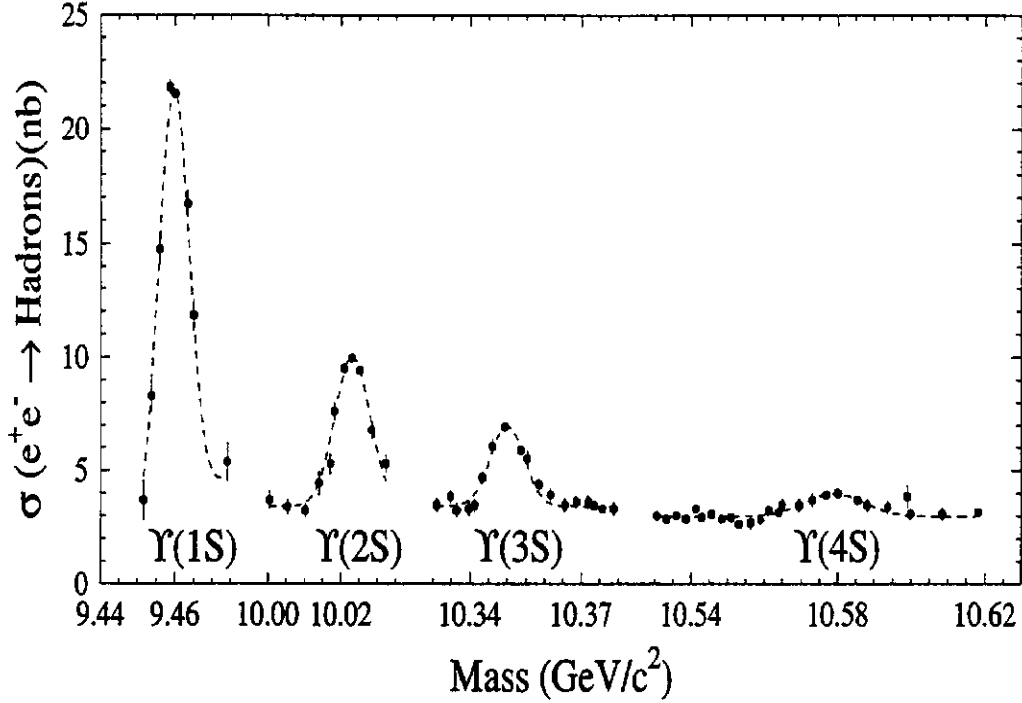


Figure 1: Hadronic cross-section in the 10 GeV energy region.

To set the scale, extrapolating a visible cross-section of approximately 10pb for the process $D^{*+} \rightarrow D^0 \pi^+$; $D^0 \rightarrow K^- \pi^+$ to a 30/fb sample of data, a CLEO-type detector should have 300K such decays observed. I will comment in the Conclusions Section on which physics topics are more well-suited for a fixed-target or a tau-charm Factory experiment. For other charm-physics environments (hadron colliders or RHIC, e.g.), I refer the interested reader to the appropriate write-ups in these proceedings [6, 7].

3 Detector design, CLEO-II to CLEO-II.5 to CLEO-III

A schematic of the CLEO-II detector is shown in Figure 2. The specifications of the present CLEO-II detector are given in Table 2. These performance specifications set the baseline for future upgrades of tracking, particle identification, and calorimetry.

3.1 Installation of Silicon

As with most general purpose particle detectors, a silicon-based tracking system close to the production point will be an essential element of the new detector. Not only will this provide substantially improved vertexing resolution, but it will also improve the angle measurement on charged tracks by at least a factor of two. Endview and sideview schematics of this detector are presented in Figure 3.

The advantage to be gained in background reduction from the silicon vertex detection system is illustrated in Figure 4, based on Monte Carlos of the present tracking system

Particle	Continuum Inclusive σ	B \bar{B} Inclusive σ
$c\bar{c}$	1.1 nb	1.2 nb
$D^0 + \bar{D}^0$	2×0.55 nb	2×0.60 nb
$D^+ + D^-$	2×0.25 nb	2×0.28 nb
$D^{*+} + \bar{D}^{*-}$	2×0.40 nb	2×0.45 nb
$D_s^+ + D_s^-$	2×0.15 nb	2×0.15 nb
$D_s^{*+} + D_s^{*-}$	2×0.07 nb	(2×0.07) nb
$D_1^0 + \bar{D}_1^0$	2×0.10 nb	$(< 2 \times 0.07)$ nb
$D_2^{*+} + D_2^{*-}$	2×0.15 nb	
$\Lambda_c^+ + \bar{\Lambda}_c^-$	2×0.10 nb	2×0.05 nb
$\bar{\Lambda}_c^{*+} + \Lambda_c^{*-}$	2×0.01 nb	$(< 2 \times 0.01)$ nb
$\Xi_c + \bar{\Xi}_c$	2×0.03 nb	2×0.045 nb
$\Omega_c + \bar{\Omega}_c(^*)$	2×0.01 nb	(2×0.01) nb
ψ	0.04 pb	1 pb

Table 1: Inclusive cross-sections for the production of charmed hadrons for e^+e^- collisions (nb). Cross-sections given are the sum of both particle and antiparticle production. Values in parentheses are estimated and not yet measured.

(without silicon) and the future tracking system including silicon. Shown is the vertexing resolution with the present CLEO-II inner tracking system, consisting of a six-layer straw tube chamber using DME as the drift gas and a 10-layer high precision vertex detection system occupying the region $7.5\text{cm} < r < 17.5\text{ cm}$, where r is the radial coordinate measured from the beam line. Also shown is the vertexing resolution expected after installation of the silicon tracking system. Note that the simulation is for charmed particles produced from the continuum, and not from B-decay. Typical lab momenta (and, therefore decay lengths) of charm from B-decay are a factor of 2 smaller than those from the continuum. Typical gains in signal to noise for D^+ decays can be read off of the two plots, and are roughly an order of magnitude.

4 From CLEO-II.5 into the B-Factory Era

The assumptions that I will make are that the proposed B-Factory era experiment will have:

- the ability to handle high trigger rates ($> 10^2$ Hz written to tape, based on a design luminosity of $\mathcal{L} = 2 - 3 \times 10^{32}/\text{cm}^2/\text{s}$) with small dead time,
- charged track reconstruction performance at least as good as CLEO-II at present ($(\frac{dp}{p})^2 \leq (0.0015)^2 + 0.005^2$),

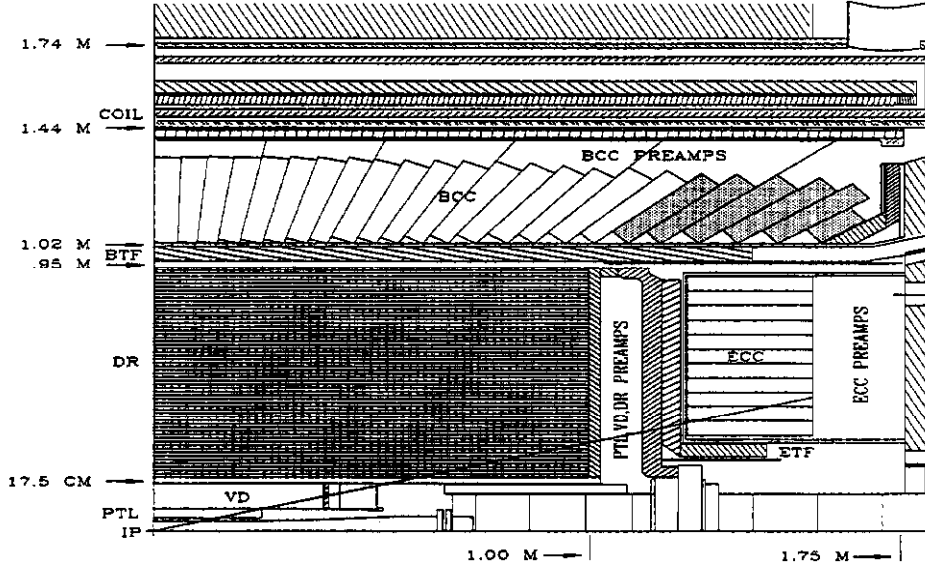


Figure 2: Cutaway picture of present CLEO-II detector

- silicon with typical vertexing resolutions of $40\mu\text{m}$, which will significantly improve S:N for charm and offers the possibility of perhaps measuring the D^* and Σ_c widths through the application of vertex constraints (not to mention the benefits in B-physics),
- photon reconstruction based on CsI with performance specifications at least as good as CLEO-II at present (3.9%(1.1%) at 100(5000) MeV),
- a particle ID system with $\geq 3\sigma$ π/K separation at $p=2.8$ GeV/c; this requirement is dictated by the necessity to separate $B \rightarrow \pi^+\pi^-$ from $B \rightarrow K^+\pi^-$. By comparison, the present CLEO-II particle ID system achieves 1.8σ π/K separation in the dE/dx relativistic-rise region.

The projections in Table 4 for event yields assume a detector capable of meeting the above requirements.

5 Particle ID in the B-factory era

At present, three particle identification options are being considered for the CLEO-III detector. These are: a) a fast RICH counter, b) high pressure threshold gas tubes, and c) an aerogel detector. The Babar detector will feature a DIRC detection system, operating on the principle of total internal reflection of Cerenkov light through a light path of known length. Simulations are underway at CLEO to evaluate the impact of each particle-ID option on the physics we would like to do. As an example, Figure 5 shows a Monte Carlo simulation of the discrimination between $D^0 \rightarrow \pi^-\ell^+\nu_\ell$ and $D^0 \rightarrow K^-\ell^+\nu_\ell$ which we can achieve with

Device	#	R(cm)	Z (cm)	cos θ	Resolution
PTL	6	4.7-7.2	25	0.96	50 μ m (DME @6mm H ₂ O)
VD CT (1)	1	7.6	19	0.92	1.3mm (5.85mm strips)
VD	10*	8.5-16.0	35	0.91	90 μ m (Ar-Eth @ 6 PSIG)
VD CT (2)	1	17.1	33	0.90	1.3mm (6.85mm strips)
DR CT (1)	1	18.6	48	0.92	1.2mm (1.00mm strips)
DR	51**	19.9-90.1	97	0.71	120 μ m (Ar-Eth @6mm H ₂ O)
DR CT (2)	1	91.6	91	0.71	1.2mm (0.95mm strips)
Full CD	67/4	4.7-90.1	-	0.92	$\frac{\sigma_p}{p}[\%] = \sqrt{(0.15p)^2 + 0.5^2}$ $\sigma_{dE/dx}(e) = 6.3\% @ 5 \text{ GeV}$
Barrel TF	64	96-101	140	0.77	$\sigma_t(\pi) = 154 \text{ ps; (2PMTs/ctr)}$ $2\sigma \pi-K \text{ for } p_t < 1.1 \text{ GeV}/c$
Endcap TF	2 \times 28	31-89	120-125	0.81-0.96	$\sigma_t(e) = 240 \text{ ps; (1PMT/ctr)}$
Barrel CC	6144	102-132	167	0.82	$\frac{\sigma_E}{E}[\%] = \frac{0.35}{E^{0.75}} + 1.9 - 0.1E$ $\sigma_\phi[\text{mrad}] = 2.8/\sqrt{E} + 1.9$
Endcap CC	2 \times 828	33-91	125-155	0.81-0.98	$\frac{\sigma_E}{E}[\%] = 0.26/E + 2.5$
Barrel MU	3	210,246,282	240	0.71	$\approx 4 \text{ cm @ } 5 \text{ GeV}$
Endcap MU	2 \times 1	160-310	280	0.67-0.85	$\approx 5 \text{ cm @ } 5 \text{ GeV}$

Table 2: Brief description of the CLEO detector subsystems: the PTL (precision tracking layers), VD (vertex detector), CT (Cathode hoops) (two for each of the vertex detector and the drift chamber), DR (drift chamber), CD (total central detector, i.e., PTL+VD+DR), TF (time-of-flight), CC (crystal calorimeter), and MU (muon system). Presented are the number of components, # (layers for CD, counters for TF, crystals for CC, superlayers for MU), approximate coverage in cylindrical radius R and longitudinal direction Z, polar angle coverage |cos θ |, and resolutions.

* instrumented for charge division.

** 40 axial ; 11 small angle stereo.

the present dE/dx particle identification system, compared with the upgraded particle id system including a RICH detector. In order to determine the $D \rightarrow \pi \ell \nu_\ell \frac{d\Gamma}{dq^2}$ spectrum ($q^2 = m_W^2$) over the full kinematic regime, such a particle identification system will clearly be essential. Recall that the primary obstacle to obtaining a model-independent value of the CKM matrix element V_{ub} is the requirement to extrapolate the $b \rightarrow u \ell \nu$ signal over the entire available phase space from the very limited region where there is separation from the $b \rightarrow c \ell \nu$ background. It is expected that the $c \rightarrow u \ell \nu$ differential cross-section will provide a model for understanding $b \rightarrow u \ell \nu$, provided that the former transition can similarly be probed over the entire Dalitz plot. The Figures therefore clearly illustrate the importance of an improved particle-ID system in obtaining a more model-independent value for V_{ub} .

Particle ID will also help for another, more subtle reason. The detection of semileptonic ($D \rightarrow K \ell \nu$, e.g.) and leptonic ($D_s \rightarrow \mu \nu$, e.g.) charm decays necessarily involve an unseen neutrino in the event. In the case of $D_s \rightarrow \mu \nu$, a particle ID system which allows $\pi/K/p$

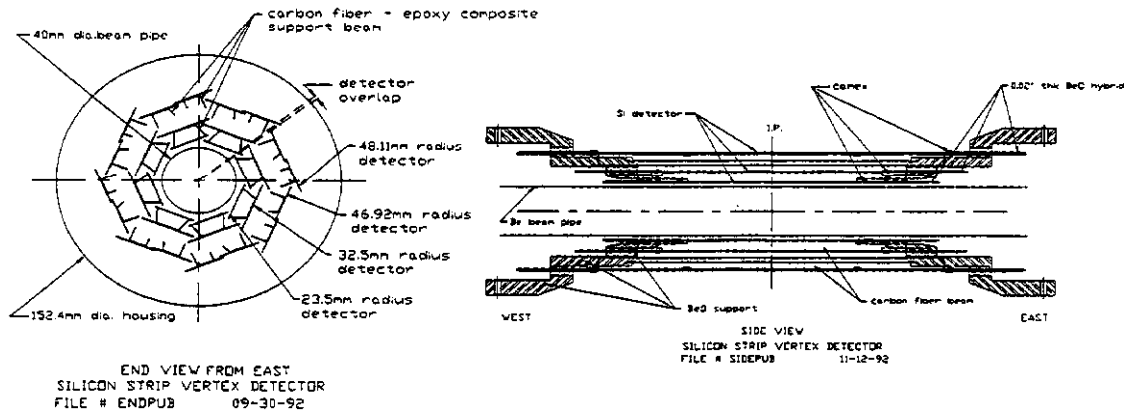


Figure 3: End view (left) and side view (right) of the silicon detector scheduled for installation into CLEO-II in Nov. 1994

separation over a large fraction of the accessible momentum range will allow a more precise determination of the total energy carried by charged tracks in an event, and will therefore sharpen the p_T estimation.

One important feature of a B-factory detector which should be kept in mind when discussing charm physics is that the detector is just that, a B-factory detector. Design is driven by achieving the physics desirable from the B-sector more than anything else, as the above specifications indicate. Although the general purpose B-factory detector would, in principle, be well-suited for general charm studies, an ideal charm detector would probably not have the detector asymmetry which must be built into a facility designed to measure CP-violation in B-decay, and would probably be more designed with an eye towards K_L^0 detection, and lepton detection at the low momenta typical of a $V - A$ $c \rightarrow s$ transition. The detectors planned for high-luminosity experiments at CESR and SLAC are displayed in Figures 6 and 7. The Babar detector (7) has its geometry matched to the beam energy asymmetry ($E_{e^+}=9$ GeV, $E_{e^-}=3$ GeV) of the planned B-factory project at SLAC.

6 Examples of physics studies at 10 GeV

To illustrate some of the accessible physics, and techniques used at 10 GeV machines, I will consider two physics topics - studies of charm semileptonic decays, as well as the determination of absolute branching ratios.

7 Consideration of semileptonic decays (by A. Freyberger)

As an example of a charm physics analysis at $\sqrt{s}=10$ GeV, we will consider the charm semileptonic decay analysis carried out with CLEO-II data with 2/fb of data, or 6% of the

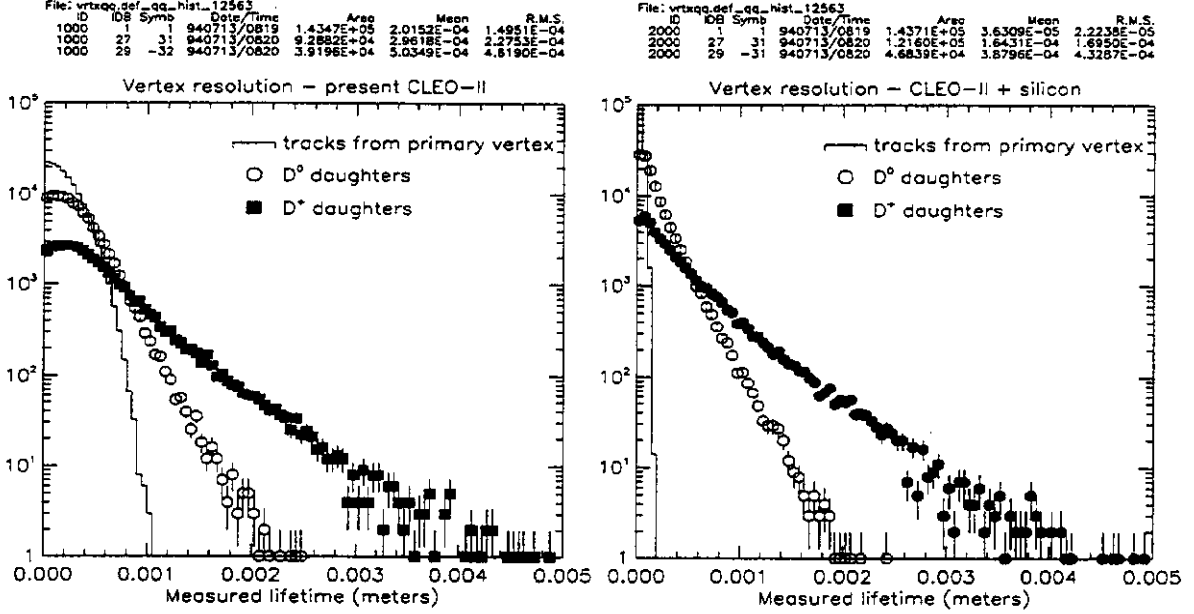


Figure 4: Vertex resolution for CLEO-II in present configuration (left), and with silicon (right).

canonical B-factory data sample of 30/fb. Interest in charm semileptonic decays is motivated by the simplicity of the decay. For example, in the decay $D^0 \rightarrow K^- e^+ \bar{\nu}$ the electron and anti-neutrino are unaffected by the strong interaction and all strong interaction effects can be absorbed in a form factor. This form factor can be thought of as the probability that the meson K will be formed as a function of the momentum transfer in the decay, $q^2 = M_W^2$. We write the differential decay rate for $D^0 \rightarrow K^- e^+ \bar{\nu}$ as:

$$d\Gamma/dq^2 = (1/24\pi^3) G_F^2 |V_{cs}|^2 f_+(q^2) P_K^3 \quad (1)$$

where G_F is the Fermi constant and $|V_{cs}|$ is the Cabibbo-Kobayashi-Maskawa (CKM) matrix element governing the $c \rightarrow s$ transition of the charm quark. The $c \rightarrow d$ transition is also allowed for the charm quark, such decays are called Cabibbo suppressed since the CKM matrix element for these decays, $|V_{cd}|$ is much smaller than $|V_{cs}|$. The form factor in Equation 1 is denoted as $f_+(q^2)$. The P_K^3 factor is the phase space term for a spin one half particle decaying into a vector and pseudo-scalar. Since the CKM matrix elements, V_{cs} and V_{cd} are known to within $\pm 1\%$ due to the unitarity constraint [8], measurements of charm semileptonic decay rates provide information on the form factors involved. These measurements can then be compared with predictions obtained from quark models, QCD sum rules and lattice gauge calculations.

Charm analysis at e^+e^- machines operating in the $\Upsilon(4S)$ resonance region uses charm events produced in continuum reactions, $e^+e^- \rightarrow c\bar{c}$. The c and \bar{c} quark fragment into a spectrum of charmed hadrons. The momentum distribution of charm hadrons from continuum production is much harder than that of charm hadrons from B decays. This fact is utilized by placing momentum cuts to reduce the combinatoric background and obtain clean

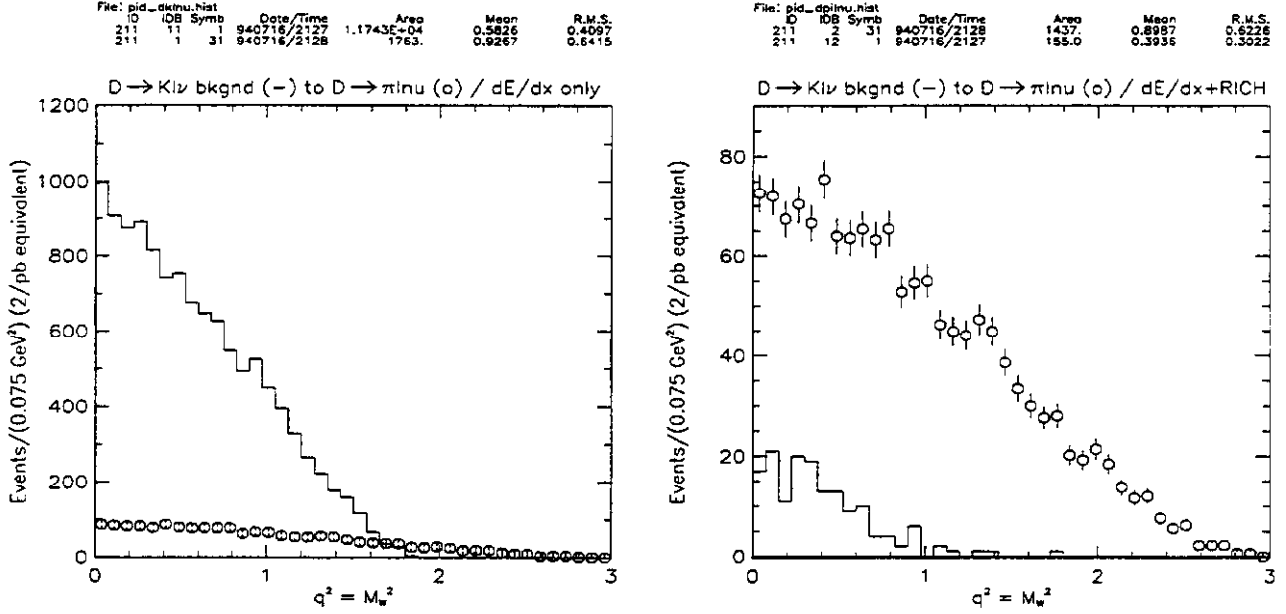


Figure 5: Simulation for the Cabibbo-suppressed semileptonic decay: $D^0 \rightarrow \pi^- \ell^+ \nu_\ell$ and the expected background from the Cabibbo-favored channel: $D^0 \rightarrow K^- \ell^+ \nu_\ell$ at present, with dE/dx as is, and in conjunction with the CLEO-III particle ID systems under consideration. The Monte Carlo data sample shown corresponds to approximately 2/fb.

signals.

7.1 The D^0 and D^+ semileptonic decays

The D^0 and D^+ mesons are the most scrutinized charm hadrons. The measurements of the semileptonic exclusive rates are becoming precise enough for detailed comparisons with the model predictions. Both CLEO [9] and ARGUS [10] rely on the initial $D^{*+} \rightarrow \pi_s^+ D^0$ decay to reduce backgrounds. CLEO also exploits their exceptional calorimeter to utilize the $D^{*+} \rightarrow \pi_s^0 D^+$ decay to gain access to the D^+ channels. This technique utilizes the fact that although the momentum of the neutrino is lost, the mass difference, $\delta m = m_{\bar{K}^{(*)} l^+ \pi_s^+} - m_{\bar{K}^{(*)} l^+}$ still peaks at the nominal value. As the mass of the $\bar{K}^{(*)} l^+$ system increases the momentum carried away by the neutrino decreases and the δm distribution becomes more sharply peaked.

The CLEO collaboration has measured yields in all four Cabibbo favored decay modes of the D^0 and D^+ , $D^0 \rightarrow K^- l^+ \bar{\nu}$, $D^+ \rightarrow \bar{K}^0 l^+ \bar{\nu}$, $D^0 \rightarrow K^{*-} l^+ \bar{\nu}$ and $D^+ \rightarrow \bar{K}^{*0} l^+ \bar{\nu}$. The \bar{K}^* channels are reconstructed through the following decay chains, $K^{*-} \rightarrow K_s^0 \pi^-$, $K_s^0 \rightarrow \pi^+ \pi^-$ and $\bar{K}^{*0} \rightarrow K^- \pi^+$. The data is split into two mass regions, low $\bar{K}^{(*)} l^+$ mass ($1.2 \leq m_{\bar{K}^{(*)} l^+} < 1.4 \text{ GeV}/c^2$) and high $\bar{K}^{(*)} l^+$ mass ($1.4 \leq m_{\bar{K}^{(*)} l^+} < 1.8 \text{ GeV}/c^2$) to take advantage of the correlation. For the $D \rightarrow \bar{K}^* l^+ \bar{\nu}$ modes a fit was performed to the $M_{K\pi}$ distributions for each bin in δm . CLEO combines the electronic and muonic yields, corrects for the phase space difference due to the different lepton masses [19], and quotes a value for

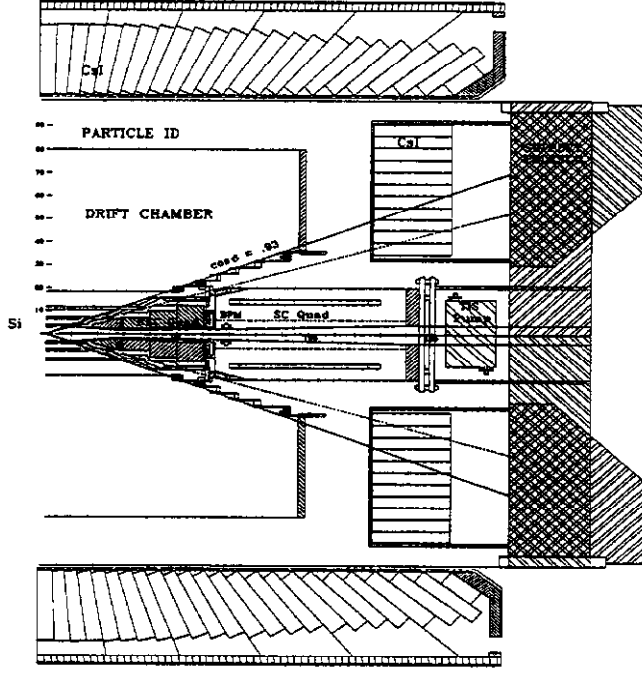


Figure 6: Schematic view of the planned CLEO-III detector, scheduled for operation in 1997.

the semi-electronic branching ratio. The yields are normalized to hadronic decay modes of the D that resemble in topology the semileptonic decay. Table 3 lists the four ratios obtained by CLEO compared with previous measurements, also included is a recent result from the ARGUS collaboration on $D^0 \rightarrow K^{*-} e^+ \bar{\nu}$. For those ratios where a common normalizing mode has been used among the experiments, the agreement is quite good.

With the large sample of $D^0 \rightarrow K^- l^+ \bar{\nu}$ decays, 1510 ± 60 events, CLEO has extracted the q^2 distribution and performed a fit to two functional forms of the form factor $f_+(q^2)$. The most common form is the pole form, $f(q^2) = f_+(0)/(1 - q^2/M_{pole}^2)$, where one extracts the value of the M_{pole} . There also exists an exponential parameterization due to Isgur *et al* (ISGW) of the form $f_+(q^2) = f_+(0)e^{\alpha q^2}$ [18].

To calculate q^2 for the event, CLEO II uses $q^2 = M_l^2 + 2[E_l E_{\bar{\nu}} - P_l P_{\bar{\nu}} \cos \theta_{l\bar{\nu}}]$ where in the Kl rest frame only $\cos \theta_{l\bar{\nu}}$ is unknown. The range of $\cos \theta_{l\bar{\nu}}$ can be restricted to reside within the two values given by $\cos \theta_{l\bar{\nu}} = \cos \theta_{\pi\bar{\nu}} \cos \theta_{\pi l} \pm \sin \theta_{\pi\bar{\nu}} \sin \theta_{\pi l}$ where $\theta_{\pi\bar{\nu}}$ is determined from δm and m_{Kl} . The value of q^2 within the allowed range that is the most probable solution based on the known decay angular distributions is then chosen. This gives a resolution in q^2 of 0.24 GeV^2 (RMS). The result of the fit is $M_{pole} = 2.00 \pm 0.12 \pm 0.18 \text{ GeV}$ or $\alpha = 0.29 \pm 0.04 \pm 0.06 \text{ GeV}^{-2}$. The pole mass agrees with the expected value of the D_s^* mass, and the value of α corresponds to $\kappa = 0.57 \pm 0.07$ which agrees with the value of $\kappa = 0.7$ used by ISGW.

By integrating $f_+(q^2)$ over the entire q^2 range, the value of $f_+(0)$ can be extracted. Using the CLEO II [26] measurement of $\mathcal{B}(D^0 \rightarrow K^- \pi^+)$ and the world average [8] for τ_{D^0} , CLEO finds $\Gamma(D^0 \rightarrow K^- e^+ \bar{\nu}) = (9.1 \pm 0.3 \pm 0.6) \times 10^{10} \text{ s}^{-1}$ for the decay width. This width

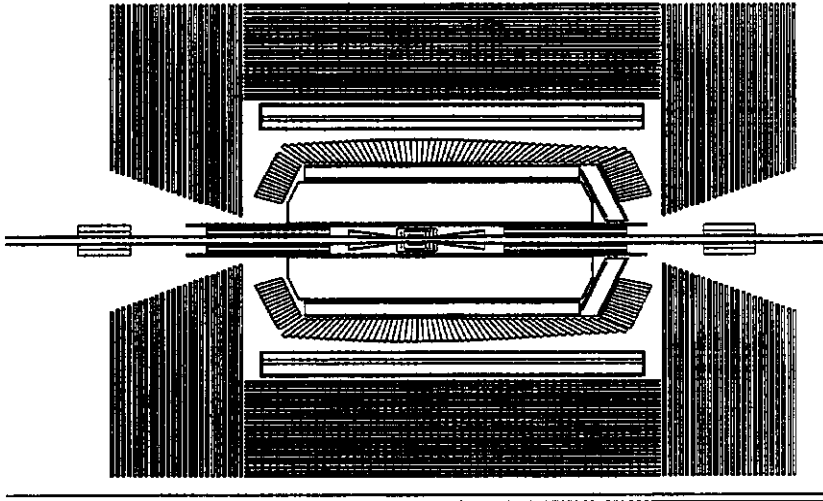


Figure 7: Schematic view of the planned Babar detector designed for the SLAC B-factory, scheduled for operation in 1998.

corresponds to $f_+(0) = 0.77 \pm 0.01 \pm 0.04$ in good agreement with the model predictions [18, 19, 20, 21, 22, 23, 24, 25]. CLEO also extracts the decay width for $D \rightarrow \bar{K}^* e^+ \bar{\nu}$ by averaging the two $D \rightarrow \bar{K}^* e^+ \bar{\nu}$ modes, they find $\Gamma(D \rightarrow \bar{K}^* e^+ \bar{\nu}) = (5.7 \pm 0.7) \times 10^{10} s^{-1}$.

With a B-Factory detector, we can expect an improvement of at least a factor of 4 in the statistical error with a 30/fb data sample. We also expect a large reduction in non-charm backgrounds as afforded by the silicon vertex detector. At this point, as indicated in Table 4, the limiting systematic errors are both the absolute tracking efficiency as well as the lepton identification efficiency.

8 Absolute branching ratios

As another example of the charm physics program that one might hope to carry out at $\sqrt{s}=10$ GeV, let's consider determination of absolute branching fractions. These have implications not only for constraining calculations of absolute partial widths, but also are crucial in understanding the $b \rightarrow c$ decay width.

8.1 $D^0 \rightarrow K^- \pi^+$

The technique pioneered by HRS[27] was to tag using the correlation of the slow pion π_{slow}^+ emitted in the decay chain: $D^{*+} \rightarrow \pi^+(D^0)$ with the thrust axis of an event to determine the total number of D^{*+} produced. By determining how often a particular D^0 mode is fully

EXPT	$\frac{B(D^0 \rightarrow K^- e^+ \bar{\nu})}{B(D^0 \rightarrow K^- \pi^+)}$	$\frac{B(D^+ \rightarrow \bar{K}^0 e^+ \bar{\nu})}{B(D^+ \rightarrow \bar{K}^0 \pi^+)}$	$\frac{B(D^0 \rightarrow K^{*-} e^+ \bar{\nu})}{B(D^0 \rightarrow \bar{K}^0 \pi^+ \pi^-)}$	$\frac{B(D^+ \rightarrow K^{*0} e^+ \bar{\nu})}{B(D^+ \rightarrow \bar{K}^0 \pi^+ \pi^+)}$
CLEO II [9]	$0.978 \pm 0.027 \pm 0.044$	$2.60 \pm 0.35 \pm 0.26$	$0.38 \pm 0.06 \pm 0.03$	$0.67 \pm 0.09 \pm 0.07$
ARGUS [10, 11]			$\frac{B(D^0 \rightarrow K^{*-} e^+ \bar{\nu})}{B(D^0 \rightarrow \bar{K}^0 \pi^+ \pi^-)}$ $0.40 \pm 0.07 \pm 0.07$	$0.55 \pm 0.08 \pm 0.10$
CLEO1.5 [12]	0.87 ± 0.07		$\frac{B(D^0 \rightarrow K^{*-} e^+ \bar{\nu})}{B(D^0 \rightarrow \bar{K}^0 \pi^+ \pi^-)}$ $0.51 \pm 0.18 \pm 0.06$	
E691 [13]	$0.91 \pm 0.07 \pm 0.11$	$0.66 \pm 0.09 \pm 0.14$		$0.49 \pm 0.04 \pm 0.05$
E687 [14]	$0.87 \pm 0.08 \pm 0.06$			$0.56 \pm 0.04 \pm 0.06$
WA82 [15]				$0.62 \pm 0.15 \pm 0.09$
E653 [16]	$\frac{B(D^0 \rightarrow K^- e^+ \bar{\nu})}{B(D^0 \rightarrow e^+ X)}$ $0.32 \pm 0.05 \pm 0.05$	$\frac{B(D^+ \rightarrow \bar{K}^0 e^+ \bar{\nu})}{B(D^+ \rightarrow \bar{K}^0 \pi^+ \pi^+)}$ $0.66 \pm 0.09 \pm 0.14$		$0.46 \pm 0.07 \pm 0.08$
MARK III [17]	$B(D^0 \rightarrow K^- e^+ \bar{\nu})$ $3.4 \pm 0.5 \pm 0.4\%$	$B(D^+ \rightarrow \bar{K}^0 e^+ \bar{\nu})$ $6.0_{-1.3}^{+2.2} \pm 0.7\%$	$B(D^0 \rightarrow K^{*-} e^+ \bar{\nu})$ $5.4_{-1.1}^{+1.9} \pm 0.6\%$	$B(D^+ \rightarrow \bar{K}^{*0} e^+ \bar{\nu})$ $4.4_{-1.0}^{+1.9} \pm 0.7\%$

Table 3: Summary of $D \rightarrow K^{(*)} l^+ \bar{\nu}$ branching ratio measurements. The use of different normalizing modes makes comparisons difficult for the $D^+ \rightarrow \bar{K}^0 l^+ \bar{\nu}$ and $D^0 \rightarrow K^{*-} l^+ \bar{\nu}$ channel.

reconstructed ($D^{*+} \rightarrow \pi_{slow}^+ D^0$; $D^0 \rightarrow K^- \pi^+$, e.g.), and normalizing to the total number of soft pions, a branching ratio for the mode of interest can be determined. The present CLEO value for this branching ratio of $(3.95 \pm 0.08 \pm 0.17)\%$ [26] is limited by the systematic uncertainty in the track reconstruction efficiency, which will hopefully be reduced (by as much as a factor of two) with more effort. Such things as decay radiation from the D^0 daughter hadrons, precise knowledge of the detector material, and noise conditions in the tracking chambers then make this difficult to push beyond 1%. This is therefore taken as the limiting systematic in this measurement.

Also possible at $B\bar{B}$ threshold is an extraction of this branching ratio using partial reconstruction of $B \rightarrow D^{*+} \ell \nu_\ell$. Here again, the decay $D^{*+} \rightarrow D^0 \pi_{slow}^+$ is tagged by observation of the π_{slow}^+ only; kinematics allow one to calculate a pseudo-B mass based on the correlation of this slow pion with the charged lepton emitted in the semileptonic B-decay.

Both of these techniques can be used, in principle, to determine the inclusive branching ratio of the D^0 into any arbitrary final state particle by observing the correlation of that final state particle with π_{slow}^+ . In this fashion, the semileptonic branching fraction $D^0 \rightarrow X^- e^+ \nu_e$ has been determined by CLEO to be $(6.97 \pm 0.18 \pm 0.30)\%$, representing a substantial improvement over the value tabulated in PDG92. With 30/fb, the statistical error on this measurement would shrink to less than 1%. Additional inclusive yields of interest are:

- $D^0 \rightarrow \phi + X$, to allow a determination of $D_s \rightarrow \phi + X$ in B-decay by subtraction of the ϕ component from B's. The $D^+ \rightarrow \phi + X$ branching ratio can be derived from the $D^0 \rightarrow \phi + X$ branching ratio by assuming equal partial widths, and using the difference

in lifetimes. This could similarly be applied to inclusive η and η' production, however, for the η mesons, the light quark components of the wave function make the extraction of the D^+ rate less reliable.

- $D^0 \rightarrow K^+ + X$ would give a measure of the fraction of times kaon-tagging for a B-factory experiment would give a false result.

Furthermore, correlations of soft π^+ with soft π^- could be used to extract the absolute $c\bar{c}$ cross-section by comparison with the inclusive (single-tag) value. Such double tags would also be interesting as a means of measuring charm-charm momentum correlations - since the soft pion momentum scales with the parent D^{*+} momentum, one can use double tags to investigate the momentum correlations of the parent D^* 's. Note that we can also get $\sigma_{c\bar{c}}$ from $\ell\bar{\ell}$ correlations using the continuum data.

8.2 $D^+ \rightarrow K^- \pi^+ \pi^+$

D^+ 's are produced in association with neutral pions in the decay: $D^{*+} \rightarrow D^+ \pi^0$. In principle, this would allow an analysis similar to that used to determine $\mathcal{B}(D^0 \rightarrow K^- \pi^+)$, but now using the correlation of soft π^0 's with the thrust axis. However, because D^0 's are also produced via $D^{*0} \rightarrow D^0 \pi^0$, when one observes a soft neutral pion correlated with the thrust axis, it is not known a priori whether the π^0 was produced in association with a charged or a neutral D^* . The soft pion trick is therefore impossible without knowing $\sigma_{D^{*+}}/\sigma_{D^{*0}}$.

We determine the $D^+ \rightarrow K^- \pi^+ \pi^+$ branching ratio by making use of the Isospin constraint that relates the ratio of D^{*+} branching ratios into neutral vs. charged D's: $R_{Isospin} = \frac{D^{*+} \rightarrow D^0 \pi^+}{D^{*+} \rightarrow D^+ \pi^0}$. By knowing the relative efficiency for slow vs. neutral charged pions, we can then determine the ratio of BR's: $\frac{D^+ \rightarrow K^- \pi^+ \pi^+}{D^+ \rightarrow K^- \pi^+} = 2.35 \pm 0.16 \pm 0.16$. Using the above tabulated value for $D^0 \rightarrow K^- \pi^+$ yields $\mathcal{B}(D^+ \rightarrow K^- \pi^+ \pi^+) = (9.3 \pm 0.16 \pm 0.16)\%$. The limiting systematic on this measurement is the ratio of the reconstruction efficiency for $\frac{\pi^0}{\pi^+}$, this can be narrowed substantially by taking data at the $\Upsilon(2S)$ resonance, and knowing that $\frac{\Upsilon(2S) \rightarrow \pi^0 \pi^0}{\Upsilon(2S) \rightarrow \pi^+ \pi^-}$ must be identically 1/2 (again, by Isospin). The limiting quoted error of 2% is the projected attainable uncertainty in this ratio of efficiencies.

8.3 $D_s^+ \rightarrow \phi \pi^+$

The most frequently invoked technique for determining the absolute branching ratio for $D_s \rightarrow \phi \pi$ involves:

1. measuring the efficiency-corrected cross-section: $\frac{\mathcal{B}(D_s \rightarrow \phi \pi^+)}{\mathcal{B}(D_s \rightarrow \phi \ell \nu_\ell)}$,
2. using the measured D_s lifetime to give the total D_s width,
3. invoking either:

- (a) equality of the $c \rightarrow s\ell\nu$ partial width for all charm decays and subtracting the rates for $D_s \rightarrow \eta\ell\nu + D_s \rightarrow \eta'\ell\nu$ to give the remainder (assumed to be $\phi\ell\nu$), or:
- (b) taking $\Gamma(D \rightarrow K^*\ell\nu) \sim \Gamma(D_s \rightarrow \phi\ell\nu)$ to obtain the branching ratio for $\phi\ell\nu$, which can then give $D_s \rightarrow \phi\pi$.

In principle, one could hope to tag the decay from the D_s^* via: $D_s^* \rightarrow D_s\gamma$; in practice this is difficult because the larger Q-value compared to the hadronic $D^* \rightarrow D\pi$ transition spoils the correlation of photon direction with the thrust axis.

Other approaches are possible if the D_s decay constant f_{D_s} is either well-measured or can reliably be taken from theory. In such a case, the $D_s \rightarrow \mu\nu$ branching ratio can be predicted with very good precision knowing the D_s lifetime. The decay $D_s \rightarrow l\bar{\nu}$ proceeds through annihilation of the $c\bar{s}$ quarks and therefore provides access to the wave function overlap of the $c\bar{s}$ quarks at zero spatial separation. This overlap is known as the meson decay constant, f_{D_s} . The decay rate for $D_s \rightarrow l\bar{\nu}$ is written as

$$\Gamma(D_s \rightarrow l^+\bar{\nu}) = \frac{1}{8\pi} G_F^2 f_{D_s}^2 m_l^2 M_{D_s} (1 - \frac{m_l^2}{M_{D_s}^2})^2 |V_{cs}|^2, \quad (2)$$

where M_{D_s} is the mass of the D_s and m_l is the mass of the lepton. The relative branching ratios for the $e\bar{\nu}$, $\mu\bar{\nu}$ and $\tau\bar{\nu}$ decay modes are $2 \times 10^{-5} : 1 : 10$. Although the $\tau\bar{\nu}$ mode has the largest relative branching ratio it is experimentally hard to detect. The $\mu\bar{\nu}$ channel is the most promising channel and there are several efforts to observe this decay both at fixed target experiments and e^+e^- experiments.

By taking the measured rate for $D_s \rightarrow \mu\nu$ relative to $B(D_s \rightarrow \phi\pi)$, one can derive the $\phi\pi$ branching ratio. Similarly, we can use double-charm decays of the B-meson, assuming factorization is valid for these decays. Factorization prescribes $\frac{\Gamma(B \rightarrow D_s D^*)}{\Gamma(B \rightarrow \ell\nu D^*)} \sim f_{D_s}$. Since the $B \rightarrow D^*\ell\nu$ rate dependence on q^2 is now rather well-studied, we can derive the value for the $\phi\pi$ branching ratio which is required by factorization. It should be mentioned, however, that the double charm decays are low Q-value; the validity of factorization valid in this limit is more questionable than in the high- q^2 limit. (There is an unpublished result from ARGUS on $B \rightarrow DD_s^*$, where the D_s^* is partially reconstructed, giving $D_s \rightarrow \phi\pi = 1.4 \pm 0.7\%$.) I have quoted an attainable error of 5% on this absolute branching ratio. This is a simple scaling of the present error up to 30/fb. With better theoretical guidance in the semileptonic sector and more precise lifetime measurements, this may be possible.

9 $\Lambda_c \rightarrow pK\pi$

As with $D_s \rightarrow \phi\pi$, we can extract this absolute branching ratio by relating a semileptonic to an hadronic width: $\frac{\Lambda_c \rightarrow pK\pi}{\Lambda_c \rightarrow \Lambda\ell\nu}$. Just as with $\phi\pi$, however, there is some model dependence in determining the fraction of the total semileptonic width which is taken up by the $\Lambda\ell\nu$ final state. Although the prejudice is that the Isospin-zero diquark remains inert in this transition and that $\Lambda\ell\nu$ should therefore saturate the semileptonic width, that has not yet

been measured precisely. $\Xi_c^0 \rightarrow \Xi^- \pi^+$ and $\Xi_c^- \rightarrow \Xi^- \pi^+ \pi^+$ also can be done analogously, using the rates into $\Xi \ell \nu$ and τ_{Ξ_c} . Here, however, there is some uncertainty owing to the different symmetry properties of the final state Ξ 's (containing two identical s-quark fermions, which must have an antisymmetrized wave function) compared to the Λ 's. For the $\Lambda_c \rightarrow \Lambda$ transition, we know that, in the $c \rightarrow s$ transition the (spin-0) ud diquark is mostly inert. In the $\Xi_c \rightarrow \Xi$ transition, the us diquark should be inert, except that the identical ss fermions in the final state will try to minimize their wave function overlap. This may make more likely the possibility of having orbitally excited Ξ 's in the final state.

Assuming that $\Xi_c \rightarrow \Xi \ell \nu_\ell$ saturates the Ξ_c semileptonic width, CLEO has recently performed this analysis and obtained branching ratios for $\Xi_c^+ \rightarrow \Xi^- \pi^+ \pi^+$ of $(1.9 \pm 0.5_{-0.6}^{+0.7})\%$ and $\Xi_c^0 \rightarrow \Xi^- \pi^+ = (0.47 \pm 0.14_{-0.13}^{+0.14})\%$. Projecting to 30/fb yields a 8% statistical error on these branching ratios.

If π /electron separation is good enough, can use tags a la $D^{*+} \rightarrow D^0 \pi^+$ and measure $\frac{\Lambda_c(2630) \rightarrow \Lambda_c \pi^+ \pi^-; \Lambda_c \rightarrow p K \pi}{\Lambda_c(2630) \rightarrow \Lambda_c \pi^+ \pi^-, \text{ all}}$. Here, the signature is a low mass dipion pair with a momentum vector lying along the event thrust axis. However, there may be a large background from $D^* \rightarrow D \gamma / \pi^0$ with photon conversion - this will fake the topology of a low-mass pair with a strong thrust axis correlation.

We can also use $B \rightarrow \text{baryons}$; however, this often requires some knowledge of the degree to which different possible mechanisms of baryon production in B-decay are actually contributing to the total $B \rightarrow \text{baryons}$ rate. As an example, consider the process $B \rightarrow \Lambda + X$. Λ 's are expected to be produced in B-decay predominantly from one of two processes: either $B \rightarrow \Xi_c \Lambda$ or $B \rightarrow \Xi_c \Lambda_c$, $\Lambda_c \rightarrow \Lambda + X$. Thus, a Λ is produced always in association with a Ξ_c . Measuring the rate for $\frac{B \rightarrow \Xi_c \Lambda; \Xi_c \rightarrow \Xi \pi}{B \rightarrow \Lambda + X}$ then gives the absolute branching ratio for $\Xi_c \rightarrow \Xi \pi$.

With enough statistics, other techniques for determining absolute branching ratios become possible. Consider D^0 's decaying to a particular final state X . Writing the fraction of times that a continuum c-quark fragments to a D^0 as f_D , the number of single tags N_X can be written as:

$$N_X = 2\sigma_{c\bar{c}} f_D \epsilon_X \mathcal{B}_X,$$

and the number of double tags $N_{X\bar{X}}$ as:

$$N_{X\bar{X}} = \sigma_{c\bar{c}} f_D^2 \epsilon_X^2 \mathcal{B}_X^2,$$

assuming no correlations between the fragmenting charm and anticharm quarks (this is almost certainly incorrect on some level, and needs further study). Given a number of single and double tags using the most common modes $D^0 \rightarrow K^- \pi^+$, $D^0 \rightarrow K^0 \pi^- \pi^+$, $D^0 \rightarrow K^- \pi^+ \pi^+ \pi^0$ and $D^0 \rightarrow K^- \pi^+ \pi^0$, one has enough information to solve for the \mathcal{B} 's as well as the $c\bar{c}$ cross-section. This is similar to what was done at threshold by MARKIII to determine absolute branching fractions.

Finally, we note that, as the individual branching ratios for $D^0 \rightarrow K^- \pi^+$ and $D^+ \rightarrow K^- \pi^+ \pi^+$ improve in precision, the unitarity constraint that $c \rightarrow (D^0 + D^+ + \Lambda_c + D_s + \Xi_c) \sim 1$ becomes an increasingly important tool in determining other charm absolute BR's, assuming the $c\bar{c}$ cross-section is known.

The expected performance of a B-factory era machine in the area of absolute branching ratios is summarized in Table 1.

10 Summary of physics Issues in the B-factory era

This topic is covered by others in these proceedings; I list in Table 4 only a couple out of my own Top Ten Reasons to Study Charm at a B-Factory. In the Table, the statistical error σ_{stat} is extrapolated from the present CLEO event statistics to the canonical B-factory sample of 30/pb. Systematic limitations of these measurements are discussed below. Possible improvements due to “new” techniques are not considered here.

11 Comment on systematic errors with 30/fb

A scan of the publications released by the CLEO-II experiment within the last four years shows a trend from statistics-limited results to precision, systematics-limited results. The study of systematics will be an increasingly time-intensive effort with a 30/fb data sample, particularly in tuning of one’s detector simulation Monte Carlo to reproduce data. As discussed in other CLEO documents [28], there are many techniques for determining absolute particle reconstruction efficiencies. The most straightforward, perhaps, is to compare a ratio of branching ratios obtained, after efficiency-correction, with the Particle Data Group value: $\frac{\eta \rightarrow \pi^+ \pi^- \pi^0}{\eta \rightarrow \gamma \gamma}$, e.g., gives a measure of $\epsilon_{\pi^\pm}^2$. Other techniques have been developed to deal with the following sources of systematic error at CLEO, which are precisely those which will have to be reckoned with in a high-luminosity B-factory experiment:

- Absolute tracking efficiency - There are currently two tracking efficiency errors which are quoted for CLEO measurements:
 - The reconstruction efficiency for simply finding a track, even if it is poorly measured. This would be relevant in determining a topological branching fraction ($\sim 0.6\%$ per track) This quantity is measured from the data and Monte Carlo using:
 - * the number of times a minimum ionizing shower in the calorimeter has a track matched to it,
 - * $\tau\tau$ events into observed lepton vs. 2 prong compared with lepton vs. 3 prong events,
 - * $\gamma\gamma \rightarrow$ two-prong events using the number of times one charged track vs. two charged tracks are observed,
 - * Studies of hadronic events with net charge of magnitude 2, 1, and 0; and assuming that the migration from the generated events (always net charge 0) to observed events with some non-zero net charge occurs through a random process of track-finding failure.

- The track reconstruction efficiency including track-fitting effects ($\sim 2\%$ per track), measured as follows:
 - * The most reliable estimate of this comes from using the “satellite” peak produced in the decay chain: $D^{*+} \rightarrow D^0 \pi^+$; $D^0 \rightarrow K^- \rho^+$; $\rho^+ \rightarrow \pi_\rho^0 \pi_\rho^+$, and using the signal observed in the $\Delta M - M(K^- \pi^0)$ scatter plot without reconstruction of the π_ρ^+ . Comparing this signal size with the signal observed for the case where the $D^{*+} \rightarrow D^0 \pi^+$; $D^0 \rightarrow K^- \rho^+$ is fully reconstructed allows an estimate of the absolute track-finding efficiency with track-fitting effects.
 - * $\pi^0 \rightarrow e^+ e^- \gamma$ can be useful when the calorimetry is as good as it is with CLEO. In principle, one can use the shower left by either the electron or the positron in the calorimeter, and, knowing the direction and magnitude of the magnetic field, determine the track parameters of a track at the origin (assuming that the calorimeter has measured the electron or positron energy well). Thus, the $\pi^0 \rightarrow e^+ e^- \gamma$ signal can be reconstructed without having to observe one of the daughter charged particle tracks. By observing how often there is, in fact, a real track matched to the shower, the absolute tracking efficiency can be inferred.
 - * Embedding Monte Carlo tracks into real events is another technique for determining losses due to event environment, as well as large scatterings through the material of the detector.
- The efficiency for reconstruction of π^0 's is measured:
 - Similar to the satellite-peak technique used to determine ϵ_{π^+} , but here determining the satellite peak signal size with and without full reconstruction of π_ρ^0 .
 - As a function of angle, by observing the $B \rightarrow \pi^0$ signal angular distribution. Since the B has such little momentum, this signal should be isotropic for real decays. This allows one to bootstrap an efficiency function from a “well-measured” regime (the barrel, in the case of CLEO-II) into a less well-measured regime (the endcaps, e.g.)

It is relevant in this context to mention that detector design is often geared towards “optimal” peak performance. However, in a systematics limited era, it may be that detectors should be designed with an eye towards minimizing systematic errors. In this light, it may be that the best magnetic field for a B-factory experiment is not necessarily that which optimizes momentum resolution (1.5 T), but that which has sacrificed slightly in tracking performance for the sake of reliability of Monte Carlo simulation (1-1.2 T, e.g.) due to greater ease in determining the drift-time relation and corresponding simplifications in pattern recognition.

12 Comparison of tau-charm vs. B-factory vs. fixed target

In this section, I briefly compare the charm physics capabilities of a tau-charm factory ($\tau c F$) vs. a B-factory vs. a fixed target program, using my own entirely subjective scheme.

The primary advantage of a B-factory lies perhaps in the diverse physics program it offers - unlike τcF , where the beam-energy is generally tuned to select a particular charm particle for study, all charmed particles are produced in e^+e^- collisions at $\sqrt{s}=10$ GeV. The situation at a fixed target program depends on the selection of target plus beam; experience shows that photoproduction experiments tend to produce the same broad assortment of charm as in e^+e^- collisions; hadroproduction generally produces a less democratic assortment of charmed particles for study. Among the advantages of τcF is that the particles are generally in a momentum range well-matched to present particle identification techniques; additionally, the beam energy constraint is extremely powerful in narrowing signal widths. As a rule of thumb, assuming the physics process is accessible to a τcF , it takes about a factor of 4-5 less luminosity to make the same measurements at τcF than at 10 GeV. Table 5 gives a comparison of the different facilities.

The three programs very nicely complement one another. The compelling argument in favor of supporting active charm physics programs at all three lies in the possibility of having redundant measurements of the same physics quantities with much different systematics. Thus, in addition to the well-established fixed target program and the proposed τcF program, there is every expectation that the charm physics program at future e^+e^- colliders above threshold (CESR, KEK, and SLAC) will continue to make strong, and necessary contributions to charm physics in the future.

13 Acknowledgments

Arne Freyberger supplied the section on semileptonic decays with some editing by myself. I would like to thank the organizers of this workshop for inviting me, as well as the person in the cafeteria who let me get an ice cream cone even though I was 10 cents short.

References

- [1] Hillary Crystal, private communication.
- [2] Arne Freyberger, presented at this conference.
- [3] M. Richard, presented at this conference and in these proceedings.
- [4] Jimmy the Greek, private communication.
- [5] I. Dunietz et al., CALT-68-1935 (1994), and I. Dunietz, presented at this conference and in these proceedings.
- [6] J. Butler, presented at this conference and in these proceedings.
- [7] S. White, presented at this conference and in these proceedings.
- [8] K. Hikasa *et al*, Review of Particle Properties Phys. Rev. D Vol 45, 1992 and references within.
- [9] A. Bean *et al*, (CLEO) to be published in Phys. Lett. B (preprint CLEO 93-18 (1993))
- [10] H. Albrecht *et al*, (ARGUS) contributed paper to the 1993 International Lepton-Photon Symposium on High Energy Physics.

- [11] H. Albrecht *et al*, (ARGUS), Phys. Lett. B255, 634 (1991).
- [12] G. Crawford *et al*, (CLEO), Phys. Rev. D44, 3394 (1991).
- [13] J.C. Anjos *et al*, (E691), Phys. Rev. Lett. 62, 722 (1989); 65, 2630 (1990).
- [14] P.L. Frabetti *et al*, (E687), Phys. Lett. B307, 262 (1993); also R. Gardner in these proceedings.
- [15] M. Adamovich *et al*, (WA82), Phys. Lett. B286, 142 (1991).
- [16] K. Kodama *et al*, (E653), Phys. Rev. Lett. 66, 1819 (1991); Phys. Lett. B286, 187 (1992).
- [17] Z. Bai *et al*, (MARK III), Phys. Rev. Lett. 66, 1011 (1991); Phys. Rev. Lett. 62 1821 (1989).
- [18] N. Isgur *et al* , Phys. Rev. D39 799 (1989).
- [19] J.G. Korner and G.A. Schuler, Z. Phys. C38, 511 (1988).
- [20] M. Wirbel *et al*, Z. Phys. C29 627 (1985).
- [21] T. Altomari and L. Wolfenstein, Phys. Rev. C37, 681 (1988).
- [22] F.J. Gilman and R.L. Singleton, Phys. Rev. D41, 142 (1990).
- [23] C.W. Bernard, A.X. El-Khadra and A. Soni, Phys. Rev. D47, 998 (1993).
- [24] V. Lubicz *et al*, Phys. Lett. B274, 415 (1992).
- [25] P. Ball, V.M. Braun and H.G. Dosch, Phys. Rev. D44, 3567 (1991).
- [26] D.S. Akerib *et al*, (CLEO) to be published in Phys. Rev. Lett. (preprint CLEO 93-16 (1993))
- [27] Art Snyder, private communication
- [28] CLEO internal note CBX 93-001, and CBX 93-96, "Measurements of Neutral and Charged Particle Tracking Efficiency in Data vs. Monte Carlo", Dave Besson, and hopefully soon-to-be-in-NIM

Process	Interest	Evt./ σ_{stat}	Systematics/ σ_{sys}
$c \rightarrow u\ell\nu_\ell$	V_{cd}, V_{ub}	10K	
$D \rightarrow \pi^0\ell\nu_\ell$	$\frac{f(u\bar{u}+d\bar{d})}{f(s\bar{s})}(\eta, \eta' f^0(975))$		
$D \rightarrow \pi^+\ell\nu_\ell$	$\frac{f_+^\pi(q^2=0)}{f_+^K(q^2=0)}$	1.5K/5%	PID(p_{lepton})
$D \rightarrow \eta^0\ell\nu_\ell$		3K/2%	PID(K/ π)
$D \rightarrow K\ell\nu_\ell$	form factors	$f(u\bar{u}+d\bar{d})/f(s\bar{s})$ 0.9K/5%	PID(p_{lepton})
$\Lambda_c \rightarrow \Lambda\ell\nu$	form factors	30K/<1%	PID(p_{lepton}) $\epsilon_{tracking} + \epsilon_{e/\mu} < 2\%$
$D_s \rightarrow \mu\nu$ (D_s^* tag)	f_{D_s}	20K/8% on f_2/f_1	$\epsilon_{tracking}$
$D \rightarrow \mu\nu$ (D^{*+} tag)	f_D	2K/5% (\mathcal{B}) 3% on f_{D_s} 500/10% (\mathcal{B})	$\epsilon_{leptons}/5\%$
$\frac{D \rightarrow K^*K}{D \rightarrow K^*\bar{K}}$	$C\bar{P}$	Unlikely	
$D \rightarrow \rho\gamma$	Penguins	< 10^{-3} evts.*	
$D \rightarrow \pi\mu^+\mu^-$	Penguins/FCNC	Unlikely	
$\frac{D^0 \rightarrow K^+\pi^-}{D^0 \rightarrow K^-\pi^+}$	DCSD	1K/3%	PID
Γ_{D^*}	$\hat{H}_{\bar{c}u}$ J=1, L=0	100 KeV	$\sigma_{MC}^{\Delta M}/500$ KeV
$\Gamma_{D^{**}}$	$\hat{H}_{\bar{c}u}$ J=1, L=1	1.4 MeV	Fitting/ $\sim \sigma_{stat}$
Spectroscopy	Potential Models	15K $D^{**} \rightarrow D^*\pi$ 3K $D_{sJ} \rightarrow D^*K$ 3K $\Lambda_c^{**} \rightarrow \Lambda_c\pi\pi$	
$c\bar{c}$ (dble tag)	correl.	6K**	
$D^0 \rightarrow K^-\pi^+$	$\mathcal{B}_{absolute}$	$\pm 1\%$	$\epsilon_{tracking}$
$D^+ \rightarrow K^-\pi^+\pi^+$	$\mathcal{B}_{absolute}$	$\pm 2\%$	$\epsilon(\frac{\pi^+}{\pi^0})$
$D_s^+ \rightarrow \phi\pi^+$	$\mathcal{B}_{absolute}$	$\pm 5\%$	$\epsilon_{tracking}$ Extraction model
$\Lambda_c \rightarrow pK\pi$	$\mathcal{B}_{absolute}$	$\pm 5\%$	Extraction model
$\Xi_c \rightarrow \Xi\pi$	$\mathcal{B}_{absolute}$	$\pm 8\%$	
$\Lambda_c \rightarrow \Lambda + X$	$W_{external}$ fraction		
$\Xi_c \rightarrow \Lambda + X$	$W_{external}$ fraction		
$\Lambda_c \rightarrow \Lambda\pi^+$	Weak asymmetries in Λ_c decays	7500	

Table 4: Physics goals of a high-luminosity B-factory experiment. Event projections represent present yields observed with CLEO-II scaled to 30/fb of luminosity, and taking into account improvements in event vertexing and particle identification (PID).

* Derived by using the CLEO result for $\Gamma(B \rightarrow K^*\gamma)$, and scaling using $\frac{m_b}{m_c})^2 \cdot (V_{cb}/V_{tb})^2$

**This is the estimated number of $((D^0 \rightarrow K^-\pi^+)(\bar{D}^0 \rightarrow K^+\pi^-))$ double tags

Physics	τcF	B-factory	Fixed target
Absolute BR's	\$\$	\$\$	\$
Fragmentation		\$\$	\$\$
$c\bar{c}$ correlations		\$\$	\$\$
Spectroscopy	\$	\$\$	\$\$
Charm semileptonics	\$\$	\$	\$
Rare modes ($D^0 \rightarrow K^+\pi^-$, eg)	\$\$	\$	\$
Lifetimes		\$	\$\$
Decay Constants	\$\$	\$	\$
Mixing + DCSD	\$	\$	\$\$

Table 5: Comparison of charm physics at three different facilities. “\$” indicates measurement is possible, “\$\$” indicates measurement is best-suited to the experiment indicated.

BES Program and Tau/Charm Factory Physics*

Walter Toki[†]

Dept of Physics, Colorado State University, Ft. Collins, CO 80523

abstract

The BES physics program is reviewed and the advantages of physics at proposed tau charm factories (Beijing, Argonne, and Dubna) are discussed. Special emphasis is given towards topics that are in competition with the charm physics programs of future fixed target experiments such as the proposed Charm 2000 and b factories. The BES group has taken e^+e^- data in the region of tau threshold ($\sqrt{s} \sim 3.55$ GeV) and recently completed a run at Ds pair threshold ($\sqrt{s} \sim 4.03$ GeV). Future BES results and the detector upgrades are discussed. Final results to be presented at the 1994 summer conferences are not given here. The experimental advantages and the physics program of a tau charm factory are summarized.

*invited talk at the Charm 2000 Workshop, FNAL, Batavia, Ill., June 7-9, 1994

[†]email: toki@lamar.colostate.edu

This work is support in part by the U.S. Department of Energy, contract number DE-FG03-94ER40788.

1.0 Current BES program

The Beijing Spectrometer Collaboration (BES) has taken data at the J/ψ resonance ($\sqrt{s} \sim 3.1$ GeV), at the ψ' resonance ($\sqrt{s} \sim 3.68$ GeV), above tau threshold ($\sqrt{s} \sim 3.552$ GeV) and most recently above Ds pair threshold ($\sqrt{s} \sim 4.03$ GeV).

During the Ds run, which ended May 1994, the total amount of integrated luminosity for useable data was 22.4 inverse picobarns. The recent performance of the machine during the January - May 1994 period was roughly ~ 10 inverse picobarns in ~ 15 weeks of running. The peak luminosity was $\sim 6 \times 10^{30} \text{ cm}^{-2} \text{ sec}^{-1}$ at 4.03 GeV. This is to be compared to the running of Mark III at SPEAR which had a peak of $\sim 1.5 \times 10^{30} \text{ cm}^{-2} \text{ sec}^{-1}$ at 4.13 GeV. During the run the integrated luminosity per day (24 hours) was as high as 200 inverse nanobarns, but the average over all was ~ 100 inverse nanobarns (including down time). In comparison, SPEAR averaged ~ 65 inverse nanobarns per day.

The BES data was analyzed both at the Institute of High Energy Physics (IHEP) in Beijing and in the U.S. mainly at the UNIX processor farm at PDSF at SSCLAB and in part at SLAC, University of Texas at Dallas and Colorado State University. The new data was transported via 8 mm tapes and reconstructed on VAX's (IHEP) and HP workstations (PDSF, CSU, UTDallas).

1.1 BES Physics Program

The BES group began with a precision tau mass measurement in 1992. The published result¹ achieved a small error of $\sim \pm 4$ MeV statistical and ± 2 MeV systematic using only the electron-muon decays from tau pairs. A new measurement prepared for the Glasgow meeting added additional modes and reduced the statistical error by a factor two.

In the ψ' run, a total of ~ 1.5 M decays have been logged to tape. In this data sample a new precision measurement of the J/ψ leptonic decay, $B(J/\psi \rightarrow e^+e^-)$, has been performed, using the decay $\psi' \rightarrow J/\psi \pi^+\pi^-$, $J/\psi \rightarrow e^+e^-$ and a new limit for the decay $\psi' \rightarrow \rho\pi$ has been made.

In the 4.03 GeV run, completed May 1994, a total of 22.4 inverse picobarns has been logged to tape. This is to be compared to the Mark III which had 6.3 inverse picobarns at 4.13 GeV. In this data the charm signals of $e^+e^- \rightarrow D_s^+D_s^-$, $D^{*0}D^0$, $D^{*0}D^{*0}$, $D^{*+}D^\pm$ and $D^{*+}D^{*\pm}$ are observed. The results to be presented in the summer conferences

¹J. Bai et al., Phys. Rev. Lett, 69,3021(1992)

Figure 1

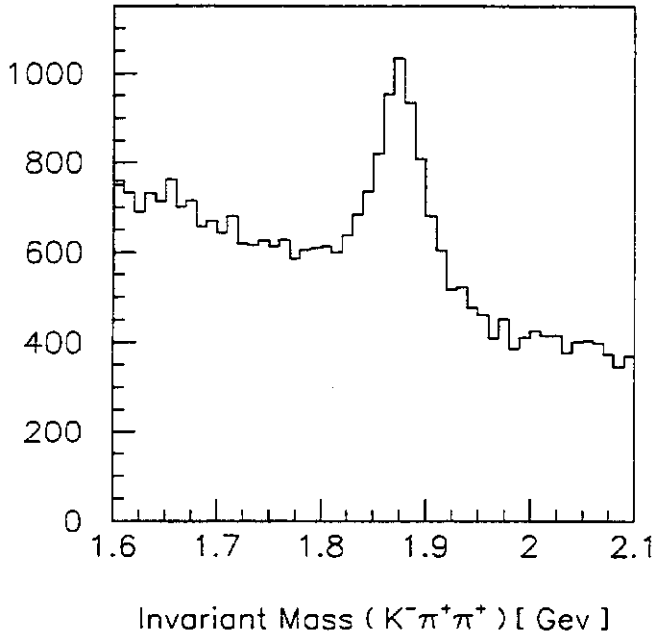
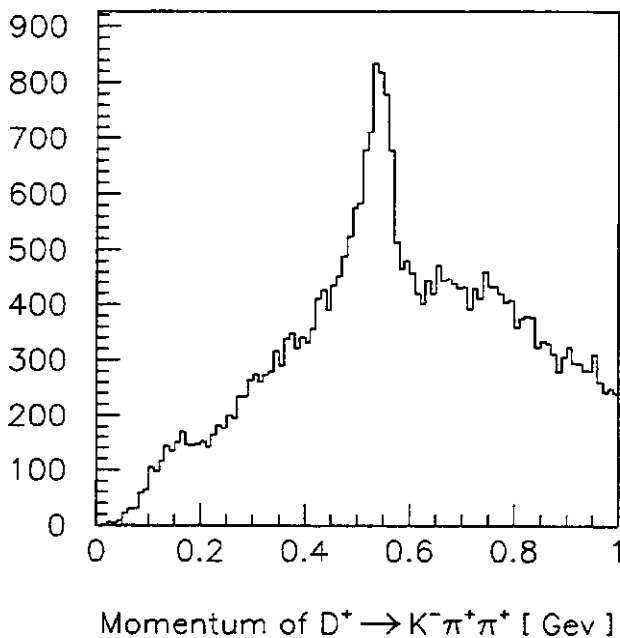


Figure 2



(Glasgow² and New Mexico³) are an absolute branching ratio measurement using double tag pairs of Ds events, evidence for leptonic decay, $D_s \rightarrow \mu \nu$ and $\tau \nu$, and a measurement of the branching ratios $D^{*\pm} \rightarrow D^0 + X$ and $D^\pm + X$. The $D^{*\pm}$ branching ratios can be obtained from a comparison of D^0 and D^\pm produced from $D^* D$.

In figures 1 and 2 is a signal of the mass and momentum of $D^\pm \rightarrow K^\mp \pi^\pm \pi^\pm$ and in figures 3 and 4 a signal of the mass and momentum of $D^0 \rightarrow K^\mp \pi^\pm$. The momentum peaks at ~ 150 MeV and ~ 550 MeV are from $ee \rightarrow D^* D^*$ and $D^* D$. The $D^* D$ peaks are composed of the direct D decays and the doppler shifted D decays from $D^* \rightarrow \gamma D$ and πD .

The current run plan for the fall 94 is to run several months at the ψ' to obtain 3-4 million events and then stop for a shutdown from early Spring 95 to late fall 95 for the upgrade installation. After the upgrade, the future running although not yet decided may possibly include ψ'' running for D meson studies.

1.2 BES Upgrade

The BES collaboration has begun an upgrade of the machine and the detector.

²see talks by Jin Li, Changchun Zhang and Joe Izen

³see talks by Mike Kelsey, Eric Soderstrom, Bruce Lowery and Oliver Bardon

Figure 3

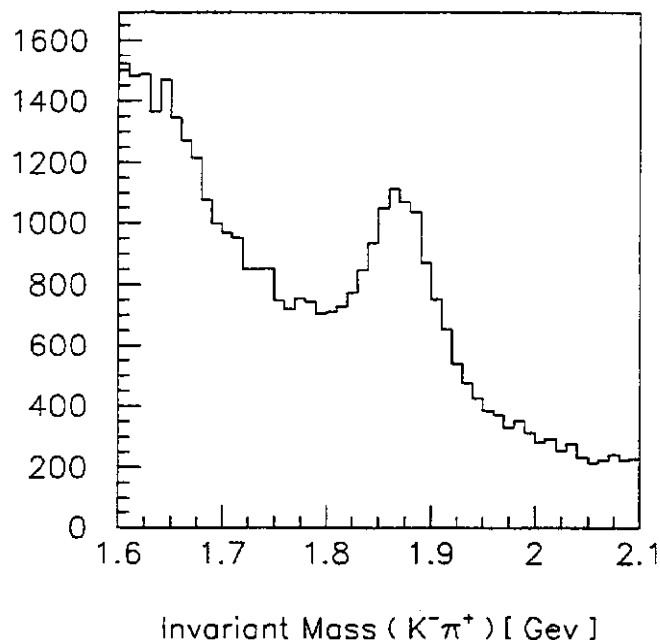
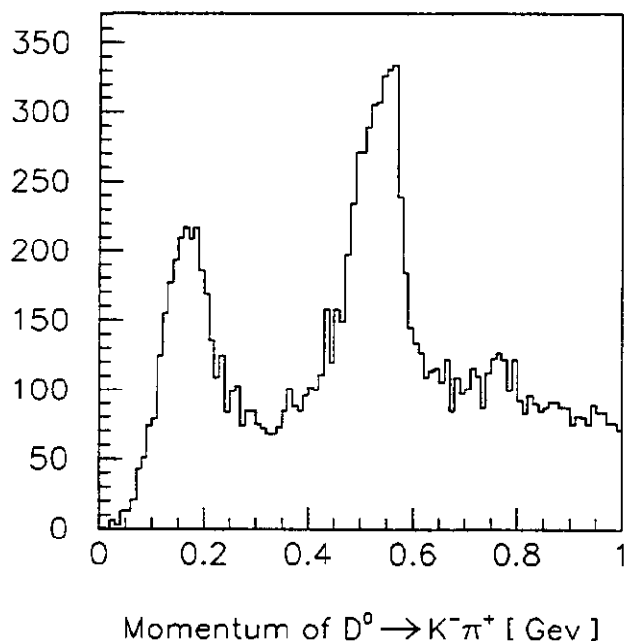


Figure 4



The upgrade is a joint IHEP and DOE supported effort. The machine will have a luminosity increase of a factor 3-4 to $2.8 \times 10^{31} \text{ cm}^{-2} \text{ sec}^{-1}$ at 4 GeV by the use of minibeta and single interaction running. The BES detector will be upgraded with the Mark III straw vertex chamber, a new main drift chamber, a new TOF scintillator counter with Hamamatsu FM PMT's and a new DAQ system.

Boston University is making the main drift chamber endplates and outer support cylinder. Caltech is building new luminosity monitors. Colorado State is refurbishing the Mark III straw chamber and fabricating the main drift chamber feed throughs. IHEP will string the main drift chamber, build the TOF system and build the new DAQ system. University of Hawaii will make the vertex chamber electronics and University of Washington will develop the trigger. The upgrade has started and should be completed by the end of 1995. In table 1 are listed the upgrade equipment.

2.0 Tau Charm Factories

The tau charm factories have been proposed to operate with a luminosity of a few times 10^{33} in the 3-6 GeV center of mass region. Below in table 2 are yields of events possible with such a machine in a year of running. For comparison we list the BES and Mark III data sets in table 3.

Table 1. BES Upgrade Detector Systems		
Item	Remarks	Group
Vertex Drift Chamber	Mark III straw Chamber	Colorado State; replacing endplates U/Hawaii; electronics U/Washington: trigger
Lum. Mon.	New monitor with FM tubes	Caltech
Main Drift Chamber	New Chamber	Endplates/support cylinder by Boston, Stringing by IHEP
TOF system	New scintillators with Hamamatsu FM PMT's	IHEP
DAQ	New VME system	IHEP

Table 2. <i>tcf</i> Physics in 1 year at 10^{33} (10^7 seconds or 10 inv. femtobarn)			
Resonance	Ecm GeV	Rate/sec	Ev./year 10^7 sec
J/ψ	3.1	1000	10 billion
ψ'	3.69	600	6 billion
$\tau^+\tau^-$	3.57	.4	4×10^6
$\tau^+\tau^-$	4.25	4	4×10^7
$D^+D^-, D^0\bar{D}^0$	3.77	5	5×10^7
DsDs	4.03	~ 0.3	3×10^6
$D^*D, D^*\bar{D}^*$		~ 5	5×10^7

Table 3. Selected recent tau/charm data sets		
Data	Mark III	BES
J/ψ	5.6 m	9 m
ψ'	.3 m	1.5 m
$\psi'' (D^+D^-, D^0\bar{D}^0)$	9 inv. pb.	0
DsDs, $D^*D, D^*\bar{D}^*$	6.3 inv. pb. (4.14)	22.4 inv. pb (4.03)

Recently a tau charm factory was proposed at SLAC⁴ and in Spain⁵. Although the physics case was compelling, tight funding in Europe caused a rejection of the Spanish machine. There has been discussions at Dubna of a tau/charm factory⁶ and very recently at Argonne⁷ and at Beijing. At IHEP, there has been discussion and agreement among the accelerator and experimental physicists that the tau charm factory is a natural next step for their physics program.

2.1 Experimental Advantages of tau charm experiments

Here we list tau charm unique capabilities, especially those experimental advantages that could be very useful when compared to B factories and fixed target experiments.

(1) Particles of interest are produced in pairs; $\tau^+ \tau^-$, $D^0 \bar{D}^0$, $D^+ D^-$, $D_s^+ D_s^-$, $D^* D$, $D^* D^*$, $\Lambda \bar{\Lambda}$. This has important advantages that if you reconstruct one flavor of the particle-antiparticle pair, you know the other recoil is of opposite flavor. This is important for normalization, flavor tagging and the search for decays that require no backgrounds (or at least backgrounds that can be precisely simulated).

(2) Kinematic Constraints. Since the center of mass energy and the absolute momentum are known exactly, these can add 4 constraints or 4-C fits to improve momentum and mass resolution.

(3) Known production distributions; Many high rate decays have known matrix elements such as $ee \rightarrow D^+ D^-$ is $\sin^2 \theta$, $ee \rightarrow ee, \mu\mu$ is QED, $J/\psi \rightarrow \rho\pi$. This enables precise comparisons between data and monte carlo simulations to test detector response.

(4) Charged and neutral tracks have low energy and low multiplicity. Lower energy allows better resolution and a better particle ID and low multiplicity reduces combinatoric backgrounds.

(5) Very High statistics calibration modes are available using the $J/\psi \rightarrow e^+ e^-$, $\mu^+ \mu^-$, $\gamma e^+ e^-$, $\gamma \mu^+ \mu^-$, $\rho\pi$, $K^* K$, $K_S K_L$. This allows better calibration of the detector response on hadron and lepton tracks. Precision checks on tracking, on angular acceptance and on the Branching ratio

⁴M. Perl, editor, SLAC Report 343, June 1989

⁵Proceedings of the Maribella Workshop, June 1993, in preparation.

⁶Proceedings of JINR workshop, May 1991.

⁷See J. Repond talk in this workshop and Argonne Report

measurements with cross checks are possible using these high statistics modes. These checks will be much needed if tests of differences in angular distributions are to be made.

A detector optimized for tau charm physics is very similar to those generic designs proposed for B factories⁸. These include (1) a low mass drift chamber to obtain high resolution for charge track momentum with little multiple scattering, (2) inner charge track detector to detect soft pions from the D* decays, (3) a crystal shower detector for low energy photons and electron detection, (4) particle ID using a combination of TOF and dEdX (possibly a DIRC detector⁹ could be far superior) and a very fast DAQ that can handle pipelining with a J/ψ rate ~1000 Hz signal. It would seem unlikely that a silicon vertex detector would have much value in a tau charm detector.

2.2 Tau Charm Physics

In this section charm physics topics are listed. For general reviews see the proceedings of the 1989 SLAC workshop¹⁰ and the 1993 Maribella workshop (to be published). Other charm reviews include those by Pich¹¹, Yaouanc et al.¹², and Bigi.¹³ Other tau charm topics¹⁴ in tau, physics, charmonium and J/ψ physics are not covered here.

Direct absolute BR The tau charm factory could measure the absolute branching ratios of the charm meson with essentially no model dependence. The technique is to use fully reconstructed events in $e^+e^- \rightarrow D^0 \bar{D}^0, D^+ D^-, D_s^+ D_s^-$ which are proportional to the product of 2 branching ratios and to compare this rate to inclusive charm meson rates which are proportional to a single branching ratio. It has been estimated that the error will be about 1% and systematics limited. This could be very important to begin closure on all decays using ~5-10M D tags to find out how much is really missing.

Leptonic Decays The tau charm factory can measure D^+ and $D_s \rightarrow \text{Lepton} + \nu$ to 1% precision. This measurement again should be relatively free of background and theoretical dependence. It could be interesting to compare $\mu\nu$ modes to $\tau\nu$. The leptonic decays of charm mesons could

⁸See the Babar Letter of Intent, SLAC-443, June 1994 and The CLEO III Detector, Design and Physics Goals

⁹B. Rarcliff, SLAC-PUB-6047, Jan. 1993.

¹⁰M. Perl, editor, SLAC Report 343, June 1989

¹¹A. Pich, CERN-TH-7066, November 1993

¹²A. Le Yaouanc et al., LPTHE-ORSAY-9249, September 1992.

¹³I. Bigi, SLAC-PUB-4349, June 1987.

¹⁴M. Perl, editor, SLAC Report 343, June 1989

also be used to extrapolate the values for B mesons (f_B) which could affect B mixing¹⁵ as this pseudoscalar constant is a factor in the calculation of mixing.

$D^0\bar{D}^0$ Mixing A tau charm factory may be the only place where mixing could be observed. CLEO has observed a large double Cabibbo suppressed decay rate which would contaminate measurements that try to detect mixing using hadronic decays. This could make the technique of using $D^* \rightarrow \pi D^0$, $D^0 \rightarrow K\pi$ very difficult. Several methods using hadronic decays could include using D^*D , D^*D^* modes which by quantum mechanics arguments can separate mixing events from double cabbibo suppressed decays. A mixing measurement of $r(D) \sim 10^{-4} - 10^{-5}$ is possible.

CP possibilities CP violation in charm is expected to be small, however direct CP could be observable in certain models. We list direct and indirect CP possibilities and Hyperon decays (strange decays) as areas of interest.

(1) Direct CP violation: For direct CP violation the search¹⁶ would look for partial decay rates where a particular $\Gamma(CP) \neq \bar{\Gamma}(CP \text{ conjugate})$. Such modes include $\Gamma(D^+ \rightarrow \bar{K}^* K^+) \neq \bar{\Gamma}$ which has been searched for by the E687 group. A value for the asymmetry of $A = 10^{-3}$ might be experimentally attainable and it almost reaches a useful theoretical level.^{17,18}

(2) Indirect CP violation with mixing: In this method one searches for $e^+e^- \rightarrow D^*D \rightarrow \gamma D \bar{D} \rightarrow \gamma(Kl\nu)$ (CP eigenstate). As in the B factory studies (B^*B) if one searches for CP eigenstates of $D \rightarrow KK$ or $\pi\pi$, the time integrated CP violating decays could be observed. Although the rate is expected to be very small, the results could be as surprising as was found in the different partial rates of $D \rightarrow KK$ and $\pi\pi$.

(3) Hyperon angular distributions: $J/\psi \rightarrow \Xi^+ \Xi^- \rightarrow \Lambda \pi \bar{\Lambda} \pi$, using a mono-chronometer (+polarized e) for getting very high J/ψ rates, a large sample of $5 \times 10^7 \Xi^+ \Xi^-$ decays/yr are possible and it could lead to asymmetry in the decays that are a factor 1-10 away from theory¹⁹. Recent calculations²⁰ by Lu, Wise and Savage indicate that CP violation may be small in this mode due to small strong phase shifts.

¹⁵J. Rosner, talk in this workshop.

¹⁶J. Fry and T. Ruf, CERN-PPE-94-20, Feb. 1994

¹⁷B. Grinstein and R. Golden, Phys. Lett., B222,501(1989)

¹⁸F. Buccella et al, Phys. Lett., B302,319, 1993.

¹⁹E. Gonzalez and J. Illana, CERN-PPE/94-33, February 1993.

²⁰M. Lu, M. Wise, and M. Savage, preprint CALT-68-1940

2.3 Concluding Remarks

For tau charm factories we need to understand first the significance of the attempted physics measurements, second the capabilities of the tau charm experiments to carry out the measurements and third what the competition from b factories and fixed target could achieve.

The physics significance needs to be answered by the theorists. Tests of the standard model are the conventional bench marks. Under these guidelines, the D mixing and the search for CP violation seem to be the most interesting measurements. It appears that D mixing is possible at the 10^{-4} - 10^{-5} rate which is at the edge of the Standard Model predictions. A tau charm factory has a unique niche where it could attempt searches free of double cabbibo suppressed contaminations when looking for hadronic decay modes. These backgrounds will limit B factories searches that use the $D^* \rightarrow \pi D$ modes, $D \rightarrow \text{hadrons}$. Fixed target experiments can measure the time evolution of this decay and might be able to reduce this background²¹. In the search for CP violation in charm decays, the predictions are very small for indirect CP violation. However, a tau charm factory could perform unique time integrated measurement using γDD from D^*D and measuring CP eigenstates. Another area (which may be hit or miss) is the search for direct CP violation in D decays. It is unclear if tau charm could compete with fixed target experiments which can measure relative branching ratios with very high statistics, although they must correct for the differences in D and \bar{D} rates in hadroproduction.

If there are attempts to measure CP violation (charm, strange or tau decays) by looking at differences in angular distributions, the ability of a tau charm factory to measure detector responses using known decays from QED and the J/ψ will be invaluable. Not only do detector efficiencies become important, but also the differences of the hadronic interactions in the detector material between the + and - charged incident track. This could be measured with the very high statistics J/ψ decays which provide all +/- particle flavors at different momenta.

An important area of tau charm factories are precision measurements of the absolute branching ratios. Early studies seem to indicate a limit of 1% systematic errors. A crucial consideration will be real understanding of the backgrounds (charged and neutral). It might be possible that by measuring more and more charm decays that the simulations of the tau charm backgrounds might in fact be fully understood and that the backgrounds in the data underneath the signal of interest could be simulated as well as the signal. The non-tau/charm backgrounds could be eventually measured by running below threshold. Since charm production is readily understood at low

²¹See Rollin Morrison talk in this workshop

energy and the running just below threshold should determine the non-charm backgrounds, it would seem tau charm factories are ideal to attempt measurements with 1% precision or less. This is to be compared to CLEO's excellent measurements²² now achieving 4% systematic errors using the soft pion decays from the D^* to tag the charged and neutral D 's.

In summary, measurements especially in the charm sector could be very complementary between tau charm factories, b factories and fixed target. As the precision increases, more and more cross checks between different experimental techniques will be needed. This is especially important if surprising experimental results are found. In many measurements high statistics limited by systematics will not be sufficient to make progress in charm physics.

Acknowledgements

The author wishes to thank John Cumalat for stimulating discussions and Dan Kaplan for an excellent workshop for future charm measurements. Also the collaboration wishes to thank support staff of the SSCLAB for the excellent work on maintaining the UNIX workstation farm for physics analysis and data reconstruction.

²²A. Fryberger, talk in this workshop

INCLUSIVE CHARM DECAYS FROM QCD

Michael Luke

Department of Physics, University of Toronto, Toronto, Canada M5S 1A7

Abstract

Some recent developments in the theory of inclusive decays of heavy hadrons are reviewed, and applications to charm decays are discussed.

1 Introduction

The inclusive decays of heavy hadrons are currently the subject of great interest, both theoretically and experimentally. In this talk, I want to review the ideas behind some of this recent theoretical work, and present some thoughts on its relevance to the charm system.

Inclusive decays are particularly clean theoretically because all final hadronic states are summed over, and so the decay is much less sensitive to the details of low-energy QCD than the decay to any particular exclusive state. Consider the semileptonic decay of a hadron containing a heavy quark Q with mass $m_Q \gg \Lambda_{QCD}$. The decay of the heavy quark is a short-distance process, with typical energies of order m_Q being released, while the hadronization occurs at a much larger distance, set by Λ_{QCD} . Therefore, up to corrections of order Λ_{QCD}/m_Q , the inclusive width of any hadron H_Q containing a single Q is expected to be given by the free quark expression

$$\sum_{X_q} \Gamma(H_Q \rightarrow X_q e \bar{\nu}) \simeq \Gamma(Q \rightarrow q e \bar{\nu}) = |V_{Qq}|^2 \frac{G_F^2 m_Q^5}{192\pi^3} f(m_q/m_Q) + \mathcal{O}(\alpha_s(m_Q)) \quad (1)$$

where $f(x) = 1 - 8x^2 + 8x^6 - x^8 - 24x^4 \log x$. It has in fact been shown [1, 2] that Eq. (1) is rigorously true, in the sense that it is the first term of a well-defined expansion in powers of Λ_{QCD}/m_Q and $\alpha_s(m_Q)$, with corrections which may be systematically computed.

Since neither the c nor the b quark is particularly heavy compared to the typical scale of strong interactions, the corrections to Eq. (1) proportional to powers of $1/m_Q$ are of great interest, and have been extensively studied for semileptonic [1, 2, 3, 4] as well as radiative [5] decays.¹ It was shown in [1, 2] that for the total semileptonic width (as well as partial widths, such as $d\Gamma/dq^2$ and $d\Gamma/dE_e$),

¹Nonleptonic decays have also been analyzed using this expansion [2]. However, this requires a somewhat stronger assumption of quark/hadron duality than semileptonic decays, and I will not discuss it here. See also [6] for a critique of this approach.

- the leading term in the $1/m_Q$ expansion reproduces the results of the spectator model, with quark (as opposed to hadron) kinematics,
- the $\mathcal{O}(1/m_Q)$ corrections to the spectator model vanish and
- at $\mathcal{O}(1/m_Q^2)$, the corrections to the spectator model may be parameterized by two nonperturbative matrix elements. In addition, one of these matrix elements is determined experimentally by the measured B and B^* mass splitting, leaving only one unknown nonperturbative parameter (in addition to the unknown quark mass).

Since this is a brief talk, I will not go into the details of the derivations of the various results. Instead, I want to sketch the reasoning behind this approach and give some of the main results. I will then discuss a few applications to the charm system.

2 Heavy Hadron Decays

The simple spectator picture clearly faces a few difficulties. First, the true final states are hadrons, not free quarks and gluons as they are in this simple picture. For charm decays, this is a particular worry since the semileptonic width is dominated by only two states, the K and K^* . Second, the decaying quark is not free, but is bound in a hadron and the decay will be affected by the interactions with the light degrees of freedom. In particular, the rate is proportional to the fifth power of the quark mass, and so is very sensitive to the definition of the quark mass used. These difficulties will be treated systematically in a manner very similar to the more familiar case of hadronic τ decays [7], although the kinematics are slightly more complicated.

Without knowing the details of low-energy QCD, the decay width to a specific final state is incalculable. However, in the rest frame of the decaying hadron H_Q the inclusive rate may be written

$$\sum_{X_q} \Gamma(H_Q \rightarrow e \bar{\nu} X_q) \sim \int [\text{phase space factors}] L^{\mu\nu} W_{\mu\nu}(q_0, q^2) \quad (2)$$

where $J^\mu = \bar{q} \gamma^\mu (1 - \gamma_5) Q$, $L^{\mu\nu} = 4(P_e^\mu P_\nu^\nu + P_e^\nu P_\mu^\mu - g^{\mu\nu} P_e \cdot P_\nu)$, q is the momentum transfer to the leptons, and all the unknown hadronic physics is contained in the hadronic tensor

$$W^{\mu\nu}(q_0, q^2) = \sum_{X_q} \frac{d^3 P_X}{(2\pi)^3 2E_X} \langle H_Q | J^{\mu\dagger} | X_q \rangle \langle X_q | J^\nu | H_Q \rangle (2\pi)^4 \delta^{(4)}(P_Q - P_X - q). \quad (3)$$

Because all possible final states X_q are summed over, the optical theorem relates $W^{\mu\nu}$ to the imaginary part of the time ordered product $T(J^{\mu\dagger}, J^\nu)$

$$W^{\mu\nu}(q_0, q^2) \propto \text{Im } T^{\mu\nu}(q_0, q^2) \equiv \text{Im} \langle H_Q | T(J^{\mu\dagger}, J^\nu) | H_Q \rangle. \quad (4)$$

This is useful because the analytic structure of $T^{\mu\nu}(q_0, q^2)$ is known: it has cuts for all complex values of (q_0, q^2) where real intermediate states may propagate between the currents in the

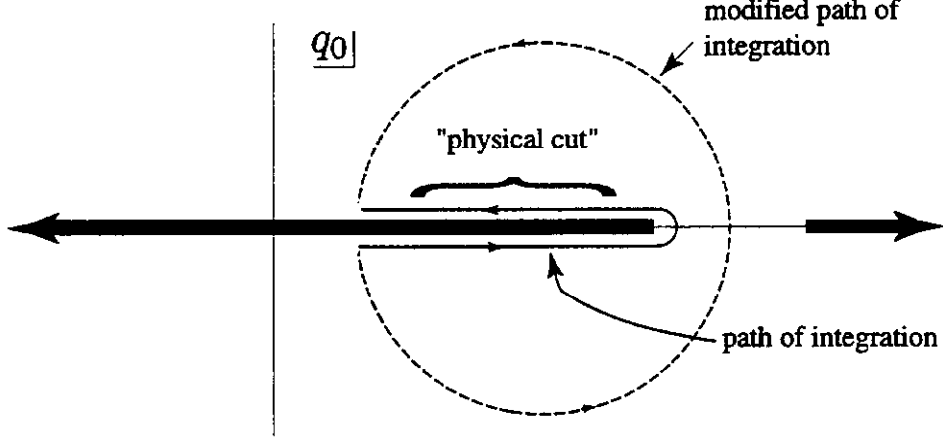


Figure 1: The complex q_0 plane (where q is the momentum transfer to the leptons) at fixed q^2 for heavy hadron decays. The phase space integral is over the region labeled “physical cut”; the other cuts correspond to different physical processes. The contour may be deformed away from the physical region where it is insensitive to the details of the physical final states.

time ordered product. At fixed q^2 , the analytic structure of $T^{\mu\nu}$ in the q_0 plane is shown in Fig. 1.

The phase space integral in (2) may now be rewritten as a contour integral around the region labeled “physical cut,” which picks out the imaginary piece of $T^{\mu\nu}$ (the other cuts correspond to other physical processes, such as lepton-hadron scattering). Close to the cut, where there are real intermediate states, $T^{\mu\nu}$ is sensitive to the details of low-energy QCD, and so is not perturbatively calculable. This corresponds to the fact that exclusive decays cannot be reliably calculated in perturbation theory. However, for the inclusive rate, the path of integration may be deformed to the modified path of integration shown in Fig. 1 which stays away from the physical region. Since $T^{\mu\nu}$ is analytic everywhere away from the cut, the integrals on the two contours are the same.

Along the deformed contour, the intermediate state is off shell by an amount $\sim m_Q^2$. Therefore, on the scale of the strong interactions the T -product is almost local, and may be evaluated using an operator product expansion. Schematically, $T^{\mu\nu}$ is written

$$T^{\mu\nu}(q_0, q^2) \sim \frac{1}{m_Q} \left[c_0(q_0, q^2) \mathcal{O}_0 + \frac{1}{m_Q} c_1(q_0, q^2) \mathcal{O}_1 + \frac{1}{m_Q^2} c_2(q_0, q^2) \mathcal{O}_2 + \dots \right] \quad (5)$$

where $\mathcal{O}_0, \mathcal{O}_1, \mathcal{O}_2, \dots$ are operators of dimension 3, 4, 5, \dots , and the coefficient functions $c_i(q_0, q^2)$ are calculable in perturbation theory. Since the typical momentum transfer is of order m_Q , the relevant scale μ_Q for α_s in the expansion is of also of order m_Q . The nonperturbative physics is contained in the matrix elements of the operators \mathcal{O}_i between hadron states.

The result is an expression for the inclusive semileptonic decay width as a double expansion in Λ_{QCD}/m_Q and $\alpha_s(m_Q)$. The additional spin and flavour symmetries of heavy quark

systems [8] greatly reduce the number of possible operators appearing in (5). At leading order the only operator is $\mathcal{O}_0 = \bar{h}h$,² which is a conserved current in the low-energy theory. It simply counts heavy quark number, so its forward matrix element is fixed, and is the same for any hadron containing a single Q quark. This term in the O.P.E. reproduces the free quark expression for the decay width. Using the equations of motion it can be shown [1] that the only operator of dimension four, $\bar{h}D^\mu h$, has a vanishing forward matrix element, so the leading nonperturbative corrections are given by operators of dimension five. Putting this together with the leading perturbative corrections yields the following expression for the semileptonic decay width of a D or B meson to $\mathcal{O}(1/m_Q^2, \alpha_s)$:

$$\sum_{X_q} \Gamma(H_Q \rightarrow e^+ \nu_e X_q) = \frac{G_F^2 m_Q^5}{192\pi^3} |V_{Qq}|^2 \left[\left(1 - \frac{2\alpha_s(\mu_Q)}{3\pi} g\left(\frac{m_q}{m_Q}\right) + \frac{\lambda_1}{2m_Q^2} \right) f\left(\frac{m_q}{m_Q}\right) - \frac{9\lambda_2}{2m_Q^2} h\left(\frac{m_q}{m_Q}\right) \right] \quad (6)$$

where $h(x) = 1 - \frac{8}{3}x^2 - 8x^4 + 8x^6 + \frac{5}{3}x^8 + 8x^4 \log x$, $g(x)$ may be found in [9, 10], and λ_1 and λ_2 are defined by

$$\begin{aligned} \lambda_1 &= \frac{1}{2m_Q} \langle H_Q | \bar{h}(iD)^2 h | H_Q \rangle \\ \lambda_2(\mu) &= \frac{1}{6m_Q} \langle H_Q | \bar{h} \left(\frac{i}{2} \right) \sigma^{\mu\nu} G_{\mu\nu} h | H_Q \rangle. \end{aligned} \quad (7)$$

As advertized, there are no $\mathcal{O}(1/m_Q)$ corrections to the free quark decay result³. A similar expression holds for the inclusive width of the Λ_Q baryon. In this case, however, the light degrees of freedom are in a spin-zero state and the analog of λ_2 vanishes.

λ_1 and λ_2 also appear in the relation between the quark and meson masses:

$$\begin{aligned} M_H &= m_Q + \bar{\Lambda} - \frac{\lambda_1 + 3\lambda_2}{2m_Q} + \mathcal{O}\left(\frac{1}{m_Q^2}\right) \\ M_{H^*} &= m_Q + \bar{\Lambda} - \frac{\lambda_1 - \lambda_2}{2m_Q} + \mathcal{O}\left(\frac{1}{m_Q^2}\right) \end{aligned} \quad (8)$$

Here, $\bar{\Lambda}$ is the energy of the light degrees of freedom in the meson and is expected to be a few hundred MeV. From the measured B and B^* masses, $\lambda_2(m_b) = 0.12 \text{ GeV}^2$, which corresponds to $\lambda_2(m_c) = 0.10 \text{ GeV}^2$. Since λ_1 contributes equally to the pseudoscalar and

²Note that in defining quark operators I am using the standard HQET heavy quark fields h . Writing the momentum of the heavy quark as $P^\mu = m_Q v^\mu + k^\mu$, where k^μ is a small “residual” momentum, h satisfies $\partial^\mu h = -ik^\mu h$. Matrix elements of higher dimension operators are therefore suppressed by powers of $k/m_Q \sim \Lambda_{QCD}/m_Q$.

³This is of course only true when the quark, rather than hadron, masses are used in the leading term. Recently, use of the quark “pole” mass in Eq. (6) has been criticized because it is formally ambiguous due to infrared renormalon effects [11, 12]. However, any such ambiguities always cancel out of physical observables. The quark mass is unobservable, and so the fact that the pole mass is formally ambiguous is irrelevant. See Ref. [13].

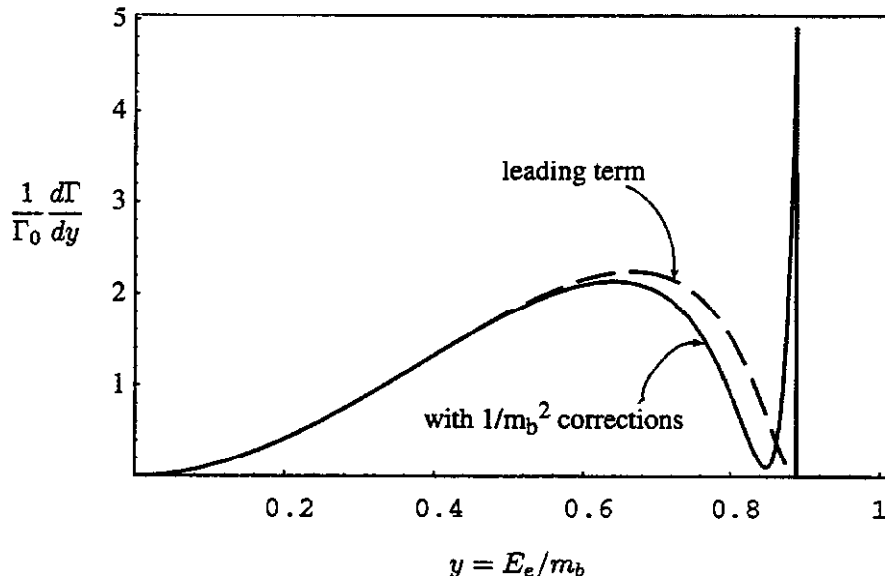


Figure 2: The electron spectrum for $B \rightarrow X_c e \bar{\nu}$ decay, at leading order and including $1/m_b^2$ corrections. The spike at the endpoint indicates that the O.P.E. breaks down in this region.

vector masses, it cannot be determined from the measured masses. By dimensional analysis, it is expected that $|\lambda_1| < 1 \text{ GeV}^2$. Note also that $\bar{\Lambda}$, λ_1 and λ_2 depend on the initial hadron, and are different for the D , D_s and Λ_c . However, because of heavy flavour symmetry [8] they are the same in the D and B , the D_s and B_s , and Λ_c and Λ_b .

The shape of the electron spectrum in inclusive heavy hadron decays may also be computed in this manner. This is of particular experimental interest in the b system, and the result is plotted (for $\lambda_1 = (300 \text{ MeV})^2$) in Fig. 2. Away from the endpoint, the corrections to free quark decay appear small and under control. However, near the endpoint the corrections grow out of control. There is of course no physics in the spike in the spectrum at the endpoint; it is simply a sign that the operator product expansion is breaking down in this region, since the subleading term has become much larger than the leading term. This is not unexpected, since near the endpoint the decay is dominated by only a few exclusive modes, and the dynamics of the decay will be governed by hadron, rather than quark, dynamics, which are not seen in the OPE. There has been much interest in the details of the endpoint of the spectrum which I will not discuss here [14, 15, 16]. If, however, we calculate a more inclusive quantity, such as the electron spectrum “smeared” with a smooth weighting function, the resulting spectrum will be smooth and the O.P.E. well behaved. Manohar and Wise [3] found that by smearing the spectrum in Fig. 2 with a Gaussian of width $\sim 500 \text{ MeV}$, a smooth spectrum was obtained which could then be compared with the experimental spectrum, smeared with the same function.

The O.P.E. has therefore enabled us to justify the spectator picture as the leading term

in a well-defined expansion of QCD, and it has provided a formalism to parameterize the subleading corrections to this picture. All corrections up to $\mathcal{O}(1/m_Q^2)$ are determined by the measured quantity λ_2 and two unknown parameters m_Q and λ_1 (or equivalently, $\bar{\Lambda}$ and λ_1).

3 Application to Charm

The focus of much of the recent work in this subject has been b decays. In this case, the spectator model is expected to work extremely well, since the leading nonperturbative corrections are suppressed by $\mathcal{O}(\Lambda_{QCD}/m_b)^2$, which is probably only a few percent. The inclusive approach may be used, for example, to extract a value for V_{bc} which is competitive with the extraction from the exclusive mode $B \rightarrow D^* e \bar{\nu}$ [17, 18].

Since the c quark is not much heavier than typical hadronic scales, it is less clear that this approach will be applicable to charm decays. The corrections to free quark decay are likely to be substantial, and it may not be sufficient to include only the leading $\mathcal{O}(1/m_c^2)$ terms. The perturbative corrections may also be a particular problem, since without a two-loop calculation of the inclusive rate the relevant scale μ_c for α_s in Eq. (6) is not determined. While it is certainly of order m_c , there is no reason it could not be as low as, for example, $m_c/3$, which would bring the validity of the perturbative expansion into question. On the other hand, it is precisely these features which make semileptonic charm decays interesting, as charm decays will allow us to test these ideas in a region where the corrections are expected to be large, but where the expansion still does not obviously break down. Since treating the c quark as heavy is a crucial ingredient in the extraction V_{bc} from exclusive B decays, it would be valuable to have additional checks on the $1/m_Q$ expansion as applied to the c system [19].

The electron spectrum from D decay is plotted in Fig. 3. Clearly, the OPE breaks down over a much larger region of the spectrum, requiring it to be smeared with a very broad smearing function in order to bring the OPE under control, and is therefore less predictive than in the b system. Therefore, in the c system this formalism is likely to be most useful for predicting quantities which are integrated over most of the available phase space, such as total decay widths and perhaps moments of the electron spectrum. I would like to close by mentioning one particularly clean prediction of this type, which would require a high precision measurement of the inclusive semileptonic widths of charmed particles.

Although the $1/m^2$ corrections in general depend on two unknown parameters, certain ratios depend only on the differences of λ_1 and $\bar{\Lambda}$ in different systems, allowing absolute predictions to be made [3]. Let us define the “spin-averaged” meson mass $\bar{m}_H = 1/4(m_H + 3m_{H^*})$. We then find

$$\bar{m}_B - \bar{m}_{B_s} - \bar{m}_D + \bar{m}_{D_s} = \frac{1}{2} (\lambda_1^u - \lambda_1^s) \left(\frac{1}{m_c} - \frac{1}{m_b} \right) \quad (9)$$

(this relation was also noted in [18]), where I denote with the superscript u parameters in the D system and with the superscript s parameters in the D_s system. Inserting the appropriate

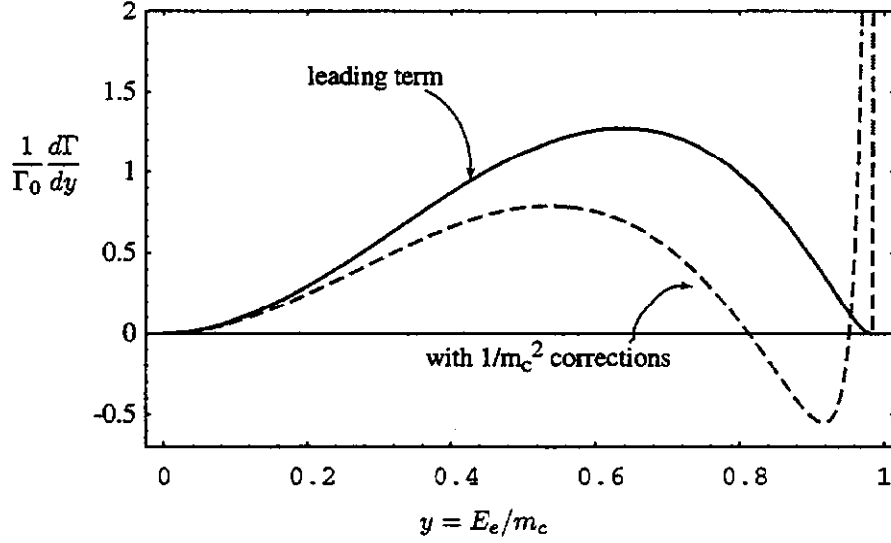


Figure 3: The electron spectrum for $D \rightarrow X_s e \bar{\nu}$ decay, at leading order and including $1/m_c^2$ corrections. The O.P.E breaks down over a much larger range of E_e than for b decays.

meson masses, this gives

$$\lambda_1^s - \lambda_1^u = (6.7 \pm 3.3) \times 10^4 \text{ MeV}^2 \quad (10)$$

which leads to a rather precise prediction for the ratio of the inclusive widths

$$\begin{aligned} \frac{\Gamma(D_s \rightarrow e \bar{\nu} X)}{\Gamma(D \rightarrow e \bar{\nu} X_s)} &= \left(1 + \frac{\lambda_1^s - \lambda_1^u}{2m_c^2}\right) - \frac{9}{2} \frac{\lambda_2^s - \lambda_2^u}{m_c^2} \frac{h(m_s/m_c)}{f(m_s/m_c)} + \mathcal{O}(1/m_c^3) \\ &= 0.995 \pm 0.005. \end{aligned} \quad (11)$$

The uncertainty of ± 0.005 corresponds only to the experimental error in the relevant meson masses, and does not include an estimate of the size of the $1/m_c^3$ terms. A similar analysis for the Λ_c baryon [3] gives the result

$$\frac{\Gamma(\Lambda_c \rightarrow e \bar{\nu} X)}{\Gamma(D \rightarrow e \bar{\nu} X)} = 1.16 \pm 0.04. \quad (12)$$

A useful feature of the predictions (11) and (12) is that the leading perturbative corrections to the individual widths cancel in the ratio, making the prediction insensitive to the scale of $\alpha_s(\mu)$, which is a significant source of uncertainty in the individual widths [17]. Precision measurements of these ratios would then provide a very clean test of the size of $1/m_c$ corrections.

Acknowledgements

The results (9–11) were derived in collaboration with M. J. Savage. I thank him for many useful conversations on this subject. I am also grateful to A. Falk, A. Manohar and M. Wise for useful discussions.

References

- [1] J. Chay, H. Georgi and B. Grinstein, Phys. Lett. **B247**, 399 (1990).
- [2] I.I. Bigi, M. Shifman, N.G. Uraltsev and A.I. Vainshtein, Phys. Rev. Lett. **71**, 496 (1993); B. Blok, L. Koyrakh, M. Shifman and A.I. Vainshtein, Phys. Rev. **D49**, 3356 (1994).
- [3] A. Manohar and M.B. Wise, Phys. Rev. **D49**, 1310 (1994).
- [4] T. Mannel, Nucl. Phys. **B413**, 396 (1994).
- [5] I.I. Bigi, N.G. Uraltsev and A.I. Vainshtein, Phys. Lett. **B293**, 430 (1992); I.I. Bigi, B. Blok, M. Shifman, N.G. Uraltsev and A.I. Vainshtein, Minnesota Report No. TPI-MINN-92/67-T (1992); A.F. Falk, M. Luke and M.J. Savage, Phys. Rev. **D49**, 3367 (1994).
- [6] I. Dunietz, A. F. Falk and M. Wise, preprint CALT-68-1933, May 1994.
- [7] see, for example, E. Braaten, S. Narison and A. Pich, Nucl. Phys. **B373**, 581 (1992).
- [8] N. Isgur and M. Wise, Phys. Lett. **B232**, 113 (1989); Phys. Lett. **B237**, 527 (1990).
- [9] N. Cabibbo and L. Maiani, Phys. Lett. **B79**, 109 (1978).
- [10] M. Jezabek and J.H. Kühn, Nucl. Phys. **B320**, 20 (1989).
- [11] I. I. Bigi, M. A. Shifman, N. G. Uraltsev and A. I. Vainshtein, preprint TPI-MINN-94-4-T, Feb 1994.
- [12] M. Beneke and V. Braun, preprint MPI-PHT-94-9, Feb 1994; M. Beneke, V. Braun and V. Zakharov, preprint MPI-PHT-94-18, May 1994.
- [13] M. Luke, A. Manohar and M. J. Savage, “Infrared Renormalons and Effective Field Theories”, to appear.
- [14] M. Neubert, Phys. Rev. **bf D49**, 3392 (1994).
- [15] A. F. Falk, E. Jenkins, A. Manohar and M. Wise, Phys. Rev. **D49**, 4553 (1994).
- [16] I. I. Bigi, M. A. Shifman, N. G. Uraltsev and A. I. Vainshtein, Phys. Lett. **B328**, 431 (1994).
- [17] M. Luke and M. J. Savage, Phys. Lett. **B32**, 88 (1994).
- [18] I. I. Bigi and N. Uraltsev, preprint CERN-TH-7063-93 (October 1993).
- [19] for a discussion of applications to charm (particularly non-leptonic decays), see B. Blok and M. Shifman, preprint TPI-MINN-93-55-T, November 1993.
- [20] I. I. Bigi, M. A. Shifman, N. G. Uraltsev and A. I. Vainshtein, preprint TPI-MINN-94-13-T, May 1994.

Charm Mixing and CP Violation in the Standard Model *

Gustavo Burdman

Fermi National Accelerator Laboratory, Batavia, Illinois 60510

ABSTRACT

The Standard Model predictions for D^0 - \bar{D}^0 mixing and CP violation in D decays are revised. The emphasis is put on obtaining the order of magnitude of the effects. In the case of mixing, the different approaches to the long-distance contributions are carefully discussed. The size of CP asymmetries is discussed in general and some specific calculations are reviewed. The possibility of using kinematic signals is briefly described.

Charm mixing and CP violation are usually thought to be negligibly small in the Standard Model (SM) when compared to the same effects in the K and B systems. The question of how small is small becomes critical when we consider the possibility of high sensitivity charm experiments which could produce 10^8 reconstructed D mesons. Although, as we will see below, in most cases the calculations are plagued with strong-interaction uncertainties making precise predictions impossible, it is of great interest to know at least the order of magnitude of the effects. This allows us to establish the existence or not of windows for the clean observation of new physics beyond the SM. This is particularly true in the case of mixing.

1 D^0 - \bar{D}^0 mixing in the Standard Model

Mixing occurs because the two weak eigenstates D^0 and \bar{D}^0 are not the mass eigenstates. If we neglect CP violation, which as we will see below is a very good approximation for D mesons, the mass eigenstates are also CP eigenstates and can be written as

$$\begin{aligned} |D_1\rangle &= \frac{1}{\sqrt{2}} (|D^0\rangle + |\bar{D}^0\rangle) \\ |D_2\rangle &= \frac{1}{\sqrt{2}} (|D^0\rangle - |\bar{D}^0\rangle). \end{aligned} \tag{1}$$

The probability that a D^0 meson produced at $t = 0$ decays as a \bar{D}^0 at time t is then given by

$$P(D^0 \rightarrow \bar{D}^0) = \frac{1}{4} e^{-\Gamma_1 t} \left\{ 1 - 2e^{-\frac{\Delta\Gamma}{2}t} \cos \Delta m t + e^{-\Delta\Gamma t} \right\}, \tag{2}$$

*Presented at the CHARM2000 Workshop, Fermilab, June 7-9, 1994.

where $\Delta m = m_2 - m_1$ and $\Delta \Gamma = \Gamma_2 - \Gamma_1$ are the mass and lifetime differences in the mass eigenstates. These two quantities determine the ratio of “wrong” final state to “right” final state in decay modes in which the final state can only be reached by one of the neutral D meson flavors. This is the case in semileptonic decays where we can define

$$r_D = \frac{\Gamma(D^0 \rightarrow l^- X)}{\Gamma(D^0 \rightarrow l^+ X)}. \quad (3)$$

This measurable quantity can be expressed in terms of Δm and $\Delta \Gamma$ by using (2) and the corresponding expression for the unmixed case. In the limit

$$\frac{\Delta m}{\Gamma}, \frac{\Delta \Gamma}{\Gamma} \ll 1 \quad (4)$$

it takes the simple form

$$r_D \approx \frac{1}{2} \left[\left(\frac{\Delta m}{\Gamma} \right)^2 + \left(\frac{\Delta \Gamma}{2\Gamma} \right)^2 \right] \quad (5)$$

As we will see, (4) is a very good approximation.

In the SM r_D is expected to be very small. The question is how small. In this workshop the possibility of having 10^8 reconstructed D 's in various experiments has been discussed [1]. It is expected that in some cases a sensitivity of 10^{-5} in r_D could be reached [2]. Several scenarios for new physics give contributions to r_D at this level. Therefore it is of great interest to establish at what level the SM contributes. It is not possible to compute r_D precisely, given the theoretical uncertainties arising from long distance dynamics. Unlike B^0 - \bar{B}^0 mixing, where r_B is completely dominated by the short-distance effects generated by the top quark, the inherently nonperturbative physics associated with these long-distance effects (e.g. propagation of light quark intermediate states) is potentially large. In what follows we review the status of our knowledge of the short and long-distance contributions to Δm . The lifetime difference $\Delta \Gamma$ is expected to be of the same order of magnitude as Δm . Given that we are interested in an order of magnitude estimate we will concentrate on Δm .

1.1 Δm_D : Short Distance

An effective $\Delta C = 2$ interaction is induced, at short distances, by one loop diagrams like the one in Fig. 1, the box diagrams. After the loop integration one obtains [3]

$$\mathcal{H}_{\text{eff}}^{\Delta C=2} = \frac{G_F}{\sqrt{2}} \frac{\alpha}{8\pi \sin^2 \theta_W} |V_{cs}^* V_{us}|^2 \frac{(m_s^2 - m_d^2)^2}{m_W^2 m_c^2} (\mathcal{O} + \mathcal{O}'), \quad (6)$$

where, in addition to the usual operator

$$\mathcal{O} = \bar{u} \gamma_\mu (1 - \gamma_5) c \bar{u} \gamma_\mu (1 - \gamma_5) c \quad (7)$$

one has to consider

$$\mathcal{O}' = \bar{u} (1 + \gamma_5) c \bar{u} (1 + \gamma_5) c \quad (8)$$

arising from the fact that the mass of the charm quark is not negligible. In (6) we

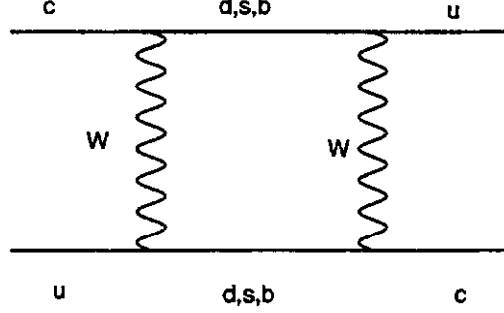


Figure 1: One of the box diagrams that induce a $\Delta C = 2$ interaction.

neglect powers of m_q/m_W with $q = d, s$ and the b quark contribution that, although enhanced by a factor of $(m_b/m_W)^2$ is largely suppressed by the factor $|V_{ub}^* V_{cb}|^2$. The GIM mechanism produces the suppression factor $(m_s^2 - m_d^2)/m_W^2$: the effect vanishes in the $SU(3)$ limit. The additional suppression $(m_s^2 - m_d^2)/m_c^2$ comes from the fact that the external momentum, of the order of m_c , is communicated to the light quarks in the loop. Both factors explain why the box diagrams are so small for D mesons relative to the K and B mesons, where the GIM mechanism enters as m_c^2/m_W^2 and m_t^2/m_W^2 and external momenta can be neglected.

The mass difference generated by the box diagrams is

$$\Delta m = 2 \langle D^0 | \mathcal{H}_{eff}^{\Delta C=2} | \bar{D}^0 \rangle, \quad (9)$$

where the matrix elements of the operators \mathcal{O} and \mathcal{O}' can be parametrized as

$$\langle D^0 | \mathcal{O} | \bar{D}^0 \rangle = \frac{8}{3} m_D f_D^2 B_D \quad (10)$$

$$\langle D^0 | \mathcal{O}' | \bar{D}^0 \rangle = -\frac{5}{3} \left(\frac{m_D}{m_c} \right)^2 m_D f_D^2 B_D'. \quad (11)$$

The vacuum insertion approximation, corresponding to the saturation of a sum over intermediate states by the vacuum state, gives $B_D = B_D' = 1$. Corrections to this simplified approach to the matrix elements are potentially large, but are not expected to change the order of magnitude of the effect. Therefore the box diagram contribution to the mass difference is

$$\Delta m_D^{s,d} \approx 0.5 \times 10^{-17} \text{ GeV} \left(\frac{m_s}{0.2 \text{ GeV}} \right)^4 \left(\frac{f_D}{f_\pi} \right)^2. \quad (12)$$

With the D^0 lifetime from [4] we have $\Gamma = (1.59 \pm 0.02) \times 10^{-12} \text{ GeV}$. Taking into account that the short-distance contribution to $\Delta\Gamma$ is of the same order as (12), we use (5) to obtain the short-distance contribution to the mixing parameter to be

$$\tau_D^{s,d} \approx 10^{-10} - 10^{-8}, \quad (13)$$

which is extremely small.

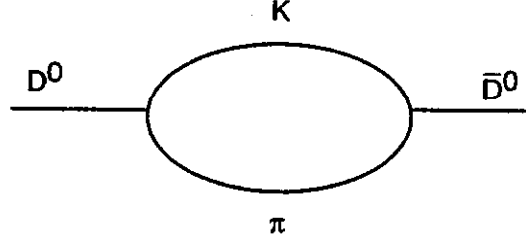


Figure 2: Two pseudoscalar intermediate state. There can be also KK and $\pi\pi$.

1.2 Δm : Long Distance

1.2.1 Dispersive Approach.

It has been argued that the fact that the main contributions to intermediate states in D meson mixing come from light quarks signals the presence of large long-distance effects. They correspond to hadronic intermediate states propagating between the D mesons. It is, in principle, not possible to calculate these effects given their essentially nonperturbative character. However it is crucial to estimate their order of magnitude. In order to obtain it the authors of Ref. [5] make use of dispersive techniques. They consider sets of n -particle intermediate states related by $SU(3)$. In the $SU(3)$ limit the contribution from each of these sets must vanish. For instance, consider the intermediate states involving two charged pseudoscalars: K^-K^+ , $\pi^-\pi^+$, $K^-\pi^+$, $K^+\pi^-$. Their contribution to mixing comes from diagrams like the one in Fig. 2. Calculating the loop one typically obtains

$$\Sigma(p^2) = A(g) [\ln(-p^2) + \dots], \quad (14)$$

where p is the external momentum and $A(g)$ depends on the form of the interaction and on the coupling g . The ellipses denote constant terms that also depend on the form of the vertex. However the logarithm gives an imaginary part that is related to the partial width of the on-shell intermediate state. That is, using

$$\ln(-p^2) = \ln p^2 + i\pi, \quad (15)$$

the relation

$$\text{Im} [\Sigma(p^2)] = \Gamma/2 \quad (16)$$

fixes the coefficient of the logarithm. Keeping only this term and properly adding all the charged pseudoscalar states one obtains

$$\begin{aligned} \Delta m_D^{l.d.} \approx & \frac{1}{2\pi} \ln \frac{m_D^2}{\mu^2} \left[\Gamma(D^0 \rightarrow K^-K^+) + \Gamma(D^0 \rightarrow \pi^-\pi^+) \right. \\ & \left. - 2\sqrt{\Gamma(D^0 \rightarrow K^-\pi^+) \Gamma(D^0 \rightarrow K^+\pi^-)} \right], \end{aligned} \quad (17)$$

where μ is a typical hadronic scale ($\simeq 1$ GeV). In order to get an estimate for the long-distance effect we would need more information on the doubly Cabibbo-suppressed mode $D^0 \rightarrow K^+\pi^-$. If we define

$$\frac{\Gamma(D^0 \rightarrow K^+\pi^-)}{\Gamma(D^0 \rightarrow K^-\pi^+)} = a \times \tan^4 \theta_c, \quad (18)$$

then in the $SU(3)$ limit one would expect $a = 1$. However, a recent measurement by the CLEO collaboration gives [6]

$$a = 2.95 \pm 0.95 \pm 0.95, \quad (19)$$

signaling a possibly large breaking of $SU(3)$. Although the value of Δm_D must be proportional to the amount of $SU(3)$ breaking, the value of (19) does not mean the effect is necessarily large. Large $SU(3)$ breaking also occurs in the ratio [4]

$$\frac{\Gamma(D^0 \rightarrow K^+K^-)}{\Gamma(D^0 \rightarrow \pi^+\pi^-)} \simeq 3, \quad (20)$$

thus allowing for a partial cancellation of large $SU(3)$ breaking effects in (17). In the end the result can be expressed as

$$\frac{\Delta m_D^{l.d.}}{\Gamma} \simeq 8 \times 10^{-4} (1.4 - \sqrt{a}) \simeq -2.5 \times 10^{-4}, \quad (21)$$

where the last number corresponds to taking the central value in (19). However it can be seen that within the large error bars in (19) the effect is consistent with zero and more data are needed.

One could imagine computing, in the same fashion, contributions from other $SU(3)$ related sets of intermediate states: pseudoscalar-vector, vector-vector, three pseudoscalars, etc. All of these are proportional to the amount of $SU(3)$ breaking in the set. The relative signs of these contributions are unknown and although there could be cancellations one would expect the order of magnitude to stay the same.

1.2.2 Heavy Quark Effective Theory (HQET).

The applicability of the HQET ideas to D - \bar{D} mixing rests on the assumption that the charm quark mass is much larger than the typical scale of the strong interactions. It was first pointed out in Ref. [7] that in this case there are no nonleptonic transitions to leading order in the effective theory since they would require a large momentum transferred from the heavy quark to the light degrees of freedom. This means that, in the effective low energy theory, mixing is a consequence of matching the full $\Delta C = 2$ theory at the scale m_c with the HQET and then running down to hadronic scales ($\ll m_c$). In other words, there are no new operators at low energy and the only “long-distance” effects come from the renormalization group running below the matching scale m_c . As a consequence, Δm_D can be computed in the HQET using quark operators and restricting the nonperturbative physics only to their matrix elements, which in Ref. [7] are estimated using naive dimensional analysis.

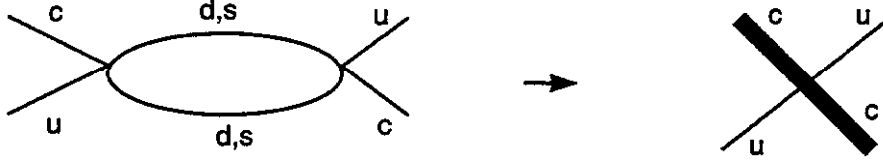


Figure 3: Diagrams generating four-quark operators in HQET.

First let us consider the four-quark operators generated from the box diagrams by integrating out the W 's. These and their matching diagrams in the effective theory are shown in Fig. 3. The contribution of these operators to the mass difference behaves like [7]

$$\Delta m_D^{(4)} \sim \frac{1}{16\pi^2} \frac{m_s^4}{m_c^2}, \quad (22)$$

where the first factor comes from the loop and m_d is neglected. This is nothing but the HQET version of the box diagrams.

There will also be higher dimension operators. In principle they will be suppressed by additional powers of $1/m_c$. However, as we see below, they can give important contributions. For instance, six-quark operators are suppressed by one of such powers. We can think that they arise by “cutting” one of the light quark lines in the loop in Fig. 4 and then shrinking the connecting line leftover when going to the effective theory given that the momentum flowing through it is large ($\sim m_c$). As a consequence, we get rid of two powers of m_s and the contribution from six-quark operators goes like

$$\Delta m_D^{(6)} \sim \frac{1}{m_c} \frac{m_s^2}{m_c^2} (m_s f^2), \quad (23)$$

where the last factor comes from taking the hadronic matrix elements and f is the pseudo-goldstone boson decay constant.

Finally, eight-quark operators are obtained by cutting the remaining light quark line and bridging the two four quark pieces with a gluon. The resulting contribution goes like

$$\Delta m_D^{(8)} \sim \frac{\alpha_s}{4\pi} \frac{1}{m_c^2} \frac{(m_s f^2)^2}{m_c^2}. \quad (24)$$

As one can see from (24), this is the least GIM-suppressed contribution. However it is suppressed by $1/m_c^2$ and most importantly by the factor $\alpha_s/4\pi$. Relative to the box diagram this is

$$\frac{\Delta m_D^{(8)}}{\Delta m_D^{(4)}} \simeq \frac{\alpha_s}{4\pi} \frac{(4\pi f)^4}{m_s^2 m_c^2} \simeq \frac{\alpha_s}{4\pi} \times 20. \quad (25)$$

Therefore there is no enhancement due to these operators. In Ref. [7] it is argued that these contributions correspond to the intermediate states taken into account by the dispersive approach. Thus the suppression factor $\alpha_s/4\pi$ in (24) suggests that there are cancellations among the different sets of states.

The six-quark operators give an enhancement of the order of

$$\frac{\Delta m_D^{(6)}}{\Delta m_D^{(4)}} \simeq \frac{(4\pi f)^2}{m_s m_c} \simeq 3 \quad (26)$$

A complete calculation in this approach, including QCD corrections to one loop, is performed in Ref. [8]. Their results can be summarized as

$$\begin{aligned} \Delta m_D^{(4)} &\simeq (0.5 - 0.9) \times 10^{-17} \text{GeV} \left(\frac{m_s}{0.2 \text{GeV}} \right)^4 \\ \Delta m_D^{(6)} &\simeq (0.7 - 2.0) \times 10^{-17} \text{GeV} \left(\frac{m_s}{0.2 \text{GeV}} \right)^3 \\ \Delta m_D^{(8)} &\simeq (0.1 - 0.6) \times 10^{-17} \text{GeV} \left(\frac{m_s}{0.2 \text{GeV}} \right)^2. \end{aligned}$$

In sum, the HQET approach to Δm_D predicts

$$\frac{\Delta m_D}{\Gamma} \simeq (1 - 2) 10^{-5}. \quad (27)$$

The uncertainty in (27) is mostly due to the uncertainty in the relative signs of the various contributions. However it is clear that HQET predicts no large enhancements with respect to the box diagram, which implies a mixing parameter of the order of

$$r_D \approx 10^{-10} - 10^{-9}. \quad (28)$$

In conclusion, with the current data on DCSD there seems to be no large disagreement between the dispersive approach of Ref. [5] and the HQET estimate of the mixing parameter for D mesons [7, 8]. A conservative upper limit can then be established for the SM contribution to D^0 - \bar{D}^0 mixing to be

$$r_D^{SM} < 10^{-8}. \quad (29)$$

2 CP Violation

In order for CP violation to occur there must be at least two amplitudes interfering with non-zero relative phases. There are two mechanisms that can produce this interference. In the first case the two amplitudes correspond to a D^0 decaying as a D^0 at time t and a D^0 decaying, after mixing, as a \bar{D}^0 at time t , both to the same final state f . This is called indirect CP violation and is theoretically clean. That is, the hadronic uncertainties cancel in the asymmetry given that they are the same for both amplitudes. However, as we have seen in the previous section, the mixing amplitude is extremely small in the SM and therefore the induced CP violation is negligible.

More generally, CP violation can occur directly in the decay amplitude. Let us assume two amplitudes contribute to a given D decay mode. Then

$$A_f = A_1 e^{i\delta_1} + A_2 e^{i\delta_2}, \quad (30)$$

where A_1 and A_2 are the two amplitudes after factoring out the strong interaction phases δ_1 and δ_2 . When the CP conjugate is taken the weak phases included in $A_{1,2}$ change but the strong phases stay the same:

$$\bar{A}_f = A_1^* e^{i\delta_1} + A_2^* e^{i\delta_2}. \quad (31)$$

The CP asymmetry is then

$$a_{CP} = \frac{|A_f|^2 - |\bar{A}_f|^2}{|A_f|^2 + |\bar{A}_f|^2} = \frac{2\text{Im}[A_1^* A_2] \sin(\delta_1 - \delta_2)}{|A_1|^2 + |A_2|^2 + 2\text{Re}[A_1^* A_2] \cos(\delta_1 - \delta_2)}. \quad (32)$$

From (32) we see that in order to have a nonzero asymmetry the two amplitudes must have different weak as well as strong phases. The predictions for a_{CP} are then plagued with hadronic uncertainties coming from the amplitudes and the final-state-interaction phases.

The interesting question is what is the typical size of the effect in the SM. Before going into the more detailed analysis let us remember that any CP-violating effect in the SM must be proportional to the rephasing-invariant quantity

$$J = \text{Im}[V_{ij} V_{kl} V_{ik}^* V_{jl}^*] \quad (33)$$

for any choice of $i \neq l$ and $j \neq k$. With the current values of the CKM phases and taking for the CP violating phase $\sin \delta = 1$ we know that $J \leq 10^{-4}$. From (32) we can see that CP asymmetries are larger the more suppressed is the mode. For instance, for Cabibbo-suppressed decays we have an enhancement of $\sin^{-2}(\theta_c)$ and then an order of magnitude estimate for the asymmetry is

$$a_{CP} \sim 10^{-3}. \quad (34)$$

In D decays all tree level diagrams contributing to a given final state have the same CKM matrix element combination. They will interfere only with the one loop diagrams called penguins. Cabibbo-favored D modes do not have penguins and then we are left with Cabibbo-suppressed decays, for which the asymmetry is estimated in (34). However the fact that one of the amplitudes is likely to be much smaller, the penguin in this case, largely reduces the size of the asymmetry. The relative size of the penguin to the tree level diagrams is not a settled issue but one should consider (34) to be on the rather optimistic side unless there is a large enhancement from strong-interaction dynamics, in the same fashion as in the $\Delta I = 1/2$ rule. This possibility is raised in Ref. [9].

On the other hand, in D_s decays it is possible to have two tree-level amplitudes with different weak phases. For instance in $D_s \rightarrow K\pi$ the spectator and annihilation diagrams are proportional to $V_{cd}^* V_{ud}$ and $V_{cs}^* V_{us}$ respectively. Therefore, if the annihilation diagram is not suppressed relative to the spectator, asymmetries of the order of (34) are expected.

As was mentioned above, the calculation of the asymmetries involves the knowledge of hadronic matrix elements and strong-interaction phases. This is done, for instance, in

Refs. [10] and [11]. In the first case, the relative strong phases are provided by the quark diagrams and final-state interactions are neglected.

In the work of Ref. [11], large final-state-interaction phases are provided by nearby resonances. This tends to give larger asymmetries. The typical result in this case is a few $\times 10^{-3}$. For instance, for the decay $D^+ \rightarrow \bar{K}^* K^+$ $a_{CP} = 2.8 \times 10^{-3}$. In D_s decays the most interesting mode is $K^* \eta'$ with $a_{CP} = -8.1 \times 10^{-3}$.

In any event, all calculations of direct-CP-violation asymmetries are very uncertain. The SM can give at most an effect of the order of 10^{-3} but more precise predictions are not possible with our current imprecise knowledge of hadronic physics.

Finally, we mention the possibility of kinematic CP-violation signals. For instance, in decays to two vector mesons $D(p) \rightarrow V_1(k)V_2(q)$ [12, 13], it is possible to construct CP-odd correlations of the two polarizations and one of the momenta. A triple-product correlation $\langle k \cdot \epsilon_1 \times \epsilon_2 \rangle$ is T odd. However a non-vanishing value of this quantity is not necessarily a signal of CP violation: the effect could be entirely due to strong-interaction phases. In order to have a truly CP-odd correlation one has to compare with the CP-conjugate state: the sum of

$$N_f = \frac{N(k \cdot \epsilon_1 \times \epsilon_2 > 0) - N(k \cdot \epsilon_1 \times \epsilon_2 < 0)}{N_{total}} \quad (35)$$

and the corresponding quantity for the CP-conjugate state, $N_{\bar{f}}$, should vanish if CP is conserved. Similar correlations but for semileptonic decays are discussed in [14]. Another type of kinematic signal can be obtained in neutral three-body decays like $D^0 \rightarrow M^+ M^- N^0$ [15]. In general the partial decay rate of a given neutral D flavor need not be symmetric in the energies E_+ and E_- . However when adding all reconstructed neutral D 's from the final state without identifying the D flavor, the Dalitz plot must be symmetric in E_+, E_- unless CP is violated. That is, given the expression

$$\Gamma[(D^0 + \bar{D}^0) \rightarrow M^+ M^- N^0] = a + b(E_+ - E_-), \quad (36)$$

a nonzero value of b signals a net energy asymmetry and therefore CP violation.

In all cases, the kinematic asymmetries are also plagued with hadronic uncertainties as in the case of partial-rate asymmetries in charged D decays. However it is important that they are taken into account given that in some cases they might be easier to observe.

To summarize, the SM predicts that CP violation in charm decays proceeds via the direct mechanism given the small value of r_D . Asymmetries are expected to be at most of order 10^{-3} in modes with branching fractions of 10^{-3} . This implies the need of at least 10^8 reconstructed D 's in order to observe a 3σ effect.

3 Conclusions

We have seen that the SM predicts extremely small values for the mixing parameter r_D . The effect, even after including possible long-distance enhancements, seems to be in the range $10^{-10} - 10^{-8}$. These effects had been previously overestimated in [16] giving therefore the impression that any observation of D^0 - \bar{D}^0 mixing would be contaminated by long-distance dynamics. However this is not the case. An observation

of D mixing at the level of $10^{-4} - 10^{-5}$, which is going to be probed at high-sensitivity experiments, would be a signal of new physics [17].

On the other hand, CP violation in the SM might be marginally observable in some cases. Signals from new physics could then be mixed with these. However, there are models where sizeable asymmetries occur in Cabibbo-favored modes, giving a clear signal over the SM background [17].

References

- [1] R.J. Morrison, these proceedings.
- [2] T. Liu, these proceedings.
- [3] H. Cheng, Phys. Rev. **D26**, 143 (1982);
A. Datta and D. Kumbhakar, Z. Phys. **C27**, 515 (1985).
- [4] Particle Data Group, Phys. Rev. **D45**, 1 (1992).
- [5] J.F. Donoghue, E. Golowich, B.R. Holstein and J. Trampetic, Phys. Rev. **D33**, 179 (1986).
- [6] M. Whitherell, proceeding of the XVI International Symposium on Lepton-Photon Interactions, Cornell University, Ithaca, New York, August 1993.
- [7] H. Georgi, Phys. Lett. **B297**, 353 (1992).
- [8] T. Ohl, G. Ricciardi and E.H. Simmons, Nucl. Phys. **B403**, 605 (1993).
- [9] M. Golden and B. Grinstein, Phys. Lett. **B222**, 501 (1989).
- [10] L.L. Chau and H. Cheng, Phys. Rev. Lett. **53**, 1037 (1984).
- [11] F. Buccella *et al.*, Phys. Lett. **B302**, 319 (1993).
- [12] G. Valencia, Phys. Rev. **D39**, 3339 (1989).
- [13] J.R. Dell'Aquila and C.A. Nelson, Phys. Rev. **D33**, 80 (1986).
- [14] E. Golowich and G. Valencia, Phys. Rev. **D40**, 112 (1989).
- [15] G. Burdman and J.F. Donoghue, Phys. Rev. **D45**, 187 (1992).
- [16] L. Wolfenstein, Phys. Lett. **B164**, 170 (1985).
- [17] S. Pakvasa, these proceedings.

Charm as Probe of New Physics

Sandip Pakvasa
Department of Physics
University of Hawaii
Honolulu, HI 96822

1 Introduction

In this talk I would like to discuss two aspects of charm physics. One is to show that many standard model predictions for rare decay modes (along with $D^0 - \bar{D}^0$ mixing and CP violation) are extremely small thus opening a window for new physics effects[1]; and the other is to review the expectations from several plausible and interesting new physics possibilities.

The standard model will be taken to be defined by the gauge group $SU(3)_c \times SU(2)_L \times U(1)$ with three families of quarks and leptons, one Higgs doublet and no right handed neutrinos (thus $m_{\nu_i} = 0$). We will review predictions for D mixing, CP violation in the D system and then discuss rare decays of D's.

Everything in this talk is based upon joint on-going work with Gastavo Burdman, Eugene Golowich and JoAnne Hewett; many details and complete results will appear in a forthcoming review.

2 $D - \bar{D}$ Mixing and CP Violation

As already discussed by Burdman,[2] $D^0 \bar{D}^0$ mixing differs from $K^0 - \bar{K}^0$ and $B^0 - \bar{B}^0$ mixing in several ways. In the box diagram, the s-quark intermediate state dominates; this is in spite of the suppression by the factor $(m_s/m_c)^2$ resulting from the external momenta (i.e. the fact that $m_c > m_s$)[3]. The final result for δm from the box diagram is extremely small, one finds

$$\delta m_D \sim 0.5 \cdot 10^{-17} \text{ GeV} \quad (1)$$

for $m_s \sim 0.2 \text{ GeV}$ and $f_D \sqrt{B_D} \sim 0.2 \text{ GeV}$; leading to

$$\delta m_D / \Gamma_{D^0} \sim 3 \cdot 10^{-5} \quad (2)$$

One should worry whether long distance contributions would give much larger contributions. The contribution from two body states $K^+ K^-$, $K^- \pi^+$, $K^+ \pi^-$, $\pi^+ \pi^-$ was carefully evaluated by Donoghue et al. [4] With the current experimental values, this is rather small,

of the same order as above. A very different calculation of the matrix element resulting from the box diagram due to Georgi et al. [5] employing HQET also yields an enhancement of no more than a factor of 4-5 over the short distance result. Even if none of these arguments are completely convincing it is likely that the SM $\delta m/\Gamma$ is not enhanced by more than an order of magnitude over the short distance value of $3 \cdot 10^{-5}$. Since the current experimental limit [6] is 0.083, there is plenty of room for new physics effects to show up.

CP violation in mixing is described by ϵ_D and the asymmetry a in e.g. $e^+e^- \rightarrow D^0 \bar{D}^0 \rightarrow \ell^+ \ell^+ x, \ell^- \ell^- x$ defined by $a = (N^{++} - N^{--})/(N^{++} + N^{--})$ goes as $2Re \epsilon_D$ for small ϵ_D . $2Re \epsilon_D$ is given by

$$2Re \epsilon_D = \frac{2Im(M_{12}\Gamma_{12}^*)}{|(Im M_2)|^2 + |(Re\Gamma_{12})|^2} \quad (3)$$

It is always possible to choose a phase convention for the KM matrix such that $Im\Gamma_{12} = 0$. Then

$$2Re \epsilon_D \leq \left(\frac{Im M_{12}}{(Re\Gamma_{12})} \right) \quad (4)$$

the left hand side is given by $\left(\frac{m_b m_c}{m_s^2} \right)^2 Im(U_{cb} U_{bu}^*)^2 / \theta_c^2$ and hence

$$2Re \epsilon_D \leq 10^{-2}. \quad (5)$$

This is the maximum value for the CP violating charge asymmetry (due to mixing) in the SM. The actual value lies between $5 \cdot 10^{-3}$ and $5 \cdot 10^{-4}$.

Direct CP violation can also be looked for in partial rate asymmetries of charge conjugate states. Such rate asymmetries are proportional to $\sin(\phi_i - \phi_j) \sin(\delta_i - \delta_j)$ where ϕ_i are weak CP phases, δ_i are final state interaction phases and i, j are strong interaction eigenstates [7]. In SM for D (and Ds) decays there can be no CP violating rate asymmetries for the Cabibbo allowed decay modes (and for the double Cabibbo-suppressed modes as well) to the lowest order. In Cabibbo-suppressed modes there can be interference between the quark decay diagram and Penguin (and/or annihilation) diagram leading to CP violating partial rate asymmetries. The main difficulty is evaluating the final state interaction phases. Several groups have estimated these phases[8] and based on these the more promising candidates seem to be $D_s^+ \rightarrow K^{*+} \eta(\eta')$ and $D^+ \rightarrow \bar{K}^{*0} K^+(\rho^0 \pi^+)$ with asymmetries in the range of $(2-8)10^{-3}$.

3 Rare Decays

There are a number of "rare" (one-loop) decay modes of D[9] which have extremely small rates when evaluated in SM; thus providing a potential window for new physics contributions.

(i) $D^0 \rightarrow \mu^+ \mu^-$

At one loop level the decay rate for $D^0 \rightarrow \mu^+ \mu^-$ is given by

$$\Gamma(D^0 \rightarrow \mu^+ \mu^-) = \frac{G_F^4 m_W^4 f_D^2 m_\mu^2 m_D}{32\pi^3} |F|^2 \sqrt{1 - 4m_\mu^2/m_D^2} \quad (6)$$

where

$$F = \frac{U_{us}U_{cs}^* (x_s + 3/4 x_s^2 \ell_n x_s)}{U_{ub}U_{cb}^* (x_b + 3/4 x_b^2 \ell_n x_b)} \quad (7)$$

and $x_i = m_i^2/m_W^2$. This yields a branching fraction of 10^{-19} . There are potentially large long distance effects; e.g. due to intermediate states such as $\pi^0, K^0, \bar{K}^0, \eta, \eta'$ or $(\pi\pi, K\bar{K})$ etc. Inserting the known rates for $P_i \rightarrow \mu^+ \mu^-$ and ignoring the extrapolation the result for $B(D^0 \rightarrow \mu^+ \mu^-)$ is $3 \cdot 10^{-15}$. This is probably an over-estimate but might give some idea of the long distance effects.

(ii) $D^0 \rightarrow \gamma\gamma$

The one loop contribution to $D^0 \rightarrow \gamma\gamma$ can be calculated in exactly the same way as above and the amplitude A is found to be approximately $4.6 \cdot 10^{-14}$ GeV, where A is defined by the matrix element $A q_{1\mu} q_{2\nu} \epsilon_{1\rho} \epsilon_{2\sigma} \epsilon^{\mu\nu\rho\sigma}$.

The decay rate is $\Gamma = |A|^2 m_D^3/64\pi$ and the branching fraction is 10^{-16} . The single particle contributions due to (π, K, η, η') yield $3 \cdot 10^{-9}$ but again are grossly over estimated.

(iii) $D \rightarrow \nu\bar{\nu}x$.

The decay rate for $c \rightarrow u\nu\bar{\nu}$ (for 3 neutrino flavors) is given by

$$\Gamma = \frac{3G_F^2 m_c^5}{192\pi^3} \left[\frac{\alpha}{4\pi x_w} \right]^2 |A_\nu|^2. \quad (8)$$

Inserting the one loop value for A_ν , one finds for the branching fractions:

$$\begin{aligned} B(D^0 \rightarrow \nu\bar{\nu}x) &= 2 \cdot 10^{-15} \\ B(D^+ \rightarrow \nu\bar{\nu}x) &= 4.5 \cdot 10^{-15} \end{aligned} \quad (9)$$

For the exclusive modes $D^0 \rightarrow \pi\nu\bar{\nu}$ and $D^+ \rightarrow \pi^+\nu\bar{\nu}$ an estimate of the long distance contributions yields

$$\begin{aligned} B(D^0 \rightarrow \pi^0\nu\bar{\nu}) &\sim 5.6 \cdot 10^{-16} \\ B(D^+ \rightarrow \pi^+\nu\bar{\nu}) &\sim 8 \cdot 10^{-16} \end{aligned} \quad (10)$$

(iv) $D \rightarrow \bar{K}(K)\nu\bar{\nu}$

These modes have no short distance one loop contributions. Estimates of long distance contributions. Estimates of long distance contributions due to single particle poles yield branching fractions of the order of 10^{-15} .

(v) $D \rightarrow \ell\bar{\ell}x$.

The one loop contributions from γ , Z and WW intermediate states give for the inclusive decay mode $c \rightarrow u\bar{l}\bar{l}$ a rate which corresponds to a branching fraction for D^+ of the order

$$B.R.(D^+ \rightarrow \bar{l}x) = 2.10^{-10} \quad (11)$$

This corresponds to a fraction for D^0 of B.R. ($D^0 \rightarrow \bar{l}x$) = 10^{-10} . The exclusive modes $D^+ \rightarrow \pi^+\bar{l}\bar{l}$ and $D^0 \rightarrow \pi^0\bar{l}\bar{l}$ are expected to have somewhat smaller branching fractions in the range of a few times 10^{-11} .

(vi) ($D \rightarrow \gamma x$)

The Penguin diagram can give rise to $c \rightarrow u\gamma$ at one loop level and (before short distance QCD corrections) gives a rate for $c \rightarrow u\gamma$ corresponding to a branching fraction of B.R. ($D \rightarrow \gamma x$) of about 10^{-16} . This would yield branching fractions for exclusive channels such as $D^0 \rightarrow \rho^0\gamma, \omega^0\gamma$ at a level of 10^{-17} or so. It is expected that the QCD corrections will enhance this rates (these calculations are in progress)...

On the other hand, if the precise partial wave structure in the amplitude for the decays such as $D \rightarrow \phi\rho$ (as well as the total rates) were known, it is possible to estimate the rates for $D^0 \rightarrow \phi^0\gamma, D \rightarrow \rho\gamma$ etc. At present only upper bounds can be obtained e.g.

$$\begin{aligned} B.R.(D^+ \rightarrow \rho^+\gamma) &< 2.10^{-4} \\ B.R.(D^0 \rightarrow \rho^0\gamma) &< 2.10^{-5} \\ B.R.(D^0 \rightarrow \phi\gamma) &< 2.10^{-4} \end{aligned} \quad (12)$$

If these long distance contributions turn out to be much larger than the Penguin contributions (even after QCD correction) then the Penguin will remain invisible in D decays. I suspect that this is the case.

From the data on $D^0 \rightarrow \bar{K}^{*0}\rho^0$ [6] and VMD one obtains B.R. ($D^0 \rightarrow \bar{K}^{*0}\gamma$) $\sim 1.6.10^{-4}$. From the data on $D^+ \rightarrow \bar{K}^{*0}\rho^+$, assuming that $|A_1| \gg |A_3|$ and that there is no particular enhancement in DCSD mode $D^+ \rightarrow K^{*+}\rho^0$, one finds B.R. ($D^+ \rightarrow \bar{K}^{*+}\rho^0$) $\sim 1.4.10^{-4}$ and in turn B.R. ($D^+ \rightarrow \bar{K}^{*+}\gamma$) $\sim 3.10^{-7}$.

I should stress that in all of the above the short distance QCD corrections have not yet been incorporated. Since these tend to enhance the decay rates and the long distance values tend to be over-estimates, the gap between the two will be smaller than it appears here.

4 New Physics Scenarios

(i) Additional Scalar Doublet

One of the simplest extensions of the standard model is to add one scalar Higgs doublet[10]. If one insists on flavor conservation there are two possible models: in one (model I) all quarks get masses from one Higgs (say ϕ_2) and the other ϕ_1 does not couple to fermions; in the other ϕ_2 gives masses to up-quarks only and ϕ_1 , to down-quarks only. The new unknown

parameters are $\tan\beta (= v_1/v_2, \text{ the ratio of the two vevs})$ and the masses of the additional Higgs scalars, both charged as well as neutral.

In the charmed particle system, the important effects are in δm_D and the new contributions due to charged Higgses to rare decays such as $D^0 \rightarrow \mu^+\mu^-$, $D \rightarrow \pi\ell\bar{\ell}$, $D \rightarrow \gamma\gamma$, $D \rightarrow \rho\gamma$ etc.

The mass of the charged Higgs is constrained to be above 50 GeV by LEP data and there is a joint constraint on m_H and $\tan\beta$ from the observation of $B \rightarrow K^*\gamma$. For large $\tan\beta$, δm_D can be larger than the SM results[11].

(ii) Fourth Generation

If there is a fourth generation of quarks, accompanied by a heavy neutrino ($M_{N0} > 50$ GeV to satisfy LEP constraints) there are many interesting effects observable in the charm system.

In general $U_{ub'}$ and $U_{cb'}$ will not be zero and then the b' -quark can contribute to δm_D as well as to rare decays such as $D^0 \rightarrow \mu\bar{\mu}$, $D \rightarrow \ell\bar{\ell}x$, $D \rightarrow \pi\nu\bar{\nu}$ etc. (A singlet b' quark as predicted in E6 GUT has exactly the same effect). A heavy fourth generation neutrino N^0 with $U_{eN0}U_{\mu N}^* \neq 0$ engenders decays such as $D^0 \rightarrow \mu\bar{e}$ as well.

For $U_{ub'}U_{cb'} \gtrsim 0.01$ and $m_{b'} > 100\text{GeV}$, it is found that[12]

- (a) $\delta m_D/\Gamma > 0.01$;
- (b) $B(D^0 \rightarrow \mu\bar{\mu}) > 0.5 \cdot 10^{-11}$;
- (c) $B(D^+ \rightarrow \pi^+\ell\bar{\ell}) > 10^{-10}$; etc.

For a heavy neutrino of mass $M_{N0} > 45$ GeV, the mixing with e and μ is bounded by $|U_{Ne}U_{N\mu}^*|^2 < 7 \cdot 10^{-6}$ [13] and we find that branching fraction for $D^0 \rightarrow \mu^-e^+, \mu^+e^-$ can be no more than $6 \cdot 10^{-22}$! This is also true for a singlet heavy neutrino unaccompanied by a charged lepton. To turn this result around, any observation of $D^0 \rightarrow \mu e$ at a level greater than this must be due to some other physics, e.g. a horizontal gauge (or Higgs) boson exchange.

(iii) Flavor Changing Neutral Higgs

It has been an old idea that if one enlarges the Higgs sector to share some of the large global flavor symmetries of the gauge sector (which eventually are broken spontaneously) then it is possible that interesting fermion mass and mixing pattern can emerge. It was realized early that in general this will lead to flavor changing neutral current couplings to Higgs[14]. As was stressed[15] then and has been emphasized recently[16], this need not be alarming as long as current limits are satisfied. But this means that the Glashow-Weinberg criterion will not be satisfied and the GIM mechanism will be imperfect for coupling to scalars. This is the price to be paid for a possible "explanation" of fermion mass/mixing pattern. Of course, the current empirical constraints from $\delta m_K, K_L \rightarrow \mu\mu, K_L \rightarrow \mu e$ etc. must be observed. This is not at all difficult. For example, in one early model, flavor was exactly conserved in the strange sector but not in the charm sector[14]!

In such theories, there will be a neutral scalar, ϕ^0 of mass m with coupling such as

$$(g\bar{u}\gamma_5 c + g'\bar{c}\gamma_5 u)\phi^0 \quad (13)$$

giving rise to a contribution to δm_D

$$\delta m_D \sim \frac{gg'}{m^2} f_D^2 B_D m_D (m_D/m_C) \quad (14)$$

With a reasonable range of parameters, it is easily conceivable for δm_D to be as large as 10^{-13} GeV. There will also new contributions to decays such as $D^0 \rightarrow \mu\bar{\mu}$, $D^0 \rightarrow \mu e$ which will depend on other parameters.

There are other theoretical structures which are effectively identical to this, e.g. composite technicolor. The scheme discussed by Carone and Hamilton leads to a δm_D of 4.10^{-15} GeV[17].

(iv) Family Symmetry

The Family symmetry mentioned above can be gauged as well as global. In fact, the global symmetry can be a remnant of an underlying gauged symmetry. A gauged family symmetry leads to a number of interesting effects in the charm sector[18].

Consider a toy model with only two families and a $SU(2)_H$ family gauge symmetry acting on LH doublets; with $\begin{bmatrix} (c)_L \\ (s)_L \end{bmatrix}$ and $\begin{bmatrix} (\nu_\mu)_L \\ (\bar{\mu})_L \end{bmatrix}$ assigned to $I_H = 1/2$ doublets. The gauge interaction will be of the form:

$$g \left[(\bar{d} \bar{s})_L \gamma_\mu \bar{\tau} \bar{G} \mu \begin{pmatrix} d \\ s \end{pmatrix}_L + \dots \right] \quad (15)$$

After converting to the mass eigenstate basis for quarks, leptons as well as the new gauge bosons, we can calculate contributions to $\delta m_K, \delta m_D$ as well as to decays such as $K_L \rightarrow e\mu$ and $D \rightarrow e\mu$. The results are:

$$\begin{aligned} \delta m_D / \delta m_K &= \frac{f_D^2 B_D m_D \left[\frac{\cos^2 2\theta_u}{m_1^2} + \frac{\sin^2 2\theta_u}{m_2^2} - \frac{1}{m_3^2} \right]}{f_K^2 B_K m_K [d \rightarrow u]} \\ m(K_L^0 \rightarrow e\mu) &= \frac{1}{2\sqrt{2}} g^2 f_K m_\mu \left[\frac{\cos 2\theta_d \cos 2\theta_e}{m_1^2} + \frac{\sin 2\theta_d \sin 2\theta_e}{m_2^2} \right] \bar{\mu} (1 + \gamma_5) e. \\ m(D^0 \rightarrow e\mu) &= \frac{1}{4} g^2 f_K m_\mu [d \rightarrow u] \bar{\mu} (1 + \gamma_5) e. \end{aligned} \quad (16)$$

where θ_d, θ_u are θ_e are the mixing angles in the $d_L - s_L$, $u_L - c_L$ and $e_L - \mu_L$ sectors and are not measured experimentally and m_i are the gauge masses. It is possible to obtain $\delta m_D \sim 10^{-13}$ GeV and $B(D^0 \rightarrow e\mu) \sim 10^{-13}$ while satisfying the bounds on δm_K and $B(K_L^0 \rightarrow e\mu)$.

(v) Supersymmetry

In the Minimal Supersymmetric Standard Model new contributions to δm_D come from gluino exchange box diagram and depend on squark mixings and mass splittings. To keep δm_K^{SUSY} small the traditional ansatz has been squark degeneracy. In this case δm_D^{SUSY} is also automatically suppressed, no more than 10^{-18} GeV [19]. Recently it has been proposed[20]

that another possible way to keep δm_K^{SUSY} small is to assume not squark degeneracy but proportionality of the squark mass matrix to the quark mass matrix. It turns out in this case that δm_D can be as large as the current experimental limit. In some non-minimal SUSY theories certain radiative decay modes can have large rates[21].

(vi) Left-Right Symmetric Models

In a very nice paper[22], the Orsay group has pointed out that in left-right symmetric extensions of the SM, there can be sizable CP violating asymmetries in the Cabibbo allowed decay modes (which is impossible in the SM). I would like to illustrate this but in a different kind of model, the model of Gronau and Wakaizumi[23].

Recall that the basic premise of the model is that the suppression of $b \rightarrow c\ell\nu$ decays is not due to a small mixing U_{bc} but due to the decay proceeding via W_R exchange and the smallness of the ratio $(m_{W_L}/m_{W_R})^2$. This is accomplished by enlarging the gauge group to $SU(2)_L \times SU(2)_R \times U(1)$ but without manifest left-right symmetry and assuming the two mixing matrices to be

$$U_L = \begin{pmatrix} 1 & \lambda & \rho\lambda^3 \\ -\lambda & 1 & 0 \\ -\rho\lambda^3 & -\rho\lambda^4 & 1 \end{pmatrix} \quad (17)$$

$$U_R = \begin{pmatrix} e^{i\alpha} & 0 & 0 \\ 0 & se^{i\delta} & ce^{i\beta} \\ 0 & ce^{i\gamma} & -se^{i(\beta+\gamma)} \end{pmatrix} \quad (18)$$

where λ and ρ are the usual Wolfenstein parameters and U_L is real. As is evident, the current $b \rightarrow c$ is pure RHC. For successful phenomenology and a good fit to all the data there are a number of constraints on the model; e.g. ν_R must have a mass in the range of few MeV, $\rho \sim 0.2$ to 0.7 , $m_{W_R} > 400$ GeV, $c > 0.8$, $s < 0.6$. All CP violation comes from the RH sector and ϵ and ϵ' require that: $\sin(\gamma - \alpha) > 0.1$, $\sin(\delta - \alpha) < 0.5$ and $\sin(\alpha + w) < 0.7$; thus the constraints on the phases in U_R are rather weak.

In this model, for a decay such as $D \rightarrow \bar{K}\pi$, in addition to the W_L mediated decay there is an additional amplitude due to W_R which now carries a CP phase. Because of the larger W_R mass, the QCD coefficients for the RR operators are different from the LL operators resulting in a different ratio for the $I = 3/2$ to $1/2$ final states from the two operators; hence $a_{3R}/a_{1R} \neq a_{3L}/a_{1L}$. Then the CP partial rate asymmetry for the decay mode $D^0 \rightarrow K^-\pi^+$ and $\bar{D}^0 \rightarrow K^+\pi^-$ is given by

$$\frac{\Gamma - \bar{\Gamma}}{\Gamma + \bar{\Gamma}} = \frac{s(a_{3R} - a_{1R})}{a_{1L}} \sin(\delta_1 - \delta_3) \sin(\alpha - \delta) \quad (19)$$

where we have taken from data $a_{1L} \sim a_{3L}$. If, for simplicity, we take $a_{1R} \gg a_{3R}$, then the RHS becomes

$$s(m_{W_L}/m_{W_R})^2 \sin(\delta_1 - \delta_3) \sin(\alpha - \delta). \quad (20)$$

Taking $s \sim 0.5$, $\sin(\alpha - \delta) \sim 0.5$ in the allowed range, $\delta_1 - \delta_3 \sim 0(90^\circ)$ from data, and $(m_{W_L}/m_{W_R})^2 \sim 0.04$ the asymmetry is of the order 0.01 to be compared to 0 in SM. As shown in Ref. [22] similar values obtain in other left-right symmetric models as well making this a generic result in Left-Right Symmetric theories. Incidentally, the new contributions to δm_D are no larger than in SM.

5 Conclusion

To summarize, in the charm system several phenomena (such as δm , CP, loop induced decays) which are easily observed in K and B system are greatly suppressed in SM and there is a window of opportunity for new physics to show up.

Of course, even when there is new physics beyond the standard model (BSM) it is not guaranteed that there are interesting signals large enough to be seen. Probably the most likely place for some new physics to show up in δm_D . To disentangle the origin some other effects have to be seen. CP violation (in channels forbidden in SM) and rare decays such as $D^0 \rightarrow \mu\bar{\mu}, \gamma\gamma, \nu\nu x$ etc. would come a close second. Decays such as $D^0 \rightarrow \mu e$ are probably unlikely to occur at rates large enough to be seen in the near future but who knows?

6 Acknowledgements

I am most grateful to my collaborators Gustavo Burdman, Eugene Golowich and JoAnne Hewett for providing insight and wisdom. I thank Dan Kaplan for the invitation to participate in CHARM2000 and the Rare Decay, CP and δM Working Groups for enjoyable and stimulating discussions. This work was supported in part by USDOE Grant #DE-FG 03-94ER40833.

References

- [1] I. Bigi, Charm Physics Symposium, Beijing, 1987, p. 339; K. S. Babu, X-G He, X-Q. Li and S. Pakvasa, Phys. Lett. B205, 540 (1988); X-H. Gao and X-Q. Li, BIHEP-TH-90, S. Egli *et al.*, ETZ-IMP PR/92-1; A. Le Yaouanc *et al.*, LPTHE Orsay 92/49; A.J. Schwartz, Mod. Phys. Lett. A8, 967 (1993).
- [2] G. Burdman, These Proceedings.
- [3] A. Datta and D. Kumbhakar, Z. Phys. C27 (515) 1985; H. -Y. Cheng, Phys. Rev. D26, 143 (1982).
- [4] J. Donoghue *et al.*, Phys. Rev. D33, 179 (1986).
- [5] H. Georgi, Phys. Lett. 297, 353 (1992); T. Ohl *et al.*, Nucl. Phys. B403, 605 (1993).
- [6] K. Hikasa *et al.*, PDG, Phys. Rev. D45 S1 (1992).
- [7] T. Brown *et al.*, Phys. Rev. Lett. 51, 1823 (1983).
- [8] L-L. Chau and H-Y. Cheng, Phys. Rev. Lett. 53 1037 (1984); F. Buccella *et al.*, Phys. Lett. B302, 319 (1993).
- [9] The basic formulae for these are given in T. Inami and C. S. Lim, Prog. Theoret. Phys. 55, 297 (1981).

- [10] L. F. Abbott *et al.*, Phys. Rev. **D21**, 179 (1980); V. Barger *et al.*, Phys. Rev. **D41**, 3421 (1990).
- [11] J. Hewett (Private Communication).
- [12] K. S. Babu *et al.*, Phys. Lett. **205B**, 540 (1988).
- [13] A. Acker and S. Pakvasa, Mod. Phys. Lett. **A7**, 1219 (1992).
- [14] S. Pakvasa and H. Sugawara, Phys. Lett. **B73**, 61 (1978).
- [15] S. Pakvasa, H. Sugawara and Y. Yamanaka, Phys. Rev. **D25**, 1895 (1982).
- [16] L. Hall and S. Weinberg, Phys. Rev. **D48**, 979 (1993). S. Pakvasa, Discovery of Neutral Currents, Santa Monica, CA 1993; AIP Conf. Proc. 300, Ed. A. K. Mann and D. Cline AIP (1994), p. 426.
- [17] C. D. Carone and R. T. Hamilton, Phys. Lett. **301**, 196 (1993).
- [18] G. Volkov *et al.*, Yad. Fis. **34**, 435 (1981).
- [19] J. S. Hagelin *et al.*, Nucl. Phys. **B415**, 293 (1994) and references therein.
- [20] Y. Nir and N. Seiberg, Phys. Lett. **B309**, 337 (1993).
- [21] I. Bigi *et al.*, Z. Phys. **C48**, 633 (1990).
- [22] A. Le Yaouanc *et al.*, Phys. Lett. **B292**, 353 (1992).
- [23] M. Gronau and S. Wakairumi, Phys. Rev. Lett., **68**, 1814 (1992); See also W-S. Hou and D. Wyler, Phys. Lett. **B292**, 364 (1992); T. Hattori *et al.*, TOKUSHIMA-93-06.

Hadrons with two heavy quarks

Jean-Marc Richard
Institut des Sciences Nucléaires
Université Joseph Fourier, CNRS-IN2P3
53, avenue des Martyrs, 38026 Grenoble Cedex, France

Abstract

We review the spectroscopy and some properties of hadrons containing two charmed quarks, or more generally, two heavy quarks. This includes heavy baryons such as (bcu) , and possible exotic multiquark states.

1 Introduction

Baryons with two heavy quarks and one light quark, hereafter denoted (QQq) , intimately combine two extreme regimes of hadron structure. There is first the slow relative motion of the two heavy quarks, very similar to the quark–antiquark motion in charmonium and bottomonium. In both cases, the heavy constituents experience an adiabatic potential generated by the light degrees of freedom. The second aspect of (QQq) is the relativistic motion of the light quark q , which is presumably very similar for (ccq) , (bcq) , and (bbq) , providing another example of heavy quark symmetry.

A rich spectrum is expected. There are excitations of the relative motion of the two heavy quarks in the lowest Born–Oppenheimer potential. One can also get excitations of the light quark, or a combined excitation of both degrees of freedom.

The ground state of each flavour configuration cannot do anything but decay weakly, by disintegration of one of the heavy quarks, and sometimes by exchange of a W -boson between the constituents. A variety of final states are accessible, with no, some, or more Cabibbo suppression. We have here an ideal laboratory for studying weak interactions and subsequent hadronisation.

If (QQq) spectroscopy becomes accessible to experiment, it will also be possible to look at exotic mesons with two heavy quarks, $(QQ\bar{q}\bar{q})$. They have been predicted to be stable on the basis of the flavour independence of the static interquark potential. Other approaches

have led to similar conclusions. Current models gives stability for ratios (M/m) of quark masses corresponding to ($bb\bar{q}\bar{q}$) or higher. However, reasonable long-range forces might well push down this ratio, so that some ($cc\bar{q}\bar{q}$) could become serious candidates to stability.

In this review, I shall briefly summarize these aspects of double heavy-flavour spectroscopy. General references are [1, 2, 3, 4] for (QQq) spectroscopy in potential models, [4, 5] for decays of these (QQq), [6, 7] for ($QQ\bar{q}\bar{q}$) exotics in simple models, while a comparison with atomic physics is attempted in [8], and another approach is discussed in [9, 10]. It is hoped that this Workshop will stimulate further investigations.

2 Relations among ground state masses

The value of a peculiar (QQq) mass is interesting only when compared with that of other flavour configurations. In the past, regularities have been noticed in the baryon spectrum, such as the Gell-Mann–Okubo mass formula, or the equal-spacing rule of the decuplet. One possible interpretation in the modern language is based on *flavour independence*. The binding potential is the same whatever quark experiences it. This property is a consequence of the gluons being coupled to the colour rather than to the isospin, or hypercharge, or mass of the quarks, at least before any relativistic correction is written down. We shall come back on flavour independence in Sec. 5, and stress the analogy with atomic physics, where the same $-1/r$ potential binds positronium, hydrogen and protonium atoms.

In the meson sector, we expect the lowest ($b\bar{c}$) meson approximately half between J/Ψ and Υ . In a flavour-independent potential, this is in fact a lower bound [11], i.e., we have

$$2(b\bar{c}) \geq (c\bar{c}) + (b\bar{b}). \quad (1)$$

If one knows the excitation spectrum of ($c\bar{c}$) and ($b\bar{b}$), one can extract model-independent bounds on the average kinetic energy in the ground state, which governs the evolution of the ground-state energy when the reduced mass varies. This leads to an upper bound on the lowest ($b\bar{c}$) state [4], and all predictions of realistic potentials nicely cluster near 6.26 GeV/ c^2 [12] in between the lower and the upper bounds provided by flavour independence.

Similar regularity patterns are expected in the baryon sector (the mathematics of the 3-body problem is of course more delicate than that of the 2-body one, and sometimes requires some mild conditions on the shape of the confining potential, which are satisfied by all current models [3]). For instance, one expects an analogue of (1)

$$2(ccq) \geq (ccq) + (qqq) \quad (2)$$

which leads to an upper bound (ccq) \leq 3.7 GeV for the centre of gravity of the ground-state multiplet of (ccq). A upper bound can also be derived for (ccs). On the other hand, the convexity relation

$$2(bcq) \geq (ccq) + (bbq), \quad (3)$$

cannot be tested immediately, as well as the even more exotic-looking [13]

$$3(bcq) \geq (bbb) + (ccc) + (qqq), \quad (4)$$

and its analogue with $q \rightarrow s$. Of more immediate use is the relation

$$(bcq) \geq (bqq) + (cqq) - (qqq), \quad (5)$$

which leads to a rough lower bound $(bcq) \geq 6.9 \text{ GeV}/c^2$, if one inputs the following rounded and spin-averaged values: $(bqq) = 5.6$, $(cqq) = 2.4$, and $(qqq) = 1.1 \text{ GeV}/c^2$.

To derive these inequalities, one uses the Schrödinger equation, even for the light quarks. Very likely, the regularities exhibited by flavour-independent potentials also hold in more rigorous QCD calculations and in the experimental spectrum. Any failure of the above inequalities would be very intriguing.

Sometimes, one can be more precise, and derive inequalities that include spin-spin corrections, for instance relations between $J^P = (1/2)^+$ baryons with different flavour content. See [3] for details.

Another mathematical game triggered by potential models consists of writing inequalities among meson and baryon masses. The basic relation is [3]

$$2(q_1 q_2 q_3) \geq (q_1 \bar{q}_2) + (q_2 \bar{q}_3) + (q_3 \bar{q}_1), \quad (6)$$

obtained by assuming that the potential energy operators fulfill the following inequality

$$2V_{qqq}(\mathbf{r}_1, \mathbf{r}_2, \mathbf{r}_3) \geq \sum_{i < j} V_{q\bar{q}}(|\mathbf{r}_i - \mathbf{r}_j|), \quad (7)$$

which holds (with equality) for a colour-octet exchange, in particular one-gluon exchange, and for the simple model

$$V_{q\bar{q}}(r) = \lambda r, \quad V_{qqq} = \lambda \min_j (d_1 + d_2 + d_3) \quad (8)$$

where d_i is the distance from the i -th quark to a junction J whose location is adjusted to minimize V_{qqq} [14]. We obtain for instance [1] $(ccq) \geq 3.45 \text{ GeV}/c^2$ for the $(1/2)^+$ state. This is rather crude, not surprisingly. Years ago, Hall and Post [15] pointed out in a different context that the pairs are not at rest in a 3-body bound state, and that their collective kinetic energy is neglected in inequalities of type (6).

3 Spectrum of doubly flavoured baryons

Computing the (QQq) energies in a given potential model does not raise any particular difficulty. The 3-body problem is routinely solved by means of the Faddeev equations or variational methods. On the other hand, successful approximations often shed some light on the dynamics. In particular, the Born–Oppenheimer method works very well for large ratios (M/m) of the quark masses. At fixed QQ separation R , one solves the 2-centre problem for the light quark q . The energy of q is added to the direct QQ interaction to generate the effective potential $V_{QQ}(R)$ in which the heavy quarks evolve. One then computes the QQ

energy and wave function. Note that one can remove the centre-of-mass motion exactly, and also estimate the hyperfine corrections.

The physics behind the Born–Oppenheimer approximation is rather simple. As the heavy quarks move slowly, the light degrees of freedom readjust themselves to their lowest configuration (or stay in the same n -th excitation, more generally). At this point, there is no basic difference with quarkonium. The $Q\bar{Q}$ potential does not represent an elementary process. It can be viewed as the effective interaction generated by the gluon field being in its ground-state, for a given $Q\bar{Q}$ separation.

The results shown in Table 1 come from the simple potential

$$V = \frac{1}{2} \sum_{i < j} \left[A + B r_{ij}^\beta + \frac{C}{m_i m_j} \boldsymbol{\sigma}_i \cdot \boldsymbol{\sigma}_j \delta^{(3)}(\mathbf{r}_{ij}) \right], \quad (9)$$

with parameters $\beta = 0.1$, $A = -8.337$, $B = 6.9923$, $C = 2.572$, in units of appropriate powers of GeV. The quark masses are $m_q = 0.300$, $m_s = 0.600$, $m_c = 1.905$ and $m_b = 5.290$ GeV. The $1/2$ factor is a pure convention, although reminiscent from the discussion of inequalities (6) and (7). The smooth central term can be seen as a handy interpolation between the short-range Coulomb regime modified by asymptotic-freedom corrections and an elusive linear regime screened by pair-creation effects. The spin-spin term is treated at first order to estimate M_0 . This model fits all known ground-state baryons with at most one heavy quark.

Table 1: Masses, in GeV, of (QQq) baryons in a simple potential model. We show the spin-averaged mass \bar{M} , and the mass M_0 of the lowest state with $J^P = (1/2)^+$.

State	ccq	ccs	bcq	bcs	bbq	bbs
\bar{M}	3.70	3.80	6.99	7.07	10.24	10.30
M_0	3.63	3.72	6.93	7.00	10.21	10.27

A more conventional Coulomb-plus-linear potential was used in Ref. [1], with similar results. One remains, however, far from the large number of models available for $(b\bar{c})$ [12], and the non-relativistic treatment of the light quark might induce systematic errors. The uncertainty is then conservatively estimated to be ± 50 MeV, as compared to ± 20 MeV for $(b\bar{c})$. Note also that the b -quark mass m_b is tuned to reproduce the experimental mass of Λ_b at 5.62 GeV/ c^2 , and this latter value is not firmly established.

The Born–Oppenheimer framework leaves room for improvements. A relativistic treatment of the light quark was attempted in [1], using the bag model. For any given QQ separation, a bag is constructed in which the light quark moves. The shape of the bag is adjusted to minimize the energy. In practice, a spherical approximation is used, so that the radius is the only varying quantity. The energy of the bag and light quark is interpreted as the effective QQ potential. Unlike the rigid MIT cavity, we have a self-adjusting bag, which

follows the QQ motion. Again, this is very similar to the bag model picture of charmonium [16].

Unfortunately, there are variants in the bag model, with different values of the parameters, and with or without corrections for the centre-of-mass motion. These variants lead to rather different values for the (ccq) masses [1]. This contrasts with the clustered shoots of potentials models, and deprives the bag model of predictive power in this sector of hadron spectroscopy.

It is hoped that the QQ potential will be calculated by lattice or sum-rule methods.

The excitation spectrum of (QQq) baryons has never been calculated in great detail, at least to our knowledge. In Ref. [1], an estimate is provided for the spin excitation (ground state with $J^P = (3/2)^+$), the lowest negative-parity level, and the radial excitation of the ground state.

The spin excitation is typically 100 MeV above the ground state, and thus should decay radiatively, with an $M1$ transition. The orbital and radial excitations of ccq are unstable, since they can emit a pion. The radial excitation of ccs can decay into $(ccq) + K$, but the orbital excitation cannot, and thus should be rather narrow, since restricted to $(ccs) + \gamma$, or to the isospin-violating $(ccs) + \pi^0$.

4 Decay of heavy baryons

The ground state of (QQq) decays weakly, with a great variety of final states. For instance, the remaining heavy flavour can stay in the baryon, or join the meson sector. Moreover, we have Cabibbo allowed, suppressed, or doubly suppressed modes. We refer to Savage et al. [5] for a comprehensive survey of 2-body channels of interest.

Inclusive decay rates are also of great importance. The difference between the D^0 and D^+ lifetimes tells us that the charmed quark, while decaying, does not ignore its environment. The main process is $c \rightarrow s + W$, and $W \rightarrow u\bar{d}$ for hadronic modes, but one should also consider W -exchange contribution for D^0 , interferences between the two \bar{d} in D^+ decay, $c\bar{s}$ annihilation for D_s , etc.

The lifetimes of single-charm baryons have been analysed by Guberina et al. [17]. The annihilation diagram requires antiquarks from the sea, and presumably does not play a very important role. On the other hand, W -exchange does not suffer from helicity suppression. We also have two types of interferences: between constituent u and u from W decay, and between constituent s and s from c transmutation. The prediction of [17]

$$\tau(\Omega_c^0) \lesssim \tau(\Xi_c^0) < \tau(\Lambda_c^+) < \tau(\Xi_c^+), \quad (10)$$

seems confirmed by recent data. If one extrapolates their analysis toward the (ccq) sector, one predicts [1]

$$\tau(\Xi_{cc}^+) < \tau(\Omega_{cc}^+) < \tau(\Xi_{cc}^{++}). \quad (11)$$

5 Exotic mesons with two heavy quarks

The situation and the perspectives for the pentaquark will be reviewed by Moinester [18]. The pentaquark is an exotic baryon ($B = 1$) with charm (or heavy flavour) $C = -1$, i.e., a $(\bar{Q}qqqq)$ structure. We shall discuss another possible multiquark, the tetraquark, with $B = 0$ and $C = 2$. The main difference, besides these quantum numbers, is that the pentaquark is tentatively bound by chromomagnetic forces, while the tetraquark uses a combination of flavour-independent chromoelectric forces, and Yukawa-type of long range forces.

Recently, Törnqvist [9], and Manohar and Wise [10] studied pion-exchange between heavy mesons, and stressed that, among others, some DD^* and BB^* configurations experience attractive long-range forces. By itself, this Yukawa potential seems unlikely to bind DD^* , but might succeed for the heavier BB^* system.

Years ago, Ader et al. [6] showed that $(QQ\bar{q}\bar{q})$ should become stable for very large quark-mass ratio (M/m), a consequence of the flavour independence of chromoelectric forces. The conclusion was confirmed in subsequent studies [7].

In the limit of large (M/m) , $(QQ\bar{q}\bar{q})$ bound states exhibit a simple structure. There is a localized QQ diquark with colour $\bar{3}$, and this diquark forms a colour singlet together with the two \bar{q} , as in every flavoured antibaryon. In other words, this multiquark uses well-experienced colour coupling, unlike speculative mock-baryonia or other states proposed in “colour chemistry” [19], which contain clusters with colour 6 or 8.

The stability of $(QQ\bar{q}\bar{q})$ in flavour-independent potentials is analogous to that of the hydrogen molecule [8]. If one measures the binding in units of the threshold energy, i.e., the energy of two atoms, one notices that the positronium molecule ($e^+e^+e^-e^-$) with equal masses is bound by only 3%, while the very asymmetric hydrogen reaches 17%. This can be understood by writing the molecular Hamiltonian as

$$\begin{aligned} H &= H_S + H_A \\ &= \left(\frac{1}{4M} + \frac{1}{4m} \right) (\mathbf{p}_1^2 + \mathbf{p}_2^2 + \mathbf{p}_3^2 + \mathbf{p}_4^2) + V \\ &\quad + \left(\frac{1}{4M} - \frac{1}{4m} \right) (\mathbf{p}_1^2 + \mathbf{p}_2^2 - \mathbf{p}_3^2 - \mathbf{p}_4^2) \end{aligned} \quad (12)$$

The Hamiltonian H_S , which is symmetric under charge conjugation, has the same threshold as H , since only the inverse reduced mass $(M^{-1} + m^{-1})$ enters the energy of the (M^+m^-) atoms. Since H_S is nothing but a rescaled version of the Hamiltonian of the positronium molecule, it gives 3% binding below the threshold. Then the antisymmetric part H_A lowers the ground-state energy of H , a simple consequence of the variational principle.

In simple quark models without spin forces, we have a similar situation. The equal mass case is found unbound, and $(QQ\bar{q}\bar{q})$ becomes stable, and more and more stable, as (M/m) increases. One typically needs $(bb\bar{q}\bar{q})$, with $q = u$ or d , to achieve binding with the nice diquark clustering we mentioned. However, if one combines this quark attraction with the long-range Yukawa forces, one presumably gets binding for $(cc\bar{q}\bar{q})$ with DD^* quantum numbers. A more detailed study is presently under way [20].

The experimental signature of tetraquark heavily depends on its exact mass. Above DD^* , we have a resonance, seen as a peak in the DD^* mass spectrum. Below DD^* , one should look at $DD\gamma$ decay of tetraquark. If it lies below DD , then it is stable, and decays via weak interactions, with a lifetime comparable to that of other charmed particles.

Acknowledgements

I would like to thank C. Quigg, S. Narison and D. Kaplan for having revived my interest in double-flavour spectroscopy, the organizers of the "Charm2000" Workshop for their invitation, and T. Mizutani for several discussions and a visit at Virginia Tech., where this review was prepared.

References

- [1] S. Fleck and J.-M. Richard, *Progr. Theor. Phys.* **82** (1989) 760.
- [2] S. Fleck and J.-M. Richard, *Part. World* **1** (1990) 67.
- [3] J.-M. Richard, *Phys. Rep.* **212** (1992) 1.
- [4] E. Bagan, H.G. Dosch, P. Gosdzinsky, S. Narison and J.-M. Richard, preprint CERN-TH 7141/94 (hep-ph 9403208).
- [5] M.J. Savage and M.B. Wise, *Phys. Lett.* **B248** (1990) 177;
M.J. Savage and R. P. Springer, *Int. J. Modern Phys.* **A6** (1991) 1701.
- [6] J.-P. Ader, J.-M. Richard and P. Taxil, *Phys. Rev.* **D25** (1982) 2370.
- [7] S. Zouzou et al., *Z. Phys.* **C30** (1982) 457;
L. Heller and J.A. Tjon, *Phys. Rev.* **D32** (1985) 755; **D35** (1987) 969;
J. Carlson, L. Heller and J.A. Tjon, *Phys. Rev.* **D37** (1988) 744;
L. Heller, in *The Elementary Structure of Matter*, Proc. Les Houches Workshop, 1987, ed. J.-M. Richard et al. (Springer Verlag, Berlin, 1988);
H.J. Lipkin, *Phys. Lett.* **B172**, 242 (1986).
- [8] J.M. Richard, *Phys. Rev.* **A49** (1994) 3579.
- [9] N.A. Törnqvist, *Phys. Rev. Lett.* **67** (1991) 556; *Z. Phys.* **C61** (1994) 525.
- [10] A.V. Manohar and M.B. Wise, *Nucl. Phys.* **B399** (1993) 17.
- [11] R.A. Bertlmann and A. Martin, *Nucl. Phys.* **B168** (1980) 111.
- [12] E. Eichten and C. Quigg, preprint Fermilab-pub-94-0320-T (hep-ph 9402210).
- [13] A. Martin, *Phys. Lett.* **B287** (1992) 251.
- [14] H.G. Dosch and V.F. Müller, *Nucl. Phys.* **B116** (1976) 470;
D. Gromes and I.O. Stamatescu, *Z. Phys.* **C3** (1979) 43;
P. Hasenfratz, R.R. Horgan, J. Kuti and J.-M. Richard, *Phys. Lett.* **B94** (1980) 401;
E. Bagan, J.I. Latorre, S.P. Merkuriev and R. Tarrach, *Phys. Lett.* **B158** (1985) 145;
J. Carlson, J. Kogut and V.R. Pandharipande, *Phys. Rev* **D27** (1983) 233; **D28** (1983) 2807.
- [15] R.L. Hall and H.R. Post, *Proc. Phys. Soc.* **90** (1967) 381.
- [16] P. Hasenfratz et al., *Phys. Lett.* **95B** (1980) 299.

- [17] B. Guberina, R. Rückl and J. Trampetic, Z. Phys. **C33** (1986) 297;
 see, also M.B. Voloshin and M.A. Shifman, Sov. Phys. JETP **64** (1986) 698;
 V. Gupta and K.V.L. Sarma, Int. J. Mod. Phys. **A5** (1990) 879.
- [18] M. Moinester, contribution to this Workshop.
- [19] Chan Hong-Mo, in Proc. IV European Antiproton Symposium, Barr, France, 1978, ed. A. Fridman
 (CNRS, Paris, 1979).
- [20] N.A. Törnqvist and J.-M. Richard, in preparation.

Future of Charm Photoproduction at Fermilab in the Next 3 Years and Beyond

John P. Cumalat

Department of Physics, University of Colorado, Boulder, Colorado 80309

Abstract

Fermilab charm photoproduction experiment E831 is described. The required E831 changes to both the E687 spectrometer and the wideband photon beam are explained. Several possible upgrades to E831 are discussed and a method for increasing the photon yield is presented. A much higher photon flux cannot be achieved without an accelerator energy upgrade.

1 The Features of an Incident Photon Beam

There are several good features to using a photon beam as compared to an incident hadron beam. First, a neutral beam passes through the spectrometer without interacting thereby reducing the singles rate in the spectrometer. Second, the charm production mechanism is well described by the photon-gluon fusion model. The background under the charm signals (outside the target) is well represented by a charm-anticharm Monte Carlo. Third, very few primary tracks are produced. Photoproduction experiment E687 has presented primary interaction charged track multiplicities that demonstrate that the mean charge track multiplicity (not including the charmed particles) is only 2.2. This small number of produced primary tracks in charm events makes photons an excellent system for examining excited charm baryon and meson states. It also allows for a quick reconstruction of the event. Fourth, the photoproduced charm cross section is roughly 1% of the total photon hadronic cross section. This charm to total cross section ratio is about 5 times higher than in a hadron beam.

The main bad feature of a photon beam is the large e^+e^- production rate relative to the hadronic interaction rate. For a beryllium target the e^+e^- rate is 500 times larger than the photon total cross section rate. This means that the experiment must resort to low Z (not so dense) target material. Another disadvantage of a photon beam is the beam flux limitation and the difficulty in collimating the beam. The large beam size might well be an advantage in high rate experiments.

2 Experiment E831

2.1 Introduction

Experiment E831 is based on photoproduction experiment E687 in which roughly 100,000 charm particles were reconstructed. Experiment E687 studied the production and decay of charm particles in a highly segmented and instrumented spectrometer. The E687 two-magnet spectrometer has 300 threshold Cerenkov cells, a 10 meter neutral Vee decay volume, gamma and pizero identification, electron and muon identification, a large charged particle acceptance covering the entire forward hemisphere, and most importantly, 12 microstrip planes with a total of 8256 pulse height analyzed strips. For more information on the E687 spectrometer the interested reader is directed to reference 1.

The E831 broadband photon group plans to accumulate 10^6 fully reconstructed charm particles. This represents a factor of 10 improvement in charm yield over E687. The study of the feasibility of this experiment was conducted at the 1989 Breckenridge meeting [2] and at the Snowmass 1990 meeting [3].

The physics of the experiment [4] will involve high precision studies of the D semileptonic decays, QCD studies of double D events, a measurement of the absolute branching fraction for the D^0 , D^+ , and the Λ_c^+ particles, searches for D^0 mixing, CP violation, rare and forbidden decays, fully leptonic decays of the D^+ and D_s^+ , and a systematic investigation of charm baryons and their lifetimes.

The new experiment will run at 5 times the previous photon flux. This increase in flux will be attained by reducing the secondary electron (positron) energy from 350 GeV to 250 GeV, running both positron and electron beams simultaneously, removing material in the beamline, and by increasing the incident proton intensity per pulse from 3×10^{12} to 4.5×10^{12} . Another factor of two increase in events is derived from a reduction in the experiment's deadtime and from improved spectrometer efficiency.

2.2 Spectrometer Upgrades

2.2.1 *Changes For Increased Rates*

The spectrometer requires several upgrades to handle the increased rate. (The instantaneous rate in E831 will be about $7 \times$ higher than in E687.) The muon gas proportional tubes in the experiment will be changed to scintillators. The Iarocci tubes used for the hadron calorimeter will also be changed to scintillator. The Proportional Wire Chambers will be changed to have lower gain and less noise. The central wires will be deadened and straw tubes will be installed in front of MWPC's P0, P1, and P2 to ensure that there are no dead tracking regions. Finally, the silicon microstrip system will be speeded up. A schematic drawing of the E831 spectrometer is presented in figure 1.

The critical change is obtaining a fast hadron calorimeter. The hadron calorimeter will

be used at the first level in triggering and should dramatically reduce the electromagnetic contamination in the triggers. The fast readout should allow the spectrometer to trigger on lower energy and hence the overall efficiency should improve. In addition, the tower geometry of the hadron calorimeter will allow identification of neutrons and K_L^0 's.

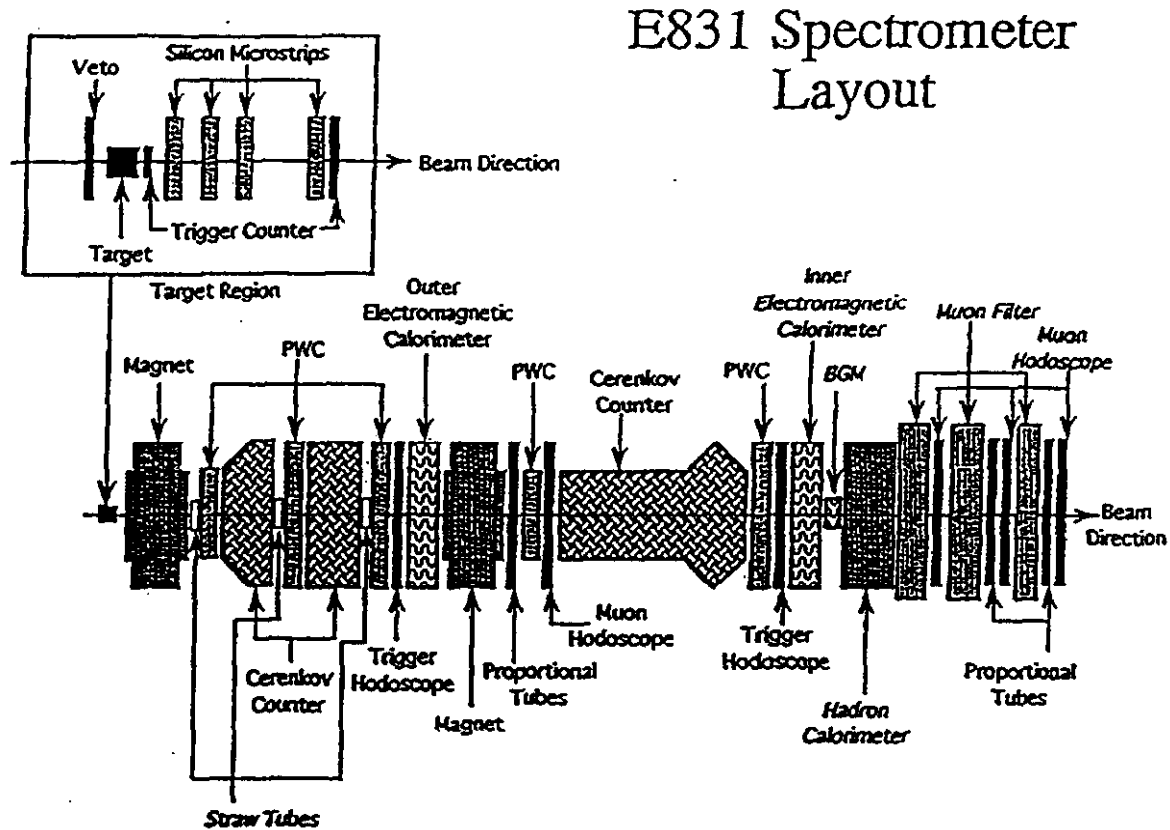


Figure 1: A Schematic Layout of the E831 Spectrometer

2.2.2 Changes For Improved Performance

Other significant upgrades to the E831 Spectrometer involve segmenting the experimental target and reducing the thickness of each silicon microstrip plane, building redundancy into and making finer the segmentation of the inner muon system to reduce muon misidentification, and replacing the inner electromagnetic calorimeter with lead glass.

The target segmentation is a major improvement. We have learned that decays outside of the target are entirely due to charm particles (see Figure 2). Inside the target there is additional background due to secondary interactions and probably background from strange particle production. Once the charm particle decays outside of the target a factor of 4 or more improvement in signal to noise is achieved. In E687 a 4 cm long block of beryllium has been used as the target. In this configuration only 14% of the reconstructed D^0 's decay in a material free region. Table 1 shows the increase in decays outside of the target under different

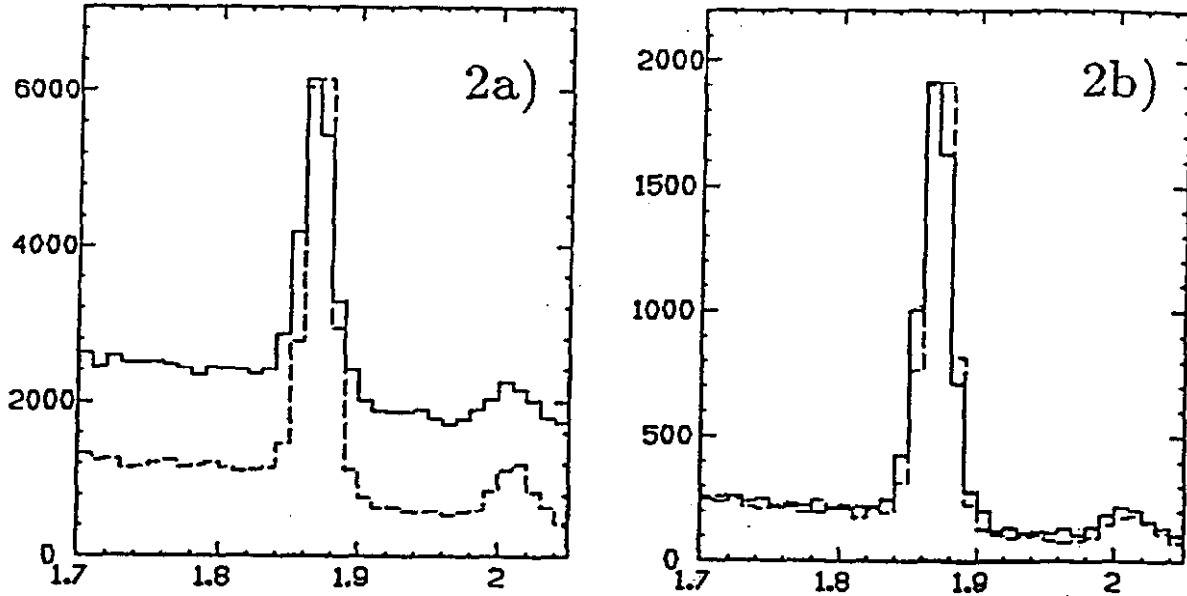


Figure 2: A mass plot of $D^+ \rightarrow K^- \pi^+ \pi^+$ with an $l/\sigma > 7$. Figure 2a only includes decays which occur inside the target. Figure 2b is the same mass distribution for decays occurring outside the target. The dashed curves are results from a $c\bar{c}$ Monte Carlo. The Monte Carlo matches the background outside the target, but falls short when the decay is inside the target.

conditions. As one can see it is possible to increase the number of D^0 's decaying outside the target by a factor of 3. It is also possible to increase the number of D^+ 's decaying outside the target by a factor of 2. By changing the target material from beryllium to diamond the signal to noise for reported signals should be significantly improved. The E831 collaboration is still evaluating the optimum arrangement of the target, but it is clear that large gains can be made.

Table 1: Percentage of Decays Outside the Target

Configuration	D^0	D^+
Solid 4cm long Be	14.3	32.9
Be segmented in 2 parts	26.9	47.3
Be segmented in 3 parts	37.3	51.0
Diamond (2 parts)	40.3	60.6
Diamond (3 parts)	49.3	63.0

Another significant improvement will be to reduce the amount of material in the target region. In E687 a thin scintillator, TR1, was placed between the beryllium target and the silicon microstrip. A hit in TR1 indicated that an interaction had occurred in the beryllium

target. In E831 this trigger counter will be removed to reduce the extrapolation error of the microstrip to the target.

The E687 silicon microstrip system is composed of 12 planes of 310 micron thick silicon. Every single channel is pulse height analyzed and a signal to noise for minimum ionizing tracks of about 30 to 1 is obtained. In E831 we plan to reduce the thickness of the silicon to cut down on multiple scattering. The impact parameter resolution at the target is limited by multiple scattering in the microstrip (a problem at low energy). By reducing the thickness of the silicon by 30% the impact parameter error for a 5 GeV track at the target is lowered by 15%. Our group is presently studying two planes from Micron Semiconductor, one of the planes is 140 microns thick while the other is 240 microns thick. The thickness of the planes was dictated by what the company had available. In figure 3 is presented the improvement in impact parameter in the x view as a function of momentum for the case of the removed trigger counter, TR1, and for the case of a 30% reduction in the silicon thickness.

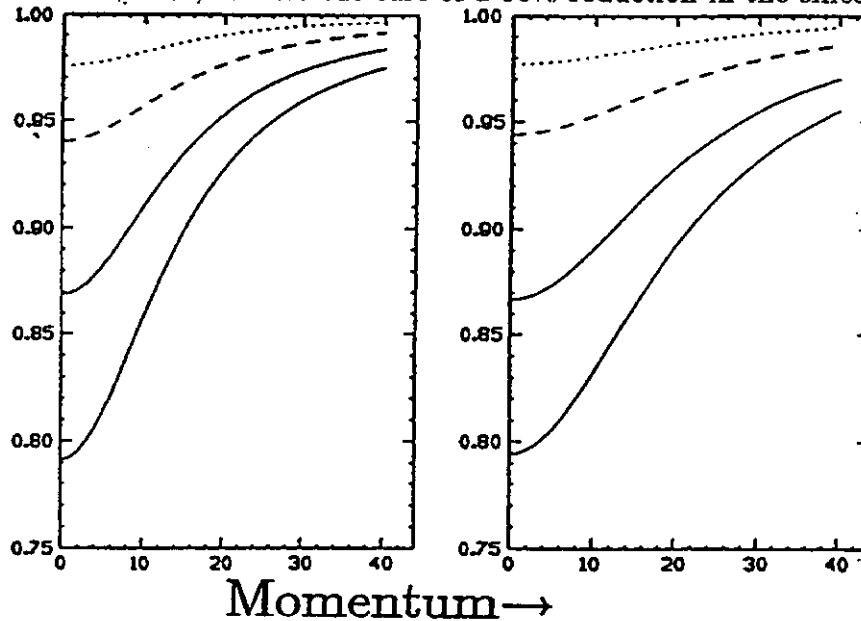


Figure 3: Reduction in Vertex resolution for the x and y views versus momentum. The upper dotted curve shows the improvement in the vertex resolution with the multiple scattering from the target removed. The dashed curve shows the effect of removing TR1. The upper solid curve is the change with the microstrip thinned by 30% while the lower solid curve is the improvement with both TR1 removed and the microstrip thinned.

Another major upgrade to the spectrometer will be to the muon system. The E831 muon identification is accomplished in two separate systems. The "inner" muon system identifies muons which pass through both magnets, while the "outer" muon system identifies muons which are only tracked through the first magnet. In E687 the outer muon system was not operational due to poor performance of phototubes in the magnetic field. In E831 fiber readout will be used to move phototubes to a lower field region. This change should result in a 50% increase in muon coverage.

The inner muon system in E687 consisted of 7 detector planes with 4 gas proportional tubes and 3 scintillator arrays located at two locations (See figure 1). Unfortunately, the

performance of this system was diminished because of a hole to transport the neutral beam to an experiment behind E687. For E831 the hole will be filled in, an additional 24 inches of steel will be added to reduce hadronic punchthrough from the calorimeter, and a third x-y array of scintillators will be added downstream of the hadron calorimeter. In this system alone we expect a factor two improvement in efficiency and a factor of $4\times$ improvement in pion misidentification. For charm decays containing muons we expect a factor of $20\times$ improvement beyond E687.

Lastly, the electromagnetic calorimetry will be changed from a strip readout scintillator detector to a tower geometry lead glass array. This modification will allow for better electron identification and much improved γ and π^0 identification.

3 Beyond the E831 Spectrometer

At the Breckenridge, 1989 study where the goal was 10^7 reconstructed charm particles it was concluded that an accelerator upgrade was necessary to increase the photon flux. If sufficient photon flux could be achieved, then there were several modifications that were needed to allow the spectrometer to survive the high rates. In this section the spectrometer upgrades necessary to survive the high rates will be presented followed by a discussion of possible improvements to the beam.

3.1 Improvements to the E831 Spectrometer

In order to be able to withstand high rates it is necessary that all detectors be fast and radiation hard. In particular all trigger counters need to have single bucket resolution. For the target region the beam will need to be spread out if silicon strip detectors are to be used or one may wish to count on diamond strip detectors being a proven technology.

3.1.1 Possible Target Region Improvements

For the target region segmented targets will be crucial to improve the signal to noise and to ensure that the background is well understood. With high rates where redundancy is important, it is beneficial to have all detector elements instrumented. Thus, the target should probably be instrumented. A good target would be a microstrip diamond detector where it might also be possible to look at the Cerenkov light. The ability to examine the Cerenkov light is interesting as the readout would not be sensitive to target fragments.

3.1.2 Target Region Tracking

The post target tracking will be accomplished with a microstrip detector, but the pitch in the detectors should be reduced from $25\mu\text{m}$ to $10\mu\text{m}$. The reduction in pitch has numerous advantages. First, the target can be moved closer to the first tracking device. This move will

improve the vertex resolution from the shortened extrapolation. Second, the background from the opposite charm particle will be reduced. Third, the instantaneous rate in each detector will be reduced. The microstrip detectors will also need to be made larger to increase the acceptance.

3.1.3 Spectrometer Tracking

The E687/E831 spectrometer traces particles with multiwire proportional chambers. In the higher rate environment of E831 there are 5 cm of wires that will need to be deadened. In a higher rate experiment the wire chamber system will have to be replaced with either straw tubes or scintillating fibers. An added benefit of changing to straw tubes or scintillating fibers is that the position resolution and hence, momentum resolution will be improved.

3.1.4 Particle Identification

The particle identification could be improved with the addition of a RICH counter. The RICH counter might take the place of C1 and C2.

Presently, the "outer" spectrometer in E831 does not have a hadron calorimeter. A hadron calorimeter could be added to identify K_L^0 's and neutrons in the outer spectrometer.

The electron identification of the electromagnetic calorimeters could be enhanced with the addition of TRD's.

3.1.5 Triggering

At high rates a better trigger will be necessary. For a first level master gate it would be possible to use a transverse energy trigger. This trigger has been shown in previous studies to enhance the charm production relative to the total hadronic cross section by a factor 5 or more. For the second level trigger an impact parameter trigger would be needed.

3.2 Photon Flux Improvements

It is difficult to imagine a major improvement in photon yield per incident proton without a change in the accelerator energy. Peter Kasper has calculated the photon flux as a function of primary proton energy and secondary electron energy. His results are presented in figure 4. If a 2 TeV proton energy was available, then a factor of 50 increase in yield is attainable. Peter Kasper's numbers do not include secondary interactions in the primary target and hence, further improvements are expected.

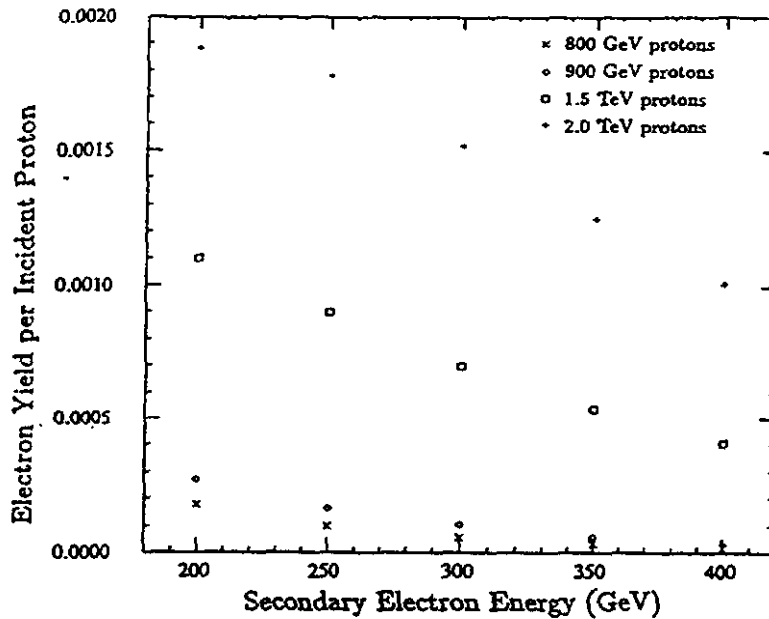


Figure 4: Electron yields for various incident proton energies.

4 Conclusions

In the next fixed target running period E831 will obtain 10^6 or better reconstructed charm particles. In experiment E831 it is anticipated that the signal to noise for charm signals will be improved over E687. Final states containing electrons or muons should see a larger than $10\times$ gain in yield.

It is my opinion that to achieve the CHARM2000 goal of 10^8 reconstructed charm particles a major accelerator upgrade is required.

5 Acknowledgements

I would like to thank the entire E687 and E831 collaborations for helping to design the E831 spectrometer. In putting together this talk I would especially like to thank Will Johns for reading this document, Peter Kasper for his work in calculating photon yields, and Jim Wiss for his comments on the target layout.

References

- [1] E687 Collab. P.L. Frabetti *et al.*, Nucl. Instrum. Methods A 320, 519 (1993).
- [2] "Physics at Fermilab in the 1990's", p.418-472, Breckenridge, August 15-25, 1989.
- [3] "Research Directions for the Decade", p.617-625, Snowmass, June 25-July 13, 1990.
- [4] "A High Statistics Study of States Containing Heavy Quarks Using the Wideband Photon Beam and the E687 Multiparticle Spectrometer", proposal P831 submitted to Fermilab, November, 1992.

CHARM BARYON PHYSICS - PRESENT AND FUTURE

J.S. Russ*

Physics Department
Carnegie Mellon University
Pittsburgh, PA 15213

Abstract

Current charm experiments still report meson samples that are 10 times larger than the most copious baryon sample, $\Lambda_c \rightarrow pK^-\pi^+$ reported from CLEO II or E687. Important results on the weak decay behavior of charm baryons are, nonetheless, starting to emerge. Next-run fixed target experiments at Fermilab promise to increase charm baryon statistics by factors > 10 for Λ_c^+ modes and even more for charm-strange baryons. Prospects for increases beyond these new projections are discussed.

1 Introduction

E781 [1] is designed to make a systematic study of charm baryon production and decay physics. As previous speakers at this conference have emphasized, charm baryon physics is now becoming a significant new source of information about the weak decays of hadrons containing a charm quark. In addition, recent observations of excited states of the Λ_c^+ [2] open the door to a rich spectroscopy of charm baryons, testing important aspects of Heavy Quark Effective Theory (HQET) or other confinement models.

One feature of the recent data is that it all comes from photoproduction, either real photons (E687) or virtual photons (Argus, CLEO II continuum charm). In both situations the charm baryon samples are dominated by Λ_c^+ states. The suppression of charm-strange baryons (Ξ_c^+ , Ξ_c^0 , Ω_c^0) in photoproduction *may* not have any physical reason; it may be purely instrumental. Nevertheless, the available information on charm-strange baryons is marginal. The E687 lifetime measurement of the Ξ_c^+ has about 30 events [3] compared to ≈ 1500 events in the Λ_c^+ lifetime sample [4]. CLEO II reports similar 100-event samples of charm-strange modes.

In contrast, early evidence from hadron experiments reports similar cross sections for charm-strange and Λ_c^+ states in modes whose branching ratios should be comparable [5]. The

*for the E781 Collaboration

original discovery experiment for the Ξ_c^+ was WA62, the CERN hyperon beam experiment at 135 GeV/c, which had acceptance only at large x_F [6]. Recently, first results have been reported at Moriond from the current CERN hyperon beam experiment WA89 [7]. Because results are available only as preliminary conference proceedings, I only cite the essential experimental features of those data. For details, one should consult the authors [7]. The intriguing new features of production by hyperons seen in their data include the following:

- i) Larger yield of $\Lambda_c^+ \rightarrow pK^-\pi^+$ than of $D^- \rightarrow K^+\pi^-\pi^-$, with a harder x_F distribution for the baryons than for the mesons.
- ii) Evidence of leading production of Σ_c^0 compared to Σ_c^{++} from the incident Σ^- beam.
- iii) Yields of $\Xi_c^+ \rightarrow \Xi^-\pi^+\pi^+$ and $\Xi_c^0 \rightarrow \Lambda^0 K^-\pi^+$ (first observation) are comparable to those of $\Lambda_c^+ \rightarrow pK^-\pi^+$.

These features suggest that hadronic production will be an extremely effective way to develop large samples of charm baryon decays.

2 Goals of Charm Baryon Studies

Broadly speaking, the physics goals of charm baryon studies fall into three principal categories:

- Weak Decay systematics, to illustrate the nature of non-factorizing contributions to the weak decay amplitude.
- Comparison of meson and baryon spectroscopy, to illustrate the degree to which the heavy nature of the charm quark regularizes the excitation spectrum for different charm hadrons.
- Understanding production systematics, including differences in “leading” behavior for different states - baryon versus meson - and different beam particles.

2.1 Weak Decays

Ultimately, the goal of the Weak Decay study is to achieve a complete description of charm hadronic processes on the basis of QCD calculations, either complete or on the lattice. This is not likely to be achieved soon, given the complexity of the problem. However, in order to guide theoretical development, it is important to have a comprehensive data set to highlight regularities. For charm mesons the development of the Mark III data, supplemented by E691 measurements, gave a huge impetus to the evolution of the weak decay picture in the late 1980's. Progress came from the comparison of D^+ , D^0 , and D_s^+ decays and excitation spectra, not from detailed studies of single states. Bigi, among others, has emphasized the need to include charm baryon results in this comparison [8].

For baryons, the semileptonic decays play an especially important role because of the reduction of strong-interaction corrections to the fundamental process. From the HQET viewpoint, this feature should make baryon decays look rather similar to meson decays. However, we note that the spin-orbit corrections for the baryon system are likely to be much smaller than the corresponding ones for mesons. In mesons, the hyperfine interaction determines the splitting from the lowest pseudoscalar ground states to the first vector excited states. For the Λ^0 the first excitation is a spin-orbit state, the $\Lambda(1405)^0$. How much does this excitation contribute to the semileptonic decay? It will surely be a function of q^2 . What does the Dalitz plot look like for this mode? A recent CLEO II study of partially-reconstructed modes showed that most of the Λ_c^+ semileptonic decays went to the ground state mode $\Lambda_c^0 e^+ \nu$, averaged over the Dalitz plot [9]. To make further progress will take much higher statistics, with large average efficiency per mode for all four stable charm baryon states.

2.2 Spectroscopy

The spectroscopy of the charm baryons is expected to look very much like the meson excitation spectrum, if HQET ideas are confirmed. However, the extra degrees of freedom in the baryon sector increase the complexity due to the interplay of the spin-orbit interaction of the heavy quark and the light di-quark system, compared with the spin-spin interaction when the di-quark is excited to spin 1 instead of spin 0. Lattice calculations, potential-model calculations and HQET have made predictions for these splittings in the meson case [10]. Some work has been done for the baryon sector, especially the simple case for the Λ_c^+ [11]. Extending the baryon data set to include excitations in the charm-strange sector is an important move to push further understanding.

2.3 Strong Production Physics

As discussed in Ridolfi's talk at this conference, charm production physics presents great technical problems for QCD analysis because the mass of the charm quark is of the same order as the QCD scale parameter μ_0 . This leads to uncertainties in the theoretical calculation that are large. In addition non-perturbative effects like "leading particle" behavior appear in the data, but are hard to treat in theory. Some enlightenment may come from measuring charm pair characteristics along with single charm distributions.

Nevertheless, charm production physics has many interesting features that require a lot more work to understand. We have alluded to the striking features of charm baryon production by hyperons as reported by WA62 and WA89. NA32 has reported that Λ_c^+ and $\bar{\Lambda}_c^+$ are produced with comparable rates for forward x_F from a π^- beam. E791 will soon have the data to make a statement about this effect at 500 GeV/c. Having an anti-baryon at large x_F is very hard to understand on the basis of perturbative QCD processes. At this conference Tang has reminded us of higher-twist effects that have been invoked to explain features of J/Ψ production for $x_F > 0.9$ via the Drell-Yan process. Whether this kind of an explanation can be applied to strong production processes to account for leading antibaryons is not at

all clear. Alternatively, Brodsky and Vogt have resurrected the *intrinsic charm* model to account for leading effects in charm meson production [12]. It remains to be developed for charm baryon states. The recent WA89 report of significant leading effects in charm baryon production by hyperons raise new questions about the ability of the intrinsic charm picture to account for apparent differences between proton, pion and hyperon beams.

3 Projections for Charm Baryon Physics at Fermilab

In the upcoming fixed target run E831(photoproduction) and E781(hadroproduction) plan to accumulate samples of about 10^6 reconstructed charm. Each will attack the weak decay physics and spectroscopy, with different emphases, reflecting differences in the meson/baryon balance and production mechanism effects. Previous talks at this conference have emphasized the impressive capabilities of E831. Let me advertise E781's potential and then make projections about future charm experiments.

3.1 E781 Design

E781 is a general charm experiment, emphasizing charm baryons and charm pair production. It uses a 3-stage magnetic spectrometer and provides good particle identification with a Ring-Imaging Cherenkov (RICH), electron TRD, and lead glass photon detectors that cover the forward hemisphere in the charm decay frame. The layout is shown in Figure 1 for the experiment in the Fermilab Hyperon Hall.

The hyperon beam is very flexible in particle composition. By changing the operating momentum, one can change the Σ/π ratio by a factor of 10, as can be seen from Figure 2. A momentum shift of this sort does not affect the charm production cross section significantly. E781 will run with a Σ flux of 10^6 Hz. Including deadtime effects, the data sample will be 3×10^{10} interactions per 1000 hours of data-taking.

The three stages of the spectrometer in Figure 1 are designed to perform the following functions:

- Stage 1: Large acceptance spectrometer with 2.5 GeV/c momentum cutoff. Designed for soft pions from excited state decays for spectroscopy, soft particles from decay of *partner charm* for charm pair studies.
- Stage 2: Forward spectrometer with 15 GeV/c momentum cutoff. Designed for efficient trigger and large acceptance for charm baryons having $x_F > 0.1$. Includes lepton identification via TRD (e) and RICH (e, μ), useful π/K separation from 20 to 225 GeV/c, K/p separation from 40 to 480 GeV/c.
- Stage 3: Final measurement of ultra-high momentum charged tracks, measurement of proton momenta from downstream $\Lambda \rightarrow p\pi^-$ decays.

- Beam region: Silicon strip detector coverage of the beam region, to provide precision tracking for high momentum, small angle tracks. This is important not only for charm physics, but for small- t physics for which this spectrometer is also ideally suited.
- Vertex region: highly redundant 20-plane, 4-view silicon strip system with VLSI read-out. Measured performance in E781 test run and in WA89 proved high efficiency and excellent resolution (4 μm for planes with 20 μm pitch).

3.2 Charm trigger

E781 plans to select charm candidates from the overall data stream *before* writing them to tape. This is, of course, a two-edged sword:

It greatly reduces the offline analysis load following the experiment, but
it requires an online physics monitor to ensure that the data are not lost.

For E781 the key is the operation of the 2-stage magnetic spectrometer to reduce the total number of tracks that the charm trigger stage must process. As Jeff Appel showed in his introductory talk at this conference, hadronic interactions usually produce about 15 tracks within a forward 150 mrad cone. For E781 non-charm interactions generally have only 5 tracks after the second magnet (M2). In only 10% of cases are there more than 3 *positive* tracks, so this provides the first stage hardware trigger with a rejection factor of 8-10 against non-charm interactions. Full readout occurs at this stage and takes less than 30 μs .

The charm trigger is *primarily* topological, based on evidence for a secondary vertex. In E781 this requirement is imposed by projecting every M2 track segment back upstream into the silicon vertex detector, to ask if there is a silicon segment that points back toward the intersection of the beam track with the center of one of the 5 production targets. Each target foil is at most 1.5 mm thick, so that smearing of the transverse resolution due to finite target thickness is small. Because the angular acceptance of M2 is 30 mrad, the worst-case geometric effect is 22 μm . We have found by simulation studies that a 30 μm cut on this variable, called *miss distance*, keeps the non-charm background trigger rate below 1%, *assuming perfect tracking*. This says that the fake trigger rate will be dominated by tracking mistakes, not measurement errors.

To establish the fake trigger rate, we are now making a full GEANT simulation, using silicon detector noise and response data from the E781 test run. That test experiment studied interactions from 400 GeV pions in a single thick target (6% λ_{int} Al). The fake track probability/event inferred in that analysis was $< 5\%$ [13]. This already meets the needs for E781. The full vertex detector will do better.

This trigger is efficient for charm hadron decays with lifetimes greater than 100 fs. Because it is done in software, we can merge other triggers that select characteristic decay modes, e.g., multiple strangeness in Ξ_c^0 or Ω_c^0 decays. If we use the RICH to select events that

have both a K^- and a proton or, even better, a K^- and a Λ decay candidate, our simulations indicate that we will achieve the required software rejection of hyperon beam inelastic events without using a miss-distance cut. Thus, we can improve sensitivity to exotic final states or very short lifetime decays. This flexibility indicates the power of the computational trigger to respond to different kinds of information from the detector in making a trigger decision.

Other aspects of the trigger should be noted. The topological trigger makes no discrimination between mesons and baryons. E781 expects to have the largest sample of meson semileptonic decays of any experiment, present or planned, among other aspects of the data. To address the *anti-baryon* production question raised earlier, we note that while our trigger requires 3 positive tracks after M2, the hardware trigger efficiency for the decay $\bar{\Lambda}_c^+ \rightarrow \bar{p}K^+\pi^-$ is more than half that of the corresponding baryon decay. This sensitivity to charm states with only *one* positive track in the final state occurs because of the extra tracks from the non-charm portion of the interaction. The software trigger will still require a suitable miss-distance from such events in order to pass the tape-writing selection.

3.3 Event Isolation

The software trigger for most charm states includes a miss-distance cut of 30 μm . This automatically imposes a cut on the statistical significance of the separation between primary and secondary vertices, one of the standard charm discriminants in fixed target experiments. As a consequence, *most* of the events listed in Table 2 will be useful for analysis. To illustrate this, we show in Figure 3 the L/σ plot for $\Lambda_c^+ \rightarrow pK^-\pi^+$ at $x_F = 0.3$. This distribution looks very similar at other x_F values. Note that small L/σ values, corresponding to difficult-to-analyze short decay lengths, are suppressed by the trigger. The present analysis does not yet include constraints on the primary vertex error imposed by the thin target structures.

3.4 Yields

The goal of E781 is to accumulate more than 10^6 reconstructed charm, half of them baryons. Because this is a new experiment, we have to take a conservative point of view in estimating yields. For pion data, we have used the 230 GeV results from NA32, scaled up by a factor of 2 in cross section, with a slightly steeper x_F distribution and the same p_T spectrum. For Σ^- data we use the WA89 cross section at 330 GeV with *no* scaleup for energy *and* with no scaleup to extend the x_F range below their quoted limit of 0.2.

To convert these to E781 yields, we choose 1000 hours of data, 1000 seconds/hour [12 weeks of good data at 83 useful hours/week], 4% inelastic interaction probability, and $A^{1/3}$ scaling of charm production compared with inelastic interactions. For E781, the target \bar{A} is 32.8. An overall operating efficiency of 80% for the experiment is assumed. This gives a sensitivity of 2300 charm events/nb of cross section for 100% efficiency. Table 2 gives the major factors affecting E781 efficiencies for the various modes as *currently* calculated by our simulation and converts to yields. Note that the trigger efficiency is weighted by the cross

beam	Mode	Expt	x_F power	$\sigma \cdot BR$ (nb)	E781 $\sigma \cdot BR$	E781 x_F power
π^-	$\Lambda_c^+ \rightarrow pK^-\pi^+$	NA32	3.5 ± 0.5	180 ± 36	360	4.2
π^-	$\Xi_c^+ \rightarrow \Xi^-\pi^+\pi^+$	NA32	?	130 ± 95	240	4.2
π^-	$D_s^+ \rightarrow K^+K^-\pi^+$	NA32	3.7 ± 0.25	67 ± 15	130	4.2
π^-	$D^0 \rightarrow K^-\pi^+$	NA32	3.7 ± 0.2	230 ± 40	460	4.2
Σ^-	$\Lambda_c^+ \rightarrow pK^-\pi^+$	WA89	3.7 ± 1.3	300 ± 180	330	4.2

Table 1: Selected charm cross section parameters

section form

$$d\sigma/dx_F = (1 - x_F)^{4.2}$$

for *all* states. The reconstruction efficiency is the geometric reconstruction including detector resolution and multiple Coulomb scattering in targets and detectors. It does not yet include effects of pattern recognition mistakes. It does include:

- a) primary vertex track assignment, x_F -averaged
- b) secondary vertex search and track assignment, x_F -averaged

The efficiencies quoted include only events in which all charm tracks are correctly assigned to the decay vertex by purely geometric analysis. There are additional event candidates with one additional track that can be excluded by kinematic analysis or further selection. Such steps would raise this efficiency for all-charged events but may not be possible for states with neutrals.

Mode	$\epsilon_{trigger}$	ϵ_{track}	ϵ_{recon}	E781 yield	yield including anticharm
$\Lambda_c^+ \rightarrow pK^-\pi^+$	0.19	0.88	0.55	75,000	$\leq 115,000$
$\Xi_c^+ \rightarrow \Xi^-\pi^+\pi^+$	0.16	0.80	0.5	40,000	$\geq 40,000$
$D_s^+ \rightarrow K^+K^-\pi^+$	0.24	0.88	0.64	36,000	55,000
$D^0 \rightarrow K^-\pi^+$	0.15	0.92	0.6	86,000	170,000

Table 2: E781 efficiency factors and yields in selected modes from π^- beam

This table includes anti-particle yields based on the NA32 report. For mesons this is likely to be a good approximation. For baryons E791 results will update the situation. In most cases from the pion beam, the anti-particles have a relative trigger efficiency that is 0.5-1.0 of that quoted for the particle. Thus, the overall sample is larger by a factor of 1.5-2.0, as shown in the last column. There are many modes with significant branching ratios and good acceptance factors that are not included in this sampling. The point of this table is to demonstrate the broad range of final states to which E781 has good sensitivity and to reinforce the argument that we do expect 10^6 reconstructed charm.

It is more difficult to project the range of charm yields from the hyperon beam, just because cross section information is just now starting to emerge from the WA89 analysis.

However, we can do something equivalent: scale yields based on acceptance, rejection factors and numbers of triggered events. At this stage such projections are good only to a factor of 2-3, but they are indicative. To make the comparison carefully requires knowing details of the analyses. We assume the following about WA89 data processing:

- WA89 average efficiency for $\Lambda_c^+ \rightarrow pK^-\pi^+$ is 1% in 1991 data, 2.5% in 1993 and 1994 data for $x_F > 0.2$ and the same cuts.
- WA89 trigger rejection factor compared to inelastic interactions is 5
- WA89 L/σ cut is 5, comparable to E781 software trigger.

The WA89 data sample is 100M triggers from 1991, 200M from 1993, and another 200M expected in 1994. With these assumptions, we can project WA89 observed signals in particular final states to E781 yields:

- WA89 observes 2×10^9 total interactions in all runs; E781 will have 30×10^9 .
- E781 average efficiency/mode is 8%.
- Operation at 600 GeV increases the cross section by a factor 1.5.
- Both WA89 and E781 will improve the 1991 acceptance factor for Ξ_c^0 by a factor of 2 due to improved vertex detectors.

Mode	WA89 (1991)	WA89(total)	E781 (estimated)
$\Lambda_c^+ \rightarrow pK^-\pi^+$	65	650	50,000
$\Xi_c^+ \rightarrow \Lambda K^-\pi^+\pi^+$	42	400	30,000
$\Xi_c^+ \rightarrow \Xi^-\pi^+\pi^+$	38	400	30,000
$\Xi_c^0 \rightarrow \Lambda K^-\pi^+$	32	600	50,000

Table 3: WA89 and E781 projected yields in selected modes from Σ^- beam

Comparing the overall yields, one sees that the π^- and Σ^- beams will give comparable numbers of charm baryons in comparable amounts of times. The differences expected include:

- comparable anti-charm yields from π^- but not from Σ^-
- suppressed meson production from Σ^- compared to π^-
- enhanced leading effects for Σ^- compared to π^-

The ability of E781 to operate with both beams in the same apparatus at the same time *and* to compare physics with online analysis will be of great importance in optimizing the charm information from a given running time.

4 Conclusion

Charm baryon physics is beginning to achieve the statistical sensitivity to theoretical predictions that has characterized charm meson physics for the past five years. Measuring the familial characteristics of charm baryon decay modes will sharply limit the kinds of theoretical explanations needed to account for the large range of charm baryon lifetimes. Precision measurements of the lifetimes and the semileptonic branching ratios for all charm hadrons, both mesons and baryons, is a stringent test of the fundamental idea of HQET to charm. Particularly in the charm-strange sector, E781 is poised to make a vital contribution.

There are also a number of strong-interaction questions to be addressed. The flexibility of the hyperon beam to deliver pions, hyperons, or protons will permit detailed comparisons of the large- x_F behavior of charm production, where some new effects have been proposed. Also, the high sensitivity of the experiment should allow the observation of doubly-charmed baryons. Models discussed at this conference by Richard predict the spectrum and general decay features of these states, based on QCD potential models. Finally, having good acceptance for charm pairs will improve the data for studying QCD in the difficult limit of charm hadroproduction. Currently the data are too sparse to tell what the effects of the scale uncertainty in the model calculations might do, as Ridolfi described at this conference.

There is much work to be done. E781 will make a large step forward in charm baryon physics.

5 Prospects for the Future

It is presumptuous to discuss how to improve an experiment that has not yet run. However, at this stage in the planning for E781, we can address the question of how to aim for a charm experiment to produce 10^8 reconstructed charm. First, from Table 1 one sees that the charm baryon cross sections from π^- and Σ^- beams are comparable. The charm *meson* cross sections are suppressed in the Σ^- beam, having a much steeper x_F spectrum, according to WA89. Therefore, Σ^- production is favored for a charm *baryon* experiment, π^- production for a *general* charm experiment. Because available pion beams can be at least an order of magnitude more intense than a hyperon beam, due to focussing, the π^- beam is probably favored for ultra-high-statistics charm. Another advantage of a π^- beam is that no beam particle identification is required. At high intensity, a sizeable fraction of RF buckets are likely to have more than one particle. Beam particle *counting* is a big problem, let alone identification.

A second point for discussion is the trigger rejection ratio. The E781 trigger scheme is deadtime limited, despite careful attention to fast-response readout systems. For higher-statistics experiments, details like drift times in gas detectors may become serious limitations. Pipelined front end electronics will be important, but even then it will be hard to run an open trigger. For E781 the front end bandwidth is 130 MB/sec. This is dominated by the loose hardware trigger, prompted by a relatively open charm trigger. To improve the charm

on tape by a factor of 100, one will have to improve the combination of front-end data rate and hardware rejection factor by a factor of 100 in some ratio. This is a formidable challenge.

References

- [1] E781 Collaboration: Carnegie Mellon University, Fermilab, University of Iowa, University of Rochester, University of Washington, Petersburg Nuclear Physics Institute, ITEP(Moscow), IHEP(Protvino), Moscow State University, University of São Paulo, Centro Brasileiro de Pesquisas Físicas, Universidade Federal de Paraíba, IHEP (Beijing), University of Bristol, Tel Aviv University, Max-Planck-Institut für Kernphysik-Heidelberg, Universidad Autonoma de San Luis Potosi.
- [2] H. Albrecht *et al.*, Phys. Lett. B 317, 227 (1993); P. L. Frabetti *et al.*, Phys. Rev. Lett. 72, 961 (1994); cf. M. Battle *et al.* and D. Acosta, *et al.* in Proceedings of the International Symposium on Lepton and Photon Interactions, Ithaca, New York, (1993).
- [3] P.L. Frabetti *et al.*, Phys. Rev. Lett. 70, 1381 (1993).
- [4] P.L. Frabetti *et al.*, Phys. Rev. Lett. 70, 1755 (1993).
- [5] S. Barlag *et al.*, Phys. Lett. B 233, 522 (1990); *ibid.*, B 247, 113 (1990).
- [6] S.F. Biagi, Phys. Lett. 122B, 455 (1983); *ibid.*, 150B, 230 (1985).
- [7] A. Simon, Moriond presentation, March, 1994.
- [8] I. I. Bigi, CERN-TH.7050.93.
- [9] T. Bergfeld *et al.*, Phys. Letters B323,219 (1994).
- [10] cf N. Isgur and M. B. Wise, Phys. Rev. Lett. 66, 1130 (1991).
- [11] see also N. Isgur and G. Karl, Phys. Rev. D 18, 4187 (1978); L. A. Copley, *et al.*, Phys. Rev. D 20, 768 (1979); T. DeGrand, *et al.*, Phys. Rev. D 12,2060 (1975).
- [12] R. Vogt and S. J. Brodsky, SLAC-PUB-6468, April, 1994.
- [13] J. Russ *et al.*, in DPF '92, C. H. Albright, P. H. Kasper, R. Raja, J. Yoh, eds., (World Scientific) 1746 (1992).

J. Lach, J. Russ
 July 3, 1994
 H-460R5

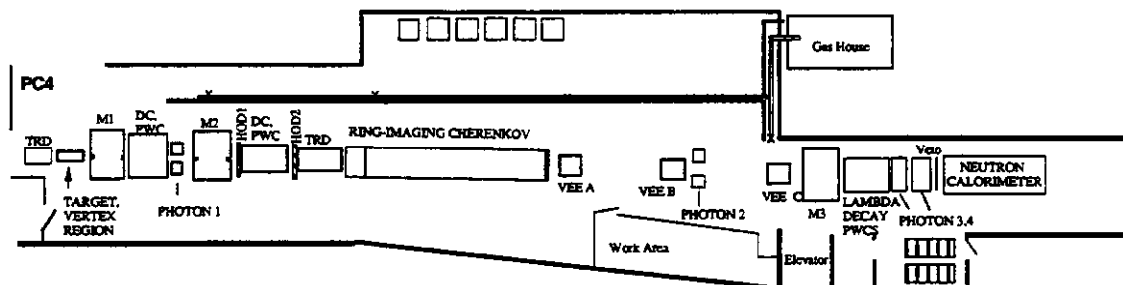


Figure 1: E781 layout in Fermilab Hyperon Area

Negative Beam Fraction at $P_t=0$, $z=10\text{m}$

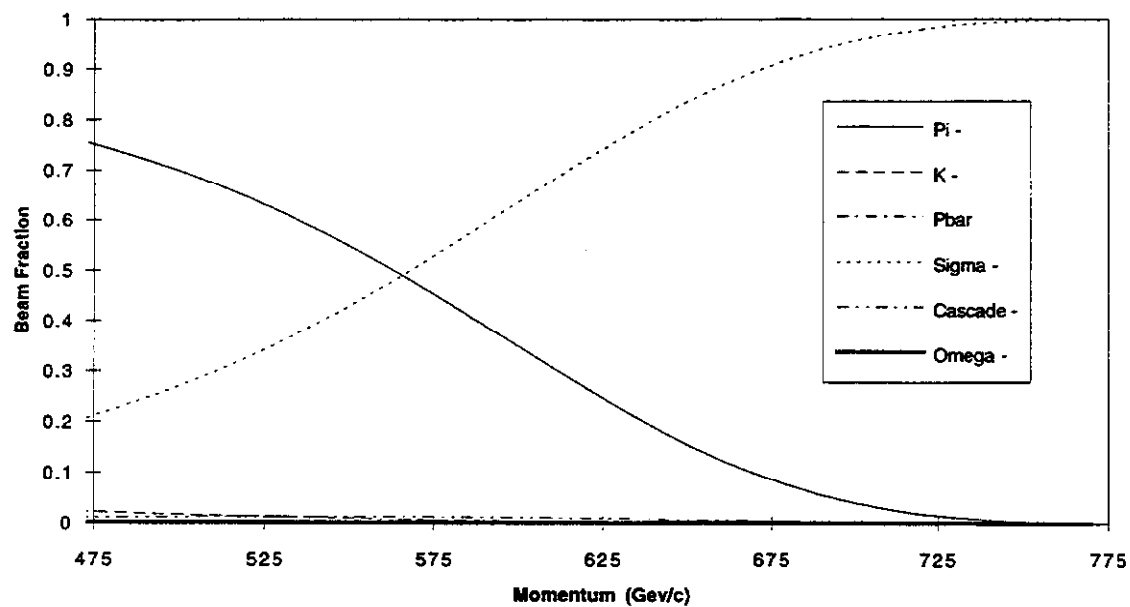


Figure 2: E781 Hyperon Beam Composition versus Momentum

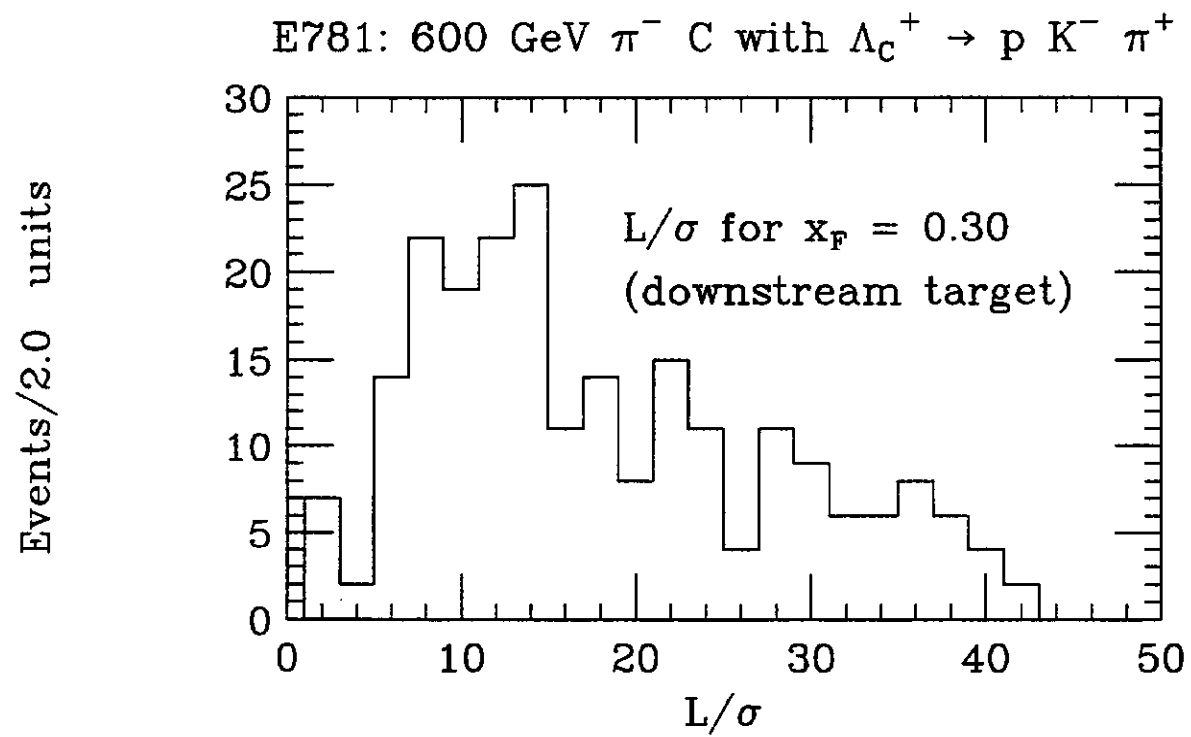


Figure 3: E781 Vertex significance at $x_F = 0.3$

Channeling Spin Precession as a Technique for Measuring Charm Baryon Magnetic Moments

Richard A. Carrigan, Jr.

Fermi National Accelerator Laboratory, Batavia, IL 60150, USA

Vincent J. Smith

H. H. Wills Physics Laboratory, University of Bristol, UK

Abstract

Measurements of hyperon magnetic moments have provided interesting insights into quark models. Charm baryon magnetic moment measurements could provide direct information on the magnetic moment of the charm quark. A recent demonstration of spin precession using channeling in a bent crystal offers the interesting possibility of a technique to measure magnetic moments of charm baryons. Accumulating evidence indicates the tools used for hyperon magnetic moment measurements, polarized production and decay asymmetries, will also be available for charm baryons. Channeling measurements may be possible but they will require challenging beam conditions.

1 Charm Baryon Magnetic Moment Predictions

The non-integer values of the proton and neutron magnetic moments are good evidence that baryons are composite particles. An early success of the simple quark model was the explanation of these magnetic moments in terms of the inferred magnetic moments of the valence quarks. This model was extended to hyperon magnetic moments by taking the expectation values of the valence quark magnetic moments in the baryon wave-function [1]. This gives the following relations for the magnetic moments :

$$p = uud = \frac{4}{3}u - \frac{1}{3}d \quad n = ddu = \frac{4}{3}d - \frac{1}{3}u \quad \Lambda = uds = s.$$

The measured values of the proton, neutron and Λ moments,

$$\mu(p) = 2.793 \text{ nuclear magnetons (nm)} ; \mu(n) = -1.913 \text{ nm} ; \mu(\Lambda) = -0.613 \text{ nm}$$

can be used to estimate the quark moments :

$$\mu(u) = 1.852 \text{ nm} \quad \mu(d) = -0.972 \text{ nm} \quad \mu(s) = -0.613 \text{ nm}$$

These values of quark magnetic moments are then used to predict the magnetic moments of the other hyperons [2]. For example, $\Sigma^+ = uus = \frac{4}{3}u - \frac{1}{3}s = 2.673 \text{ nm}$ (experimentally [3], this is $2.461 \pm 0.005 \text{ nm}$.)

These predictions, and the experimental values, are plotted by the PDG on p VII.59 of the 1992 'Particle Properties' [4]. It is seen that the values are in agreement with the simple quark model at the 10% level : the deviations must hold more information about the quark

structure of baryons. There are many theoretical strategies for extensions to the simple quark model (for a review and list, see the thesis of A. Morelos [5]). Examples include changing the effective quark mass in the different baryons, adding non-valence quarks (polarized sea), carrying out bag model calculations, or with lattice QCD. But at the 10% level, the SQM results are satisfactory for making initial predictions in the charm sector.

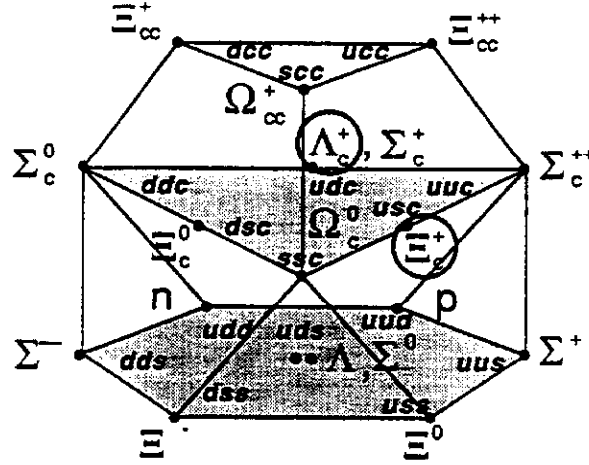


Figure 1: 20-plet with SU(3) octet showing singly-charged charm baryons that can be measured.

The stable single-charm baryons are members of the $J = \frac{1}{2}$ 20-plet of SU(4) (fig.1). They are on the center level, while the familiar octet baryons of SU(3) lie below.

In order to make predictions of the magnetic moments of these baryons, it is necessary to assume a value of $\mu(c)$: if the charm quark is a Dirac particle with charge $=\frac{2}{3}e$ and mass $\approx 1.68 \text{ GeV}/c^2$, then $\mu(c) = 0.37 \text{ nm}$.

However, only 4 single-charm states are stable :

Λ_c^+	Ξ_c^+	Ξ_c^0	Ω_c^0
<u>udc</u>	<u>usc</u>	<u>dsc</u>	<u>ssc</u>

(An underlined pair of quarks represents an antisymmetric (spin singlet) combination, with no net magnetic moment from this pair.)

Furthermore, only positively charged particles are suitable for measurement by the channeling method. Thus it appears that Λ_c^+ and Ξ_c^+ are the only charm baryons able to be measured by the channeling method, and that they should have very similar magnetic moments ($\approx 0.37 \text{ nm}$).

It is important to note that it is not just the magnetic moment itself which determines the precession angle, but the g -factor of the particle under study : $g = 2 \frac{\mu}{Q} \frac{m_R}{m_P}$

$$g(\Lambda_c^+) = 2 \times 0.37 \times \frac{2265}{940} = 1.80 \quad g(\Xi_c^+) = 2 \times 0.37 \times \frac{2467}{940} = 1.95.$$

(These values should be compared with $g(\text{proton}) = 2\mu(p) = 5.586$)

So both are expected to be very close to $g = 2.0$, which would mean very little precession (see below).

Motivated by the deviations from the simple model in the case of hyperon magnetic moments, a number of theoretical predictions for Λ_c^+ and Ξ_c^+ have been made (see table 1.)

		Λ_c^+, Ξ_c^+
Independent quark model following DGG [2]	Pandit <i>et al.</i> [19]	0.370
Independent quark model log V in spirit of Quigg and Rosner [23]	Jena and Rath [20]	0.352
MIT bag model	Bose and Singh [21]	0.503
Topological soliton	Oh <i>et al.</i> [22]	0.28–0.31

Table 1: Some charm baryon magnetic moment predictions (in nuclear magnetons)

2 Requirements for a Charm Magnetic Moment Measurement

To measure a charm baryon magnetic moment it is necessary to produce a substantial spin rotation in the short life of the particle. Since charm lifetimes are typically a thousand times shorter than hyperons, the conventional approach would require magnetic fields of order 1000 tesla for charm particles with momenta in the 0.5–1 TeV/ c range. Channeling in a bent crystal can provide such spin rotation within the charm particle lifetime, as is discussed in the next section. Three other elements are needed: 1) a production mechanism that produces polarized, short-lived baryons, 2) a decay mode with a non-zero asymmetry parameter to use as a polarization analyzer, and 3) samples of channeled, polarized short-lived baryons on the order of 10,000 events or more.

A group working with the BIS-2 spectrometer at Serpukhov [6] has reported a limit on the polarization of Λ_c^+ produced by 40-70 GeV neutrons that is about two σ away from zero and in line with hyperon polarizations. More recently Jezabek *et al.* [7] have reported evidence for polarization in a 121 event sample from the ACCMOR detector at CERN (NA32). E687, a high-statistics charm production experiment at Fermilab, and WA89, a hyperon beam charm production experiment at CERN, may shed more light on production polarization in the near future.

The ACCMOR analysis was based on the decay mode $\Lambda_c^+ \rightarrow pK^-\pi^+$, a mode with a branching ratio of 3.2%. Because this is a three-body decay they must use a technique similar to the approaches suggested by Berman and Jacob [8] or Bjorken [9]. The Bjorken approach extends the alpha, beta, gamma formalism used for two-body hyperon decays to multi-body modes. Note that information on the final charm baryon spin direction could

also be inferred from observation of the decay of the daughter baryon. For example, the Λ^0 will carry information on the spin direction of its parent.

Groups at Cornell [10] and DESY [11] have now reported measurements of the Λ_c^+ decay asymmetry parameter for the decay $\Lambda_c^+ \rightarrow \Lambda^0 \pi^+$. Both groups get values of $\alpha \approx 1.0 \pm 0.4$ so that the asymmetry is pleasingly large. This is also in line with theoretical estimates. The branching ratio to this channel is about 0.6%. Small branching ratios to two body-states are a general problem for charm baryon studies. On the other hand, the Bjorken formalism may be able to be exploited for the other states.

A sample of about ten thousand polarized charm baryons is needed for a measurement. The largest sample of $\Lambda_c^+ \rightarrow p K^- \pi^+$ so far published for fixed target running in a hadron beam is 154 events by ACCMOR in 1990 [12], the data set used for the Jezabek *et al.* analysis. Currently the published world sample of Λ_c^+ is less than 2000. E791 now has an order of magnitude more data on tape than the ACCMOR sample. (However there may be little or no polarization since the baryons are produced by pions at small angles.)

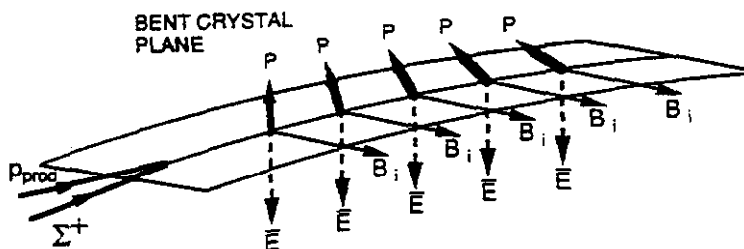


Figure 2: Schematic illustration of channeling spin precession.

3 Channeling Spin Precession

When a positively-charged particle moves through a crystal close to a plane or an axis, it is channeled [13]. For an angle smaller than the so-called critical angle the particle glides back and forth between the planes, repelled by the higher positive charge density near the nuclear centers. The critical angle is small, so that the angular acceptance for channeling is small.

Energy loss for channeled particles is smaller than random particles because there are, on average, fewer electrons in the channel. Measurement of the energy loss of channeled particles using detectors implanted in semiconducting material provides a useful indicator of channeling behavior.

Down to a certain radius of curvature, the Tsyanov radius, a channeled particle in a bent crystal follows the bend. In the extreme relativistic limit the Tsyanov radius is:

$$R_T = pc/eE_c$$

where e is the charge of the electron and E_c is the critical field at which the particle no longer channels. In practical experiments the radius of curvature must be several times larger than

the Tsyganov radius to avoid significant dechanneling. The Tsyganov radius is proportional to $1/Z$ where Z is the nuclear charge of the crystal material. Increasing from $Z=14$ (Si) to $Z=32$ (Ge) or $Z=74$ (W) could give substantially higher fields as well as larger channeling critical angles. However, crystals with low dislocation densities are needed for high energy channeling. It is here that Si excels.

The average centripetal electric field in the crystal giving rise to the bend transforms into a magnetic field in the particle center of mass. This field is equivalent to the field that would deflect the particle through the angle of the bent crystal.

The spin of a channeled particle moving in a bent crystal should precess through an angle ϕ given by:

$$\phi = \gamma\theta(g - 2)/2$$

for $\gamma \gg 1$, where γ is the Lorentz factor, g is the gyromagnetic ratio, and θ is the deflection angle of the channeled particle [14]. The channeling spin precession process is illustrated schematically in fig.2. The crystal bend produces an average electric field that points in to the center of curvature. This results in the net effective magnetic field perpendicular to the plane of curvature. The spin of a particle moving in the channel precesses around that effective field.

Equivalent fields up to 1000 tesla are possible. In the recent demonstration of channeling spin precession done in E761 at Fermilab [15], the equivalent field was 45 tesla. The equivalent magnetic field for bent crystal channeling for the case $\gamma \gg 1$ is:

$$B = p/0.3R$$

(here B is in tesla, p , the momentum, is in GeV/c, and R , the radius of curvature, is in m).

Because they produce large deflections in a short length of crystal, the high effective magnetic fields associated with bent crystal channeling offer a unique possibility for the measurement of charm particle magnetic moments. On the other hand, the angular acceptance for planar channeling is small, typically 10 μ rad at 400 GeV/c, because the channeling critical angle is small. This should be compared to typical particle production distributions which are in the 1 mrad range. The channeling angular acceptance is a significant limitation for applying channeling to magnetic moment measurements.

In the recent Fermilab spin precession demonstration polarized Σ^+ from the Fermilab charged hyperon beam were channeled in two 4.5 cm long silicon crystals with 1.65 mrad bends, resulting in a spin precession of $60 \pm 17^\circ$. This was in agreement with the predicted value of 62° based on the world average of the measurements of the Σ^+ magnetic moment.

The E761 experiment is shown in fig.3. A vertically polarized beam with a polarization of $12 \pm 1\%$ was produced by pitching the incident beam horizontally by ± 4 mrad. A 7 m long magnet after the target selected the Σ^+ momentum. The Σ^+ fraction was about 1% 10 m from the target. A hyperon spectrometer consisting of a magnet and silicon planes determined the Σ^+ direction. A downstream baryon spectrometer measured the proton from the decay $\Sigma^+ \rightarrow p\pi^0$.

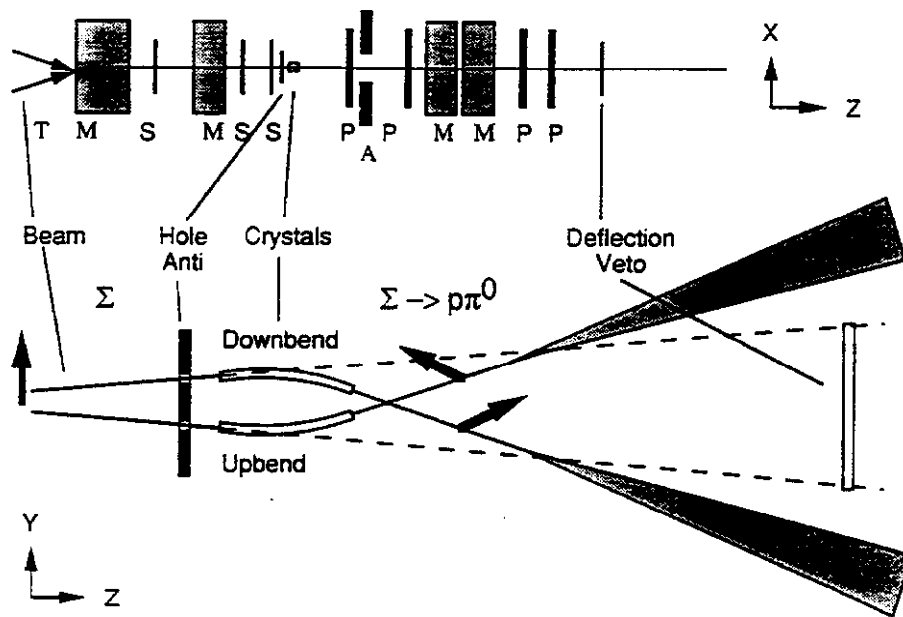


Figure 3: Schematic of the E761 spectrometer showing the overall hyperon spectrometer above and the channeling spin apparatus below.

The lower portion of fig.3 illustrates the channeling apparatus. Several silicon crystals with one of their (111) planes close to the horizontal were positioned after the hyperon spectrometer. An anti-counter with holes over the active region of the crystals cut the overall 'start' signal rate. A second 'deflection' veto after the baryon spectrometer eliminated beam-associated particles.

The bends in the crystals above the center of the beam line were arranged to deflect down through 1.6 mrad while those below deflected particles up. The curvature around the horizontal axis perpendicular to the beam direction (the x axis) produced the effective magnetic field B_x to precess the hyperon spin in the (y, z) plane. Eight diodes implanted along the 45 mm long, 400 μm thick crystals measured the energy loss of the beam particles.

The data was gathered in runs totaling seventy hours of beam time. Channeling Σ^+ events were selected by cutting out events without a vertex and eliminating events outside of the $\Sigma^+ \rightarrow p\pi^0$ decay region. A cut was also made for small energy loss in a middle pad to select channeling events. Σ^+ were selected by determining the missing mass of the recoil particle. The mass resolution was the same as that achieved with more conventional techniques.

At high energy, polarization is relatively small. The secret of unfolding polarization effects with modest polarization has been bias canceling. In E761 this proceeded through several stages. One was periodic polarization reversal by changing the incident beam direction. The second was the partition of the incident hyperon beam phase space into small bins so that angular acceptance biases of the baryon spectrometer were minimized.

Improvements such as the use of crystals with more active area and five to ten times the bending angle would have permitted this experiment to match precision experiments done in the 1980s with a factor of three more running time (200 hours).

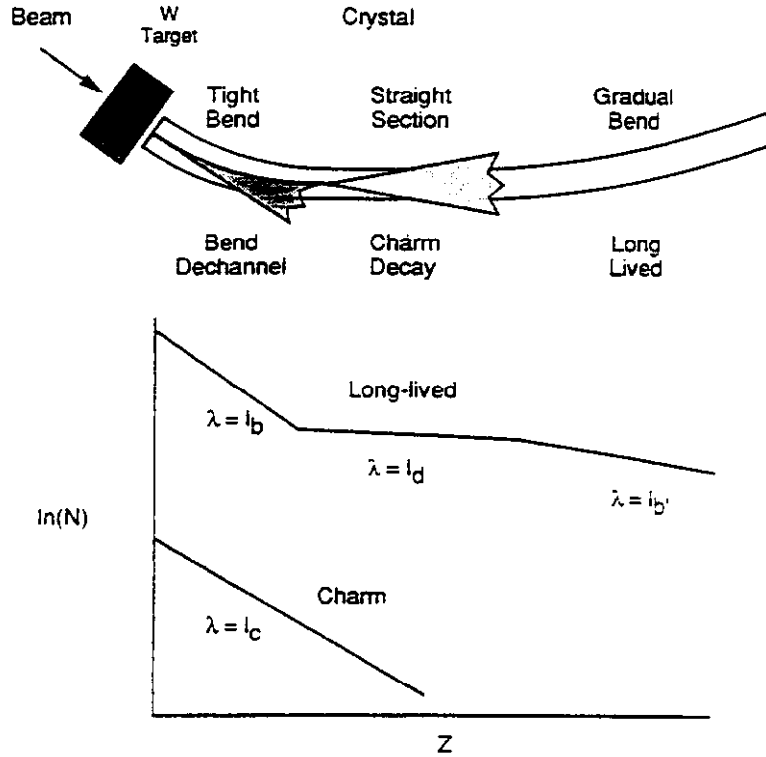


Figure 4: Schematic of an experiment to measure charm baryon magnetic moments.

4 A Conceptual Charm Magnetic Moment Measurement

An experiment for a charm magnetic moment would look quite different than the channeling Σ^+ measurement. Since the charm lifetime is short, there is not a beam of charm baryons in the conventional sense. A geometry for a possible experiment is shown in fig.4. Charm baryons would be produced in a thin, high Z amorphous target upstream of the bent crystal. An amorphous target must be used since particles produced on nuclei in the channeling planes of a crystal cannot channel. The charm particle angle relative to the direction of the production beam would be established by the crystal critical angle. Different polarization orientations arising from the production asymmetry could be realized by using two crystals with opposite bends or rotating a crystal. The crystal bend may enrich the trigger, since the charm particles are deflected somewhat from the forward cone. The long-lived channeled particles go much further around the bend so they will not be as large a background on the channeled charm side beam. The figure illustrates a conceptual variation with a small straight section to direct many of the channeled particles to one angle.

4.1 Rate Calculations

In order to find how many beam particles are needed to achieve the required number of measured, channeled, charm decays, and thus how long the experiment will take, some details of the experiment design have to be assumed [16].

Daniels and Lach [17] approached this by factoring the charm moment experiment production process into eight elements: 1) production, 2) charm fraction decaying to selected mode, 3) charm particle fraction not decaying, 4) channeling acceptance, 5) channeling surface acceptance, 6) fraction not undergoing normal dechanneling, 7) fraction not dechanneling from bending, and 8) a p_T sufficient to polarize. It is convenient to put these in 3 groups : a 'production factor' ($p_1 \times p_2 \times p_3$), a 'channeling factor' ($p_4 \times p_5 \times p_6 \times p_7$) and a 'decay factor' (p_3).

Thus, the number of polarized, channeled, charm baryons =

$$\begin{aligned} & (\text{production factor}) \times (\text{channeling factor}) \times (\text{decay factor}) \\ & \quad p_1 p_2 p_3 \quad \quad \quad p_4 p_5 p_6 p_7 \quad \quad \quad p_3 \\ & \times \text{number of incident beam particles} \end{aligned}$$

A careful optimisation is required, since these parameters vary strongly with momentum : the 'production' and 'channeling' factors favor low momentum, whereas the 'decay' factor favors high momentum. Furthermore, the number of charm baryons required to make a measurement of given precision is reduced at higher momentum, since the precession angle increases, again favoring high momentum.

The effects of these parameters can be illustrated by some particular design choices for an experiment at current energies, designed to make a 10% measurement of the magnetic moments of (a) Λ_c^+ and (b) Ξ_c^+ , before making an extrapolation to possible Charm2000 conditions :

(a) Λ_c^+ experiment, using a primary proton beam of 10^{11} s^{-1} , a tungsten target of length 6 mm, a silicon crystal of length 2.0 cm and bend angle of 15 mrad, with a mean charm baryon momentum of 300 GeV/c :

Taking the $\Lambda_c^+ \rightarrow p K^- \pi^+$ mode, with $\sigma B = 2 \times 10^{-6}$ barn and requiring p_T to be above 1 GeV/c to give polarized Λ_c^+ , the production factor is estimated as 8.3×10^{-8} .

For the channeling factor, the angle acceptance, $p_4 = 4 \times 10^{-3}$; the channeling surface acceptance, $p_5 = 0.5$; the dechanneling factor, $p_6 = 0.84$, and the bend dechanneling, $p_7 = 0.33$. This gives a factor $p_{4567} = 7.2 \times 10^{-4}$. (This factor in the E761 setup was 4×10^{-4} .)

For the decay factor, the mean momentum is 300 GeV/c, the mean distance travelled is 2.3 cm, so $p_3 = \exp(-1/\lambda) = 0.05$. A more realistic calculation, averaging over a range of momenta, yields a value of $p_3 = 1.2 \times 10^{-2}$.

Thus the overall factor is $p_{1\dots 8} = 7 \times 10^{-13}$ for Λ_c^+ , which translates to a running time of 300 hours in these (challenging !) beam conditions.

(b) Ξ_c^+ experiment, using a beam of Σ^- hyperons at a rate of 10^6 s^{-1} , a tungsten target of 6 mm, a silicon crystal of length 2.0 cm and a lower bend angle of 5 mrad, with a mean charm momentum of 300 GeV/c. At first sight, it might appear that it would be advantageous to use a beam of *polarized* Σ^- , hoping to produce polarized Ξ_c^+ by spin transfer (as was successfully exploited by E800 [18] to make polarized Ω^- from polarized neutral hyperons.) But since the spin of the Λ_c^+ and Ξ_c^+ are carried entirely by the c quark, it seems that any polarization will have to be created in the same interaction as creates the charm quark. Thus the charm baryon must be produced at a finite angle, with the corresponding loss of cross-section. Nevertheless, it is expected that there will be advantages in using a Σ^- beam, even if spin transfer does not work : a heavy quark in the projectile may be more effective for producing a heavier quark in the interaction. This is something that can be tested experimentally when Fermilab E781 takes data.

This time the production factor is $\approx 2.5 \times 10^{-7}$, the channeling factor is $\approx 10^{-3}$ and the decay factor is 0.11 (longer mean life for Ξ_c^+), leading to an overall factor of 2.8×10^{-11} . The estimated running time, in these much more favorable experimental conditions, is a wholly unrealistic 50,000 hours (2000 days !)

4.2 Extrapolation to Higher Energy

The factors giving rise to the yield in an experiment depend on the production beam momentum in different ways (fig.5). Above threshold, charm production rises approximately linearly with momentum. The effect of the charm decay length increasing with momentum is somewhat complicated. The functional form for a reasonable set of parameters is shown in fig.5. The angular acceptance is determined by the critical angle which is proportional to $1/\sqrt{p}$. Ordinary dechanneling is small and can be ignored. Bending dechanneling is also complicated. A practical experiment will always bend near the Tsyganov radius so that the factor $p\theta_b$ must be kept constant. This means that the net bend has to decrease as the energy increases. Application of the Baryshevskii formula shows that the effective yield of particles goes as $(p\theta_b)^2$. Since the ratio is constant there is no increase or decrease with energy.

Of course, it will be very important to see whether the polarization phenomenon (which is inadequately understood) persists at higher energy, since it is essential to these measurements.

5 Conclusions

The conclusions from these studies are rather sobering. First-- only two charm baryons, Λ_c^+ and Ξ_c^+ , are likely to be measurable (it will be a long time before cc and ccc states are seen). Second--both of them will show small precession angles. Third--in the simple quark

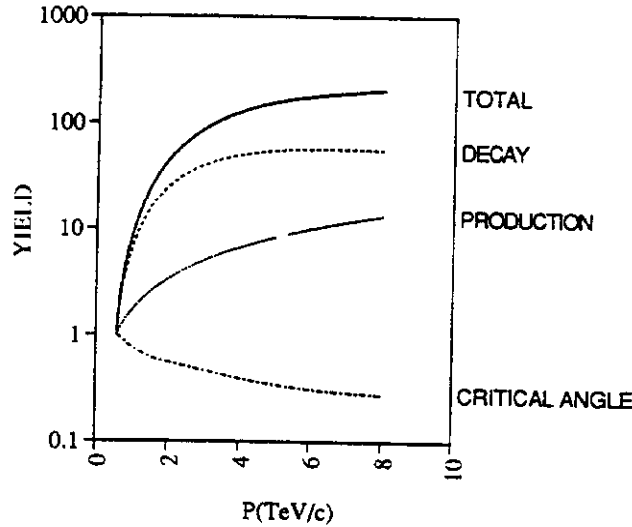


Figure 5: Effective yield with momentum for a charm magnetic moment measurement.

model they will have the same magnetic moment. However, any mixing of the Ξ_c^+ will change its magnetic moment, so measuring both Λ_c^+ and Ξ_c^+ is interesting. Fourth—there is no hope to measure beauty baryon magnetic moments since there are no stable positively charged states. Finally, this study suggests we are about three orders of magnitude away from being able to do the experiment.

In spite of the very challenging situation, the possibility of charm baryon magnetic moment measurements with channeling is worth keeping under review as experience is gained with channeling and with charm baryon production, polarization, and decay asymmetries since the subject of charm baryon magnetic moments remains interesting.

We wish to thank the other members of Fermilab E761 for their help. In particular, D. Daniels (Harvard), J. Lach (Fermilab), and V. Samsonov (PNPI) have made significant contributions to this study. This work was supported in part by the U.S. Department of Energy under contract DE-AC02-76CH0300, the Russian Academy of Sciences and the UK Particle Physics and Astronomy Research Council.

References

- [1] S. Coleman and S. L. Glashow, Phys. Rev. Lett. **6**, 423 (1961);
see also: D. H. Perkins, 'Introduction to High Energy Physics', Addison-Wesley, 2nd Ed. (1982) p.187
and J. Lach, Fermilab-Conf-91/200 (1991).
- [2] A. DeRújula, H. Georgi and S. L. Glashow, Phys. Rev. D **12**, 147 (1975).
- [3] A. Morelos *et al.*, Phys. Rev. Lett. **71**, 3417 (1993).
- [4] Particle Data Group, Phys. Rev. D **45**, 1 (1992).
- [5] A. Morelos, PhD thesis, CINVESTAV-IPN, Mexico (1992).
- [6] A. Aleev *et al.*, Yad. Fiz. **43**, 619 (1986) [Sov. J. Nucl. Phys. **43**, 395 (86)].

- [7] M. Jezabek, K. Rybicki, and R. Rylko, Phys. Lett. B286, 175 (1992).
- [8] S. Berman and M. Jacob, Phys. Rev. 139, B1023 (1965).
- [9] J. Bjorken, Phys. Rev. D40, 1513 (1989).
- [10] P. Avery, *et al.*, Phys. Rev. Lett. 65, 2842 (1990).
- [11] H. Albrecht, *et al.*, DESY 91-091 (1991).
- [12] S. Barlag *et al.*, Z. Phys. C49, 555 (1991).
- [13] See, for example, Relativistic Channeling, eds. R. A. Carrigan, Jr. and J. E. Ellison (Plenum, New York, 1987).
- [14] V. G. Baryshevskii, Pis'ma Zh. Tekh. Fiz. 5, 182 (1979), Sov. Tech. Phys. Lett. 5, 73 (1979),
L. Pondrom, private communication and Proc. of the 1982 DPF Summer School on Elementary Particle
Physics and Future Facilities, p. 98, eds. R. Donaldson, R. Gustafson, and F. Paige, Snowmass, CO
(1982),
V. L. Lyuboshits, Yad. Fiz. 31, 986 (1980) [Sov. J. Nucl. Phys. 31, 509 (1980)],
and I. J. Kim, Nucl. Phys. B229, 251 (1983).
- [15] D. Chen *et al.*, Phys. Rev. Lett. 69, 3286 (1992).
- [16] These estimates are described in more detail in
V. V. Baublis *et al.*, Nucl. Instr. and Meth. B90, 112 (1994)
and V. J. Smith, Hyperon Note H-687 (E761 collaboration, unpublished).
- [17] D. Daniels and J. Lach, Hyperon Note H-569 (E761 collaboration, unpublished).
- [18] H. T. Diehl *et al.*, Phys. Rev. Lett. 67, 804 (1991).
- [19] P. N. Pandit *et al.*, Acta. Phys. Austriaca 53, 211 (1981)
(NB These authors use Ξ_c^+ for the particle we refer to as Ξ_c^+).
- [20] S. N. Jena and D. P. Rath, Phys. Rev. D34, 773 (1980).
- [21] S. K. Bose and L. P. Singh, Phys. Rev. D34, 196 (1986).
- [22] Y. Oh *et al.*, Nucl. Phys. A534, 493 (1986).
- [23] C. Quigg and J. L. Rosner, Phys. Lett. 71B, 153 (1977), Phys. Rep. 56, 167 (1979).

A Tau - Charm - Factory at Argonne

JIM NOREM AND JOSÉ REPOND

*High Energy Physics Division
Argonne National Laboratory
Argonne, IL 60439, U.S.A.*

Abstract

In this paper we explore the possibility of building a tau-charm-factory at the Argonne National Laboratory. A tau-charm-factory is an e^+e^- collider with a center-of-mass energy between 3.0 GeV and 5.0 GeV and a luminosity of at least $1 \times 10^{33} \text{cm}^{-2} \text{s}^{-1}$. Once operational, the facility will produce large samples of τ pairs, charm mesons, and charmonium with either negligible or well understood backgrounds. This will lead to high precision measurements in the second generation quark and the third generation lepton sectors that cannot be done at other facilities. Basic physical properties and processes, such as the tau neutrino mass, rare tau decays, charm decay constants, rare charm meson decays, neutral D^0 -meson mixing, and many more will be studied with unique precision.

An initial design of the collider including the injector system is described. The design shows that a luminosity of at least $1 \times 10^{33} \text{cm}^{-2} \text{s}^{-1}$ can be achieved over the entire center-of-mass energy range of the factory.

I. Introduction

Progress in High Energy Physics (HEP) is achieved on two complementary frontiers, one requiring higher energies to discover new quanta and the other requiring higher precision to find violations of the selection rules of the Standard Model. Whereas the first frontier leads to the need for larger and larger machines, the second frontier requires higher particle production rates and high resolution detectors. Both approaches have been essential to the progress of the field.

The Tau-Charm-Factory (τcF) is an e^+e^- collider running at a center-of-mass energy between 3.0 and 5.0 GeV and with a very high luminosity of at least $1 \times 10^{33} \text{cm}^{-2}\text{s}^{-1}$. The energy range covers the thresholds for the production of charmonium, τ pairs, and charm mesons. Running the collider above and below the different thresholds creates data samples with well understood backgrounds and, therefore, results in measurements with very small systematic errors. The number of produced particles compared to a Z- and a B-factory is compiled¹ in Table I for one year running at the design luminosity. The table shows that a τcF produces a factor of five more charm mesons and τ pairs, and is unique in producing high rates of charmonium states. The goal of the Charm2000 workshop was to study experiments capable of collecting 10^8 reconstructed charm mesons. This is clearly within the reach of a τcF .

II. Physics Case

Depending on the beam energy setting, the τcF will be optimized to study physics with τ leptons, with charm mesons, or with charmonium states. The following is a short overview of the physics topics. The projected sensitivities are taken from Ref. 2(3) for the τcF (B-factory).

A) Tau Lepton Physics

The observed properties of the τ lepton are consistent with it being a sequential lepton, a heavier version of the electron and muon, with its own neutrino partner ν_τ . With a mass of 1777 MeV, the τ lepton is the only lepton sufficiently heavy to decay into hadrons: approximately 64% of its decays contain hadrons. This makes it an ideal tool to study hadronic weak interactions under very clean conditions and to search for deviations from the predictions of the Standard Model.

The optimal center-of-mass energy to study the production and the decay of τ leptons is around 3.57 GeV, i.e. below the ψ' resonance and the open charm thresholds. The cross section is large, approximately 1 nb, and therefore high statistics data samples of τ pairs may be collected. The decay branching ratios, the Michel parameters, the τ neutrino mass, and the τ dipole moment can be determined with unmatched precision. A search for rare decay modes not expected in the Standard Model can be made to very small branching ratios of the order of 10^{-8} . Other rare decay modes, such as $\tau \rightarrow \eta\pi\nu$, can be measured accurately if occurring at the rate predicted by the Standard Model.

Table II shows a comparison of the status of recent measurements (taken from reports at the 1993 Cornell conference), the projected sensitivity of a τ cF as advertised during the 1993 workshop,^{2,4} and the sensitivity to be achieved at a B-factory.³

The production rate of τ pairs is only a factor five larger at a τ cF compared to a B-factory. Nevertheless, the measurements at a τ cF are significantly more precise. This advantage is mostly due to: a) the unique possibility to control the systematic errors by running above and below the production threshold, b) the absence of charm meson backgrounds, and c) the high efficiency for identification of background-free τ pairs.

B) Charm Meson and Charmonium Physics

The charm quark, c , is the only heavy charge $2/3$ quark accessible to precise experiments. Its variety of weak decays (Cabibbo allowed, Cabibbo forbidden, doubly Cabibbo forbidden, rare second-order weak decays, ...) can be used to probe the interplay of the weak and strong interactions, including precise tests of quantum chromodynamics (QCD) at the interface of perturbative and non-perturbative dynamics^{1,4}. Mixing in the $D^0 - \bar{D}^0$ system and studies of CP non-invariance in the charge $2/3$ sector would be of great interest, distinct from the studies of $K - \bar{K}$ and $B - \bar{B}$ mixing and related CP non-invariance that involve charge $-1/3$ quarks. In addition, decays of the J/ψ , ψ' , and other charmonium systems provide important insight into light meson and gluonium spectroscopy.

With the increase in event rate expected at B factories and high-luminosity investigations at the Z⁰, the precision attainable in specific rare processes will be limited by backgrounds and systematic uncertainties. At a τ cF, adjustment of the beam energy above or below a particular threshold permits measurements of backgrounds directly. Data samples are pure, free from contamination from heavier flavor decays. Near threshold, heavy flavors are produced in simple particle-antiparticle final states (e.g. $D^0 \bar{D}^0$, $D^+ D^-$, ...). If the decay of one particle is observed, its companion is tagged cleanly. Operation of a τ cF at the ψ'' (3.77 GeV) would yield pure $D^0 \bar{D}^0$ and $D^+ D^-$ states, without contamination from other charm meson or baryon states. At 4.03 GeV, tagged D_s^\pm (cs) states can be studied, while at 4.14 GeV, $D_s^{*\pm}$ states can be investigated via associated production of $D_s^{*\pm} D_s^\mp$. Operation at the J/ψ (3.10 GeV) would provide an intense clean source of gluonic states and light-quark hadrons. Table III shows a compilation of the estimated sensitivity of a τ cF in the charm and charmonium sector.

III. Design of the Collider

An initial design of the collider to determine a preliminary set of parameters and the approximate cost of the facility is presented. The design shows that a luminosity in excess of $1 \times 10^{33} \text{cm}^{-2} \text{s}^{-1}$ can be achieved with a center-of-mass energy in the range between 3 and 5 GeV with beam-beam tunes less than 0.04.

The operational characteristics of the machine were defined by the design of the interaction region, which determines the charge per bunch and the bunch separation, and by the machine lattice, which determines the equilibrium emittance. The initial parameters assume two rings with a vertical separation of one meter, and one collision point halfway between the rings. The beams will be steered to the collision point using vertical bends, similar to the Spanish/CERN design⁵.

The ring is oval, approximately 38 m wide and 100 m long with two zero dispersion straight sections and a circumference of about 300 m. One straight section contains the interaction point and the other is used for injection and RF acceleration. The length of the straight sections is determined by the optics that is required to couple the arcs to the interaction region.

Despite the relatively low beam energy, the large circulating beam currents, approximately 1.4 A, produce about 400 kW of synchrotron radiation per beam. This high radiation is responsible for the production of considerable gas in the arcs. Following the design of Argonne's Advanced Photon Source (APS)⁶, distributed pumping is used to remove this gas. The vacuum chamber is assumed to be a copper extrusion incorporating non evaporable getter (NEG) tapes. Using the parameters of the vacuum chamber, the design of the magnets and power supplies were based on algorithms developed for the APS.

The RF system serves two purpose: replacement of the energy in the beams lost due to synchrotron radiation and reduction of the bunch length. Superconducting cavities provide the required power and voltage in a system which has a large internal diameter. Higher order modes are minimally excited and can be damped.

The parameters of the interaction point are constrained by the nearest quadrupoles, which are located within the detector. These are large aperture superconducting magnets with concentric higher order multipole correctors. The beams are separated by long electrostatic separators. Masking of the synchrotron radiation is somewhat easier than in B-factories^{7,8} due to the lower beam energies and the approximate collinearity of the beams.

The storage ring will be provided with a full energy injector. A number of options for the injector system are being considered, including a small synchrotron supplied by an electron/positron linac.

The conventional construction will include the shielding requirements for the beams, a large hall for the detector, the work and assembly areas, the counting house and the run control rooms, as well as buildings housing the power supplies, the refrigeration plant, and the safety systems associated with the storage ring operation. The rings could be located underground and shielded by dirt. Additional shielding will be required for the straight section used for injection and acceleration of the beams and the injection beam lines.

IV. Cost and Schedule

A preliminary survey of the beam optics, the vacuum system, the ring magnets, the power supplies, the RF system, and the interaction point has been completed, permitting some preliminary cost estimates of the systems and identification of the critical issues. The cost estimates are in fair agreement with extrapolations based on existing facilities, but preliminary. The major costs of the collider are associated with the vacuum system, the magnets, and the RF system. The costs of the collider and the detector are roughly equal.

The construction time of the facility is estimated to be about four years from approval, assuming the existence of a fairly complete design.

V. Conclusions

After evaluating the scientific and technical matters that are described above, we reached the following principal conclusions:

1. Physics potential: A τ cF will be the most powerful tool anywhere for precise experimental study of the properties of the τ lepton and the charm quark. Its combination of high production rate and low background will provide major advantages compared to similar experiments at B-factory machines, and will be of particular importance for the study of rare decay modes and for sensitive searches for new processes and new states.
2. Collider design and the Argonne site: the Argonne site offers important advantages for the design, construction and operation of a τ cF. A conceptual design of the collider including several options for the injector system is in preparation. A document describing the design and the costs is expected to be released within the next few months.
3. Overall assessment: A τ cF can be expected to be a unique, powerful, and cost-effective tool in HEP research for many years. Whether such a project could be funded in a timely way at ANL (or anywhere else) is not clear, in view of current budget uncertainties and the abrupt termination of the SSC project by the US Congress. Nevertheless, a τ cF would provide excellent research opportunities in a very cost effective way and contribute significantly to the productivity and the vitality of the U.S. HEP community.

Acknowledgements

We would like to thank Edmond Berger, Tom Fields, David Grosnick, and Paul Schoessow from Argonne's High Energy Physics Division and Edwin Crosbie, Frederick Mills, and Lee Teng from Argonne's Advanced Photon Source for their many contributions which made this paper possible. This work was supported by the US Department of Energy, Division of High Energy Physics, under contract W-31-109-ENG-38.

References

1. Antonio Pich, Proceedings of the Tau-Charm Factory Workshop in Marbella, Spain. CERN - TH. 7066/93 (1993).
2. " τ - Charm Factory Update," the Tau-Charm Factory Proto-Collaboration, J.Kirkby et al. (unpublished, 1993).
3. "Status Report on the Design of a Detector for the Study of CP Violation at PEP-II at SLAC," SLAC-419 (1993).
4. "Proceedings of the Tau-Charm Factory Workshop, June 1-6, 1993, Marbella, Spain," editor Jasper Kirkby.
5. "Lattice and Interaction Region Design for Tau-Charm Factories," J.M. Jowett, US/CERN School on Particle Accelerators, Benalmedena, Spain (1992).
6. "7 GeV Advanced Photon Source," Conceptual Design Report, Argonne, ANL 87-15 (1987).
7. "PEP-II: An Asymmetric B Factory," Conceptual Design Report, LBL Pub 5379 (1993).
8. "CESR-B: Conceptual Design for a B-Factory Based on CESR," Cornell University (1993)

Table Captions

- I Comparison of τ -charm data samples at the Z, B and τ -charm factories to be collected in one year of data taking. The quoted numbers correspond to integrated luminosities of 2 fb^{-1} ($\mathcal{L} = 2 \times 10^{32} \text{ cm}^{-2} \text{ s}^{-1}$) for the Z factory and 10 fb^{-1} ($\mathcal{L} = 1 \times 10^{33} \text{ cm}^{-2} \text{ s}^{-1}$) for the B - and τ -charm factories.
- II Comparison of the status of some important measurements in τ physics with the projected sensitivities of both τ -charm and B-factories.
- III Estimated sensitivity of a τcF in the charm and charmonium sector.

Table I

Particle	Z Factory	B Factory	$\tau c\Gamma$
D^0 (single)	1.2×10^7	1.5×10^7	5.8×10^7 (ψ'')
D^+ (single)	0.5×10^7	0.7×10^7	4.2×10^7 (ψ'')
D_s^+ (single)	0.3×10^7	0.3×10^7	1.8×10^7 (4.14 GeV)
$\tau^+\tau^-$ (pairs)	0.3×10^7	0.9×10^7	0.5×10^7 (3.57 GeV)
			2.4×10^7 (3.67 GeV)
			3.5×10^7 (4.25 GeV)
ψ	-	-	1.7×10^{10}
ψ'	-	-	0.4×10^{10}

Table III

Topic	Measurement	Sensitivity
CKM Matrix Elements	V_{cd}/V_{cs}	$\sim 1\%$
Weak Decay Constants	f_D, f_{D_s}	2%
New Physics	Rare Decay Branching Ratios	$O(10^{-8})$
$D - \bar{D}$ Mixing	Semileptonic Decays	$\tau_D < 2 \times 10^{-5}$
—”—	Hadronic Decays	—”—
CP Violation	Decays into CP Eigenstates	$\sim 1\%$
Absolute Branching Ratios	D Mesons	$O(1\%)$
—”—	$D_s, \Lambda_c, \Xi_c, \dots$ Mesons	$O(5\%)$
Charmonium	Spectroscopy	$O(10^3)$ More Statistics
—”—	Electromagnetic Coupling	—”—
—”—	Gluonium Search	—”—

Table II

Measurement	1993 Cornell	τ cF 1993	SLAC BF 1993
m_τ	± 0.3 MeV	± 0.1 MeV	?
τ_τ	$\pm 1.0\%$	-	$\pm 0.3\%$
m_{ν_τ}	< 32.6 MeV CL=95%	< 1 MeV CL=95%	< 5.5 MeV CL=95%
ρ	$\pm 3.9\%$	$\pm 0.02\%$	$\pm O(0.1)\%$
τ Polarization	$\pm 10\%$	-	-
d_τ	-	$< 1 \times 10^{-17}$ ecm	?
Universality	$O(0.5)\%$	0.1%	0.5%
$e\nu\nu$	$\pm 0.8\%$	$\pm 0.1\%$	$\pm 0.5\%$
$\mu\nu\nu$	$\pm 0.9\%$	$\pm 0.1\%$	$\pm 0.5\%$
$\pi\nu$	$\pm 2.2\%$	$\pm 0.1\%$	$\pm 0.5\%$
$K\nu$	$\pm 10\%$	$\pm 0.8\%$?
$\rho\nu$	$\pm 1.3\%$?	?
$3\pi\nu$	$\pm 2.4\%$?	?
$\pi 2\pi^0\nu$	$\pm 3.6\%$?	?
$5\pi\nu$	$\pm 16\%$?	?
$5\pi\pi^0\nu$	$\pm 43\%$?	?
$\pi\pi^0\eta\nu$	$< 1.1 \times 10^{-2}$ CL=95%	$< 10^{-7}$	$< 10^{-6}$
$e\gamma$	$< 1.7 \times 10^{-4}$ CL=90%	$< 10^{-7}$	$< 10^{-6}$
$\mu\gamma$	$< 4.2 \times 10^{-6}$ CL=90%	$< 10^{-7}$	$< 10^{-6}$
3μ	$< 1.7 \times 10^{-5}$ CL=90%	$< 2 \times 10^{-8}$ CL=90%	$< 5 \times 10^{-7}$ CL=90%
$\pi\eta\nu$	$< 0.9 \times 10^{-2}$ CL=95%	$\sim 1 \times 10^{-5}$	$< 5 \times 10^{-5}$ CL=95%

CHARM Yields in a dedicated B experiment at RHIC

M. Atiya and S. White

Brookhaven National Laboratory, Upton, New York 11973

M. Marx

SUNY, Stony Brook, New York 11794

presented by Sebastian White
at CHARM2000

Abstract

We consider the prospects for high statistics charm measurements as a byproduct of a dedicated hadron collider B-experiment. At RHIC energies ($\sqrt{s} = 500\text{GeV}$) roughly 10 % of charm production is expected to originate from sequential decays of B mesons. Improved triggerability and reconstruction efficiency of these sequential decay events could offset the rate advantage of the bulk of $c\bar{c}$ production sources. An efficient B-trigger could yield a large sample of unbiased, tagged charm decays from the 1×10^{10} B's which will be produced in a 2×10^6 sec pp run at RHIC.

1 Introduction

The physics potential of an experiment designed to focus on the production and decays of particles containing a b-quarks at hadron colliders has been widely recognized. The main experimental challenges are those of triggering on soft leptons in the decay chain $b \rightarrow c+l\nu$ as well as the more general tag of a secondary displaced vertex. Such an experiment must have the capability of reconstructing charmed particle masses and identifying secondaries (mostly π vs. K-mesons) to discriminate against random combinatorial backgrounds. It possible that any such experiment would be well matched also to the direct study of charm and with minor corrections to the trigger could be adapted to yield a very large sample of reconstructed charm decays.

In this paper we consider the more intriguing possibility that the charm sector could most effectively be explored by continuing to focus on B's. An experiment running at a high luminosity insertion when RHIC is colliding protons at full energy will have the opportunity to record a large fraction of the 1×10^{10} b's produced in an

expected pp run . This assumes a production cross section of $12 \mu b$. The inclusive charm cross section is expected to be $100 \mu b$ but there is both larger theoretical and experiential uncertainty on this number than in the b case. On the experimental side, this is because charm decay secondaries have relatively low momenta making vertex detection and mass reconstruction particularly difficult.

Even though hadron collider experiments have a big advantage in production rate over fixed target experiments, only a handful of D mesons have been reconstructed in collider experiments(CDF) and those have been found by their association with a B decay.

2 RHIC pp running

The RHIC project at BNL is being constructed, and will be operated by the Nuclear Physics program of the DOE, starting operations in 1999. In addition to a complement of 4 experiments to study heavy ion physics, the BNL scientific program committee has approved a program of spin physics to measure high energy parity violation and structure functions using 250-on-250 Gev polarized protons, and also an experiment to measure pp total cross sections and elastic scattering. The constraint on this HEP program is that it should be limited to the approximately 12 weeks not scheduled for the nuclear program, and the incremental costs must be borne by HEP. These costs are currently estimated at less than \$ 1M/week. Using an estimate of 2×10^6 seconds of actual running (1 month), and the expected luminosity that can be achieved for 250-on-250 Gev protons on protons($4 \times 10^{32} sec^{-1} cm^{-2}$), results in a total B production of 10^{10} . The running conditions at RHIC also provide the attractive features of a short luminous region ($\sigma_z = 9$ cm) and a bunch spacing of 110 nsec, with about 1 interaction per crossing at the highest expected luminosity. Finally, there is an available intersection region, which has the foundations for a major detector facility and 20m of free space between the splitting dipoles. The main parameters for RHIC operation are shown in Table 1.

Table 2 shows comparisons of B production at various current and planned facilities, utilizing advertised design luminosities. Planning advice from FNAL now suggests using 50% of the luminosity shown in the table, and experience suggests it might take several years to reach the full luminosity of the B-factory. This table illustrates one of the major features of hadroproduction - approximately half of the B-flavored hadrons produced are not available in 4S running at a B-factory. Of the 10^{10} B's produced in a 1-month run at RHIC, 15% are B_s , 0.1% are B_c , and 10% are B-baryons. The other advantage for hadron colliders is the nearly 3 orders of magnitude more B_u and B_d produced per run. Initially it will be more difficult to exploit these mesons fully, due to higher backgrounds and trigger requirements , but

Parameter	Value
\sqrt{S}	500 GeV
L_{peak}	4×10^{32}
β^*	1 m
ϵ	$15\pi \times 10^{-6}$ m
Number of bunches	114
Bunch separation	110 nsec
Luminous region (Initial)	$\sigma_z = 9$ cm $\sigma_{x,y} = 110\mu\text{m}$
Free space between splitting dipoles	± 10 m

Table 1: RHIC machine parameters .

once one learns how to extract them, the ultimate precision measurements of CKM matrix elements will probably be made at hadron colliders.

	RHIC	Tevatron Post MI	ABF SLAC	LEP (Z^0 pole)
L ($\text{cm}^{-2}\text{sec}^{-1}$)	4×10^{32}	5×10^{31}	10^{34}	2×10^{31}
σ (μb)	12.5	50	10^{-3}	7×10^{-3}
Sec/year	2×10^6	10^7	10^7	10^7
Total B's	10^{10}	2.5×10^{10}	10^8	10^5
$B_{u,d}$	5×10^9	1.25×10^{10}	10^8	4×10^6
B_s	1.5×10^9	4×10^9	0	8×10^5
B_c	10^7	2.5×10^7	0	4×10^3
Λ_b	10^9	2.5×10^9	0	4×10^5

Table 2: Comparison of B production for hadronic and e^+e^- machines.

The main feature of B-production at RHIC is best illustrated by Figure 1 ,which shows the acceptance of a detector for $\bar{B}B$ pairs in which a tag lepton from one semileptonic decay and the decay products of another nonleptonic decay (assumed to be $B \rightarrow \Psi K_s$) are measured. The total number of accepted events for a 1 month RHIC run are plotted vs. lepton rapidity coverage for different ranges of barrel spectrometer coverage.

The availability of such large samples of B-flavored hadrons makes possible important studies of the spectroscopy of B_s , the much rarer B_c , and B-baryons. The

B_c in particular, will be the first quark-antiquark system with two heavy quarks providing a unique testing ground for potential models and HQET. In addition, with 2×10^9 B_u and B_d mesons available per run, many important rare decay modes can be studied. For the B_s system, decays like $B_s^0 \rightarrow K^* l^+ l^-$ and $B_s^0 \rightarrow \phi l^+ l^-$ test the limits of the Standard Model and provide important new windows to extensions of the SM. This is also true of the FCNC decay $B_s \rightarrow K^* \mu^+ \mu^-$, and even more interesting lepton-number violating decays like $B_s \rightarrow K^* \mu^+ e^-$, which are completely independent of current searches in K and μ -decay, since the B decays sample effects due to the third generation which have never been explored. While these rare decays are challenging, most provide straight-forward triggers.

3 A central detector geometry

Both forward and central geometry detectors have been considered at RHIC. A forward proposal (COBEX) [1] has emphasized a first level trigger based on secondary vertex identification. Figure 2 shows an alternate approach which would capitalize on the predominantly central production at RHIC. Whether or not a better yield could be realized with this central geometry is now under study.

In the remainder of the paper we consider the central detector. The current design of the magnet which resembles the Axial Field Spectrometer at the ISR and PHENIX at RHIC, yields a field integral which varies from 0.75 Tm at 90 deg to 0.4 Tm at 25 deg to the beam direction [2]. Expected advantages over a solenoidal magnet are the high bending power near the forward direction (due to the pole piece design) and the relatively open geometry making possible a barrel particle id detector. Since the magnetic field falls off rapidly at large radii ($B = 0.06$ T at $r = 2.5$ m), this system could use standard PMT readout. In addition to the particle id system, the detector will consist of a Silicon Vertex Detector, low mass tracking chambers and a barrel EM calorimeter. We expect to have extended lepton (μ) coverage into the plug region. In what follows, we assume a barrel coverage of ± 1.5 in η and a lepton tag covering ± 3.0 units

4 Comparison of CHARM yields:

We now consider the acceptance for charm from sequential decays and compare to a strategy where one triggers on the semileptonic decay of the associated D from $c\bar{c}$ production.

1. $b \rightarrow cl\nu$: trigger on the lepton which can then also be used for tagging in a search for nonstandard mixing or CP violation. Consider as an example for acceptance

calculations $D \rightarrow K\pi\pi$.

2. $c\bar{c} \rightarrow (l\nu X)(D \rightarrow K\pi\pi)$. Here we trigger on the semileptonic decay of one of the c's.

The production rate for 2) is expected to be 1×10^{11} whereas for 1) it is 1×10^{10} . In both cases we take the semileptonic branching ratio $2 \times 11\%$ (assuming capability for both e and μ) and $\times 2$. (taking into account that the lepton could come from either b as it could from either c in 2)).

In what follows we consider yield statistics after cuts in the case of these two sources.

4.1 lepton trigger efficiency

The p_t spectrum for leptons from 1) is harder than that from direct decays (2)). This is illustrated in Figure 3 , where the direct Charm spectrum is already biased by a p_t cut on the charm jet at 2 GeV/c. In the 2 distributions shown a p_t cut of 2 GeV/c on the lepton, 1) has a factor of 10 higher acceptance (20.% vs.2.%) .

We then conclude that 1) charm production via sequential decays of B's will yield events with at least 1 lepton having $p_t \geq 2.0$ GeV/c at a level of $8 \times 10^8 \text{ events} = L\sigma \times 2 \times 10^6 \text{ sec} \times 2 \times br \times 20.\%$.

To calculate the yield from direct $c\bar{c}$ production with the same lepton cut we have also to multiply the 2% lepton cut acceptance by the fraction ($\sim 25\%$)of charm jet production above $p_t = 2\text{GeV}/c$ [3]. This results in a total yield of 2×10^8 events for the same running period.

So after this lepton trigger requirement, sequential decays lead to a factor of 4 higher yield in the detector geometry we've considered. We now consider further differences between these two classes of events which favor sequential decays for the study of charm.

4.2 other considerations

- Acceptance for the nonleptonic decay: Independent of the lepton tag efficiency, the inclusive D production spectrum also differs in the 2 cases and we find, as a result, a factor of 2 higher acceptance in the case of sequential decays - again we expect another factor of 4 to account for the fraction of c jets above our p_t threshold.

- The correlation in η between c , \bar{c} produced at RHIC will be very weak, with $\sim 50\%$ of events having $\Delta\eta \geq 1.4$. Therefore, the acceptance for charm decay with a lepton tag should be as high or larger in sequential decays where the tag lepton comes from the same b-jet.
- Secondary vertex identification: Charm and Beauty decays have similar lifetimes but since b-jets have higher momenta than charm jets, as well as higher track multiplicity and q-value, secondary vertex measurement will probably always be more efficient in the latter case.

5 Summary

A dedicated detector for efficiently triggering on and recording B-decays at a hadron collider would be a rich source of Charm with the added feature of providing a relatively unbiased lepton tag. Perhaps this detector would more appropriately be called the "Beauty and Charm Detector (BCD)".

References

- [1] P. Schlein, et al., "A collider B experiment for RHIC" RHIC Proposal, September 1993
- [2] S. Kahn, RHIC detector note, in preparation.
- [3] F. Paige, Private Communication, For example the isajet leading order QCD calculation with $m_c=1.5$ GeV gives a total charm production cross section of $166 \mu\text{barn}$ when integrated above $p_t = 0.5$ GeV/c and $42 \mu\text{barn}$ above 2.0 GeV/c.

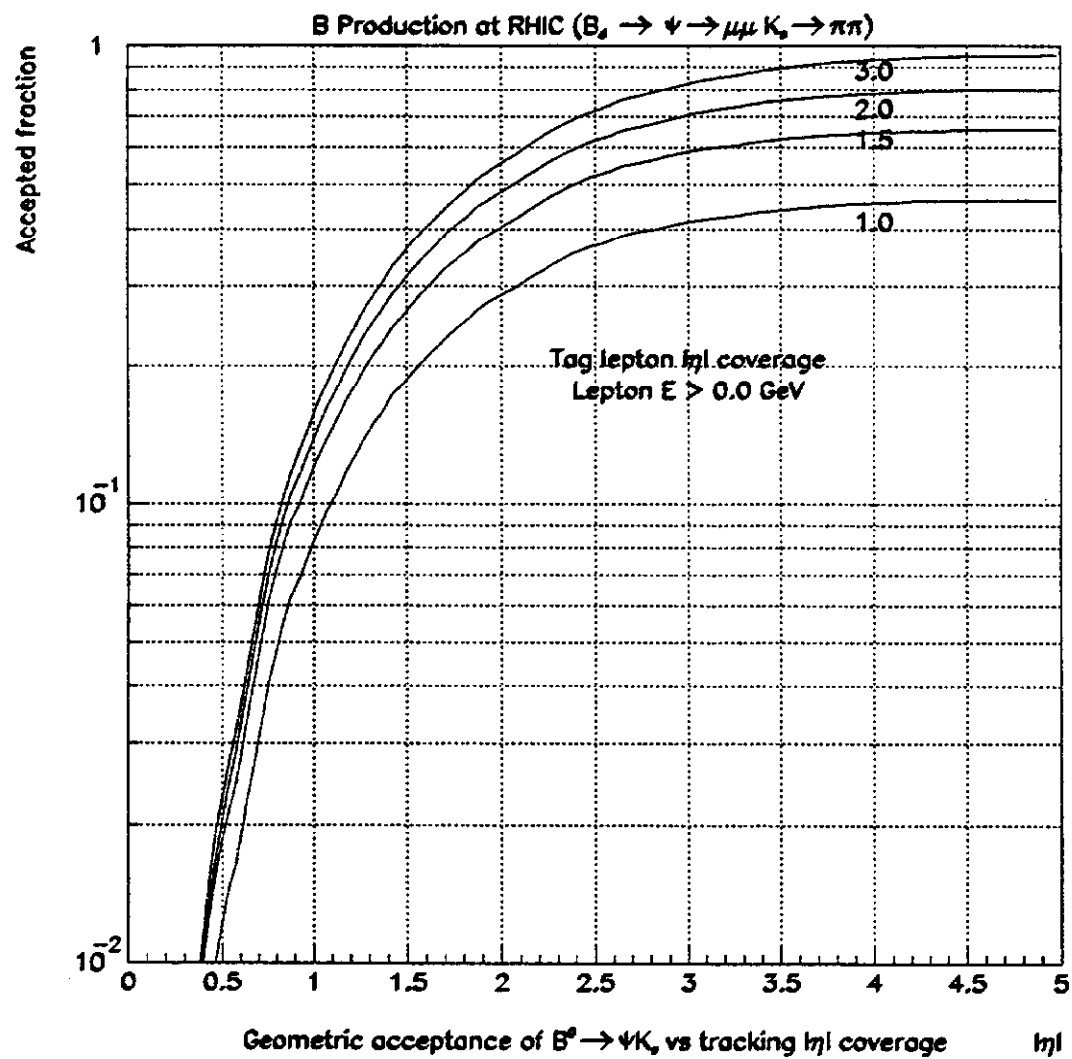


Figure 1: Geometric acceptance of typical tagged B events

Possible B detector magnet at RHIC

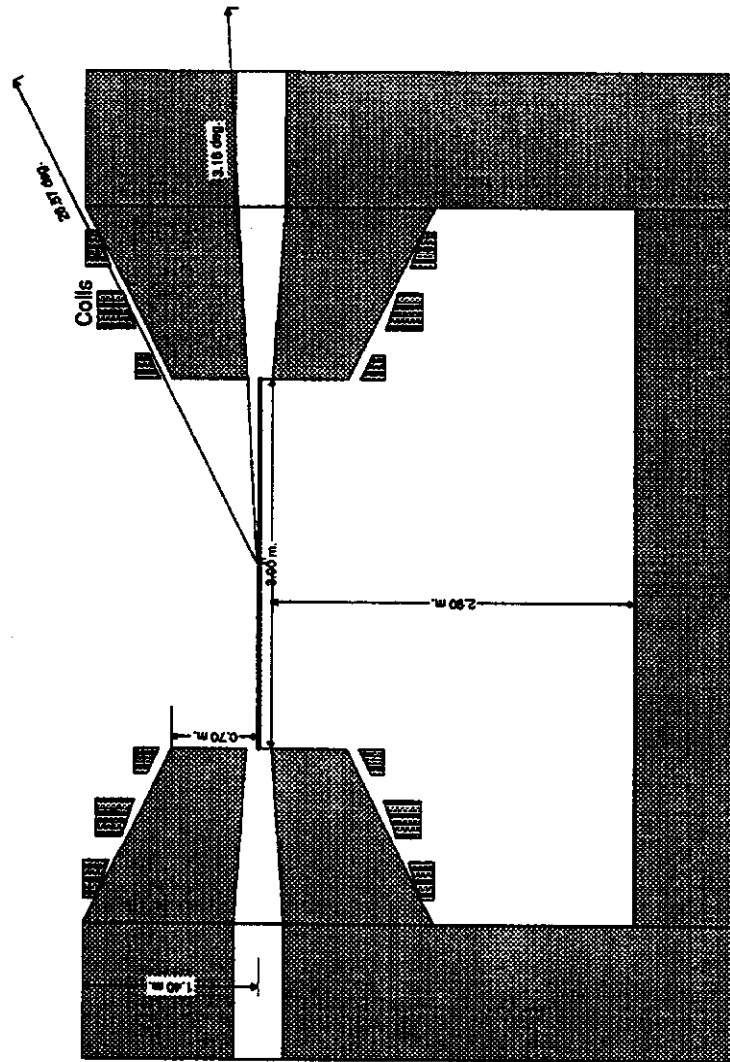


Figure 2: Sketch of a possible central B detector magnet at RHIC

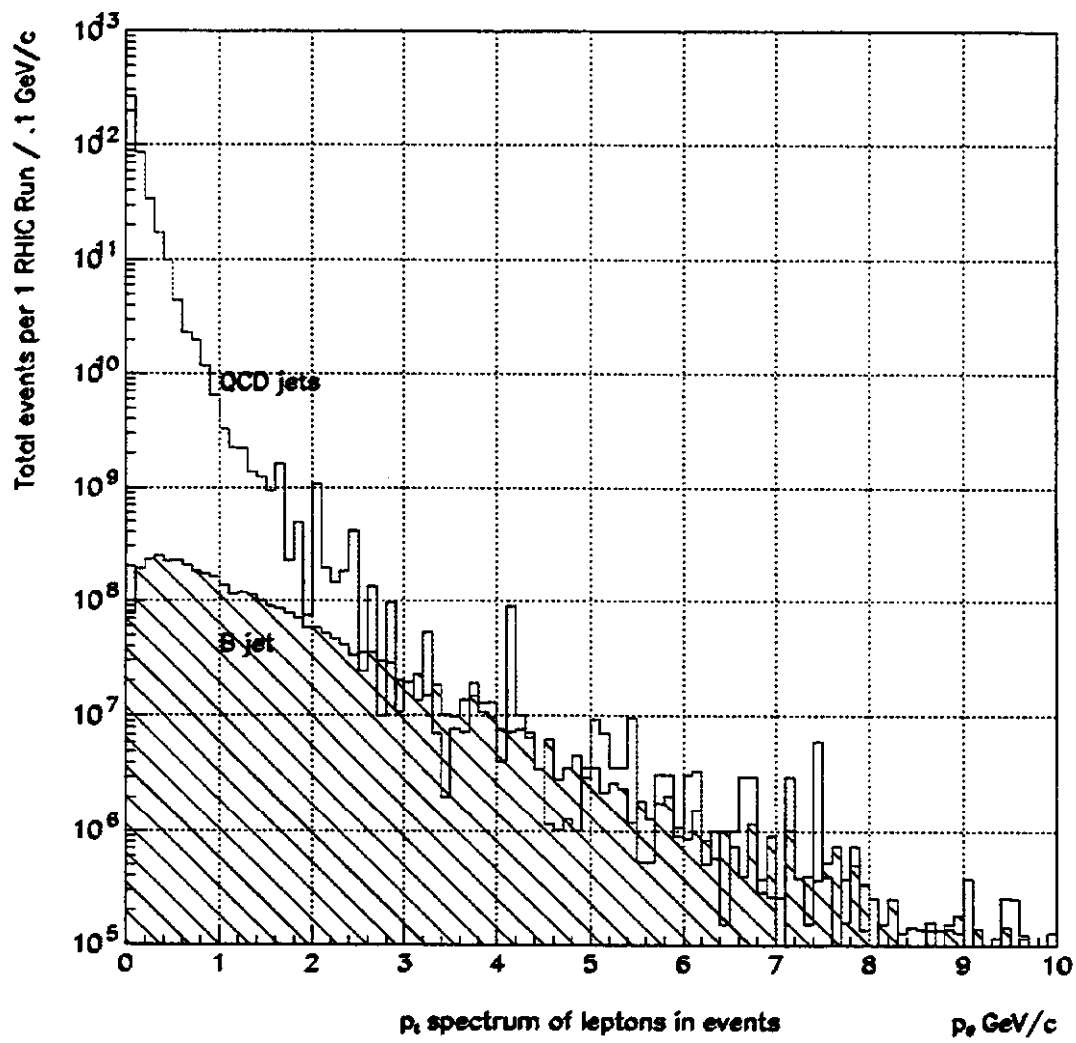


Figure 3: p_t distribution for leptons in QCD and B jets at RHIC

Perspectives on vertex detectors (Fixed target scenario)

Luigi Moroni
I.N.F.N. Milano, via Celoria 16

Abstract

Target configuration and vertex detector structure are discussed in the context of a high luminosity charm experiment. Several key issues about microvertex resolution and its role in charm selection are examined. The impact of pixel detectors on this scenario is also discussed on the basis of the present status and the related R&D programs.

1 Introduction

High luminosity experiments on charm in the Main Injector era have to face and solve a crucial problem, the background and its reduction.

It is very well known indeed that the background plays a fundamental role in high precision measurements. In particular, rare process limits are expected to improve as $1/N$ for a negligible level of background, or as $1/\sqrt{N}$ only, when the background is present.

More generally, systematics are mainly dominated by background modeling; our experience suggests that inferring the background from the signal sidebands turns out to be very problematic for a variety of reasons.

The reduction and a better understanding of the background will then be a key issue for the success of a future high statistics experiment in the charm sector.

As a consequence, the figure of 10^8 fully reconstructed charms, as the main goal for CHARM2000, is by itself vague or at least misleading; one would prefer to express the sensitivity of a charm experiment as S signal events, over N background events.

Paradoxically, depending on the level of background underlying the signal, 10^7 reconstructed charms could be even better than 10^8 ; in other words, one has to find the right compromise between the quality of the events and their quantity.

In this paper I would try to answer the following question: for a fixed number of produced charms, which are the structural features of the vertex detector that can enhance the quality of the events?

2 What can be learned from previous experiments?

In E687, we demonstrated that a dramatic reduction of non-charm background can be achieved by requiring the charm decay vertex to lie outside the target, in vacuum; furthermore, the remaining irreducible charm background can be well reproduced by a $c\bar{c}$ Monte Carlo.

To illustrate this, we present in Fig. 1 the $D^0 \rightarrow K^-\pi^-\pi^+\pi^+$ signal as found by E687 for a certain set of cuts; the global signal, shown in the first histogram (Fig. 1a), is then split into its two components having the interaction vertex in the first half of the target (Fig. 1b) and in the second half (Fig. 1c) respectively. The dotted lines represent the corresponding $c\bar{c}$ Monte Carlo signals normalized to the peak values of the data. In all cases, the Monte Carlo is not able to track the data, indicating the presence of a non-charm component in the background.

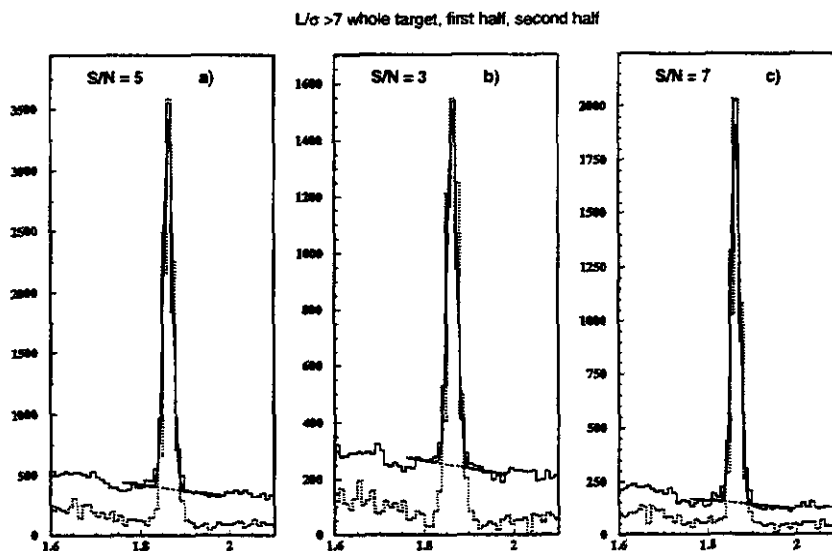


Fig. 1: $K\pi\pi\pi$ invariant mass (continuous line: data - dotted line: Monte Carlo)

As soon as the decay is required to happen downstream of the target, Fig. 2, the agreement between data and Monte Carlo becomes evident.

Meanwhile, the significance of the signal goes from a $S/N = 5$ to 32 for increasing cuts on the significance of the distance between the decay vertex and the downstream end of the target, D/σ_D (> 0 , > 5 and > 15 in Fig. 2a, 2b and 2c respectively).

The situation is even more striking for multipion decays; Fig. 3 and 4 show the same sequence of histograms for the $D^0 \rightarrow \pi^-\pi^-\pi^+\pi^+$ decay.

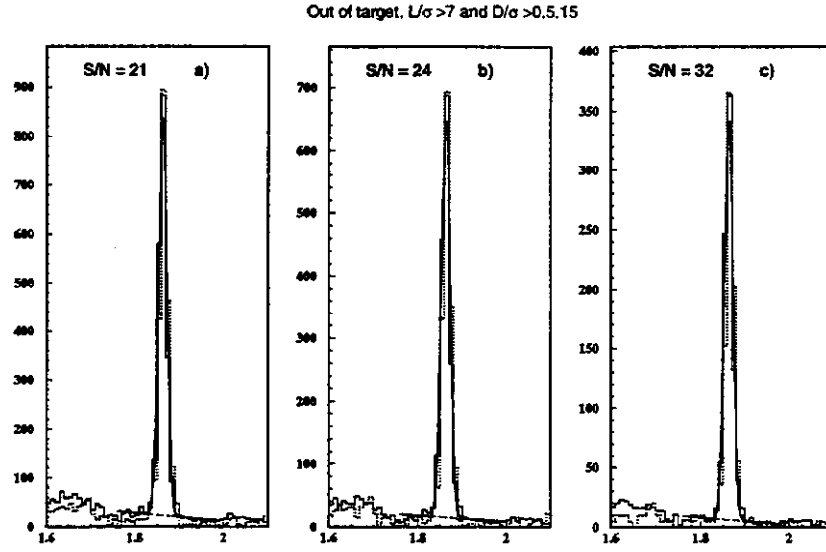


Fig. 2: $K\pi\pi\pi$ invariant mass (out of target) (continuous line: data - dotted line: Monte Carlo)

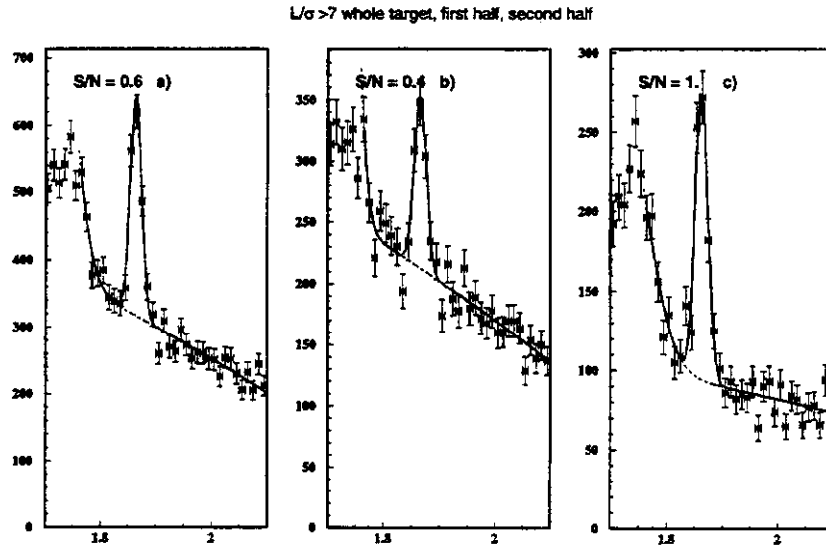


Fig. 3: $\pi\pi\pi\pi$ invariant mass

Again, the evidence of the signal for the decays in vacuum is spectacular and the only surviving background comes from charm reflections.

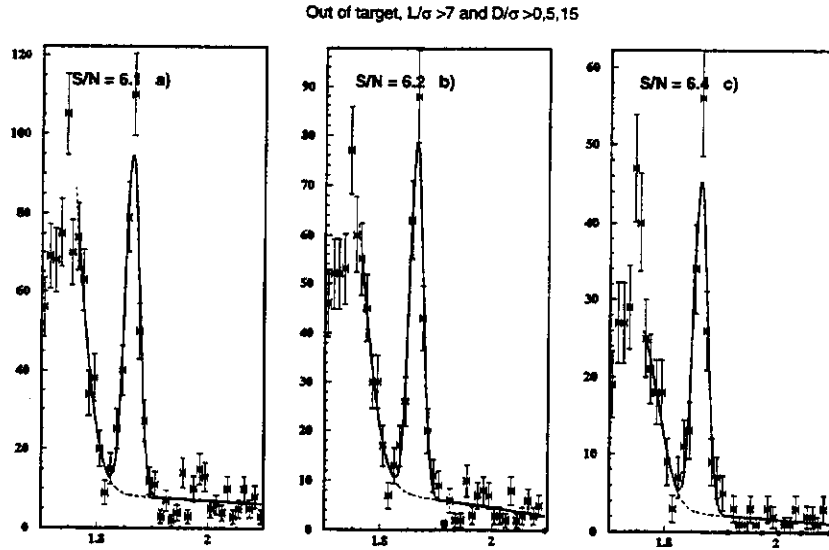


Fig. 4: $\pi\pi\pi\pi$ invariant mass (out of target)

In Fig. 5 the $\pi^-\pi^-\pi^+\pi^+\pi^+$ invariant mass is plotted with and without the target cut (the second and the first histogram respectively). In this case, one has to require the decays outside the target just to establish the D^+ and D_s signals, which, otherwise, would be hidden by the huge background.

In conclusion, selecting the class of charm signals reconstructed in the vacuum, one can get a spectacular reduction of the background, a simultaneous increase of the signal significance and an insight into the dominant part of the remaining background.

I believe that this constitutes a crucial issue to carry on charm physics at fixed target in the next millennium.

3 Target configurations

Following the previous considerations, a hypothetical architecture for a vertex detector has to maximize the fraction of decays outside the target.

In this perspective, I foresee two extreme configurations:

- a) Segmented light target (*à la E831*); Fig. 6a
- b) Thin and dense target; Fig. 6b

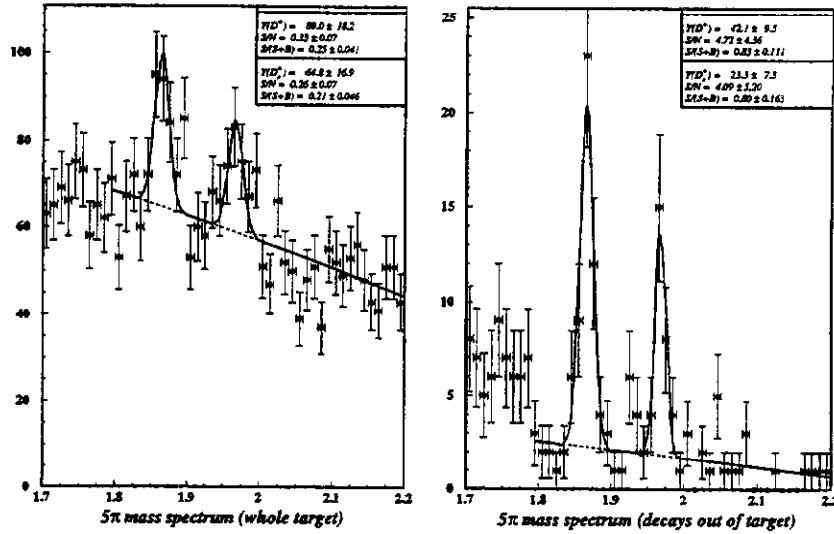


Fig. 5: 5π invariant mass

Configuration a), depending on the particular experimental conditions, greatly enhances the percentage of decays in the vacuum but introduces slabs of material in the tracking volume, which degrade the track extrapolation error at low momenta. One has then to maximize the L_{int}/L_{rad} ratio of the target in order to keep this effect within reasonable limits; Be or Diamond would be two possible choices for the target material. One could even extend the tracking into the target region by adding suitable tracking elements in the most crucial points. In order to leave as much free space as possible, one could place strip detectors immediately upstream of each target segment; much higher resolution detectors are needed because of their proximity to the interaction point.

In such a way, configuration a) is viable also for photoproduction; in particular, for a high luminosity photoproduction experiment, one can spread the e^+e^- flux over a wider transverse area.

Configuration b) represents the optimum solution to maximize the fraction of decays in the vacuum. Although it employs a very dense material, the primary vertex reconstruction is not problematic because of the very short lever arm in track extrapolation into the target. It is very well suited for hadroproduction, but is certainly inconceivable for photoproduction.

The merits of a) vs b) would definitely depend on the kind of environment chosen for the experiment, i.e. hadro vs photoproduction.

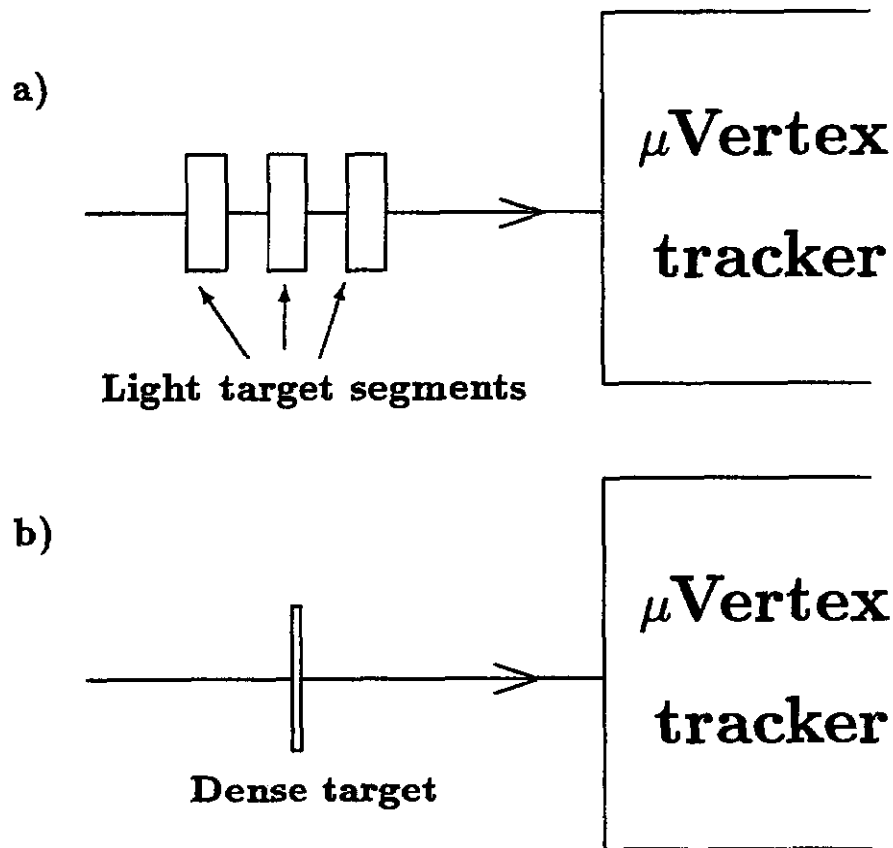


Fig. 6: Possible target configurations

4 General problems related to the microvertex tracker

I discuss two aspects of this problem which are crucial for the reconstruction of charm decays, namely:

- the track extrapolation error
- the resolution in pointing back, i.e. how well the charm reconstructed momentum vector can be traced back to the primary interaction vertex.

The extrapolation error has a critical dependence on the radiation length of the tracking medium: thin and light detector planes are preferable. In this respect, Diamond strip detectors are very promising.

For the same reason, the number of tracking elements should be kept as small as possible.

As a candidate vertex detector for the following discussion, I would propose a triplet of $(x, y)(u, v)$ double sided silicon strip detectors, arranged in the configuration sketched in Fig. 7.

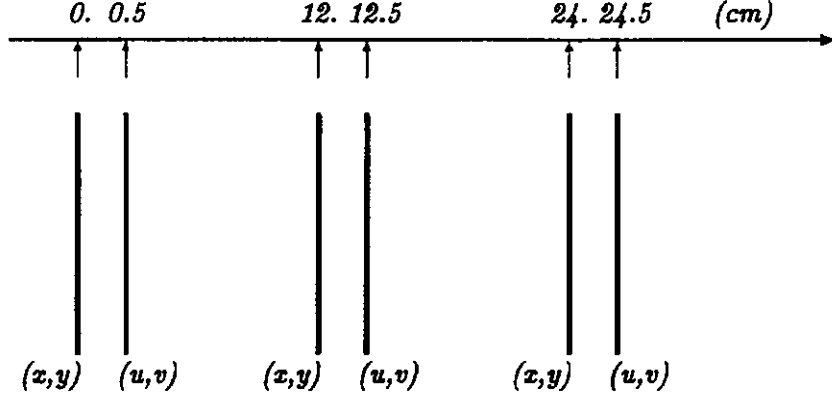


Fig. 7: A candidate vertex detector for CHARM2000

For this system, the calculated asymptotic errors at 7 cm upstream of the first plane are shown in Table 1 in pitch units and in Table 2 for a 50 μm microstrip pitch.

Errors	value	units
σ_x	0.2597	pitch
$\sigma_{x'}$	0.0120	pitch/cm

Table 1: Asymptotic errors at 7 cm from the first plane

Errors	value	units
σ_x	13.	μm
$\sigma_{x'}$	60.	$\mu\text{radians}$

Table 2: Asymptotic errors at 7 cm from the first plane for 50 μm pitch detectors

To investigate the effects of Multiple Coulomb Scattering, we express the errors in the effective momentum form:

$$\sigma = \sigma_{\infty} \sqrt{1 + \left(\frac{P^*}{P}\right)^2},$$

where the two uncorrelated components are explicitly given: the first one, σ_{∞} , is the asymptotic error at infinite momentum depending on the intrinsic resolution of the detectors, while

the second one, $\sigma_\infty \times \frac{P^*}{P}$, represents the momentum dependent MCS contribution. P^* is, therefore, the momentum value at which the two contributions are equal.

The dependence of P^* on the detector thickness for the considered configuration with 50 μm pitch is quoted in Table 3.

Detector thickness (μm)	P_x^* (GeV)	$P_{x'}^*$ (GeV)
200	9.0	24.0
300	11.0	29.3

Table 3: Effective momentum values for 50 μm pitch detectors

In general, P^{*2} turns out to be a linear function of the detector thickness.

Now, for a fixed detector configuration, i.e. same geometry and detector thickness, on varying the pitch the following relation holds:

$$\sigma_\infty \times P^* = \text{constant}$$

In other words, for a fixed MCS environment, a finer pitch improves the asymptotic resolution, but it increases in the same proportion the corresponding effective momentum, P^* . For instance, going from a 50 μm pitch to a 10 μm pitch would boost P_x^* from 11 GeV to 55 GeV and $P_{x'}^*$ to the considerable value of 147 GeV. This means that, for a certain range of momentum, further improvements of the detector resolution beyond a certain value would be rendered vain by MCS effects.

Another crucial tool in charm selection is based on pointing the reconstructed momentum of the charm candidate back to the primary vertex. The precision in this process (Pointing Back, PB) increases the rejection against background and reflections from charm decays with different multiplicity, which are expected to miss the primary.

To be accurate, pointing back needs precision in both track reconstruction and momentum. In fact, the error on the direction of the charm momentum vector in a projection can be expressed for a decay into n prongs as:

$$\delta^2(\text{Slope}_{PB}) = \sum_{i=1}^n (f_i \delta^2(\theta_i) + g_i \delta^2(p_i)),$$

where $\delta(\theta_i)$ are the errors on the prong slopes as reconstructed by the microvertex detector and $\delta(p_i)$ those on their momenta. For sake of simplicity, we have ignored any correlation between $\delta(p_i)$ and $\delta(\theta_i)$.

In order to quantify how the momentum accuracy affects the pointing-back direction, we can calculate the critical momentum resolution, that is to say, the momentum resolution whose contribution to the pointing-back error equals that of the tracking.

Explicitly, for an n -body decay and small θ_i , equating the two error components, one obtains:

$$\sum_{i=1}^n \theta_{i,x}^2 \delta^2(p_i) = \sum_{i=1}^n p_i^2 \delta^2(\theta_{i,x})$$

where $\theta_{i,x}$ is the angle in the x projection of the i^{th} prong relative to the flight direction of the parent, chosen as z -axis.

Very roughly, for a *typical* isotropic decay in the center of mass transverse plane

$$p_i \sim p \Rightarrow \delta^2(p_i) \sim \delta^2(p)$$

and, for $m_i \ll M(\text{parent})$,

$$\langle \sum_{i=1}^n \theta_{i,x}^2 \rangle \sim M^2 / (2np^2)$$

Hence, because $\delta^2(\theta_{i,x}) = \delta^2(\theta_x)$,

$$n^2 \delta^2(\theta_x) = \frac{M^2}{2p^2} \frac{\delta^2(p)}{p^2}$$

Now, since $\delta^2(p)/p^2 \propto p^2$,

$$\frac{M^2}{2p^2} \frac{\delta^2(p)}{p^2} \sim \text{invariant}$$

for decays of the same charm particle.

This means that the strongest constraint on critical momentum resolution comes from two body decays.

It is then possible to get an estimate of the critical momentum resolution just considering the decay $D^0 \rightarrow K\pi$, with $p_D = 200$ GeV and $p_K, p_\pi \sim 100$ GeV.

In this case

$$\delta p/p = \frac{\sqrt{2}}{\sqrt{\theta_{1,x}^2 + \theta_{2,x}^2}} \delta(\theta_x) = \frac{\sqrt{2}}{8.7 \times 10^{-3}} \delta(\theta_x)$$

and, for $\delta(\theta_x) = 6 \times 10^{-5}$ as in the example of Table 2, the critical momentum resolution turns out to be:

$$(\delta(p)/p)^* \sim 1\% \quad \text{at } 100 \text{ GeV}$$

A worse resolution would definitely degrade the accuracy in pointing back and, hence, the effectiveness of this tool in charm selection.

5 Impact of pixel detectors on this scenario

To complete the picture on vertex detectors, I have to consider the new possibilities offered by pixel detectors. It is difficult to draw conclusions now because of the continuous evolution of pixel R&D programs.

I would prefer to discuss the present status of pixel detectors and examine the possible applications for a CHARM2000 experiment.

The pixel detector I will consider is the so-called "intelligent pixel", capable of providing full sparse readout.

The minimum pixel size, so far achieved, is of the order of $15000\mu m^2$ and is limited by the dimensions of the electronics; obviously, VLSI technology plays a fundamental role in this context.

This relatively large pixel area can be arranged in an asymmetric fashion, for instance, $50 \times 300\mu m^2$, which is natural in a barrel-collider detector, but not in a fixed-target experiment.

Nevertheless, the unambiguous coordinate information makes pixels attractive also for fixed-target applications. Track reconstruction would surely benefit from them and would yield a superior track purity (percentage of reconstructed fake tracks).

Moreover, their impact on the elaboration of a fast trigger based on track reconstruction would be dramatic. In this perspective, the present readout schemes are already fully compatible for applications to the second level trigger for CHARM2000. More problematic would be the use of pixels in making a first level trigger: the main limitation comes from the time needed to transfer the information from pixels to the periphery at each interaction. Depending on the readout architecture and the nature of the information desired, i.e. digital or analog, the rate capabilities of the pixels, at the first level trigger, would vary over a wide range. However, this particular kind of application would require important changes of the readout schemes so far developed and, hence, would need a specific R&D program.

In conclusion, pixel detectors offer unique features, that would be of high impact on the CHARM2000 scenario; on the other hand, a major effort to fully exploit their potential has still to be made. One should remember that pixel R&D programs have made impressive progresses during the last quinquennium; hopefully, we can expect great news on pixels in the time frame of CHARM2000.

Diamond Detectors

R. J. Tesarek*

*Department of Physics and Astronomy
Rutgers University, Piscataway, NJ 08855*

Abstract

Results from high intensity fixed target experiments question whether silicon microstrip detectors can survive the rigors of the next generation of high sensitivity experiments. In light of this, alternate detector technologies are being explored for microvertex detectors in the next generation of charm experiments. The current status of one such technology is summarized here, namely the use of commercially grown diamond film as an active detector medium. Particular emphasis is placed on the development of diamond microvertex detectors with preliminary results from a beam test at CERN of the first such device. Also presented are early results of radiation hardness studies of diamond detectors.

1 Introduction

Diamond for use as an ionizing radiation detector offers several beneficial features which make it an attractive detector material in high rate, high radiation environments. Diamond is radiation hard with fast rise and recovery times, typically collecting charge over 300 μm thickness in 1 ns [1, 2, 3]. The radiation length of diamond is 60% that of silicon which admits less multiple scattering of charged tracks than an equivalent silicon detector. A smaller dielectric constant and extremely high resistivity help to minimize noise in amplifier electronics. The high resistivity and large band gap imply that no p-n junction is required to make a detector. The high resistivity also allows one to use ohmic contacts to read out the charge produced by ionizing radiation which makes a simple design of double sided detectors from single wafers possible. Diamond is chemically inert and physically robust which makes handling easier. A high thermal conductivity allows the detector to heat sink its readout electronics. Table 1 provides a numerical comparison of the properties discussed above with those of silicon.

Large area diamond films are currently grown by the process of chemical vapor deposition (CVD). In this process hydrogen and simple hydrocarbon gases such as methane or acetylene are mixed with a small amount of oxygen and ionized to form a plasma. The plasma flows past a carbide forming substrate on which the diamond grows. When the diamond film reaches the desired thickness, the substrate is chemically removed leaving a diamond film. This film is polycrystalline in nature with columnar grains whose features range from 1 μm

*for the DIAMAS collaboration

Table 1: Comparison of Diamond properties with Silicon.

Property	Silicon	Diamond	Units
Band Gap	1.1	5.5	eV
Resistivity	10^5	$> 10^{12}$	$\Omega \cdot \text{cm}$
Breakdown Field	10^3	10^7	V/cm
Electron Mobility	1500	1800	$\text{cm}^2/\text{V} \cdot \text{s}$
Hole Mobility	500	1200	$\text{cm}^2/\text{V} \cdot \text{s}$
Dielectric Const.	11.7	5.6	-
Energy/e-h pair	3.6	13	eV
Density	2.3	3.5	g/cm^3
Radiation Length	21.8	42.7	g/cm^2
$-\frac{dE}{dX}$	1.20	1.32	$\text{MeV}/\text{g} \cdot \text{cm}^2$
# e-h/100 μm	7800	3600	-
Thermal Conductivity	1.68	≈ 26	$\text{W}/\text{cm} \cdot \text{K}$

on the substrate side to 50 μm on the growth side. One should note that the raw materials for producing diamond in this fashion are abundant and inexpensive, thus making diamond potentially inexpensive.

2 Diamond Detectors

The principle of operation of diamond as an ionizing radiation detector is illustrated in Figure 1. One applies an electric field across the diamond using electrodes on either side of the wafer. When a charged particle passes through the material, electron-hole pairs are created. The charges separate in the applied electric field and induce a signal on the surface electrodes which is read out through a charge sensitive amplifier. Since diamond is an excellent insulator, the leakage current for such a device is negligible even for fields $> 10^4$ V/cm. Typical leakage currents for the devices discussed here range between 10 pA and 1 nA.

Detector grade diamond is categorized in terms of its *collection distance*, d_c . The collection distance is the average distance an electron-hole (e-h) pair separate under the applied electric field. In terms of other measureable quantities:

$$d_c = \mu E \tau, \quad (1)$$

where μ is the average carrier mobility, E is the applied electric field, and τ is the average carrier life time. The charge collected from a detector is proportional to the collection distance, namely:

$$Q_{\text{measured}} = Q_{\text{generated}} \times \frac{d_c}{t} \quad (2)$$

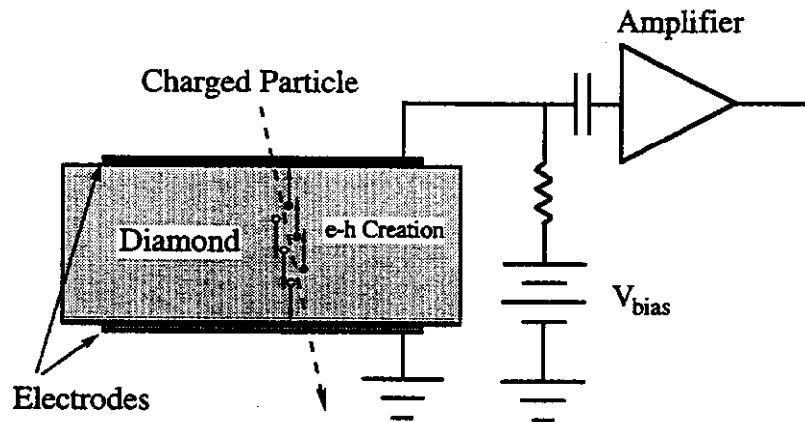


Figure 1: Schematic of diamond detector operation.

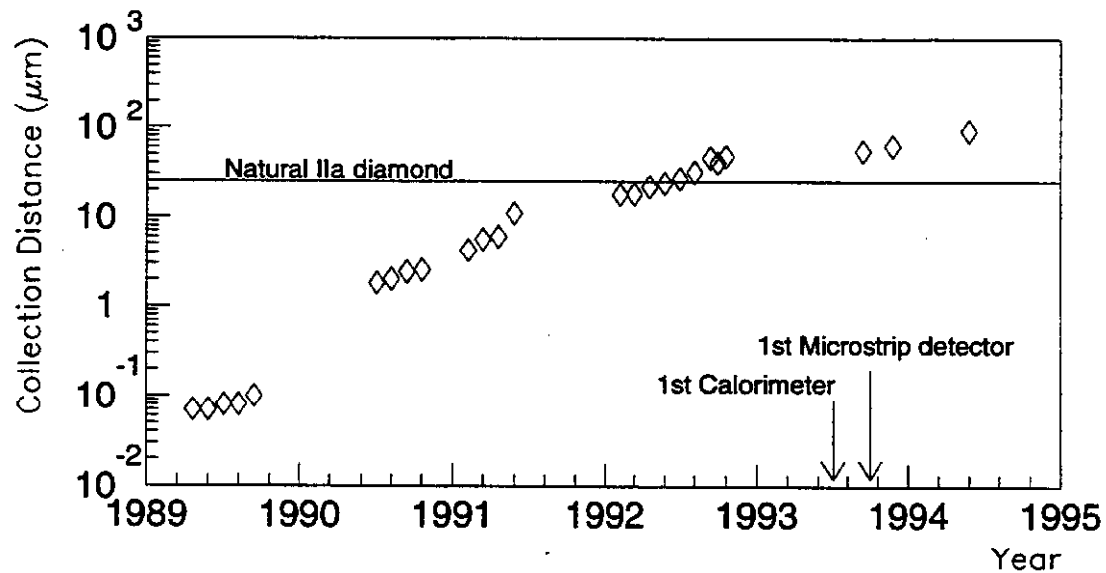


Figure 2: Collection distance of CVD samples as a function of year. The collection distance numbers are normalized to that achieved with an applied field of 10 kV/cm.

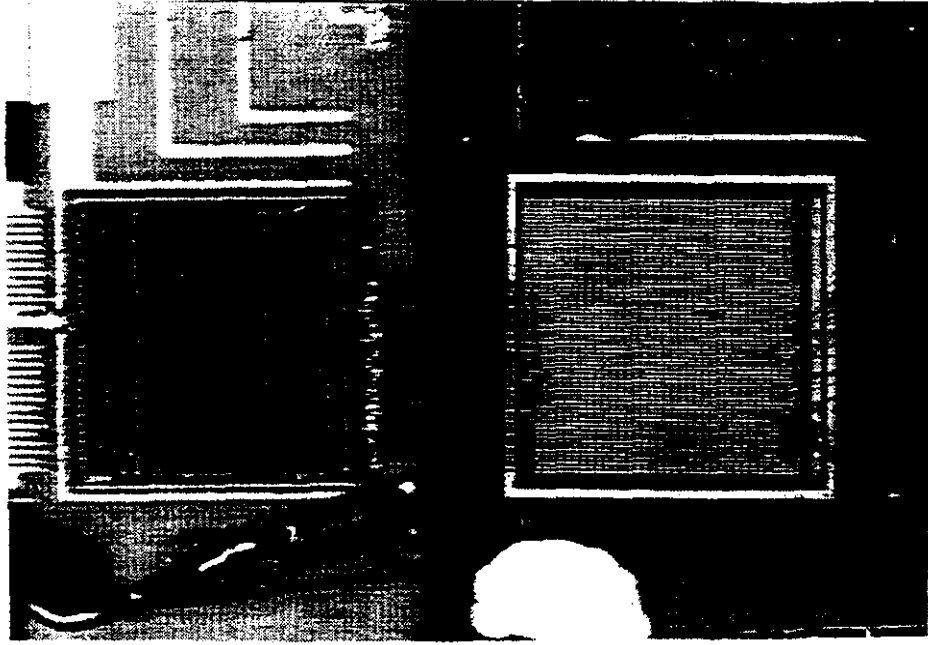


Figure 3: The first diamond microstrip detector. The diamond with 100 μm pitch strips is on the right. The VIKING readout chip is on the left.

where t is the thickness of the material and $Q_{\text{generated}}$ is given by:

$$Q_{\text{generated}} = -\frac{dE}{dx} \cdot \frac{t}{13 \text{ eV/e} \cdot \text{h pair}} \quad (3)$$

Figure 2 plots the collection distance of commercially grown diamond over the past 5 years demonstrating an improvement of over three orders of magnitude. The figure shows that the collection distance of commercially grown diamond has surpassed that of natural diamond. The figure also shows two important milestones in the development of diamond detectors: the testing of the first diamond/tungsten sampling calorimeter and the first diamond microstrip detector.

The diamond/tungsten calorimeter demonstrated the first application of large amounts of detector grade, commercially grown diamond in a prototype HEP detector. The calorimeter consisted of 30 layers of $3.0 \times 3.0 \text{ cm}^2$ detectors, 270 cm^2 total area. It should be pointed out that about half of the diamond for the calorimeter was grown and processed the week before the beam test. The energy resolution for 0.5–5.0 GeV electrons measured with this device was:

$$\frac{\sigma_E}{E} = \frac{(4.7 \pm 2.7)\%}{E} \oplus \frac{(19.13 \pm 0.86)\%}{\sqrt{E}} \oplus (2.3 \pm 1.8)\% \quad (4)$$

where \oplus denotes addition in quadrature. The energy resolution of this device agrees very well with results from an EGS simulation and with results from the same calorimeter using silicon photodiodes in place of the diamond detectors [4].

In late October of 1993, it became apparent that a microstrip detector could be made with only small modifications to materials of the same quality as that used in the calorimeter.

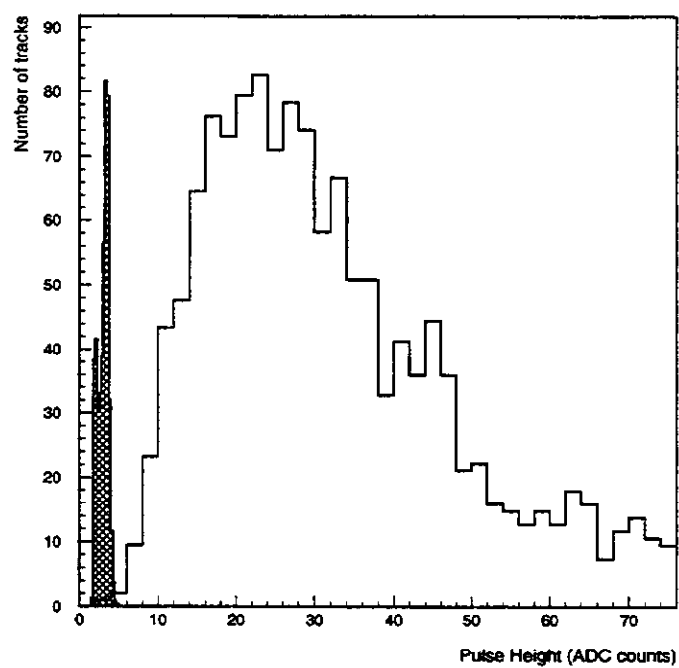


Figure 4: Pedestal width (hatched region) and signal distributions for a diamond microstrip detector.

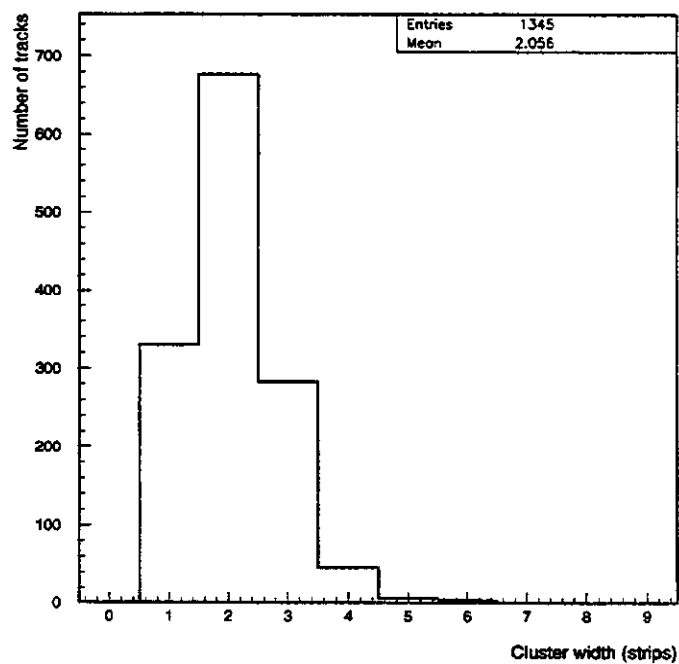


Figure 5: Number of hit strips for a minimum ionizing particle.

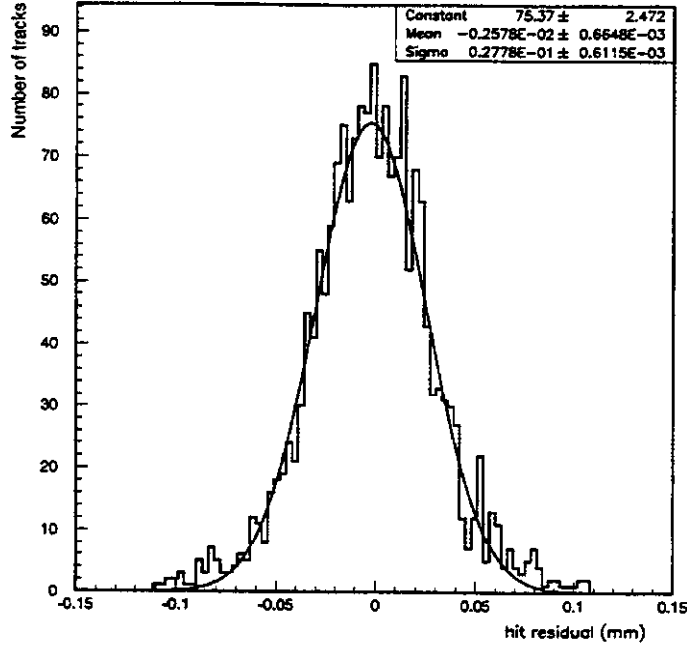


Figure 6: Position resolution of first diamond microstrip detector.

The first diamond microstrip detector measured 1 cm on a side with 100 μm strip pitch on a 200 μm thick diamond wafer. Each strip had an electrode width of 50 μm and was wire bonded to special, low noise readout electronics (VIKING) developed at CERN. The collection distance of this diamond was measured at approximately 50 μm . Figure 3 is a picture of the detector and the readout electronics. The electronic noise measured for this setup was approximately 140 electrons using a 2 μs shaping time in the preamplifier-shaper electronics. Preliminary results of a beam test at CERN using 50 GeV pions indicate a signal/noise of approximately 6:1, where the signal is the total charge collected on the strips while the noise is from a single strip. Figure 4 shows signal and pedestal width distributions from these data. From the same data, the number of strips hit is shown in figure 5. Figure 6 a residual distribution for tracks passing through the diamond detector giving a spacial resolution of 27 μm . More information about the beam test and materials may be found in reference [5]. More recently grown diamond samples have shown collection distances approaching 100 μm . These samples have been fabricated into new detectors and were recently tested in 125 GeV beams at CERN.

3 Radiation studies

In conjunction with the fabrication of prototype detectors, we are studying the response of diamond detectors to large doses of radiation. To date, three studies have been performed with many more soon to be performed. These studies include exposures to:

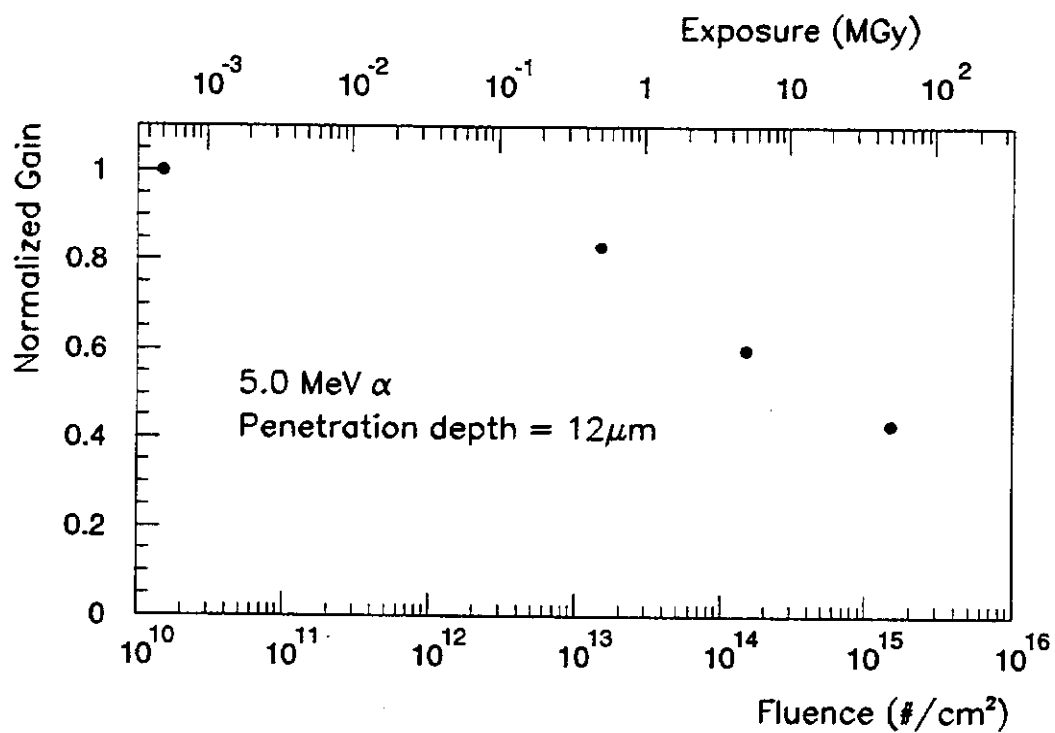


Figure 7: Normalized collection distance (gain) as a function of exposure to 5.0 MeV α particles.

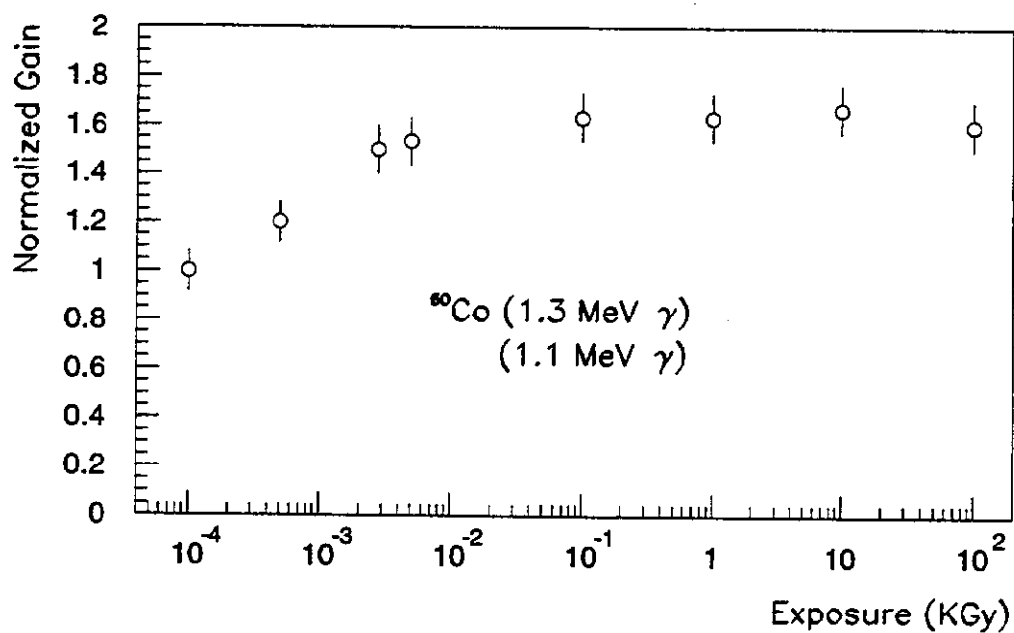


Figure 8: Normalized collection distance (gain) as a function of exposure to a ^{60}Co (γ) source.

- ^{90}Sr source (2.3 MeV β^-). These studies provide information on short term and long term low exposure effects and serve as a control for the other studies.
- 5.0 MeV α particles. The penetration depth of the alpha particles is only 12 μm so these studies provide information on surface damage effects with massive amounts of energy deposited in the material (up to 100 MGy).
- ^{60}Co source (1.1 and 1.3 MeV γ). These studies give information about damage to the bulk material induced by photons. These data also provide background information for future neutron studies using a reactor.

Data from both of the later studies are shown in figures 7 and 8. The ^{60}Co data indicate that diamond may actually improve with moderate exposure to radiation. For very large doses of radiation, $\approx 10^6$ Gy, the observed signal size begins to decrease, with a loss of approximately 60% of the original signal size, with exposure of 100 MGy.

4 Summary and Conclusions

Diamond now appears to be a viable technology for use in detectors for future high energy physics experiments. Commercially grown diamond has shown an improvement of over three orders of magnitude in the collection distance over the past 5 years. Large scale diamond detectors are now feasible, and a working prototype calorimeter and microstrip detectors have been demonstrated. New results from microstrip detectors fabricated with the best diamond available are eagerly anticipated. Early studies of the radiation hardness of diamond indicates a high degree of radiation tolerance and even improvement with moderate exposures. Diamond now represents a ripening technology with good prospects for applications in future HEP experiments.

References

- [1] L.S. Pan *et al.*, Journal of Applied Physics, 74 (1993) 1086.
- [2] S. Zhao, Ph.D. Thesis, Ohio State University, 1994 (unpublished).
- [3] M. Franklin *et al.*, Nuclear Instruments and Methods, A315 (1992) 39.
- [4] R.J. Tesarek *et al.*, accepted by Nuclear Instruments and Methods A (April, 1994).
- [5] F. Borchelt *et al.*, submitted to Nuclear Instruments and Methods A.

Low-Pressure MSGC and a Search for a High-Efficiency Secondary-Electron Emitter

D.F. Anderson and S. Kwan

Particle Detector Group

Fermi National Accelerator Laboratory

Batavia, IL 60510, USA

Abstract

The operation of a low-pressure micro-strip gas chamber with a thick CsI secondary-electron emitting surface as the source of primary ionization is presented. Fast signals are produced and improvements in gain and timing resolutions of over an order of magnitude, compared to atmospheric devices, are achieved with reduced sensitivity to discharges. Such devices should have little or no angular dependence in their position and timing resolution, or on their efficiency.

There is currently a great deal of activity in the development of micro-strip gas chambers (MSGC) for tracking in high energy physics[1-3]. Their attractions are position resolutions as good as 30 μm for particles at normal incidence, a rate capability of up to $10^6 \text{ s}^{-1}\text{mm}^{-2}$, and radiation hardness. The MSGC also lends itself to the coverage of large areas.

There are shortcomings of the conventional MSGC, particularly in high-rate environments. The typical gas gain considered safe from discharges is only 3000. Also, the collection of the charge liberated across a 3 mm gap requires a collection time of 50-70 ns, requiring shaping times of the low-noise amplifiers to be 40-50 ns in order to maintain high efficiency. Although a timing resolution of 9 ns rms has been achieved[2], resolutions of ≥ 17 ns are more typical[3].

A big problem for MSGC in a 4π experiment is that their efficiency, position resolution, and timing resolution degrade rapidly with increasing angle of incidence. As an example, a measurement of the position resolution of 40 μm at 0° resulted in a resolution of only 300 μm at 30° .

To address many of these problems we proposed and demonstrated the use of low-pressure MSGC using secondary-electron emission (SEE) from a surface as the source of ionization[4]. With this approach, we have been able to increase the gas gain to $>10^5$, improve the timing resolution to better than 0.9 ns, and achieve a reduced sensitivity to discharges. In principle, this

technique also eliminates dependence of position resolution, efficiency, and timing resolution on the angle of the incident particle.

The key to making the low-pressure MSGC a viable technique for high energy physics is finding an efficient and stable secondary-electron emitter that can be operated in a non-vacuum environment. To date the best emitter has been porous CsI. The best efficiency that we have been able to achieve for a porous CsI emitter operated in a low pressure chamber is 30%, including a 4% contribution from the interaction of the minimum-ionizing particle with the gas. For non-porous CsI the efficiency is only 2-3%.

In search of a secondary-electron emitter with high efficiency, we were led to the study of chemical vapor deposited (CVD) polycrystalline diamond films by two facts: 1) diamond is an insulator in which free charge can be transported easily, and 2) with the right surface treatment it has been shown in vacuum that the surface can be made to have a negative electron affinity (positive work function). So in principle, though not yet in practice, electrons liberated by a traversing particle should drift in the electric field in the diamond and exit the material into the gas to be counted.

References

1. F. Angelini, et al., Nucl. Phys. B 23A (1991) 254.
2. F. Angelini, et al., Nucl. Instr. and Methods A315 (1992) 21.
3. RD-28 Collaboration, "Development of the Micro-Strip Gas Chamber for Radiation Detection and Tracking at High Rates", CERN/DRDC/93-34, 1993.
4. D. F. Anderson, et al., Nucl. Instr. and Methods A346 (1994) 102.

FIBER TRACKING

RANDY RUCHTI

Department of Physics, University of Notre Dame, Notre Dame, IN 46556

for the

D0 Fiber Tracking Group

D. Adams, M. Adams, B. Baumbaugh, I. Bertram, A. Bross, D. Casey, S. Chang,
M. Chung, C. Cooper, C. Cretsinger, R. Demina, G. Fanourakis, T. Ferbel,
S. Grünendahl, J. Hinson, B. Howell, H. Johari, J. S. Kang, C. L. Kim, S. K. Kim,
D. Koltick, F. Lobkowicz, J. Marchant, S. Margulies, J. Moromisato, M. Narain,
C. H. Park, Y. M. Park, S. Reucroft, R. Ruchti, J. Solomon, E. VonGoeler,
J. Warchol, M. Wayne, E. Won, and Y. Yu

*Fermi National Accelerator Laboratory, University of Illinois at Chicago
Korea University, Kyungsung University, Northeastern University
University of Notre Dame, Purdue University, Rice University
University of Rochester, and Seoul University*

ABSTRACT

A large tracking detector consisting of scintillating plastic optical fibers has been chosen by the D0 collaboration as a part of a planned upgrade at the Fermilab Tevatron. The tracker will utilize multicladd scintillating fibers and optical waveguides and state of the art photosensors called Visible Light Photon Counters (VLPC). In this paper we present some general characteristics of fiber detectors and then describe recent measurements of system performance based on data from the 3072 channel cosmic ray test stand. Based upon these studies, fiber detectors are expected to perform very well for collider operation, and excellent performance is also expected for fixed target applications.

INTRODUCTION

A scintillating fiber (SciFi) detector combines the old technology of scintillating plastics with the new technology of fiber optics. Fig. 1 shows a schematic view of a generic SciFi detector for a colliding beam experiment. Plastic optical fibers doped with scintillating dyes are precisely placed on support cylinders which surround the point where two beams collide. Charged particles which

are produced in the collision pass through the fibers and deposit energy, which is converted into scintillation light. A fraction of that light is optically trapped in the fiber and travels to the end of the cylinder, where the doped fiber is mated to a clear optical fiber, which in turn "pipes" the light over some distance to a photodetector.

A variety of technically demanding challenges must be met in order for this technique to work well as a particle detector. The location of the active fibers must be precisely known. The scintillating dyes must produce enough light to be detected while maintaining a low level of self-absorption. Fiber-to-fiber interconnections need to have optical transmissions of near 100%, the clear fiber must transmit light over large distances, and the photodetector is required to have good efficiency and high rate capability.

Several scintillating fiber detectors have been proposed and are under development around the world, each with its own unique way of attacking the challenges listed above.¹ Perhaps the most ambitious of these detectors is the tracker being built as part of the upgrade of the D0 experiment at Fermilab.² This fiber tracker will contain 80,000 fibers and VLPC channels.

THE D0 SCIFI TRACKER

A quarter-section view of the upgraded D0 central detector is shown in Fig. 2. The D0 detector is designed to measure the production of both charged and neutral particles over nearly the entire 4π solid angle. The SciFi detector surrounds a compact silicon strip vertex detector, and both are situated within a superconducting solenoid. The solenoid provides a 2 Tesla magnetic field to deflect the charged particles and enable momentum measurement. In the region outside the magnet (not shown) are located the liquid argon calorimetry and muon toroids.

Table I lists some of the parameters of the D0 SciFi tracker. Each of the four support cylinders contain 8 layers of scintillating fibers, four in the axial direction and two each at small stereo angles($\pm\theta$). This fiber "superlayer" gives a 3-dimensional space point and a "mini-vector" in $r\phi$ space at each cylinder. The clear waveguide fibers are about 8 meters in length in order to pipe the scintillation light from the D0 active volume to the photodetectors, which are located outside the central calorimetry.

Table I. Parameters of the D0 fiber tracker

Barrel	Radius (cm)	Length (cm)	# of Fibers	Stereo Angle
Superlayer1	20	166	11,566	± 1.3 deg
Superlayer2	30	190	17,333	± 2.0 deg
Superlayer3	40	215	23,111	± 2.7 deg
Superlayer4	50	240	28,888	± 3.3 deg
TOTAL			80,888	

A great deal of progress has been made recently towards optimizing the individual components which make up this detector. The details of several of these developments are reviewed in the following subsections, after which the latest results from tests of scintillating fiber tracking systems are presented.

Scintillator

Over the past several years, extensive research has been carried out to find the optimal scintillating dyes applicable to fiber tracking. Desired characteristics include high light output and a fast decay constant. In D0, the active fibers are doped with a combination of 1% p-terphenyl (PTP) and 1500 PPM of 3-hydroxyflavone (3HF).³ Energy deposited in the polystyrene fiber core is transferred non-radiatively to the primary dye, PTP, followed by a waveshift from the primary to the secondary dye, 3HF. The fluorescence of 3HF has a decay constant of 7.8 nsec. The light emission of 3HF peaks at a wavelength of 530 nm, in the yellow-green part of the visible spectrum. At these wavelengths, attenuation lengths of 4.5m have been routinely observed in scintillating fiber of 830 μ m diameter.

Optical Fiber

Scintillating fibers and clear optical waveguide fibers are of the step-index type. The polystyrene core of the fiber is surrounded by a cladding of lower index of refraction, so that light striking the core-cladding interface below the critical angle is trapped inside the core and propagates along the fiber. The fibers used in D0 make use of an important new development in plastic fibers, multi-clad construction. As shown in Fig. 3, the polystyrene core is surrounded by two claddings - first an acrylic of index $n=1.49$, then a fluorinated material of index $n = 1.42$. The benefit of adding this second cladding is substantial improvement of the fraction of light trapped by internal reflection, 5.3% for multiclad as compared to 3.1% for single clad fiber. An additional benefit is that the multi-clad fiber is mechanically more flexible and robust than single-clad fiber. This performance improvement has been verified in several measurements, using photodiodes and VLPCs.⁴

Ribbons, Cylinders and Connectors

Before scintillating fibers are placed onto support cylinders, they are first made into ribbons. The "standard" ribbon is a doublet structure, 128 fibers wide (Fig. 4). The 830 μ m diameter active fibers are spaced by 870 μ m center-to-center. The two layers in the doublet are offset by 1/2 fiber diameter relative to each other, to provide an overall high detection efficiency per doublet. The inherent position resolution of a ribbon doublet is 120 μ m if the fibers are treated as a digital system, i.e. a fiber is either "on" or "off". The resolution can be further improved by ~50% using pulseheight information from the fibers. Two methods of ribbon manufacture have been developed. In the first, a layer of fibers is placed in a machine-grooved plate. The second layer of

fibers are laid in the spaces between the fibers making up the first layer, and whole doublet is glued to make a ribbon.⁵ In the second method, two separate singlet layers are made with grooved plates and glued to thin fiberglass backing material. The two backing layers are then glued together to make the doublet ribbon. In both methods, the center-to-center spacing can be maintained to within an RMS of less than 10 μm along the entire length of a 3 meter ribbon. The average thickness of a doublet ribbon is about 0.4% of a radiation length.

The support cylinders to be used in D0 will be made of Hexcel covered by a carbon-fiber skin. This creates a cylinder which is relatively light, strong and adds a minimal amount of inactive material to the tracking detector. Test cylinders have been constructed and measured values of roundness and sag are well within the required specifications.⁶ The technique developed to accurately mount the ribbons onto their support cylinders utilizes a large coordinate measuring machine (CMM) which can measure the ribbon's location relative to the cylinder throughout the mounting process.⁶

Although the design details are still under development, the D0 fiber tracker will have at least two fiber-to-fiber connections per channel, one at the end of the cylinder and another at the photodetector. These connections are required to be mechanically robust, reliable over time and they must have a good optical throughput. The two techniques under discussion involve: a) splicing clear fiber "pigtailes" onto the ribbons and mating these to the 8-meter-long clear fibers with connectors, or b) mate the scintillating fibers to the 8-meter-long clear fibers directly with connectors. With either technique the long clear fibers will have a diameter of 965 μm (compared to 830 μm diameter scintillating fiber) to lessen the demands on fiber-to-fiber alignment within the connectors.

In either scheme, connectors mating large numbers of fibers (32-128) are required. Light transmission measurements have been performed with connectors made from Delrin plastic. These connectors are made up of two mating pieces, each with a matched, rectangular array of 128 machined holes, or alignment grooves. The fibers are glued into the holes (or grooves) and connector faces are finished with a diamond fly-cutter. The two pieces are screwed together, with alignment pins for precise registration. Repeated tests of such a connector show that the average optical throughput across the connector is better than 95%.⁷

Visible Light Photon Counter (VLPC)

There are stringent requirements on any photosensor to be used in a fiber tracking detector. The photodetector must be capable of detecting single photons with a high efficiency, at high rates and with large gain. D0 has chosen to use the Visible Light Photon Counter (VLPC), developed by Rockwell International Science Center.^{8,9} Several of the key parameters of these devices are listed in Table II. The 1mm diameter pixel active area, fast rise time, high gain and good quantum efficiency (QE) make them an excellent match to the needs of the fiber tracker.

Table II. Geometric and operating characteristics of the VLPC.

VLPC Parameter	Value
Active Area	1 mm diameter
Pulse rise time	< 5 ns
Average gain	10,000-20,000
Gain dispersion	< 30 %
Effective QE at 560 nm	≥ 60 %
Dead time	none (continuous)
Dark pulse rate	≤ 50 kHz
Saturation pulse rate	25 MHz
Average power	1.6 mW/channel
Operating bias voltage	6-8 V
Operating temperature	6-8 K

The VLPC's are produced in the form of a bare die containing an array of 8 pixels. Each array is then mounted onto an aluminum-nitride substrate. (See Fig.5.) Once mounted, wire bonds connect the active area of the pixel to readout pads located on the substrate to form a "hybrid". This VLPC-substrate hybrid is then mounted into a molded Torlon carrier. The carrier has 8 holes which are precisely aligned with the VLPC pixels, and into which the clear optical fibers carrying the scintillation light to the VLPC's are permanently glued.

The use of special materials for mounting and bonding to the VLPCs is necessitated by the cryogenic operating temperature of the devices of 6-8 K. In the current design, 16 VLPC arrays are housed in a container known as a "cassette", shown schematically in Figure 6a. The VLPC arrays are mounted on a copper isotherm at the bottom of the cassette. Short lengths of clear fiber bring the light signals down from an optical connector at the top of the cassette, and special low-capacitance ribbon cables take the VLPC output signals back up to the preamplifier cards operating at room temperature and mounted outside the cassette volume. The cassettes are operated in a liquid helium cryostat, also shown schematically in Fig. 6b. The cassettes are mounted into cylindrical tubes which sit in the helium volume. The cold helium vapor rising up the walls of these tubes intercepts heat flow and keeps the VLPC's at their operating temperature. Currently a cryostat containing 24 cassettes, supporting a total of 3072 channels of VLPC, is being operated as part of a large-scale cosmic ray test located at Lab 6 at Fermilab.

The first study of large numbers of VLPC arrays has recently been completed at Fermilab.¹⁰ A special test cassette was constructed in which 8 VLPC arrays could be inserted, tested and then removed. Light from an LED was optically mixed and then distributed by clear fibers to each of the 64 pixels. Figure 7 shows typical ADC spectra obtained from an 8-pixel VLPC array. Clearly visible are the first few individual photopeaks in response to the LED light. The distance between the peaks measures the relative gain of the pixel, while the ratio of 2nd to 3rd photopeak areas

provides a measure of relative quantum efficiency. In this way the relative performance of 5000 channels of VLPC were studied as a function of operating temperature and bias voltage. As an example, Fig. 8 shows the variation of relative quantum efficiency as a function of bias voltage for several operating temperatures. The points plotted are averages over all the measured VLPC channels. The results were consistent with expectations for these devices. By comparing the VLPC response to that of photodetectors of known QE, the mean quantum efficiency of the 5000 channels was measured to be approximately 60% at a bias voltage of 6.5 V and temperature of 6.5 K. The total number of bad pixels was less than 250, corresponding to a good channel yield of over 95%.

This 5000 channel characterization study proved that the current design of VLPC (HISTE-IV) performs adequately for fiber tracking. Even so, a new run of devices is underway at Rockwell in which the chips will be further optimized to obtain higher QE and a reduced single-photon noise rate. The new devices (designated HISTE-V) will be characterized in the same way and results should be available by late 1994. Also under development is a new cassette design which incorporates the VLPC arrays at a higher density. This will be necessary because of the limited space available for cryostats in the D0 upgrade.

Readout

In the current fiber tracking tests, the VLPC outputs are sent to a charge sensitive preamplifier based on the QPA02 chip. The amplified signal is in turn digitized by a separate ADC. For the final tracking detector, a single chip is desired which will amplify, shape and digitize the signal from each VLPC output. The VLPC gain of 10,000 - 20,000 means that the charge input to the preamp is about the same as for silicon strip detectors, so D0 is planning to build electronic readout systems for both the silicon and fiber tracking detectors based on the SVX-II chip at Fermilab. One added feature of the fiber electronics will be a fast digital pick-off for the axial fiber channels. This will allow the fiber tracker to participate in the fast triggering of the D0 detector.

TESTS OF SCIFI TRACKING SYSTEMS

The preceding section described the status of research and development of the key components that make up a scintillating fiber tracking detector. The results clearly show that the performance and understanding of these components is at an advanced stage. Even so, it is essential to prove that the individual parts can be assembled together and operated as a system. Several tests aimed at demonstrating the viability of fiber tracking have been performed recently. Key goals of these tests have been to measure the position resolution and light yield of a fiber system. Since the number of photons produced in a fiber by a charged particle obeys statistical laws, the mean number of photons must be large enough to insure that all tracks are detected efficiently. For the D0 fiber tracker, a minimum of 2.5 detected photoelectrons per fiber is required.

Proof of Concept

Beam tests involving small numbers of scintillating fibers were carried out at Fermilab¹¹ and BNL.¹² The measured tracking resolutions were as expected, but observed light yields were too low for efficient tracking. However, both of these tests used single-clad fibers and an early version of VLPC designated HISTE-III. In summer 1993, a series of tests carried out at Notre Dame⁴ examined the light yield of 3 meter lengths of multi-clad fiber doped with 1500 PPM of 3HF, read out through 8 meters of clear multi-clad fiber into VLPC's of a newer version, HISTE-IV. The active fibers were excited with a ²⁰⁷Bi source or triggered on cosmic rays. The diamond-finished ends of the scintillating and clear fibers were mated by pressing them together in lucite ferrules. Measurements of the light yield were taken for source or cosmic ray locations at the near and far ends of the scintillating fiber. The effect of mirroring the non-readout end of the scintillating fibers was also studied - the mirroring was accomplished with an aluminized mylar foil. The results of these measurements is summarized in Table III. In the worst case, a mean number of 6-7 photoelectrons was observed from the far end of the fiber, with no mirroring. However, in the D0 fiber tracker, the lowest photon yields are expected for particles passing through the fibers in the middle of the tracker, at a distance of only 1.4 meters from the clear fiber splice. These particles traverse the fibers at a 90° angle with respect to the fiber axis - the shortest possible path length in the fiber. Tracks passing through the far end of the scintillating fibers will give more light because those particles traverse the fiber at an oblique angle and thus deposit more energy in the fiber. In addition, the non-readout ends of the fibers will be mirrored in D0. Detailed simulations of the D0 fiber detector show that fully efficient tracking is achieved when the mean number of photoelectrons is greater than 2.5.¹³ Table III shows that the tracker designed for D0 should have adequate light yield to track efficiently, with a safety factor of at least 4.

Table III. Photo yield results for 3HF scintillating fibers spliced to clear waveguide fibers and read out by VLPC's.

Mirroring	Source Location	Excitation	Most Probable PE Yield
Unmirrored	Near End	Beta	7.8
Unmirrored	Far End	Beta	6.8
Unmirrored	Far End	Cosmic Rays	6.2
Mirrored	Near End	Beta	12.2
Mirrored	Far End	Beta	11.0
Mirrored	Far End	Cosmic Rays	10.2

Large Scale Operation: The Cosmic Ray Test Stand

The aforementioned tests have proven that the fiber tracking concept works well, at least for small numbers of channels. The next step is to demonstrate that a large scintillating fiber system can be operated stably over an extended period of time. For this purpose a cosmic ray test has been

commissioned at Fermilab.¹⁴ The test detector contains 3 fiber superlayers (24 layers and 3072 channels total) - one mounted at the top of a 2-meter-long support cylinder, one at the bottom of the cylinder and the third (or middle superlayer) on a flat board at the cylinder symmetry axis. As shown in Fig. 9, the fiber detector sits upon a 2-meter stack of steel with trigger counters above and below. The steel filters out low momentum particles and gives a minimum trigger threshold of about 2.5 GeV/c. The scintillating fibers are mated to 8-meter-long clear waveguide fibers with diamond-finished connectors made of Delrin plastic. The clear fibers pipe the light to VLPC's mounted in the cassettes and cryostat discussed above.

The cosmic ray experiment tests essentially all the key components of the fiber tracker as an integrated system, under realistic operating conditions. The three-superlayer configuration enables detailed measurements of tracking efficiency, position resolution and light yields. All of the 24 total cassettes are installed and running. The cryostat is operating stably and is capable of controlling the temperatures of individual cassettes to ± 15 mK.

Preliminary results on the light yield and tracking efficiency are consistent with expectations. Figs. 10 and 11 display the observed photoelectron yields for individual fibers and for fiber doublet layers. The far ends of the fibers are mirrored in each case. The mean values of these distributions, 10.8 and 19.7 photoelectrons, indicate that very high photodetection efficiency is achieved consistent with the earlier studies.

The inherent tracking ability of the fiber system is evident in Fig. 12, an event display which shows a "zoom" view of part of the middle superlayer. This superlayer is made up of two axial doublets which are separated by 1.5 cm, with the two stereo doublets directly on top of the upper axial doublet. Only fibers with ADC counts greater than 800 (~ 2 -3 photoelectrons) are drawn, and the cosmic ray track is clearly seen with no background. The number of photoelectrons detected in the hit fibers range from 8 to 15, and seven of the 8 possible fiber layers show hits.

From track reconstruction of the test stand data, the intrinsic spatial resolution of a fiber doublet can be determined as shown in Fig. 13. Currently for tracking studies, the fibers are treated as digital elements: that is fibers are either "on" or "off". If a single fiber is hit, the coordinate is taken to be the fiber center. If a fiber and its nearest neighbor in the offset layer are both hit, the coordinate is taken as the mean position. A resolution of $137\mu\text{m}$ is indicated. We expect a value near $120\mu\text{m}$ with improved fiber ribbon construction. Once pulse height information from the fibers is incorporated into the analyses, in conjunction with expected improvements in fiber ribbon construction, we anticipate a limiting resolution for fiber doublet layers of $\sim 80\mu\text{m}$.

Fig. 14 displays the efficiency of a fiber doublet ribbon, and the efficiency of the individual singlet layers of which the doublet is composed. The lower efficiency of the singlets is a consequence of the separation (gaps) between individual fibers which make a layer. The fiber doublet structure fills in these gaps. Ultimately, a doublet efficiency in excess of 99% is expected

from the high photostatistics which we observe, once geometric construction of the fiber ribbons is perfected.

SUMMARY

Particle physics tracking detectors based on scintillating optical fibers are being proposed for a variety of experiments around the world. Several features of SciFi detectors, including good position resolution, excellent time response, uniformity of material and relative ease of operation, make them attractive choices for experiments studying high-rate, complex events at present and future accelerators. The D0 collaboration has chosen to build a scintillating fiber tracker as part of a major detector upgrade. The key components of this detector are well understood, and recent system tests indicate that the D0 fiber tracker will be able to track particles at the Fermilab Tevatron with very high efficiency and excellent position resolution. Comparable or even better performance should be expected in fixed target applications, where scintillating fiber and waveguide lengths may be shorter due to more favorable geometry and accessibility, and hence higher detected light levels are to be expected.

REFERENCES

1. J.-M. Gaillard, *Proceedings of the Workshop on Scintillating Fiber Detectors - SciFi 93*, edited by A.Bross, R. Ruchti and M. Wayne (World Scientific Press, to be published).
2. The D0 Collaboration, D0 Note Nos. **1733 & 1993**, Fermilab, (1993).
3. B. Abbott et al., "Scintillating Fiber Detectors", *Proceedings of the Symposium of Detector Research and Development for the Superconducting Super Collider*, Fort Worth, TX (1990), pp. 90-99.
4. B. Baumbaugh et al., NIM **A345** (1994) 271-278.
5. D. Koltick et al., D0 Note No. **1687**, Fermilab, (1993).
6. B. Howell et al., D0 Note Nos. **2008 & 2009**, Fermilab, (1993).
7. C.L. Kim, Fermilab, and S. Margulies, UI Chicago, (private communication).
8. M.D. Petroff and M.G. Stapelbroek, IEEE Trans. Nucl. Sci. **36**, No. 1(1989) pp. 158-162.
9. M.D. Petroff and M. Atac IEEE Trans. Nucl. Sci. **36**, No. 1(1989) pp. 163-164.
10. D. Casey, *Proceedings of the Workshop on Scintillating Fiber Detectors - SciFi 93*, edited by A.Bross, R. Ruchti and M. Wayne (World Scientific Press, to be published).
11. B. Abbott, et al., NIM **A327** (1993), pp. 319-327.
12. B. Abbott, et al., NIM **A339** (1994), pp. 439-448.
13. D. Adams, SDC-92-279, (1992) and D0 Note No. **1437**, Fermilab, (1992).
14. C.L. Kim, *Proceedings of the Workshop on Scintillating Fiber Detectors - SciFi 93*, edited by A.Bross, R. Ruchti and M. Wayne (World Scientific Press, to be published), D0 Note No. 2042, Fermilab, (1993).

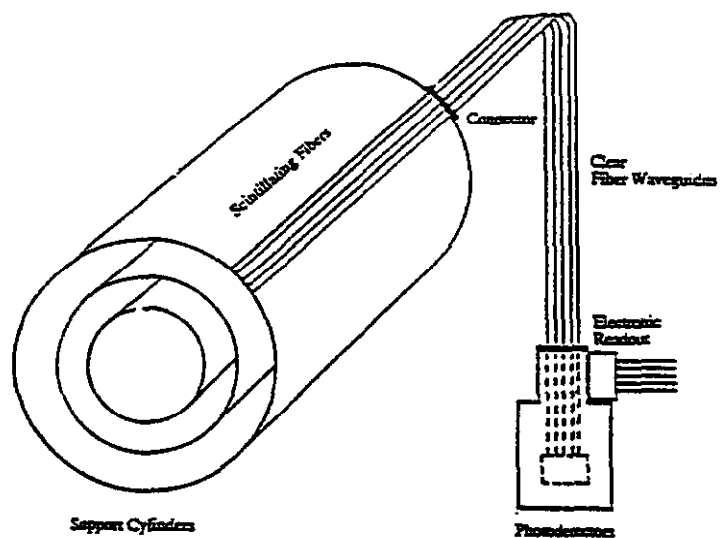


Figure 1. Schematic view of a generic scintillating fiber tracking detector.

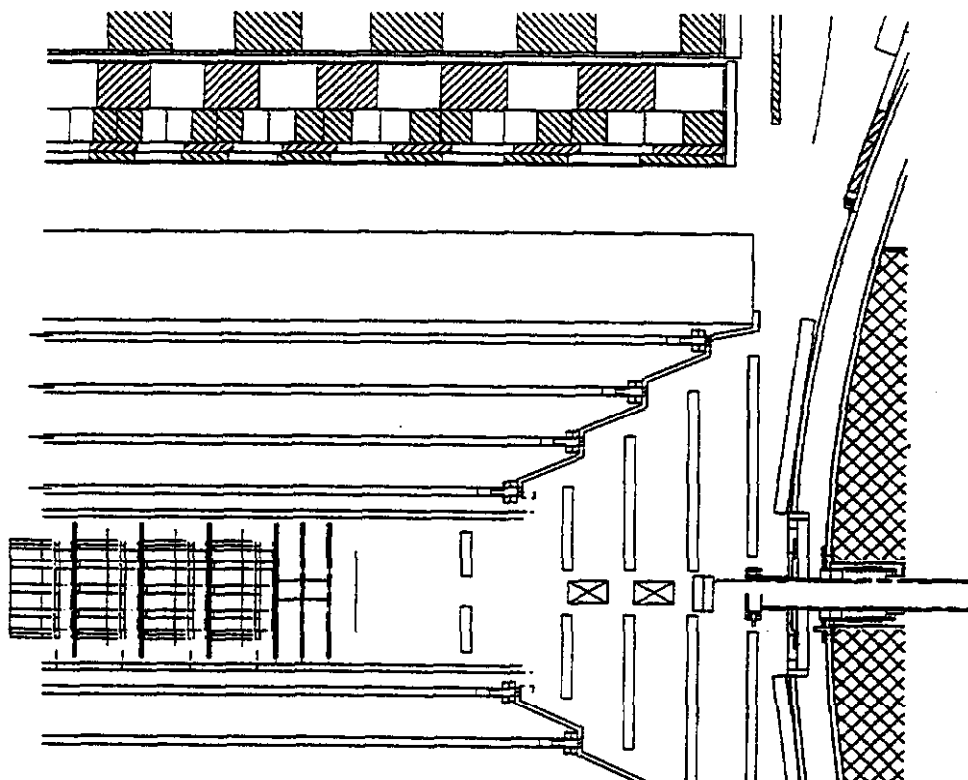


Figure 2. Quarter-section view of the D0 upgrade central detector.

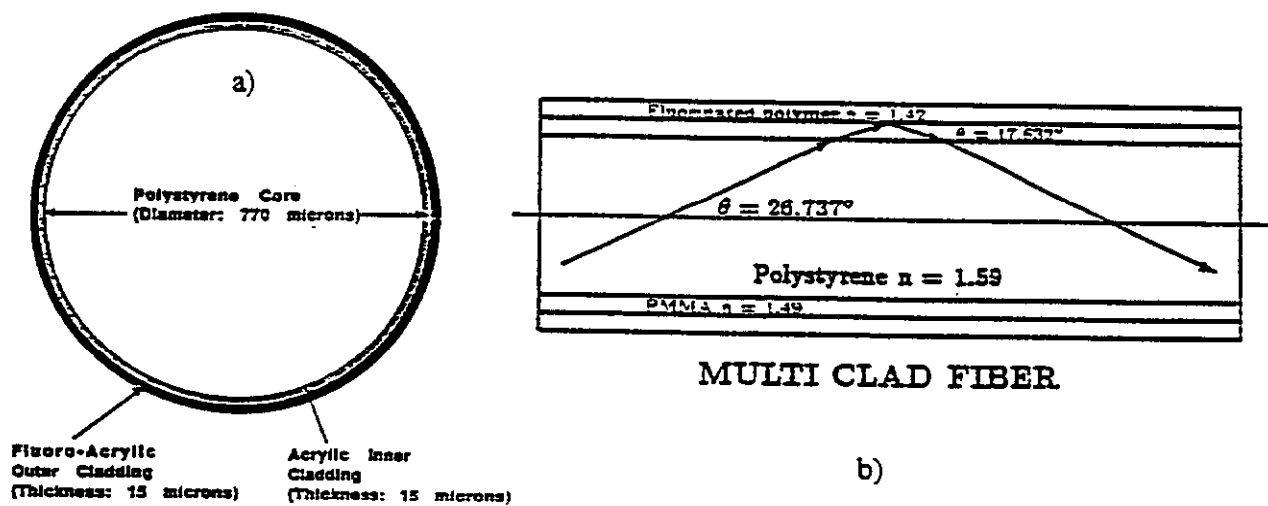


Figure 3. (a) Construction of multi-clad fiber. (b) Critical angles of multi-clad fiber, illustrating the additional light trapping.

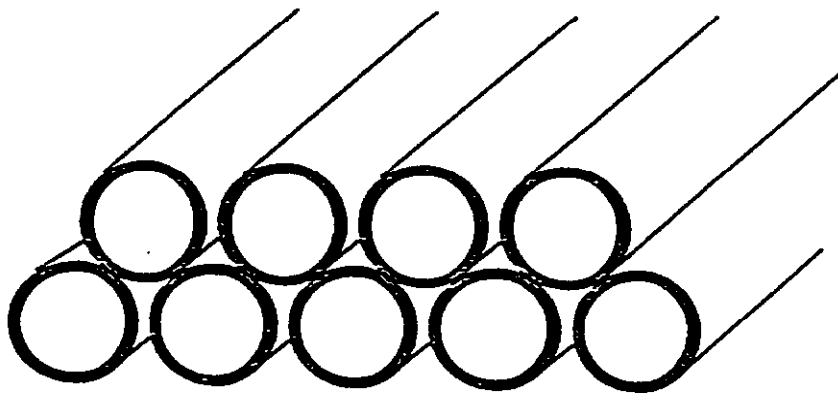


Figure 4. Schematic of a fiber doublet ribbon.

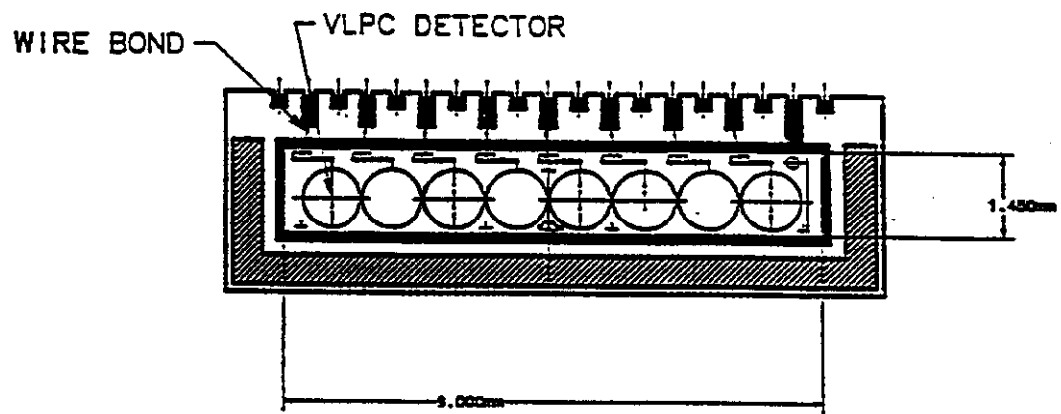


Figure 5. Layout of an 8 channel VLPC array, mounted on a support substrate.

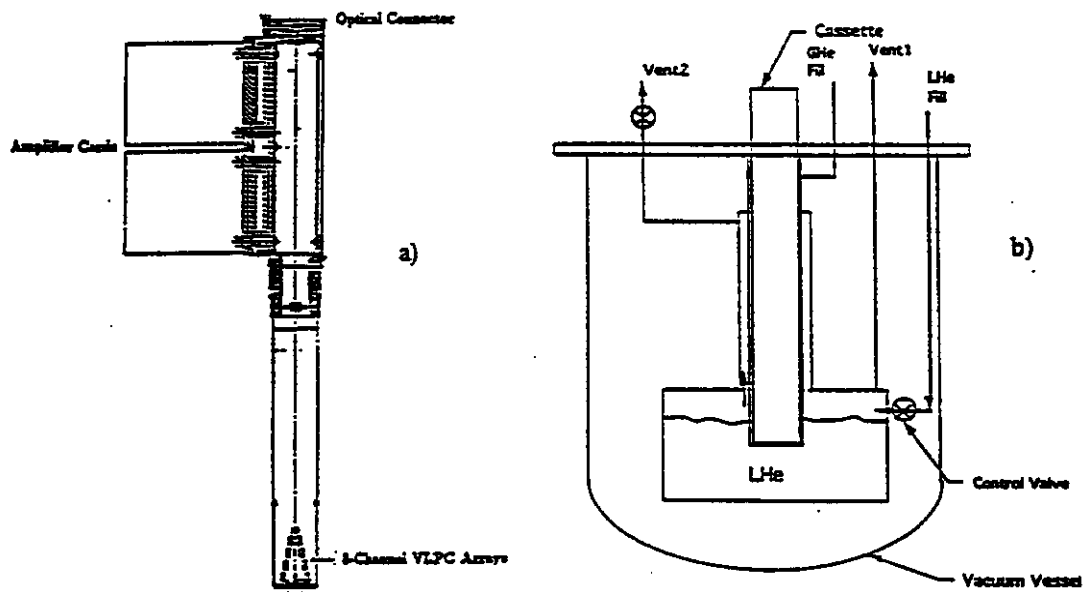


Figure 6. Schematic views of a (a) VLPC cassette and (b) cryostat.

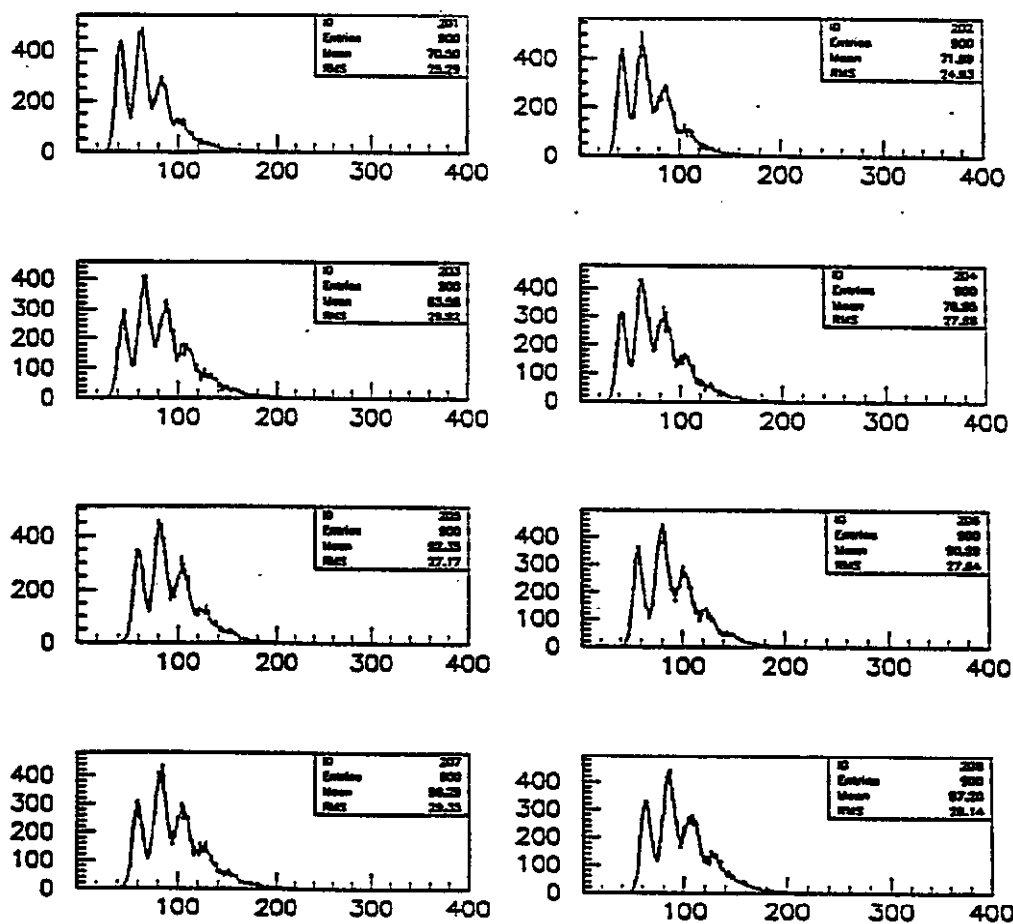


Figure 7. Typical ADC spectra of 8 VLPC pixels illuminated by LED light.

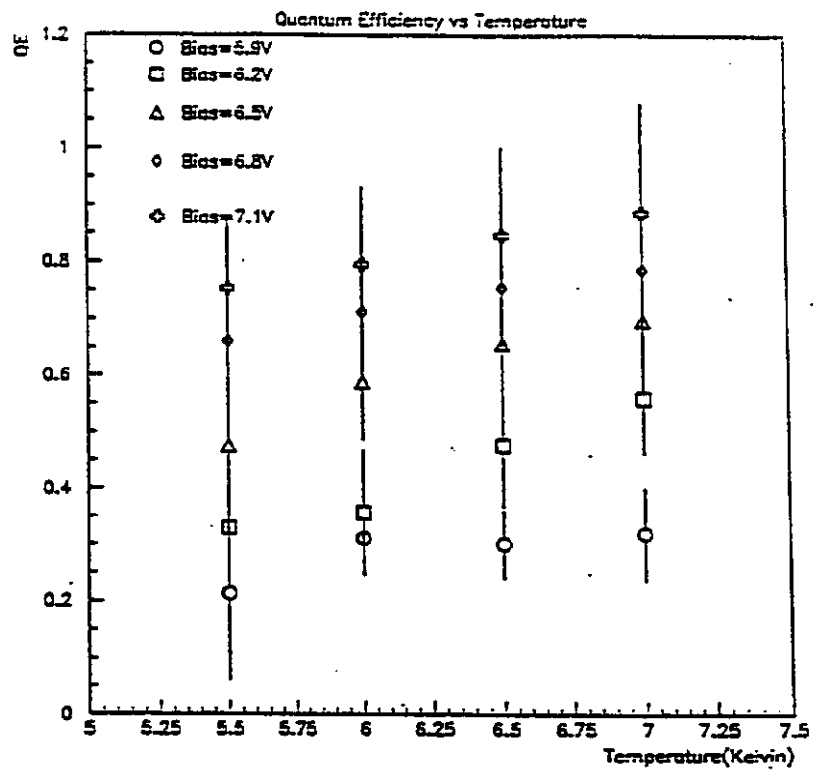


Figure 8. VLPC QE as function of temperature for several bias voltages.

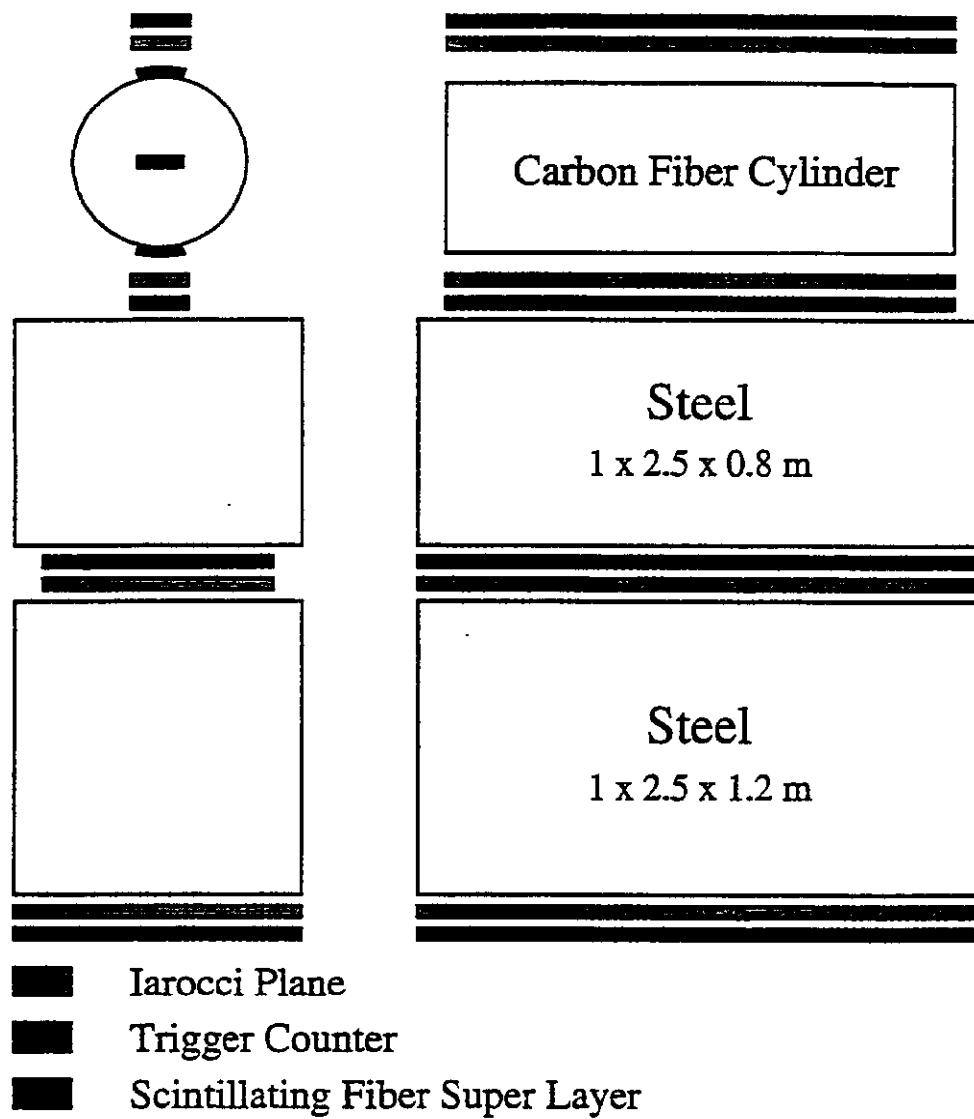


Figure 9. Schematic of the Cosmic Ray Test Stand. End View and Elevation View.

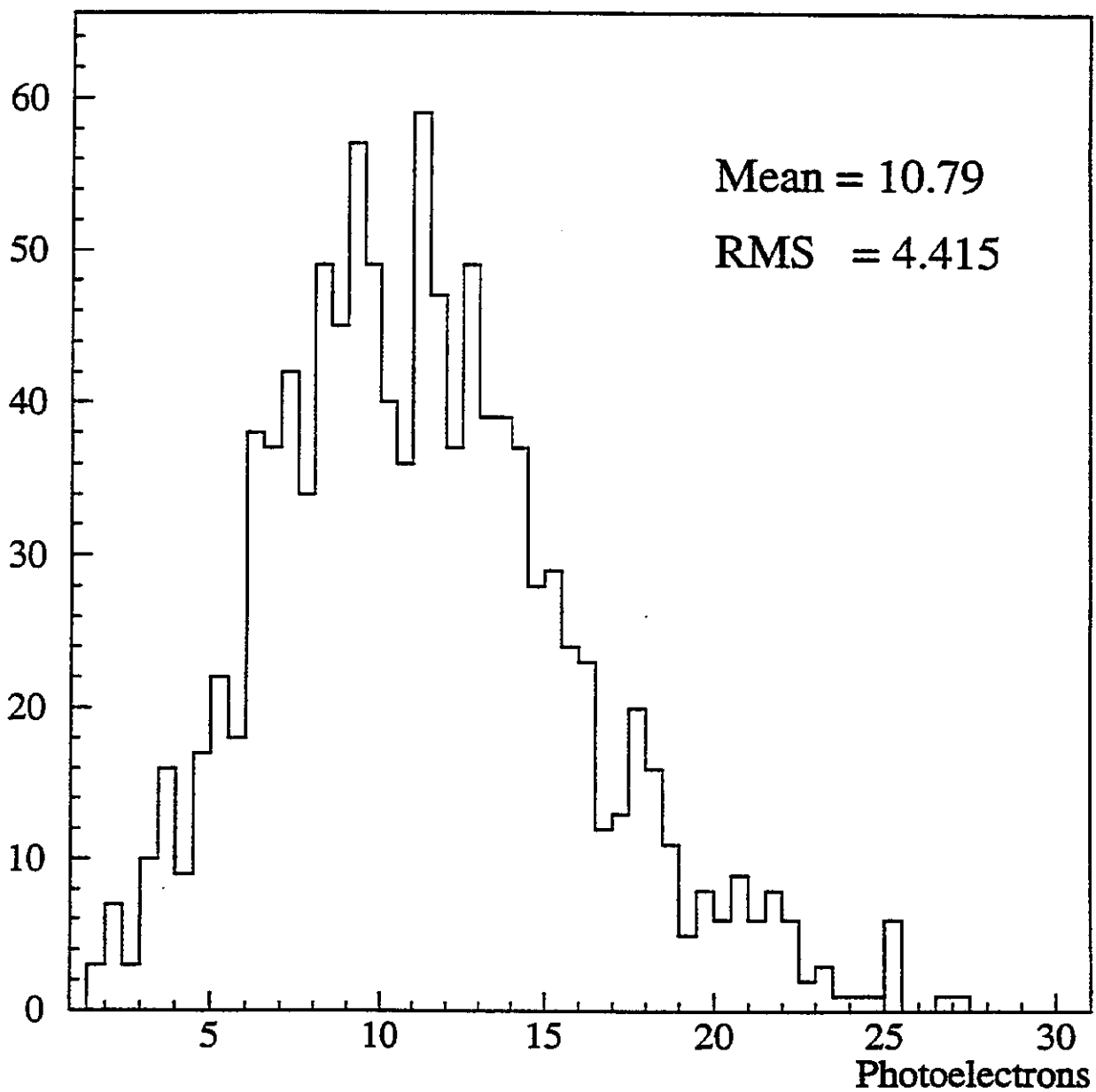


Figure 10. Detected photoelectron yield from a single-layer of fibers having mirrored ends.

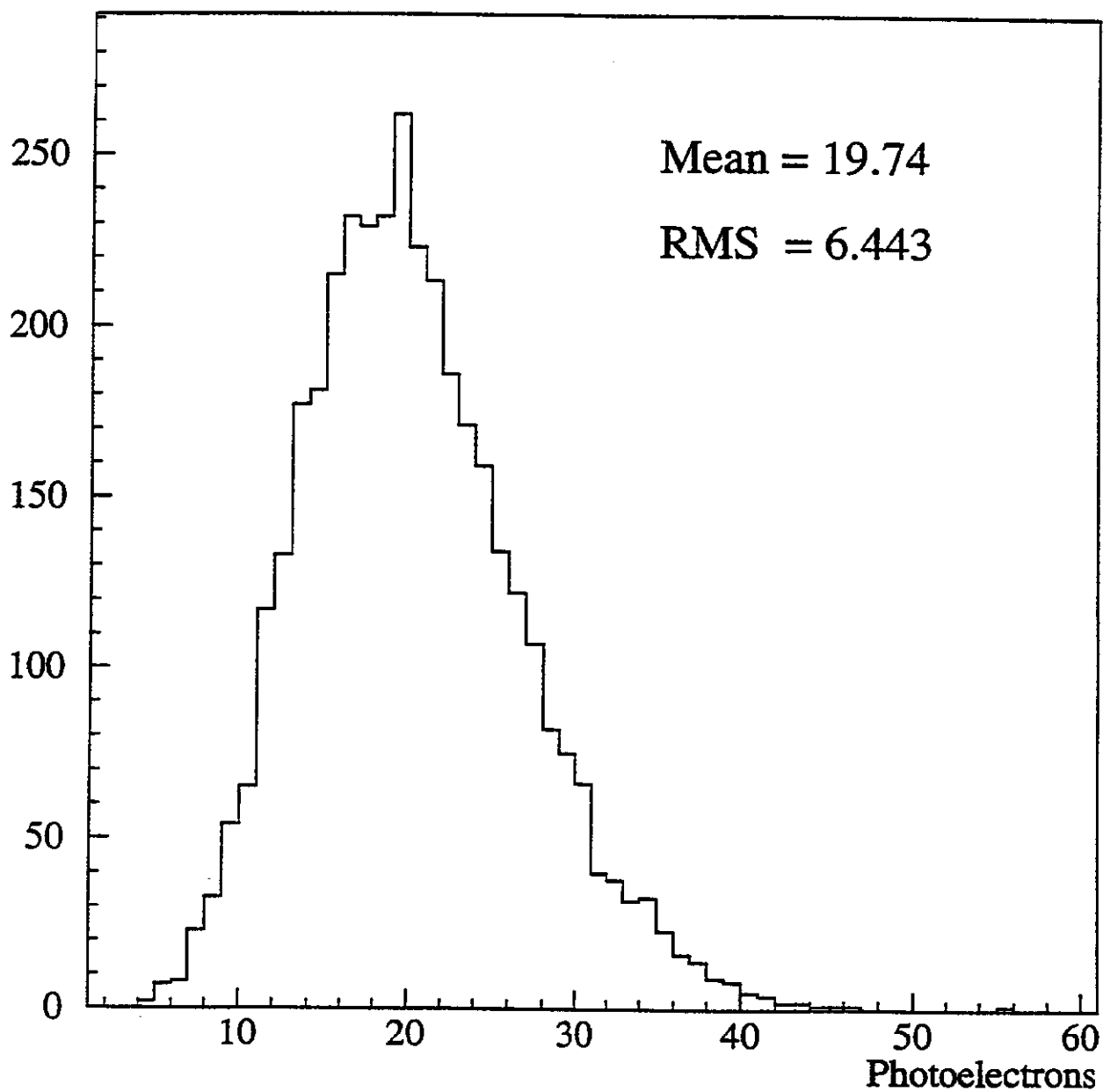


Figure 11. Detected photoelectron yield from a doublet-layer of fibers having mirrored ends.

RUN
EVENT

○
○

ZOOM

650 - 1060

1060 - 1470

1470 - 1880

1880 - 2290

2290 - 2702

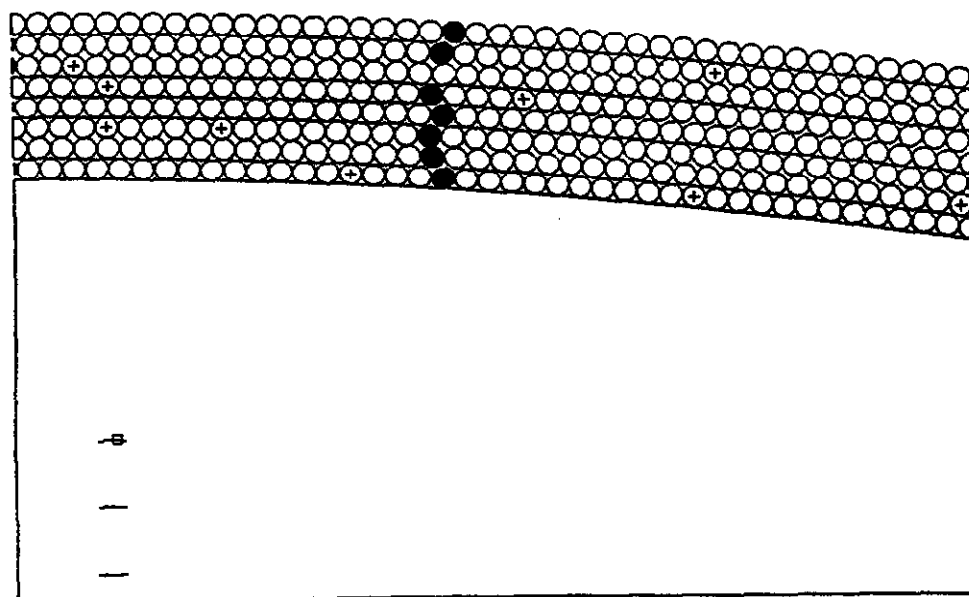


Figure 12. Event display of a cosmic ray track seen in the D0
SciFi test detector.

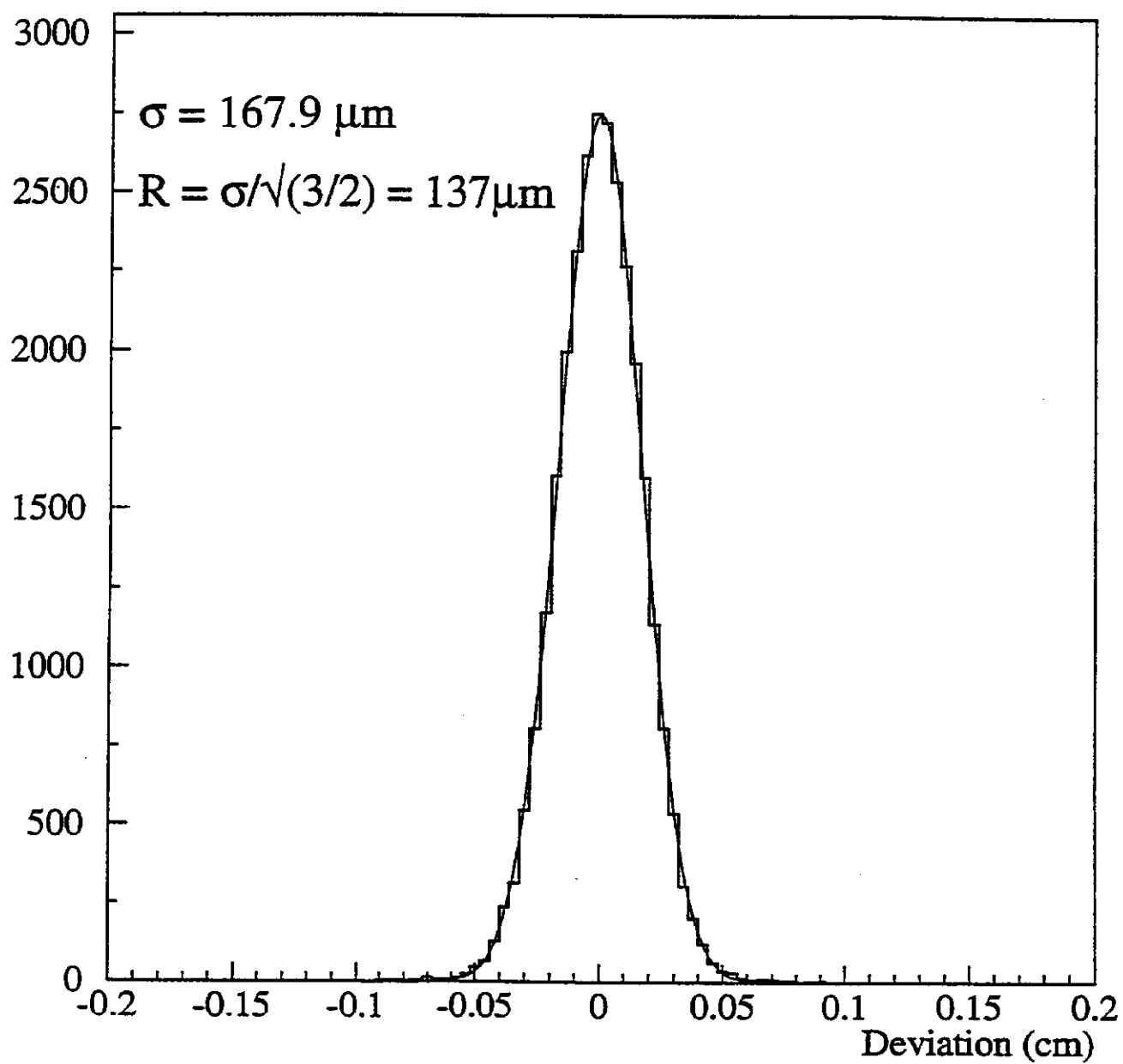


Figure 13. Measured spatial resolution of a fiber doublet layer.

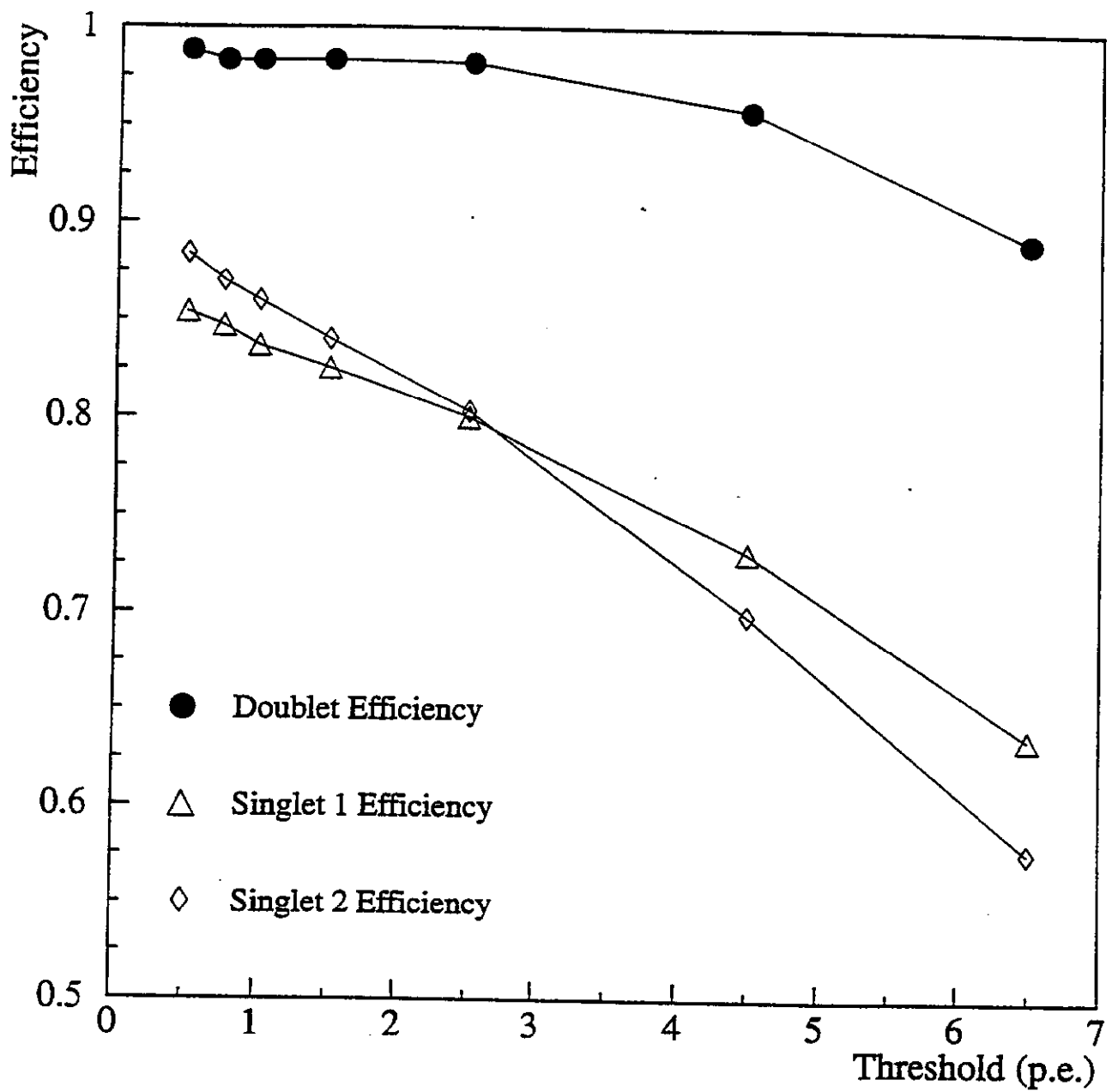


Figure 14. Efficiency of a fiber doublet layer compared to the efficiency of the component singlet layers.

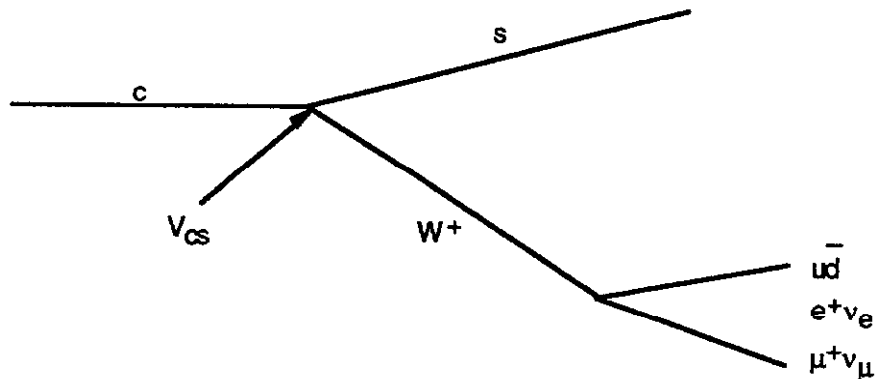
Particle Identification Issues for Charm 2000

E. I. Rosenberg
Department of Physics & Astronomy, Iowa State University
Ames, Iowa 50011-3160

We briefly summarize some topics concerning particle identification in a high-rate fixed target environment, such as might be envisioned for Charm 2000. This outline of topics served to focus the discussion in the Particle Identification working group.

Introduction:

The dominant decay mode of the charmed quark is

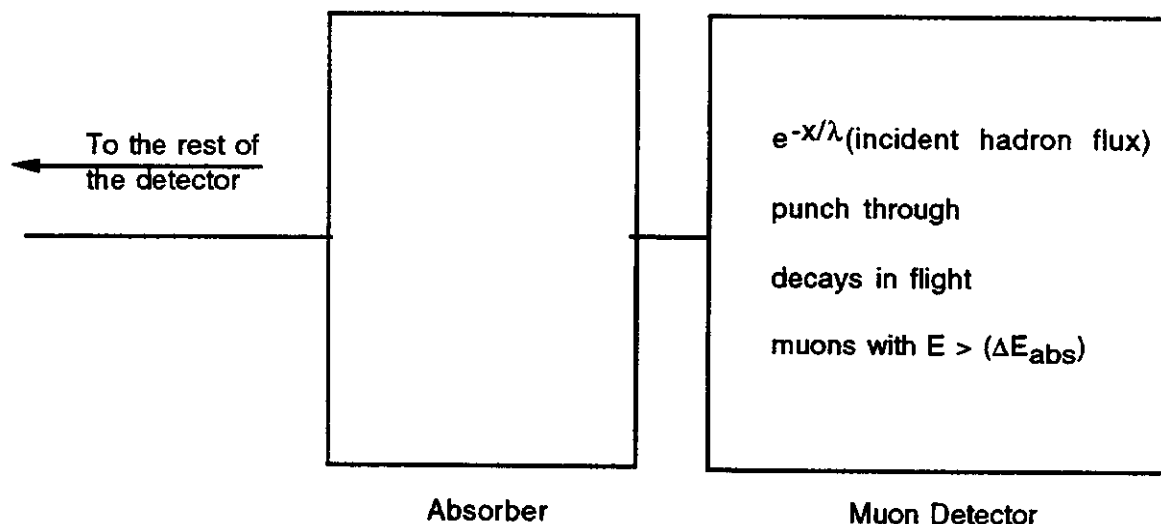


where $V_{cs} \approx 1$ and the leptonic final states occur about 30% of the time. Thus identification of electrons, muons and strange hadrons are all required to select the charm decay candidates out of the copious hadronic background. Fermilab experiment E-791, which collected about 20 billion triggers, had a sample of about 200,000 charm events (i.e. about 1 in 10^5). Thus incorporation of particle identification into the trigger is important. When discussing particle identification systems the capability of generating fast signals usable in the early stages of the trigger needs to be addressed.

Most of the issues relevant to charm decay are relevant to b decay and were discussed in detail at last summer's Snowmass Workshop on B Physics at Hadron Accelerators¹. I have borrowed freely from the summary talks of E. C. Dukes², N. R. Stanton³ and the hadron identification working group⁴.

Muon Identification

Identification of muons is relatively straightforward and typically uses an iron absorber. In the discussions of the working group, it was felt that the absorber could be instrumented as a hadron calorimeter to help in the identifications of K_L s. However, as indicated in the figure below, what emerges downstream of the absorber consists of more than just muons.



The size (and more importantly the cost of materials) of the muon system scales with the overall detector length. However, the muon system is typically the downstream most element and to first order can be treated independently of the rest of the detector. The major issue in designing a muon identification system is its level of sophistication. As indicated in the figure hadronic punch-through and muons resulting from the decay in flight of pions and kaons are a serious source of background. These backgrounds can be reduced if the muon candidate is measured twice, once upstream of the absorber and once downstream of the absorber. This means that the muon detector itself is a magnetic spectrometer. If one is interested in studying the semi-leptonic charm decays, a double momentum measurement would seem to be essential. By having the first momentum measurement as upstream as possible, the decays in flight can also be suppressed.

A simple muon tag is easily incorporated into the trigger. The more sophisticated tag which demands consistence between an upstream and downstream momentum measurement requires at the very least a lookup table in the trigger hardware. As noted in the discussion of the SFT at the Snowmass Workshop⁵, both the p and p_T of the muon can be cut on independently in the trigger.

Electron Identification

Table I is taken from a transparency shown by E.C. Dukes at the Snowmass Workshop summary and list the tools available for electron identification, the momentum range over which they are efficient and at what level they can be brought into the trigger. Some of the other issues for the particle identification working group can be outlined as follows.

Calorimetry :

What choice of materials best suits the electromagnetic calorimeter? Crystals, lead-glass and lead-scintillator are the leading candidates. To answer this question, we need physics simulation input for the proposed experiment so as to determine the energy and spatial resolution required from the calorimeter. The minimum constraint is that the energy resolution from the calorimeter should match the momentum resolution for charged particles.

Table 1 Electron Identification Tools

<u>Technique</u>	<u>Applicable Momenta</u>	<u>Incorporation into Trigger Levels</u>		
		Level 1	Level 2	Level 3
Calorimetry				
•Electromagnetic				
Long. Shower Shape	1-1000 GeV	✓	✓	✓
Lat. Shower Shape		✓	✓	✓
Preradiator		✓	✓	✓
Shower max. detector	3-1000 GeV	✓	✓	✓
•Hadronic				
Lat. Shower Shape	1-1000 GeV	✓	✓	✓
Hadronic/EM energy		✓	✓	✓
Tracking	1-1000 GeV	≈	✓	✓
E/p	1-300 GeV		✓	✓
TRD	1-100 GeV		✓	✓
Cherenkov Radiation	0.5-60 GeV			
•Threshold		✓	✓	✓
•RICH				✓
dE/dx	<5 GeV			✓
Time of Flight	<≈1 GeV			✓
Synchrotron Radiation	10-1000 GeV			✓

The issue of segmentation for such a calorimeter is a convolution of the lateral shower size, i.e. Molière radius, and the cell, or tower, occupancy. The uniform particle distribution in rapidity space implies a $1/r$ dependence on the distance from the beam. Occupancy of the innermost cells dictates how far downstream the calorimeter must be placed to avoid saturation. This means the cells closer to the beam need to be as small as possible; the Molière radius puts a lower limit on this value. Cells further from the beam can be larger. Coupled to the occupancy question is the issue of radiation hardness. In the P-865 Letter of Intent, a cumulative dose of 7 MRad was anticipated for the innermost cells. While the measurements of Bross and Pla-Dalmau⁶ indicate that 3HF-doped polystyrene can withstand such doses, the use of such scintillator forces the use of multialkali photocathode phototubes and increases the per channel readout cost. It may be advisable to design the calorimeter mechanics so that replacement of these innermost cells can be easily done.

The shower position resolution requirements need to be addressed. An energy weighted centroid of the struck cells may not give adequate resolution. However, the introduction of a shower maximum position detector has implications for the longitudinal segmentation and the cost of the associated readout electronics. There is also the issue of a pre-shower detector. The material

upstream of the calorimeter, especially an hadronic flavor identification system, may lead to a significant pair conversion rate. Two other issues that need study are the resolution of the readout electronics and the attainable calibration accuracy. In considering the former, both the requisite dynamic range and electronic noise need to be addressed.

Transition Radiation:

This subject is being addressed in the talk immediately following this one⁷. Two matters of concern for a transition radiation detector are the amount of material it will represent and the overall length of such a detector.

RICH:

The issue here is whether one detector, such as a RICH counter, can do it all— $e/\pi/K/p$ identification or whether the electron identification is separate from the hadron identification. RICH counters will be discussed below in terms of hadron identification.

Hadron Blind Detectors:

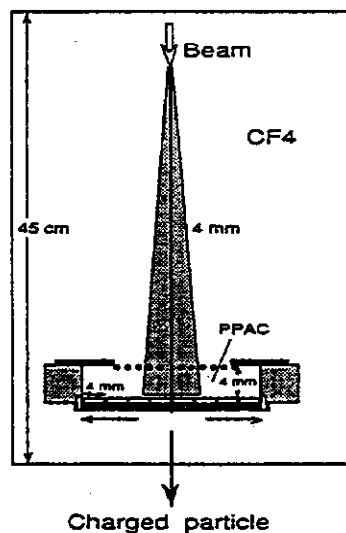


Figure 1 The Hadron Blind Detector

A new approach has been suggested by Giomataris and Charpak⁸ and test results are available⁹. In this approach electrons in a high hadronic background are detected using Cherenkov light to both identify the electrons and measure their trajectories. The test device is shown in figure 1. The same gas (CF_4 plus a noble gas) is used for the radiator and detector, so that the device is windowless. A thin CsI photocathode is used to convert the Cherenkov light to photoelectrons. A Parallel Plate Avalanche Chamber (PPAC) amplifies the photoelectrons for collection by the anode wires. Energy weighted signals from the cathode pads are used to localize the electrons. The performance of this device is shown in figures 2 and 3.

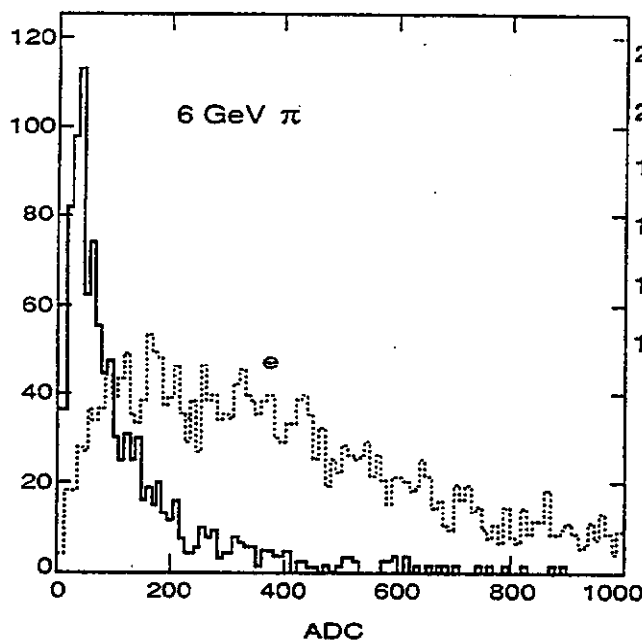


Figure 2 Pulse Height Distribution from the Hadron Blind Detector for 6 GeV e's and π 's

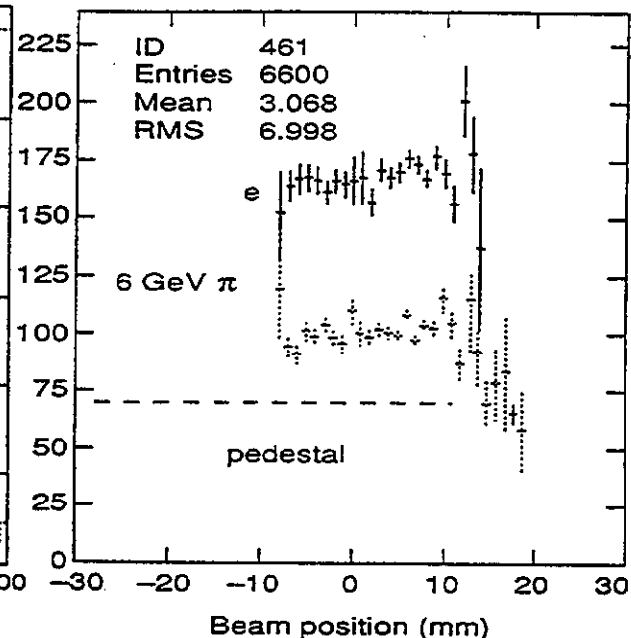


Figure 3 Pulse Height versus transverse beam position in the Hadron Blind Detector

Hadron Identification

The primary issue in hadron identification is the separation of strange particles, primarily but not exclusively K mesons, from the pion background. Some issues to be considered for candidate detectors are enumerated below.

Calorimeters

To a large extent hadron calorimetry is more of a trigger issue than a strict particle identification issue since the need for a transverse energy trigger will govern the nature of this device. However, a hadron calorimeter is necessary to tag both neutrons and, as noted earlier, K_L^0 's. The question of integrating the hadron and electromagnetic calorimeters is an important one which will effect the overall design.

Threshold Cherenkov Counters

In order to cover the momentum range anticipated at Charm 2000, a system of multiple threshold Cherenkov counters with media of varying indices of refraction are required. The question is how many are required and of what overall length? The Tagged Photon Laboratory (TPL) uses two multicell threshold counters one of index $n-1=3.089 \times 10^{-4}$ and the other of index $n-1=9.01 \times 10^{-5}$. The BaBar Collaboration is considering the use of aerogel of different densities. Clearly an important issue for the downstream detectors, e.g. the electromagnetic calorimeter, is the amount of material these will represent. Of particular importance are the mirrors and their supports, which will need to be of low density materials.

In his presentation at the Snowmass Workshop, Simon Kwan¹⁰ reported the actual detection efficiencies attained by the TPL threshold counters were only 3.1% and 6%. He further went on to compare the resolution of threshold counters, where the Cherenkov angle is inferred from the number of photoelectrons, and that of ring imaging counters, where the Cherenkov angle is directly measured. His conclusion was that for the least chromatic radiators, the resolution of a RICH counter could be as much as 250 times better than that of a threshold counter.

RICH Counters

While RICH counters have intrinsically higher resolution and can do particle separation over a wide momentum range, the general experience in keeping them operating efficiently has not been uniformly good. At Charm 2000, the issue will be complicated by the need for high rate capability, i.e. fast readout. Two possibilities are worth discussing.

•FAST RICH

The FAST RICH was originally proposed for use at the high-luminosity B-factory at the PSI¹¹. What distinguishes the FAST RICH is the use of fast photon detectors with pad readout. The BaBar collaboration is considering a liquid freon radiator, C_6F_{14} , with quartz windows, a proximity gap, and a pad readout chamber based on a solid CsI photocathode¹². A possible choice for the radiator material is the one by DELPHI in their forward RICH counters, C_4F_{10} , but this gives a kaon threshold of 9 GeV. The quantum efficiency of the CsI is an area which needs clarification. Reported values range from 10% to 31%. Another area needing investigation is that of aging of CsI or of any proposed readout chamber. In the high rate environment of Charm 2000, aging issues become more important.

•VLPC RICH¹³

The FAST RICH has the advantage of eliminating the need for TMAE. This proposal for a TMAEless RICH involves the use of Visible Light Photon Counters (VLPCs) which were described at this workshop by R. Ruchti. L. D. Isenhower gave a detailed presentation on this proposal during the particle identification working group session. The principle advantage of this technique is that it works in the visible part of the spectrum. The idea would be to place Winston light cones at the image plane and couple these to an array of VLPCs via clear optical fibers. Such a counter has the advantage of being radiation hard and having a time resolution <20 ns.

Again a major question is how much material would these represent to the downstream detectors.

References

- ¹ P. McBride and C. Shekhar Mishra, eds., **Proceeding of the Workshop on B Physics at Hadron Accelerators**, SSCL-SR1225/FERMILAB-CONF-93/267 (1993).
- ² E.C. Dukes, *ibid*, p. 505.
- ³ N.R. Stanton, *ibid*, p. 531.
- ⁴ K. Nelson et al., *ibid*, p. 551.

- 5 S. Connetti et al., *ibid*, p. 595.
- 6 A. D. Bross and A. Pla-Dalmau, "Radiation Effect in Intrinsic 3HF Scintillator," FERMILAB-
PUB-92/247 (1992).
- 7 M. Sheaff, these proceedings.
- 8 Y. Giomataris and G. Charpak, NIM **A310**, 589 (1991).
- 9 M. Chen et al., CERN PPE/93-161 (1993).
- 10 S. Kwan, "Comparison of Particle Identification Methods," **Proceeding of the Workshop
on B Physics at Hadron Accelerators**, SSCL-SR1225/FERMILAB-CONF-93/267 p. 557
(1993)
- 11 R. Eichler et al., PSI Report PR 86-13 (1993).
- 12 D. Boutigny et al., "Letter of Intent for the Study of CP Violation and Heavy Flavor Production
at PEP-II," SLAC 443 (1994).
- 13 D.M. Kaplan et al., NIM **A343**, 316 (1994).

TRANSITION RADIATION DETECTORS (TRD's)*,**

M. Sheaff
Physics Department
University of Wisconsin
Madison, Wisconsin, 53706

1. INTRODUCTION

Transition Radiation Detectors (TRD's) have been used successfully for particle identification in high energy physics experiments over approximately the last ten years. They have been utilized in a variety of experimental environments, including the Intersecting Storage Rings at CERN¹, hadron collider experiments at the CERN Sp \bar{p} S and at the Fermilab Tevatron², and an internal gas jet target experiment at the Sp \bar{p} S³ as well as fixed target experiments at both laboratories^{4,5,6,7,8}. The primary application has been electron identification^{1,2,3,4,5,6}, but, more recently, they have been used to identify hadrons as well, including both primary beam particles⁷ and secondaries in the very forward region of a multiparticle spectrometer⁸. These versatile detectors show great promise for use in the identification of heavy quark decay products in future experiments.

There is a wide window over which TR can be used to identify electrons with little contamination from other species. This is because the total TR energy radiated is proportional to the Lorentz factor, γ , of the charged particle. Thus, a TRD which "turns on" for electrons between 1 and 2 GeV demonstrates the same response to pions only when they reach an energy of 250-500 GeV.

This is demonstrated in Figure 1, which shows the expected average number of TR photons radiated and detected per module of the E769/791 TRD⁷ for electrons, pions, kaons, and protons incident as a function of particle energy. The numbers shown have been calculated using the simulation package developed for modeling this detector⁹, which was found to reliably predict the actual detector performance. The measured efficiency for the x-ray capture signal to be above the 4 keV threshold set on the electronic readout circuit, which was 83%, has been included in the numbers shown. Comparisons to the results of Reference 4 indicate that saturation is not modeled correctly in the simulations, so it has

*Talk presented at the Workshop on the Future of High-Sensitivity Charm Experiments (CHARM2000), Fermilab, June 7 and 8, 1994

**Work supported under NSF PHY-86-15287 and PHY-89-01274, and DOE DE-AC02-76-ER00881-Task D and DE-AC02-76-CHO-3000.

been put in by hand at the gamma value corresponding to that for pions at an energy of 500 GeV. This seems prudent, since no experimental data are available from the E769/791 detector at higher pion energies than this. Tests run during E791 indicated that saturation does not occur below this value, although this is somewhat above the saturation energy for pions of 430 GeV predicted using the method discussed in Reference 10. (Note the author's comments on the reliability of this estimate, however.) The dashed line on the plot shows the drop in response for the pions due to the use of a latch for readout. The crosses, which show the measured response at 250 GeV and 500 GeV, are to be compared to this. An enhanced performance, closer to the solid curve, could be achieved by instead recording all electronically separable clusters using a pipelined readout as is proposed for SSC experiments¹¹.

2. TWO EXAMPLES OF PRACTICAL TRD's AT FERMILAB

The E769/791 detector is an example of a typical, practical TRD. It was made from 24 identical modules, one of which is shown schematically in Figure 2. Each contains a radiator made from 200 $12.7 \mu\text{m}$ polypropylene (CH_2) foils stacked alternately with nylon net spacers, which are $180 \mu\text{m}$ thick. The nylon net was cut away in the region of the beam since it was found to attenuate the TR x-rays by a factor of approximately 2. The radiator volume was flushed with helium during the E769 run but was run with air during the E791 tests, since the difference is not significant. The radiator is followed by a two-plane proportional chamber with single cell depth .635 cm, and active area 76 mm wide by 65 mm high. The 64 sense wires (anodes) are spaced at 1 mm and all are oriented horizontally since the chambers were not used to measure position. The wires are $10.2 \mu\text{m}$ gold-plated tungsten and the cathodes are $12.7 \mu\text{m}$ mylar with 140 \AA of aluminum sputtered onto both sides. The chamber gas used was xenon bubbled through methylal at 0°C , which results in a mixture that is approximately 90% xenon. There is a .3175 cm buffer volume filled with nitrogen in front and in back of the two-plane chamber. The gas volumes were maintained at equal pressure to keep the chamber gains uniform across the planes.

Because it is comprised of many layers, each with a relatively small number of foils in the radiator stack followed by two chamber planes that are shallow in depth, this detector is an example of a "fine-sampling TRD"^{11,12}. This means that at most one x-ray is likely to be captured per plane, which is the reason that the latch readout, although not optimum, sufficed. Also, because of the short integration time of the electronics circuits used, which shaped the pulses from the very localized ionization of an Fe_{55} source to 26 ns full width at half maximum, this TRD discriminates using the technique of "cluster counting"^{12,13}. This has been shown to give better separation between species than the method of total charge collection.

The length of the detector as built was 2.79 m. The total amount of material in the detector was 8.7% of an interaction length and 16.9% of a radiation length including two .3175 cm scintillation counters used for gating. It would be difficult to reach the 90% efficiency for pions coupled with a factor of 30 in background rejection (in this case protons, since the kaons were separately tagged by means of a Differential Isochronous Self-Focusing Cerenkov

counter [DISC]¹⁴) that was achieved with this detector with much less material than this. The method by which the pion sample was selected is illustrated in Figure 3, which shows the distribution of TRD planes hit per event for all events in which the beam particle was not tagged by the DISC as a kaon from a typical E769 data run. As shown by the curves in the figure, the proton and pion peaks were each fit with a double binomial on a run-by-run basis. A plane count cut was chosen such that 90% of the integrated pion distribution lay above it. Then, the background above this cut was calculated using the proton curve. The technique was verified using plane count distributions made for the protons and pions separately during special runs in which the DISC pressure was set to tag them. Further details about the E769/791 detector are contained in Reference 7.

The second example I would like to discuss is the TRD which was designed and built at the Leningrad Nuclear Physics Institute for E715⁴ at Fermilab. This detector was used successfully to identify the electrons resulting from the beta decay of Σ^- hyperons, $\Sigma^- \rightarrow ne^- \nu$. The branching fraction for this decay is three orders of magnitude smaller than that of the non-leptonic decay mode, $\Sigma^- \rightarrow \pi \pi^-$, which has a branching fraction close to 100%. Thus, in order to obtain a beta decay sample with only a few percent hadron contamination it was necessary to achieve a better rejection of pions than could be accomplished by the use of a calorimeter alone.

Since the momentum range of the decay pions and electrons from 250 GeV/c Σ^- is 5-80 GeV/c, the detector was designed with foil and gap thicknesses such that saturation was reached for electrons just below 5 GeV/c. Thus the efficiency for electron detection was uniform throughout the range of interest and also the pion rejection factor, since, even at 80 GeV/c, the pions are well below the threshold for TR.

The E715 TRD was made from 12 identical radiator-chamber assemblies. Each radiator stack contained 210 foils made from the same material as in the E769 TRD, CH_2 , but both the thickness of the foils and the depth of the air-filled gaps were larger, 17 μm and 1 mm. This is the reason that saturation is reached at higher electron energy. Since the chambers were in the region downstream of the experiment target and behind the analysis magnets, they were not exposed to very high rates. Thus they did not need to have such narrow wire spacing or shallow cell depth as the E769 detector. Thus, for the E715 detector, the wire spacing was 2 mm and the depth of the chambers, which were filled with xenon-methane 70/30, was 1.6 cm. The increased cell depth resulted in a somewhat better efficiency for capture of the TR x-rays, especially the higher energy x-rays, in the chamber. In this detector, the wires were ganged in sets of 8 and input to electronics circuits very similar to the ones in the E769 detector. However, a scaler was put on the output of each discriminator to allow the registering of all clusters seen in the cell for each event. The combination of several factors, including the fact that the E715 detector was above saturation, had chambers with deeper cells, and had electronics circuits capable of counting all (electronically separable) x-ray capture clusters, resulted in the excellent separation of electrons from pions in this 12-layer TRD. This separation is shown in Figure 4, reproduced from Reference 11. As shown in a), the calorimeter alone does not pick out the beta decay signal. The addition of the information from the TRD as shown in b) results in a signal for $\Sigma^- \rightarrow ne^- \nu$ which has a background of only 3%¹⁵.

3. USE OF TRD's TO IDENTIFY HADRONS IN FIXED TARGET OR FORWARD COLLIDER

TRD's are useful in the very forward region of a fixed target spectrometer for the identification of hadron secondaries resulting from charm decays at energies above those where Cerenkov counters work well for hadron identification. This technique was actually used for this purpose in one experiment using the OMEGA spectrometer at CERN. Figure 5 displays the distributions in the number of hits above the 4 keV threshold expected per track for protons (dotted line), kaons (dot-dash line), and pions (solid line) traversing a detector with 24 radiator-chamber modules identical in construction to the E769/791 detector. The curves shown are for particle energies of 200, 400, 600, 800, and 1000 GeV, respectively. The rejection for kaons or protons versus efficiency for pions is good over the range shown.

4. USE OF TRD's TO IDENTIFY ELECTRONS IN THE CENTRAL AND MODERATELY FORWARD COLLIDER

Since electrons radiate TR and hadrons do not over a two order of magnitude range in momentum, the momentum window over which it is possible to discriminate electrons from hadrons is large. A TRD can be designed to saturate at just below 2 GeV for electrons, so that above that value, the efficiency for electrons is constant. In the same detector, since the effect goes as γ , pions do not radiate appreciable TR until they are at energies near that same value of γ , in the range of hundreds of GeV. When used in combination with an electromagnetic calorimeter, the two can provide a background rejection of $\sim 10^{-4}$ with good selection efficiency for electrons.

Figure 6 shows the expected hit distributions for electrons (solid line) and pions (dotted line) at 0.5, 1.0, 1.5, and 2.0 GeV/c in a possible future TRD to be used for the identification of electrons from charm decay. The curve shown for 2.0 GeV/c also represents the situation all the way out to energies of 150 GeV/c, since above 2.0 GeV/c the detector is saturated for electrons and below 150 GeV/c pions are not yet at a high enough energy to radiate. The simulations were carried out assuming 24 modules, each with a radiator made from 50 $12.7 \mu\text{m}$ foils followed by a single-plane xenon-filled detector .635 cm in depth. The results indicate that a TRD could be built with total depth less than half a meter which is capable of discriminating electrons from pions at as low a momentum as 1 GeV/c.

Not only can TRD's be used offline to discriminate between electrons and hadrons, but they should also make it possible to trigger on electrons online at the first trigger level providing the cell sizes are small and the drift time in the gas and the electronics can be made fast enough. Since they are constructed using narrowly spaced wire chambers, TRD's are also capable of identifying electrons inside jets, which makes them well suited for identifying b and c jets in collider experiments. And, they can simultaneously be used as high resolution tracking detectors and for particle identification by splitting the wire signals and subjecting them to multiple thresholds¹⁶. The down side of TRD's is that they represent a significant amount of material, especially in radiation lengths. Further research is in progress to optimize the separation relative to the amount of material utilized.

5. ACKNOWLEDGMENTS

The assistance of Timothy Meyer, a Fermilab summer student who is an undergraduate at Johns Hopkins University, with the simulations and the plots is gratefully acknowledged.

6. REFERENCES

- [1] J. Cobb et al., "Transition Radiators for Electron Identification at the CERN ISR", NIM 140 (1977) 413.
- [2] R. Ansari and B. Merkel, "Transition Radiation Detectors for Hadron Colliders", talk given by B. Merkel at the "Symposium on Particle Identification at High Luminosity Hadron Colliders", Fermilab, April 5-7, 1989, published in the proceedings of the symposium edited by Treva Gourlay and Jorge Morfin, p. 359.
- [3] A. Vacchi, "Large-Area Transition Radiation Detectors for Electron Identification in the UA6 Experiment at the CERN $p\bar{p}$ Collider", NIM A252 (1986) 498.
- [4] A. V. Kulikov et al., "Performance of the E715 Transition Radiation Detector", talk given at the First Annual Meeting (New Series) of the Division of Particles and Fields of the American Physical Society, Santa Fe, New Mexico, Oct 31 - Nov 3, 1984. Published in the proceedings edited by T. Goldman and Michael Martin Nieto, World Scientific Publishing Co. Pte. Ltd.
- [5] G. Barr et al., "The NA31 Transition Radiation Detector", IEEE Transactions on Nuclear Science 36 (1989) 66.
- [6] M. Clemen (representing the Helios collaboration), "The Helios Transition Radiation Detector", talk given at the "Symposium on Particle Identification at High Luminosity Hadron Colliders", Fermilab, April 5-7, 1989, published in the proceedings of the symposium edited by Treva Gourlay and Jorge Morfin, p. 339.
- [7] "Use of a Transition Radiation Detector in a Beam of High Energy Hadrons", D. Errede et al., NIM A309 (1991) 386.
- [8] M. Baake et al., "A Transition Radiation Detector for Kaon/Pion Separation", NIM A281 (1989) 325.
- [9] The simulation package has two parts. The first is a calculation of the average number of TR photons as a function of energy produced by the radiators including detection in the xenon chamber planes. See L. C. Myrianthopoulos et al., "Status Report on the University of Maryland Transition Radiation System for Beam Particle Identification", University of Maryland, MdDP-TR-80-106, May 1980, unpublished, for details. Since the Monte Carlo part of that program was appropriate for the total charge method as opposed to "cluster counting", the method used in the E769/791 TRD, the part of the package that generates the detector hits was written by our group. The simulations take into account the fact that signals were simply latched and not scaled, so that two clusters seen in the same chamber plane would be recorded as one.

- [10] X. Artru et al., "Practical theory of the multilayered transition radiation detector", Phys. Rev. D12 (1975) 1289, discusses these and other properties of Transition Radiation. See p. 1297 for a discussion of saturation.
- [11] B. Dolgoshein, "Transition Radiation Detectors and Particle Identification", NIM A252 (1986) 137.
- [12] T. Ludlam et al., "Particle Identification by Electron Cluster Detection of Transition Radiation Photons", NIM 180 (1981) 413.
- [13] C. Fabjan et al., "Practical Prototype of a Cluster-Counting Transition Radiation Detector", NIM 185 (1981) 119.
- [14] M. Benot et al., "Cerenkov Counters for Particle Identification at High Energies", NIM 105 (1972) 431.
- [15] S.Y. Hsueh et al., "Measurement of the Electron Asymmetry in the Beta Decay of Polarized Σ^- Hyperons", Phys. Rev. Lett. 54 (1985) 2399.
- [16] J. T. Shank et al., "Test-beam Performance of a Tracking TRD Prototype", NIM A309 (1991) 377.

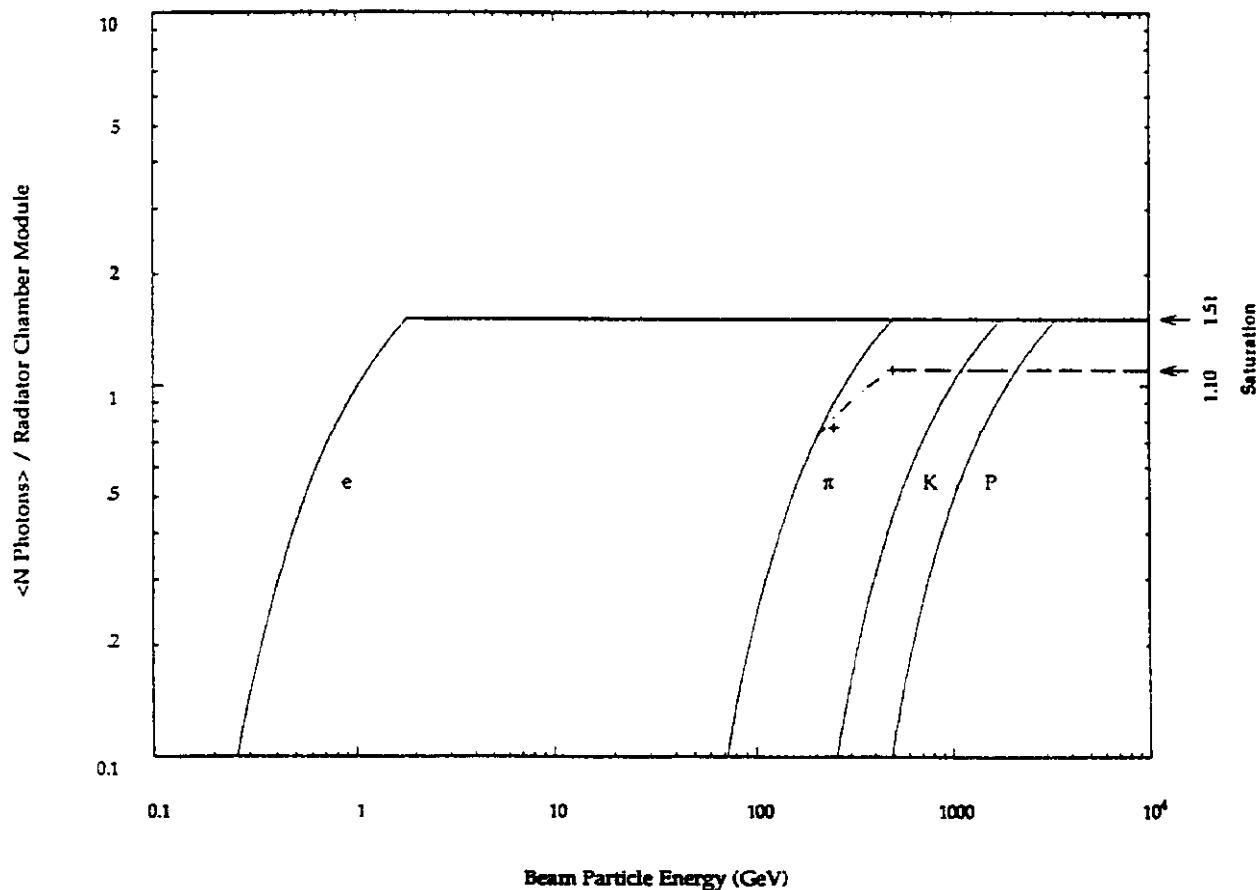


Figure 1. Expected average number of photons detected above the 4 keV threshold in each module of the E769/791 TRD for electrons, pions, kaons, or protons incident as a function of particle energy. The dashed line shows the degradation in performance due to readout by means of a latch. The crosses indicate the measured performance of the detector at 250 and 500 GeV.

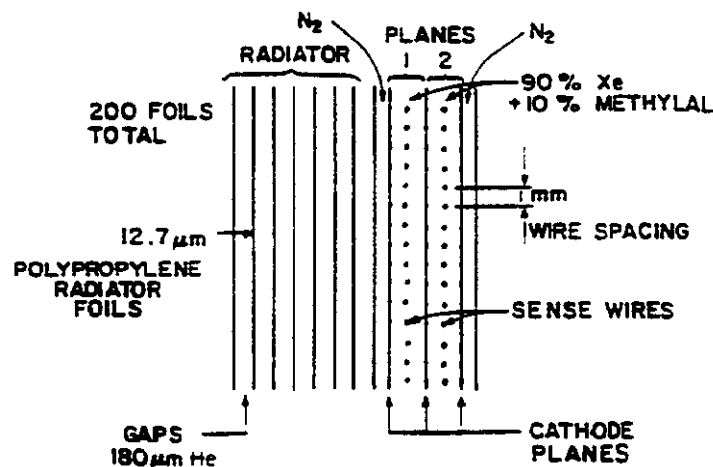


Figure 2. Schematic of one module of the E769/791 TRD in elevation view. The beam is incident from the left in the figure.

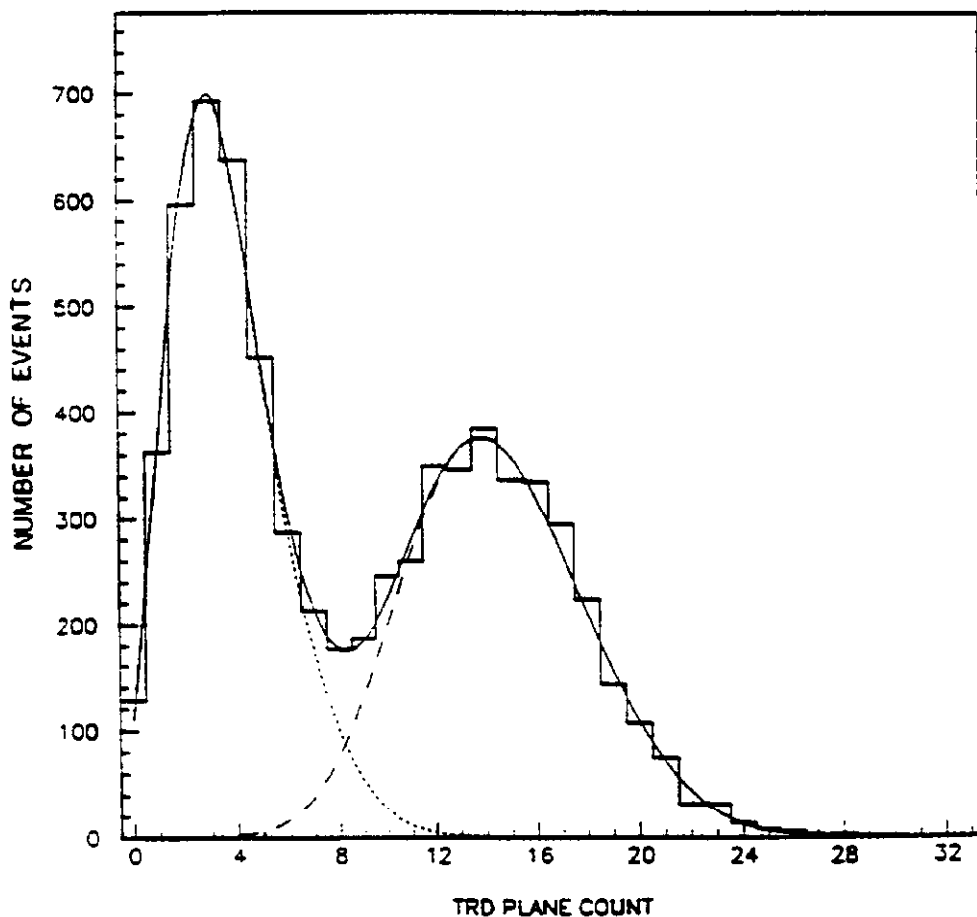


Figure 3. TRD plane count distributions for all event triggers on a typical E769 data tape for which the incident beam particle was not tagged as a kaon by the DISC Cerenkov counter. The peak to the left contains protons and the one to the right, pions. The results of the double binomial fits to each of the two peaks are indicated by the curves on the plot.

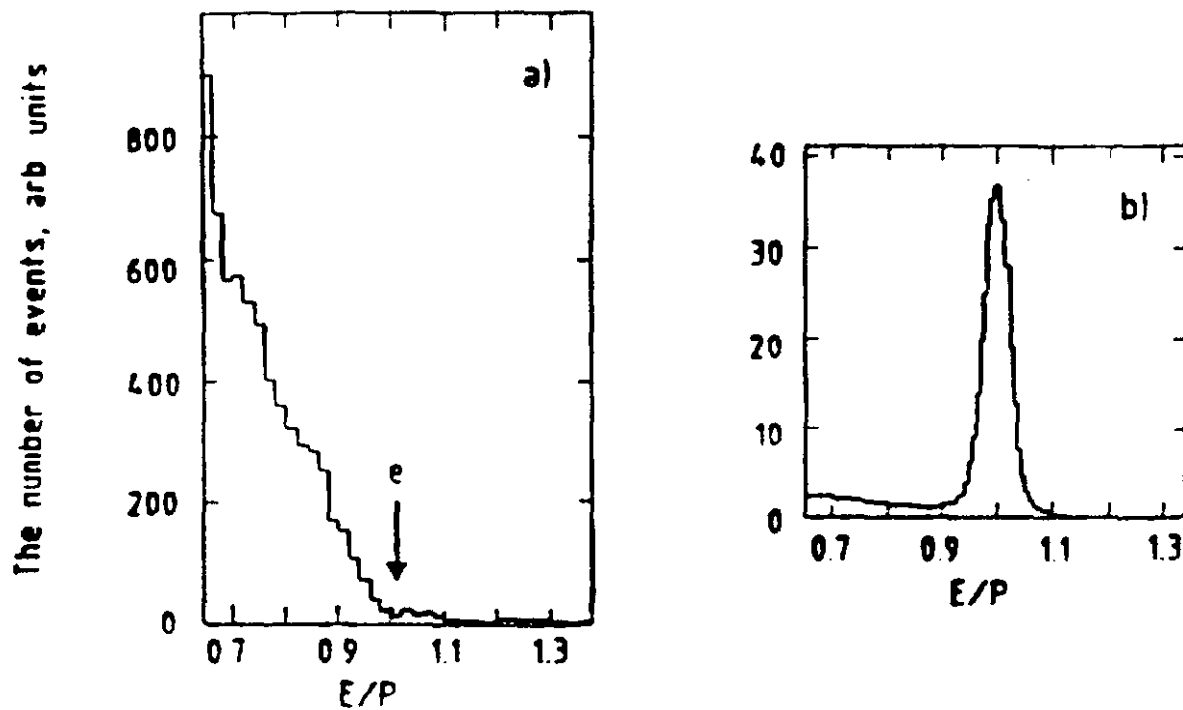


Figure 4. Electron secondaries from $\Sigma \rightarrow p e \nu$ candidates from E715 a) before, and b) after making a cut on electron identification using the transition radiation detector.

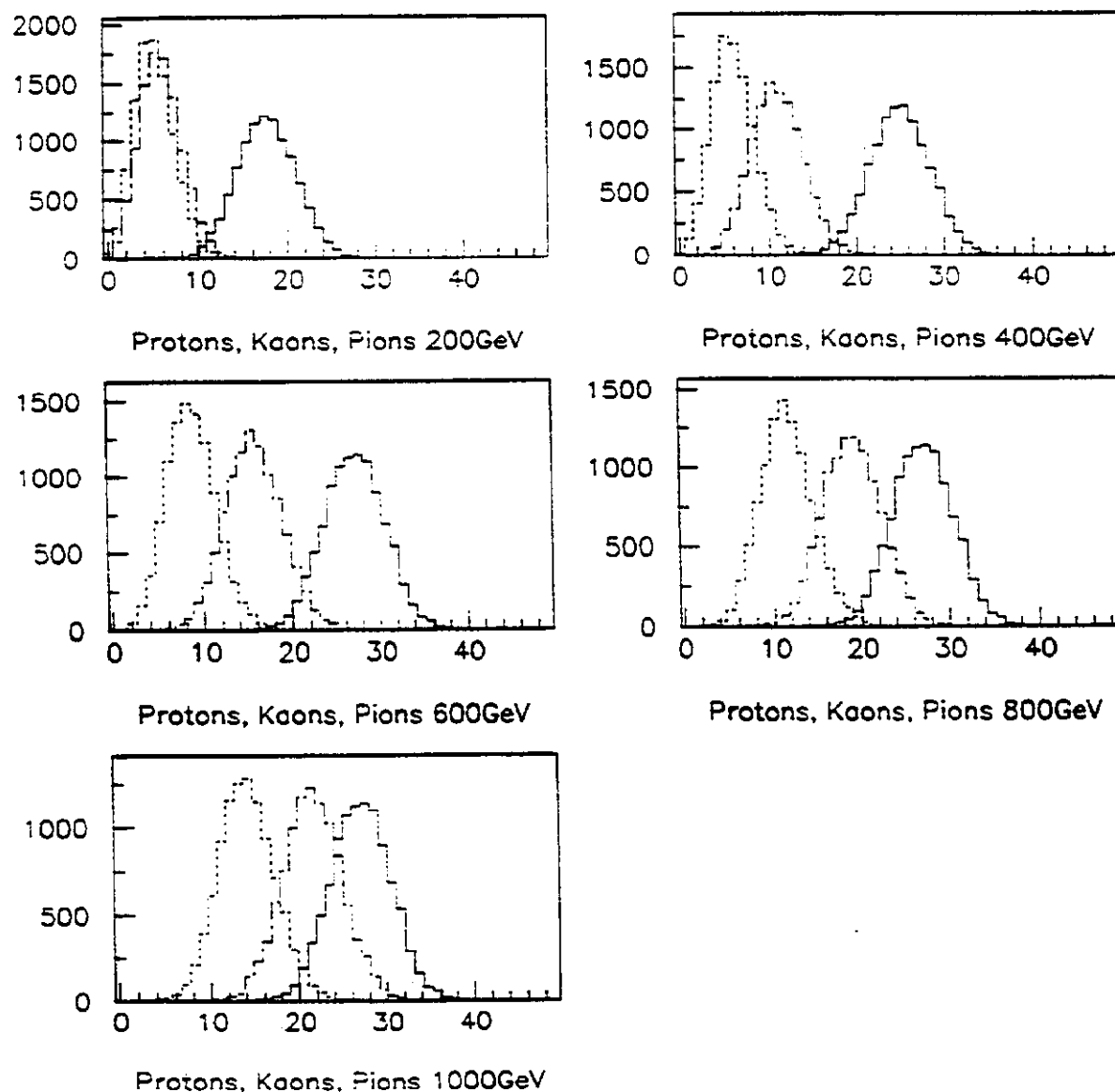


Figure 5. Expected hit distributions above the threshold for TR per track for protons (dotted line), kaons (dot-dash line), and pions (solid line) at 200, 400, 600, 800, and 1000 GeV. The simulations assume a TRD identical in construction to the E769/791 detector. Saturation for pions at 500 GeV/c results in poorer K/pi separation at higher momenta.

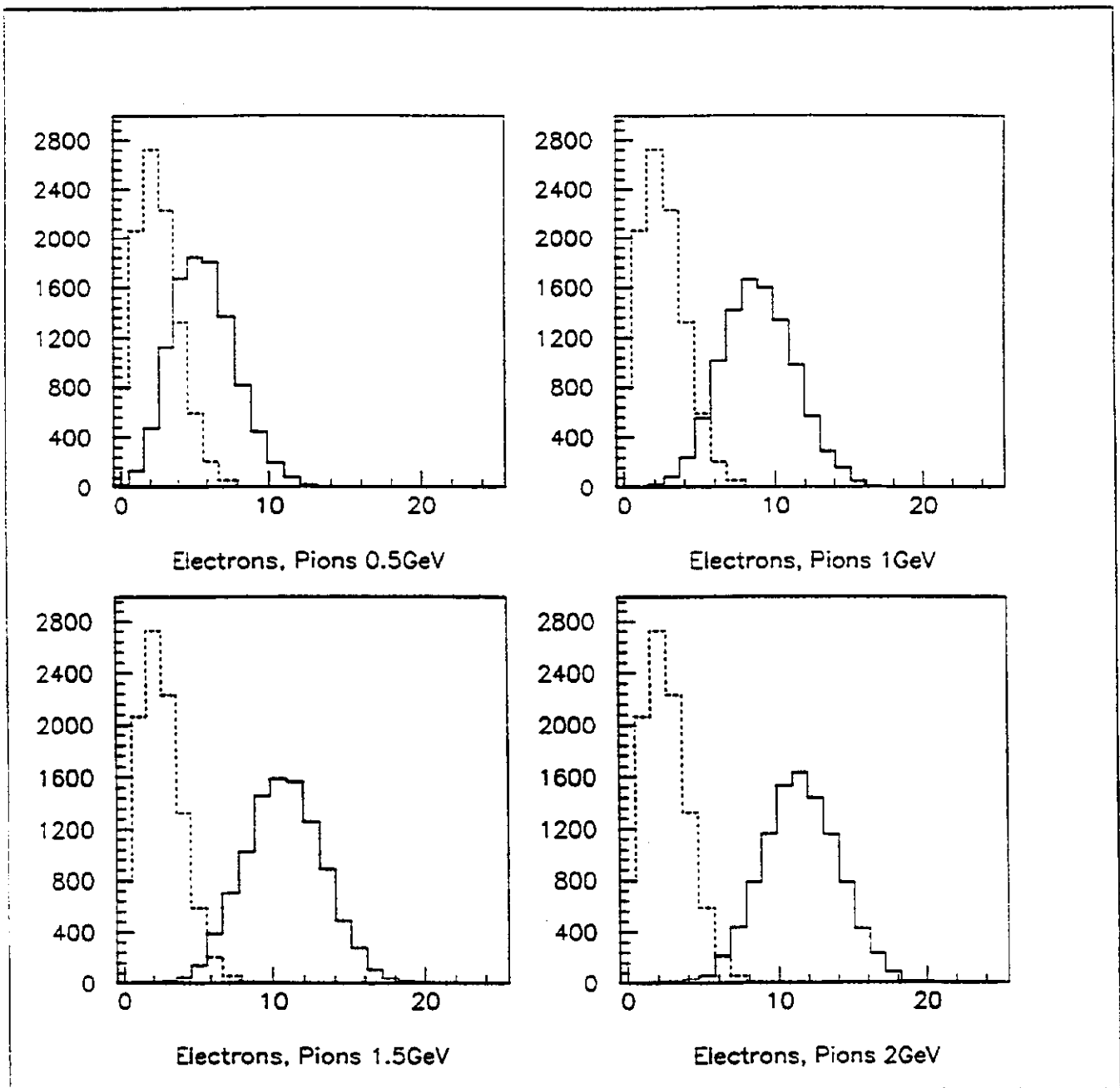


Figure 6. Expected hit distributions for electrons (solid line) and pions (dotted line) at 0.5, 1.0, 1.5, and 2.0 GeV in a “fine-sampling” TRD built from 24 modules, each with a radiator composed of 50 $12.7 \mu\text{m}$ CH_2 foils followed by a single-plane xenon-filled MWPC with cell depth .635 cm.

A Secondary Vertex Trigger for Beauty Search: Results from the BEATRICE/WA92 Experiment

Dario Barberis

University and INFN Genova (Italy)

representing the BEATRICE Collaboration:

M. Adamovich⁶, M. Adinolfi³, Y. Alexandrov⁶, C. Angelini⁷, C. Bacci¹⁰, D. Barberis³, D. Barney⁵, J. Batten⁵,
W. Beusch², C. Bruschini³, R. Cardarelli⁹, A. Cardini⁷, V. Casanova³, F. Ceradini¹⁰, G. Ciapetti⁸, M. Dameri³,
G. Darbo³, A. Di Ciaccio⁹, A. Duane⁵, J.P. Dufey², Ph. Farthouat², V. Flaminio⁷, A. Forino¹, B.R. French²,
A. Frenkel⁸, C. Gemme³, R. Gessaroli¹, K. Harrison³, R. Hurst³, A. Kirk², F. Lacava⁸, C. Lazzeroni⁷,
L. Malferrari¹, S. Maljukov⁴, G. Martellotti⁸, P. Martinengo², P. Mazzanti¹, J.G. McEwen¹¹, I. Minashvili⁴,
P. Nechaeva⁶, A. Nisati⁸, D. Orestano⁸, B. Osculati³, M. Passaseo⁸, G. Penso⁸, E. Petrollo⁸, L. Pontecorvo⁸,
A. Quareni¹, P. Ragni⁸, H. Rotscheidt², V. Ryzhov², C. Roda⁷, L. Rossi³, N. Russakovich⁴, C. Salvo³,
R. Santonico⁹, G. Schuler², A. Semenov⁴, A. Solovjev⁴, M. Torelli⁸, S. Veneziano⁸, M. Verzocchi⁸, D. Websdale⁵,
M. Weymann², L. Zanello⁸, M. Zavertyaev⁶
*Bologna¹, CERN², Genova³, JINR-Dubna⁴, London ICSTM⁵, Moscow LPI⁶,
Pisa⁷, Roma I⁸, Roma II⁹, Roma III¹⁰, Southampton¹¹*

Abstract

We describe the trigger and the finely segmented silicon microstrip detector used in the WA92 fixed-target experiment at the CERN Omega spectrometer and give preliminary results on their performance during the 1992 and 1993 data-taking periods and on the search for beauty decay topologies.

1 Introduction

Experiment WA92 [1, 2], which took data in 1992 and 1993 at the Ω spectrometer at the CERN SPS, has been designed to study the hadroproduction and the decays of particles containing b quarks. Two factors are important for finding a beauty signal in a fixed-target environment: the selectivity of the trigger and the reconstruction efficiency for decay vertices. A large acceptance for beauty particles and high background rejection have been achieved using the apparatus and the trigger we describe in this paper.

The apparatus consisted of a Si microstrip beam telescope, a 2 mm Cu/W target, the Decay [3] and Vertex [4] detectors, 15 modules of MWPC's in the 1.8 T vertical field of the Ω magnet, 2 drift chamber modules, the Olga electromagnetic calorimeter [5] and the RPC muon detector [6].

The Decay Detector (DD) is made of 17 planes of Si microstrip detectors with $10\mu\text{m}$ pitch covering an area of $5 \times 5\text{mm}^2$. The spacing along the beam direction is 1.2 mm for

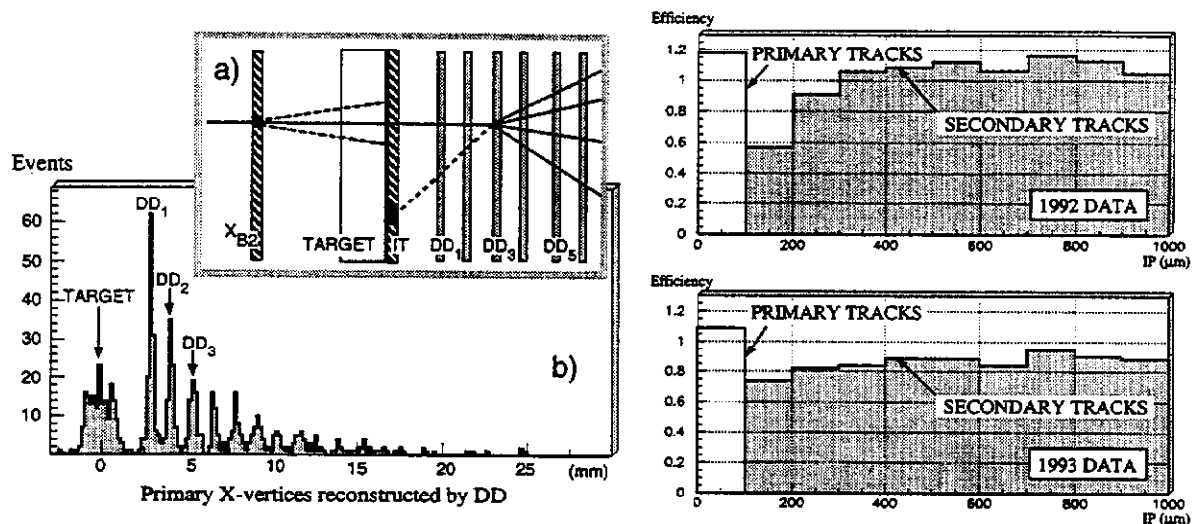


Figure 1: a) Primary interaction in a DD plane with low-energy back-scattered particle. b) Distribution of reconstructed primary interactions in DD planes which do not satisfy the correlation between hits in X_{B2} and IT. c) BCT track reconstruction efficiency as function of true track impact parameter (from simulation).

the first 14 planes and 5 mm for the following ones; the first 6 detectors are $150\ \mu\text{m}$ thick and the rest $300\ \mu\text{m}$ thick. Thirteen planes (12 in 1993) measure the Z (vertical) coordinate, 2 (3) the Y (horizontal) coordinate and 2 are inclined for projection matching. All strips are individually read out into 8-bit ADC's; with thresholds set for each strip at 4 times the pedestal RMS we obtain efficiencies of 93% and 97% for the thin and thick planes respectively with a noise level of 10^{-3} per strip. The measured single-point resolution is between 2 and $3\ \mu\text{m}$ and the two-track resolution is of the order of $30\ \mu\text{m}$. The DD was designed to allow the reconstruction of a decay chain with secondary and tertiary vertices which is an important characteristic of beauty events.

The Vertex Detector consists of 12 planes (6 per projection) of $25\ \mu\text{m}$ pitch Si microstrip detectors spaced by 2.5 cm and 5 inclined planes with $50\ \mu\text{m}$ pitch; all detectors cover an area of $5.12 \times 5.12\ \text{cm}^2$ and have a digital read-out. The 6 Z planes are equipped with a fast read-out and are used in the impact parameter trigger.

2 Trigger

To counter the unfavorable signal-to-noise ratio ($\sigma_{b\bar{b}}/\sigma_{tot} \simeq 10^{-6}$ at $\sqrt{s} = 26\ \text{GeV}/c^2$) we used of a combination of several independent trigger components:

- *High transverse momentum Trigger:*

This trigger selects, in less than 250 ns, events having particles with $P_t \geq 0.6\ \text{GeV}/c$ with respect to the beam direction, which can be produced in decays of high-mass particles. The trigger uses two so-called butterfly hodoscopes [7]; as a result of the

deflection in the magnetic field of the Ω spectrometer, a charged particle that originates in or close to the target can cross the butterfly hodoscopes, and thus give a trigger, only if it has P_t larger than the set threshold ($0.6 \text{ GeV}/c$).

- *Muon trigger:*

This trigger takes advantage of the large semi-leptonic branching ratio of B mesons. The μ -trigger [6] is based on two hodoscopes built with resistive-plate chambers, each hodoscope having two chambers to measure the vertical coordinate (Z view) and one chamber to measure the horizontal coordinate (Y view). Using only information for the Z view, a coincidence matrix logic [8] selects in 250 ns muon tracks coming from the target region.

- *Secondary-vertex trigger:*

The secondary-vertex trigger or beauty contiguity trigger (BCT) exploits the long B lifetime ($c\tau \simeq 450 \mu\text{m}$) which allows decay vertices to be well separated from the primary interaction point. The BCT hardware and the implemented algorithm have been extensively described elsewhere [4, 9, 10] and only their performance will be discussed here, with emphasis on the 1993 upgrades.

2.1 Secondary-Vertex Trigger

The secondary-vertex trigger uses 9 silicon strip detectors, providing views of events in the Z projection, where tracks are not affected by the magnetic field:

- two planes of $20 \mu\text{m}$ pitch microstrips that measure the incoming beam trajectory, one plane at $X_{B1} \simeq -71 \text{ cm}$ and one plane at $X_{B2} \simeq -11 \text{ cm}$ upstream of the 2 mm target (half of the 1992 data were recorded with a W target, the rest of the 1992 data and all the 1993 data were recorded with a Cu target). The two coordinates of the primary vertex position (X_V, Z_V) are given respectively by the X_{TG} position of the target centre and by the linear extrapolation to X_{TG} of the track defined by the hits measured in the two beam planes.
- one $200 \mu\text{m}$ pitch silicon strip detector, placed $50 \mu\text{m}$ after the target, fires if a charge equivalent to at least five minimum-ionizing particles (m.i.p.) is released in one of the strips. This condition is satisfied by $\sim 90\%$ of interactions occurring in the target and by only $\sim 4\%$ of interactions occurring in the DD planes. This detector is referred to as the in-target counter (IT).
- six planes of $25 \mu\text{m}$ pitch microstrips with $5.12 \times 5.12 \text{ cm}^2$ active area cover a region extending from $X_{V1} \simeq 6 \text{ cm}$ to $X_{V6} \simeq 42 \text{ cm}$. Using the hits recorded in these six planes, tracks with at least 5 hits are reconstructed by the BCT and classified according to their impact parameters (IP) with respect to the primary vertex and dip angles.

The trigger algorithm is executed by the BCT in $35 \mu\text{s}$, which is about 3 to 4 orders of magnitude better than is achieved when running a similar algorithm on an off-line computer. The

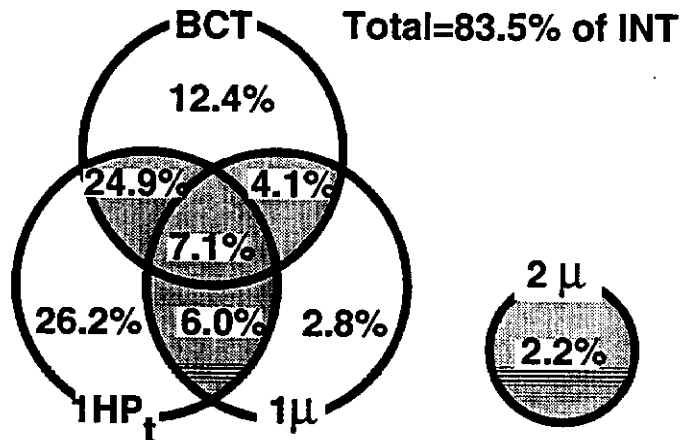


Figure 2: The shaded region of the diagram represents the 1992 WA92 trigger. The numbers are the beauty acceptance with respect to the INT trigger, which had an efficiency of 75% for beauty events occurring in the target.

BCT condition used required the presence of at least three primary tracks ($IP \leq 100 \mu\text{m}$), to re-enforce the primary-vertex constraint, and two secondary tracks ($IP \geq 100 \mu\text{m}$), to indicate the existence of a secondary vertex.

We recognized that a weak point of the BCT in the 1992 configuration was the primary vertex definition, where triggering conditions were likely to be satisfied if the primary vertex was not correctly reconstructed. For example, when two or more beam particles arrived during the live time of the front-end electronics (about 200 ns), the wrong (X_V, Z_V) could be found. Also, the existence of a primary vertex in the target could be wrongly flagged because of heavily ionizing nuclear fragments emerging from primary interactions in the DD planes and travelling backwards (see Fig. 1.a). For 1993 we required a spatial correlation between the firing IT strip and the extrapolated (X_V, Z_V) . As an example of the improvement achieved, we show in Fig. 1.b the X position of the primary vertex for those events that were rejected by the 1993 BCT configuration but would previously have been accepted.

2.2 Trigger Performance

In triggering on secondary vertices there is a trade-off between beauty acceptance and background reduction, and some attention is needed to avoid (or at least reduce) possible trigger biases. In designing the BCT track-reconstruction algorithm we were careful to minimize the effects of detector inefficiencies and noise and to correctly count and classify tracks according to their IP. In Fig. 1.c the BCT track-finding efficiency is shown as a function of IP class for simulated beauty events. The double counting of tracks falling in two neighbouring IP classes that in 1992 led to an apparent efficiency of greater than one was

largely eliminated in 1993 by an improved BCT algorithm. Also, the peak of the primary tracks, associated with a deeper valley in the first IP class, was reduced in 1993. We then obtained a trigger providing an IP selection that is uniformly efficient between $100\mu\text{m}$ and 1mm .

To understand the trigger behaviour we have fully simulated minimum-bias, $c\bar{c}$ and $b\bar{b}$ events. Minimum-bias events were generated using Fluka [11] as interfaced with Geant 3.21 [12]. This reproduces well the experimentally measured charged particle multiplicities and kinematics, and also the production of heavily ionizing particles, which is important for the simulation of the response of the in-target counter. We generate $c\bar{c}$ and $b\bar{b}$ events using a combination of Pythia 5.4 [13] and Fluka. In the generation process up to 98.5% of the centre-of-mass energy is available for the simulation of hard processes by Pythia; the remaining energy is used to simulate soft processes with Fluka. The passage of generated particles through the experimental apparatus is simulated in detail using Geant 3.21. Non-interacting beam particles, detector inefficiencies and random noise are added in accordance with experimental measurements.

In Table 1 we present the trigger rates obtained for background and signal with the different triggers and in Fig. 2 we represent the beauty acceptance of the 1992 trigger for the Cu target data. The interaction pretrigger (INT) required the presence of an incoming beam particle, incident on the target, and outgoing interaction products, together with a signal of more than 5 m.i.p. in the IT; the 1μ (2μ) trigger required the presence of at least one (two) muon(s); the $1HP_t$ ($2HP_t$) trigger required that there should be at least one (two) particle(s) having a transverse momentum with respect to the beam $\geq 0.6\text{ GeV}/c$; the BCT required at least three primary and two secondary tracks. The 1992 trigger was the logical 'OR' of the 'AND' of any two of the 1μ , HP_t , BCT triggers; all events satisfying the 2μ trigger were accepted. The $1HP_t$ ($2HP_t$) trigger condition was used with the Cu (W) target.

Trigger Type	Data	Min.Bias	$c\bar{c}$	$b\bar{b}$
INT/σ_{tot}	65 %	67 %	75 %	75 %
$1\mu/INT$	2.8 %	2.5 %	7.8 %	20.0 %
$2\mu/INT$	0.07 %	0.1 %	0.6 %	2.2 %
$1HP_t/INT$	40 %	40.5 %	40.8 %	64.2 %
$2HP_t/INT$	12 %	11.2 %	10.4 %	28.1 %
BCT/INT	5.8 %	5.1 %	15.2 %	48.5 %
1992 Tri/ σ_{tot}	2.5 %	2.2 %	8.2 %	31.6 %

Table 1: Trigger rates for 1992. The first column is for real data, the others are from simulation. For the definition of the trigger components see the text.

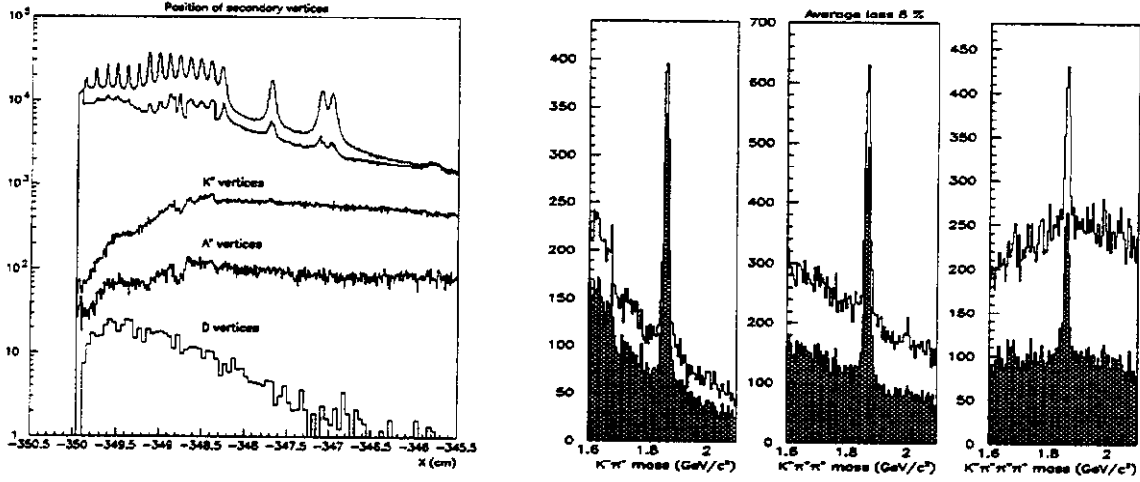


Figure 3: a) *Position of reconstructed secondary vertices in the DD region. The vertices between the two upper curves are rejected as due to secondary interactions in the Si planes.* b) *D^0 and D^\pm invariant mass distributions showing the effect of the algorithm rejecting secondary interactions.*

3 Rejection of secondary interactions

As shown in Fig. 3.a, most secondary vertices reconstructed in the decay detector region are hadronic interactions in the silicon planes. The DD represents 0.6% of a π interaction length and 4.5% of a radiation length. Given the small beauty production cross-section, the ratio between the number of secondary vertices due to beauty cascade decays and those due to secondary interactions in minimum bias events is of the order of 10^{-5} . A simple cut on the vertex position cannot be used because of the small spacing between the DD planes; we have developed a method based on the large energy release due to nuclear fragments and slow tracks which accompany most of the interactions in the Si planes. Cuts based on the distance between the reconstructed vertex position and the centroid of the large energy deposits reject 91% of the vertices due to secondary interactions while losing only 3% of K_s^0 and Λ^0 and 8% of $D^{0,\pm}$ decays (Fig. 3.b). Some secondary vertices are due to coherent or low-multiplicity hadronic interactions surviving the pulse height cuts and others are fake vertices due to high hit densities (mostly interactions).

4 Search for beauty decays

In the 1992 run we have recorded on tape $80 \cdot 10^6$ events; among these the Trident reconstruction program [14] found $12 \cdot 10^6$ events with a secondary vertex, containing an estimated sample of 750 beauty events (assuming a cross-section of 5 nb/nucleon and a linear dependence on the atomic number). The cut on hadronic interactions has reduced the data sample to $2 \cdot 10^6$ events. The events have then been separated into 3 streams to be

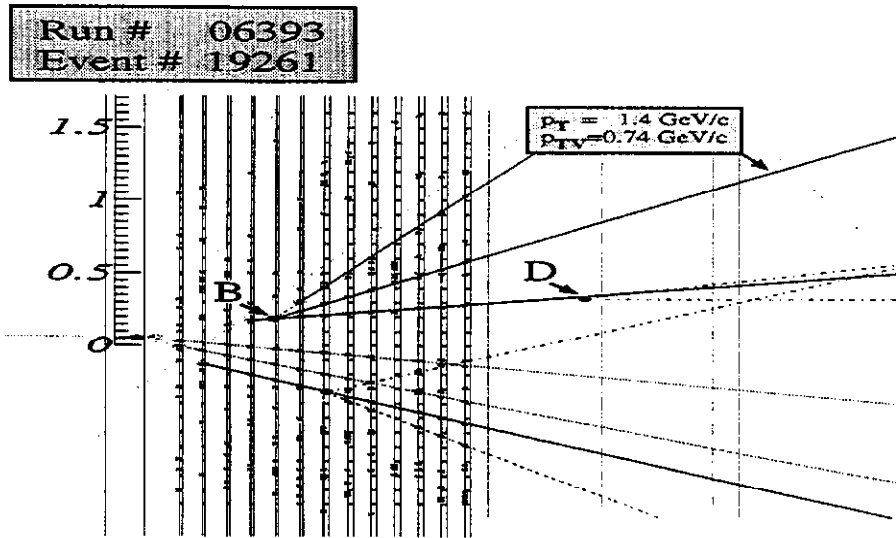


Figure 4: Display of a beauty multi-vertex candidate event, 1992 data, Cu target. Both $B \rightarrow D$ decay chains are clearly visible.

analyzed with a graphical display program, in order to exploit the visualizing capabilities of the decay detector:

- events with at least 3 secondary vertices in the decay detector region;
- events with a fully reconstructed charm meson NOT pointing to the primary vertex and accompanied by additional secondary activity;
- events with a high transverse momentum muon NOT associated with the primary vertex and accompanied by additional secondary activity.

These strict selection criteria give, for the Cu target sample, about 5000 events amongst which we expect to observe 20 beauty decays. The use of the DD information in the graphical analysis of these events has significantly enhanced the S/N ratio and has led to the selection of events with cascade decays such as the one shown in Fig. 4. The graphical analysis allows us to check the reconstruction of the tracks and vertices in the DD region, to correctly measure the transverse momenta relative to the line of flight and to search for additional secondary activity and kinks. It is therefore possible to improve on the selection based on the kinematical information alone (transverse momentum of the tracks in the lab frame, invariant mass of tracks attached to a secondary vertex, presence of leptons), and thus obtain a larger background reduction. The background evaluation in the final sample is still in progress, but the observation of events with properties strongly characteristic of beauty decays gives us confidence that we are actually observing beauty decays and that only a small fraction of the final sample may be ascribed to background.

5 Conclusions

A fast trigger looking for secondary vertices has been used for the first time in an experiment to search for beauty particles. The BCT trigger was able, in $35\mu\text{s}$, to reject 94.2% of the background keeping $\sim 50\%$ of the beauty signal (the background rejection and the acceptance for beauty were, respectively, 97.5% and 32% for the global 1992 trigger configuration).

A high precision ($10\mu\text{m}$ pitch) Si telescope has been operated and used to observe directly the cascade decays of beauty particles. Secondary hadronic interactions can be rejected efficiently with cuts correlating the vertex position to the large energy deposits.

The topological trigger, together with the high resolution of the decay detector, enabled us to see beauty events in the data analyzed so far with the help of interactive graphics. More sophisticated code is being developed to improve the event selection and allow us to relax some cuts, thus gaining in acceptance and efficiency.

References

- [1] M. Adamovich et al., *Nucl. Phys. B* **27** (1992) 251-256.
- [2] M. Adamovich et al., "The WA92 experiment: apparatus designed to trigger and detect short-lived decays produced by $350\text{ GeV}/c\ \pi^-$ interactions on a fixed target", *to be submitted to Nucl. Instr. and Meth. Phys. Res.*
- [3] M. Adinolfi et al., *Nucl. Instr. and Meth. Phys. Res. A* **329** (1993) 117-124.
- [4] A. Beer, et al., *Nucl. Instr. and Meth. Phys. Res. A* **337** (1994) 280-294.
- [5] E. Augé, "Photoproduction de π^0 et de photons directs de grande impulsion transverse", *Thesis, University of Orsay (1989)*.
- [6] C. Bacci et al., *Nucl. Instr. and Meth. Phys. Res. A* **324** (1993) 83-92.
- [7] W. Beusch et al., *Nucl. Instr. and Meth. Phys. Res. A* **249** (1986) 391-398.
- [8] E. Petrolo and S. Veneziano, *Nucl. Instr. and Meth. Phys. Res. A* **315** (1992) 95-101.
E. Gennari, E. Petrolo and S. Veneziano, *IEEE Trans. Nucl. Sci.* **NS-39** (1992).
- [9] G. Darbo and L. Rossi, *Nucl. Instr. and Meth. Phys. Res. A* **289** (1990) 584-591.
- [10] C. Bruschini, "Studio di un Trigger rapido su vertici secondari per la ricerca di particelle dotate di Beauty", *Thesis, University of Genova*.
- [11] A. Fassò et al., "FLUKA: present status and future developments", proceedings of the IV International Conference on Calorimetry High Energy Physics, la Biodola, Italy, 21-26 September 1993.
- [12] GEANT Detector Description and Simulation Tool, CERN Program Library Long Writeup W5013 (1994).
- [13] H.-U. Bengtsson and T. Sjöstrand, *Comput. Phys. Commun.* **46** (1987) 43-82.
- [14] J.-C. Lassalle et al., *Nucl. Instr. and Meth. Phys. Res. A* **176** (1980) 371-379.
D. Barberis, M. Dameri and B. Osculati, *private communication*.

TRIGGERS FOR A HIGH SENSITIVITY CHARM EXPERIMENT

David C. Christian
Fermilab, Batavia, IL 60521

Abstract

Any future charm experiment clearly should implement an E_T trigger and a μ trigger. In order to reach the 10^8 reconstructed charm level for hadronic final states, a high quality vertex trigger will almost certainly also be necessary. The best hope for the development of an offline quality vertex trigger lies in further development of the ideas of data-driven processing pioneered by the Nevis/U. Mass. group.

1 Introduction

In his introductory talk, Jeff Appel stressed that two technical developments have been crucial to the success of the Fermilab fixed target charm program. He cited the use of silicon microstrip detectors, which allow the selection of charm candidates through the detection of separated decay vertices, and the use of inexpensive high density tape and powerful offline computing farms. However, he also expressed the opinion that the exponential increase in the yield of charm reaped in the Fermilab fixed target program will not continue past the upcoming run without another technical breakthrough. Detector technology is continuing to evolve which will meet the needs of a "10⁸ reconstructed charm" experiment. The breakthrough which is required is an offline-quality vertex trigger which will allow background events to be rejected in real time without losing a significant number of reconstructible charm decays.

In this talk I will review the short list of triggers that have been used successfully by charm experiments, and then present a partial review of development work related to vertex triggers.

2 E_T Triggers

The only unbiased trigger which has been shown to be effective for both photoproduction and hadroproduction of charm is the requirement of "large" global event E_T . A series of experiments in the Tagged Photon Laboratory have used E_T triggers, with different thresholds [1]. Experiment 831 (in the wideband photon beam) will use an E_T trigger in the next fixed target run [2]. For FNAL proposal 829 [3] we studied the use of the E791 calorimetry for an E_T trigger¹. E791 ran with a 500 GeV/c π^- beam and triggered on E_T , but with a

¹Most of this work was done by Ai Nguyen, Tom Carter, and Mike Halling.

threshold of 4 GeV/c, which rejected only about $\frac{1}{4}$ of the total cross section and was close to 100% efficient for charm. All of the information available to the E_T trigger logic was written to tape for every event, so it was possible to study what would have happened with higher E_T thresholds. We determined the fraction of events rejected as a function of E_T threshold using an unfiltered data sample. The efficiency for a variety of charm decays was determined using DST's culled from approximately $\frac{1}{3}$ of the full E791 data set. The charm efficiency as a function of E_T did not vary significantly depending on which decay mode was chosen. Figure 1 shows that a threshold of 8.6 GeV/c would have accepted only 20% of the total cross section, but would have retained 69% of the $D^{*\pm} \rightarrow D^0 \pi^\pm (D^0 \rightarrow K^\mp \pi^\pm)$ decays reconstructed by E791, yielding a charm enrichment of $3\frac{1}{2}$.

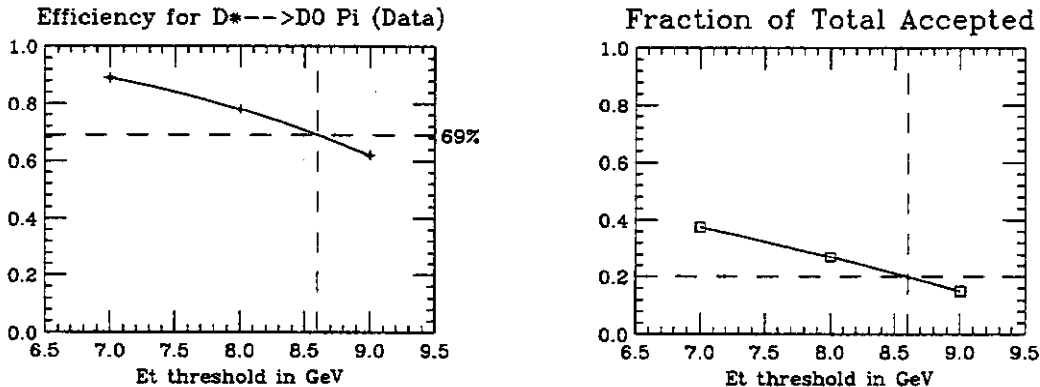


Figure 1: E_T trigger study for FNAL P829 performed using E791 data.

We also studied the effect of triggering on the sum of $|p_T|$ of tracks found by the E791 reconstruction programs. It was possible to achieve a slightly larger charm enrichment using this variable than using the measured E_T . It is likely that more modern calorimetry than that used by E791 would yield a slightly better E_T trigger².

The bottom line is: *E_T works as a charm trigger and can "easily" provide an enrichment of 3-5 while rejecting 80-90% of σ_{tot} .*

3 Muon Triggers

The other charm trigger which has been used successfully and has been widely proposed for future use is a μ trigger. E653 triggered on the presence of a μ with $p > 5$ GeV/c, and selected about $\frac{1}{30} \times \sigma_{tot}$ for 600 GeV/c π^- interactions in a nuclear emulsion target [4]. The E653 spectrometer was unusually short, specifically to minimize π decays in flight. A longer spectrometer would not get quite as large a rejection from a μ trigger without detecting and rejecting decays in flight. The inefficiency of a μ trigger is typically not much worse than the offline reconstruction inefficiency for μ identification, so a μ trigger need not introduce

²A similar study of E_T triggers, using Monte Carlo data, has been done by Kennedy, Karchin, and Harr in the context of possible fixed target b and c experiments at the Tevatron and at the SSC. Their memos were presented to the Trigger Group of this workshop.

bias, at least not for the study of semi-muonic decays. Moreover, since approximately 10% of charmed meson decays yield a μ , the trigger can yield an enriched sample of all charm decays, provided that the spectrometer acceptance for the “other” charmed particle is adequate. The combination of an E_T trigger and a μ trigger could likely reject 99.5% of σ_{tot} while being $\approx 50\%$ efficient for semi-muonic charm decays³. Given an interaction rate of 5 MHz, this would yield 25 kHz to be read out and written to tape. This is easily within the reach of current technology. *If one wants to concentrate on semi-muonic decays, this combination will be very hard to beat - and there is no need for a triggering breakthrough.*

4 Vertex Triggers

It is almost uniformly accepted that all future fixed target charm studies will employ a very high resolution vertex detector and require that every charm candidate have a distinct decay vertex. If one could construct a vertex trigger that identified all reconstructible decay vertices online, one could substantially reduce the number of events which needed to be written to tape without throwing away any reconstructible charm. The E791 offline software filter accepts 9% of the events that passed the loose online E_T trigger, based on the existence of a secondary vertex seen in the silicon vertex detector⁴. If one used an E_T trigger to reduce the raw trigger rate by a factor of 5 and then rejected 90% of those triggers with an online vertex trigger, then a 5 MHz interaction rate would yield 100 kHz to be read out and written to tape. This is a factor of 5 higher rate than was envisioned in P829, and a factor of ten more than actually read out by E791, but not impossible to consider in the year 2000.

4.1 Simple/Fast Vertex Triggers

Vertex triggers may be divided into two types; those that don't require data from tracking detectors, and those that do. Triggers that don't require data from tracking detectors put much less strain on the front-end data acquisition system, but they generally have inefficiencies that are different from the inefficiencies of an offline event reconstruction algorithm. Significant progress has been made in the past few years on two types of fast vertex triggers which do not require information from tracking detectors.

4.1.1 Multiplicity Jump

Some of the first high energy physics experiments to use silicon detectors attempted to trigger on a multiplicity increase between planes, as a signal of a charm decay between the planes [5]. These attempts, and many subsequent attempts to trigger on a multiplicity step, were not very successful. The problem was that the the signal was due to energy loss, and

³This implies an enrichment of less than 5 for all charm decays, but as much as 100 for semi-muonic decays.

⁴This is with a cut at $dz > 6\sigma_{dz}$ for the dominant two prong vertices. Many E791 analyses employ a more stringent vertex separation cut.

the amount of energy lost per particle has large fluctuations. Moreover, the presence of slow nuclear fragments, which are very heavily ionizing, makes the trigger even more problematic. Halling and Kwan have suggested avoiding these problems by using the Cherenkov light produced in two quartz plates to estimate multiplicity [6]. This method is sensitive only to relativistic charged particles and the fluctuations are given simply by the Poisson statistics of the detected light. A beam test of this idea was performed using the E791 spectrometer during the last FNAL fixed target run. The amount of light detected per track was not large enough to provide an efficient charm trigger. If one increased the amount of light detected per track, either by using higher quantum efficiency photodetectors, or by using a radiator with a higher index of refraction, this might become a practical charm trigger. However, the Cherenkov radiator plates add material upstream of the silicon tracking detectors, which degrades the vertex resolution of the spectrometer. In addition, since a decay must occur between the radiator plates, this trigger is likely to be inefficient for the shortest lifetime charmed particles.

4.1.2 *Optical Impact Parameter*

The other fast vertex trigger that is being developed [7] also uses Cherenkov light, but in this case it is the uniqueness of the Cherenkov angle that is the key feature. The idea is to use a solid radiator made from two concentric spherical shells in contact with one another, placed so that the (point-like) interaction target is at its center. The two shells are made of materials chosen so that the difference of their refractive indices allows total internal reflection only for Cherenkov light made by tracks which do not originate at the center of the shells. The detection of the light produced by these nonradial tracks provides the trigger. Unfortunately, one can show that only light made along a length of radiator approximately equal to the particle's impact parameter with respect to the target is internally reflected. In addition, the materials chosen for the two shells must not only have appropriate refractive indices; their dispersion relations must also match. If the dispersion relations do not match, then one must use only a narrow band of wavelengths - outside of which tracks from the target may contribute totally internally reflected light and tracks with non-zero impact parameter may not contribute. These details severely limit the amount of light which can be detected per nonradial track. Much more development is needed before this idea is practical as a charm trigger.

4.2 Tracking Triggers

The second class of vertex triggers is those that require information from some or all of the tracking detectors. If such a trigger is to operate at level two in an experiment running with a 5 MHz interaction rate and approximately 1 MHz of level one triggers, it will require a much faster front-end data acquisition system than is familiar to most physicists. However, there are systems that either have been built, or soon will be built, that are more than fast enough. For example, the E771 silicon strip readout system is capable of digitizing

and reading out more than 3 MHz of high multiplicity interactions with zero deadtime [8]. The digital phototube readout conceived for SDC and under construction for KTeV will be capable of similar or higher rates [9].

4.2.1 *Stored-Program Processor Farm*

Conceptually, the simplest way to implement an offline quality vertex trigger is to use a farm of conventional computers running the same program as is used for offline reconstruction. This is exactly the approach being taken by E781, which will run in the next FNAL fixed target run [11]. E781 does not plan to implement full vertex reconstruction online, but forward positive tracks will be found and projected with full offline precision to the production target so that an impact parameter can be calculated and cut upon.

Even with today's fastest processors it typically takes many milliseconds to reconstruct a single event. This implies that to implement a trigger similar to the E791 filter program, a farm would require thousands of nodes to process 1 MHz of level one triggers. This approach will probably be prohibitively expensive, even in the year 2000. Moreover, the problem of routing events into idle processors in such a farm would be quite challenging ⁵.

4.2.2 *Memory Lookup*

If a processor farm represents one end of the spectrum of possible tracking triggers, the other end is memory lookup. This approach is conceptually easy and typically very fast. One "simply" precomputes all patterns of hit data that represent legal tracks, and then uses the hit pattern from an event to access the memory and retrieve track parameters⁶. The limitation of this approach is that as the number of tracks per event and measurements per track are increased, the required memory size becomes enormous. It is currently far from possible to match offline precision with memory lookup. Nonetheless, the integration scale of VLSI memory continues to increase, the cost continues to drop exponentially, and progress continues to be made on "content addressing" schemes [12].

4.2.3 *Data-Driven Processor (Nevis/U.Mass.)*

The most promising prospect for implementing an offline quality tracking trigger for a high rate charm experiment is a data-driven processor of the type developed over the last decade at Columbia University Nevis Laboratories and the University of Massachusetts [14]. The Nevis/U.Mass. data-driven processor is a special purpose digital computer whose function is determined not by a stored program, but rather by its constituent modules and the interconnections between the modules. Data and control information flow from module to module and sequential steps in a calculation occur in sequential modules in the processor

⁵Perhaps this could be accomplished using one or more high speed switches similar to the type used by telephone companies [10].

⁶A related idea used in WA92 was described at this workshop by Dario Barberis [13].

pipeline. Data flows only on transitions of a synchronous clock which is centrally generated and fanned out to every module. All other control is local. The absence of shared resources such as central memory or I/O paths eliminates possible bottlenecks and makes the structure almost arbitrarily expandable. The processor is naturally parallel in that calculations that do not depend on one another can be done in parallel; however, most of the tremendous speed that is achievable derives from the pipelined architecture.

The processor implemented for FNAL E690 [15] consisted of approximately 800 functional modules of 45 different types. It was capable of track finding and least squares fitting at a rate of approximately $1\mu\text{s}$ per fit track. Track reconstruction of the full 5 billion event E690 data sample was performed in approximately 100 days.

The same processor modules have been used in E789 to trigger on charm decay vertices seen in a closed geometry spectrometer [16], and in a test at CERN (RD21) intended to demonstrate the use of a data-driven processor as the primary trigger for a collider b experiment (COBEX [17]). In that test, straight line tracks were found using information from silicon strip detectors. The tracks were then fit to the hypothesis that all of the tracks originated at a common vertex. Most events with b decays would fit this hypothesis poorly, whereas the vast majority of all interactions fit well. There was provision to avoid triggering on events with multiply scattered low momentum tracks by eliminating the one or two tracks contributing most to χ^2 ; finally events were selected with a large χ^2 . The average time per 16 track event was $12\mu\text{sec}$. Since the COBEX design calls for a vertex detector which consists of four separate quadrants, the tracks in each quadrant could easily be found simultaneously in separate processor pipelines. This would reduce the time per event to approximately $3\mu\text{sec}$.

As an exercise for this workshop I have worked out another possible trigger algorithm. My goal was to find an algorithm that could operate at level two in our strawman 10^8 charm experiment, which I took to mean that it should be able to process 1 MHz of level one triggers. My approach was to try to avoid a loop over N^2 combinations for an event with N tracks. Here is what I came up with:

- Require the interaction point to be known in at least two dimensions.
- Locate the target in a weak magnetic field such that tracks below a momentum cut-off curve enough not to be found as straight lines (These tracks will often have large impact parameter because of multiple scattering).
- Eliminate points on straight lines between the primary vertex and one measurement plane (Requires only N cycles + the number of cycles to empty the pipeline).
- Find straight lines with the remaining hits (Requires $n \times m$ steps where n and m are the number of hits remaining in two seed planes).
- Trigger on events in which at least one (or two...) tracks are found with an impact parameter within a predefined window (The calculation of impact parameter is very

fast, requiring only about one clock cycle per track not originating at the primary vertex).

Assuming an average of 16 hits per plane, 5 of which do not lie on straight line trajectories from the primary vertex, I estimate that this algorithm would require no more than about 40 clock cycles in any given subroutine using existing processor modules. With a 30 nsec. clock cycle, this translates to 1.2 μ sec/event - very close to 1 MHz.

The current Nevis/U.Mass. processor modules are based on 10 year old technology (all ECL 10K and 10KH). It would be possible to construct an even faster and more powerful data-driven pipeline if one were to update the processor using modern technology and larger scale integration (FIFO's, DSP's, ASIC's, etc.). This would also yield a system that would require fewer modules to perform a given calculation.

The principles of the Nevis/U.Mass. data-driven processor are well matched to the needs of a fast vertex trigger. Hopefully these ideas will continue to be developed. Fermilab participation in this development could be crucial.

4.3 Conclusions

The triggering tools are in hand now for a 10^8 level charm experiment which focusses on semi-muonic decays. In order to reach this level of sensitivity for hadronic decay modes, a breakthrough in triggering is required. The best hope for this breakthrough is the continued development of data-driven processing.

References

- [1] J.A. Appel *et al.*, Nucl. Instr. & Meth. **A243**, 361 (1986).
- [2] S. Bianco *et al.*, "A High Statistics Study of States Containing Heavy Quarks Using the Wideband Photon Beam and the E687 Multiparticle Spectrometer," J. Cumalat, spokesperson, September 1, 1992.
- [3] B. Meadows *et al.* "P829: Continued Study of Heavy Flavors at TPL," D. Christian and M. Sokoloff, spokesperson, October, 1993.
- [4] Byron Lundberg, private communication.
- [5] See for example, E. Meroni, "Use of Active Targets in the NA1 Experiment" in Como 1983, Proceedings, Physics in Collision/Search for Heavy Flavours, pp 443-449.
- [6] A. M. Halling and S. Kwan, Nucl. Instr. & Meth. **A333**, 324 (1993).
- [7] G. Charpak, L. M. Lederman, and Y. Giomataris, Nucl. Instr. & Meth. **A306**, 439 (1991); D. M. Kaplan *et al.*, *ibid.* **A330**, 33 (1993); G. Charpak *et al.*, *ibid.* **A332**, 91 (1993).
- [8] C. Swoboda *et al.*, IEEE Trans. Nucl. Sci. **37** #2, 342 (1990).
- [9] R.J. Yarema *et al.*, Fermilab-CONF-92-148, Published in Chestnut Ridge Collid. 1992: 131-142 (QCD183:C66:1992)
- [10] D. Black *et al.*, Fermilab-CONF-91-303 (1991).

- [11] R. Edelstein *et al.*, "A Proposal to Construct -SELEX- Segmented Large-x Baryon Spectrometer" J. Russ, spokesperson, November 8, 1987.
- [12] F. Morsani *et al.*, Nucl. Instr. & Meth. **A315**, 446 (1992).
- [13] D. Barberis *et al.*, "A Secondary Vertex Trigger for Beauty Search: Results from the BEATRICE/WA92 Experiment", these proceedings.
- [14] B. Knapp, Nucl. Instr. & Meth. **A289**, 561 (1990).
- [15] M. Church *et al.*, "Study of Hadronic Production and Spectroscopy of Strange, Charm, and Bottom Particles at the Tevatron" B. Knapp, spokesperson, January, 1981.
- [16] C. Lee *et al.*, IEEE Trans. Nucl. Sci. **38** 461, (1989).
- [17] S. Erhan *et al.*, Nucl. Instr. & Meth. **A333**, 101 (1993).

A High-Rate Fixed-Target Charm Experiment

Daniel M. Kaplan
Northern Illinois University, DeKalb, IL 60115

Abstract

A fixed-target experiment capable of reconstructing $> 10^8$ charm decays is described.

1 Introduction

In the P865 Letter of Intent [1], we have proposed a fixed-target experiment aimed at achieving high sensitivity to decays both of charm and of beauty. I describe here a revised version which is somewhat more optimized for charm and less so for beauty. The rationale for this change of emphasis is two-fold: by the time a new fixed-target experiment might run (\approx Year 2000), it is likely that studies of beauty at the level proposed in P865 will no longer be competitive; furthermore, it may well be that charm is even more interesting than beauty, since the background to rare processes beyond the Standard Model is so much smaller in charm than in beauty. At this workshop, Pakvasa has emphasized that rare and forbidden processes such as D^0 mixing, charm-changing neutral currents, and lepton-family-violating currents must exist at some level if we are ever to have an understanding of the fermion masses and mixings; some extensions of the Standard Model predict effects detectable at the level of sensitivity discussed here.

2 Beam and Target

To achieve charm sensitivity three orders of magnitude beyond that achieved in E687 and E791 and two orders of magnitude beyond that expected from CLEO, E831, and E781, i.e. $\gtrsim 10^8$ reconstructed decays, probably requires a primary proton beam, since it may be difficult to produce a sufficient rate of high-energy photons, pions, or hyperons. For the sake of discussion, I therefore assume a beam of 800 GeV protons.¹ Then given $\sigma(pN \rightarrow DX) + \sigma(pN \rightarrow \bar{D}X) \approx 40 \mu\text{b}/\text{nucleon}$ at 800 GeV [2] and $\sigma(pN \rightarrow D^0 X) \propto A^{1.0}$ [3], and assuming that the cross section to produce D_s and charmed baryons is $\approx 15\%$ that of D mesons, I estimate that charmed particles are produced at the rate of $7 \times 10^{-3}/\text{interaction}$ if a high- A target (e.g. Au) is used. A 1 mm Au target is suitable, representing 1% of an interaction length and on average 14% of a radiation length for outgoing secondaries. Alternatively (as suggested at this workshop by D. Summers), a low- Z target such as ^{13}C -diamond may be favored to minimize scattering of low-momentum pions from D^* decay;

¹Though 900 GeV or more may become available, this is unlikely to occur by the Year 2000.

then a 2 mm target is suitable, representing $\approx 1\%$ of an interaction length and $\approx 1\%$ of a radiation length and producing charm at the rate 3×10^{-3} /interaction.

Based on experience in ACCMOR, E672, E687, E789, and E791, a single short target is desirable. This allows attention to be focused on decays occurring in air or vacuum downstream of the target, and decays inside the target (for which backgrounds are substantially larger²) to be excluded, and it simplifies secondary-vertex triggers. Given the typical Lorentz boost $\gamma \approx 20$, a 1-2 mm target is short enough that a substantial fraction even of charmed baryons will decay outside it.

I take as a benchmark a 5 MHz interaction rate, which then requires 500 MHz of beam or 10^{10} protons per 20 s Tevatron spill, an intensity easily attainable.

3 Spectrometer Design

3.1 Rate capability

A significant design challenge is posed by radiation damage to the silicon detectors. To configure detectors which can survive at the desired sensitivity, we choose suitable maximum and (in one view) minimum angles for the instrumented aperture, arranging the detectors along the beam axis with a small gap through which pass the uninteracted beam and secondaries below the minimum angle (Figs. 1, 2).³ Thus the rate is spread approximately equally over several detector planes, with large-angle secondaries measured close to the target and small-angle secondaries farther downstream. Along the beam axis the spacing of detectors increases approximately geometrically, making the lever arm for vertex reconstruction independent of production angle. Since small-angle secondaries tend to have high momentum, the multiple-scattering contribution to vertex resolution is also approximately independent of production angle. The instrumented angular range is $|\theta_x| \leq 200 \text{ mr}$, $4 \leq \theta_y \leq 175 \text{ mr}$, corresponding to the center-of-mass rapidity range $|y| \lesssim 1.9$ and containing over 90% of produced secondaries.

To maximize the rate capability of the spectrometer, the tracking is performed entirely with silicon and scintillating-fiber planes. The rate per unit area (and hence the radiation fluence) in a detector element can easily be estimated based on the uniform-pseudorapidity approximation. Fig. 3 shows the rate calculation for an annular area dA located a transverse distance r from the beam and of thickness dr . Since the operational limit of present-day silicon detectors is 10^{14} particles/cm², the charged multiplicity per unit pseudorapidity in 800 GeV proton-nucleus collisions is $n \approx 4$ for high- A targets [4] (less for C), and a typical run will yield up to $n_{\text{int}} \equiv (5 \times 10^6 \text{ interactions/s}) \times (4 \times 10^6 \text{ s}) = 2 \times 10^{13}$ interactions, we

²This has been emphasized by several other speakers at this workshop, notably J. Cumalat and L. Moroni; see also Proposal 829 [10].

³An alternative approach with no gap may also be workable if the beam is spread over sufficient area to satisfy rate and radiation-damage limits, however the approach described here probably allows smaller silicon detectors and is "cleaner" in that the beam passes through a minimum of material.

can derive the “minimum survivable” inner detector radius

$$r_{\min} = \left(\frac{n}{2\pi} \frac{n_{\text{int}}}{10^{14}} \right)^{\frac{1}{2}},$$

or $r_{\min} = 3.5$ mm, which we set as the half-gap between the two detector arms. This ensures that the detectors will survive for the entire run (or at most will need to be replaced once⁴). To cover the desired angular range, we configure 14 double-sided silicon strip detectors⁵ above and 14 below the beam as shown in Fig. 2, such that at all angles of interest there are at least six measurements per track (and more at small angles where the occupancy is highest).

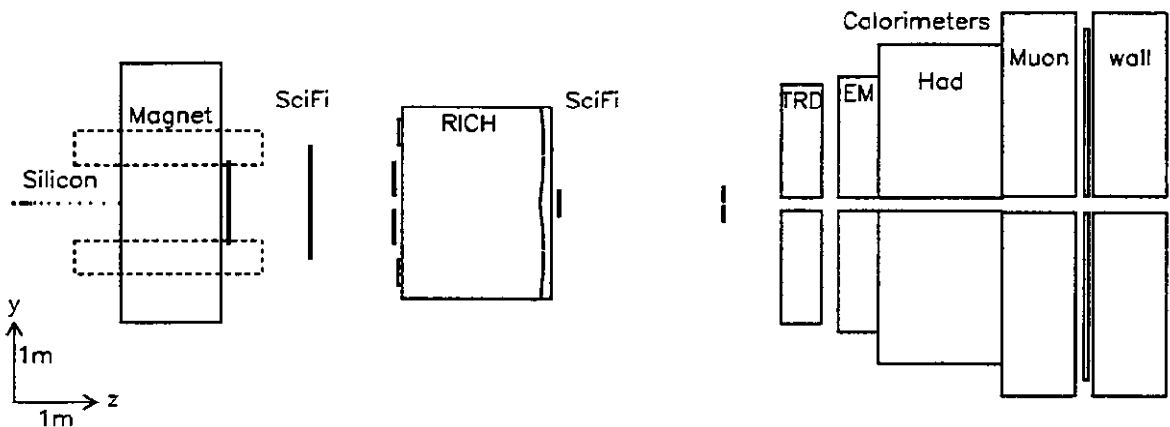


Figure 1: Spectrometer layout (bend view).

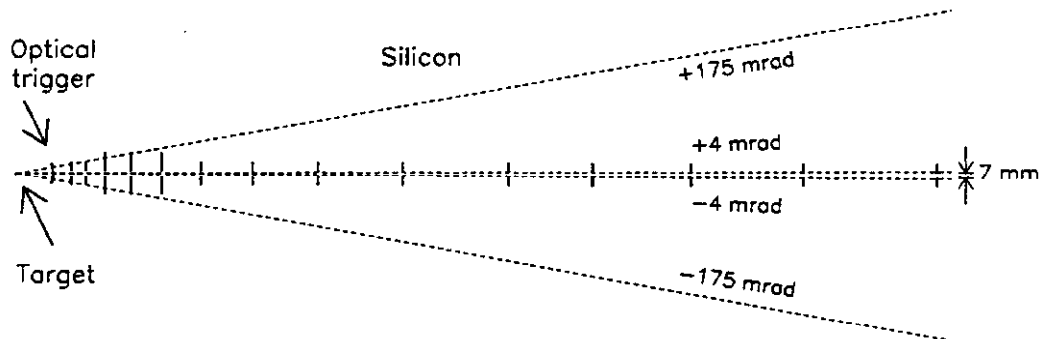
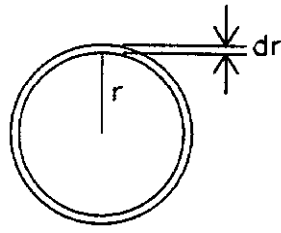


Figure 2: Detail of vertex region (showing optional optical impact-parameter trigger).

The green-scintillating 3HF/PTP fibers are deployed in staggered doublets in three views. They are read out using cryogenic solid-state “visible-light photon counters” (VLPCs) [5], which feature high quantum efficiency (up to 85% for green light [6]), low noise, and high speed: up to 30-MHz rate capability has been demonstrated, with single-electron noise rates

⁴In E789 we operated silicon detectors at fluence up to $\approx 5 \times 10^{13} \text{ cm}^{-2}$ with negligible efficiency loss.

⁵I assume silicon strip detectors for definiteness, but silicon pixel detectors would be better if available with sufficient readout speed and radiation hardness; because of their radiation hardness, diamond detectors, if available, should also be considered (see talk by Tesarek at this workshop).



$$\begin{aligned}\frac{dN}{d\eta} &\doteq \text{constant} \equiv n \\ d\eta &= \frac{dr}{r} \\ dA &= 2\pi r dr \\ \frac{dN}{dA} &= \frac{dN}{d\eta} \frac{d\eta}{dA} \\ &= n/2\pi r^2\end{aligned}$$

Figure 3: Calculation of rate per unit area in an annulus.

of several kHz [7]. At this workshop Ruchti has reported the successful operation of a large scintillating-fiber tracking system with VLPC readout in a cosmic-ray test carried out for D0. The long fibers (3 m of scintillator with 8 m of clear waveguide) used in that test with 99% efficiency represent a more challenging application than that discussed here. Since the fibers are more radiation-hard than silicon detectors [1], and (due to occupancy; see below) the beam gap between fiber planes is larger than that in the silicon, radiation damage of the fibers is not anticipated to be a problem.

We assume 1-bucket (< 19 ns) recovery times for all detectors, so that there is no pile-up due to out-of-time interactions. Designs capable of this performance have been presented [1, 4, 8] for all detectors except the TRD.⁶

Detector-element occupancies also follow from the derivation of Fig. 3. For an element of height dy located a transverse distance y from the beam and covering $-x_{\max} < x < x_{\max}$, the occupancy per event (neglecting magnetic bending) is

$$\frac{n}{\pi} \frac{dy}{y} \arctan \frac{x_{\max}}{y}.$$

For 800 μm fiber diameter, this implies $\approx 16\%$ occupancy at $y = 1$ cm, $\approx 8\%$ at 2 cm, and $\approx 4\%$ at 4 cm. A full trackfinding simulation will be required to assess the maximum acceptable occupancy, but this suggests ≈ 1 cm as the minimum acceptable half-gap in the scintillating-fiber planes. The fibers near the gap could be split at $x = 0$ and read out at both ends, halving their occupancies. Since shorter fibers have less attenuation, a smaller diameter could be used near the gap, reducing occupancy still further.

3.2 Spectrometer performance

I have carried out a simple Monte Carlo simulation of the spectrometer sketched above. Assuming a 1.2-m-long analyzing magnet with pole pieces tapered to give 0.5 GeV p_t kick, I obtain $(56 \pm 1)\%$ geometrical acceptance for $D^0 \rightarrow K^-\pi^+$ decays and $(44 \pm 1)\%$ for $D^{*+} \rightarrow D^0\pi^+ \rightarrow K^-\pi^+\pi^+$, comparable to those of existing open-geometry spectrometers despite the beam gap. With silicon detectors of 25 μm pitch read out digitally (i.e. no

⁶It may be that a TRD for electron identification is not cost-effective and a hadron-blind detector [9] or preshower detector should be used instead.

pulse-height information) and $800\text{ }\mu\text{m}$ scintillating-fiber pitch, and assuming $\pm 10^\circ$ stereo, Gaussian fits to the reconstructed distributions give rms resolutions of 6 MeV in mass (a factor ≈ 2 better than that of existing spectrometers) and $11\text{ }\mu\text{m}$ (bend-view) and $21\text{ }\mu\text{m}$ (nonbend-view) in impact parameter, giving 40 fs decay proper-time resolution, comparable to that of existing spectrometers. Since the mass resolution is dominated by scattering, minimization of material is crucial, for example use of helium bags and avoidance of threshold Cherenkov counters employing heavy gas mixtures. The performance parameters just given are a snapshot of work in progress and probably can be improved with further optimization.

4 Trigger

While the most successful previous charm hadroproduction experiments (E769 and E791) used very loose triggers and recorded most inelastic interactions, this approach is unlikely to extrapolate successfully by three orders of magnitude! (Consider that E791 recorded 2×10^{10} events – tens of terabytes of data – on 20,000 8 mm tapes.) Thus our sensitivity goal requires a highly selective trigger. However, we wish to trigger on charm-event characteristics which bias the physics as little as possible. Lepton triggers, used successfully by E653, while capable of great selectivity ($\sim 10^3$ rejection for minimum-bias events), have only $\sim 10\%$ charm efficiency. The E_t triggers used by E769 and E791, while highly efficient for charm, have poor selectivity ($\lesssim 10$ minimum-bias rejection). I therefore assume a first-level trigger requiring calorimetric E_t OR'ed with high- p_t -lepton and lepton-pair triggers. At second level, secondary-vertex requirements can be imposed on the E_t -triggered events to achieve a rate ($\sim 100\text{ kHz}$) which is practical to record.

Analyses of the efficacy of an E_t trigger carried out using E791 data [10] and the PYTHIA Monte Carlo [11] agree on minimum-bias rejection vs. charm efficiency (though due to nuclear effects not simulated in PYTHIA, they differ as to the E_t threshold corresponding to a given rejection). Fig. 4 shows the efficiencies for charm and minimum-bias events as a function of the PYTHIA E_t threshold. A considerable degradation results if there is significant probability for two interactions to pile up in the calorimeter. Given the 53 MHz rf structure of the Tevatron beam and the typical $\approx 50\%$ effective spill duty factor, at the benchmark 5 MHz mean interaction rate there is a $\approx 20\%$ probability for a second simultaneous interaction. Thus at a 5 GeV PYTHIA E_t threshold (corresponding to a $\approx 10\text{ GeV}$ actual threshold [10]), the minimum-bias rejection factor is 5, i.e. pile-up degrades the rejection by a factor ≈ 2 , even for a calorimeter with one-bucket resolution. The charm efficiency at this threshold is about 50%, for a charm enrichment of ≈ 2.5 . (These are rough estimates based on a relatively crude calorimeter [11], and an optimized calorimeter may provide better rejection.) Such an E_t trigger yields a 1 MHz input rate to the next level.

While it may be technically feasible by the Year 2000 to record events at a 1 MHz rate, an additional factor ≈ 10 in trigger rejection is desirable and can be achieved by requiring evidence of secondary vertices. Existing custom trackfinding trigger processors [12], while perhaps capable of this rejection, typically fall short by \approx one order of magnitude in speed. At $\sim 1\text{ MIPS-s/event}$, an on-line farm of commercial processors would need a capacity of

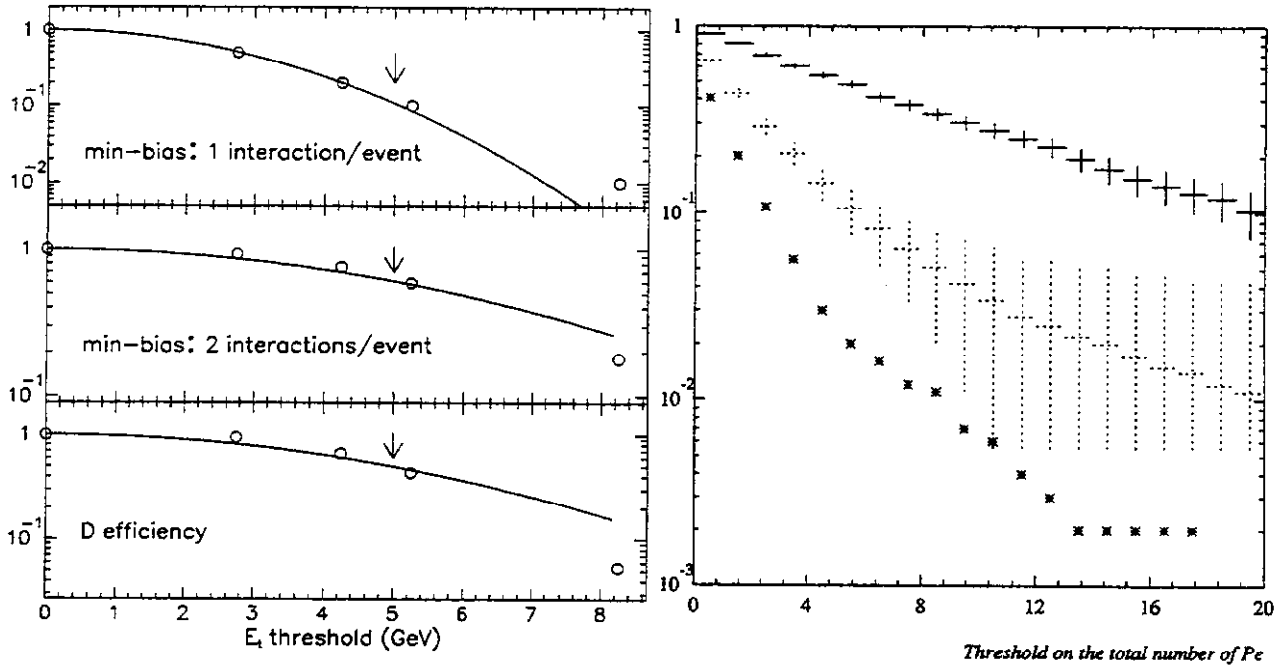


Figure 4: Left: minimum-bias and D efficiencies vs. E_t threshold; points are from PYTHIA simulation of Ref. [11], curves are fits of the form $\exp(-aE_t^2)$, and arrows indicate the 5 GeV threshold discussed in text. Right: estimated optical-trigger efficiency for minimum-bias (solid crosses), PYTHIA charm (dashed crosses), and $B^0 \rightarrow \pi\pi$ events (stars) vs. threshold in photoelectrons (from [1]).

$\sim 10^5 - 10^6$ MIPS, which may be prohibitive even in the Year 2000. It is likely that by then a sufficiently fast custom trackfinding processor can be developed. This would require fast buffering (~ 100 ns) and readout (~ 1 μ s) of event information in order not to impose excessive deadtime. Trackfinding secondary-vertex triggers benefit from the use of focused beam and a single thin target, which allow simplification of the algorithm since the primary vertex location is known *a priori*. Since low- p_t tracks have poor vertex resolution [13], a trigger which discriminates p_t is more effective than one which is purely topological; such discrimination may be simply accomplished by placing the vertex detectors in a weak magnetic field and looking for straight tracks.⁷

As an alternative to iterative trackfinding at a 1 MHz event rate, three other approaches also appear worth pursuing. The first is a secondary-vertex trigger implemented using fast parallel logic, e.g. PALs, neural networks, or pre-downloaded fast RAMs, to look quickly for patterns in the silicon detectors corresponding to tracks originating downstream of the target. The others are fast secondary-vertex trigger devices originally proposed for beauty: the optical impact-parameter trigger [14] and Cherenkov multiplicity-jump trigger [15]; while results from prototype tests so far suggest undesirably low charm efficiency, these might with further development provide sufficient resolution to trigger efficiently on charm. For example, Fig. 4 shows the efficiency for minimum-bias, charm, and beauty events projected for a version of the optical trigger [1], indicating 40% charm efficiency for a factor 5 minimum-

⁷As suggested by D. Christian.

Table 1: Estimated yields of reconstructed events (antiparticles included)

mode	charm frac.	BR	accept.	trigger eff.	reconst. eff.	yield
$D^0 \rightarrow K\pi$	0.6	0.0365	0.56	0.2	0.5	1.2×10^8
$D^+ \rightarrow K^*\mu\nu$ $\rightarrow K\pi\mu\nu$	0.3	0.027	0.4	0.5	0.5	8×10^7
all	1	≈ 0.1	≈ 0.4	≈ 0.2	≈ 0.5	4×10^8

bias rejection. The resulting ≈ 200 kHz event rate can be processed or recorded using existing technology.

5 Yield

The charm yield is straightforwardly estimated. Assuming a Au target and a typical fixed-target run of 3×10^6 live beam seconds, 10^{11} charmed particles are produced. The reconstructed-event yields in representative modes are estimated in Table 1 assuming (for the sake of illustration) that the optical trigger is used for all-hadronic modes (but not for leptonic modes, for which the first-level trigger rate should be sufficiently low to be recorded directly) and performs as estimated above. Although due to off-line selection cuts not yet simulated, realistic yields could be a factor $\approx 2 - 3$ below those indicated, the total reconstructed sample is in excess of 10^8 events. Given the factor ≈ 2 mass-resolution improvement compared to E791, one can infer a factor ~ 50 improvement in statistical significance in a typical decay mode. Since the charm cross section at 120 GeV proton-beam energy may be several % of that at 800 GeV, and the geometrical acceptance remains $\approx 50\%$, interesting charm sensitivity may also be available using Main Injector beam during Tevatron Collider running; at the least, there will be opportunity to debug and test the spectrometer thoroughly so that full-energy beam may be used with optimal efficiency.

6 Summary

A fixed-target hadroproduction experiment capable of reconstructing in excess of 10^8 charm events is feasible using detector, trigger, and data acquisition technologies which exist or are under development. A typical factor ~ 50 in statistical significance of signals may be expected compared to existing experiments. The cost of the design sketched here has been estimated at under \$10M [1]. I anticipate an exciting future for charm physics at the turn of the century.

References

- [1] L. D. Isenhower *et al.*, "P865: Revised Letter of Intent for a High-Sensitivity Study of Charm and Beauty Decays," D. M. Kaplan, spokesperson, April 2, 1993.

- [2] I average together measurements of charged- and neutral- D production from R. Ammar *et al.*, Phys. Rev. Lett. **61**, 2185 (1988); K. Kodama *et al.*, Phys. Lett. **263B**, 573 (1991); and Ref. [3].
- [3] M. J. Leitch *et al.*, Phys. Rev. Lett. **72**, 2542 (1994).
- [4] H. Albrecht *et al.*, "An Experiment to Study CP Violation in the B System Using an Internal Target at the HERA Proton Ring," (HERA- B Letter of Intent), DESY-PRC 92/04, October 1992.
- [5] M. D. Petroff and M. Atac, IEEE Trans. Nucl. Sci. **36** (1989) 163; M. Atac *et al.*, Nucl. Instr. & Meth. **A314** (1992) 56; M. Atac *et al.*, Nucl. Instr. & Meth. **A320** (1992) 155.
- [6] M. G. Stapelbroek, M. D. Petroff, and R. Bharat, "Visible Light Photon Counters for Astronomy," in *Proceedings of an ESA Symposium on Photon Detectors for Space Instrumentation*, ESA/ESTEC, Noordwijk, The Netherlands, 10–12 November 1992.
- [7] M. D. Petroff and W. G. Stapelbroek, IEEE Trans. Nucl. Sci. **NS-36** (1989) 158.
- [8] see e.g. D. M. Kaplan *et al.*, Nucl. Instr. & Meth. **A343**, 316 (1994); D. F. Anderson, S. Kwan, and V. Peskov, *ibid.*, p. 109; N. S. Lockyer *et al.*, *ibid.* **A332**, 142 (1993).
- [9] Y. Giomataris and G. Charpak, Nucl. Instr. & Meth. **A310**, 589 (1991); M. Chen *et al.*, "Results of a First Beam Test of Hadron Blind Trackers", CERN-PPE-93-191, Aug. 1993.
- [10] J. C. Anjos *et al.*, "Continued Study of Heavy Flavors at TPL," Fermilab Proposal 829, D. C. Christian and M. Sokoloff, co-spokespersons (1994); see also paper by D. C. Christian, these Proceedings.
- [11] C. J. Kennedy, R. F. Harr, and P. E. Karchin, "Simulation Study of a Transverse Energy Trigger for a Fixed Target Beauty and Charm Experiment at Fermilab," Sept. 9, 1993 (unpublished).
- [12] C. Lee *et al.*, IEEE Trans. Nucl. Sci. **38** 461, (1989); M. Adamovich *et al.*, *ibid.* **37** No. 2, 236 (1990); B. C. Knapp, Nucl. Instr. & Meth. **A289**, 561 (1990).
- [13] W. Selove, in *Proceedings of the Workshop on B Physics at Hadron Accelerators*, P. McBride and C. S. Mishra, eds., Fermilab-CONF-93/267 (1993), p. 617.
- [14] G. Charpak, L. M. Lederman, and Y. Giomataris, Nucl. Instr. & Meth. **A306**, 439 (1991); D. M. Kaplan *et al.*, *ibid.* **A330**, 33 (1993); G. Charpak *et al.*, *ibid.* **A332**, 91 (1993).
- [15] A. M. Halling and S. Kwan, Nucl. Instr. & Meth. **A333**, 324 (1993).

Testing QCD in Charm Production

G. Ridolfi

CERN TH-Division, CH 1211 Geneva 23, Switzerland

S. Frixione

INFN Sezione di Genova, Genoa, Italy

M.L. Mangano

INFN Sezione di Pisa, Pisa, Italy

P. Nason

CERN TH-Division, on leave from INFN Sezione di Milano, Milan, Italy.

Abstract

We present recent theoretical results in heavy-quark production, and we show some comparisons between theoretical predictions and experimental data in hadroproduction and photoproduction of charmed particles.

1 Introduction

Next-to-leading order calculations of heavy quark production cross sections have been developed in the last ten years by various authors [1]-[11]. In particular, in refs. [3, 10] a full next-to-leading calculation of double-differential distributions was performed. On the other hand, a large amount of experimental data is now available, and it has become possible to undertake the task of a systematic comparison between the full next-to-leading theoretical results and experiments (see ref. [12] for a complete bibliography).

In the present talk we will deal with total, single-inclusive and double-differential cross sections for charm production in hadron-hadron and photon-hadron collisions. Our aim is twofold. On one hand we will try to understand whether there are inconsistencies between perturbative QCD predictions and experimental results. This requires a thorough analysis of the theoretical uncertainties. As a second objective, we would like to see if, by a simple parameterization of the most important nonperturbative effects, one can give an adequate description of the observed phenomena. We therefore present results where effects like the primordial transverse momenta of the incoming partons and the fragmentation effects are taken into account.

2 Total cross sections

In fig. 1 we plot the $c\bar{c}$ and $b\bar{b}$ cross sections, computed in QCD at next-to-leading order, as functions of the beam energy, for πN collisions, together with some of the most recent experimental results. The E789 collaboration [13], using an 800 GeV proton beam colliding on a Be or Au target, studied neutral D meson production near $x_F = 0$ to investigate the A dependence of the results. As a by-product, they obtain

$$\sigma(D^0/\bar{D}^0) = 17.7 \pm 0.9 \pm 3.4 \mu b. \quad (1)$$

In figs. 1-3 three different bands are shown, each corresponding to a different value of the heavy quark mass. The cross sections are calculated using the parton distribution set HMRSB [14] for the nucleon and the central set SMRS2 [15] for the pion. The bands in the figure are obtained as follows. We varied the renormalization scale μ_R between half and twice the heavy quark mass. The factorization scale, in the case of charm, was kept fixed at $2m_c$, since available parameterizations of parton densities are usually given for Q^2 larger than 5 or 10 GeV². For this reason, the bands shown in the figure are only an underestimate of the uncertainties involved in the computation of charm production cross sections. The bands represent the maximum variation of the cross sections in this parameter range. The bands in the figure take also into account variation of Λ_{QCD} and of parton density parameterizations.

Observe the considerable improvement in predictivity, after inclusion of next-to-leading order corrections, that takes place when going from charm to bottom. Observe also the strong mass dependence of the charm result.

The results of the same analysis for a proton beam and for a photon beam are shown in figs. 2 and 3 respectively. Most of the considerations made in the case of the pion beam also apply to the cases of protons and photons. This is certainly true for the large overall range of values allowed by the uncertainties of the calculation.

As one can see, experimental results on total cross sections for charm and bottom production at fixed target are in reasonable agreement with theoretical expectations, if the large theoretical uncertainties are taken into proper account. The uncertainties in the case of photoproduction are smaller than in the hadroproduction case. We can also see that the data are compatible with a value of 1.5 GeV for the charm quark mass.

3 Single-inclusive differential distributions

We consider here the p_T^2 and x_F single-inclusive distributions in charm production. The experimental collaborations fit their data using the following parameterization:

$$\frac{d\sigma}{dx_F} = A(1 - x_F)^n \quad (2)$$

for the x_F distribution, and

$$\frac{d\sigma}{dp_T^2} = C e^{-bp_T^2} \quad (3)$$

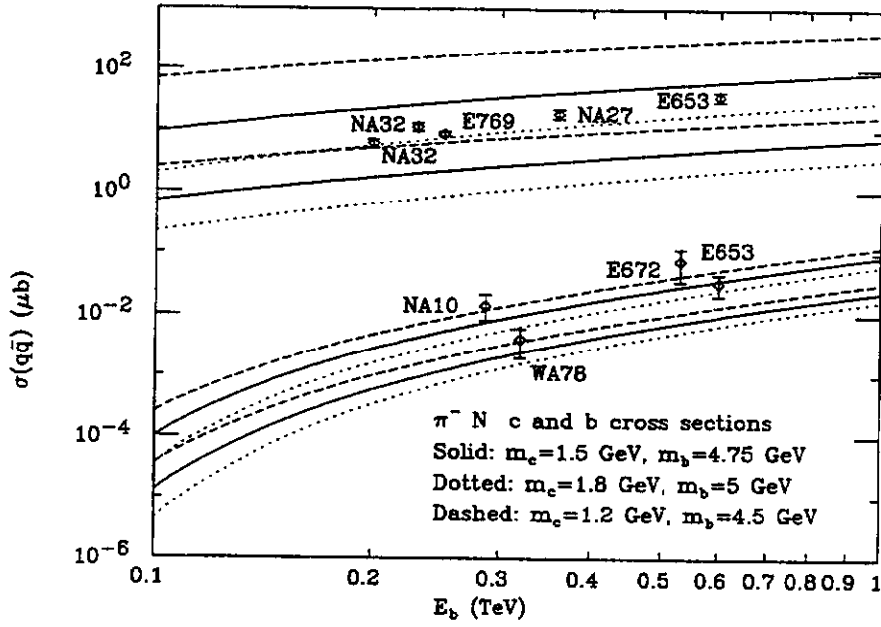


Figure 1: Cross sections for b and c production in πN collisions versus experimental results.

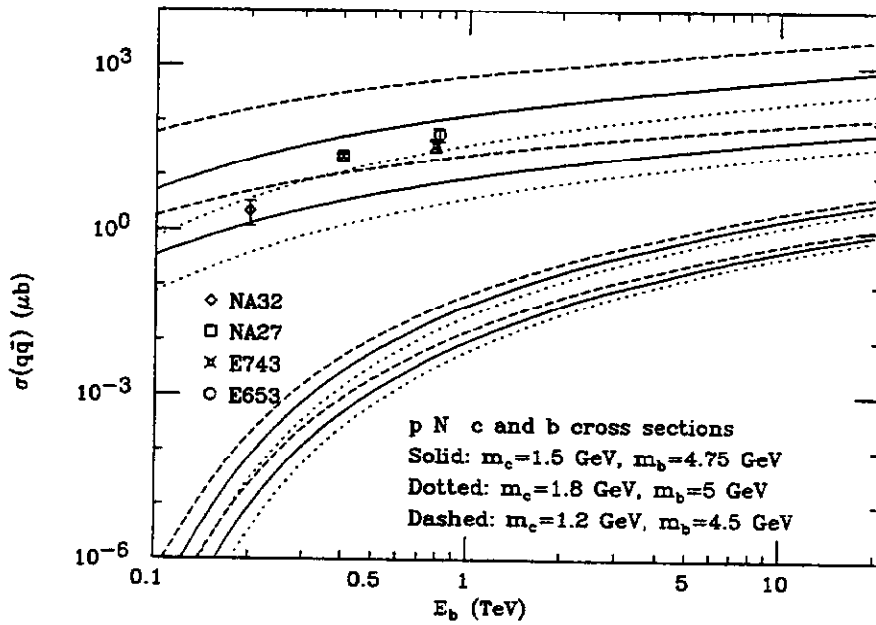


Figure 2: Cross sections for b and c production in pN collisions versus experimental results.

for the p_T^2 distribution. The data are then presented in the form of measured values for the parameters n and b . A possible way of comparing the experimental results with QCD predictions is that of fitting the theoretical distributions using the same functional forms,

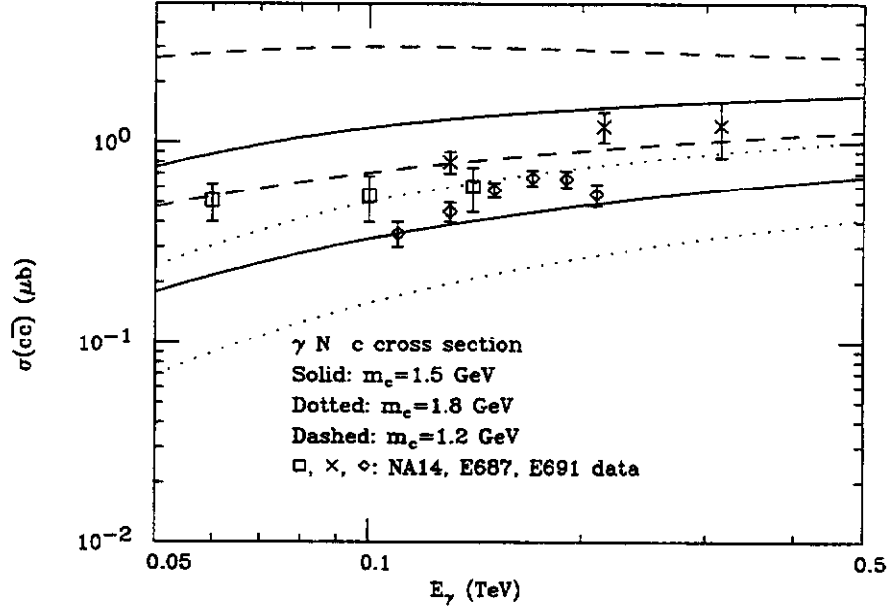


Figure 3: Cross sections for c production in γN collisions versus experimental results.

eqs. (2) and (3), and then comparing the values of the fit parameters obtained in this way with the measured ones. We have therefore fitted the x_F and p_T^2 single-inclusive distributions for charm production computed at next-to-leading order in perturbative QCD, using the forms in eqs. (2) and (3). The values of b that we find for our theoretical curves are in reasonable agreement with the measured values, while the experimental measurements seem to suggest values of n which are smaller than the purely perturbative QCD result, both for the pion and the proton cases. In principle, some description of the hadronization phenomena should be added to the perturbative calculation in order to compare it with the data. These problems were considered in ref. [11], where the hadronization phenomena were studied using the parton shower Monte Carlo HERWIG [16]. In ref. [11] the conclusion was reached that the combined effects of perturbative higher orders and nonperturbative (partonic intrinsic transverse momentum and hadronization) contributions eventually result in a hardening of the x_F distribution, that is, in a smaller value of n . In ref. [11] it was also argued that the usual approach of complementing the perturbative calculation with a fragmentation function in order to describe the x_F distribution is completely unjustified, since the factorization theorem holds only in the large p_T region.

We find that the parameter b , that characterizes the p_T^2 distributions, is very sensitive to the upper bound of the p_T^2 range. This is due to the fact that the fall-off of the cross section at large p_T is not exponential, but it rather follows a power-law. Experimental data show a similar trend (see for example fig. 8 in ref. [17]). We find that the form

$$\frac{d\sigma}{dp_T^2} = \left(\frac{C}{bm_c^2 + p_T^2} \right)^\beta \quad (4)$$

provides an excellent fit to the theoretical distributions in the whole p_T range.

Almost all the experimental collaborations observe, in pion-nucleon collisions, the so-called leading particle effect, that is, an enhanced production of the D mesons whose light valence quark is of the same flavour of one of the valence quarks of the incoming pion. We have found that the QCD prediction is in better agreement with the available data for non-leading particles than they are in the case of the full D meson sample. For proton-nucleon collisions the situation is less clear. Some collaborations explicitly state that no leading effect is observed.

Another, perhaps more significant, possibility is to compare the experimental and theoretical distributions directly. This is done in fig. 4 for the single-inclusive p_T^2 distribution measured by the WA82 collaboration [17] in πN collisions. In this case, the agreement with

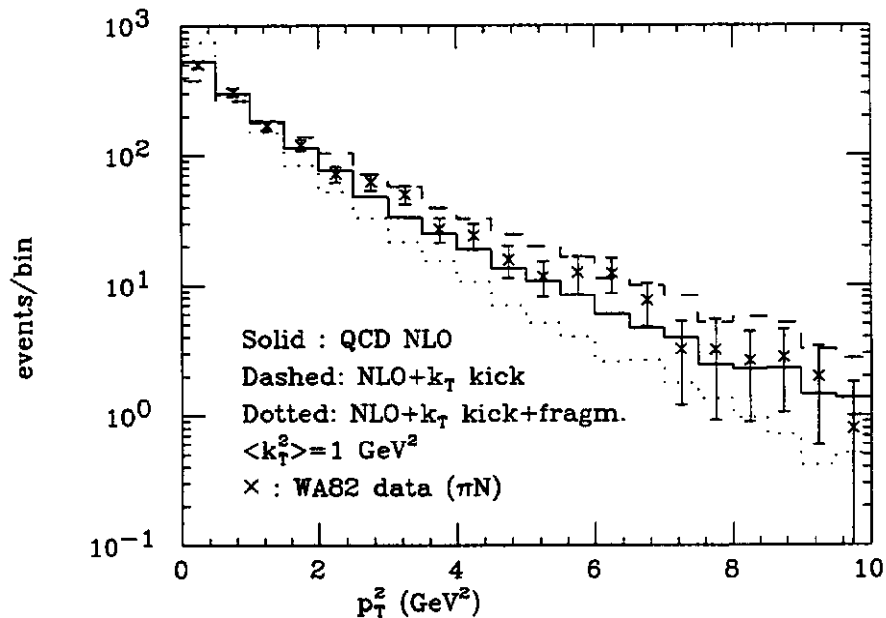


Figure 4: Experimental p_T^2 distribution compared to the next-to-leading order QCD prediction, for $m_c = 1.5$ GeV, with and without the inclusion of nonperturbative effects.

the next-to-leading order QCD calculation is almost perfect over the whole p_T^2 range explored by the experiment, although no higher-order or nonperturbative effects are included in this theoretical curve.

Due to the low mass of the charm quark, we can however expect that nonperturbative effects may play an important rôle. We therefore included in our calculation an intrinsic transverse momentum for the incoming partons. The inclusion of this effect results in a hardening of the single-inclusive p_T^2 distribution.

Another nonperturbative effect that must be accounted for is the hadronization process. Thanks to the factorization theorem, this effect can be described by convoluting the partonic

cross section with a fragmentation function, which we choose to be of the Peterson form [18]. This degrades the parent charm quark momentum, and results in a softening of the p_T distribution.

Both effects are shown in fig. 4, for an average intrinsic transverse momentum of the incoming partons $\langle k_T^2 \rangle = 1 \text{ GeV}^2$. The parameter ϵ_c that characterizes the Peterson fragmentation function was set at its central value of 0.06. We have verified that the result does not change substantially if we use the smaller value $\epsilon_c = 0.04$. From inspection of fig. 4, we can conclude that perturbative QCD, supplemented with some parameterization of the most important nonperturbative effects, leads to a prediction in qualitative agreement with the experimental single-inclusive p_T^2 distribution measured by the WA82 collaboration. We have checked, however, that, in order to reproduce the WA82 data, an average intrinsic transverse momentum $\langle k_T^2 \rangle = 2 \text{ GeV}^2$ is needed. This value for $\langle k_T^2 \rangle$ is rather large, and we will comment later upon its effect on other observables. One may attempt to use larger values of the charm quark mass in order to get better agreement with data without the need of a large $\langle k_T^2 \rangle$. In fact, a larger m_c would harden the p_T spectrum of the quark. As better data will become available, it will be certainly worth comparing the data with QCD predictions at different values of the charm quark mass.

In fig. 5 we present the x_F distributions measured by WA82 in πN collisions, for D^- and D^+ mesons, compared with the theoretical QCD NLO curve for charm quarks. We can see that the experimental data show a harder behaviour, and that the agreement with the theoretical distribution is satisfactory in the case of the non-leading hadron (D^+ in this case). This is another indication that non perturbative phenomena (such as color drag effects) are present in production of leading particles.

Single-inclusive distributions for charm production have also been measured by photon-nucleon collision experiments. In the case of photoproduction, we expect QCD predictions to be more reliable than in the hadroproduction case, since only one hadron is present in the initial state (see refs. [7] and [10] for a detailed discussion).

In figs. 6 and 7 we show the p_T^2 distribution measured by the E687 [19, 20] and E691 [21] collaborations respectively. We also show the next-to-leading order QCD prediction, and the QCD prediction supplemented with Peterson fragmentation and an intrinsic transverse momentum for the incoming partons with $\langle k_T^2 \rangle = 0.5 \text{ GeV}^2$, 1 GeV^2 and 2 GeV^2 . It is interesting to notice that, in this case, the fragmentation effect, combined with a moderate intrinsic transverse momentum of the initial state partons, is sufficient to reproduce the experimental distribution. Contrary to what happens in the hadroproduction case, this distribution is now less sensitive to the choice of the $\langle k_T^2 \rangle$, and it can accommodate any value between 0.5 and 2 GeV^2 .

4 Double-differential distributions

Correlations between charmed particles in hadro- and photoproduction have been studied by many experiments, which reported distributions of the azimuthal distance between the

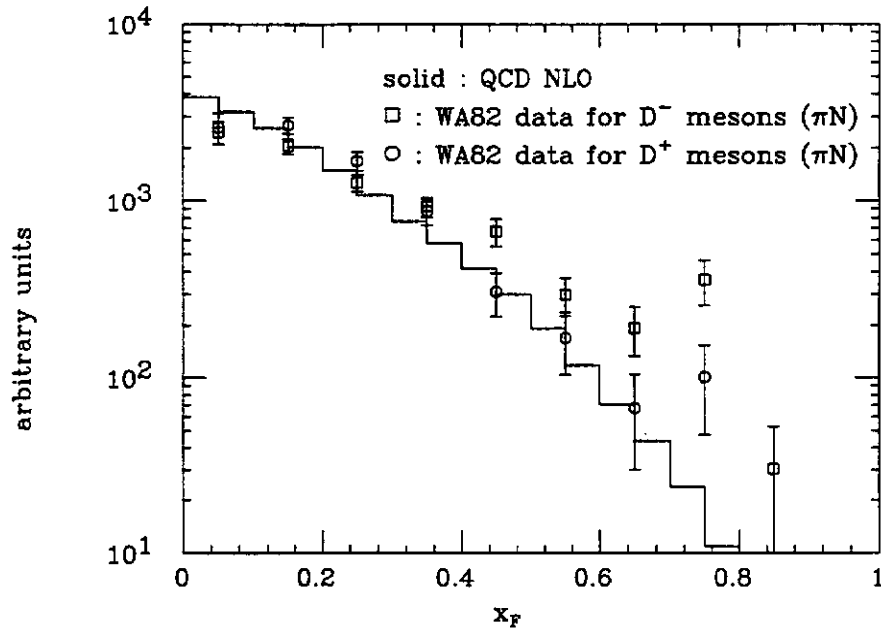


Figure 5: Experimental x_F distribution for D^- and D^+ mesons, compared to the next-to-leading order QCD prediction for charm quarks ($m_c = 1.5$ GeV).

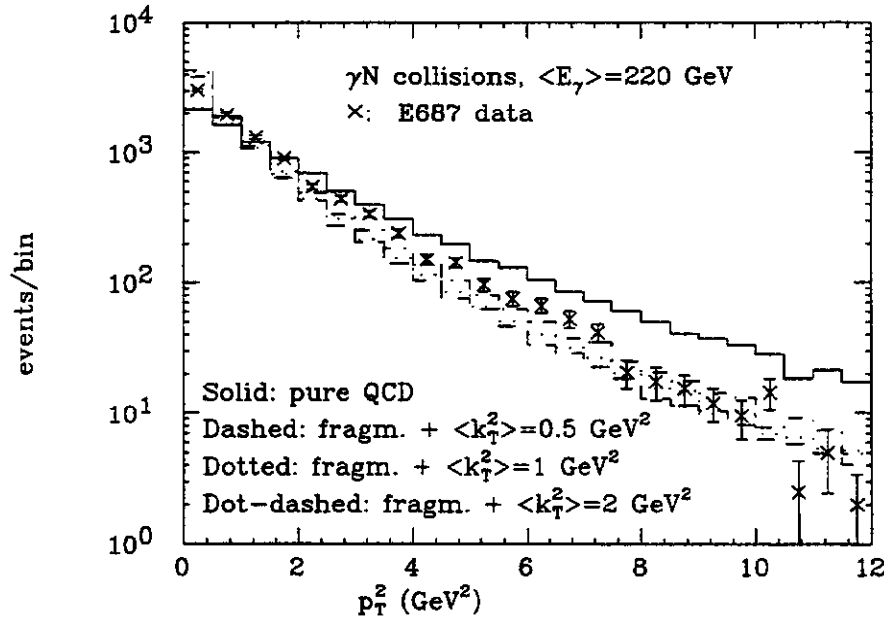


Figure 6: Experimental p_T^2 distribution compared to the next-to-leading order QCD prediction, with and without the inclusion of nonperturbative effects, in γN collisions at $\langle E_\gamma \rangle = 220$ GeV ($m_c = 1.5$ GeV).

charmed hadrons, the rapidity difference, the invariant mass and the p_T of the pair. In what

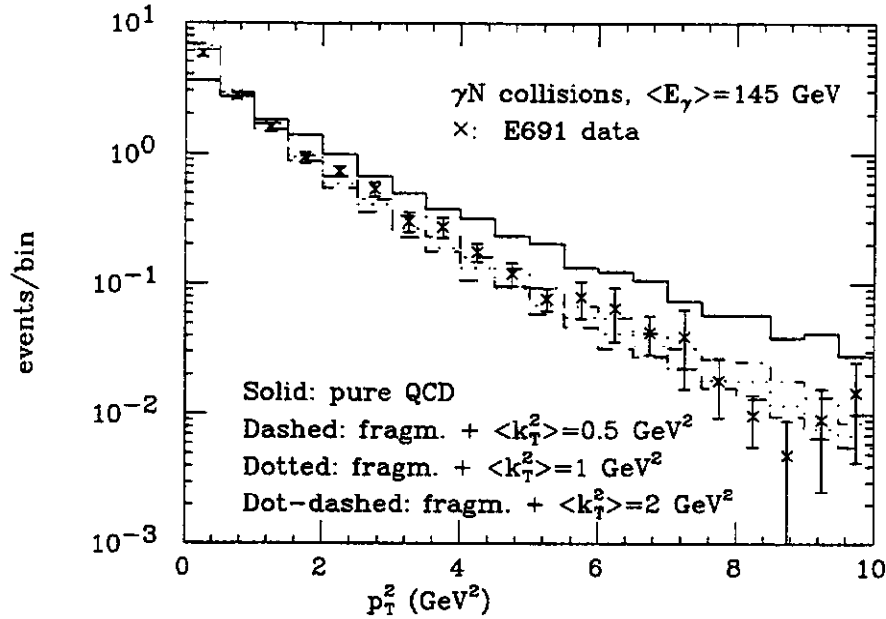


Figure 7: Experimental p_T^2 distribution compared to the next-to-leading order QCD prediction, with and without the inclusion of nonperturbative effects, in γN collisions at $\langle E_\gamma \rangle = 145$ GeV ($m_c = 1.5$ GeV).

follows we will focus on the distributions of $\Delta\phi$, defined as the angular difference between the transverse momenta of the heavy quark and antiquark, and of the transverse momentum of the pair. Leading-order QCD predicts that the heavy-quark pair be produced exactly in the back-to-back configuration, corresponding to $\Delta\phi = \pi$ and $p_T(Q\bar{Q}) = 0$. Next-to-leading order corrections, as well as nonperturbative effects, can cause a broadening of these distributions, as illustrated in refs. [10] and [11]. In the hadroproduction case, the data show some enhancement of the $\Delta\phi$ distribution around π . There is however no sound agreement on the significance of the enhancement observed by different experiments. For example, the WA75 collaboration [22] favours a relatively flat distribution. The E653 collaboration [23] has mild evidence for a peak in the $\Delta\phi = \pi$ bin. A recent analysis performed by the WA92 collaboration [25] shows clear evidence of a back-to-back enhancement of the distribution.

We addressed the question, can next-to-leading order QCD predictions account for the available experimental data? We have chosen, as an illustration, the cases of the WA75 and the WA92 results, which have both been obtained in $\pi^- N$ collisions at the same energy, $E_b = 350$ GeV. In both cases, the experimental data are broader than the pure QCD NLO calculation. One should however take into account also nonperturbative effects, as in the case of single-inclusive distributions. We have computed the $\Delta\phi$ distribution in perturbative QCD with an intrinsic transverse momentum of the incoming partons (the use of a fragmentation function has no effect on the $\Delta\phi$ distribution, since it does not affect momentum directions). An average value $\langle k_T^2 \rangle = 0.5$ GeV² allows to achieve a rather consistent description of the heavy-flavour azimuthal correlation in the case of the WA92 data, while a higher $\langle k_T^2 \rangle$ is needed in order to reproduce WA75 data, as shown in fig. 8. The WA75 collaboration also

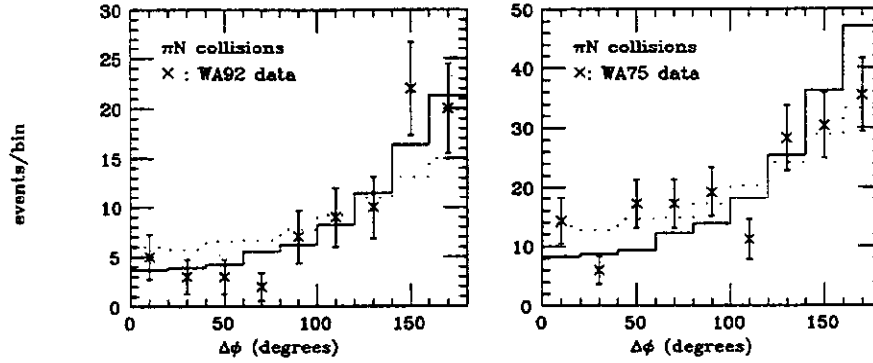


Figure 8: Next-to-leading order QCD result (for $m_c = 1.5$ GeV) supplemented with a primordial transverse momentum for the incoming partons of 0.5 GeV^2 (solid) and 1 GeV^2 (dotted), compared with the WA92 and WA75 data.

published in ref. [22] the distribution of the transverse momentum of the heavy quark pair. This distribution is very hard, and in this case the theoretical prediction supplemented with a parton primordial transverse momentum with $\langle k_T^2 \rangle = 1 \text{ GeV}^2$ is insufficient to reproduce the data, as displayed in fig. 9. Unlike the azimuthal correlation, the pair transverse momentum

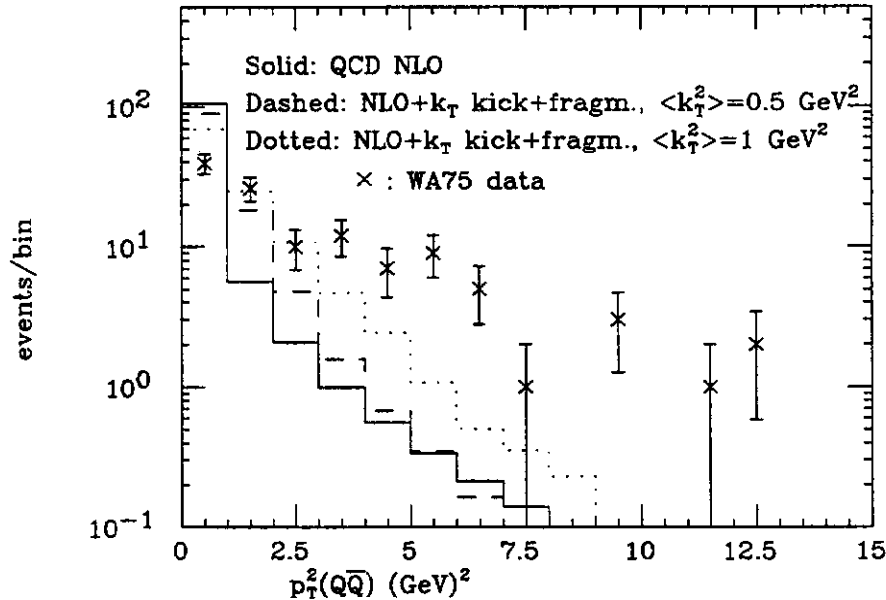


Figure 9: Next-to-leading order QCD result (for $m_c = 1.5$ GeV) for the $p_T^2(Q\bar{Q})$ supplemented with a primordial transverse momentum for the incoming partons compared with the WA75 data.

distribution is affected by fragmentation effects, since these effects can randomly degrade the momenta of the quark and antiquark by different amounts. Fragmentation effects, however, have also the effect of moderating the pair transverse momentum arising from gluon radiation,

or from an intrinsic parton transverse momentum. We have verified that at the end, at $E_b = 350$ GeV, the fragmentation effect always tends to soften the pair transverse momentum distribution. Summarising, the WA75 data, both for the azimuthal correlation and for the pair transverse momentum, require a very large intrinsic transverse momentum of the incoming parton. On the other hand, the $\Delta\phi$ distribution measured by WA92 is consistent with a reasonably moderate intrinsic k_T distribution. Clarification of this issue requires more experimental information.

We observe that the procedure of adding an intrinsic transverse momentum to the incoming partons to the perturbative computation is not theoretically well defined. In fact, the perturbative expansion itself does provide, via gluon emission, a transverse momentum to the partons that enter the hard subprocess. We find for example that changing the renormalization scale μ_R to lower values leads to a broader $\Delta\phi$ distribution. This is illustrated in fig. 10, where we see that for a choice of $\mu_R = \mu_0/2$ there is no need of an intrinsic transverse momentum in order to reproduce the WA92 data. As an additional remark, we mention that in ref. [11] we verified, using the Monte Carlo HERWIG [16], that perturbative higher order effects do not affect significantly the shape of the $\Delta\phi$ distributions.

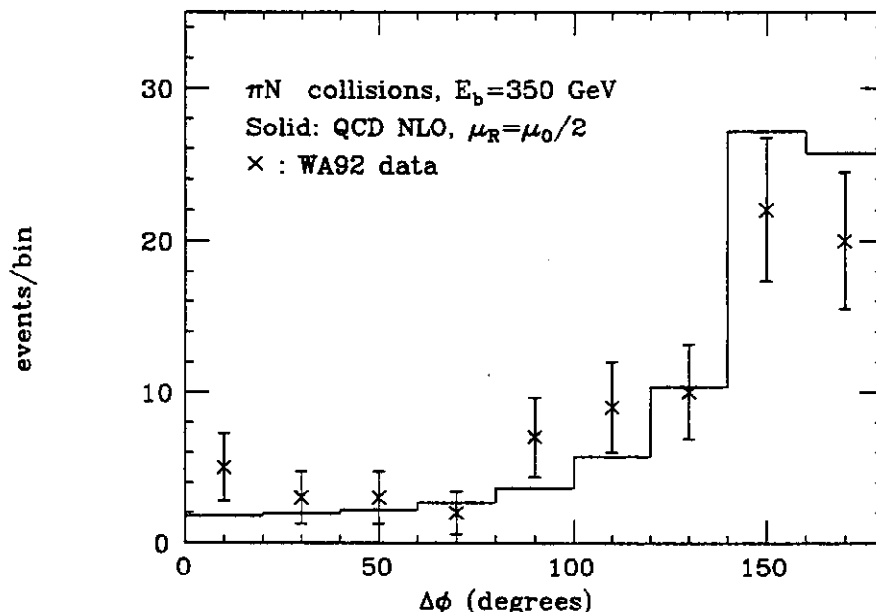


Figure 10: Next-to-leading order QCD result (for $m_c = 1.5$ GeV) calculated with $\mu_R = \mu_0/2$ compared with the WA92 data.

Photoproduction of heavy quarks [24] is another example in which a k_T kick would induce broader correlations. It can therefore be used to see what is the value of the parton intrinsic transverse momentum favoured by the photoproduction data. In fig. 11 the azimuthal correlation measured in photoproduction experiments is given, together with the next-to-leading order result, with and without the addition of an intrinsic k_T of the incoming partons with $\langle k_T^2 \rangle = 0.5$ GeV² and $\langle k_T^2 \rangle = 1$ GeV². As one can see, the data do not require

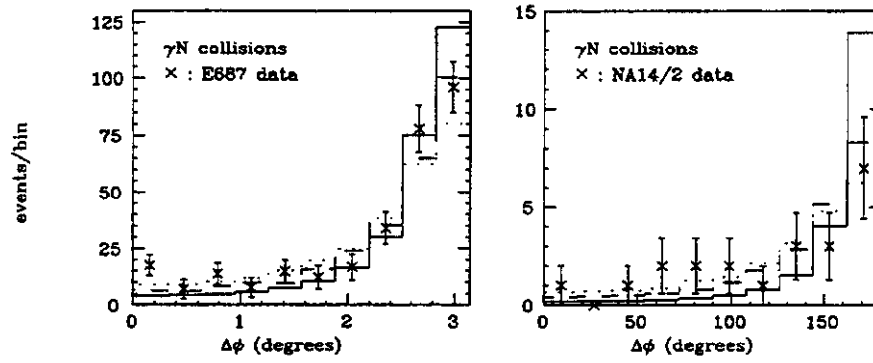


Figure 11: Azimuthal correlation of $D\bar{D}$ pair versus the perturbative result in photoproduction for the E687 and NA14 experiments. Solid: pure QCD ($m_c = 1.5$ GeV); dashed: $\langle k_T^2 \rangle = 0.5$ GeV²; dotted: $\langle k_T^2 \rangle = 1$ GeV².

a large intrinsic transverse momentum. Both curves give a reasonable representation of the data, the one with $\langle k_T \rangle = 0.5$ GeV² being slightly better.

Another distribution which is very sensitive to the intrinsic transverse momentum of the partons is the transverse momentum of the heavy quark pair, displayed in fig. 12. Even in

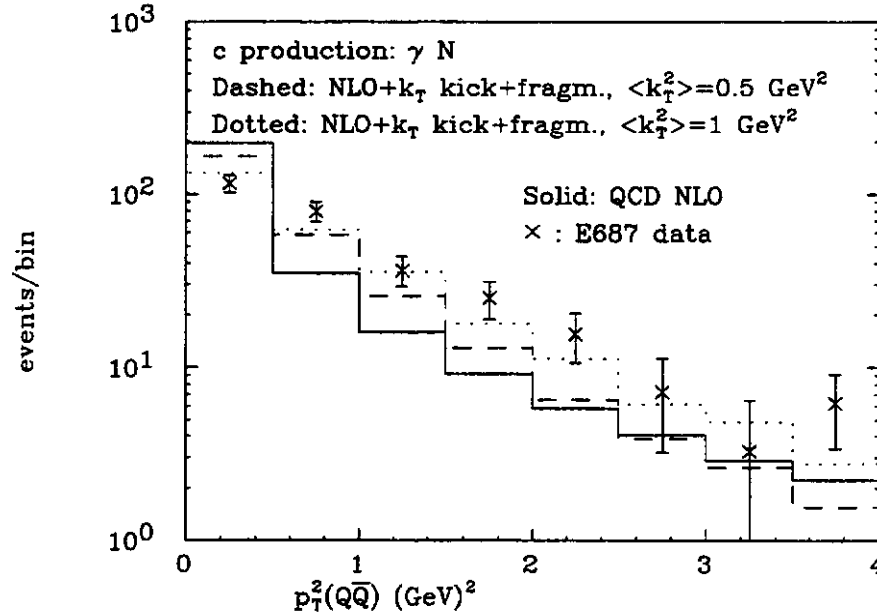


Figure 12: Transverse momentum distribution of the $D\bar{D}$ pair versus the perturbative result (for $m_c = 1.5$ GeV) for the E687 experiment.

this case, we see that the data favour a reasonably small intrinsic transverse momentum.

5 Conclusions

We have presented a comparison between charm production data and theoretical predictions. All the most recent total-cross-section data are in reasonable agreement with the QCD next-to-leading-order predictions, once the large theoretical uncertainties are properly taken into account. The measurements for charm production in pion-nucleon, proton-nucleon and photon-nucleon collisions are consistent with a quark mass value of 1.5 GeV.

We have shown that the pure QCD perturbative results are not adequate to describe the observed charmed meson distributions, and that the inclusion of nonperturbative effects is necessary. We attempted to model these effects by giving a randomly distributed transverse momentum (k_T -kick) to the partons entering the hard subprocesses, and by applying to the final-state heavy quarks a Peterson fragmentation function in order to model hadronization.

For the single-inclusive transverse momentum distribution, the agreement with the photoproduction data is quite satisfactory for values of $\langle k_T^2 \rangle$ between 0.5 and 2 GeV². These distributions are not very sensitive to the value of $\langle k_T^2 \rangle$. They seem however to favour large values of $\langle k_T^2 \rangle$, at least for $m_c = 1.5$ GeV. In the hadroproduction case we were able to perform a meaningful comparison only for the data of the WA82 collaboration. We get a good agreement with the WA82 data for $\langle k_T^2 \rangle$ around 2 GeV².

We have also shown that the measured x_F distribution can be reproduced by the perturbative QCD next-to-leading-order result only for the non-leading D -meson hadroproduction. Due to the failure of the factorization theorem in the high- x_F region, we were not able to supplement our perturbative calculation with a description of the hadronization phenomena. In ref. [11] this problem was studied using a parton shower approach, which led to harder distributions, possibly consistent with the data.

We also compared theoretical predictions with experimental measurements in the case of double-differential distributions. We considered the distribution in the transverse momentum of the heavy-quark pair, and the distribution in the azimuthal distance between the two heavy quarks. For the transverse momentum of the heavy-quark pair, we find that a value of $\langle k_T^2 \rangle = 1$ GeV² fits the photoproduction data of the E687 experiment well, while in the hadroproduction case the experimental distribution (measured by the WA75 experiment) is much harder than the theoretical one for any plausible value of $\langle k_T^2 \rangle$. For the $\Delta\phi$ distribution we found that in almost all cases a definite choice of $\langle k_T^2 \rangle$ is sufficient to reproduce the data. However, different data sets favour different values of $\langle k_T^2 \rangle$, ranging from 0.5 GeV² for the WA92 experiment to 1 GeV² for WA75. Photoproduction data are well described by both values.

Acknowledgement

One of us (GR) would like to thank Dan Kaplan and the Fermilab Theory Group for their kind hospitality during the CHARM2000 Workshop.

References

- [1] P. Nason, S. Dawson and R. K. Ellis, *Nucl. Phys.* **B303**(1988)607; **B327**(1988)49.
- [2] W. Beenakker et al., *Nucl. Phys.* **303**(1991)507; *Phys. Rev.* **D40**(1989)54.
- [3] M.L. Mangano, P. Nason and G. Ridolfi, *Nucl. Phys.* **B373**(1992)295.
- [4] E. Laenen, J. Smith and W.L. van Neerven, *Nucl. Phys.* **B369**(1992)543.
- [5] E. Berger and R. Meng, *Phys. Rev.* **D49**(1994)3248.
- [6] M. Cacciari and M. Greco, preprint FNT/T-93/43 (University of Pavia), hep-ph/9311260 (1993).
- [7] R.K. Ellis and P. Nason, *Nucl. Phys.* **B312**(1989)551.
- [8] J. Smith and W.L. Van Neerven, *Nucl. Phys.* **B374**(1992)36.
- [9] E. Laenen, S. Riemersma, J. Smith and W.L. Van Neerven, *Nucl. Phys.* **B392**(1993)162 and 229.
- [10] S. Frixione, M.L. Mangano, P. Nason and G. Ridolfi, *Nucl. Phys.* **B412**(1994)225
- [11] M. Mangano, P. Nason and G. Ridolfi, *Nucl. Phys.* **B405**(1993)507.
- [12] S. Frixione, M.L. Mangano, P. Nason and G. Ridolfi, preprint CERN-TH.7292/94, GEF-TH-4/1994.
- [13] M. J. Leitch et al., E789 Coll., *Phys. Rev. Lett.* **72**(1994)2542.
- [14] P. Harriman, A. Martin, R. Roberts and J. Stirling, *Phys. Rev.* **D37**(1990)798.
- [15] P.J. Sutton, A.D. Martin, R.G. Roberts and W.J. Stirling, *Phys. Rev.* **D45**(1992)2349.
- [16] G. Marchesini and B.R. Webber, *Nucl. Phys.* **B310**(1988)461.
- [17] M.I. Adamovich et al., WA82 Coll., *Nucl. Phys. (Proc. Suppl.)* **B27**(1992)212.
- [18] C. Peterson, D. Schlatter, I. Schmitt and P. Zerwas, *Phys. Rev.* **D27**(1983)105.
- [19] G. Bellini, proceedings of "Les Rencontres de Physique de la Vallee d'Aoste", La Thuile, Aosta Valley, March 6-12, 1994.
- [20] R. Gardner, private communication.
- [21] J.C. Anjos et al., E691 Coll., *Phys. Rev. Lett.* **62**(1989)513.
- [22] S. Aoki et al., WA75 Coll., *Progr. Theor. Phys.* **87**(1992)1315;
S. Aoki et al., WA75 Coll., *Phys. Lett.* **B209**(1988)113.
- [23] K. Kodama et al., E653 Coll., *Phys. Lett.* **B263**(1991)579.
- [24] M.P. Alvarez et al., NA14/2 Coll., *Phys. Lett.* **B278**(1992)385,
V. Arena et al., E687 Coll., *Phys. Lett.* **B308**(1993)194;
J.C. Anjos et al., E691 Coll., *Phys. Rev. Lett.* **65**(1990)2503;
M.I. Adamovich et al., Photon Emulsion Coll., *Phys. Lett.* **B187**(1987)437 and references therein.
- [25] A. Cardini, WA92 Coll., to appear in the Proceedings of the XXIX Rencontres de Moriond, 19-26 March 1994, Meribel, France; Ph.D thesis, unpublished, Pisa University.

Anomalous Charm Production at Large x_F ¹

W.-K. Tang²

*Stanford Linear Accelerator Center
Stanford University, Stanford, CA 94309*

Abstract

We show that the new QCD production mechanisms which were proposed by S. J. Brodsky, P. Hoyer, A. H. Mueller and the author can explain at least some of the anomalous behavior of open and/or closed charm production at large x_F .

1 Introduction

Charm production at large x_F is a very fascinating regime which provides a lot of information about the internal structure, especially the higher Fock state components of the projectile in the question [1, 2]. No matter whether it is deep inelastic scattering, pion nucleus collisions, open charm or hidden charm production [3, 4, 5, 6, 7, 8, 11, 13, 12, 14], all of them show anomalous behavior which cannot be explained by leading twist PQCD. In fact, in the $x \rightarrow 1$ limit, there is a new hard scale $\Lambda_{QCD}^2/(1-x)$, and the corrections to leading twist terms are of order $\Lambda_{QCD}^2/(1-x)Q^2$. Actually, in the combined limit,

$$\left. \begin{array}{l} Q^2 \rightarrow \infty \\ x \rightarrow 1 \end{array} \right\} \quad \text{with } \mu^2 \equiv (1-x)Q^2 \text{ fixed,} \quad (1)$$

the twist expansion breaks down and higher twist terms are no longer suppressed and can become dominant.

This paper is organized as follow: in section 2, we will review some of the experimental data which shows that higher twist effects are important at large x_F . It is well known that higher twist terms are suppressed by $\mathcal{O}(1/M^2)$ so it raises the question why they become dominant at large x_F . Thus, we need to understand the physical origin of the suppression of higher twist terms at moderate x_F and this is reviewed in section 3. We then explain in section 4 why in the new limit, $x_F \rightarrow 1$ and $M^2 \rightarrow \infty$ but with $\mu^2 = (1-x_F)M^2$ fixed, higher twist terms are not suppressed. We will argue in section 5 that in this new QCD limit, the cross section for freeing the $c\bar{c}$ pair is not small due to the fact that the dominant contribution comes from peripheral processes in which slow spectator quarks interact with the target. These new production mechanisms are then applied to different processes and can explain at least some of anomalous behavior observed. Finally, we give our conclusion in the last section.

¹Invited talk presented at Workshop on the Future of High Sensitivity Charm Experiments: Charm2000, Fermilab, Batavia, IL, June 7-9, 1994

²Work supported by the Department of Energy, contract DE-AC03-76SF00515

2 Anomalous behavior of open and/or hidden charm production at large x_F

(a) It is reported by EMC [3] that the $c(x)$ distribution measured at large x_{bj} is anomalously high. The CERN measurements disagree with photon-gluon fusion by a factor of 20 to 30 at $Q^2 = 75 \text{ GeV}^2$ and $x_{bj} = 0.422$ as shown in Fig. 1a and b. One should notice that the measured x_{bj} is the fractional longitudinal momentum for one charm quark only. The total x_{bj} for the $c\bar{c}$ pair should be nearly double which is 0.85, very close to 1. In Fig. 1a and b, one can see that photon-gluon fusion fits the data well for x_{bj} less than 0.3, but badly for x_{bj} larger than 0.4.

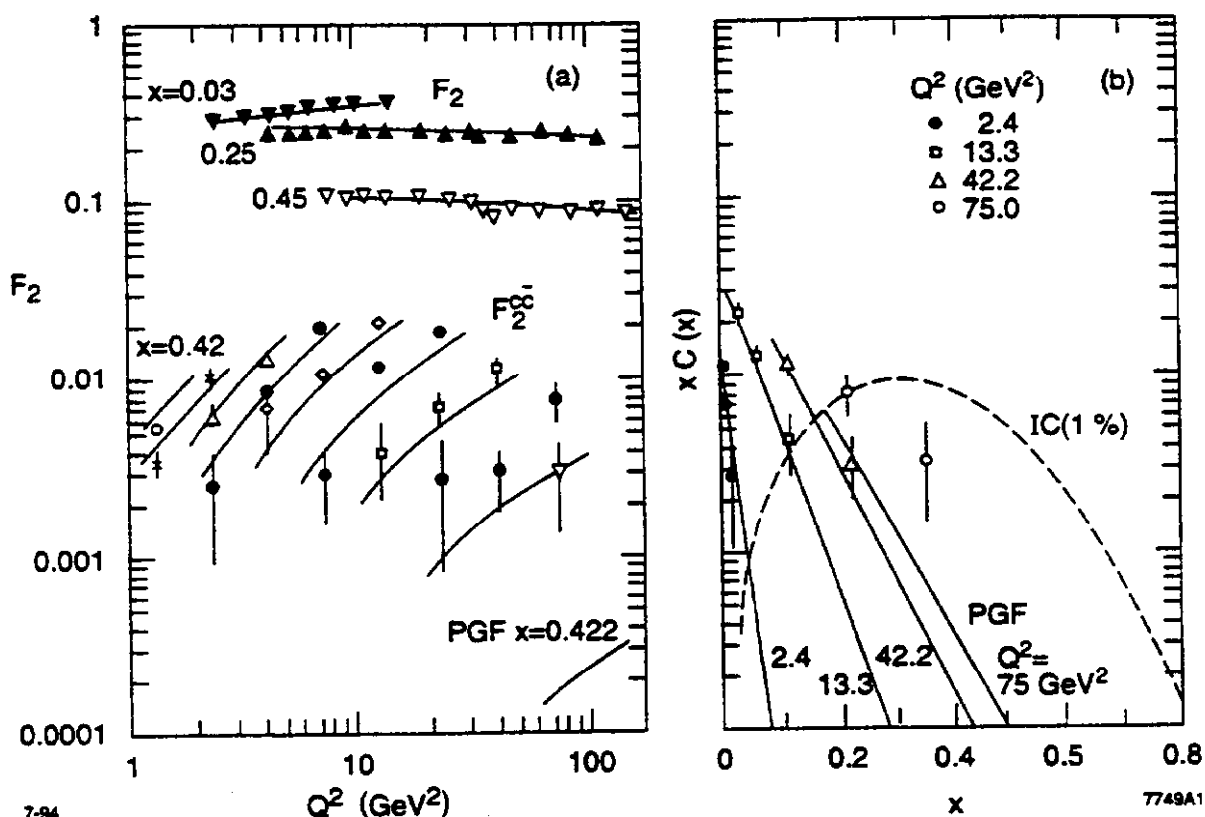


Figure 1: Fig. 1a shows the value of F_2^{cc} versus Q^2 for fixed x : \circ ($x=0.00422$), \times ($x = 0.00750$), \triangle ($x = 0.0133$), \otimes ($x = 0.0237$), \diamond ($x = 0.0422$), \bullet ($x = 0.0750$), \square ($x = 0.133$), \oplus ($x = 0.237$), ∇ ($x = 0.422$). Please notice the large disagreement between experimental data ∇ and the PGF prediction (smooth curves). In Fig. 1b the charm quark momentum density distribution $xc(x)$ as a function of x and Q^2 is plotted. The PGF prediction (smooth curves) does not fit the data when x is large. The data is from Ref.[3].

(b) A sudden change in polarization of the J/ψ is reported by CIP [4] and E537 [5] at large x_F in πN collisions. The polarization of the J/ψ is determined by the angular distribution of its decay muons in the J/ψ rest frame. By rotational symmetry and parity, the angular distribution of massless muons, integrated over the azimuthal angle, has the

form

$$\frac{d\sigma}{d\cos\theta} \propto 1 + \lambda \cos^2\theta \quad (2)$$

where θ is the angle between the μ^+ and the projectile direction (i.e., in the Gottfried-Jackson frame). The parameter λ is directly related to the polarization of the J/ψ particle, i.e.,

$$\lambda = \begin{cases} 1 & \text{transverse } J/\psi \\ 0 & \text{unpolarized } J/\psi \\ -1 & \text{longitudinal } J/\psi. \end{cases} \quad (3)$$

In Fig. 2, where λ is plotted against x_F , one can clearly see that the polarization of the produced J/ψ changes sharply from unpolarized to longitudinally polarized around $x_F \sim 0.85$. This dramatic effect is inconsistent with leading order QCD.

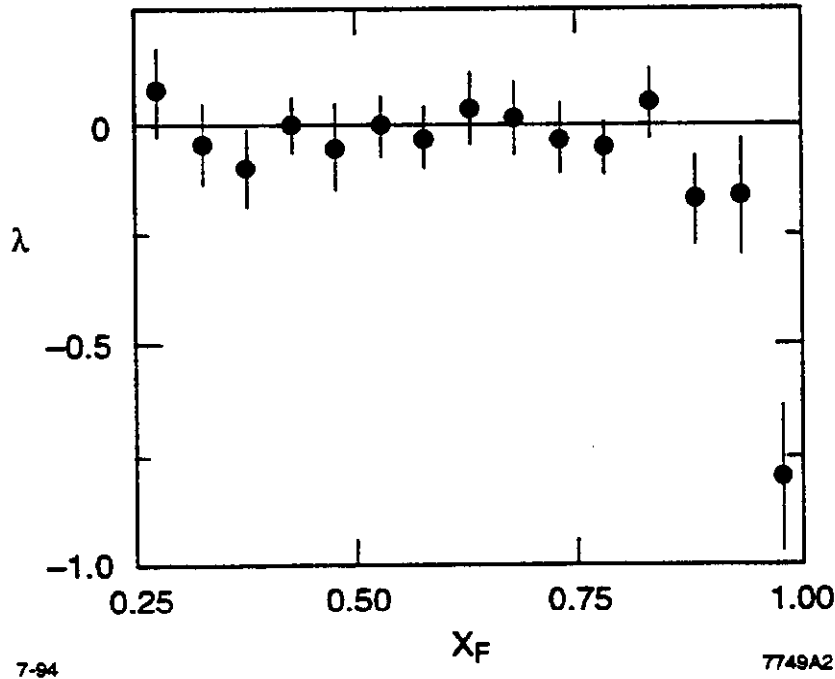


Figure 2: CIP data: x_F dependence of λ fitted to the J/ψ decay. Please notice the sudden change of the J/ψ polarization around $x_F \sim 0.85$.

(c) The measurement from NA3 [6] shows that double J/ψ pairs are hadroproduced only at large x_F . In the NA3 experiment, 6 $\psi\psi$ are found at 150 GeV and 7 $\psi\psi$ at 280 GeV in π^- beam scattering with a platinum target. In table 1, we list the x_F of the $\psi\psi$ pair of all 13 events in ascending order. The mean x_F of the pair is 0.71 (150 GeV) and 0.53 (280 GeV) which is very large.

The data also indicates strong correlations in the production mechanisms. The transverse momentum of the $\psi\psi$ pair is 0.9 ± 0.1 GeV for the 280 GeV beam; whereas uncorrelated pairs from a Monte Carlo study have a much larger mean transverse momentum of 1.7 GeV. Also amazingly, the mean value of the individual J/ψ transverse momenta in the $\psi\psi$ events,

P_π	x_F of $\psi\psi$ pair						
150 GeV	0.58	0.61	0.75	0.75	0.77	0.78	
280 GeV	0.39	0.47	0.47	0.48	0.51	0.65	0.75

Table 1: The x_F of the $\psi\psi$ pair of all 13 events in ascending order. The data are from Ref. [6].

1.5 GeV, is significantly higher than the mean transverse momentum of the $\psi\psi$ pair, so there is strong correlation of between the transverse momenta of two J/ψ 's produced.

To make a quantitative statement about the correlation, we should compare the measured double J/ψ cross section per nucleon $\sigma_{\psi\psi}$ with $A^{1/3}(\sigma_\psi/\sigma_{tot})^2\sigma_{tot}$, which is the theoretical estimate assuming that the ψ 's are produced uncorrelated. Here σ_ψ/σ_{tot} is the probability of producing a J/ψ in a pion nucleon collision. The extra $A^{1/3}$ dependence takes into account the nuclear effect. In table 2, we compare the two cross sections and find that the theoretical prediction is off by three orders of magnitude! This strongly indicates that we need a new production mechanism in order to account for the large disagreement. The leading charm hadroproduction and the nuclear dependence, being reviewed in the following paragraphs, give us hint of the nature of this new mechanism.

P_π	$\sigma_{\psi\psi}$ [pb]	σ_ψ [nb]	σ_{tot} [mb]	$A^{1/3}(\sigma_\psi/\sigma_{tot})^2\sigma_{tot}$ [10^{-2} pb]
150 GeV	18 ± 8	6.5	~ 25	1.0
280 GeV	30 ± 10	8.7	~ 25	1.7

Table 2: Cross sections per nucleon for double J/ψ production in π^-N collisions and the theoretical prediction assuming the J/ψ 's are produced uncorrelated. The data is from Ref. [6].

(d) Dramatic leading particle effects in hadronic D production are observed by WA82 [7] and E769 [8] experiments. In $\pi^-(\bar{u}d)$ interactions with hadrons or nuclei, the $D^-(\bar{c}d)$ and $D^0(c\bar{u})$ are referred to as "leading" charm mesons while the $D^+(c\bar{d})$ and $\bar{D}^0(u\bar{c})$ are "nonleading". The asymmetry between leading and nonleading charm, which has been used in the analyses of the WA82 and E769 collaborations, is defined as

$$\mathcal{A} = \frac{\sigma(\text{leading}) - \sigma(\text{nonleading})}{\sigma(\text{leading}) + \sigma(\text{nonleading})} \quad (4)$$

Both experiment find that the measured $\mathcal{A}(x_F)$ increases from ~ 0 for $x_F \leq 0.4$ to ~ 0.5 around $x_F = 0.65$ (Fig. 3). Therefore, the leading charm asymmetry is localized at large x_F only.

According to leading twist QCD, the hadroproduction cross section of D mesons is given by

$$\frac{d\sigma_{AB \rightarrow DX}}{dx_a dx_b dz_1} \propto \sum_{ab} f_{a/A}(x_a) f_{b/B}(x_b) \hat{\sigma}_{ab \rightarrow c\bar{c}} D_{D/c}(z_1). \quad (5)$$

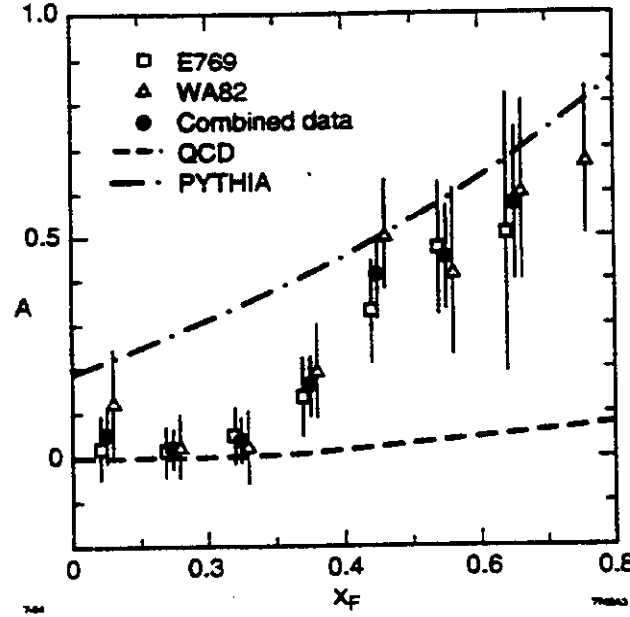


Figure 3: Leading charm asymmetry versus x_F . A substantial asymmetry is observed at large x_F .

The structure functions of the initial hadrons, $f_{a/A}(x_a)$, are process independent while the fragmentation functions $D_{D/c}(z_1)$ are independent of the quantum numbers of both the projectile and the target. Thus, leading twist QCD predicts the leading charm asymmetry to be nearly zero.³ The observed large leading charm asymmetry breaks QCD factorization which strongly suggests that it is a higher twist effect.

(e) The data [11, 12, 13] on J/ψ production in hadron-nucleus collisions exhibits a surprising result. The NA3 and E772 data give direct evidence for the breakdown of the leading twist approximation at large x_F . Following the argument of Ref.[14], by the factorization theorem, the cross section of J/ψ production in πA collisions is,

$$\frac{d\sigma_{\pi A \rightarrow J/\psi X}}{dx_1 dx_2} = f_{a/\pi}(x_1) f_{b/A}(x_2) \hat{\sigma}(ab \rightarrow J/\psi) \quad (6)$$

For simplicity we just assume gluon gluon fusion to be dominant. For $\sqrt{s} \gg M_\psi^2$ and $x_F > 0$, approximately $x_1 \simeq x_F$, $x_2 \simeq M_\psi^2/x_F s$. In the factorized formula (6), the nuclear A -dependence appears only through the target function $f_{b/A}(x_2)$. Hence, ratios $R = A\sigma(pp \rightarrow J/\psi + X)/\sigma(pA \rightarrow J/\psi + X)$ of J/ψ production should be independent of c.m. energies \sqrt{s} when \sqrt{s} and x_F varied in such a way as to keep x_2 constant. However, as shown in Fig. 4, the NA3 data [11] shows that the ratio for H/Pt is consistent with *Feynman scaling*, i.e., scales with x_F but not with x_2 . A clear energy dependence is seen at small values of x_2 . Thus the leading twist factorization fails at large Feynman x of the J/ψ , since $x_2 \simeq M_\psi^2/x_F s$. A similar result was observed by combining pA data from NA3 and E772 [12].

The same anomalous behavior is also observed if one studies the nuclear A -dependence of the J/ψ production cross section through the parametrization $\sigma_A = \sigma_p A^\alpha$. The effective

³Next-to-leading order calculation do give rise to a small charge asymmetry between \bar{c} and c production due to qg and $q\bar{q}$ interference [9, 10].

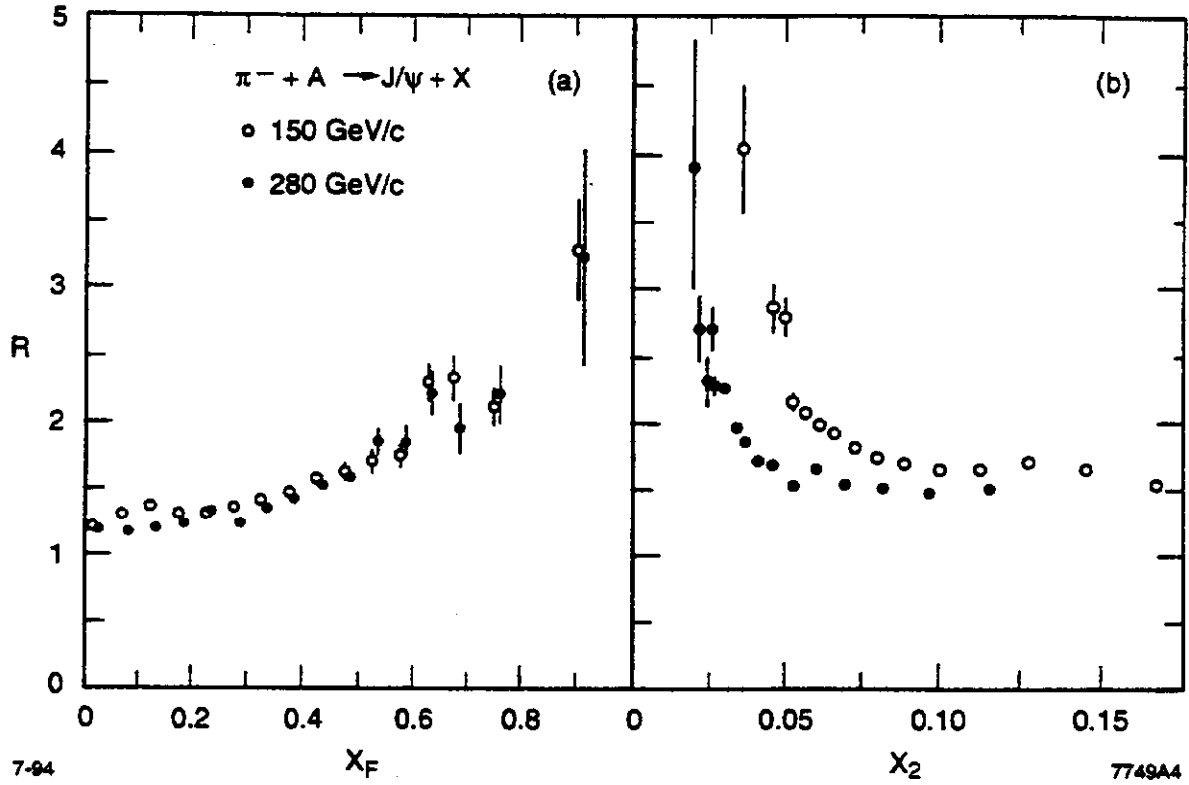


Figure 4: The ratio $R = A\sigma(pp \rightarrow J/\psi + X)/\sigma(pp \rightarrow J/\psi + X)$ of inclusive J/ψ production on Hydrogen and Platinum [11]. In (a) the ratio is plotted as a function of x_F of J/ψ , and in (b) as a function of x_2 .

power α at different energies show that indeed $\alpha = \alpha(x_F)$, i.e., the nuclear suppression obeys Feynman scaling [12], and is not a function of x_2 . The power α decreases from 0.97 at $x_F = 0$ to 0.7 as $x_F \rightarrow 1$ [11, 12, 13] (see Fig. 5), i.e., becomes surface dominated at large x_F .

The above nuclear A -dependence and the leading charm asymmetry directly contradict leading-twist PQCD factorization and suggest that higher twist effects play an important role at large x_F . But it is a well known fact that higher twist effects are suppressed by $\mathcal{O}(1/M^2)$. This raises the question of how the higher twist effects survive and become dominant at large x_F . In the next section we will review the physics of higher twist terms and point out a way to overcome the usual suppression.

3 Physical Picture of Higher Twist Terms

Let us take the well known process, Deep Inelastic Scattering (DIS), to illustrate the physics of 'leading twist' and 'higher twist' terms. In leading twist diagrams (Fig. 6a), only the active (hit) parton interacts with the external photon and there is no connection between the spectator partons and the active parton. On the other hand, there are strong interactions between the active parton and the spectator partons in higher twist diagrams (Fig. 6b).

If we take the 'infinite momentum frame' in which the parton language is valid, the

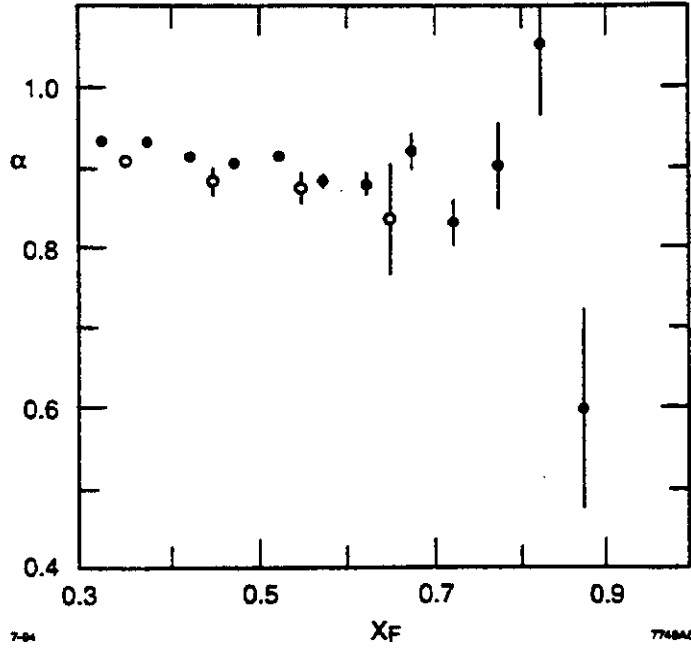


Figure 5: The effective power α of the A -dependence of J/ψ production : E789 (●) and E772 (○) data.

proton is boosted to very high momentum along the z axis with four momentum given by $P = (p + m^2/2p, 0, p)$. In this frame, the photon momentum can be taken as $q = (Q^2 p/m^2 x, q, Q^2 p/m^2 x)$ and the virtuality of the photon is $Q^2 = q^2$; i.e., the resolving power in transverse dimension. In other words, the transverse dimension of the partons that interact, directly or indirectly, with the photon is of the order of $1/Q$. With the above pictures in mind, it is easy to understand why the higher twist terms are suppressed by $1/Q^2$ in the usual Bjorken limit $Q^2 \rightarrow \infty$ with x fixed. As the interaction time τ of the hard subprocess $eq \rightarrow eq$ scattering is very short, only of the order of $1/Q$, any interaction between the active parton and the spectator partons must occur within this short time interval τ and so they must be within transverse distance of $r_\perp \sim 1/Q$ (Fig. 7). This immediately leads to the conclusion that higher twist terms are suppressed by $1/Q^2$ as the probability of finding two partons with dimension $1/Q^2$ within an area of $1/Q^2$ is given by the geometrical factor $1/Q^2 R^2$, with R the size of proton.

However, there is an exception to the above conclusion. Suppression of higher twist terms depends a lot on the size of proton, which is of order of 1 fm, much larger than the size of the parton, which is $1/Q$. If somehow the initial proton or meson is already very small, of the same size as the parton, then there is no suppression. But how can that be realized? The answer to that question lies on the large x kinematic region and we will review that region in the next section.

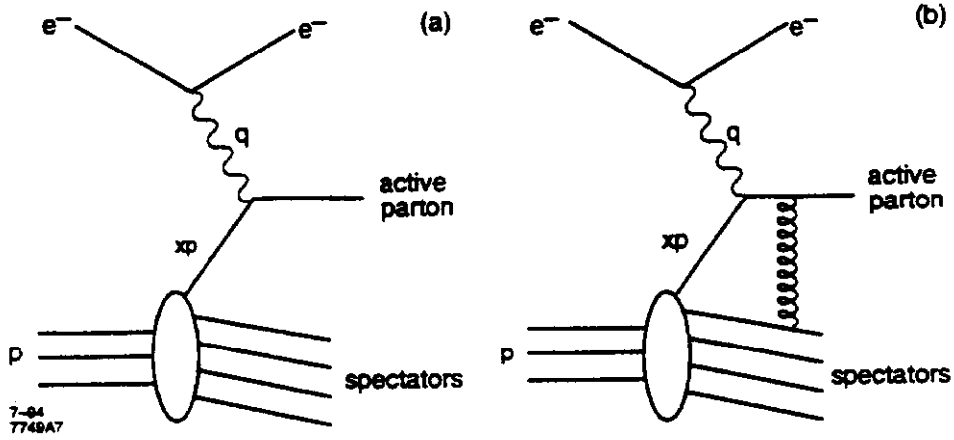


Figure 6: DIS scattering: (a) leading twist and (b) higher twist.

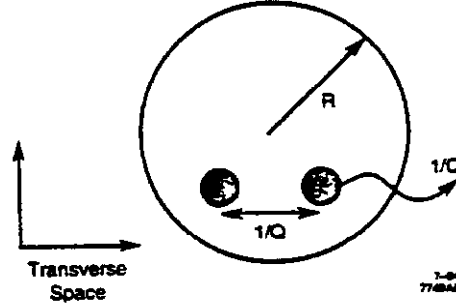


Figure 7: The transverse view of the partons in the hadron in the infinite momentum frame.

4 The combined limit : $x \rightarrow 1$ and $Q^2 \rightarrow \infty$ with $(1 - x)Q^2$ fixed

In the large x kinematic region, besides the usual hard scale Q^2 , another new scale $\Lambda_{QCD}^2/(1-x)$, which reflects the hardness of this new limit, emerges [2, 1]. In fact, this new hard scale actually is the transverse size of the meson; i.e., $r_\perp^2 \sim (1-x)/\Lambda_{QCD}^2$. If the two scales are comparable; i.e., taking the combined limit as in equation (1), higher twist contributions will not be suppressed assuming $\mu^2 \sim \Lambda_{QCD}^2$. In this new limit, higher and leading twist are of the same order,

$$\frac{1/Q^2}{r_\perp^2} \sim \frac{\Lambda_{QCD}^2}{(1-x)Q^2} \sim \frac{\Lambda_{QCD}^2}{\mu^2} \sim 1.$$

But how does the new hard scale $\Lambda_{QCD}^2/(1-x)$ emerge in the limit $x \rightarrow 1$? Let us consider Fig. 8 which gives the probability amplitude for the $x \rightarrow 1$ perturbative distribution of the meson. The soft non-perturbative distribution is described by the wavefunction $\phi(y, p_\perp)$ which is suppressed in the extreme kinematic limit $y \rightarrow 0, 1$ or $p_\perp \rightarrow \infty$. The perturbative contribution comes from diagrams where one or more gluons are exchanged between the two

quarks. For simplicity, we just consider exchanging one gluon between the quarks in Fig. 8.

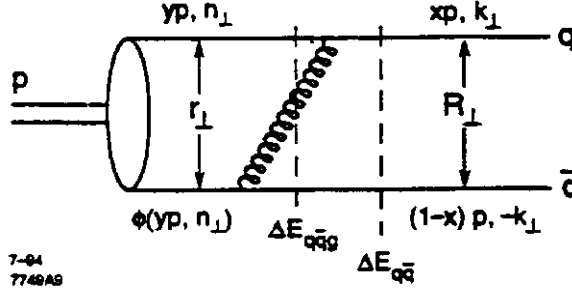


Figure 8: The $x \rightarrow 1$ limit of a hadron structure function generated by perturbative gluon exchange.

The separation between the two quarks r_\perp can be estimated by considering the intermediate state $q\bar{q}g$. The virtuality of this state is given by

$$\begin{aligned} 2p\Delta E_{q\bar{q}g} &\simeq -\frac{m_q^2 + n_\perp^2}{y} - \frac{m_q^2 + k_\perp^2}{1-x} - \frac{(n_\perp - k_\perp)^2}{x-y} \\ &\simeq \frac{m_q^2 + k_\perp^2}{1-x} \end{aligned} \quad (7)$$

when

$$n_\perp^2 \leq \mathcal{O}\left(\frac{k_\perp^2}{1-x}\right). \quad (8)$$

Since $\Delta E_{q\bar{q}g}$ is independent of n_\perp , the perturbative tail is

$$\begin{aligned} \int_{\frac{k_\perp^2}{1-x}}^{\frac{k_\perp^2}{1-x}} dn_\perp \phi(y p, n_\perp) &\simeq \int_0^\infty dn_\perp \phi(y p, n_\perp) \\ &\simeq \phi(y p, r_\perp = 0) \end{aligned} \quad (9)$$

which shows that the transverse distance between the two quarks is $r_\perp^2 \sim (1-x)/k_\perp^2$, very compact at the moment of creation. For a typical value, $k_\perp \sim \Lambda_{QCD}$, we find the new hard scale $\Lambda_{QCD}^2/(1-x)$ as promised.

Another interesting physical quantity is the transverse distance R_\perp between the two quarks after the exchange of the gluon, i.e., when one of the quark carries nearly all the longitudinal momentum. The life time of this intermediate state is very brief,

$$\Delta\tau \simeq \frac{1}{\Delta E_{q\bar{q}g}} \simeq \frac{2p(1-x)}{k_\perp^2 + m_q^2} \quad (10)$$

Nevertheless, during this short life time, the 'slow' quark can move a transverse distance

$$R_\perp \simeq v_\perp \Delta\tau = \frac{k_\perp}{p(1-x)} \frac{2p(1-x)}{k_\perp^2 + m_q^2} \simeq \frac{2k_\perp}{k_\perp^2 + m_q^2} \quad (11)$$

which for $k_{\perp} = \mathcal{O}(\Lambda_{QCD})$ can be of the order of 1 fm. Hence, the specific large x kinematic region selects a very compact Fock state component of the meson at the moment of creation and then it expands very quickly to its normal size of 1 fm. The large transverse size R_{\perp} of the light quarks has a very important implication in the production of heavy quarks.

5 Dynamics in the new QCD Limit

In the previous section, we showed that there is a new scale $\Lambda_{QCD}^2/(1-x)$ at large x and that the transverse size of the light quarks R_{\perp} can be as large as 1 fm. In this section, we want to exploit these properties in the production of heavy quarks at large x . As the transverse size R_{\perp} of the light quarks is very large, one can imagine that the heavy quark pair can be freed easily by deflecting the slow light quark. This phenomenon has been studied in Ref.[1] in the case of heavy quark production on nuclear target. The new limit in this case is defined by:

$$\left. \begin{array}{l} M^2 \rightarrow \infty \\ x \rightarrow 1 \end{array} \right\} \quad \text{with } \mu^2 \equiv (1-x)M^2 \text{ fixed} \quad (12)$$

where M is the mass of the heavy quark pair. To understand the physics in this new limit, let us consider the “extrinsic” and “intrinsic” diagrams as shown in Figs 9a and 9b. In the extrinsic diagram the produced heavy quark pair couples directly to only one parton in the projectile while in the intrinsic case it couples to several.

The energy difference in the extrinsic diagram is given by

$$2p\Delta E \sim \frac{k_{\perp}^2}{1-x} + M^2. \quad (13)$$

The first term $k_{\perp}^2/(1-x)$ comes from the effectively stopped light valence quarks $q\bar{q}$ as the produced $Q\bar{Q}$ pair carries almost all of the momentum ($x \rightarrow 1$) while the second term comes from the virtuality of the gluon which is of the order of the mass of the heavy quark pair. In order to get a large production cross section, the energy difference should be minimized and thus the two terms in equation (13) are of the same order, *i.e.*,

$$k_{\perp}^2 \sim (1-x)M^2 = \mu^2 \quad (14)$$

Now we have a very nice result. The transverse momentum square of the light quarks are of the order of μ^2 and so these states can be resolved by a target gluon of transverse momentum l_{\perp} of order of μ . Hence the hardness of the scattering from the target is not M^2 as one would expect in the leading twist calculation, but instead it is $\mu^2 = (1-x)M^2$. Actually, the transverse size of the stopped light quark pair is given by $1/k_{\perp} \sim 1/\mu$. This explains why the scattering dominantly occurs off the light quarks. Therefore, we can conclude that heavy quarks can be, and are, produced at large x by soft peripheral scattering and so the cross section is large. These new production mechanisms can help to explain the various anomalous behaviors of charm production as described in section 2.

In leading twist diagrams, the usual lowest order diagram describing the fusion process $gg \rightarrow Q\bar{Q}$ is shown in Fig. 10. Although the size of the light quark pair is large, the heavy quark pair $Q\bar{Q}$ still has a small transverse size $h_{\perp} \sim 1/M$. A target gluon can resolve the

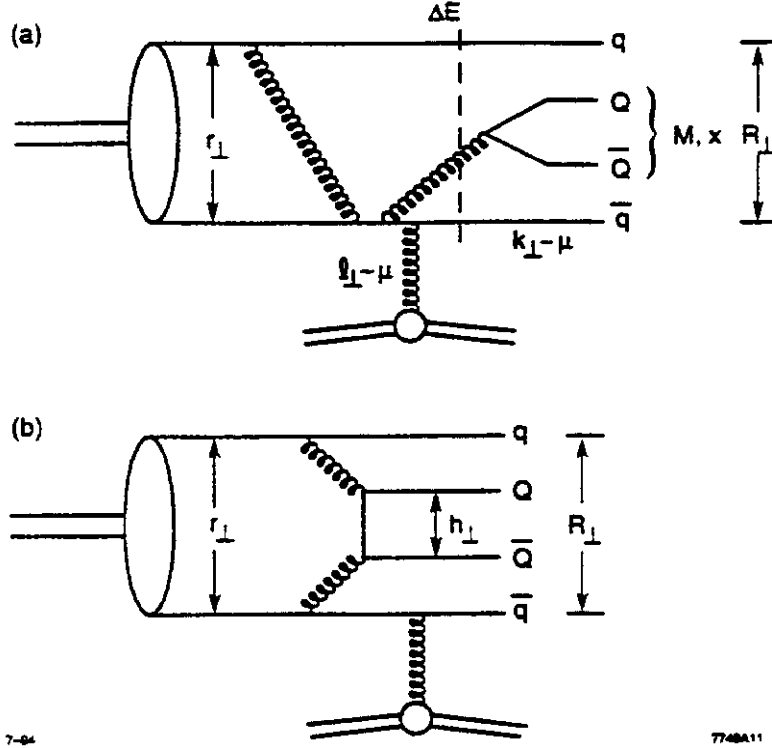


Figure 9: Leading order diagrams in heavy quark production in the new limit (12): (a) extrinsic diagram and (b) intrinsic diagram.

$Q\bar{Q}$ pair only provided that it has a commensurate wavelength, i.e., $l_\perp \sim M$ as indicated in Fig. 11. This is much larger than the $l_\perp \sim \mu$ required to resolve the light quarks. Hence the leading twist is actually suppressed by $1/M$ compared to the new mechanisms in the new limit.

One can also go through the same argument as described in the previous section and conclude that the Fock state of the projectile hadron from which the heavy pair is produced has a small transverse size $r_\perp^2 \sim (1-x)/\mu^2 \sim 1/M^2$. Because of the smallness of the transverse size, the intrinsic diagram as shown in Fig. 9b, where an extra gluon is attached to the heavy quark pair, is not suppressed relative to the extrinsic diagram Fig. 9a. Therefore, the distinction between extrinsic and intrinsic processes essentially disappears.

6 Applications of the New Mechanisms

Let us summarize the physics in the new limit (12) before we go on to apply it to the anomalous charm production. In the combined limit, the Fock states are very compact and small. The transverse radius square of the states has a typical value of $(1-x)M^2$. Because of the compactness of the Fock states, intrinsic diagrams and extrinsic diagrams are of the same order. But the intrinsic diagrams can numerically dominate the extrinsic contributions

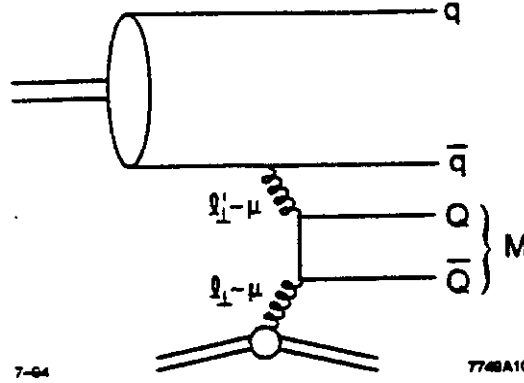


Figure 10: Leading twist diagram in heavy quark production: $gg \rightarrow Q\bar{Q}$.

because of the large combinatoric factor. The heavy quark pair can be freed easily by stripping away the slow light spectator quark in the projectile through an interaction with the target. The hardness scale of the collision is given by $(1-x)M^2$. It is a soft peripheral process and so the cross section is large. This picture can provide a QCD framework for understanding the puzzling features of the large x data mentioned in section 2:

(a) The larger than expected charm structure function of the nucleon at large x_b reported by EMC [3] can be understood by the large intrinsic charm contribution in the proton. In this case, $Q^2 = 75 \text{ GeV}^2$ (for the data point with $x_b = 0.422$) is fixed and the photon can resolve the charm quark easily. But as discussed above, the intrinsic production of the charm pair at large x_F (which is nearly twice of x_b) can numerically dominate the usual extrinsic production considered in PGF calculation and boost up the charm structure function a lot.

(b) The longitudinally polarized J/ψ at large x_F in πN collisions has a natural explanation by the new production mechanisms [15]. The dominant contributions to the polarization of J/ψ at large x_F are the intrinsic diagrams as shown in Fig. 11. The initial state pion valence quarks naturally have opposite helicities. There is a factor $1/(1-x_F)$ enhancement for the emission of transversely polarized gluon with same sign of helicity as the radiated quark. Thus the two gluons coupled to the charm pair have opposite helicity. In order to form a bound state, the transverse momenta of the gluons and thus of the charm pair should be small. In that case, the initial $J_z = 0$ and thus the formed J/ψ is in longitudinally polarized state. Here, we have made the assumption that the formation of the J/ψ through the radiation of an extra gluon does not change the polarization of the charm quarks. In the large x_F limit, the radiated gluon must be soft and this justifies our assumption.

The counting rules in powers of $1-x_F$ are presented in Ref.[15]. The cross section for producing a longitudinally polarized (Fig. 12a) and a transversely polarized (Fig. 12b) J/ψ is proportional to $(1-x_F)^3$ and $(1-x_F)^4$ respectively. We find that the basic reason for the dominance of the intrinsic polarization amplitude (Fig. 12a) is that it allows two helicity flips of the heavy quarks, each contributing a power of $M \sim 1/\sqrt{1-x_F}$ in our analysis. Thus, the longitudinal polarization of the J/ψ at large x_F is mainly due to intrinsic charm production mechanisms.

(c) The anomalous double J/ψ production can be understood qualitatively by consid-

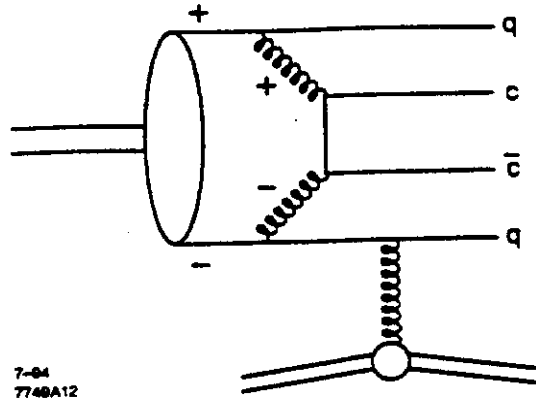


Figure 11: Dominant diagram in heavy quark production. The plus and minus signs refer to the particle helicities.

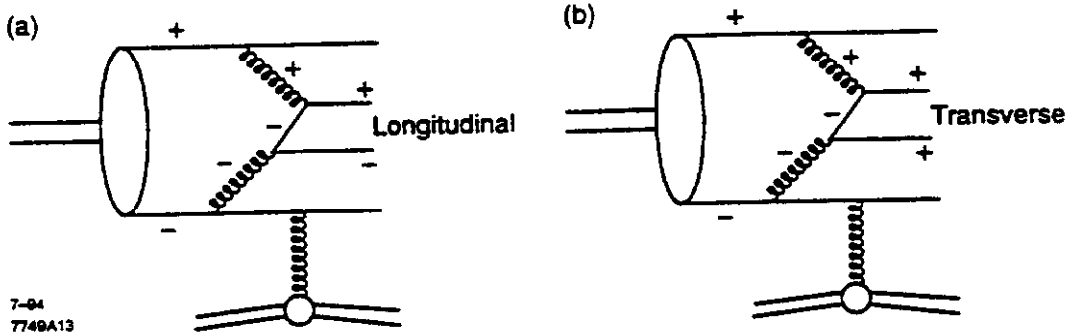


Figure 12: The production of (a) longitudinal and (b) transverse J/ψ .

ering intrinsic production as shown in Fig. 13. The two J/ψ 's produced as shown in the diagram clearly are strongly correlated. The cross section for freeing the pairs becomes large at large x_F as it is a soft peripheral scattering from the target. This helps to explain why the J/ψ pairs produced at large x_F only. Intrinsic charm production (Fig. 13) has another nice feature. The total transverse momentum square of the J/ψ pair is of the order of $\mu^2 = (1 - x_F)M^2$ only, i.e., of the same order as that of the light quarks. However, the individual J/ψ 's can have transverse momenta up to the mass scale M . In fact, if one uses the measured mean value of x_F , which is 0.53, from the NA3 280 GeV beam data and the measured mean transverse momentum of the individual J/ψ 's, $M \sim k_{\perp} = 1.5$ GeV, one gets $\mu = 1.0$ GeV which is close to the measured value of $\langle p_{\perp}^{J/\psi} \rangle = 0.9 \pm 0.1$ GeV. Obviously, one cannot take this number too seriously. Nevertheless, it indicates that all these features fit nicely with the data and the proposed new mechanisms may play an important role in double J/ψ production.

(d) The leading charm asymmetry has been studied in detail by R. Vogt and S. J. Brodsky [16] using a two-component model. The first component is the usual leading twist fusion process while the second component is based on the model discussed above.

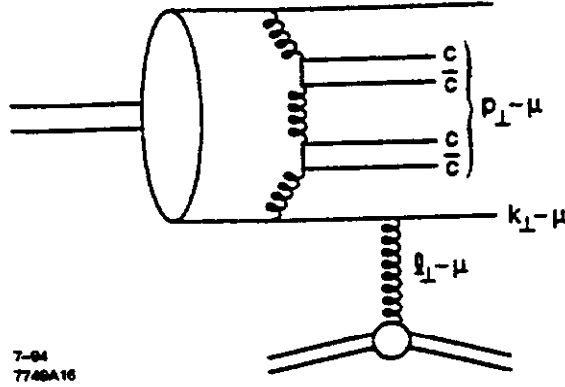


Figure 13: Intrinsic diagram that may account for double J/ψ production at large x_F .

In the usual leading twist fusion subprocess, there is a finite probability that the produced charm quark will combine with a spectator valence quark in the final state to produce a leading hadron. Such final state coalescence mechanisms have been incorporated into PYTHIA, a Monte Carlo program based on the Lund string model [17]. In that model, the “string acceleration” of slow heavy quarks by fast valence quarks can boost the fast charm rate. However, such a mechanism overestimates the observed asymmetry $\mathcal{A}(x_F)$ at low x_F . The Lund string model is strictly a final state coalescence. However, the model we propose is an initial state coalescence. The pion can fluctuate into higher Fock states as shown in Fig. 14. All the partons have nearly the same velocity in order to minimize the invariant mass of the state. As the charm and the valence quark have the same rapidity, it is easy for them to coalesce to form a large D meson state without paying much penalty. Thus, it can produce a strong leading particle correlation at large x_F .

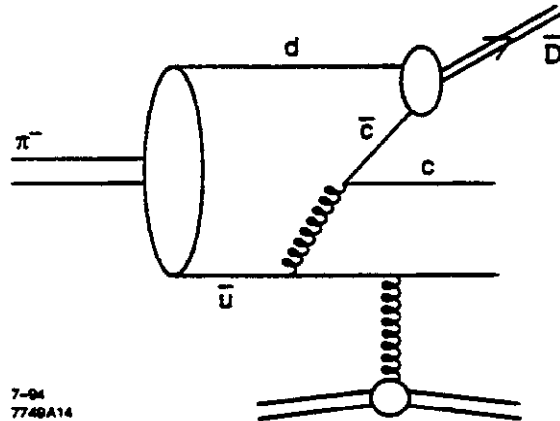


Figure 14: Initial state coalescence producing a D meson through the intrinsic charm fluctuation at large x_F .

Figure 15 shows the results of the two-component model. The parameter ξ determines the relative importance of the leading twist and intrinsic charm components. All the calculations reproduce the general trend of the data.

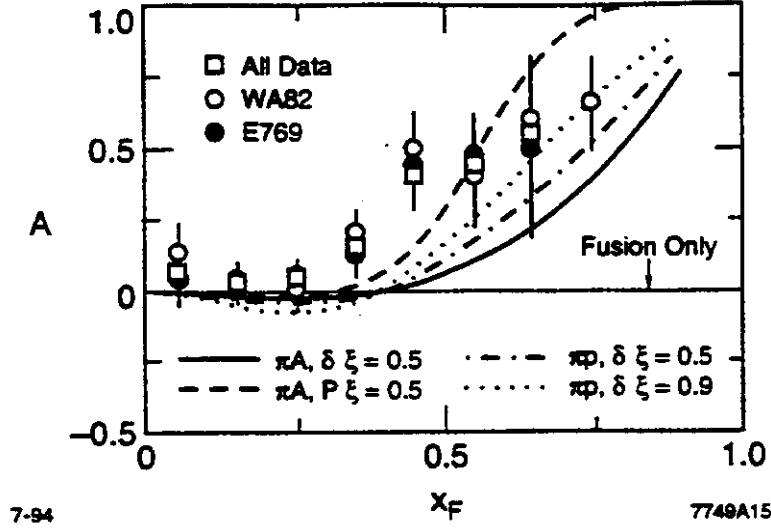


Figure 15: The prediction of the two-component model. The figure is from [16]

(e) The new production mechanisms have all the novel features observed in the nuclear dependence of J/ψ production. QCD factorization is invalid in the combined limit since there is no relative suppression of interactions involving several partons in the projectile. The nuclear A^α -dependence is a function of x_F rather than a function of x_2 of the target-parton momentum fraction. Because of the rapid transverse size expansion of the spectators, production cross sections in nuclear targets becomes surface dominated at large x_F .

7 Conclusion

We have reviewed the experimental status of charm production at large x_F and observed a lot of anomalous behaviors in this kinematic limit. Both the leading charm asymmetry and the nuclear J/ψ production show that factorization breaks down at large x_F . Higher twist effects becomes dominant because a new scale $\Lambda_{QCD}^2/(1 - x_F)$ emerges, which reflects the small transverse size of the Fock state, in the $x \rightarrow 1$ limit. In the combined limit (12), the heavy quark pair can be freed easily as the coherence of the Fock state is easily broken by soft interactions of finite transverse momentum because of the rapid expansion of the transverse size of the spectators. This new production mechanism helps to explain the anomalous phenomena observed at large x_F . This new picture of hadron formation opens up a whole new avenue for studying the far-off-shell structure of hadrons. It is thus critical that a new measurement of the charm and beauty structure functions be performed in future experiments.

References

- [1] S. J. Brodsky, P. Hoyer, A. H. Mueller and W.-K. Tang, Nucl. Phys. **B369**, 519 (1992).

- [2] P. Hoyer, Acta Phys.Polon. **B23**, 1145 (1992)
- [3] EMC: J. J. Aubert *et al.*, Nucl. Phys. **B213**, 31 (1983).
- [4] CIP: C. Biino, *et al.*, Phys. Rev. Lett. **58**, 2523 (1987).
- [5] E537: C. Akerlof, *et al.*, Phys. Rev. **D48**, 5067 (1993).
- [6] NA3: J. Badier, *et al.*, Phys. Lett. **B114**, 457 (1982).
- [7] WA82: M. Adamovich, *et al.*, Phys. Lett. **B305**, 402 (1993).
- [8] E769: G. A.Alves, *et al.*, Phys. Rev. Lett. **72**, 812 (1994).
- [9] W. Beenakker, *et al.*, Nucl. Phys. **B351**, 507 (1991).
- [10] P. Nason, S. Dawson, and R. K. Ellis, Nucl. Phys. **B327**, 49 (1989).
- [11] NA3: J. Badier, *et al.*, Z. Phys. **C20**, 101 (1983).
- [12] E772: D. M. Alde, *et al.*, Phys. Rev. Lett. **66**, 133 (1991).
- [13] E789: M. S. Kowitt, *et al.*, Phys. Rev. Lett. **72**, 1318 (1994).
- [14] P. Hoyer, M. Vanttinen and U. Sukhatme, Phys. Lett. **B246**, 217 (1990).
- [15] M. Vanttinen, P. Hoyer, S. J. Brodsky and W.-K. Tang, in preparation.
- [16] R. Vogt and S. J. Brodsky, SLAC and LBL preprint, SLAC-PUB-6468 and LBL-35380, April 1994.
- [17] H.-U. Bengtsson and T. Sjöstrand, Comput. Phys. Commun. **46**, 43 (1987).

Direct Measurements of V_{cd} and V_{cs}

T. Bolton

Columbia University, New York, N.Y. 10027

and

Department of Physics, Kansas State University, Manhattan, KS 66506

Abstract

The current status of direct measurements of the CKM matrix elements V_{cd} and V_{cs} is reviewed. Future prospects for improving these measurements towards the unitary limit are summarized.

1 Introduction

The CKM parameters $|V_{cd}|$ and $|V_{cs}|$ can presently only be directly measured via the neutrino production of charm at high energies. This paper summarizes the current state of knowledge of these parameters and estimates the possible precision that will be achieved in future experiments.

In the standard three generation CKM matrix, unitarity and the precise determinations[1] of $|V_{ud}| = 0.9744 \pm 0.0010$ and $|V_{us}| = 0.2196 \pm 0.0023$ tightly constrain $|V_{cd}|$ and $|V_{cs}|$. This can be easily appreciated in the Wolfenstein parameterization,[2] in which $\sin \theta_{12} = \lambda$, $\sin \theta_{23} = A\lambda^2$, and $\sin \theta_{13}e^{i\delta} = A\lambda^3(\rho + i\eta)$. In this scheme

$$\left| \frac{V_{cd}}{V_{us}} \right| = 1 + A^2\lambda^4\left(\rho - \frac{1}{2}\right) \simeq 1 + (2.4 \times 10^{-3})A^2\left(\rho - \frac{1}{2}\right),$$

and

$$\left| \frac{V_{cs}}{V_{ud}} \right| = 1 - \frac{1}{2}A^2\lambda^4 \simeq 1 - (1.2 \times 10^{-3})A^2.$$

Since A and ρ are known to be of order unity from measurements of V_{cb} and V_{ub} at CLEO and Argus, $|V_{cd}|$ and $|V_{cs}|$ must be within a few parts per thousand of $|V_{ud}|$ and $|V_{us}|$.

On the other hand, if three generation unitarity is not assumed, the coupling of $|V_{cd}|$ to $|V_{us}|$ is much less tight. For example, in a four generation unitary CKM matrix, mixing between the second and fourth generation ($\sin \theta_{24}$) could allow $|V_{us}| - |V_{cd}| \leq 0.03$ while

maintaining $|V_{ud}|^2 + |V_{us}|^2 \simeq 1$. To summarize, the standard model predicts $|V_{cd}|$ and $|V_{cs}|$ to a level of $\sim \pm 0.1\%$. Any larger deviation would indicate new physics, and deviations as large as 10% are interesting.

2 Charmed Hadron Decay

At first sight, it would seem that the way to measure $|V_{cd}|$ and $|V_{cs}|$ is from the study of D_{e3} decays of charmed mesons, for example

$$\frac{\Gamma(D^0 \rightarrow \pi^- e^+ \nu_e)}{\Gamma(D^0 \rightarrow K^- e^+ \nu_e)}$$

should provide a measure of $\left|\frac{V_{cd}}{V_{cs}}\right|^2$. Unfortunately the semi-leptonic widths depend on transition form factors that cannot be separately measured or calculated yet with any reliability. Mark III[3] and CLEO[4] have measured

$$\begin{aligned} \left|\frac{V_{cd}}{V_{cs}}\right|^2 &= (0.057^{+0.038}_{-0.015} \pm 0.005) \left|\frac{f_+^K(0)}{f_+^\pi(0)}\right|^2 \text{ (Mark III),} \\ \left|\frac{V_{cd}}{V_{cs}}\right|^2 &= (0.085 \pm 0.027 \pm 0.014) \left|\frac{f_+^K(0)}{f_+^\pi(0)}\right|^2 \text{ (CLEO).} \end{aligned}$$

Current models give a range for the form factor ratio of 0.7-1.4[5]; a useful calculation needs to be accurate to the percent level.

It also does not seem possible to measure the form factor ratio independent of the CKM matrix elements. It may be, however, that other ratios of suppressed to favored decays depend on a less model dependent ratio. A possible example is

$$\frac{\Gamma(D_S^+ \rightarrow K^0 e^+ \nu_e)}{\Gamma(D^+ \rightarrow \bar{K}^0 e^+ \nu_e)}.$$

3 Measurements of V_{cd} and V_{cs} in νN Production of Charm

The cross sections for the production of charm in neutrino and antineutrino interactions can be written

$$\frac{d\sigma(\nu N \rightarrow \mu^- c X)}{dx dy} = \frac{G_F^2 M E}{\pi} \times \left\{ \begin{aligned} &|V_{cd}|^2 F_V [q_V(\xi, Q_0^2), \alpha_S(Q_0)] + |V_{cd}|^2 F_S [q_S(\xi, Q_0^2), \alpha_S(Q_0), G(\xi, Q_0^2)] + \\ &|V_{cs}|^2 F_{SS} [s(\xi, Q_0^2), \alpha_S(Q_0), G(\xi, Q_0^2)] \end{aligned} \right\}$$

and

$$\frac{d\sigma(\bar{\nu} N \rightarrow \mu^+ \bar{c} X)}{dx dy} = \frac{G_F^2 M E}{\pi} \times \left\{ |V_{cd}|^2 F_S [\bar{q}(\xi, Q_0^2), \alpha_S(Q_0), G(\xi, Q_0^2)] + |V_{cs}|^2 F_{SS} [s(\xi, Q_0^2), \alpha_S(Q_0), G(\xi, Q_0^2)] \right\}.$$

The terms multiplying the CKM elements represent valence quark scattering (F_V), light sea quark scattering (F_S), and strange sea quark scattering (F_{SS}). Unlike the charmed hadron case, these non-calculable terms can be determined independently at some reference momentum transfer Q_0^2 from the measured inclusive charged current structure functions. Furthermore, as indicated schematically by the arguments of F_V , F_S and F_{SS} , QCD calculations, available to next-to-leading order[6], reliably predict the Q^2 evolution and the charm mass threshold dependence of the cross sections. In practice, only $|V_{cd}|$ can be currently measured. This is because the strange quark distribution $s(\xi, Q^2)$ can thus far only be determined in the same charm production process. The size of the strange sea in the nucleon is conventionally parameterized by

$$\kappa = \frac{2 \cdot \int_0^1 dx \cdot x \bar{s}(x, Q^2)}{\int_0^1 dx \cdot x \bar{u}(x, Q^2) + \int_0^1 dx \cdot x \bar{d}(x, Q^2)},$$

where in the SU(3) limit, $\kappa = 1$.

Thus far the only high statistics samples of charm in neutrino scattering are from the CDHS[7] and CCFR[8] experiments, each of which is sensitive to charm only through its muonic decay, the signature in the detector being an opposite sign dimuon pair. The more complete and up-to-date CCFR analysis will be briefly described; a much fuller account is available in the reference. A key point about the dimuon measurements is that they require information about charm production and decay. This information can be summarized by a mean inclusive muonic decay fraction for charmed hadrons produced in neutrino scattering, B_c .

The CCFR dimuon sample from FNAL E744/770 consists of 5048 neutrino induced and 1068 anti-neutrino induced events. Backgrounds from π/K decay have been accurately measured in hadron test beams and are at the level of 16% for neutrinos and 11% for antineutrinos. The only other significant experimental issue is the antineutrino/neutrino confusion that remains after kinematic identification of the incident lepton. Monte Carlo calculations indicate that 1.2% of the nominal neutrino and 25.6% of the nominal antineutrino sample are mis-identified.

Three kinematic variables enter the subsequent analysis: E_{vis} , the energy of the neutrino; x_{vis} , the fraction of the nucleon's momentum carried by the struck quark; and z_{vis} , the ratio of the secondary muon momentum from the charm decay to the total hadronic energy. The subscript 'vis' denotes the fact there is missing energy in the event carried away by the neutrino from the charm semi-leptonic decay. Using the formalism of reference [6], a fit is performed to binned distributions of the three kinematic quantities. The z_{vis} distribution is sensitive to the charm quark fragmentation and allows an *in situ* determination of the fragmentation model parameters. The E_{vis} distribution is sensitive mainly to the threshold behavior of the cross section and provides a measure of the charm mass of

$$m_c = 1.70 \pm 0.17 \pm 0.09 \text{ GeV}/c^2.$$

The agreement of the " m_c " measured in neutrino interaction with the " m_c " determined by next-to-leading order QCD analyses of photon-gluon fusion [9] is evidence of the fact that this parameter can be meaningfully identified as the mass of the charm quark, and

X	$f(X)(\%)$	$B_\mu(X)(\%)$
D^0	58 ± 6	7.91 ± 1.1
D^+	26 ∓ 6	17.2 ± 1.9
D_s^+	7 ± 5	5.0 ± 5.4
Λ_c^+	7 ± 4	4.5 ± 1.7

Table 1: Production Fractions and Semi-muonic branching fractions for charmed hadrons.

lends confidence in the theoretical description of the charm production process. The x_{vis} distribution is sensitive to the relative amount of production of charm off d -quarks vs. s -quarks, and hence to V_{cd} and V_{cs} . Roughly speaking, the low x_{vis} data from the anti-neutrino data determines V_{cs} , while the high x_{vis} neutrino data determines V_{cd} . The actual quantities extracted are, for $E_{\text{vis}} > 30$ GeV,

$$|V_{cd}|^2 B_c = (5.34 \pm 0.39 \pm 0.24_{-0.51}^{+0.25}) \times 10^{-3},$$

$$\frac{\kappa}{\kappa+2} |V_{cs}|^2 B_c = (2.00 \pm 0.10 \pm 0.06_{-0.14}^{+0.06}) \times 10^{-3}.$$

The first error in each of the quantities is the statistical uncertainty and the second the experimental systematic uncertainty. The latter is dominated by imprecise knowledge of charm quark fragmentation. The third error is the QCD scale error; it is relatively large because an absolute rate is being used to determine the fit parameters.

The final determination of $|V_{cd}|$ requires B_c from other measurements. This parameter can be written:

$$B_c = f(D^0)B_\mu(D^0) + f(D^+)B_\mu(D^+) + f(D_s^+)B_\mu(D_s^+) + f(\Lambda_c^+)B_\mu(\Lambda_c^+),$$

where contributions from Ξ_c and Ω_c are neglected. The $f(X)$ are the production fractions of the charmed hadron “ X ”. They have been measured by one experiment, FNAL E531[10], which recorded 122 charm events in an emulsion target. Of these, only three were examples of anti-neutrino production. An assumption must thus necessarily be made that the antineutrino mean branching ratio is the same as that for neutrinos. The $B_\mu(X)$ are the branching ratios for $X \rightarrow \mu$ plus anything. Most of these measurements[1] are actually for $X \rightarrow e$ plus anything. No correction is made to convert these to muonic branching ratios. Table 1 summarizes the vales for the $f(X)$ and $B_\mu(X)$. It is remarkable how dated and imprecise these important measurements are.[11]

The result for the average branching ratio is

$$B_c = 0.099 \pm 0.008 \pm 0.009,$$

where the first error is the contribution from the production fractions and the second is the contribution from the hadron branching ratios. Using this value of B_c results in

$$|V_{cd}| = 0.232 \pm 0.019.$$

The error contains contributions from the experimental statistics (± 0.009), charm fragmentation and other experimental systematics (± 0.007), the QCD scale uncertainty (± 0.009), the charm production fractions (± 0.009), and the charmed hadron branching fractions (± 0.010).

The CKM parameter $|V_{cs}|$ requires an independent determination of the strange sea fraction κ , which is currently unavailable. Using the value of B_c given above and making the conservative assumption that $\kappa \leq 1$ implies that

$$|V_{cs}| > 0.69 \text{ at } 90\% \text{ C.L.}$$

There is a possibility that κ will be independently determined from a refined analysis of inclusive charged current scattering underway at Columbia. The analysis is based on the fact that, to leading order, the difference in the parity violating structure functions between neutrino and antineutrino is related to the strange sea:

$$xF_3^\nu(x, Q^2) - xF_3^{\bar{\nu}}(x, Q^2) = 2 [s(x, Q^2) - c(x, Q^2)].$$

Once κ is known at some level, it will be better to convey the information about $|V_{cs}|$ through the ratio $\left| \frac{V_{cd}}{V_{cs}} \right|$. This ratio is independent of B_c , and it should have much less uncertainty associated with the QCD scale. A 20% measurement of κ will provide a 10% measurement of the CKM matrix element ratio.

4 Future Neutrino Determinations of V_{cd} and V_{cs}

Four high energy neutrino experiments are either now running or are approved to run in the next six years. While none of the experiments is optimized for the study of neutrino charm production, all have the potential to improve the CKM matrix element measurements. The experiments are summarized in Table 2. The Nomad[12] and Chorus[13] experiments at CERN are designed to search for $\nu_\mu \rightarrow \nu_\tau$ oscillations. Nomad features a low mass target with very good tracking and electron identification. This experiment should be able to detect charm in both di-lepton modes ($\mu\mu$ and μe). Their excellent tracking may also allow for the identification of charm via the $D^* \rightarrow D\pi$ trick. Chorus is a hybrid emulsion spectrometer. It's major virtue is its ability to reconstruct charm inclusively via the identification of the charm decay vertex. This feature serves to boost statistics, and, more importantly, largely eliminates the need to know the production, fragmentation, and decay properties of the charmed hadrons. Fermilab E815[14] uses the E744/770 Lab E neutrino detector. The experiment is optimized for precision studies of neutral current interactions. The feature most relevant for charm studies is the new sign-selected neutrino beam. This will eliminate the $\nu/\bar{\nu}$ confusion in the dimuon channel which will allow for a cleaner measurement of $|V_{cs}|$, assuming that the strange sea is measured by then.

The ultimate neutrino charm production experiment is FNAL E803[15]. Like Chorus, this experiment is designed for a high sensitivity search for $\nu_\mu \rightarrow \nu_\tau$ oscillations using a hybrid emulsion spectrometer. E803 will have a factor of twenty higher statistics than Chorus; and

Experiment	Target	Start	CC Sample	Charm Sample
Nomad (CERN)	low mass	1994	1×10^6	$2 \times 10^4 (e\mu, \mu\mu, D^*)$
Chorus (CERN)	emulsion	1994	3×10^5	2×10^4 (inclusive)
E815 (FNAL)	iron	1996	5×10^6	$3 \times 10^4 (\mu\mu)$
E803 (FNAL)	emulsion	1999	6×10^6	3×10^5 (inclusive)

Table 2: Future Neutrino Experiments. Event samples are rough estimates.

its spectrometer will have three times better resolution. The higher resolution is crucial to reduce backgrounds, particularly in one-prong decays of charm. E803 might be able to achieve a resolution of $\sim 2\%$ on $|V_{cd}|$. This is estimated by assuming: a sample of 50,000 reconstructed charm events, which reduces the statistical error to ± 0.003 ; a $\times 5$ reduction in the experimental systematic errors due to the elimination of fragmentation uncertainties and background; a $\times 5$ reduction in the QCD scale error via the normalization of charm to single muon production that is possible with higher statistics; and a $\times 10$ reduction in production fraction and branching ratios achieved by the ability to inclusively reconstruct charm. The total ± 0.004 error on $|V_{cd}|$ will be comparable to that on $|V_{us}|$; and one will thus be able to test the unitarity property of the CKM matrix at a level that is sensitive to new physics.

5 Acknowledgements

I would like to thank Andy Bazarko for fruitful discussions, and for allowing me to include his soon-to-be published CCFR results.

References

- [1] M. Aguilar-Benitez *et al.* (Particle Data Group), Phys. Rev. D45, Part 2 (1992).
- [2] L. Wolfenstein, Phys. Rev. Lett., **51** (1983) 1945.
- [3] J. Adler *et al.* (Mark III Collaboration), Phys. Rev. Lett. **62** (1989) 1821.
- [4] M.S. Alam *et al.* (CLEO Collaboration), Phys. Rev. Lett. **71** (1993) 1311.
- [5] N. Isgur *et al.*, Phys. Rev. D39 (1989) 799; M. Bauer, B. Stech, and M. Wirbel, Z. Phys. C34 (1987) 103; C.A. Dominguez, Phys. Lett. B207 (1988) 499; T.M. Aliev, A.A. Ovchinnikov, and V.A. Slobodenyuk, Triest Report No. IC/89/382; M. Crisafulli, *et al.*, Phys. Lett. B223 (1989) 90; G.P. Lepage and S.J. Brodsky, Phys. Rev. D22 (1980) 2157.
- [6] M.A.G. Aivazis, F.I. Olness, and W.-K. Tung, S.M.U. Preprint S.M.U.-HEP/93-16, (1993).
- [7] H. Abromowicz *et al.* (CDHS Collaboration), Z. Phys. C15 (1982) 19.
- [8] A. O. Bazarko *et al.* (CCFR Collaboration), Nevis Preprint 1502 (1994) Submitted to Phys. Lett. B.
- [9] J.C. Anjos *et al.* (E691 Collaboration), Phys. Rev. Lett. **65** (1990) 2503.
- [10] N. Ushida *et al.* (E531 Collaboration), Phys. Lett. B206 (1988) 375. A kinematic cut of $E_{vis} > 30$ GeV is applied to the E531 data. A small bias is also removed from the production fraction extraction. See T. Bolton, Nevis-Preprint-1502, 1994.

- [11] The CLEO Collaboration has recently reported a substantially improved measurement of the D^0 inclusive electronic branching ratio: $B(D^0 \rightarrow e^+ X) = (6.97 \pm 0.18 \pm 0.30)\%$. (See contribution by A. Freyberger, these proceedings.) This new measurement changes the value of the mean muonic branching fraction used in the CKM analysis to $B_c = (9.3 \pm 1.1)\%$ and the matrix element to $|V_{cd}| = 0.239 \pm 0.019$.
- [12] P. Astier *et al.*, "Search for the Oscillation $\nu_\mu \rightarrow \nu_\tau$ ", CERN-SPSLC/91-21 (11 March 1991).
- [13] N. Armenise *et al.*, "A New Search for $\nu_\mu \rightarrow \nu_\tau$ Oscillations", CERN-SPSC/90-42 (15 December 1990); M. deJong *et al.*, "A New Search for $\nu_\mu \rightarrow \nu_\tau$ Oscillations", CERN-PPE/93 (19 July 1993).
- [14] T. Bolton *et al.*, "Precision Measurements of Neutrino Neutral Current Interactions Using a Sign Selected Beam", Fermilab-Proposal-P-815 (1990).
- [15] K. Kodama *et al.*, "Muon-Neutrino to Tau-Neutrino Oscillations", Fermilab-Proposal-P-803 (1993).

Pentaquark Search with Energetic Hadron Beams

M. A. Moinester,⁽¹⁾ D. Ashery,⁽¹⁾ L. G. Landsberg,⁽²⁾ H. J. Lipkin^(1,3)

⁽¹⁾Raymond and Beverly Sackler Faculty of Exact Sciences, School of Physics
Tel-Aviv University, 69978 Ramat Aviv, Israel

⁽²⁾Institute for High Energy Physics, 142284 Protvino, Russia

⁽³⁾Department of Nuclear Physics, Weizmann Institute of Science, 76100 Rehovot, Israel

Abstract

The strange-anticharmed Pentaquark is a $uud\bar{c}s$ or $udd\bar{c}s$ five-quark baryon that is expected to be either a narrow resonance, or possibly even stable against strong decay. We describe this hyperon here; its structure, binding energy and lifetime, resonance width, production mechanisms and decay modes. We estimate production cross sections, techniques to reduce backgrounds in search experiments, and how to optimize experiments to observe it. Possibilities for enhancing the signal over background in Pentaquark searches are investigated by examining predictions for detailed momentum and angular distributions in multiparticle final states. General model-independent predictions are presented as well as those from two models: a loosely bound $D_s^- N$ "deuteron" and a strongly-bound five-quark model. Fermilab E791 data, currently being analysed, may be marginal for showing definitive signals. Future experiments with more than 10^5 reconstructed charmed baryon events should have sensitivity to determine whether or not the Pentaquark exists.

1 Introduction

Ordinary hadrons are mesons or baryons, whose quantum numbers can be described by quark-antiquark or three-quark configurations. Unusual hadrons that do not fit this picture would constitute new forms of hadronic matter - exotic hadrons. Such hadrons may have significant multiquark configurations such as $qq\bar{q}\bar{q}$ and $qqqq\bar{q}$. Exotic hadrons can have anomalous quantum numbers not accessible to a three-quark or quark-antiquark structures (open exotic states) or even usual quantum numbers (cryptoexotic states). Cryptoexotic hadrons can be identified only by their unusual dynamical properties (anomalously narrow decay widths, anomalous decay branching ratios, etc.). The discovery of exotic hadrons would have far-reaching consequences for quantum chromodynamics, for the concept of confinement, and for specific models of hadron structure (lattice, string and bag models). Detailed discussions of exotic hadron physics can be found in recent reviews [1].

We consider here possible exotic hadronic states with heavy quarks (c, b), which contain quarks with four different flavors (e.g. u, d, s, c). Their properties follow from the general hypothesis of "flavor antisymmetry" [2], by which quark systems characterized by the maximum possible antisymmetry of quark flavors (both quarks and antiquarks) are the

most strongly bound. For instance, this means that the $u\bar{u}d\bar{s}$ system would be more bound than the $uud\bar{s}$ one, etc.

Jaffe [3] predicted in this spirit that for dibaryons with six light quarks, the most bound is the Hexaquark $H = [u,u,d,d,s,s]$ combination, for which not more than two quarks are in states with identical flavors. Lipkin [4] and Gignoux *et al.* [5] showed that 5-quark “anticharmed” baryons (Pentaquarks) of the $P^0 = [uud\bar{c}s]$ and $P^- = [udd\bar{c}s]$ type, or analogous “anti-beauty” baryons, are most bound in the 5-quark sector. There are also predictions [6] for the most bound tetraquark exotic meson, the $\tilde{F}_s = [cs\bar{u}\bar{d}]$.

2 Binding Energy of the Pentaquark

Some of these exotic states with heavy quarks may be bound. The masses would be below the threshold for strong decays (i.e., $M(P^0) < M(D_s^-) + M(p)$). Such quasi-stable bound states would decay only via weak interactions, with typical weak decay lifetimes. Resonant states with masses above the strong decay threshold would decay strongly. In the present work, we focus on experimental searches for the Pentaquark, both bound and resonant varieties.

The binding potential of a system is given by the difference between the Color Hyperfine CH interaction in the system and in the lightest color-singlet combination of quarks into which it can be decomposed. The wave function of the H may be written as:

$$\Psi_H = \alpha_1 \Psi_{6q} + \beta_1 \Psi_{(\Lambda\Lambda)} + \gamma_1 \Psi_{(\Sigma-\Sigma^+)} + \delta_1 \Psi_{(\Xi^-p)}. \quad (1)$$

The lightest color singlet combination is the $\Lambda\Lambda$ system at 2231 MeV. The CH contribution to the binding energy of the H is about 150 MeV, in simple models of the CH interaction. Similarly, the P^0 and P^- wave functions can be written as:

$$\Psi_{P^0} = \alpha_2 \Psi_{5q} + \beta_2 \Psi_{(D_s^-p)} + \gamma_2 \Psi_{(\Sigma^+D^-)} + \delta_2 \Psi_{(\Lambda\bar{D}^0)}, \quad (2)$$

$$\Psi_{P^-} = \alpha_3 \Psi_{5q} + \beta_3 \Psi_{(D_s^-n)} + \gamma_3 \Psi_{(\Sigma^-\bar{D}^0)} + \delta_3 \Psi_{(\Lambda D^-)}. \quad (3)$$

Here the lightest color singlet is the $D_s^- N$ system at 2907 MeV. The CH contribution to the mass splitting $M(D_s^- p) - M(P^0)$ is the same as for the H particle, again in simple models of the color hyperfine interaction. The anti-Pentaquarks are defined in a similar way and, in general, whatever will be said about the Pentaquarks will also hold true for the charge-conjugate particles.

The calculations of ref. [7] account for the $SU(3)_F$ breaking. It was shown that as the symmetry breaking increases, the P always retains a larger binding potential than the H and that the binding can be several tens of MeV. The total binding energy includes the internal kinetic energy. Because the c quark is massive, the kinetic energy in the P is smaller than in the H by about 15 MeV. This improves the prospects of the P to be bound.

More recently, Takeuchi, Nussinov and Kubodera [8] studied the effects on the Pentaquark and Hexaquark systems of instanton induced repulsive interactions for three quarks

in flavor antisymmetric states. They claim in this framework that both Pentaquark and Hexaquark are not likely to be bound. Also, Zouzou and Richard [6] reconsidered previous bag model calculations for the tetraquark and pentaquark. Their new calculation has weaker chromomagnetic attractions at short distances and a larger bag radius for multiquark states compared to ordinary hadrons. They find that the Pentaquark is unbound by 80 MeV, while the \bar{F} tetraquark is unbound by 230 MeV. Similar conclusions for the P and H were given by Fleck *et al.* [7]. Riska and Scoccola [9] recently described the Pentaquark in a soliton model, using different parameter sets. One set gives a bound state, while another gives a near threshold resonance. Considering all the uncertainties in knowing the Pentaquark binding energy, our experimental approach is to search for both strongly and weakly bound Pentaquarks, as well as unbound Pentaquark resonances.

A very weakly bound $D_s^- p$ deuteron-size bound state just below threshold with a structure very different from that of the strongly bound proton size Pentaquark might still be consistent with these recent calculations, considering all the model uncertainties. The $D_s^- p$ system does not have Pauli blocking and repulsive quark exchange interactions which arise in all hadron-hadron systems where quarks of the same flavor appear in both hadrons. Thus, even a comparatively weak short range interaction could produce a relatively large size bound state analogous to the deuteron, with a long $D_s^- p$ tail in its wave function and a good coupling to the $D_s^- p$ system. The attraction is due to a short range interaction, not long-range one-pion exchange. This long attractive tail will also assist in the production mechanism. Because in the Pentaquark, unlike the deuteron, there is no short range repulsion, its structure at short distances will be quite different from that of the deuteron. This component too has its influence on the production mechanism. These issues are discussed in subsection 4.2. The deuteron-like state will be stable against strong and electromagnetic decays. Since the $D_s^- p$ pair is some 50-75 MeV lower mass than other meson-baryon cluster components in the Pentaquark, it will be the dominant component in a weakly bound deuteron-like Pentaquark.

3 Structure and Decay Modes of the Pentaquark

There are different possibilities for the internal structure of observable (not very broad) exotic hadrons. They can be bound states or near threshold resonance structures of known color singlet sub-systems ($\Lambda\Lambda$ for the H [10] or $D_s^- p$ for the P^0). But they can have more complicated internal color structure; such as baryons with color octet and sextet bonds $[(qqq)_{8c} \times (q\bar{q})_{8c}]$ and $[(qq\bar{q})_{\bar{6}c} \times (qq)_{6c}]$ (see ref. [11]). We designate all such structures as direct five quark configurations. If color substructures are separated in space by centrifugal barriers, then exotic hadron resonances can have not very large or even anomalously narrow decay widths, because of complicated quark rearrangements in the decay processes. If these exotic hadrons are bound strongly, they can be quasistable, with only weak decays.

The wave function of the Pentaquark contains two-particle cluster components, each corresponding to a pair of known color singlet particles; and also a direct five quark [non-cluster] component. The Pentaquark production mechanism and its decay modes depend on these components. The P^0 can be formed for example by the coalescence of pD_s^- , $\Lambda\bar{D}^0$, pD_s^{*-} , $\Sigma^+ D^-$ +

$\Sigma^0 \bar{D}^0, \Lambda \bar{D}^{*0}, \Sigma^+ D^{*-} + \Sigma^0 \bar{D}^{*0}$; or by a one-step hadronization process. Let us consider three color-singlet components of the $P^0 : D_s^- p$ (2907 MeV), $D^- \Sigma^+$ (3058 MeV) and $\bar{D}^0 \Lambda$ (2981 MeV). The relative strengths of these components depend strongly on the binding energy, as discussed above for the deuteron-like Pentaquark. Pentaquark searches in progress in E791 [12, 13] are based on charged particle decay modes of different Pentaquark components: $D_s^- p \rightarrow \phi \pi^- p$ (B=3%), $D_s^- p \rightarrow K^{*0} K^- p$ (B=3%), $D^- \Lambda \rightarrow K^+ \pi^- \pi^- \Lambda$ (B=8%), $\bar{D}^0 \Lambda \rightarrow K^- \pi^+ \Lambda$ (B=4%) and $\bar{D}^0 \Lambda \rightarrow K^- \pi^+ \pi^+ \pi^- \Lambda$ (B=8%). The indicated branching ratios are those of the on-shell D-meson. Weak decays of virtual color singlet substructures in bound states are possible, ΛD^0 or $\Sigma^+ D^-$ for example, if their masses are smaller than the $D_s^- p$ threshold. In other cases, there would be strong decays through quark rearrangement $(\Sigma^+ D^-)_{bound} \rightarrow D_s^- + p$, and so on. Even if the masses are smaller, the phase space favors decay to the lightest system. The phase space factor would cause the partial width for any decay mode to be smaller than for the on-shell decay, making the total lifetime longer.

The decay through the direct five quark [non-cluster] component can open many additional channels; such as two-particle $\pi^- p$, $K^- p$, and $\Xi^- K^+$ final states. These additional decay modes can shorten the lifetime of the Pentaquark, which would reduce the experimental possibilities to observe it. Such relatively simple final states are more prone to contamination by large combinatoric backgrounds.

Consider the resonant Pentaquark possibility. Yields can be high, as one measures the total strong decay, rather than a particular weak decay mode. The width is the crucial parameter that determines the possibility to observe a resonance. Chances for observation would be good if it is of the order of 50-100 MeV or lower, similar to widths of excited D^* mesons and widths estimated by Greenberg and Lomon [14] for the lowest lying strangeness -1 dibaryon resonances. Our attitude is to support experimental searches for narrow exotic Pentaquark resonances.

4 Experimental Pentaquark Search

An experimental program to search for the Pentaquark should include:

- (1) Reactions likely to produce the Pentaquark, complemented by an estimate of the production cross section.
- (2) Experimental signatures that allow identification of the Pentaquark.
- (3) Experiments in which the backgrounds are minimized.

These points will be further discussed in the following subsections.

4.1 Experimental Considerations

All charm experiments require vertex detectors consisting of many planes of silicon microstrips with thousands of channels. E791 used 23 such planes. Some of the planes are upstream of the target. These detectors allow a high efficiency and high resolution for reconstruction of both primary (production) vertex and secondary (decay) vertex. The position resolution of

the vertex detectors is typically better than 300 microns in the beam direction. By measuring the yield of a particle as a function of the separation between the two vertices, the lifetime of the particle is obtained. Other major components of the spectrometers are dipole magnets for momentum analysis, wire chambers for track reconstruction, cerenkov counters for particle identification, and Electromagnetic and Hadronic calorimeters. Muon detectors are included for studies of leptonic decays. The invariant mass resolution for typical charm masses in such spectrometers is about 10 MeV. Different spectrometers are sensitive to different regions of Feynman- x values.

In hadronic production, the charm states produced are preponderantly charm mesons at low x . The triggers for such experiments vary. In E791, the requirement was to ensure an interaction in the target (using signals from various scintillators) and a transverse energy (E_t) larger than some threshold. The rest of the charm selection was done off-line. Increased charm sensitivity can be achieved as in E781 [15] by a trigger condition that identifies a secondary vertex. A good charm trigger can produce an enriched sample of high x charm baryons with improved reconstruction probability because of kinematic focusing and lessened multiple scattering. Charm2000 experiments will also require charm enhancement triggers [16]. The present E791 and future E781 and Charm2000 experiments [17] complement each other in their emphasis on different x regions, incident particle types, statistics and time schedules.

4.2 Pentaquark Production Mechanisms

We consider possible mechanisms for P formation. For the central hadron-nucleus charm production at several hundred GeV/c, the elementary process is often associated with $q\bar{q} \rightarrow c\bar{c}$ or $gg \rightarrow c\bar{c}$ transitions. The produced charmed quarks propagate and form mini-jets as they lose energy. Hadronization associated with each jet proceeds inside the nucleus, and to some extent also outside the nucleus; depending on the transverse momentum of the jet. The propagating charmed quarks may lose energy via gluon bremsstrahlung or through color tube formation in a string model, or by other mechanisms, as discussed in ref. [18] and references therein. One may form a meson, baryon, Pentaquark, according to the probability for the charmed quarks to join together with appropriate quarks and antiquarks in the developing color field. One can estimate Pentaquark production cross sections via one-step and also two-step hadronization. All such estimates are very rough. Our aim is to account for major ingredients in estimating the cross section, and to give a conservative range of values. For one-step hadronization, the \bar{c} joins directly to the other quarks. The one-step is the usual mechanism for meson and baryon formation. For two-step, the first involves meson and baryon hadronization, while the second involves meson-baryon coalescence.

We first consider estimates for the central production cross section assuming a meson-baryon coalescence mechanism, expected to be the main mechanism for production through the long-range (deuteron-like) component of the Pentaquark wave function. We make a crude estimate relative to the D_s^- , an anticharmed-strange meson ($\bar{c}s$). The weakly bound P (deuteron type structure) can be produced by coalescence of a proton or a neutron with

a D_s^- , analogous to the production of a deuteron by coalescence of a neutron and a proton. The data [19] give roughly 10^{-3} for the $\sigma(d)/\sigma(p)$ production ratio. This ratio can also be applied to $\sigma(P)/\sigma(D_s^-)$ production. The reason is that in both cases, the same mass (nucleon mass) is added to the reference particle (proton or D_s^-), in order to form a weakly bound deuteron-like state.

We now consider the one-step hadronization of a Pentaquark, expected to be the main mechanism for the production through the short-range component of the Pentaquark wave function. We rely here on an empirical formula which reasonably describes the production cross section of a mass M hadron in central collisions. The transverse momentum distribution at not too large p_t follows a form given as [20]:

$$d\sigma/dp_t^2 \sim \exp(-B\sqrt{M^2 + p_t^2}), \quad (4)$$

where B is roughly a universal constant $\sim 5 - 6 \text{ (GeV)}^{-1}$. The exponential fit has inspired speculation that particle production is thermal, at a temperature $B^{-1} \sim 200 \text{ MeV}$ [20]. One can also include a $(2J+1)$ statistical factor to account for the spin of the hadron. To illustrate the universality of B , we evaluate it for a few cases. For Λ_c and Ξ^0 , empirical fits to data give $\exp(-bp_t^2)$, with $b=1.1 \text{ GeV}^{-2}$ and $b=2.0 \text{ GeV}^{-2}$, respectively [21, 22]. This corresponds to $B= 5.0 \text{ GeV}^{-1}$ for Λ_c , and $B= 5.3 \text{ GeV}^{-1}$ for Ξ^0 . For inclusive pion production, experiment gives $\exp(-bp_t)$ with $b = 6 \text{ GeV}^{-1}$ [23]; and $B \sim b$, since the pion mass is small. Therefore, $B= 5-6 \text{ GeV}^{-1}$ is valid for Λ_c , Ξ^0 hyperon, and pion production. We expect therefore that eq. 4 should be also applicable to Pentaquark production. After integrating over p_t^2 , we estimate the ratio:

$$\sigma(P)/\sigma(D_s^-) \sim \exp[-5[M(P) - M(D_s^-)]] \sim 10^{-2}. \quad (5)$$

For illustration, let us consider the ratio of Λ_c to D_s^- total production cross sections by sufficiently energetic baryon beams. This ratio is roughly 0.23, comparing the Λ_c cross section [21] with incident Σ^- to the D_s^- cross section [25] with incident neutron. Eq. 5 with the masses of these particles, including a spin statistical factor, gives about the same ratio. In applying eq. 5 to Pentaquark production, we assume that the suppression of cross section for the heavy P as compared to the light D_s^- is due to the increased mass of P . The particular one-step hadronization process is not relevant. However, as the size of the P increases, this formula would be less and less reliable. Cross section estimates for P production have been given previously [12, 13], based on other arguments, and are consistent with the ratio given by eq. 5.

All the various reaction mechanisms described above can contribute to the production cross section, which is estimated in the range of $\sigma(P)/\sigma(D_s^-) = 10^{-3} - 10^{-2}$. In actual measurements, the product $\sigma \cdot B$ for a particular decay mode is measured, and estimates of the P lifetime and branching ratios may be necessary as well.

4.3 Pentaquark Expected Yield

We proceed with count rate estimates. Analysis of a part of the E791 data (500 GeV/c π^- beam) already yielded a preliminary upper limit $\sigma(P^0)/\sigma(D_s^-) < 6\%$ for Pentaquark

production [24]. This was done for the $D_s^- \rightarrow \phi\pi^-$ and $P^0 \rightarrow \phi\pi^-p$ decays assuming the same branching ratios. It was based on a small fraction of the data and measured D_s^- yield. With the full data sample, several tens of Pentaquarks may be observed if the cross section is in the range estimated in the previous section. For the planned E781 and charm2000, when both use Baryon beams, we rely on previous measurements done with similar beams. With 600 GeV/c neutrons, the D_s^- was measured [25] in the $D_s^- \rightarrow \phi\pi^-$ decay mode with $\sigma B = 0.76 \mu\text{b}/N$ for $0.05 < x < 0.3$, where x designates the Feynman x -value. For Baryon beams the cross section should be proportional to $(1-x)^n$, with n between 4.5 and 5.5, based on the WA89 experiment [21] with a 300 GeV/c Σ^- beam. These data and x -dependence correspond to $\sigma \cdot B$ values for the whole range of $x > 0$ of roughly $1. \mu\text{b}/\text{nucleon}$. With the $\sigma(P)/\sigma(D_s^-)$ factors given above, we estimate $\sigma \cdot B = 1 - 10 \text{ nb}/N$, for each of P^0 and P^- . For E781, scheduled for 1996, the experimental conditions should allow reconstructed Pentaquark events at a rate of roughly 200 events/nb. These expectations are based on a contribution to this workshop by J. Russ [15], which cites an expected yield of 2300 charm events/nb of cross section for 100% efficiency. The efficiencies include a tracking efficiency of 96% per track, a trigger efficiency averaged over x of roughly 18%, and a signal reconstruction efficiency of roughly 50%. We therefore assume an overall average Pentaquark reconstruction efficiency of $\epsilon \simeq 8\%$. We then estimate an expected yield of $N(P^0) = 200 - 2000$ in E781. If we assume a rate of 2000 events/nb for charm2000, the Pentaquark yield may reach the 2000 - 20,000 range. These projections depend critically on the value used for the D_s production cross section. We note that the value quoted in [25] is exceptionally large.

It is still possible that different mechanisms for charm production contribute in different x regimes. For example, there is evidence for leading production of charmed hadrons in WA89 and FNAL E769 [26], which suggests diffractive contributions. For charm2000, one could study [10] the pair diffractive production reaction $p + N \rightarrow (P^0 D_s^+) + N$, with possible D_s^+ tag or without such tag. For the diffractive pair production cross section, one can compare to the diffractive cross section for the reaction $p + N \rightarrow (\Lambda K^+) + N$ at 70 GeV; about $4 \mu\text{b}$ after subtraction of isobar contributions [27]. Estimates are needed but are not available for the cross section ratio $\sigma(P^0 D_s^+)/\sigma(\Lambda K^+)$. For the ratio of 10^{-3} , with $B = 3\%$, one would obtain around 240 reconstructed P^0 baryons with charm2000. There is the D_s^+ tag possibility for this process. The efficiency for tagged versus untagged events is reduced, but tagging may improve the signal to background ratio.

4.4 Pentaquark Decay Signatures

(1) Mass and Width and Decay Modes:

Searches for the Pentaquark are easiest via modes having all final decay particles charged. With all charged particles detected, the invariant mass of the system can be determined with high resolution. One signature of the Pentaquark is a peak in the invariant mass spectrum somewhat lower than 2907 MeV if the system is bound, and above if it is a resonance. The position of the peak should be the same for several decay modes. It's width should be determined by the experimental resolution if it is bound, and broader if it is a resonance.

The selection of the decay modes to be studied is made primarily by considering detection efficiency and expected branching ratios. Since the $D_s^- p$ system is the lightest it is expected to be preferred from phase space arguments. Also, two of its decay modes have four charged particles in the final state (e.g. $K^+ K^- \pi^- p : \phi \rightarrow K^+ K^-$, $K^* \rightarrow K^+ \pi^-$). We describe how this signature is implemented. First, two distinct vertices are identified: a production vertex and a decay vertex. From the decay vertex, four tracks are identified and associated with $K^+ K^- \pi^- p$. By reconstructing the invariant mass of the $K^+ K^-$ pair, one can require only ϕ mass events. One then reconstructs the invariant mass of all four particles. If there is a peak in the resulting spectrum, it will be one of the identifying characteristics of the Pentaquark. One can also study a strong decay into $D_s^- p$, if the P is a resonance. For this strong decay, the proton and D_s^- come from primary vertex, and the D_s^- decay forms the secondary vertex. Both weak and strong decay modes coming from the $D_s^- p$ and the $\bar{D}^0 \Lambda$ components of the P are currently being studied in E791.

(2) One General Signature - A Spectator Baryon:

We first note a striking signature for Pentaquark decay which may be useful for discrimination against background. This signature is predicted by both of two very different Pentaquark models (1) a loosely-bound $D_s^- p$ deuteron-like state and (2) a strongly-bound five-quark state. Both models predict decay modes into a baryon and two or more mesons, in which the three quarks in the baryon are spectators in the decay process and remain in the final state with a low momentum which is just the fermi momentum of the initial bound state.

That the baryon is a spectator is obvious in the deuteron model, in which the decay is described as an off-shell D_s^- decaying with a nucleon spectator. In the five-quark model, a similar situation arises in the commonly used spectator model with factorization. Here, the charmed antiquark decays into a strange antiquark by emission of a W^- which then creates a quark-antiquark, which hadronizes into mesons. The strange antiquark combines with one of the four spectator quarks to form one or more mesons, while the three remaining spectator quarks combine into a baryon.

In both cases, it seems that the final state should show a low-momentum baryon in the center-of-mass system of the Pentaquark and the invariant mass spectrum of the remaining mesons peaked at the high end near the kinematic limit. Thus in the particular cases of the $p\phi\pi^-$, $K^{*0}K^-p$ and $\Lambda K^+\pi^-$ decay modes, the $\phi\pi^-$, $K^{*0}K^-$ and $K^+\pi^-$ invariant mass distributions respectively should show this peaking near the kinematic limit.

Note that in the particular case of the $p\phi\pi^-$ decay mode, a low momentum proton in the center of mass system means that the π^- and ϕ are back to back with the same momentum and therefore that the pion carries off most of the available energy. Thus one might reduce background with a cut that eliminates all pions with low momentum in the center of mass.

(3) Some Model-Dependent Branching Ratio Predictions:

The $\phi\pi^-p$ decay mode is the most convenient for a search, since the ϕ signal is so striking. We now examine the lowest order predictions from the two extreme models for the

branching ratios of other modes relative to $\phi\pi^-p$.

In experiments sensitive only to charged particles the $\phi\pi^-p$ decay mode is observed in the four-prong final state $K^+K^-\pi^-p$. The $K^{*0}K^-p$ decay mode is also observable in this same four prong final state. The $K^{*0}K^-p$ decay mode arises naturally in the deuteron model, since the $K^{*0}K^-$ decay is observed for D_s^- decays with a comparable branching ratio to $\phi\pi^-$. In this model, the ratio of the two decays is predicted from observed D_s^- decay branching ratios with phase space corrections. However, the $K^{*0}K^-p$ decay mode does not occur in the five quark spectator model, where the spectator strange quark can only combine with the \bar{s} produced by the charm decay to make a ϕ or with two spectator nonstrange quarks to make a hyperon. Comparing the two decays thus tests the decay model.

The $K\pi\Lambda$ and $K^*\pi\Lambda$ decay modes arise naturally in the five quark spectator model. However, they should not be expected in a very weakly bound deuteron model with mainly a D_s^-p structure. In that case, the D_s^- decays into mesons containing one strange quark-antiquark pair and the baryon spectator has no strangeness.

(4) Angular Momentum Constraints and Angular Distributions for P Decays:

We can give a model-independent prediction. The Pentaquark has spin 1/2 and this total angular momentum is conserved in the decay. Since the production process is a strong interaction which conserves parity, the Pentaquark will not be produced with longitudinal polarization. Its polarization in the beam direction must also vanish. Therefore, the angular distribution in the center-of-mass system of the Pentaquark must therefore be isotropic for the momentum of any final state particle in any decay mode with respect to either the incident beam direction or the direction of the total momentum of the Pentaquark. The background does not necessarily have these constraints.

We also give a model-dependent prediction. We first consider the deuteron model. The D_s^- has spin zero, and spin is preserved in the decay. Thus, in the center of mass frame of all the D_s^- decay products, the angle between the proton momentum and the momentum of any particle emitted in the D_s^- decay must have an isotropic angular distribution.

A further prediction is obtainable for the case of a vector-pseudoscalar decay mode of the D_s^- ; e.g. $\phi\pi^-$ or $K^{*0}K^-$. The vector meson must be emitted with zero helicity in the rest frame of the D_s^- . The zero helicity can be seen in the $\phi\pi$ decay by measuring the angle $\theta_{K\pi}$ between the kaon momenta in the ϕ rest frame and the pion momentum. The prediction is to have a $\cos^2 \theta_{K\pi}$ distribution. By contrast, the five-quark model for the Pentaquark favors helicity one over helicity zero for the vector meson by just the 2:1 ratio needed to give an isotropic distribution in $\theta_{K\pi}$. Here again the background does not necessarily have these constraints.

4.5 Reducing Background

There is much background from central interactions. When low x production is studied, the momenta of P^0 decay products are also lower. As a result, the background rate increases

faster than the charm signal. It is known [27] that the combinatoric background in inclusive processes is significantly reduced in the fragmentation region ($x \geq 0.6$). The produced particles and the decay fragments from the P , especially for high- x production, are all focused in a forward cone in the laboratory system. One has therefore a good efficiency for detecting all particles in the final state. The diffractive pair production reactions with low combinatoric background also contribute in this high x region. One would expect more favorable background conditions at high x for the identification of resonance P baryon states.

High quality particle identification (PID) for the largest possible energy range of the outgoing particles is important for reducing backgrounds associated with incorrect identification of tracks. This is available in E781, for example, via ring imaging Cerenkov (RICH) and transition radiation detector (TRD) PID systems. The separation of vertices is very important also for reducing the combinatoric backgrounds, as the majority of particles come from the primary vertex. These and other experimental techniques to reduce backgrounds are described in more detail in the contribution of J. Russ [15].

5 Heavy Baryons with Hidden Charm

In recent years, several candidates were reported for baryon states with unusual properties (narrow decay widths, large branching ratios for the decays with strange particles). There are candidates for cryptoexotic baryons with hidden strangeness $B_\phi = |qqqs\bar{s}\rangle$ ($q = u$ or d quarks) [28]. Although the existence of such a baryon is not yet confirmed [29], the suggestions raise the question of the possible existence of heavy cryptoexotic baryons with hidden charm $B_\psi = |qqqc\bar{c}\rangle$. If $M(B_\psi) < M(\eta_c) + M(p) \simeq 3.9$ GeV, the B_ψ decays would be OZI suppressed and the width of this cryptoexotic baryon would be quite narrow (≤ 1 MeV). To search for such B_ψ states, it was proposed [30] to use the diffractive production reaction $p + N \rightarrow B_\psi^+ + N$; with possible decays of B_ψ baryons $B_\psi^+ \rightarrow p + (J/\psi)_{virt} \rightarrow p + (l^+l^-)$ or $B_\psi \rightarrow p + (\eta_c)_{virt} \rightarrow p + (K^+K^-\pi^+\pi^-; 2\pi^+2\pi^-; K\bar{K}\pi; \eta\pi\pi)$. The $\sigma \cdot B$ was estimated as roughly 1.5 nb [30]. Assuming the expected Charm2000 efficiency of 2000 events/nb would hold for these events too, this would correspond to the detection of roughly 3000 events.

If $M(B_\psi) > 4.3$ GeV, there would be OZI allowed decays $B_\psi^+ \rightarrow p + J/\psi; \Lambda_C + D^0$, etc. Because of a complicated internal color structure of this baryon (see Introduction), one expects a narrow decay width (≤ 100 MeV). Such resonance states may be observable in diffractive production reactions.

6 Conclusions

We described the expected properties of Pentaquarks. Possibilities for enhancing the signal over background in Pentaquark searches were investigated. General model-independent predictions were presented as well as those from two models: a loosely bound $D_s^- N$ “and a strongly-bound five-quark model. While the current E791 may have marginal sensitivity, future experiments with more than 10^5 reconstructed charmed baryon events should have sensitivity to determine whether or not the Pentaquark exists.

7 Acknowledgements

Thanks are due to J. Appel, P. Cooper, L. Frankfurt, S. Gavin, D. Kaplan, M. A. Kubantsev, J. Lach, J. Lichtenstadt, S. May-Tal Beck, S. Nussinov, J. Russ, and B. Svititsky for stimulating discussions. This work was supported in part by the U.S.-Israel Binational Science Foundation, (B.S.F.) Jerusalem, Israel.

E-mail addresses of authors are: murray@tauphy.tau.ac.il, ashery@tauphy.tau.ac.il, lgl@mx.ihep.su, ftlipkin@weizmann.weizmann.ac.il

References

- [1] L.G. Landsberg, *Surveys in High Energy Phys.* **6** (1992) 257; K. Peters, *Proceed. of LEAP-92 Conf.*, Courmayeur, Aosta Valley, p.93, September 14-19, 1992, Eds. C. Guaraldo et al., 1993, North-Holland; L.G. Landsberg, *Yad.Fiz.* **57** (1994) 47
- [2] H.J. Lipkin, *Phys. Lett.* **B70** (1977) 113
- [3] R.L. Jaffe, *Phys. Rev. Lett.* **38** (1977) 195; **38** (1977) 1617E
- [4] H.J. Lipkin, *Phys. Lett.* **B195** (1987) 484; *Nucl. Phys.* **A478** (1988) 307c
- [5] C. Gignoux, B. Silvestre-Brac and J. M. Richard, *Phys. Lett.* **B193** (1987) 323
- [6] S. Zouzou and J.-M. Richard, *Few-Body Systems* **16** (1994) 1
- [7] S. Fleck *et al.*, *Phys. Lett.* **B220** (1989) 616
- [8] S. Takeuchi, S. Nussinov, K. Kubodera, *Phys. Lett.* **B318** (1993) 1
- [9] D.O. Riska and N.N. Scoccola, *Phys. Lett.* **B299** (1993) 338
- [10] M.A. Moinester, C.B. Dover, H.J. Lipkin, *Phys. Rev.* **C46** (1992) 1082
- [11] H. Høgaasen, P. Sorla, *Nucl. Phys.* **B145** (1978) 119; M. De Crombrugghe, *Nucl. Phys.* **B156** (1979) 347
- [12] D. Ashery, *Proc. 6th Lake Louise Winter Institute*, World Scientific, B.A. Campbel, A.N. Kamal, P. Kitching, F.C. Khanna, eds., (1991), p. 280
- [13] J. Lichtenstadt, (Proc. Suppl.) *Nucl. Phys.* **B21** (1991) 264
- [14] W.R. Greenberg, E.L. Lomon, *Phys. Rev.* **D47** (1993) 2703
- [15] J. Russ, Spokesman, FNAL Experiment 781, in CHARM2000, (these Proceedings)
- [16] J. Appel, in CHARM2000, (these Proceedings)

- [17] D. Kaplan, in CHARM2000, (these Proceedings)
- [18] F. Niedermayer, *Phys. Rev. D* **34** (1986) 3494
- [19] W. Bozzoli *et al.*, *Nucl. Phys. B* **144** (1978) 317
- [20] H. Grote, R. Hagedorn, J. Ranft, "Atlas of Particle Production Spectra", CERN preprint, 1970
 R. Hagedorn, in Quark Matter 84, ed. K. Kajantie, Lecture Notes in Physics Vol. 221 (Springer-Verlag, New York, 1985)
 P. V. Ruuskanen, *Acta Phys. Polon. B* **18** (1987) 551
 A. Casher, H. Neuberger and S. Nussinov, *Phys. Rev. D* **20** (1979) 179
 N. K. Glendenning, T. Matsui, *Phys. Rev. D* **28** (1983) 2890
 A. K. Kerman, T. Matsui, B. Svetitsky, *Phys. Rev. Lett.* **56** (219) 1986
 T. Matsui, *Nucl. Phys. A* **488** (535c) 1988
- [21] A. Simon, (for CERN WA89), Moriond presentation, (March 1994)
- [22] F. S. Rotondo, *Phys. Rev. D* **47** (1993) 3871
- [23] S. D. Ellis and R. Stroynowski, *Rev. Mod. Phys.* **49** (1977) (753)
- [24] S. May-Tal Beck, (for FNAL E791), DPF Annual Meeting, Albuquerque, N.M. (Sept. 1994)
- [25] C. Shipbaugh *et al.*, *Phys. Rev. Lett.* **60** (1988) 2117
- [26] G.A. Alves *et al.*, Preprint Fermilab-Pub-93/310-E, Oct. 1993, submitted to *Phys. Rev. Lett.*
- [27] L.G. Landsberg, M.A. Moinester, M.A. Kubantsev, Preprint IHEP 94-19, TAUP 2153-94, Protvino and Tel Aviv, 1994
- [28] V.F. Kurshetsov, L.G. Landsberg, Preprint IHEP 94-07, Protvino, 1994; *Yad. Fiz.* (in press) 1994;
 D.V. Vavilov *et al.*, Preprint IHEP 94-06, Protvino, 1994, *Yad. Fiz.* (in press), 1994; D.V. Vavilov *et al.*, *Yad. Fiz.* **57**(1994) 253
- [29] M. Ya. Balatz *et al.*, *Z. Phys. C* **61** (1994) 223; 399
- [30] L.G. Landsberg, Preprint IHEP 93-149, *Yad. Fiz.* (in press), 1994

Reducing Systematic Effects in High-Sensitivity Charm Experiments

Krishnaswamy Gounder and Donald Summers
Department of Physics and Astronomy
University of Mississippi
Oxford, Mississippi, 38677. U. S. A.

Abstract

The sensitivity of present charm measurements are still limited mostly by statistics. With a proposed charm sample of 10^8 (CHARM2000), the systematics will dominate the sensitivity of many charm measurements such as $D^0-\bar{D}^0$ Mixing, FCNC and other rare decays. Global design considerations as well as specific detector design issues in reducing systematic effects in such measurements are explored.

I. Introduction

For the past decade or so, our understanding of charm physics has improved steadily. The size of fully reconstructed charm samples have grown from a few tens in the early eighties to a few hundred thousands available at present. This impressive progress can be attributed to the development of silicon vertex detection techniques, high rate parallel data acquisition systems, advancements in computing, and accelerator technology. The availability of such large charm samples have made it possible: (a) to accurately measure the masses and lifetimes of charm mesons and baryons; (b) to discover rare decay modes and excited states; (c) to make accurate measurements of decay and standard model parameters; (d) to probe CP violation and flavor changing neutral current decays (FCNC) in the charm sector; and (e) to investigate the mechanism of charm production as well.

In spite of the remarkable growth in the size of the reconstructed charm data samples, the accuracy of present charm physics measurements are still limited by statistics. But the prospect of CHARM2000 aiming to generate three orders of magnitude more than the current samples raises interesting possibilities. With such a large fully reconstructed data sample, it is likely that the systematic effects will limit the sensitivity for rare charm decays. This can be extrapolated from the current limits as addressed in the next sections. Therefore, to apply severe tests on the standard model, the requirement will be not only high statistics but also high precision. Moreover, lower systematic contributions will greatly improve the accuracy of all measurements. Therefore, an experiment such as CHARM2000 should be designed to reduce and control the systematic effects along with producing a high statistics charm sample.

In section II, we outline our general approach to the design of high precision measurements. Sections III and IV address the issues for reducing the systematic effects in observing D^0 - \bar{D}^0 mixing and flavor changing neutral current decays. A number of viable solutions are attempted. The relevant issues in charged particle tracking, neutral particle reconstruction, and particle identification are outlined in section V. Section VI deals with the global design considerations that will contribute to systematic effects. Finally in section VII, we briefly outline the outlook for proposing a high sensitivity charm experiment such as CHARM2000.

II. Reducing Systematic Effects

The systematic effects can arise due to myriad of factors during all phases of an experiment - design, running, and reconstruction. In the design stage, the aim should be for finer resolution and higher efficiency detector components. The spectrometer has to be well controlled, monitored, and maintained at peak performance during the data acquisition stage. Beyond this stage, a number of factors such as reconstruction algorithms, calibration techniques and the quality of Monte Carlo simulations can also contribute to systematic effects.

During the design stage, the motivation should be for improving the sensitivity for rare and forbidden processes such as those listed below. Therefore, the reconstruction efficiency for the relevant decay modes should be greatly enhanced by the design of detector elements.

★ **D^0 - \bar{D}^0 Mixing:** $D^{*+} \rightarrow D^0 \pi^+$, $D^0 \rightarrow K^- \pi^+$, $D^0 \rightarrow K^- \pi^+ \pi^+ \pi^-$,
 $D^0 \rightarrow K^- \mu^+ \nu_\mu$, $D^0 \rightarrow K^- e^+ \nu_e$

Present Limits: DCSD/Mixing Ratio - 0.47% @ 90% CL [E791 - preliminary result using 1/3 data sample] [1]; $(0.77 \pm 0.25 \pm 0.25)\%$ [CLEO] [4].

★ **FCNC:** $D^+ \rightarrow \pi^+ \mu^+ \mu^-$, $D^0 \rightarrow \mu^+ \mu^-$

Present Limit: $\leq 4.6 \times 10^{-5}$ @ 90% CL for D^+ [E791] [2]; $\leq 3.1 \times 10^{-5}$ @ 90% CL for D^0 [E789] [3]

★ **Lepton Family Number Violation:** $D^0 \rightarrow e^\pm \mu^\mp$;

Present Limit: $\leq 1.0 \times 10^{-4}$ [ARGUS]

In the next two sections, we specifically address the issues for improving the sensitivity for D^0 - \bar{D}^0 mixing and FCNC decays. In each case, we attempt possible solutions to enhance the reconstruction efficiency and thus, improving the sensitivity for the relevant decay processes.

III. $D^0-\bar{D}^0$ Mixing

The soft pion in the decay $D^{*+} \rightarrow \pi^+ D^0$ tags the D meson as a D^0 or \bar{D}^0 when produced. By looking for wrong sign decays (e.g. $D^0 \rightarrow K^+ \pi^-$, $K^+ \pi^- \pi^- \pi^+$ or $K^+ \pi^- \pi^0$), one may be able to measure $D^0 \leftrightarrow \bar{D}^0$ mixing, if the D meson can be tagged. The hadronic wrong sign decays are also allowed via the doubly Cabbibo suppressed mechanism (DCSD). Recently, CLEO has reported that DCSD in the mode $K^+ \pi^-$ is about 1% [4] of the Cabbibo favored rate. The relative magnitude of this term and the interference term (DCSD and mixing) is an additional complication for hadronic decays. While the semi-leptonic modes, $D^0 \rightarrow K^- \mu^+ \nu_\mu$ and $K^- e^+ \nu_\mu$, are free of DCSD, the missing neutrino broadens the D^0 mass region. Besides DCSD, many other factors contribute systematic effects such as soft pion reconstruction efficiency, K- π misidentification, vertex and momentum resolutions, and accidental pions at the primary.

To improve the soft pion reconstruction, the direction and the magnitude of its momentum has to be measured accurately. By minimizing the error in the mass difference, $M(D^{*+}) - M(D^0)$, many background events can be rejected which would otherwise contaminate the mixing measurement. How much could the mass difference error be minimized? A typical value at fixed target experiments today is 1.2 MeV/c². Experimentally the 90% CL upper limit to $\Gamma(D^{*+})$ is 131 KeV [5]. Theoretically $\Gamma(D^{*+})$ ranges from this value down to 25 KeV [6]. The uncertainty is dominated by the error on the branching fraction of the radiative decay $B(D^{*+} \rightarrow D^+ \gamma) = 1.1^{+1.4}_{-0.7}$ % [7]. The bottom line is that the natural width is far from the reach of today's spectrometers.

The soft pion dominates the mass difference error. Consider a *typical* $D^{*+} \rightarrow \pi^+ D^0$ decay. Let $E_{\pi^+} = 3.0$ GeV, $E_{D^0} = 40.0$ GeV, and the opening angle $\theta = 0.806^\circ$. Now let the soft pion travel through 2mm of ¹³C with a density 3.9 g/cc. This diamond [8,9,10] provides a dense, low Z target which allows the D meson to exit before decaying. Decays in air, rather than in the target material, reduce background arising from secondary interactions. This 2mm diamond target amounts to 1.7% of a radiation length. One can next calculate the multiple scattering angle and its effect on the mass difference.

$$\delta(\theta) = \left(\frac{0.0136}{p}\right) \sqrt{X_0} [1. + 0.2 \text{LOG}_{10} X_0]$$

$$M_{D^{*+}} = \sqrt{M_{D^0}^2 + M_{\pi^+}^2 + 2E_{D^0}E_{\pi^+}(1. - \beta_{D^0}\beta_{\pi^+}\cos(\theta))}$$

Thus the multiple scattering leads to a shift of the D^{*+} mass of 65 KeV/c². Changing the magnitude of the soft pion momentum by 1% leads to a 70 KeV/c² D^{*+} mass shift. So the targets must be thin. If multiple targets are required, they must be interspersed with silicon microstrip detectors. A possible configuration is shown in Figure 1.

Misidentifying kaons and pions can also wreck havoc with a mixing measurement. A noteworthy development in the field of Čerenkov counters is the E781-SELEX RICH [11]

based on phototubes. Phototubes work. Phototubes which can distinguish single photons, such as the 1- $\frac{1}{8}$ " EMI 9124A, are getting down to the \$100 range.

To boost the mixing sample one may wish to look for $D^0 \rightarrow K^+ \pi^- \pi^0$ decays with an electromagnetic calorimeter. This detector is also useful for $D^0 \rightarrow K^+ e^- \bar{\nu}_e$ decays. DAΦNE [12,13] is developing a lead - scintillating fiber calorimeter. Particles intersect the calorimeter perpendicular to the fiber direction. The volume is 83% lead and 17% scintillating fiber. The total thickness for $20 X_0$ is 14cm. Showers are thus narrow. Because this thickness corresponds to 0.6 interaction lengths, hadrons tend to pass through. The resolution at 1 GeV is 5%, worse than CsI, but the shower isolation from the thinness may outweigh raw resolution.

Due to the absence of DCSD, mixing could be better observed by searching for the wrong sign semi-leptonic mode $D^0 \rightarrow K^+ \mu^- \bar{\nu}_\mu$. The relevant issues for this decay mode such as muon identification, kaon and pion decays in flight are addressed in the next sections.

Target-Silicon Planes Configuration: Schematic Diagram

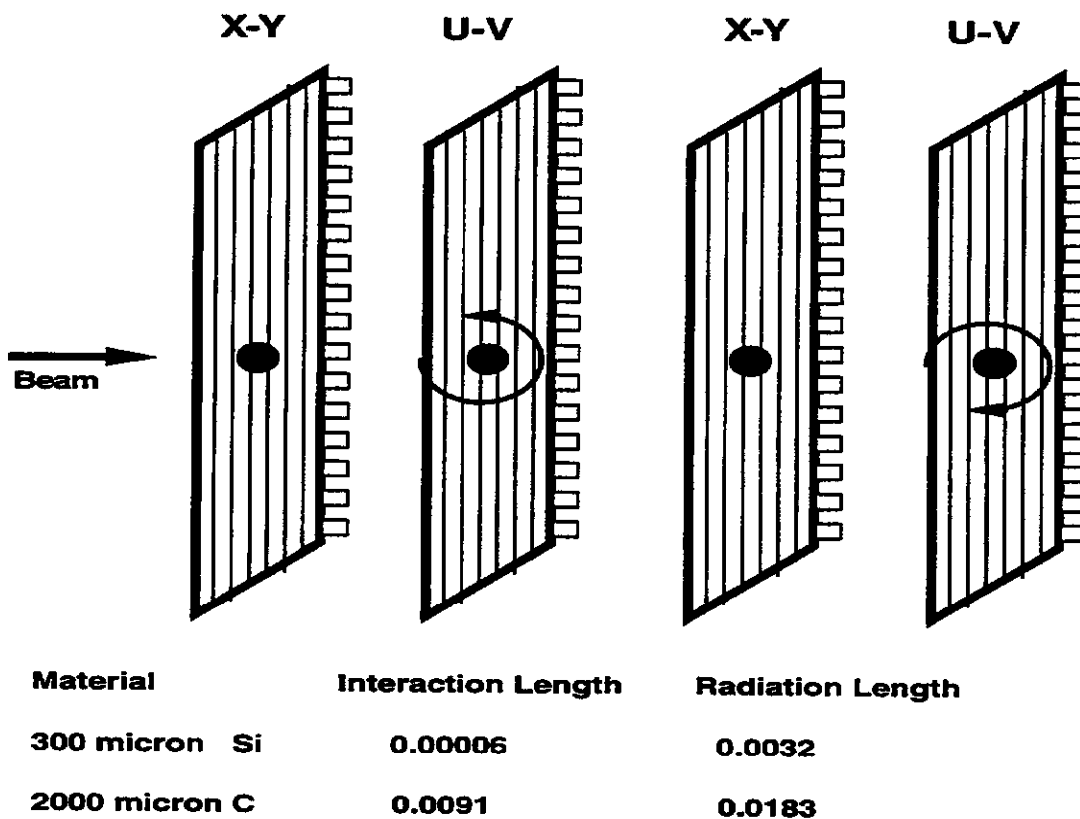


Figure:1

IV. Flavor Changing Neutral Current Decays

The standard model predicts that the FCNC decays $D^+ \rightarrow \pi^+ \mu^+ \mu^-$, $D^0 \rightarrow \mu^+ \mu^-$ should proceed at the level of 10^{-9} . To improve the present limits, the systematics due to misidentification, decays in-flight, vertex, mass resolutions and calorimeter punchthrough have to be overcome.

In addition to an excellent muon identification system, the in-flight decays of kaons and pions to muons have to be minimized. The flight path should be minimized. The pions only lose about 20% of their momenta when they decay as shown in Figure 3. A fairly accurate second momentum measurement as part of a muon detector might help. An iron toroid may not be adequate [14,15]. An air magnet would provide the best resolution. A schematic solution is shown in Figure 2. To minimize multiple scattering in the hadron absorber upstream of the muon system, Al_2O_3 may be preferable to iron. There is, however, a premium on a short hadrometer, so that pions in showers do not have time to decay into energetic muons. To minimize punchthrough, neutrons should be thermalized with hydrogen and then stopped with boron. A sophisticated tracking system with high efficiency in the non-bend view can also help to reconstruct the in-flight decays (kinks).

Secondary Muon Tracking System: Schematic Diagram

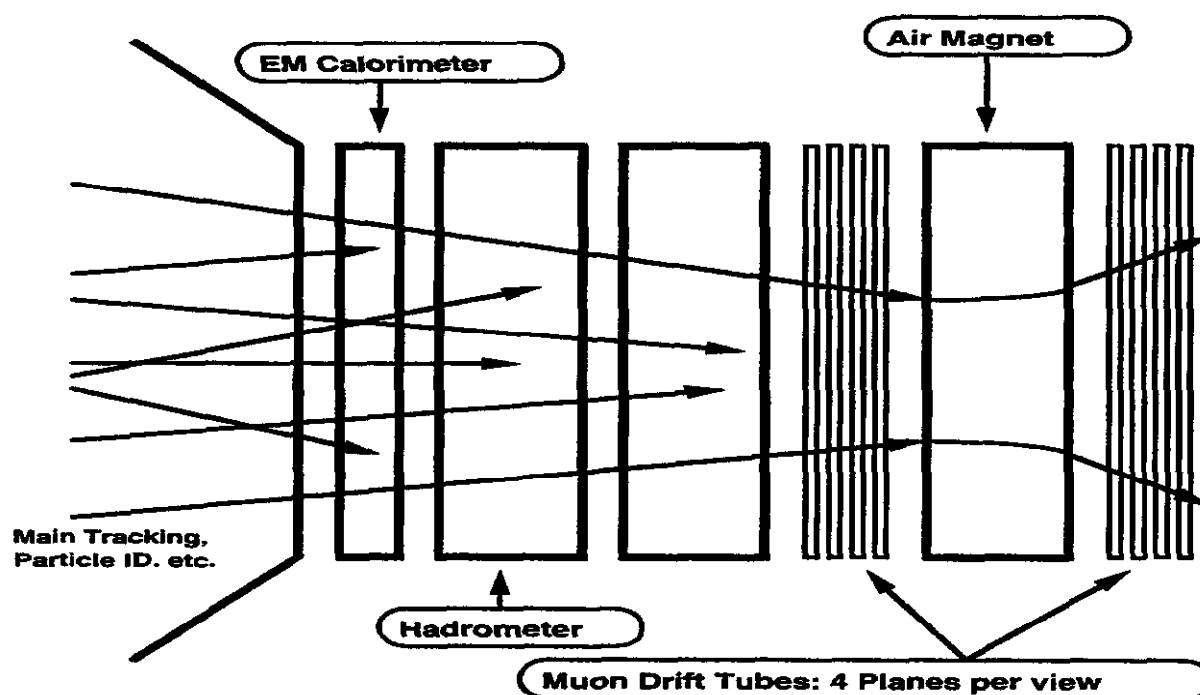


Figure: 2

V. Detector Design Issues

The specific design of each spectrometer component can be motivated to reduce the final systematic effects. The design goals should be the optimization of efficiencies and resolutions for tracking, vertexing, particle identification etc.. To reduce multiple scattering, detector elements and light weight support structures should be opted wherever possible. Below we briefly outline the major detector design issues to be considered for an optimal performance.

★ **Mass Resolution:** The present high-statistics charm experiments have mass resolutions of the order of 10-12 MeV for D^0 . By using a superconducting magnet instead of a conventional one, magnetic fields of 3 Tesla or higher can be produced in a smaller region of space. This will also lower the detector volume (decay volume). Combined with a finer resolution tracking system, the mass resolution can be improved by a factor of 2-4. The mass resolution also depends on the amount of multiple scattering present in the detector volume which is addressed below.

★ **Tracking:** To improve tracking efficiency, ideally we would like to have redundant planes in all views. Also, the overall tracking efficiency should be a weak function of individual plane efficiencies. Present tracking chambers have a resolution of few a hundred microns. Using straw tube or gas microstrip chambers can improve this resolution by a factor of 2 or more. Presence of more materials in the decay volume unavoidably causes more multiple scattering. This can be somewhat overcome by building tracking chambers with gold plated silicon carbide wires, aluminum field wires [16] or scintillating fibers. Also recent development with helium based drift chamber gases [12] (e.g. He:C₄H₁₀:CF₄ (80:19:1)) should prove useful. The empty portions of the decay volume can be filled with low Z gas such as helium. The total tracking system should be designed with an appropriate pattern recognition algorithm that helps to optimize the tracking efficiency and resolution.

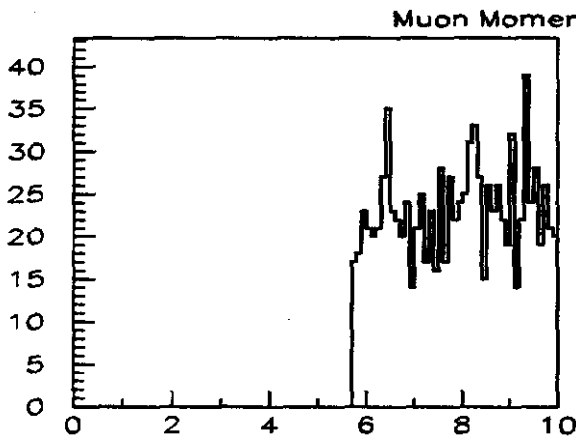


Figure 3A — 10 GeV Pion Decay

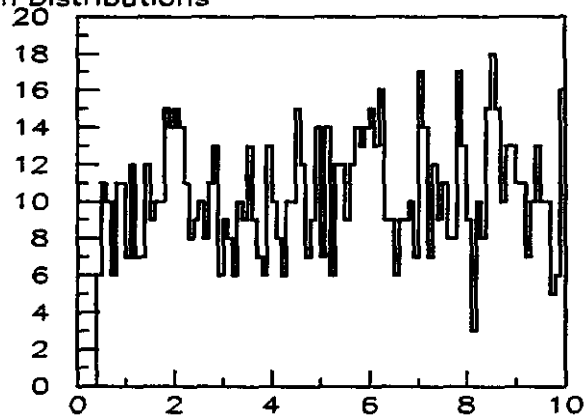


Figure 3B — 10 GeV Kaon Decay

★ **Vertexing:** The goal for vertex resolution should be about 200-250 microns. The present silicon microstrip vertex detectors fall short by a factor of 2 or more. The present day technology offers two-sided silicon strips with a pitch of 10 microns. Again the configuration of different tracking views should be motivated by pattern recognition as outlined above. The design of a good beam tracking system can improve the transverse vertex resolutions considerably. Segmented targets and minimization of materials upstreams are necessary to improve resolution by reducing the amount of multiple scattering.

★ **Particle Identification:** Particle misidentification is a major systematic factor contributing to both signal and background. On general principles, less systematic effects can be achieved using redundant particle identification systems and high efficiency devices (Detection of Internally Reflected Cerenkov Counters, Aerogel Threshold Counters) in the required kinematical region. In the particular case of the decay, $D^+ \rightarrow \pi^+ \mu^+ \mu^-$, $\pi - \mu$ separation is crucial. Along with excellent muon identification, a secondary tracking system is essential for this as discussed in the last section.

★ **Neutral Particle Reconstruction:** The goal of obtaining excellent resolution for neutral particle reconstruction such as π^0 , neutron and K_L^0 is an optional issue for a high-sensitivity charm experiment such as CHARM2000. The CLEO collaboration [15] has demonstrated a resolution of 1.5 % at 5 GeV of photon energy and 3.5 % at 100 MeV for their barrel CsI calorimeter. Also recently, the BABAR collaboration [17] has chosen CsI over other options such as BaF, liquid krypton, and scintillating fiber. Using a uranium-scintillator based hadrometer, the ZEUS has obtained a resolution of $32\%/\sqrt{E}$ [18]. It should be noted that the high efficiency for neutral particle reconstruction is very expensive costing tens of millions of dollars.

★ **Trigger Bias:** One of the key challenges for a high-sensitivity charm experiment is that of a development of a trigger that will contribute less systematic errors. For example a mild E_T trigger introduces lower bias for the lifetime distributions than a vertex trigger. Vertex triggers are likely to enrich the long lifetime events. On the other hand, an E_T trigger will adversely affect the systematic contributions for the study of charm production properties. Consequently, it is necessary to design a trigger that will have less dependence on the chosen physics goals and contribute minimum systematics bias. A mild E_T trigger might be a suitable candidate for FCNC decays and $D^0 - \bar{D}^0$ Mixing studies. Also, it has been long known that E_T trigger of 5-6 GeV produces an enrichment factor of 2-4 in the hadro-production of charm.

VI. Global Design Considerations

A number of global issues such as backgrounds, particle-antiparticle asymmetries, experimental control and monitoring, alignment systems, calibration techniques, and reconstruction algorithms should be considered in detail during the design phase of a high-

sensitivity experiment. These factors play important roles in reducing the overall systematic effects. Below, we briefly consider each of these factors:

★ **Physics Backgrounds:** Physics backgrounds can arise due to similar decay topology and decay properties such as lifetime. For example, the decay $D^+ \rightarrow \pi^- \pi^+ \pi^+$ is an unavoidable background to the FCNC decay $D^+ \rightarrow \pi^+ \mu^+ \mu^-$ as discussed in section IV. In this case, the design emphasis should be placed on obtaining premium efficiency for muon, kaon and pion identification while optimizing the tracking for reconstruction of kinks (secondary kaon and pion decays).

★ **Production Asymmetries:** Production asymmetries are caused by the nature of beam and target. For example, a negative pion beam produces more D^- mesons than D^+ mesons. A residual beam polarization in hyperon experiments can cause systematic effects in the final polarization measurements. Sufficient design emphasis in determining the beam parameters such as momentum, polarization etc. is necessary.

★ **Particle-Antiparticle Acceptance:** In a highly sensitive CP violating decays, it will be essential to have an understanding of the differences in particle and antiparticle acceptance corrections. These differences will vary with momentum and the amount of material present in their tracks. The difference in the interactions of K^- and K^+ in the calorimeter is a well known example.

★ **Experimental Control and Monitoring:** There is a multitude of experimental parameters such as high and low voltages, gas pressures, temperatures, magnet currents etc. that determine the efficiency of any given spectrometer. A well designed, robust control and monitoring system (such as EPICS [19]) will be essential for peak spectrometer performance and the proper calibration of detector elements.

★ **Alignment Systems and Calibration Techniques:** The complete knowledge of detector geometry is of paramount importance for finer resolutions and higher efficiencies. There are sophisticated available laser systems [20] that provide alignment of tracking devices to a few hundred microns. Improper calibration schemes for detector readouts such as ADCs, TDC's etc. can dilute the detector efficiencies and contribute systematic effects.

★ **Reconstruction Algorithms:** The efficiency for reconstruction of an event directly depends on the reconstruction algorithms for tracking and vertexing. For example, a good pattern recognition algorithm can make a considerable improvement in the tracking efficiency. This reduces random background and thus contributes less systematic effects. Even a small change in single track efficiency can make a large impact on the reconstruction of multi-particle decays. Therefore, a considerable amount of effort should be placed on developing such algorithms.

VII. Outlook for CHARM2000

Is it possible to realize a generic charm experiment capable of producing a reconstructed charm sample of 10^8 during early 2000's? Before answering, we should also consider the potential competition from three approved B-factories - i.e., BABAR, KEK, and CLEO III. The B mesons and baryons mostly decay into intermediate charm states making them also huge charm factories! CLEO is already on-line while BABAR and KEK are supposed to be producing physics by the year 2000!

We feel that a better alternative for a generic charm 10^8 experiment would be to opt for a high statistics and high precision FCNC or $D^0-\bar{D}^0$ mixing search. In the case of FCNC search, an efficient lepton trigger can be developed. This might also prove cost effective and has less competition from the B-factories. A much detailed design for such an experiment addressing issues such as rate limit, radiation protection, trigger design, sensitivity etc. would be an excellent theme for a future workshop.

VIII. Acknowledgements

The authors are grateful to Prof. Lucien Cremaldi, Fermilab E791 and E789 colleagues for many years of collaboration and enrichment. They also like to thank Prof. Dan Kaplan and the organizing committee for a successful workshop. This work was supported by the US Department of Energy under contract DE-FG05-91ER40622.

IX. References

1. M. Purohit *et al.*, " $D^0 - \bar{D}^0$ Mixing and Doubly Cabibbo-Suppressed Decays of D^+ ", ICHEP94 Reference 0490, Presented at the International Conference on High Energy Physics, Glasgow, Scotland, July 20-27, 1994.
2. A. Nguyen *et al.*, "Recent Results from Fermilab E-791" Presented at the 5th Conference on the Intersections of Particle and Nuclear Physics, St. Petersburg, Florida, May 31 - June 6, 1994.
3. S. Mishra *et al.*, "Search for the Decay $D \rightarrow \mu\mu$ ", FERMILAB-Pub-94/083-E.
4. D. Cinabro *et al.*, Phys. Rev. Lett. 72, 1406 (1994).
5. S. Barlag *et al.* (ACCMOR), Measurement of the Mass and Width of the Charmed Meson D^{*+} (2010), Physics Letters B278 (1992) 480-484.
6. James F. Amundson, C. Glenn Boyd, Elizabeth Jenkins, Michael Luke, Aneesh V. Manohar, Jonathan L. Rosner, Martin J. Savage, and Mark B. Wise, Radiative D^* Decay Using Heavy Quark and Chiral Symmetry, Physics Letters B296 (1992) 415-419.

7. M. Aguilar-Benitez et al. (Particle Data Group), Review of Particle Properties, Physical Review D50 (1994) 1173.
8. Karl E. Spear and John P. Dismukes, editors, SYNTHETIC DIAMOND: Emerging CVD Science and Technology, Wiley (1994) ISBN 1-53569-3.
9. Norton Diamond Film, Goddard Road, Northboro, Massachusetts 01532.
10. Genasystems, General Electric, 6325 Huntley Road, Worthington, Ohio 43085.
11. M. Pommot Maia, P.S. Cooper, L. Stutte, V. Solyanik, I. Filimonov, and A. Nemitkin (E781-SELEX), A Phototube RICH Detector, Nuclear Instruments and Methods A326 (1993) 496-507.
12. S. Berolucci et al., A PB-SCI.FI. Calorimeter for DAΦNE, Workshop on Physics and Detectors for DAΦNE, Frascati (9-12 April 1991) 557-562.
13. Jasper Kirkby, Detectors for Phi, Tau-Charm, and B Factories, CERN-PPE/93-85; Presented at the Joint US-CERN School on Particle Accelerators: Course on Frontiers of Particle Beams: Factories with $e^+ e^-$ Rings, Benalmadena, Spain (29 Oct - 4 Nov 1992)
14. R. L. Gluckstern, Uncertainties in Track Momentum and Direction, Due to Multiple Scattering and Measurement Errors, Nuclear Instruments and Methods 24 (1963) 381-389.
15. Konrad Kleinknecht, Detectors for Particle Radiation, Cambridge University Press (1987) Chapter 7, ISBN 0-521-35852-3.
16. Y. Kubota et al., The CLEO II Detector, Nuclear Instruments and Methods A320 (1992) 66-113.
17. D. Boutiguy et al. (BABAR), Letter of Intent for the Study of CP Violation and Heavy Flavor Physics at PEP-II, SLAC-443 (June 1994) 108.
18. R. Yoshida, "The ZEUS Uranium Calorimeter", in the proceedings of the Third International Conference on Calorimetry in High Energy Physics, edited by Phyllis Hale and James Siegrist, World Scientific, 1993.
19. "Experimental Physics and Industrial Control System (EPICS)", Argonne National Laboratory and Los Alamos National Laboratory, 1992.
20. R. Fabbretti et al., The Laser Beacon: A Survey System for the Torsion Free Alignment and Monitoring of the L3 Muon Spectrometer Octants, NIM A280 (1989) 13-24.

What Charm Can Tell Us About Beauty

Jonathan L. Rosner
Enrico Fermi Institute and Department of Physics
University of Chicago, Chicago, IL 60637

Abstract

A number of ways are reviewed in which the study of charmed particles can answer corresponding questions about particles containing b quarks. Topics include the properties of resonances, the magnitude of decay constants, the size of spin-dependent effects, and the hierarchy of lifetime differences.

1 Introduction

The study of charmed particles is of interest not only in its own right, but for the information it can provide about particles containing b quarks.

Charmed particles are relatively easy to produce. In the standard electroweak picture, their weak decays are unlikely to exhibit detectable CP-violating effects, and are noticeably affected by strong interactions. The good news is that these strong interactions are rich and easily studied.

Particles containing b quarks are much harder to produce. Their weak interactions (again, in the conventional view) are expected to be a rich source of observable CP-violating phenomena, and to be less polluted by the strong interactions. However, these strong interactions are still important (for example, one needs to know B meson decay constants), but their study is hampered by a lack of statistics. Here, charmed particles can be very helpful.

Many questions regarding B hadrons can benefit from the corresponding studies of charmed particles. These include resonances, spin-dependent effects, lifetime differences, and form factors for heavy-to-light weak transitions. Moreover, since weak decays of B hadrons often involve charm, the branching ratios of charmed particles are crucial in determining the corresponding B branching ratios.

This brief article touches upon some of the ways in which information about charmed particles can be applied to the corresponding states containing b quarks. In Section 2 we

review the relevant aspects of heavy quark symmetry permitting an extrapolation from charm to beauty. Section 3 is devoted to the open questions facing the study of CP violation in B decays, with emphasis on parallels with charm. Section 4 is devoted to strange B 's: their production, masses, and mixings, and the corresponding questions for charm. Heavy meson decay constants, for which we have partial information in the case of charm, are treated in Section 5. Heavy baryon spectra are discussed in Section 6, while Section 7 treats lifetime differences. We summarize in Section 8.

2 Heavy quark symmetry

In a hadron containing a single heavy quark, that quark ($Q = c$ or b) plays the role of an atomic nucleus, with the light degrees of freedom (quarks, antiquarks, gluons) analogous to the electron cloud. The properties of hadrons containing b quarks (we shall call them B hadrons) then can be calculated from the corresponding properties of charmed particles by taking account [1] of a few simple "isotope effects." For example, if q denotes a light antiquark, the mass of a $Q\bar{q}$ meson can be expressed as

$$M(Q\bar{q}) = m_Q + \text{const.}[n, \ell] + \frac{\langle p^2 \rangle}{2m_Q} + a \frac{\langle \sigma_q \cdot \sigma_Q \rangle}{m_q m_Q} + \mathcal{O}(m_Q^{-2}) \quad (1)$$

Here the constant depends only on the radial and orbital quantum numbers n and ℓ . The $\langle p^2 \rangle / 2m_Q$ term expresses the dependence of the heavy quark's kinetic energy on m_Q , while the last term is a hyperfine interaction. The expectation value of $\langle \sigma_q \cdot \sigma_Q \rangle$ is $(+1, -3)$ for $J^P = (1^-, 0^-)$ mesons. If we define $\bar{M} \equiv [3M(1^-) + M(0^-)]/4$, we find

$$m_b - m_c + \frac{\langle p^2 \rangle}{2m_b} - \frac{\langle p^2 \rangle}{2m_c} = \bar{M}(B\bar{q}) - \bar{M}(c\bar{q}) \simeq 3.34 \text{ GeV} \quad (2)$$

so $m_b - m_c > 3.34 \text{ GeV}$, since $\langle p^2 \rangle > 0$. Details of this picture which are of interest include (1) the effects of replacing nonstrange quarks with strange ones, (2) the energies associated with orbital excitations, (3) the size of the $\langle p^2 \rangle$ term, and (4) the magnitude of hyperfine effects. In all cases there exist ways of using information about charmed hadrons to predict the properties of the corresponding B hadrons.

3 CP violation and B mesons

3.1 The CKM matrix

3.1.1 Parameters and their values

In a parametrization [2] in which the rows of the CKM [3, 4] matrix are labelled by u, c, t and the columns by d, s, b , we may write

$$V = \begin{pmatrix} V_{ud} & V_{us} & V_{ub} \\ V_{cd} & V_{cs} & V_{cb} \\ V_{td} & V_{ts} & V_{tb} \end{pmatrix} \approx \begin{bmatrix} 1 - \lambda^2/2 & \lambda & A\lambda^3(\rho - i\eta) \\ -\lambda & 1 - \lambda^2/2 & A\lambda^2 \\ A\lambda^3(1 - \rho - i\eta) & -A\lambda^2 & 1 \end{bmatrix} \quad (3)$$

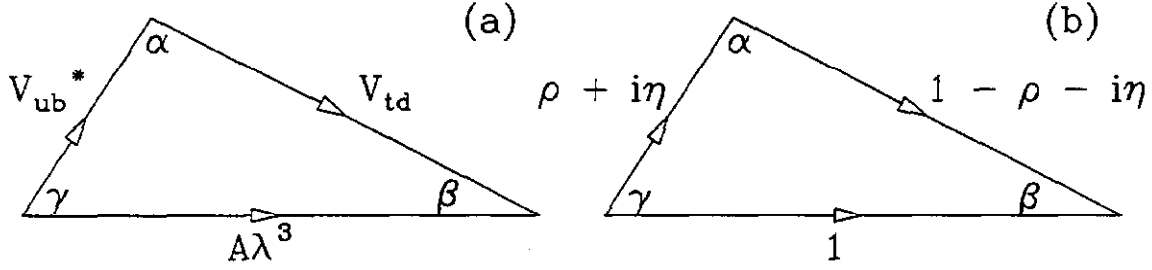


Figure 1: The unitarity triangle. (a) Relation obeyed by CKM elements; (b) relation obeyed by (CKM elements)/ $A\lambda^3$

Note the phases in the elements V_{ub} and V_{td} . These phases allow the standard $V - A$ interaction to generate CP violation as a higher-order weak effect.

The parameter λ is measured by a comparison of strange particle decays with muon decay and nuclear beta decay, leading to $\lambda \approx \sin \theta \approx 0.22$, where θ is just the Cabibbo [3] angle. The dominant decays of b -flavored hadrons occur via the element $V_{cb} = A\lambda^2$. The lifetimes of these hadrons and their semileptonic branching ratios then lead to estimates in the range $A = 0.7 - 0.9$. The decays of b -flavored hadrons to charmless final states allow one to measure the magnitude of the element V_{ub} and thus to conclude that $\sqrt{\rho^2 + \eta^2} = 0.2 - 0.5$. The least certain quantity is the phase of V_{ub} : $\text{Arg}(V_{ub}^*) = \arctan(\eta/\rho)$. We shall mention ways in which information on this quantity may be improved, in part by indirect information associated with contributions of higher-order diagrams involving the top quark.

The unitarity of V and the fact that V_{ud} and V_{tb} are very close to 1 allow us to write $V_{ub}^* + V_{td} \simeq A\lambda^3$, or, dividing by a common factor of $A\lambda^3$, $\rho + i\eta + (1 - \rho - i\eta) = 1$. The point (ρ, η) thus describes in the complex plane one vertex of a triangle whose other two vertices are $(0, 0)$ and $(0, 1)$. This triangle and conventional definitions of its angles are depicted in Fig. 1.

3.1.2 Indirect information

Indirect information on the CKM matrix comes from $B^0 - \bar{B}^0$ mixing and CP-violating $K^0 - \bar{K}^0$ mixing, through the contributions of box diagrams involving two charged W bosons and two quarks of charge $2/3$ (u, c, t) on the intermediate lines. Evidence for the top quark with a mass of $m_t = 174 \pm 10^{+13}_{-12} \text{ GeV}/c^2$ has recently been reported [5], reducing the errors associated with these box diagrams.

The original evidence for $B^0 - \bar{B}^0$ mixing came from the presence of “wrong-sign” leptons in B meson semileptonic decays [6]. The splitting Δm_B between mass eigenstates is proportional to $f_B^2 m_t^2 |V_{td}|^2$ times a slowly varying function of m_t . Here f_B is the B meson decay constant. The contributions of lighter quarks in the box diagrams, while necessary to cut off the high-energy behavior of the loop integrals, are numerically insignificant.

The CKM element $|V_{td}|$ is proportional to $|1 - \rho - i\eta|$. Thus, exact knowledge of Δm_B , f_B

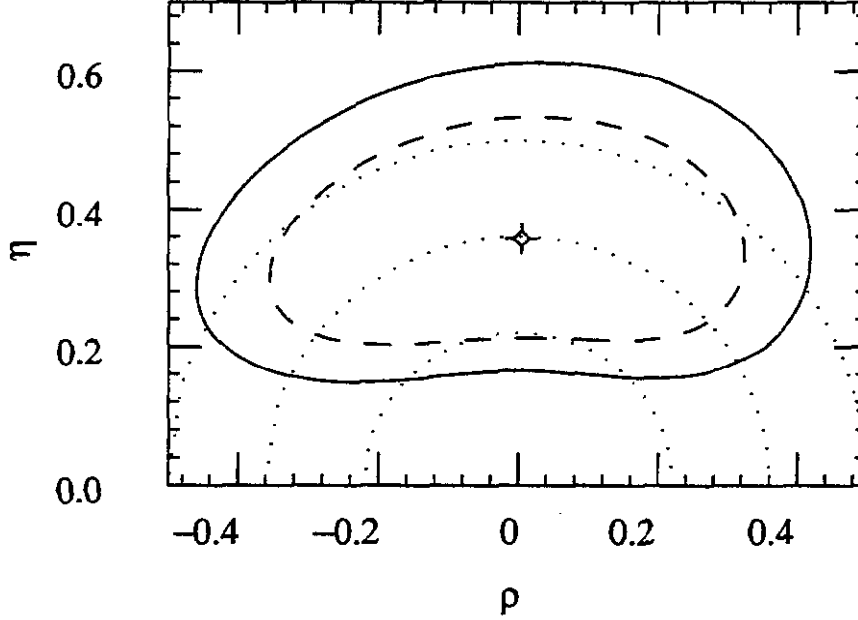


Figure 2: Contours of 68% (inner curve) and 90% (outer curve) confidence levels for regions in the (ρ, η) plane. Dotted semicircles denote central value and $\pm 1\sigma$ limits implied by $|V_{ub}/V_{cb}| = 0.08 \pm 0.03$. Plotted point corresponds to minimum $\chi^2 = 0.17$, while (dashed, solid) curves correspond to $\Delta\chi^2 = (2.3, 4.6)$

and m_t would specify a circular arc in the (ρ, η) plane with center $(1, 0)$. Errors on all these quantities spread this arc out into a band. Present averages [7] give $(\Delta m_B / \Gamma_B) = 0.71 \pm 0.07$. This value (close to 1) is nearly optimal for observing CP-violating asymmetries in B^0 decays.

Similar box diagrams govern the parameter ϵ in CP-violating $K^0 - \bar{K}^0$ mixing. Here the dominant contribution to the imaginary part of the off-diagonal mass matrix element is proportional to $f_K^2 m_t^2 \text{Im}(V_{td}^2)$ times a slowly varying function of m_t . Charmed quarks also provide a small contribution.

The kaon decay constant is known: $f_K = 160$ MeV. The imaginary part of V_{td} is proportional to $\eta(1 - \rho)$. Knowledge of ϵ thus specifies a hyperbola in the (ρ, η) plane with focus at $(1, 0)$, which is spread out into a band because of uncertainties in hadronic matrix elements.

3.1.3 Allowed (ρ, η) region

Information on $|V_{ub}/V_{cb}|$ specifies a circular band in the (ρ, η) plane. When this constraint is added to those mentioned above, one obtains the potato-shaped region shown in Fig. 2. Here we have taken $m_t = 174 \pm 17$ GeV/ c^2 , $f_B = 180 \pm 30$ MeV, $(\rho^2 + \eta^2)^{1/2} = 0.36 \pm 0.14$ (corresponding to $|V_{ub}/V_{cb}| = 0.08 \pm 0.03$), and $A = 0.79 \pm 0.09$ (corresponding to $V_{cb} = 0.038 \pm 0.005$). A parameter known as B_K describes the degree to which the box diagrams dominate the CP-violating $K^0 - \bar{K}^0$ mixing. We take $B_K = 0.8 \pm 0.2$, and set the corresponding value for B mesons equal to 1. A QCD correction [8] to the $B^0 - \bar{B}^0$ mixing amplitude has been taken to be $\eta_{\text{QCD}} = 0.6 \pm 0.1$. Other parameters and fitting methods are

as discussed in more extensive treatments elsewhere [9, 10]. Several parallel analyses [11, 12] reach qualitatively similar conclusions.

The best fit corresponds to $\rho \simeq 0$, $\eta \simeq 0.36$, while at 90% confidence level the allowed ranges are:

$$\begin{aligned} \eta \simeq 0.3 & : -0.4 \leq \rho \leq 0.4 \quad ; \\ \rho \simeq 0 & : \eta \simeq 0.3 \times 2^{\pm 1} \quad . \end{aligned} \tag{4}$$

A broad range of parameters gives an acceptable description of CP violation in the kaon system. The study of CP violation in B decays could confirm or disprove this picture.

3.2 Modes of studying CP violation in B decays

Any manifestation of CP violation requires some sort of interference. We give two of the main examples under consideration for B decays. We then discuss how charmed particles can provide useful information in both cases.

3.2.1 Self-tagging decays

Inequality of the rates for a process and its charge conjugate, such as $B^+ \rightarrow \pi^0 K^+$ and $B^- \rightarrow \pi^0 K^-$, would signify CP violation. Under charge conjugation, the weak phases change sign while the strong phases do not. A rate difference can arise if both strong and weak phases are different in two channels (here, $I = 1/2$ and $I = 3/2$). Interpretation requires knowing the strong phase shift difference $\delta \equiv \delta_{3/2} - \delta_{1/2}$.

3.2.2 Decays to CP eigenstates

Interference between a decay amplitude and a mixing amplitude can lead to rate differences between decays of B^0 's and \bar{B}^0 's to CP eigenstates such as $J/\psi K_S$ or $\pi^+ \pi^-$. Here, no strong phase shift is needed to generate an observable effect, and decay rate asymmetries can directly probe angles of the unitarity triangle. However, it is necessary to know the flavor of the initial neutral B meson.

3.3 Final-state phases

Several examples involving charmed particles can be instructive in how one obtains final-state phase shift information from decay rates. These examples turn out to have parallels in the case of B mesons, but the cases of real interest for CP violation in the B system turn out to be somewhat more complex.

The decays $D \rightarrow \bar{K} \pi$ are characterized by the quark subprocess $c \rightarrow s u \bar{d}$, which has $\Delta I = \Delta I_3 = 1$, and so there are two final-state amplitudes, one with $I = 1/2$ and one with $I = 3/2$. The amplitudes for decays to specific charge states can be written in terms of

isospin amplitudes as $A(D^+ \rightarrow \bar{K}^0 \pi^+) = A_{3/2}$; $A(D^0 \rightarrow K^- \pi^+) = (2/3)A_{1/2} + (1/3)A_{3/2}$; $A(D^0 \rightarrow \bar{K}^0 \pi^0) = \sqrt{2}(A_{3/2} - A_{1/2})/3$. The amplitudes then obey a triangle relation, and by considering the observed rates one finds the relative phase of the $I = 1/2$ and $I = 3/2$ amplitudes to be around 90° [13]. This is likely to indicate the importance of resonant structure. The $I = 1/2$ channel is “non-exotic” (it can be formed of a quark-antiquark state), while the $I = 3/2$ channel is “exotic,” requiring at least two quarks and two antiquarks. No resonances have been seen in exotic channels, while there is an $I = 1/2$ $K\pi$ resonance just around the mass of the D meson [14].

Triangle constructions similar to that mentioned above indicate that the relative phase of $I = 1/2$ and $I = 3/2$ amplitudes in $D \rightarrow \bar{K}^* \pi$ appears to be about 90° , while it appears to be about 0 in $D \rightarrow \bar{K}^* \rho$. This difference may be due to details of resonance couplings, but could not have been anticipated *a priori*. It illustrates the importance of actual measurements rather than theoretical prejudices in the evaluation of final-state phase shift differences.

The decays $D \rightarrow \pi\pi$ are governed by the subprocess $c \rightarrow du\bar{d}$ (or $c \rightarrow u$ penguin subprocesses). The $\Delta I = 1/2$ transitions lead to an $I = 0$ $\pi\pi$ final state, while the $\Delta I = 3/2$ transitions lead to an $I = 2$ $\pi\pi$ final state. Again, a triangle relation holds between amplitudes, and the $I = 0$ and $I = 2$ amplitudes are found [15] to have a relative phase consistent with 90° .

The decays $B \rightarrow \bar{D}\pi$ involve the quark subprocess $\bar{b} \rightarrow \bar{c}u\bar{d}$ and so their isospin analysis parallels that of $D \rightarrow \bar{K}\pi$. It has recently been concluded [16] that present data are consistent with a relative phase shift of zero between the $I = 1/2$ and $I = 3/2$ amplitudes.

The decays $B \rightarrow K\pi$ involve the quark subprocesses $\bar{b} \rightarrow \bar{s}u\bar{u}$ and $\bar{b} \rightarrow \bar{s}$ (penguin processes), and thus are characterized by both $\Delta I = 0$ and $\Delta I = 1$ transitions. The $\Delta I = 0$ transitions can lead only to an $I = 1/2$ final state, while the $\Delta I = 1$ transitions lead to both $I = 1/2$ and $I = 3/2$ final states. Four $B \rightarrow K\pi$ decay amplitudes then can be expressed in terms of two $I = 1/2$ and one $I = 3/2$ reduced amplitude, leading to a quadrangle relation [17]. Suggestions have been made [18] for incorporating information from $B \rightarrow \pi\pi$ decays with the help of flavor $SU(3)$ and untangling various final-state phases in the $K\pi$ channel.

3.4 Flavor tagging in neutral B decays

As mentioned above, the decays of neutral B mesons to CP eigenstates can provide crisp information on angles in the unitarity triangle if one can “tag” the flavor of the decaying B at the time of its production. One method for doing this [19] relies on the correlation of a neutral B with a charged pion.

This method [20] is already in use for tagging neutral D decays. The charged D^* resonance is far enough above the neutral D that the decays $D^{*+} \rightarrow \pi^+ D^0$ and $D^{*-} \rightarrow \pi^- D^0$ are kinematically allowed. Here one is interested in whether a given final state has arisen from mixing or from the doubly-suppressed process $c \rightarrow du\bar{s}$.

In the case of B mesons, the B^* is only 46 MeV above the B , so the decay $B^* \rightarrow B\pi$

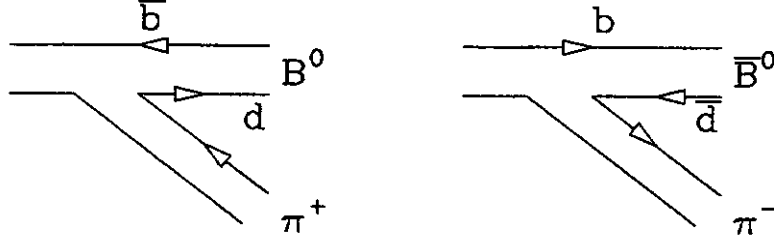


Figure 3: Quark graphs illustrating pion- B correlations. Fragmentation of a \bar{b} quark leads to a B^0 and a nearby π^+ , while fragmentation of a b quark leads to a \bar{B}^0 and a nearby π^- .

is kinematically forbidden. Nonetheless, one can expect non-trivial correlations between the flavor of a produced B and a pion nearby in phase space, either as a result of correlations in the fragmentation process or through the decays of resonances above the B^* . In both cases, the corresponding physics for charmed particles is easy to study and will provide interesting information.

3.5 Pion – B correlations

The pion- B correlation in a fragmentation picture is illustrated in Fig. 3. When incorporated into a neutral B meson, a \bar{b} quark is “dressed” with a d , leading to a B^0 . The next quark down the rapidity chain is a \bar{d} , which will appear in a pion of positive charge. Similarly, a \bar{B}^0 is more likely to be correlated with a π^- .

The existence of this correlation in CDF data is still a matter of some debate. It would be interesting to see if it exists for charmed particles. One would have to subtract out the contribution of D^* decays, of course.

3.6 B^{**} resonances and their charmed equivalents

A B^0 or B^{*0} can resonate with a positive pion, while a \bar{B}^0 or \bar{B}^{*0} can resonate with a negative pion. The combinations $B^0\pi^-$ and $\bar{B}^0\pi^+$ are exotic, and not expected to be resonant.

The lowest-lying resonances which can decay to $B\pi$ or $B^*\pi$ are expected to be the P-wave $\bar{b}q$ states. We call them B^{**} (to distinguish them from the B^* ’s). The expectations for masses of these states [19, 21], based on extrapolation from the known D^{**} resonances, are summarized in Table 1.

The known D^{**} resonances are a 2^+ state around 2460 MeV/ c^2 , decaying to $D\pi$ and $D^*\pi$, and a 1^+ state around 2420 MeV/ c^2 , decaying to $D^*\pi$. These states are relatively narrow, probably because they decay via a D-wave. In addition, there are expected to be much broader (and probably lower) D^{**} resonances: a 1^+ state decaying to $D^*\pi$ and a 0^+ state decaying to $D\pi$, both via S-waves.

Table 1: P-wave resonances of a b quark and a light (\bar{u} or \bar{d}) antiquark

J^P	Mass (GeV/ c^2)	Allowed final state(s)
2^+	~ 5.77	$B\pi, B^*\pi$
1^+	~ 5.77	$B^*\pi$
1^+	< 5.77	$B^*\pi$
0^+	< 5.77	$B\pi$

Once the masses of D^{**} resonances are known, one can estimate those of the corresponding B^* states by adding about 3.32 GeV (the quark mass difference minus a small binding correction). Adding a strange quark adds about 0.1 GeV to the mass. Partial decay widths of D^{**} states are also related to those of the B^{**} 's [21]. Thus, the study of excited charmed states can play a crucial role in determining the feasibility of methods for identifying the flavor of neutral B mesons.

4 Strange B 's

4.1 Production

It is important to know the ratios of production of different B hadrons: $B^+ : B^0 : B_s : \Lambda_b$. These ratios affect signals for mixing and the dilution of flavor-tagging methods. Aside from effects peculiar to the decays $D^* \rightarrow D\pi$, one should have similar physics in the ratios $D^+ : D^0 : D_s : \Lambda_c$.

4.2 Masses

It appears that the B_s states are about 90 MeV above the B 's [21]. One predicts a similar splitting for the strange and nonstrange vector mesons [22]. The corresponding splittings for charmed particles are about 100 MeV for both pseudoscalar and vector mesons, as well as for the observed P-wave levels. This leads to a more general question: How much mass does a strange quark add? This is an interesting "isotope effect" which in principle could probe binding effects in the interquark force.

4.3 $B_s - \bar{B}_s$ mixing

The box diagrams which lead to $K^0 - \bar{K}^0$ and $B^0 - \bar{B}^0$ mixing also mix strange B mesons with their antiparticles. One expects $(\Delta m)|_{B_s}/(\Delta m)|_{B_d} = (f_{B_s}/f_{B_d})^2 (B_{B_s}/B_{B_d}) |V_{ts}/V_{td}|^2$, which should be a very large number (of order 20 or more). Thus, strange B 's should undergo many particle-antiparticle oscillations before decaying.

Table 2: Dependence of mixing parameter x_s on top quark mass and B_s decay constant.

m_t (GeV/ c^2)	157	174	191
f_{B_s} (MeV)			
150	7.6	8.9	10.2
200	13.5	15.8	18.2
250	21.1	24.7	28.4

The main uncertainty in an estimate of $x_s \equiv (\Delta m/\Gamma)_{B_s}$ is associated with f_{B_s} . The CKM elements $V_{ts} \simeq -0.04$ and $V_{tb} \simeq 1$ which govern the dominant (top quark) contribution to the mixing are known fairly well. We show in Table 2 the dependence of x_s on f_{B_s} and m_t . To measure x_s , one must study the time-dependence of decays to specific final states and their charge-conjugates with resolution much less than the B_s lifetime (about 1.5 ps).

5 Heavy meson decay constants

5.1 The D_s

Direct measurements are available so far only for the D_s decay constant. The WA75 collaboration [23] has seen 6 – 7 $D_s \rightarrow \mu\nu$ events, and Fermilab E653 and the BES detector at the Beijing Electron-Positron Collider (BEPC) also have a handful. The CLEO Collaboration [24] has a much larger statistical sample; the main errors arise from background subtraction and overall normalization (which relies on the $D_s \rightarrow \phi\pi$ branching ratio). The actual measurement is $r \equiv B(D_s \rightarrow \mu\nu)/B(D_s \rightarrow \phi\pi) = 0.245 \pm 0.052 \pm 0.074$.

A better measurement of $B(\phi\pi) \equiv B(D_s \rightarrow \phi\pi)$ is sorely needed. One method [25] is to apply factorization [26] to the decay $B \rightarrow D_s D$, where $D_s \rightarrow \phi\pi$, to obtain the combination $f_{D_s}^2 B(\phi\pi)$. Since $r \propto f_{D_s}^2/B(\phi\pi)$, one can extract both the decay constant and the desired branching ratio. Using this and other methods, Muheim and Stone [25] estimate $f_{D_s} = 315 \pm 45$ MeV and $B(\phi\pi) = (3.6 \pm 0.6)\%$.

The large value of f_{D_s} implies a branching ratio of about 9% for $D_s \rightarrow \tau\nu_\tau$. This is good news for experiments [27] contemplating the production of ν_τ in beam dumps.

5.2 The charged D

By searching for the decay $D \rightarrow \mu\nu$ in the decays of D mesons produced in the reaction $e^+e^- \rightarrow \psi(3770) \rightarrow D^+D^-$, the Mark III collaboration has obtained the upper limit [28] $f_D < 290$ MeV (90% c.l.). The BES detector at Beijing should be able to improve upon this limit, which is not far above theoretical expectations [30, 31, 32].

The CLEO measurement of f_D , mentioned above relied on photon- D_s correlations in

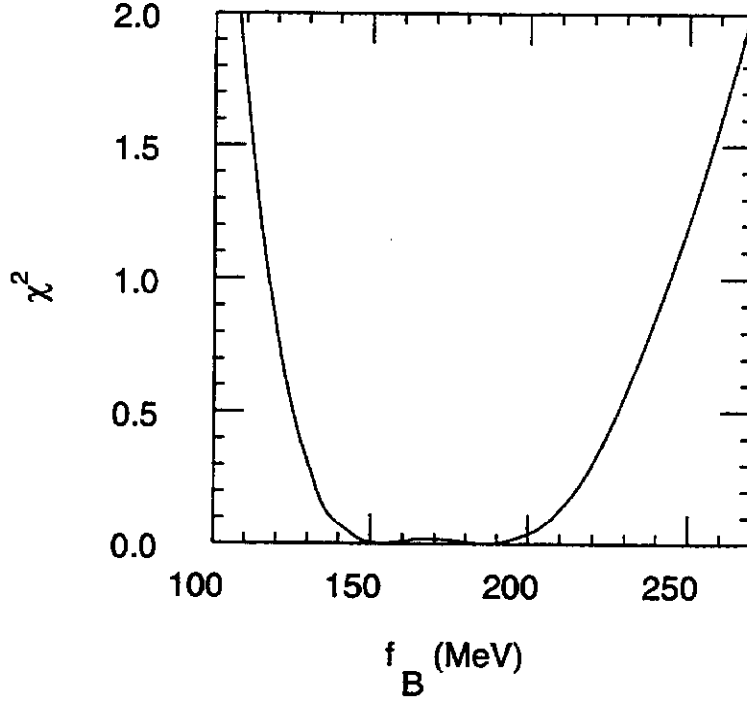


Figure 4: Variation of χ^2 in a fit to CKM parameters as a function of f_B .

the decay $D_s^* \rightarrow D_s \gamma$. One may be able to search for the decay $D^+ \rightarrow \mu \nu$ by looking for the $\pi^0 - D^+$ correlation in the decay $D^{*+} \rightarrow D^+ \pi^0$ [29].

5.3 B Meson decay constants

If f_B were better known, the indeterminacy in the (ρ, η) plane associated with fits to CKM parameters would be reduced considerably. We show in Fig. 4 the variation in χ^2 for the fit described in Sec. 3.1 when f_B is taken to have a fixed value. An acceptable fit is obtained for a wide range of values, with $\chi^2 = 0$ for $f_B = 153$ and 187 MeV.

The reason for the flat behavior of χ^2 with f_B is illustrated in Fig. 5. The dashed line, labeled by values of f_B , depicts the (ρ, η) value for the solution with minimum χ^2 at each f_B . The product $|1 - \rho - i\eta|f_B$ is constrained to be a constant by $B^0 - \bar{B}^0$ mixing. The product $\eta(1 - \rho)$ is constrained to be constant by the value of ϵ . The locus of solutions to these two conditions lies approximately tangent to the circular arc associated with the constraint on $|V_{ub}/V_{cb}|$ for a wide range of values of f_B .

The uncertainty in f_B thus becomes a major source of uncertainty in ρ , which will not improve much with better information on $|V_{ub}/V_{cb}|$. Fortunately, several estimates of f_B are available, and their reliability should improve.

Lattice gauge theories have attempted to evaluate decay constants for D and B mesons.

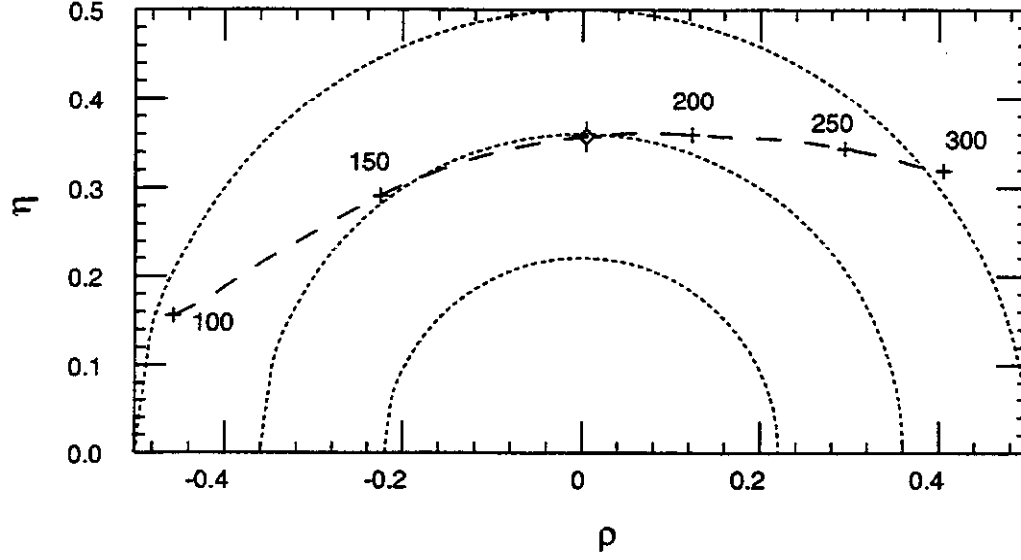


Figure 5: Locus of points in (ρ, η) corresponding to minimum χ^2 for fixed values of f_B . Circular arcs depict central value and $\pm 1\sigma$ errors for $|V_{ub}/V_{cb}|$. Solid dots denote points with $\chi^2 = 0$.

A representative set [31] is

$$\begin{aligned}
 f_B &= 187 \pm 10 \pm 34 \pm 15 \text{ MeV} , \\
 f_{B_s} &= 207 \pm 9 \pm 34 \pm 22 \text{ MeV} , \\
 f_D &= 208 \pm 9 \pm 35 \pm 12 \text{ MeV} , \\
 f_{D_s} &= 230 \pm 7 \pm 30 \pm 18 \text{ MeV} ,
 \end{aligned} \tag{5}$$

where the first errors are statistical, the second are associated with fitting and lattice constant, and the third arise from scaling from the static ($m_Q = \infty$) limit. The spread between these and some other lattice estimates [32] is larger than the errors quoted above, however.

Quark models can provide estimates of decay constants and their ratios. In a non-relativistic model [33], the decay constant f_M of a heavy meson $M = Q\bar{q}$ with mass M_M is related to the square of the $Q\bar{q}$ wave function at the origin by $f_M^2 = 12|\Psi(0)|^2/M_M$. The ratios of squares of wave functions can be estimated from strong hyperfine splittings between vector and pseudoscalar states, $\Delta M_{\text{hfs}} \propto |\Psi(0)|^2/m_Q m_q$. The equality of the $D_s^* - D_s$ and $D^* - D$ splittings then suggests that

$$f_D/f_{D_s} \simeq (m_d/m_s)^{1/2} \simeq 0.8 \simeq f_B/f_{B_s} , \tag{6}$$

where we have assumed that similar dynamics govern the light quarks bound to charmed and b quarks. In lattice estimates these ratios range between 0.8 and 0.9.

An improved measurement of f_{D_s} and a first measurement of f_D could provide a valuable check on predictions of various theories and could help pin down B meson decay constants, since ratios are expected to be more reliably predicted than individual constants [34].

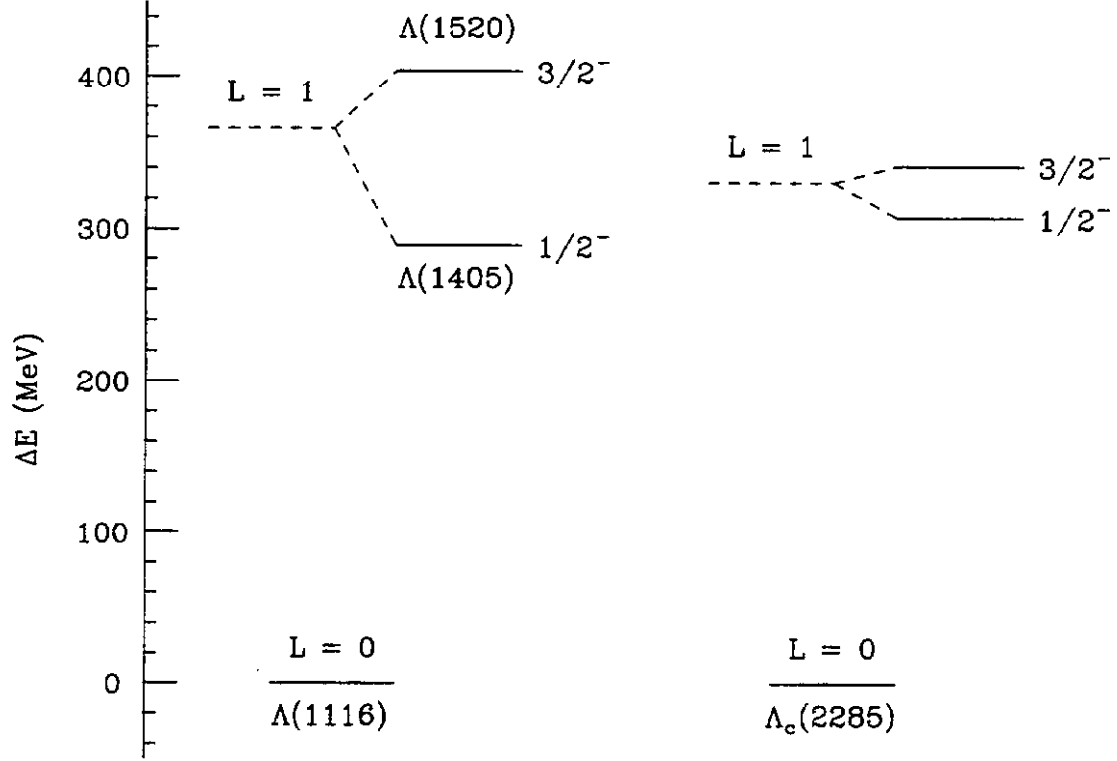


Figure 6: Ground states and first orbital excitations of Λ and Λ_c levels.

6 Charmed baryon spectra

The Λ_c baryon is a particularly simple object in heavy-quark symmetry, since its light-quark system consists of a u and d quark bound to a state $[ud]$ of zero spin, zero isospin, and color antitriplet. Comparisons with the $\Lambda_b = b[ud]$ and even with the $\Lambda = s[ud]$ are thus particularly easy.

The $[ud]$ diquark in the Λ can be orbitally excited with respect to the strange quark. The $L = 1$ excitations consist of a fine-structure doublet, the $\Lambda(1405)$ with spin-parity $J^P = 1/2^-$ and the $\Lambda(1520)$ with $J^P = 3/2^-$. The spin-weighted average of this doublet is 366 MeV above the Λ . These states are illustrated on the left-hand side of Fig. 6.

Within the past couple of years candidates have been observed [35] for a corresponding $L = 1$ doublet of charmed baryons. These are illustrated on the right-hand side of Fig. 6. The lower-lying candidate, 308 MeV above the Λ_c , decays to $\Sigma_c \pi$, while the higher-lying candidate, 342 MeV above the Λ_c , does not appear to decay to $\Sigma_c \pi$, but rather to $\Lambda_c \pi \pi$. This pattern can be understood [36] if the lower candidate has $J^P = 1/2^-$ and the higher has $J^P = 3/2^+$. The lower state can decay to $\Sigma_c \pi$ via an S-wave, while the higher one would have to decay to $\Sigma_c \pi$ via a D-wave. It would have no trouble decaying to $\Sigma_c^* \pi$ via an S-wave, however. The predicted Σ_c^* , with $J^P = 3/2^+$, has not yet been identified.

The spin-weighted average of the excited Λ_c states is 331 MeV above the Λ_c , a slightly smaller excitation energy than that in the Λ system. The difference is easily understood in terms of reduced-mass effects. The $L \cdot S$ splittings appear to scale with the inverse of the heavy quark (s or c) mass.

The corresponding excited Λ_b states probably lie 300 to 330 MeV above the $\Lambda_b(5630)$, with an $L \cdot S$ splitting of about 10 MeV.

7 Lifetime differences

Charmed particle lifetimes range over a factor of ten, with

$$\tau(\Xi_c^0) < \tau(\Lambda_c) < \tau(\Xi_c) \simeq \tau(D^0) \simeq \tau(D_s) < \tau(D^+) \quad . \quad (7)$$

Effects which contribute to these differences [37] include (a) an overall nonleptonic enhancement from QCD [38], (b) interference when at least two quarks in the final state are the same [39], (c) exchange and annihilation graphs, e.g. in Λ_c and Ξ_c^0 decays [40], and (d) final-state interactions [41].

In the case of B hadrons, theorists estimate that all these effects shrink in importance to less than ten percent [42]. However, since the measured semileptonic branching ratio for B decays of about 10 or 11% differs from theoretical calculations of 13% by some 20%, one could easily expect such differences among different b -flavored hadrons. These could arise, for example, from final-state interaction effects. As mentioned earlier [18], there are many tests for such effects possible in the study of decays of B mesons to pairs of pseudoscalars.

8 Summary

Charmed particles are a rich source of information about what to expect in the physics of particles containing b quarks, in addition to being interesting in their own right.

Some properties of charmed particles are expected to be very close to those of B hadrons, such as excitation energies. Others are magnified in the case of charm, being proportional to some inverse power of the heavy quark mass.

Charmed particles are easier to produce than B hadrons in a hadronic environment (and in photoproduction), and so are a natural area of study for fixed-target experiments such as those being performed and planned at Fermilab. The high-statistics study of charmed particles could have a broad impact on fundamental questions in particle physics.

References

- [1] E. Eichten, this workshop; M. Luke, this workshop.
- [2] L. Wolfenstein, *Phys. Rev. Lett.* 51 (1983) 1945.

- [3] N. Cabibbo, *Phys. Rev. Lett.* **10** (1963) 531.
- [4] M. Kobayashi and T. Maskawa, *Prog. Theor. Phys.* **49** (1973) 652.
- [5] CDF Collaboration, F. Abe *et al.*, Fermilab report FERMILAB-PUB-94-097-E, April, 1994, submitted to *Phys. Rev. D*, and Fermilab report FERMILAB-PUB-94-116-E, May, 1994, to be published in *Phys. Rev. Letters*.
- [6] ARGUS Collaboration, H. Albrecht *et al.*, *Phys. Lett. B* **192** (1987) 245.
- [7] W. Venus, in *Proceedings of the XVI International Symposium on Lepton and Photon Interactions*, Cornell University, August 10–15, 1993, edited by P. Drell and D. Rubin (New York, AIP, 1994), p. 274.
- [8] A. Buras, M. Jamin, and P. H. Weisz, *Nucl. Phys. B* **347** (1990) 491.
- [9] G. Harris and J. L. Rosner, *Phys. Rev. D* **45** (1992) 946.
- [10] J. L. Rosner, Enrico Fermi Institute report 93-62, to be published in *B Decays*, edited by S. Stone (World Scientific, Singapore, 1994).
- [11] A. Buras, M. E. Lautenbacher, and G. Ostermaier, Max-Planck-Institut report MPI-PH-94-14, 1994.
- [12] A. Ali and D. London, CERN report CERN-Th.7248/94, May, 1994, submitted to *Phys. Lett. B*.
- [13] S. Stone, in *Heavy Flavours*, ed. by A. J. Buras and M. Lindner (World Scientific, River Edge, NJ, 1992).
- [14] D. Aston *et al.*, LASS Collaboration, *Nucl. Phys. B* **296** (1988) 493.
- [15] CLEO Collaboration, M. Selen *et al.*, *Phys. Rev. Lett.* **71** (1993) 1973.
- [16] H. Yamamoto, Harvard University Report No. HUTP-94-A006, 1994 (unpublished).
- [17] Y. Nir and H. R. Quinn, *Phys. Rev. Lett.* **67** (1991) 541; M. Gronau, *Phys. Lett. B* **265** (1991) 389; H. J. Lipkin, Y. Nir, H. R. Quinn and A. E. Snyder, *Phys. Rev. D* **44** (1991) 1454; L. Lavoura, *Mod. Phys. Lett. A* **7** (1992) 1553.
- [18] M. Gronau, J. L. Rosner, and D. London, *Phys. Rev. Lett.* **73** (1994) 21; M. Gronau, O. F. Hernández, D. London, and J. L. Rosner, April, 1994, submitted to *Phys. Rev. D*; O. F. Hernandez, D. London, M. Gronau, and J. L. Rosner, April, 1994, to be published in *Phys. Lett. B*.
- [19] M. Gronau, A. Nippe, and J. L. Rosner, *Phys. Rev. D* **47** (1992) 1988; M. Gronau and J. L. Rosner, in *Proceedings of the Workshop on B Physics at Hadron Accelerators*, Snowmass, Colorado, 21 June – 2 July 1994, ed. by P. McBride and C. S. Mishra, Fermilab report FERMILAB-CONF-93/267 (Fermilab, Batavia, IL, 1993), p. 701; *Phys. Rev. Lett.* **72** (1994) 195; *Phys. Rev. D* **49** (1994) 254.
- [20] S. Nussinov, *Phys. Rev. Lett.* **35** (1975) 1672.
- [21] C. T. Hill, in *Proceedings of the Workshop on B Physics at Hadron Accelerators* (Ref. [19]), p. 127; C. Quigg, *ibid.*, p. 443; E. Eichten, C. T. Hill, and C. Quigg, *Phys. Rev. Lett.* **71** (1994) 4116; Fermilab Reports FERMILAB-CONF-94/117-T, 118-T, papers submitted to the CHARM2000 workshop, June, 1994.
- [22] J. L. Rosner and M. B. Wise, *Phys. Rev. D* **47** (1993) 343.
- [23] WA75 Collaboration, S. Aoki *et al.*, *Prog. Theor. Phys.* **89** (1993) 131.
- [24] CLEO Collaboration, D. Acosta *et al.*, *Phys. Rev. D* **49** (1994) 5690.
- [25] F. Muheim and S. Stone, *Phys. Rev. D* **49** (1994) 3767.
- [26] D. Bortoletto and S. Stone, *Phys. Rev. Lett.* **65** (1990) 2951; J. L. Rosner, *Phys. Rev. D* **42** (1990) 3732.
- [27] Fermilab Proposal P-872, R. Rameika, spokesperson.
- [28] Mark III Collaboration, J. Adler *et al.*, *Phys. Rev. Lett.* **60** (1988) 1375; *ibid.* **63** (1989) 1658(E).
- [29] J. Rosner, *Phys. Rev. D* **47** (1993) 3057.

- [30] J. Rosner, Enrico Fermi Institute Report No. 94-25, presented at PASCOS 94 Conference, Syracuse, NY, May 21, 1994. Proceedings to be published by World Scientific.
- [31] C. W. Bernard, J. N. Labrenz, and A. Soni, *Phys. Rev. D* **49** (1994) 2536.
- [32] See, e.g., P. B. Mackenzie, in *Proceedings of the XVI International Symposium on Lepton and Photon Interactions* (Ref. [7]), p. 634; UKQCD Collaboration, R. M. Baxter *et al.*, *Phys. Rev. D* **49** (1994) 1594; A. S. Kronfeld, in *Proceedings of the Workshop on B Physics at Hadron Accelerators* (Ref. [19]), p. 175; P. B. Mackenzie and A. S. Kronfeld, *Ann. Rev. Nucl. Part. Sci.* **43** (1993) 793.
- [33] E. V. Shuryak, *Nucl. Phys.* **B198** (1982) 83.
- [34] B. Grinstein, *Phys. Rev. Lett.* **71** (1993) 3067.
- [35] ARGUS Collaboration, H. Albrecht *et al.*, *Phys. Lett. B* **317** (1993) 227; CLEO Collaboration, M. Battle *et al.*, Paper No. 303, submitted to XVI International Symposium on Lepton and Photon Interactions (Ref. [7]); J. A. Appel, in *Proceedings of the XVI International Symposium on Lepton and Photon Interactions*, *op. cit.*, p. 568.
- [36] M. Peskin, unpublished.
- [37] M. B. Voloshin and M. A. Shifman, *Zh. Eksp. Teor. Fiz.* **91** (1986) 1180 [*Sov. Phys. - JETP* **64** (1986) 698]; M. A. Shifman, in *Proceeding of the 1987 International Symposium on Lepton and Photon Interactions at High Energies*, Hamburg, 1987, ed. by W. Bartel and R. Rückl (*Nucl. Phys. B, Proc. Suppl.*, vol. 3) (North-Holland, Amsterdam, 1988), p. 289.
- [38] M. K. Gaillard and B. W. Lee, *Phys. Rev. Lett.* **33** (1974) 108; G. Altarelli and L. Maiani, *Phys. Lett.* **52B** (1974) 351; M. K. Gaillard, B. W. Lee, and J. L. Rosner, *Rev. Mod. Phys.* **47** (1975) 277; G. Altarelli, N. Cabibbo, and L. Maiani, *Nucl. Phys.* **B88** (1975) 285.
- [39] See, e.g., Shifman, Ref. [37], and references therein.
- [40] V. Barger, J. P. Leveille, and P. M. Stevenson, *Phys. Rev. Lett.* **44** (1980) 226; S. P. Rosen, *Phys. Rev. Lett.* **44** (1980) 4; M. Bander, D. Silverman, and A. Soni, *ibid.* **44** (1980) 7; H. Fritzsch and P. Minkowski, *Phys. Lett.* **90B** (1980) 455; W. Bernreuther, O. Nachtmann, and B. Stech, *Zeit. Phys. C* **4** (1980) 257.
- [41] H. J. Lipkin, *Phys. Rev. Lett.* **44** (1980) 710; J. F. Donoghue and B. R. Holstein, *Phys. Rev. D* **21** (1980) 1334.
- [42] I. Bigi *et al.*, in *B Decays* (Ref. [10]).

Charm2000 Workshop Summary

R. J. Morrison
U.C.S.B.

I found this to be a very interesting workshop. First we heard proponents for five very different experimental environments for producing and detecting really large samples of charmed events. We heard talks by Jeff Appel and Jim Wiss on Fermilab fixed target results. E687 and E791 have on the order of 100 thousand reconstructed charmed events and future approved experiments expect an order of magnitude more. Then we heard Arne Freyberger and David Besson discuss the beautiful CLEO results and make projections for B factory charm samples at $\sqrt{s} \approx 10$ GeV. Then Walter Toki told us about BES and he and Jose Repond argued for a tau/charm factory at $\sqrt{s} \approx 4$ GeV, the region where charm was first discovered at SPEAR. Joel Butler discussed charm possibilities at the Tevatron collider and Sebastian White discussed a possible scenario at RHIC. It has only been 18 years since Gerson Goldhaber and his MARK I colleagues heroically detected the first charm events, and now we are seriously talking about reconstructed charmed samples of $\approx 10^8$ events produced and detected at five different types of accelerator environments.

I. Some highlights from the data

First I have selected just a few results from the data presented in the talks by Jim Wiss and Arne Freyberger. I focus on charm semileptonic decays.

1. There is now overwhelming confirmation of the result that

$$\frac{\Gamma(D \rightarrow \bar{K}^* l \nu)}{\Gamma(D \rightarrow \bar{K} l \nu)} \approx 0.55.$$

This implies that the axial form factor $A_1(0)$ is smaller than predictions. This is in contrast to the vector form factor $f_+(0)$ measured in decays to the pseudoscalar, which seems to be well predicted by models.

2. The new data also supports the notion that the two main Cabibbo-favored D decays plus an expected 8% for Cabibbo-suppressed D decays saturates the inclusive D semileptonic rate,

$$\Gamma(D \rightarrow \bar{K}^* l \nu) + \Gamma(D \rightarrow \bar{K} l \nu) + C.S. \approx \Gamma(D \rightarrow X l \nu)$$

3. CLEO has good measurements of semileptonic D_s decays to η and η' . They find,

$$\frac{\Gamma(D_s \rightarrow \phi l \nu)}{\Gamma(D_s \rightarrow \eta l \nu) + \Gamma(D_s \rightarrow \eta' l \nu)} \approx \frac{\Gamma(D \rightarrow \bar{K}^* l \nu)}{\Gamma(D \rightarrow \bar{K} l \nu)}.$$

This evidence suggests that the strange and nonstrange semileptonic decays are very similar, as expected, and lends credibility to two separate assumptions which can be used to estimate the D_s branching ratio scale:

- a. The D_s and D semileptonic decay rates to the vector are equal,

$$\Gamma(D_s \rightarrow \phi l \nu) = \Gamma(D \rightarrow \bar{K}^* l \nu),$$

- b. The D_s inclusive rate is equal to that of the nonstrange D's, and as with the nonstrange D's, is saturated by the lowest lying pseudoscalar and vector decays,

$$\Gamma(D_s \rightarrow \phi l \nu) + \Gamma(D_s \rightarrow \eta l \nu) + \Gamma(D_s \rightarrow \eta' l \nu) + C.S. = \Gamma(D \rightarrow X l \nu).$$

Either of these assumptions leads to approximately the estimate,

$$B(D_s \rightarrow \phi \pi) = (4.0 \pm 0.8)\%.$$

In his talk, Walter Toki mentioned that BES is measuring this branching ratio directly, and that BES is seeing very few $D_s \rightarrow \phi\pi$ decays. This could be due either to a low branching ratio or a low production crosssection. If BES measures a branching ratio much below 3%, our nice, consistent picture of D semileptonic decays will be destroyed.

II. Some theoretical issues

It has usually been assumed that HQET is not very useful for charm decays due to the low mass of the final quarks. We saw, however, at this workshop an HQET calculation by Michael Luke of the inclusive D semileptonic rate,

$$\Gamma(D \rightarrow Xe^+ \nu) = \frac{G_F^2 m_c^5}{192\pi^3} \left\{ |V_{cs}|^2 \left[\left(1 - \frac{2\alpha_s(\mu_c)}{3\pi} g\left(\frac{m_s}{m_c}\right) + \frac{\lambda_1}{2m_c^2} \right) f_1\left(\frac{m_s}{m_c}\right) - \frac{g\lambda_2}{2m_c^2} f_2\left(\frac{m_s}{m_c}\right) \right] \right. \\ \left. + |V_{cd}|^2 \left[1 - \frac{2\alpha_s(\mu_c)}{3\pi} g(0) + \frac{\lambda_1 - 9\lambda_2}{2m_c^2} \right] \right\} + \dots ,$$

where λ_1 and λ_2 are parameters related to $1/m^2$ corrections. This is certainly a great theoretical advance. On the other hand it is proportional to the charmed quark mass to the fifth power and we do not have an experimental recipe for determining this mass. Arne Freyberger has just presented the CLEO result,

$B(D^0 \rightarrow Xe \nu) = (6.97 \pm 0.18 \pm 0.30)\%$. In order to approach this precision with a prediction, using the above expression, the charmed quark mass needs to be known to a accuracy of 1%.

Jim Wiss and Arne Freyberger have pointed out that another application of HQET to charm is the prediction of the polarization parameter in the decay, $\Lambda_c \rightarrow \Lambda/\nu$, which agrees very well with the CLEO and ARGUS measurements.

At this workshop we found a growing interest in charmed baryons. Jean-Marc Richard discussed baryons with more than one charmed quark. Isi Dunietz believes that a significant type of B decay has been ignored. This involves the inner spectator diagram where the W couples to $\bar{c}s$ and there are two charmed baryons in the final state. This would explain the low B inclusive semileptonic branching ratio since it enhances the hadronic rate, and it explains the soft Λ_c momentum spectrum. Isi explained how to test his predictions with existing CLEO data and we will soon know whether his excitement is justified.

III. Near future physics

John Cumalat and Jim Russ told us about experiments which will be taking data in the fixed target run starting about Jan. 1996. Experiment E831 is a photoproduction experiment which is an enhanced continuation of the E687 program. Projecting from past experience, they expect to obtain about a million reconstructed charmed events. That is about an order of magnitude beyond the E687 and E791 data samples and will produce a wealth of physics.

E781 will focus on charmed baryons produced with a hyperon beam. The experimental layout is unique in a number of respects. It is very long, providing decay space for very high energy lambda decays. It emphasizes the large x region and it has an on-line vertex trigger. E781 expects to obtain hundreds of thousands of charmed baryon

decays, including more than five thousand Ω_c decays. The expected yields in this experiment are not based on past experience, as for E831, and therefore contain a larger uncertainty, especially since they depend upon the production cross-section at large x . This experiment should greatly improve our knowledge of charmed baryons.

IV. Very high sensitivity charm physics

As we look beyond the next Fermilab fixed target run to the more distant future we must consider the charm physics which will be coming from B factories and that which may be possible with a future very high sensitivity experiment. Roughly we can consider two categories:

A. Very good standard model physics. Here we have a very long list of important topics.

Certainly the semileptonic decays need to be studied with as much precision as possible. The q^2 dependencies of the vector form factors, and the comparisons with the D_s and Cabibbo suppressed form factors, where there is different strangeness in the initial or final state particles, are important issues requiring very high statistics. Charm baryons will be increasingly important. Jonathan Rosner has pointed out the relationship between charm and B physics. The relationship between the Cabibbo-suppressed charm form factors and Charmless semileptonic B decays is very important. The accurate extraction of $|V_{ub}|$ from B semileptonic decays may depend upon the knowledge of the appropriate charm form factors. Double Cabibbo suppressed decays (DCSD) will be very interesting. As pointed out by Ted Liu in his contribution, an understanding of the population of the DCSD Dalitz plot may be useful in observing mixing.

Of course the list of important topics is very long. Charm physics is a very rich subject. Arne Freyberger pointed out that CLEO publishes about twice as many papers on charm as it does on B physics. This will probably continue as long as increasingly useful data samples become available.

B. Nonstandard model Physics. Is there a window in the charm sector for the discovery of really new physics? Perhaps this is the most important issue discussed at the workshop.

Gustavo Burdman addressed the issue of neutral D mixing. In contrast to earlier estimates by Wolfenstein and others that long distance effects may lead to mixing at the 10^{-3} level, he calculates that within the standard model there is no mechanism leading to mixing at a level above about 10^{-8} . It was reported that Wolfenstein and others now agree with this much lower estimate. This means that searches for mixing in the neutral D system are much more important than previously thought, since any positive result means new physics.

We also heard about possibilities for observing CP violation and flavor changing neutral currents. Paul Sheldon presented a very nice review.

The talk by Sandip Pakvasa was especially interesting since he showed that in plausible models observable effects can be seen in the charm sector. For example, he showed that an extra Higgs doublet will lead to D mixing. The D_1 - D_2 mass difference is calculated in terms of two parameters in the model. A large region of this parameter space is not excluded by existing data, allowing for mixing at levels up to the existing upper limit.

V. Experimental issues regarding the search for mixing

In these two days there have been a large number of working groups and I apologize for not being able to report on the work of these groups. I did participate with the mixing group, led by Ted Liu. Since this is one of the key physics issues for high sensitivity charm, I think it is appropriate to discuss some of the mixing experimental issues. This is in the context of a future data sample which may be about one thousand

times larger than that available today. See Jim Wiss's talk for a discussion of the frustrations in setting mixing limits.

The existing limits from Fermilab fixed target experiments E691, E687, and E791, have been set by studying the time dependence of "wrong sign" D^0 decays,

$$I(t) = e^{-t} \left[\frac{r_{mix}}{2} t^2 + t \sqrt{2r_{mix}r_{DCSD}} \cos(\phi) + r_{DCSD} \right],$$

where the proper decay time, t , is measured in D^0 lifetimes, r_{mix} is the fraction of decays in the mode which are mixed, r_{DCSD} is the fraction with the "wrong sign" due to double Cabibbo suppressed decay, and ϕ is the relative phase of the two amplitudes. The particle is tagged initially as a D^0 by using D's from D^{*} 's. The sign of the slow pion from the D^{*} decay identifies the initial D^0 . The signature for mixing is a deviation from an exponential proper time distribution with the lifetime of the D^0 . The sensitivity tends to be at large times due to the factor of t for the interference term and the factor of t^2 for the mixing term.

Ted Liu of CLEO has recently observed the DCSD decay, $D^0 \rightarrow K^+ \pi^-$. This rate is significantly larger than expected, about 1% of $D^0 \rightarrow K^- \pi^+$. The interference term could, in principle, be larger than the pure mixing term but, unfortunately, the relative phase is unknown. The DCSD rates for other modes may be much smaller. Figure 1 shows how the wrong sign proper time distribution might look for the case where r_{mix} is one tenth r_{DCSD} . It can be seen that for extreme relative phases the interference leads to very characteristic proper time distributions. The interference could help in the observation of mixing, but, since the phase is unknown, complicates the setting of mixing upper limits.

There is a nasty background which also has an exponential distribution with the D^0 lifetime. This comes from the background under the mass difference peak due to choosing a wrong slow pion. This wrong pion can have either sign and so leads to wrong identification of the initial character of the D. This background, divided by the right sign signal is,

$$\frac{B}{S} \equiv \left(\frac{1}{S} \frac{dB}{dQ} \right) (2\sigma_Q),$$

where S is the number of right sign signal events, B is the number of background events, Q is the D^{*} -D mass difference and σ_Q is the mass difference resolution. The background

density, $\frac{1}{S} \frac{dB}{dQ}$, is a characteristic of the fragmentation process. It is about 0.001 MeV^{-1}

for CLEO and was about $.004 \text{ MeV}^{-1}$ for E691 using photoproduction. It is probably larger for hadroproduction. This background can be reduced by improving the mass difference resolution. This resolution is dominated by the angle measurement of the slow pion and is typically about 1 MeV. With the silicon vertex detector, CLEO expects to reduce this to about 0.3 MeV. In fixed target experiments it is important to keep the target thin to reduce the multiple scattering of the slow pion. For CLEO this background is about 1/7 the DCSD rate.

There are a number of possible approaches to the search for mixing. One, which eliminates the DCSD issues, uses semileptonic decays where there is no DCSD. One could use the D^{*} trick, with the decay $D^0 \rightarrow K^- l^+ \nu$. In this case the missing neutrino effectively broadens the signal mass difference region. This population is given as a function of the observed $K^- l^+$ mass in figure 2. The region with $K^- l^+$ mass above 1.4 GeV is rich, with about half of the total signal. For these events the neutrino has a low

energy and so the proper decay time can be reasonably well estimated obtaining the Lorentz factor from the ratio of observed momentum over observed mass. Then mixing shows up as a t^2 term in the proper decay time distribution. Unfortunately this region has an effective mass difference width about ten times larger than σ_D , so, very roughly, we expect the random pion background to be about ten times larger than for the hadronic decay described above. With very good vertex resolution this background can be reduced by obtaining the D direction as the line between the primary and decay vertices. In this case the neutrino kinematics are known, but with a quadratic ambiguity. The background will depend upon how well the D direction is measured. It was pointed out in the working group that it is the late decays which matter for mixing, and these are the ones with the best D direction measurements.

One could imagine "enhancing" the D^* tag for either method by also requiring information from the "other" charm in the event. About 20% of the "other" charm decays are semileptonic and are uncontaminated by DCSD. Requiring a lepton from the "other" charm reduces our good event rate by the factor $b_l a_l \epsilon_l$ where b_l is the semileptonic branching ratio, a_l is the acceptance for detecting the lepton from the "other" charmed particle, and ϵ_l is the efficiency for identifying the lepton as a lepton. Assuming that the "other" charm lepton has a substantial impact parameter with respect to the primary vertex, the background is probably now limited by events where a meson from the "other" charm is misidentified as a lepton. Then the background is reduced by the factor $n_m a_m \epsilon_{miss}$ where n_m is the average number of charm decay mesons of the sign opposite to that of the lepton, per charm decay, a_m is the acceptance for a meson from the "other" charm, and ϵ_{miss} is the probability of misidentifying a meson as a lepton. Requiring the lepton from the other charm then improves (or worsens) the experimental signal over root background by the factor,

$$\frac{b_l \epsilon_l a_l}{\sqrt{n_m a_m \epsilon_{miss}}}. \quad \text{The lepton identification efficiency should be about 100\%, the two}$$

acceptances should be about equal, and n_m is about 1.5. Then, very roughly, the

improvement factor is, $b_l \sqrt{\frac{a_l}{1.5 \times \epsilon_{miss}}}$. Since the other charm is usually at low x it may

be hard to obtain a large value for a_l . This method of "boosting the tag" may be useful if the lepton misidentification probability can be kept very small. If the misidentification probability can be made very small it may be necessary to suppress events with multiple charm pairs. The notion of a lepton tag from the "other" D may lead to a very useful trigger for a fixed target experiment.

The question of how to best observe mixing is a very interesting one and one which deserves a much more thorough study. My own guess is that after 30 fb^{-1} a B-factory could observe mixing at the level of 10^{-4} and that a fixed target experiment, with a sensitivity equivalent to 10^8 reconstructed charm decays, might approach 10^{-5} . With a fortunate value for the relative DCSD phase both types of experiments might be more sensitive.

VI. Comparison with B-factories

In order make an unbiased comparison between a possible very high sensitivity fixed target experiment and charm results from a B-factory, I have scaled from results of existing experiments. In the case of fixed target I have scaled from E791, since I assume that to obtain this event rate a hadron beam will be required. In the case of a B-factory I

have scaled from CLEO II. In both cases we can expect substantial improvements in the detector, which I assume roughly cancel in the comparison. The numbers I get for a few modes are given in the following table:

Comparison of numbers of events

Mode	B-factory 30 fb ⁻¹ scaled from CLEO	Charm2000 10 ⁸ reconstructed
$D^{*+} \rightarrow \pi^+ (D^0 \rightarrow K^- \pi^+)$	$4 \cdot 10^4$	$2 \cdot 10^6$
$D^+ \rightarrow K^- \pi^+ \pi^+$		10^7
$D^+ \rightarrow K^- e^+ \nu$	10^4	10^6
$D^0 \rightarrow K^- e^+ \nu$	$5 \cdot 10^5$	$2 \cdot 10^6$
$D^+ \rightarrow \pi^0 e^+ \nu$	500	
$D^0 \rightarrow \pi^- e^+ \nu$		10^5
I_{mix}	$\sim 10^{-4}$	$\sim 10^{-5}$

The table shows some interesting features. CLEO does a bad job with D^+ decays, which are a strong point of fixed target experiments due to the long lifetime. The CLEO silicon detector upgrade and the B-factory vertex detectors should help fix this problem. The B-factories and CLEO will have superb π^0 detection and it may not be sensible for fixed target experiments to try to compete. As a consequence I assume that for Cabibbo suppressed decays the fixed target experiment will focus on detecting charged pions. This will require K rejection at a level of a few tenths of a percent. With the equivalent of 10^8 reconstructed Charm decays, it looks this fixed target experiment has a sensitivity advantage of about a factor of 50 over one year of running at a B-factory.

When could such a run take place at the Fermilab? In the next table we consider the possible Fermilab schedule, and the probable situation at CLEO and the presently approved B-factories. Such a schedule is clearly very speculative and has an error of about 2 years by the year 2003.

One of the reality factors is the very long time between 800 GeV fixed target runs, about 5 years. Another possible comparison is the time averaged Fermilab rate compared with the B-factory rate, considering that there will be three B-factories. Then the sensitivity advantage is $\approx \frac{50}{3 \times 5} = 3$.

VII. Is a high sensitivity charm experiment possible? What is the goal? Design?

Defining a high sensitivity charm experiment as equivalent to 10^8 reconstructed charm decays, is it possible to carry out such an experiment with reasonable resources?

What should be the goal of the experiment? What is the experimental philosophy? What is the design?

I had the sense at this workshop that the pro's who have been making E687 and E791 work, and are producing the physics, feel that this goal is too ambitious. I take their views very seriously. On the other hand we heard a number of very interesting talks about new technologies which could possibly solve some of the problems.

Charm Highlights

1994	1995	1996	1997	1998	1999	2000	2001	2002	2003
E687 pub	E791 pub	E831 E781	Main -	Inj-----	collid- -----	er run -----	Charm 2000 run		Charm 2000 pub
CLEO ~3 fb ⁻¹	CLEO L~ 5 10 ³²		CLEO ∫ L= 15 fb ⁻¹	CLEO III L ~ 10 ³³	SLAC KEK B-fac L~ 3 10 ³³			CLEO 20 fb ⁻¹ SLAC KEK 30 fb ⁻¹ ----- tot 80 fb ⁻¹ per year	B-fac tot ∫ L= 160 fb ⁻¹

Sherwood told us about pixel detectors. I understand that pixel detectors can handle a fluence of 10^{15} tracks per cm². That is about the fluence of a beam with a cross-sectional area of a few cm² which would be necessary to produce this enormous charm sample in a thin target.

Randy Ruchti told us about the very successful cosmic ray tests of the D⁰ fiber tracking system. This might be the solution for a high rate tracking system.

We heard about Diamond detectors from Richard Tesarek, Vertex detectors from Luigi Moroni, Gas microstrips from David Anderson, Particle ID from Eli Rosenberg and Marleigh Sheaff, the WA82/92 vertex trigger from Dario Barberis, ideas about triggers by David Christian.

I found these talks very interesting. For an experiment which can not run before the beginning of the next century we should be seriously looking at new technologies.

What about the experimental arrangement? I detected a very wide range of ideas. Some think in terms of a short experiment like E691, about 16 meters. Others think long, like E781, about 60 meters. Short gives fewer muon decays, long gives more separation of particles and is naturally made of stages. Some think in terms of an open trigger recording vast quantities of data, others want to be selective. There are very different ideas about the target and vertex detector arrangements. Should the beam be tightly focused and pass through holes in detectors or should the beam be spread out in order to have an acceptable fluence as it passes through detector material?

Dan Kaplan presented his ideas for an experimental layout. It was not what I expected and I suspect that many people at this workshop would choose very different arrangements. In contrast to a B-factory, where any group of physicists would invent essentially the same detector, the fixed target environment lends itself to a variety of sensible alternatives, particularly when the goal is not defined. To be viable, there will

eventually have to be a convergence of a substantial number of physicists toward a consistent set of well defined goals, and a single experiment to carry them out.

It seems to me that some very important questions were not really addressed very well in the talks. What is the rate limit for such an experiment? Why 10^8 reconstructed charm events? Is the limit the tracking system? Is it radiation protection? Is it the data acquisition system? The trigger? Could one trigger on a lepton, for example, and get the equivalent of 10^9 reconstructed charm events? Should Charm2000 try to do everything, or should it pick a well defined physics objective, which can not be approached by the B-factories, and do it very well?

The thinking has begun. Perhaps it will lead to a great experiment.

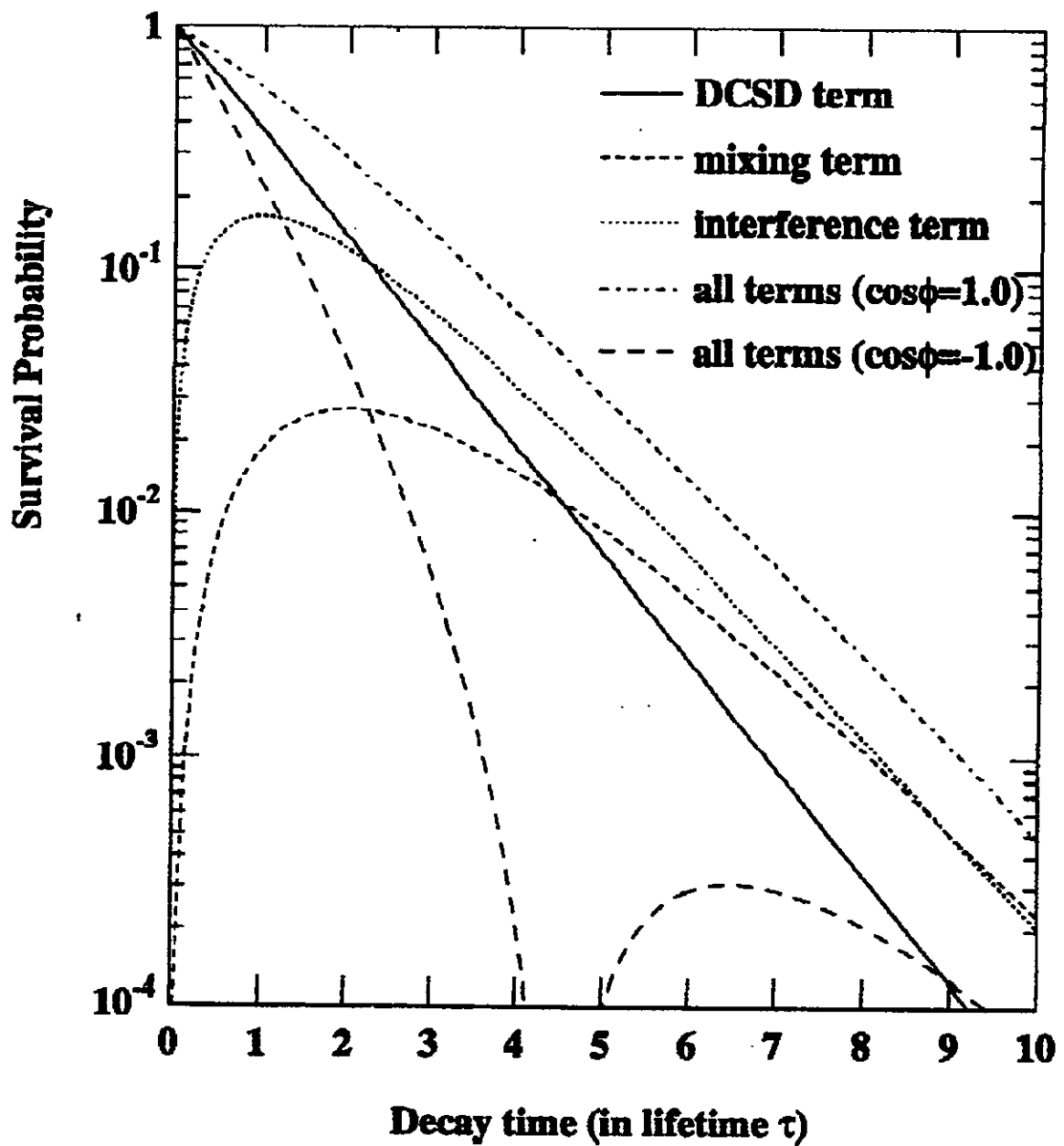


Figure 1. The “wrong sign” proper time distribution including mixing and DCSD. For this plot the mixing rate is assumed to be 0.1 that of DCSD. The interference term is shown with $\cos(\phi) = 1$. The summed distributions show the extreme cases with maximum positive and negative interference.

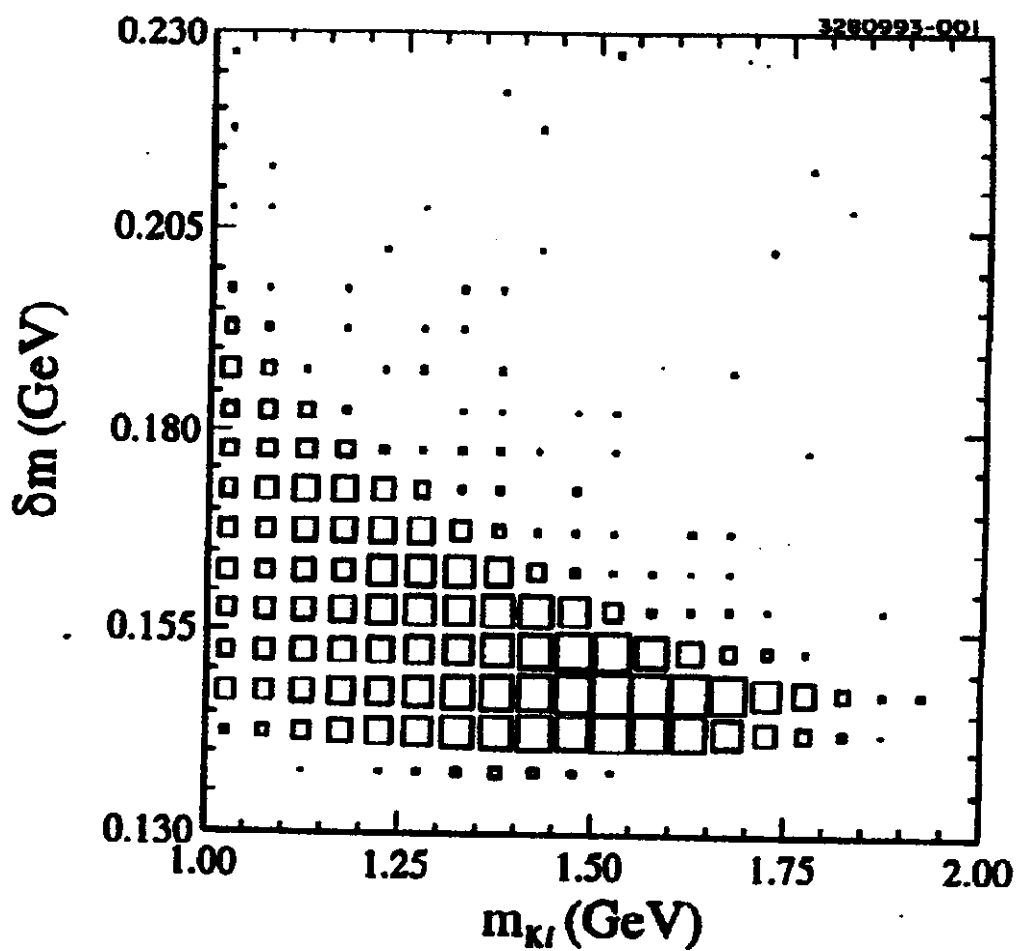


Figure 2. The mass difference vs. mass for $D^{*+} \rightarrow \pi^+ (D^0 \rightarrow K^- l^+ \nu)$ decays. The reconstructed mass is less than the D^0 mass due to the missing neutrino.

2 Contributed Papers

OPEN QUESTIONS IN CHARM DECAYS DESERVING AN ANSWER

I. I. Bigi

TH Division, CERN, CH-1211 GENEVA 23, SWITZERLAND

and

Dept. of Physics, Univ. of Notre Dame du Lac, Notre Dame, IN 46556, U.S.A.

e-mail address: IBIGI@VXCERN, BIGI@UNDHEP.HEP.ND.EDU

CERN-TH.7370/94

July 28, 1994

Abstract

A list is given of those open questions concerning the dynamics of charm decays where there exists a strong need for obtaining an answer. Such a need is based on lessons to be learnt about QCD – either in their own right or for a better understanding of B physics – or on searches for New Physics with a small background from the Standard Model. The major items on this list are: lifetimes of the $\Xi_c^{0,+}$ baryons; semileptonic branching ratios of D_s , Λ_c and Ξ_c hadrons and absolute branching ratios for those states; radiative decays $D \rightarrow \gamma K^*$, $\gamma \rho/\omega$, $D_s \rightarrow \gamma \phi/\omega$, $D \rightarrow l^+ l^- K/K^*$; $D^0 - \bar{D}^0$ oscillations down to a sensitivity below 10^{-4} and CP asymmetries in nonleptonic D decays down to 0.1 %. Ongoing and already approved experiments will produce important new insights, yet are unlikely to provide sufficient answers to all of these questions. It is discussed how a third-generation fixed-target experiment like CHARM2000 or a τ -charm factory can fill the bill.

One can always raise further issues about a physical system. Yet the mere fact that some questions still wait for an answer does not mean there exists any real need for obtaining those answers. My discussion will therefore proceed in three steps: first I will list those open questions concerning the physics of charm decays that in my judgement strongly deserve an answer; next I will try to anticipate which of those will be answered to which degree in on-going or already approved experiments including those at the asymmetric B factories; in the final step I will attempt to evaluate to which degree new initiatives like a new generation fixed target experiment – as envisioned by CHARM2000 – or a tau-charm factory can make significant new contributions.

In passing I would like to note that intriguing open questions remain also concerning charm production, like the nature of leading particle effects, the size of associated (i.e., $\Lambda_c \bar{D}$) production and of diffractive charm production, the specifics of charm-anticharm correlations etc. However I will not address them in this note.

1 Worthy Open Questions in Charm Decays

According to the Standard Model (SM) charm decays constitute a decidedly dull affair: The relevant KM parameters $V(cs)$ and $V(cd)$ are well known; for the smallness of $|V(cb)|$ and $|V(ub)|$ constrains $V(cs)$ and $V(cd)$ very tightly through KM unitarity. Slow $D^0 - \bar{D}^0$ oscillations, small CP asymmetries and tiny branching ratios for rare decays are expected.

This is actually the Pessimist's perspective; the Optimist will look at these statements and re-interpret them in a constructive way:

- Because $V(cs)$ and $V(cd)$ are well-known *a priori*, one can employ charm decays to study the workings of QCD in a novel environment under *controlled* laboratory conditions.
- Precisely because the SM promises us no drama in charm decays, one can conduct searches for $D^0 - \bar{D}^0$ oscillations, CP violation and rare charm decays as probes for New Physics (NP) with an almost zero background from the SM.
- In addition it appears now that these phenomena might become observable at the new facilities, even if they occur only at the level of the SM expectations.

Let me first summarize our present understanding of charm decays:

1.1 Lifetimes

While most predictions of charm lifetimes have historically turned out to be embarrassing for theory (or at least for the authors involved), postdictions have done much better. While this is not very surprising, it represents a non-trivial success, if it is based on a systematic and self-consistent treatment. Heavy Quark Expansions (HQE) provide us with such a framework. To be sensitive to lifetime differences among charm *mesons*, one has to go to order $1/m_c^3$. In the table below I have juxtaposed the 'Predictions' for the lifetime ratios [1, 2] with present data:

	QCD($1/m_c$ expansion)	Data
$\tau(D^+)/\tau(D^0)$	~ 2 (mainly due to <i>destructive</i> interference)	2.50 ± 0.05
$\tau(D_s)/\tau(D^0)$	$1 \pm \text{few} \times 0.01$	1.13 ± 0.05
$\tau(\Lambda_c)/\tau(D^0)$	~ 0.5	0.51 ± 0.05

In evaluating the theoretical entries in this table one has to keep in mind that the theoretical error is estimated to be around 30%; the observed value for $\tau(D^+)/\tau(D^0)$ is thus reproduced within the expected errors.

Lifetimes for charm-strange baryons have been measured as well, yet with quite unsatisfactory errors, as listed in the table below:

	QCD($1/m_c$ expansion)+ quark models [2]	Data
$\tau(\Xi_c^+)/\tau(\Lambda_c)$	~ 1.3	2.0 ± 0.7
$\tau(\Xi_c^+)/\tau(\Xi_c^0)$	~ 2.8	4.0 ± 1.5

Considering that m_c represents at best a moderately large expansion parameter, the agreement between theoretical expectations and present data is better than could have been anticipated. I can identify a need for improved experimental accuracy only in two respects: (i) Present data on the lifetimes of $\Xi_c^{0,+}$ baryons clearly leave something to be desired. A 10% accuracy on $\tau(\Xi_c^{0,+})$ represents an appropriate goal; a similar measurement of $\tau(\Omega_c)$ would be neat. Such data would provide us with valuable cross checks of the $1/m_c$ expansion for baryon decays, yield indirect information on terms of higher order in $1/m_c$ not yet computed, and allow us to make numerically meaningful extrapolations to beauty baryon lifetimes. (ii) Measuring the ratio $\tau(D_s)/\tau(D^0)$ with $\sim 1\%$ precision would provide us with a rather sensitive gauge for the impact of ‘weak annihilation’ (WA) in charm decays and for the weight of $SU(3)_{FI}$ breaking.

1.2 Semileptonic Decays of Charm Hadrons

Somewhat dated measurements have yielded

$$b_{SL}(D^+) \equiv BR(D^+ \rightarrow e^+ X) = 17.2 \pm 1.9\% \quad (1)$$

$$b_{SL}(D^0) \equiv BR(D^0 \rightarrow e^+ X) = 7.7 \pm 1.2\% \quad (2)$$

Their ratio is consistent with the observed $D^+ - D^0$ lifetime ratio. The absolute numbers are also reproduced reasonably well in the $1/m_c$ expansion [3].

$BR(D_s \rightarrow lX)$ has not been measured yet (only constrained), nor have $BR(\Xi_c^{0,+} \rightarrow lX)$; I also remain unconvinced that $BR(\Lambda_c \rightarrow lX)$ has truly been measured. It should be noted that while $\Gamma(D^+ \rightarrow lX_s) = \Gamma(D^0 \rightarrow lX_s)$ holds due to isospin invariance, no symmetry argument can be invoked for $\Gamma(\Lambda_c \rightarrow lX_s)$ vs. $\Gamma(D^0 \rightarrow lX_s)$; in the $1/m_c$ expansion one actually finds $\Gamma_{SL}(\Lambda_c) \sim (0.85 - 0.9) \times \Gamma_{SL}(D)$ through order $1/m_c^2$.

The lepton energy spectra have been measured in inclusive D decays, but not with a high degree of accuracy; the Cabibbo suppressed $c \rightarrow d$ transitions have not been identified there yet. Exclusive decays like $D \rightarrow l\nu K/K^*$ have been studied and $D^0 \rightarrow l\nu\pi$ been seen.

Yet the overall database is highly unsatisfactory and calls out for a significant improvement. The insights to be gained from it concerning the workings of QCD would be valuable not only in their own right, but would be a great asset in understanding the weak decays of beauty hadrons in general and in extracting $|V(cb)|$ and $|V(ub)|$ in particular. To be more specific: (i) The semileptonic widths of D , D_s , Λ_c and preferably Ξ_c should be measured with at least 5% accuracy. Comparing them with each other and the corresponding nonleptonic widths will illuminate the impact of WA. (ii) The observed value of $\Gamma_{SL}(D)$ yields an important calibration point for understanding the semileptonic width of B mesons as a function of

$|V(cb)|$. (iii) Analysing the lepton *spectra* in inclusive semileptonic decays separately of D^0 , D^+ and D_s mesons, in particular in the endpoint region, will provide us with rather direct information on the weight of WA and other hadronization effects.

1.3 Absolute Branching Ratios

Absolute branching ratios for D^0 and D^+ decays have been determined with 5-10% accuracy. Nothing is known in this respect about Ξ_c and precious little about Λ_c decays. Reviewing events over the last two years I feel little confidence that the absolute branching ratios for D_s decays are known to better than 30% – if even that.

I regard this situation as truly embarrassing, since the absolute charm branching ratios constitute an important ‘engineering input’ in beauty physics. The uncertainties in the charm branching ratios are emerging as the limiting factor in determining the branching ratios of beauty decays like $B \rightarrow l\nu D^{(*)}$, $B_s \rightarrow l\nu D_s^{(*)}$ and $\Lambda_b \rightarrow l\nu \Lambda_c$ with obvious consequences for extracting a numerical value for $|V(cb)|$. Any analysis of the charm content in B decays depends on the absolute branching ratios of charm hadrons, and any claim of a ‘charm deficit’ is therefore severely compromised by our ignorance in that respect.

1.4 Rare Decays

An observation of D^+ , $D_s^+ \rightarrow \mu^+\nu$, $\tau^+\nu$ will allow a reliable extraction of the values for the decay constants f_D and f_{D_s} . A battery of theoretical estimates clusters around [4]

$$f_D \sim 200 \pm 30 \text{ MeV}, f_{D_s} \sim 200 \pm 30 \text{ MeV}, f_{D_s}/f_D \simeq 1.15 - 1.2 \quad (3)$$

The Mark III upper bound on $D^+ \rightarrow \mu^+\nu$ yields $f_D \leq 290 \text{ MeV}$ at 90% C.L. Recent studies by CLEO and WA 75 on $D_s \rightarrow \mu^+\nu$ yield $f_{D_s} = 344 \pm 37 \pm 52 \pm 42 \text{ MeV}$ [5] (for $BR(D_s \rightarrow \phi\pi) = 3.7\%$) and $f_{D_s} = 232 \pm 45 \pm 20 \pm 48 \text{ MeV}$ [6], respectively. I view these as pilot studies establishing in principle that such decays can be observed and measured not only at $D\bar{D}$ threshold.

The occurrence of radiative decays like $D \rightarrow \gamma K^*$, $\gamma\rho/\omega$; $D_s \rightarrow \gamma\phi$, $\gamma\rho/\omega$ *per se* would not be remarkable theoretically since they can proceed via WA coupled with photon emission off the initial light antiquark line. Yet their observation would serve an important ulterior motive. For it has been suggested [7] that the KM parameter $|V(td)|$ can be extracted from exclusive radiative B decays: $BR(B \rightarrow \gamma\rho/\omega)/BR(B \rightarrow \gamma K^*) \simeq |V(td)|^2/|V(ts)|^2$. This is based on the assumption that both radiative transitions are dominated by the electromagnetic penguin operator. There is however a fly in the ointment for this interesting suggestion: WA coupled with photon emission also generates $B \rightarrow \gamma\rho/\omega$ transitions and this WA contribution is independent of $|V(td)|$ and estimated to be roughly comparable in size to the penguin contribution ¹! Ignoring such a contribution would lead to the extraction of an incorrect number for $|V(td)|$. Radiative charm decays on the other hand do not receive any

¹WA also contributes to $B^- \rightarrow \gamma K^{*-}$, but that can be neglected.

significant contributions from penguin operators, only from WA. Measuring $BR(D \rightarrow \gamma K^*)$ and $BR(D \rightarrow \gamma \rho/\omega)$ will provide us with an important calibration for gauging the impact of WA on $B \rightarrow \gamma \rho/\omega$. As a rough estimate one expects $BR(D \rightarrow \gamma K^*) \sim 10^{-5} - 10^{-4}$ and $BR(D \rightarrow \gamma \rho/\omega) \sim 10^{-6} - 10^{-5}$ [8].

There is actually a nice bonus to be found in measuring these charm decays: New Physics can generate $c \rightarrow u\gamma$ transitions leading to $D \rightarrow \gamma \rho/\omega$, but not to $D \rightarrow \gamma K^*$. Observing

$$\frac{BR(D \rightarrow \gamma \rho/\omega)}{BR(D \rightarrow \gamma K^*)} \neq \tan^2 \theta_c \quad (4)$$

would then signal the intervention of NP, of which non-minimal SUSY is one relevant example [9]!

1.5 $D^0 - \bar{D}^0$ Oscillations

According to the SM the rate for $D^0 - \bar{D}^0$ oscillations is quite slow, namely

$$r_D \equiv \frac{\Gamma(D^0 \rightarrow l^- X)}{\Gamma(D^0 \rightarrow l^+ X)} \sim \mathcal{O}(10^{-4}) \quad (5)$$

$D^0 - \bar{D}^0$ transitions are driven by long-distance dynamics within SM; the prediction stated in Eq. 5 therefore suffers from considerable numerical uncertainties. The best available experimental bound comes from E691:

$$r_D \leq 3.7 \times 10^{-3} \text{ (90\% C.L.)}. \quad (6)$$

There is nothing intrinsically preventing NP to intervene at this level; i.e. a measurement with improved sensitivity could reveal a positive signal. Observing a non-vanishing value for r_D between 10^{-4} and 10^{-3} would at present not constitute irrefutable evidence for NP, considering the uncertainties in the SM prediction. There is some hope that those can be reduced in the future, partly through theoretical efforts and partly through more precise and comprehensive data on $D^0 \rightarrow K^+ K^-, \pi^+ \pi^-, K^0 \bar{K}^0, \pi^0 \pi^0, \pi^- K^+, K \bar{K} \pi, 3\pi, K \bar{K} \pi \pi, 4\pi$ modes. For a more reliable estimate of $\Gamma(D^0 \rightarrow \bar{D}^0)$ can be obtained from a dispersion relation involving the measured branching ratios for the channels common to D^0 and \bar{D}^0 decays.

1.6 CP Violation in Charm Decays

CP asymmetries of very different forms and shapes can arise in charm decays: they can involve $D^0 - \bar{D}^0$ oscillations or represent direct CP violation; in the latter case they can refer to decay widths or to final state distributions like T odd correlations in $D \rightarrow K \bar{K} \pi \pi$ modes.

1.6.1 Direct CP Violation

Since direct CP asymmetries require the interference of two different weak amplitudes with different strong phases, one has the best (and within the SM only) chance to observe such an effect in Cabibbo suppressed charm decays like $D^0 \rightarrow K^+ K^-, \pi^+ \pi^-$; $D^+ \rightarrow$

$K^+K^-\pi^+$, $\phi\pi^+$. No CP asymmetry has been observed yet, with the best bounds so far coming from E687:

Decay Mode	Measured Asymmetry	90% C.L. Limit
$D^0 \rightarrow K^+K^-$	0.024 ± 0.084	$-11\% < A_{CP} < 16\%$
$D^+ \rightarrow K^-K^+\pi^+$	-0.031 ± 0.068	$-14\% < A_{CP} < 8.1\%$
$D^+ \rightarrow \bar{K}^{*0}K^+$	-0.12 ± 0.13	$-33\% < A_{CP} < 9.4\%$
$D^+ \rightarrow \phi\pi^+$	0.066 ± 0.086	$-7.5\% < A_{CP} < 21\%$

The requirement to encounter strong final state interactions does not pose any problem in principle since charm decays proceed in the resonance region below 2 GeV; yet at the same time it introduces an element of considerable numerical uncertainty into the predictions. A rough estimate suggests that within the SM direct CP asymmetries could be as ‘large’ as $\mathcal{O}(10^{-3})$ [10, 11]. Fitting a set of quark diagrams to describe a host of nonleptonic two-body modes of D mesons leads to a quite similar conclusion [12]. It is not inconceivable that NP could enhance these asymmetries somewhat, say to the 1% level.

Larger effects could surface in the Dalitz plots for $D \rightarrow K\bar{K}\pi$, 3π or in T odd correlations, like for example $\langle \vec{p}_{\pi^\pm} \cdot (\vec{p}_{K^+} \times \vec{p}_{K^-}) \rangle$ in $D^\pm \rightarrow K^+K^-\pi^\pm\pi^0$.

1.6.2 CP Asymmetries involving $D^0 - \bar{D}^0$ Oscillations

In the presence of $D^0 - \bar{D}^0$ oscillations and for a channel f common to D^0 and \bar{D}^0 decays, the required interference can occur between the amplitudes for $D^0 \rightarrow f$ and $\bar{D}^0 \rightarrow f$. Examples for such final states are $f = K^+K^-$, $\pi^+\pi^-$, $K_s\pi^0$, $K_S\omega$, $K_S\eta$. Ignoring the possibility of direct CP violation one writes down:

$$\begin{aligned}\Gamma(D^0 \rightarrow f; t) &= e^{-\Gamma_D t} |T(D^0 \rightarrow f)|^2 (1 - \text{Im} \frac{q}{p} \bar{\rho}_f \sin \Delta m_D t) \\ \Gamma(\bar{D}^0 \rightarrow f; t) &= e^{-\Gamma_D t} |T(\bar{D}^0 \rightarrow f)|^2 (1 + \text{Im} \frac{q}{p} \bar{\rho}_f \sin \Delta m_D t)\end{aligned}\quad (7)$$

with $\bar{\rho}_f = T(\bar{D}^0 \rightarrow f)/T(D^0 \rightarrow f)$ denoting the ratio of decay amplitudes and q/p reflecting $D^0 - \bar{D}^0$ oscillations. Three observations should be noted here [13]:

(i) While this CP asymmetry becomes unobservable for $\Delta m_D = 0$, it actually is proportional to $\Delta m_D/\Gamma_D$ for small values of Δm_D . The quantity r_D , introduced in eq. 5, on the other hand is given by $\frac{1}{2}(\Delta m_D/\Gamma_D)^2$. (For simplicity I ignore $\Delta\Gamma_D$ effects although within the SM one expects very roughly $\Delta\Gamma \sim \mathcal{O}(\Delta m_D)$.) Thus the experimental bound on r_D translates into $\Delta m_D \leq 0.09 \cdot \Gamma_D$ and the CP asymmetry

$$A_{CP}^f \equiv \frac{\Gamma(\bar{D}^0 \rightarrow f; t) - \Gamma(D^0 \rightarrow f; t)}{\Gamma(\bar{D}^0 \rightarrow f; t) + \Gamma(D^0 \rightarrow f; t)} \simeq \frac{\Delta m_D}{\Gamma_D} \frac{t}{\tau_D} \text{Im} \frac{q}{p} \bar{\rho}_f \quad (8)$$

could still reach values of several per cent!

(ii) No such luck arises in the SM: for reasons that are quite specific to it, one finds $\Delta m_D \sim \mathcal{O}(0.01)\Gamma_D$ and $Im(q/p)\bar{\rho} \sim \mathcal{O}(10^{-3})$; i.e. the size predicted by the SM for these kinds of asymmetry is presumably too small to be observable.

(iii) Accordingly one should vigorously search for CP asymmetries involving $D^0 - \bar{D}^0$ oscillations: their dependance on the (proper) time of decay provides a striking experimental signature; observing them – as defined in eq. 8 – with a size of 10^{-3} or above constitutes a clear sign for the intervention of NP.

Hence we arrive at the following benchmarks concerning future studies of CP violation: one should aim for achieving a 10^{-3} sensitivity for CP asymmetries involving $D^0 - \bar{D}^0$ oscillations as well as for direct CP violation. Observation of an effect unequivocally signals the presence of NP in the former case, but not necessarily in the latter.

2 Answers Expected To Be Obtained by Existing or Approved Experiments

Over the next four years I expect important new data to come from experiments at FNAL, CERN, Beijing and Cornell. Five years from now the asymmetric B factories at KEK and SLAC will start to contribute. I anticipate the most significant new information in the following areas:

- (i) A more precise determination of $\tau(D_s)$ and the first fully quantitative measurement of $\tau(\Xi_c^{+,0})$.
- (ii) The first measurement of $BR(D_s \rightarrow l + X)$ and studies of the *inclusive* lepton spectrum in semileptonic D_s decays; the first *direct* determination of $BR(D_s \rightarrow \phi\pi)$.
- (iii) Extracting the *absolute* values of $BR(D \rightarrow K\pi, K\pi\pi)$ to better than 5%.
- (iv) Possibly a measurement of *absolute* Λ_c branching ratios via a $\Sigma_c \rightarrow \Lambda_c\pi$ tag.
- (v) The first quantitative extraction of f_D and f_{D_s} from $D, D_s \rightarrow \mu\nu$.
- (vi) Mapping out the doubly Cabibbo suppressed D and D_s decays.
- (vii) A rather comprehensive analysis of Cabibbo favoured and once Cabibbo suppressed D, D_s and possibly Λ_c decays.
- (viii) Detailed studies of exclusive semileptonic decays $D \rightarrow l\nu K/K^*/\pi/\rho, D_s \rightarrow l\nu\eta/\phi/K/K^*$ and $\Lambda_c \rightarrow l\nu\Lambda/\Sigma$ with the dependance of the formfactors on the momentum transfers measured rather than assumed.
- (ix) Probing $D^0 - \bar{D}^0$ oscillations down to $\tau_D \sim 10^{-4}$ and CP asymmetries down to a few per cent.

All these anticipated data will certainly deepen our understanding of the hadrodynamics driving charm decays:

- (a) Applying a comprehensive BSW-type analysis of the two-body modes of D and D_s mesons (and preferably of Λ_c baryons as well) *separately* to Cabibbo allowed, once and twice

suppressed decays will undoubtedly reveal a clear deviations from the predictions based on factorization, presumably with a definite pattern. It will also help us to arrive at better estimates of $\Delta m_D|_{SM}$, and it will sharpen our understanding of where we can expect the largest direct CP asymmetries, and what size they can reach within the SM.

(b) It will be immensely instructive to compare detailed data on exclusive semileptonic D , D_s and Λ_c decays with predictions obtained in particular through simulations of QCD on the lattice.

(c) The improved accuracy in the measurements of $\tau(D_s)$ and $\tau(\Xi_c^{0,+})$ will provide us with a handle to arrive at a quantitative understanding of charm lifetimes and at the same time with a gauge from which to extrapolate to $\tau(B_s)$, $\tau(\Lambda_b)$ and $\tau(\Xi_b)$.

(d) Observing $D^0 - \bar{D}^0$ oscillations and/or CP violation would represent a major discovery; its ramifications would of course depend on the numerical size of the effect.

Yet despite all this progress major tasks will remain unaddressed or at least unfinished:

(i) A $\sim 5\%$ measurement of $\tau(\Omega_c)$ would be quite helpful, although this is not the major item among the unfulfilled tasks. (ii) I find it doubtful that the *absolute* branching ratios for D_s , Λ_c or Ξ_c decays will have been determined within even 10%. (iii) Likewise, f_D and f_{D_s} will not have been measured to better than 20% or so. (iv) Nothing useful will be known about the radiative decays $D \rightarrow \gamma K^*/\rho/\omega$, $D_s \rightarrow \gamma \phi/\rho/\omega$. (v) The accuracy will still be unsatisfactory with which the total semileptonic widths will be known for D , D_s and Λ_c , let alone for Ξ_c ; likewise for the *inclusive* lepton spectra.

At first sight, this list might appear like a rather pitiful collection of small morcels having falling off the main table. In particular, I have already implied that I expect all two-body channels of D and D_s mesons to have been measured with sufficient accuracy and detail, i.e. including modes with one or two neutrals. Yet I would like to state quite emphatically that the list above represents very major unresolved problems using the criteria given in the introduction:

- Weak decays of charm hadrons constitute a microscope to study the strong interaction effects crucial for a full understanding and thus exploitation of beauty decays.
- Charm decays provide a rather clean lab to search for manifestations of NP in rare D decays, $D^0 - \bar{D}^0$ oscillations and CP violation.

These two aspects will not have been treated with the ‘ultimate’ sensitivity. I therefore conclude: in all likelihood there will remain a strong and identifiable need for another major new initiative for studies of charm decays to understand hadronization effects down to the level of the QCD ‘noise’ and to probe for NP down to the SM ‘noise’ – or to better understand a signal that has emerged!

3 New Initiatives for The Next Millenium

I will attempt to evaluate the potential of two complementary facilities to provide the ‘final’ answers in the physics of charm decays, namely CHARM2000 on one hand and a τ -charm factory on the other.

3.1 CHARM2000

A next-generation experiment based on fixed-target production of charm will be able to do a superb job in measuring the *relative* branching ratios of a host of exclusive nonleptonic channels in D , D_s , Λ_c and Ξ_c accurately. I am however not convinced at all that our understanding of charm decays would improve in proportion, since I am skeptical that the theoretical ‘noise’, i.e. the irreducible uncertainties, will drop to the per cent level. I should add one caveat, though: I could see a meaningful progress to emanate from CHARM2000 measurements of (quasi-)two-body modes if previous experiments – contrary to my expectations stated above – had failed to measure channels containing two neutrals in the final state with decent accuracy.

In my opinion there are then five main challenges against which the significance and the merits of CHARM2000 can be judged:

- (1) The lifetimes of Ξ_c and preferably also of Ω_c baryons should be measured with an accuracy of at least 5%.
- (2) The decay constants f_D and f_{D_s} should be extracted from D , $D_s \rightarrow \mu\nu$ to within 10%.
- (3) CHARM2000 would again have the statistical muscle to observe the radiative decays $D \rightarrow \gamma K^*/\rho/\omega$, $D_s \rightarrow \gamma \phi/\rho/\omega$ (and also $D \rightarrow l^+l^- K/K^*/\rho/\omega$ etc.) at the transition rate expected for them. The question is whether backgrounds like $D \rightarrow \pi^0 K^* \rightarrow \gamma[\gamma] K^*$ can be controlled.
- (4) Can *absolute* branching ratios be determined to within $\sim 1 - 2\%$ for D , within $\sim 5\%$ for D_s and within $\sim 10\%$ for Λ_c decays? The strong decay $D^* \rightarrow D\pi$ can be used for calibrating the D branching ratios; for the other charm hadrons new calibration methods have to be pioneered, like $\Sigma_c \rightarrow \Lambda_c \pi$.
- (5) Can $D^0 - \bar{D}^0$ oscillations be probed down to $r_d \sim 10^{-5}$ which almost certainly should reveal a positive signal? Even more crucially, can systematics be controlled to such a degree that a comprehensive search for CP asymmetries involving $D^0 - \bar{D}^0$ oscillations and direct CP violation can be undertaken with a sensitivity for 10^{-3} or even smaller?

There is another aspect to be briefly mentioned, not – in all fairness – as a formal challenge, but rather as a potential bonus of quite significant weight: (i) Can the inclusive semileptonic widths of the different charm hadrons be measured with, say, 5% accuracy?

(ii) Can the lepton energy spectra in inclusive semileptonic charm hadron decays be measured with an accuracy that allows to extract the value of $|V(cd)|$ from the endpoint region?

3.2 τ -Charm Factory

The capabilities of a τ -charm factory are quite complementary to those of CHARM2000. Clearly charm lifetimes cannot be measured directly. What can be done – and can be done quite well – is to measure semileptonic branching ratios. For the isospin partner D^+ and D^0 one has: $\tau(D^+)/\tau(D^0) \simeq BR_{SL}(D^+)/BR_{SL}(D^0)$. Yet such a relation does not hold in general for all hadrons; in particular one expects $\tau(\Lambda_c)/\tau(D^0) \neq BR_{SL}(\Lambda_c)/BR_{SL}(D^0)$. Using tagged decays one can determine the *absolute* branching ratios of the various charm hadrons in a clean way. The lepton energy *spectra* in inclusive semileptonic decays both of mesons and of baryons can be studied quite well. Employing beam energy constraints should allow one to measure radiative charm decays like $D \rightarrow \gamma K^*/\rho/\omega$ rather reliably. Relying on quantum mechanical EPR-like correlations one can probe for $D^0 - \bar{D}^0$ oscillations, CP asymmetries involving them and direct CP violation [10].

While all of this appears feasible in principle, I see two challenges on a practical level:

- (1) Can τ_D be probed down to values $\sim 10^{-5}$? Even more importantly, can one acquire the sensitivity to search for $\sim 10^{-3}$ CP asymmetries?
- (2) The clean environment at a τ -charm factory has its price: very little charm physics can be done ‘parasitically’; i.e., D , D_s , Λ_c and Ξ_c decays have to be studied at different beam energies corresponding to $D\bar{D}$, $D^*\bar{D}/D\bar{D}^*$, $D_s\bar{D}_s$, $\Lambda_c\bar{\Lambda}_c$ and $\Xi_c\bar{\Xi}_c$ final states. The required statistics has then to be accumulated in the rather limited amount of time available at each beam energy – and these beam energies have to span, merely for charm physics, the region from the $D\bar{D}$ threshold up to at least the Λ_c and very preferably the Ξ_c threshold!

4 Summary

There is a strong and well-defined need for another new generation of charm decay experiments, like CHARM2000 and a τ -charm factory. Very specific challenges can be formulated that those projects have to overcome. Since their approaches, strenghts and drawbacks are quite complementary, it would be wonderful if both could be realised.

Acknowledgement: I have learnt a lot from many discussions with my collaborators B. Blok, M. Shifman, N. Uraltsev and A. Vainshtein; I have also benefitted from exchanges with T. Mannel, D. Kaplan, A. Nguyen and P. Sheldon. This work was supported by the National Science Foundation under grant number PHY 92-13313.

References

- [1] I.I. Bigi, N.G. Uraltsev, Phys. Lett. **B280**, 271 (1992); I.I. Bigi, N.G. Uraltsev, Z. Phys. **C62**, 623 (1994).
- [2] B. Blok, M. Shifman, preprint TPI-MINN-93/55-T, Invited talk given at the Third Workshop on the Tau-Charm Factory, Marbella, Spain, June 1993, to appear in the Proceed.
- [3] I.I. Bigi, N.G. Uraltsev, A.I. Vainshtein, Phys. Lett. **B293**, 430 (1992).

- [4] C. Sachrajda, Invited talk given at QCD 94, Montpellier, France, July 1994, to appear in the Proceed.
- [5] CLEO Collab., D. Acosta *et al.*, Phys. Rev. **D49**, 5690 (1994).
- [6] WA75 Collab., S. Aoki *et al.*, Prog. Theor. Phys. **89**, 131 (1993).
- [7] A. Ali
- [8] This observation has been made also by A. Soni, G. Eilam and H.-Y. Cheng.
- [9] I. Bigi, F. Gabbiani, A. Masiero, Z. Phys. **C48**, 633 (1990).
- [10] I.I. Bigi, in: Proceed. of the Tau-Charm Factory Workshop, Stanford, CA, May 1989, ed. by L.V. Beers, SLAC Report, p. 169.
- [11] M. Golden, B. Grinstein, Phys. Lett. **B222**, 501 (1989).
- [12] F. Buccella *et al.*, Phys. Lett. **B302**, 319 (1993).
- [13] I.I. Bigi, A.I. Sanda, Phys. Lett. **B171**, 320 (1986).

Perturbative QCD Fragmentation Functions as a Phenomenological Model for Charm Fragmentation *

Kingman Cheung

Department of Physics, Northwestern University, Evanston, Illinois 60208, U.S.A.

ABSTRACT

The perturbative QCD fragmentation functions, which have recently been calculated to predict the production rates of the heavy-heavy quark bound states (*e.g.*, J/ψ , ψ' , Υ , and B_c) at e^+e^- and hadronic colliders, could be applied phenomenologically as a model for charm and bottom quark fragmentation into heavy-light mesons. The prediction on the observables P_V , $\langle z \rangle$, and $\alpha(z)$ are compared with experimental data.

1. Introduction

It has been well known that the dominant production mechanism for mesons and baryons that contain a single heavy quark is the fragmentation of the heavy quark, in which light quark-antiquark pairs are created out of the vacuum by the color force of the heavy quark and then the heavy quark captures the light quarks to form mesons or baryons. However, in this process, the creation of light quark-antiquark pairs tells us that the nonperturbative effects are important and so the fragmentation function, which describes the process, cannot be calculated from the first principle or from perturbative QCD. But, of course, a lot of model-dependent fragmentation functions are available, *e.g.*, Peterson fragmentation function¹ and Lund fragmentation model.²

On the other hand, for the production of heavy-heavy quark bound states such as η_c , J/ψ , ψ' , Υ , and B_c mesons,³ the importance of fragmentation was not realized until Braaten and Yuan⁴ pointed out that at the large transverse momentum region, fragmentation of the heavy quark and of the gluon is the dominant production mechanism for the heavy-heavy quark bound states. They also emphasize that the production process essentially involves the creation of heavy quark-antiquark pair, which tells us that the natural scale of the process should be of order of the mass of the heavy quark created, and so the process should be calculable by perturbative QCD (PQCD). Subsequently, the fragmentation functions for $g \rightarrow \eta_c$ and J/ψ ,⁴ $c \rightarrow \eta_c$ and J/ψ ,⁵ $c \rightarrow$ polarized J/ψ ,⁶ $\bar{b} \rightarrow B_c$ and B_c^* ,^{7,8} $\bar{b} \rightarrow$ polarized B_c^* ,^{8,9} $g \rightarrow \chi_c$,¹⁰ and $\bar{b} \rightarrow$ P-wave B_c ,^{8,11} were calculated to leading order in strong coupling constant α_s , and v , where v is the typical velocity of the quarks inside the meson.

These fragmentation functions have been applied trivially to predict the branching ratios of the Z boson into the corresponding heavy-quark bound states. Among the bound states, the production of J/ψ , ψ' , χ_c 's, and B_c mesons is of great interest

*A talk given at the QCD group of the "Charm2000 Workshop", Fermilab, Illinois (June 1993).

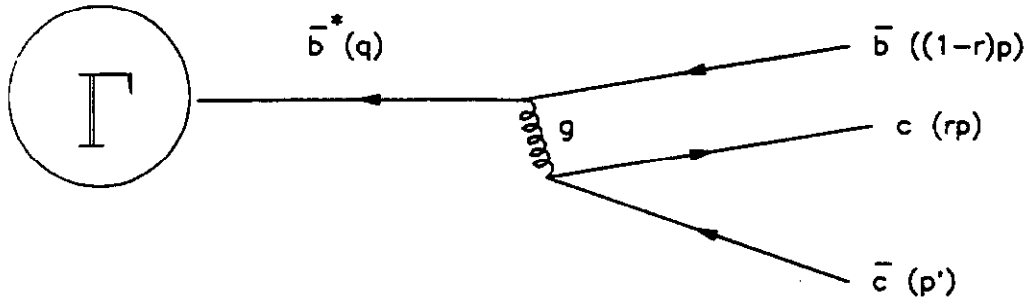


Fig. 1. The lowest order contributing Feynman diagram in axial gauge for the fragmentation of an off-shell \bar{b} antiquark into the B_c meson and \bar{c} antiquark.

to experiments. The production rates and the transverse momentum spectra for J/ψ , ψ' ,¹² and B_c mesons¹³ at hadronic colliders were also calculated by convoluting the corresponding fragmentation functions with the parton cross sections. The J/ψ production by heavy quark fragmentation can, to a great extent, explain the discrepancy between the production by the lowest order mechanism and the experimental measurement at the Tevatron.¹² The B_c meson, which has not been observed but should exist, has been predicted observable at the Tevatron because of the sufficiently large production cross section.¹³ In addition to the application that the PQCD fragmentation functions can successfully predict the production rates of heavy-heavy quark bound states without any model dependence, they can also be applied as a phenomenological model to describe the charm and bottom quark fragmentation into heavy-light mesons,⁹ e.g., $c \rightarrow D, D^*$ and $\bar{b} \rightarrow B, B^*$. Although in the fragmentation of $c \rightarrow D, D^*$ and $\bar{b} \rightarrow B, B^*$, there are probably large nonperturbative and relativistic effects that the PQCD fragmentation functions cannot take into account, these PQCD fragmentation functions can at least provide insights to understand these heavy-light systems. For the rest of the paper, we concentrate on the phenomenological applications of the PQCD fragmentation functions to charm mesons.

2. Perturbative QCD Fragmentation Functions

In this section, we briefly describe the idea of PQCD fragmentation functions with $\bar{b} \rightarrow B_c$ and B_c^* as illustrative examples. All other bound states can be calculated similarly. The lowest order contributing Feynman diagram for the fragmentation of the heavy \bar{b} antiquark is shown in Fig. 1. The bulb represents a short distance process producing a heavy \bar{b} antiquark and Γ denotes the Dirac spinor for producing the \bar{b} antiquark. The fragmentation function for $\bar{b} \rightarrow B_c$ should be independent of Γ , i.e., independent of how the \bar{b} is produced in the short distance process. The fragmentation

function can be calculated from this expression:

$$D_{\bar{b} \rightarrow B_c}(z) = \frac{1}{16\pi^2} \int ds \theta \left(s - \frac{M^2}{z} - \frac{m_c^2}{1-z} \right) \lim_{q_0/m_b \rightarrow \infty} \frac{|\mathcal{M}|^2}{|\mathcal{M}_0|^2} \quad (1)$$

where $M = m_b + m_c$ is the mass of the meson, \mathcal{M} is the amplitude for producing a B_c and \bar{c} from an off-shell \bar{b}^* with virtuality $s = q^2$, where q is the 4-momentum of the \bar{b} antiquark, and \mathcal{M}_0 is the amplitude for producing a \bar{b} with the same 3-momentum \vec{q} . The amplitude \mathcal{M} is evaluated in axial gauge with an auxiliary 4-vector $n^\mu = (1, -\vec{p}/|\vec{p}|)$, where \vec{p} is the 3-momentum of the B_c meson. In this gauge, the dominant contribution arises from the Feynman diagram depicted in Fig. 1. Other diagrams are suppressed by powers of $m_{b,c}/q_0$. In other words, factorization is manifest in this gauge.⁷ Different spin-orbital states of the B_c meson can be obtained by using the corresponding projections. After some algebraic work and integrating over s , we obtain

$$D_{\bar{b} \rightarrow B_c}(z, \mu_0) = N \frac{rz(1-z)^2}{(1-(1-r)z)^6} \left[6 - 18(1-2r)z + (21-74r+68r^2)z^2 - 2(1-r)(6-19r+18r^2)z^3 + 3(1-r)^2(1-2r+2r^2)z^4 \right], \quad (2)$$

for the 1S_0 state, and

$$D_{\bar{b} \rightarrow B_c^*}(z, \mu_0) = 3N \frac{rz(1-z)^2}{(1-(1-r)z)^6} \left[2 - 2(3-2r)z + 3(3-2r+4r^2)z^2 - 2(1-r)(4-r+2r^2)z^3 + (1-r)^2(3-2r+2r^2)z^4 \right], \quad (3)$$

for the first excited 3S_1 state. In the above equations, $N = 2\alpha_s(2m_c)^2|R(0)|^2/(81\pi m_c^3)$ and $r = m_c/(m_b + m_c)$. The results for the longitudinal and transverse B_c^* mesons and the P-wave B_c mesons can be found in Refs.^{9,11} In this case, N is a product of the strong coupling constant $\alpha_s(2m_c)$, the constituent quark masses m_b and m_c , and the wavefunction $|R(0)|$ of the bound state. The constituent quark masses can be determined from other observed quarkonia and the wavefunction can also be determined reliably from potential models.¹⁴ The scale of the strong coupling constant is set to be $2m_c$ – the minimal virtuality of the gluon propagator, and the initial scale μ_0 of the fragmentation functions is set to be $m_b + 2m_c$ – the minimal virtuality of the off-shell \bar{b} antiquark. Since the inputs to these fragmentation functions can be reliably obtained from other sources, they can be used to calculate the production rates and distributions of the mesons at high energy colliders with great predictive power.

3. As a Phenomenological Fragmentation Model

The fragmentation functions in Eqns. (2) and (3) can also be regarded as two-parameter functions with N and r as free parameters. N governs the overall normalization and $r = m_{\text{light}}/m_{\text{meson}}$ is the mass ratio, which is very similar to the parameter ϵ_Q of the Peterson fragmentation function.¹ We vary the parameter r to study the behavior of these fragmentation functions in the limit $r = m_{\text{light}}/m_{\text{meson}} \rightarrow 0$. In other

words, we expect that in this limit, $\tau \rightarrow 0$, these fragmentation functions can describe, to certain extent, the fragmentation of the heavy quark into heavy-light mesons, *e.g.*, $c \rightarrow D, D^*$ and $\bar{b} \rightarrow B, B^*$. Although in the fragmentation processes of $c \rightarrow D, D^*$ and $\bar{b} \rightarrow B, B^*$ there are probably large nonperturbative and relativistic effects that we have not taken into account, our PQCD fragmentation functions with the free parameters N and τ can at least provide some insights to these systems while precise nonperturbative fragmentation functions for charm and bottom are not available yet. These PQCD fragmentation functions as a phenomenological model to describe the charm and bottom quark fragmentation into heavy-light mesons have certain advantages over the previous fragmentation models^{1,2}:

- i. they contain the spin information for different spin-orbital states;
- ii. although the normalization of each fragmentation function is a free parameter, the ratio of the normalizations of different spin-orbital states is determined. For example, the ratio of the normalization of 3S_1 and 1S_0 states can be cancelled before the limit $\tau \rightarrow 0$ is taken;
- iii. our PQCD fragmentation functions are consistent with a general analysis using the methods of Heavy Quark Effective Theory.

Using the techniques of HQET, Jaffe and Randall¹⁵ have recently shown that at the heavy quark mass scale the fragmentation function $D_{Q \rightarrow H}(z)$ for a heavy quark Q to split into a hadron H with a single heavy quark can be expanded as a power series in τ ,

$$D_{Q \rightarrow H}(z) = \frac{a(y)}{\tau} + b(y) + \mathcal{O}(\tau), \quad (4)$$

where $a(y)$ and $b(y)$ are functions of $y = (1 - (1 - \tau)z)/\tau z$ and $\mathcal{O}(\tau)$ denotes all other terms higher order in τ . The leading term $a(y)$ is independent of the heavy quark spin and flavor; while the next-to-leading term $b(y)$ and all higher order terms contain heavy quark spin-flavor symmetry breaking effects. It was verified that our PQCD fragmentation functions can be expressed in this form.^{7,9} In fact, one can show that¹⁶ the leading order terms can be derived by using the Feynman rules of the leading operator in the HQET Lagrangian, while the $\mathcal{O}(\tau^0)$ pieces arise not only from the next-to-leading $(1/M)$ operators but also from the small component of the heavy quark spinor in the HQET.

For the following we concentrate on the charm system. The fragmentation functions for $c \rightarrow D$ and $c \rightarrow D^*$ are given in Eqns. (2) and (3), respectively, with N as a free parameter and $\tau = m_{u,d}/(m_c + m_{u,d})$, where $m_{u,d}$ is the constituent mass of the light quark inside the D and D^* mesons. We look at a few observables: P_V , $\langle z \rangle$, and $\alpha(z)$, and compare with some existing data.

a) P_V for the D and D^* system is defined as

$$P_V = \frac{D^*}{D + D^*}, \quad (5)$$

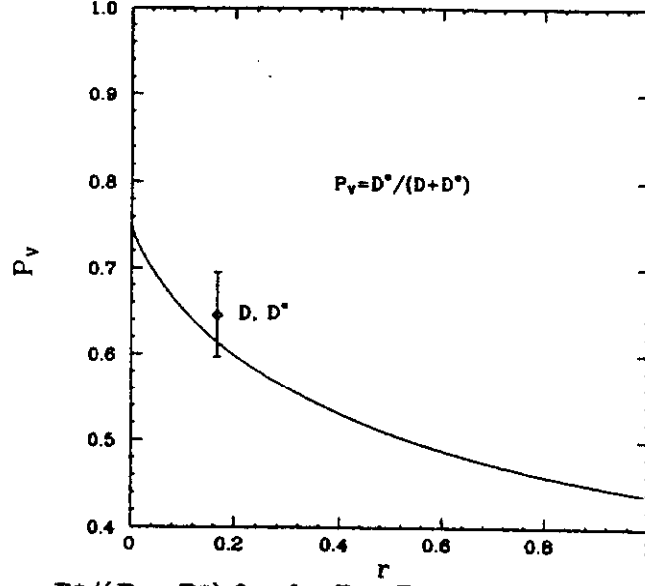


Fig. 2. The ratio $P_V = D^*/(D + D^*)$ for the $D - D^*$ system predicted by the PQCD fragmentation functions, and the comparison with the data.

which is a measure of the relative population of D^* in the production of D and D^* mesons. Since fragmentation is the dominant production mechanism, the production rates of D and D^* in Eqn. (5) can be replaced by the corresponding fragmentation probabilities as

$$P_V = \frac{P_{c \rightarrow D^*}}{P_{c \rightarrow D} + P_{c \rightarrow D^*}}, \quad (6)$$

which is a function of r only. The probabilities $P_{c \rightarrow D}$ and $P_{c \rightarrow D^*}$ can be obtained by integrating $D_{c \rightarrow D}(z)$ and $D_{c \rightarrow D^*}(z)$ over z . The prediction by our fragmentation model is shown in Fig. 2. At $r = 0$, which is the heavy quark mass limit, the ratio $P_V = 0.75$ is exactly the value given by heavy quark spin symmetry. However, the experimental data did not agree well with the heavy quark symmetry prediction of 0.75. A compilation of the data on P_V can be found in Ref.¹⁷ where the updated branching ratio, $B(D^{*+} \rightarrow D^0 \pi^+) = 0.681 \pm 0.016$ is used, and the average $P_V = 0.646 \pm 0.049$. For the charm system we choose $m_c = 1.5$ GeV and the light constituent quark mass $m_{u,d}$ inside the D and D^* mesons to be 0.3 GeV, therefore $r = 0.167$. The experimental data point ($r = 0.167, P_V = 0.646 \pm 0.049$) is also plotted in Fig. 2. We found a very good agreement between the prediction of our fragmentation model and the data. If we choose a smaller value, say 0.2 GeV, for the light constituent quark mass, we could even get a better agreement. The error in P_V certainly allows us to vary the $m_{u,d}$ more than ± 0.15 GeV such that the prediction is still within 1σ from the data point. Or, we can use the experimental value of P_V to extract the parameter r . Physically, $P_V < 0.75$ means that the production rate of D meson is larger than it should be as given by heavy quark spin symmetry, or in other words, D^* is produced less than it should be. This might be due to the hyperfine mass splitting of D and D^* mesons, which can be accounted for by the $\sigma^{\mu\nu} G_{\mu\nu}/M$ term in the HQET Lagrangian.

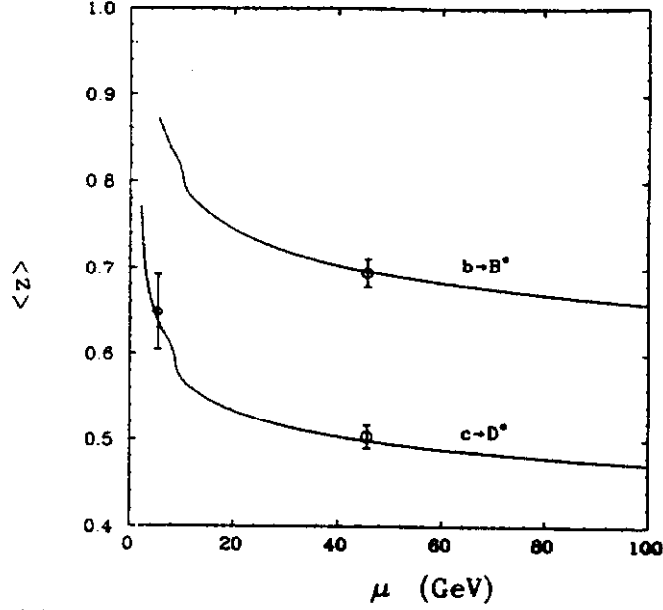


Fig. 3. The average $\langle z \rangle^\mu$ for $c \rightarrow D^*$ and for $b \rightarrow B^*$ fragmentation versus the scale μ . The experimental measurements from LEP ($\mu = m_Z/2$) and CLEO/ARGUS ($\mu = 5.3$ GeV) are also shown.

b) $\langle z \rangle$ is the average longitudinal momentum fraction that is transferred from the heavy quark to the meson. In terms of fragmentation functions, $\langle z \rangle^\mu$ at a scale μ is given by

$$\langle z \rangle_{c \rightarrow D^*}^\mu = \frac{\int dz z D_{c \rightarrow D^*}(z, \mu)}{\int dz D_{c \rightarrow D^*}(z, \mu)}. \quad (7)$$

Experimentally, the inclusive $c \rightarrow D^*$ channel was measured at LEP and at CLEO and ARGUS. The $\langle z \rangle_{c \rightarrow D^*}^\mu$ given in Eqn. (7) is the ratio of the second to the first moments of the fragmentation function at the scale μ . Since the anomalous dimensions of the moments are known explicitly, the scaling behavior of $\langle z \rangle^\mu$ can be determined to be

$$\langle z \rangle^\mu = \langle z \rangle^{\mu_0} \left(\frac{\alpha_s(\mu)}{\alpha_s(\mu_0)} \right)^{\frac{-2\gamma}{b}}, \quad (8)$$

where $\gamma = -4C_F/3$, $C_F = 4/3$, $b = (11N_c - 2n_f)/3$, $N_c = 3$, n_f is the number of active flavors at the scale μ , and $\langle z \rangle^{\mu_0}$ is the value determined at the initial scale μ_0 . Taking the inputs: $m_c = 1.5$ GeV, $m_{u,d} = 0.3$ GeV, $\mu_0 = m_c + 2m_{u,d} = 2.1$ GeV, we have $r = 0.167$, and $\langle z \rangle_{c \rightarrow D^*}^{\mu_0} = 0.77$ and $\langle z \rangle_{c \rightarrow D^*}^{\mu=m_Z/2} = 0.50$. The variation of $\langle z \rangle_{c \rightarrow D^*}^\mu$ and $\langle z \rangle_{b \rightarrow B^*}^\mu$ as functions of μ are shown in Fig. 3, where we chose $m_b = 4.9$ GeV. The curve for $\langle z \rangle_{b \rightarrow B^*}^\mu$ was also shown because we want to demonstrate that using the same $m_{u,d}$ and $m_b = 4.9$ GeV, the results predicted also agree with the data for the bottom quark fragmentation at LEP.

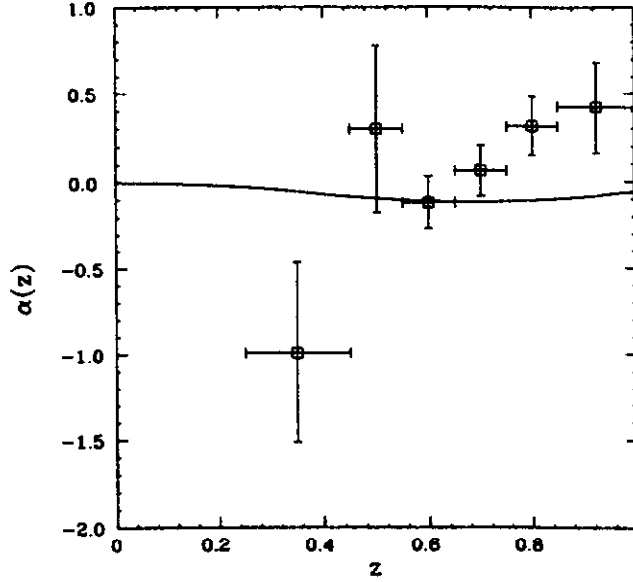


Fig. 4. The spin asymmetry parameter $\alpha(z)$ versus z for the D^* vector mesons predicted by our PQCd fragmentation model and the experimental measurement by CLEO.

The measured quantity is $\langle x_E \rangle$, which is the energy of the meson relative to one half of the center-of-mass energy of the machine, and x_E should be a good approximation to z . At LEP, measured values of $\langle x_E \rangle_{c \rightarrow D^*}$ are from OPAL (0.52 ± 0.0316), ALEPH (0.504 ± 0.0188), and DELPHI (0.487 ± 0.0158).¹⁸ The average $\langle x_E \rangle_{c \rightarrow D^*} = 0.504 \pm 0.0133$. For the bottom quark, only the inclusive hadron production has been measured. But we expect that $\langle x_E \rangle_{b \rightarrow B^*}$ should be close to $\langle x_E \rangle_{b \rightarrow H_b}$, where H_b is a bottom hadron, because the $b \rightarrow B^*$ is the dominant fragmentation mode of the bottom quark. The measured values of $\langle x_E \rangle_{b \rightarrow H_b}$ are from OPAL (0.726 ± 0.023), ALEPH (0.67 ± 0.050), DELPHI (0.695 ± 0.0326), and L3 (0.686 ± 0.017).¹⁹ The average $\langle x_E \rangle_{b \rightarrow H_b} = 0.694 \pm 0.0166$. Also, we have data on $c \rightarrow D^*$ from CLEO and ARGUS.²⁰ Combining the CLEO and ARGUS data we have $\langle x_E \rangle_{c \rightarrow D^*} = 0.648 \pm 0.043$. The scale of the measurements is taken to be one half of the center-of-mass energy of the machines, so it is $m_Z/2$ at LEP and 5.3 GeV at CLEO/ARGUS. These data are shown in Fig. 3. Excellent agreement is demonstrated. The only inputs to these comparisons are m_b , m_c , $m_{u,d}$, and μ_0 . Once they are fixed, $\langle z \rangle^{\mu_0}$ can be calculated by Eqn. (7) and evolved by Eqn. (8) to any scale μ .

c) $\alpha(z)$ is defined by

$$\alpha = \frac{2L - T}{T}, \quad (9)$$

where $L(T)$ denoted the production of the longitudinal (transverse) component of the vector meson. Since the fragmentation into the spin-orbital 3S_1 states is the dominant production mechanism for longitudinal and transverse vector mesons, α can be

expressed in terms of the fragmentation probabilities $P_{c \rightarrow D^*(L)}$ and $P_{c \rightarrow D^*(T)}$ as:

$$\alpha = \frac{2P_{c \rightarrow D^*(L)} - P_{c \rightarrow D^*(T)}}{P_{c \rightarrow D^*(T)}}. \quad (10)$$

α is then a function of r only. If we expand α as a series of r we have

$$\alpha = 0 - \frac{5}{4}r + \mathcal{O}(r). \quad (11)$$

The leading term 0 corresponds to the value given by heavy quark spin symmetry since we expect that in the heavy quark mass limit the ratio of L:T=1:2. The first nonzero term $-\frac{5}{4}r$ breaks the heavy quark symmetry. The spin asymmetry, which comes in in the order of r , is expected to be larger in the D^* meson than in the B^* meson. The z -dependence of α can also be obtained without the z integration:

$$\alpha(z) = \frac{2D_{c \rightarrow D^*(L)}(z) - D_{c \rightarrow D^*(T)}(z)}{D_{c \rightarrow D^*(T)}}. \quad (12)$$

The expressions for these polarized fragmentation functions $D_{c \rightarrow D^*(L,T)}(z)$ can be found in Ref..⁹ Experimental data of $\alpha(z)$ was available from the CLEO measurement.²¹ We choose $m_c = 1.5$ GeV, $m_{u,d} = 0.3$ GeV, and we have $r = 0.167$. We show the prediction of $\alpha(z)$ by our fragmentation model and the data from CLEO in Fig. 4. A moderate agreement is concluded as the error of the data is large.

4. Conclusions

In this paper, we have demonstrated the applications of the perturbative QCD fragmentation functions as a phenomenological model to describe the fragmentation of a heavy quark into heavy-light mesons. Explicitly, we compare the predictions by the PQCD fragmentation functions on the charm system assuming a 0.3 GeV for the light constituent quark mass in the charm mesons. Excellent agreement was found in the measurements of P_V and $\langle z \rangle$, and a moderate agreement on $\alpha(z)$. If more and more charm or bottom fragmentation data are available, we can also compare the production rates of the P-wave states, which allows a further test of the PQCD fragmentation functions as a phenomenological fragmentation model. No doubt that a more precise measurement on the spin asymmetry parameter $\alpha(z)$ is necessary.

Acknowledgements

I am indebt to my collaborators: Tzu Chiang Yuan and Eric Braaten for the results that I presented here. This work was supported by the U. S. Department of Energy, Division of High Energy Physics, under Grants DE-FG02-91-ER40684.

References

1. C. Peterson, D. Schlatter, I. Schmitt, and P. M. Zerwas, Phys. Rev. D **27**, 105 (1983).
2. B. Andersson, *et al.*, Phys. Rep. **97**, 33 (1983).

3. L. Clavelli, Phys. Rev. **D26**, 1610 (1982); V. Barger, K. Cheung, and W.-Y. Keung, Phys. Rev. **D**, (1990); C.-H. Chang and Y.-Q. Chen, Phys. Lett. **B284**, 127 (1992); Phys. Rev. **D46**, 3845 (1992).
4. E. Braaten and T.C. Yuan, Phys. Rev. Lett. **71**, 1673 (1993).
5. E. Braaten, K. Cheung, and T.C. Yuan, Phys. Rev. **D48**, 4230 (1993).
6. A. Falk, M. Luke, M. Savage, and M. Wise, Phys. Lett. **B312**, 486 (1993).
7. E. Braaten, K. Cheung, and T.C. Yuan, Phys. Rev. **D48**, R5049 (1993).
8. Y.-Q. Chen, Phys. Rev. **D48**, 5158 (1993).
9. K. Cheung and T.C. Yuan, preprint NUHEP-TH-94-7 and UCD-94-4 (April 1994).
10. E. Braaten and T.C. Yuan, preprint FERMILAB-PUB-94/040-T (March 1994).
11. T.C. Yuan, preprint UCD-94-2 (May 1994).
12. E. Braaten, M. Doncheski, S. Fleming, and M. Mangano, preprint FERMILAB-PUB-94/135-T; M. Cacciari and M. Greco, INFN preprint FNT/T-94/13.
13. K. Cheung, Phys. Rev. Lett. **71**, 3413 (1993); K. Cheung and T.C. Yuan, Phys. Lett. **B325**, 481 (1994).
14. E. J. Eichten and C. Quigg, Fermilab preprint, FERMILAB-PUB-94/032-T, February (1994).
15. R. L. Jaffe and L. Randall, Nucl. Phys. **B412**, 79 (1994).
16. E. Braaten, K. Cheung, S. Fleming, and T. C. Yuan, in preparation.
17. A. F. Falk and M. E. Peskin, SLAC preprint, SLAC-PUB-6311, August (1993).
18. OPAL Collaboration, Phys. Lett. **B262**, 341 (1991); ALEPH Collaboration, Phys. Lett. **B266**, 218 (1991); DELPHI Collaboration, Z. Phys. **C59**, 533 (1993).
19. OPAL Collaboration, Phys. Lett. **B263**, 310 (1991); ALEPH Collaboration, Phys. Lett. **B244**, 551 (1990); DELPHI Collaboration, Z. Phys. **C57**, 181 (1993); L3 Collaboration, Phys. Lett. **B261**, 177 (1991).
20. Bortoletto *et al.* (CLEO Collaboration), Phys. Rev. **D37**, 1719 (1988); Albrecht *et al.* (ARGUS Collaboration), Z. Phys. **C52**, 353 (1991).
21. Kubota *et al.* (CLEO Collaboration), Phys. Rev. **D44**, 593 (1991).

Spectra of Heavy-Light Mesons

Estia J. Eichten,^{*} Christopher T. Hill,[†] and Chris Quigg[‡]
Fermi National Accelerator Laboratory
P.O. Box 500, Batavia, Illinois 60510

May 25, 1994

Abstract

We present templates for the spectra of highly excited heavy-light ($Q\bar{q}$) mesons that are derived from potential-model descriptions of quarkonium ($Q\bar{Q}$) spectra.

When we have information about the energy levels of one family of heavy-light mesons, heavy-quark symmetry is an apt tool for mapping that information onto another heavy-light family [1]. When that information is lacking for all the heavy-light families (charmed mesons and above), we must fall back upon more model-dependent considerations. It is noteworthy that the spin-independent spectra of heavy-light mesons calculated in potentials constructed to describe the ψ and Υ spectra reproduce the known general features of the heavy-light spectra, particularly along the leading Regge trajectory. The calculated energy levels define templates that may be useful in anticipating the spectroscopy and in making preliminary assignments of levels discovered in the future.

We consider two functional forms for the potential that give reasonable accounts of the $c\bar{c}$ and $b\bar{b}$ spectra: the QCD-motivated potential given by Buchmüller and Tye [2], with (constituent) quark masses

$$\begin{aligned} m_c &= 1.48 \text{ GeV}/c^2 & m_b &= 4.88 \text{ GeV}/c^2 \\ m_s &= 0.45 \text{ GeV}/c^2 & m_u &= m_d = 0.30 \text{ GeV}/c^2 \end{aligned} ;$$

^{*}Internet address: eichten@fnal.gov

[†]Internet address: hill@fnal.gov

[‡]Internet address: quigg@fnal.gov

and a Coulomb-plus-linear potential (the “Cornell potential”) [3],

$$V(r) = -\frac{\kappa}{r} + \frac{r}{a^2} \ ,$$

with

$$\begin{aligned} m_c &= 1.84 \text{ GeV}/c^2 & m_b &= 5.18 \text{ GeV}/c^2 \\ m_s &= 0.45 \text{ GeV}/c^2 & m_u &= m_d = 0.32 \text{ GeV}/c^2 \\ \kappa &= 0.52 & a &= 2.34 \text{ GeV}^{-1} \ . \end{aligned}$$

We solve the Schrödinger equation, turning a blind eye to the fact that heavy-light mesons are far from nonrelativistic systems [4]. For each meson flavor, we adjust the 1S energy level to the value

$$M(1S) = \frac{3M(1^-) + M(0^-)}{4}$$

determined from experiment [5, 6]. The resulting spin-independent spectra of K , D , D_s , B , and B_s mesons are presented in Table 1 for the Buchmüller-Tye potential and in Table 2 for the Cornell potential. The essential features of the spectra are quite similar in the two potentials. We have not attempted to estimate spin splittings. The relativistic quark model of Godfrey and Isgur [7], which includes an estimate of spin splittings, gives similar predictions [8].

In the figures that follow, the Buchmüller-Tye spectra are compared with what is known experimentally [5, 6, 9]. The agreement encourages us to take the calculated energy levels as good first guesses for the positions of the unobserved levels. In addition to the 2^- and 3^- states whose properties we have predicted in [1], the first radial excitations of the D_s and B_s may be especially good candidates for discovery.

Fermilab is operated by Universities Research Association, Inc., under contract DE-AC02-76CHO3000 with the U.S. Department of Energy.

Table 1: Masses (in GeV/c^2) of heavy-light mesons in the Buchmüller-Tye potential. The 1S center of gravity has been adjusted to match experiment.

Level	K	D	D_s	B	B_s
1S	0.7943	1.973	2.075	5.313	5.403
2P	1.312	2.460	2.538	5.790	5.854
2S	1.592	2.710	2.761	6.029	6.064
3D	1.715	2.830	2.880	6.149	6.183
3P	1.962	3.051	3.077	6.361	6.369
4F	2.066	3.149	3.172	6.457	6.462
3S	2.205	3.269	3.271	6.569	6.552

Table 2: Masses (in GeV/c^2) of heavy-light mesons in the Cornell potential. The 1S center of gravity has been adjusted to match experiment.

Level	K	D	D_s	B	B_s
1S	0.7943	1.973	2.075	5.313	5.403
2P	1.326	2.463	2.541	5.806	5.864
2S	1.636	2.732	2.781	6.064	6.088
3D	1.749	2.843	2.893	6.176	6.200
3P	2.028	3.089	3.115	6.413	6.411
4F	2.123	3.178	3.200	6.500	6.495
3S	2.299	3.325	3.326	6.640	6.612

References

- [1] Estia J. Eichten, Christopher T. Hill, and Chris Quigg, *Phys. Rev. Lett.* **71**, 4116 (1993). For an update with additional details, see Estia J. Eichten, Christopher T. Hill, and Chris Quigg, "Orbitally Excited Heavy-Light Mesons Revisited," FERMILAB-CONF-94/118-T.
- [2] W. Buchmüller and S.-H. H. Tye, *Phys. Rev. D* **24**, 132 (1981).
- [3] E. Eichten, K. Gottfried, T. Kinoshita, K. D. Lane, T.-M. Yan, *Phys. Rev. D* **17**, 3090 (1978); *ibid.* **21**, 313E (1980); *ibid.* **21**, 203 (1980).
- [4] The surprising success of potential-model descriptions of the light hadrons is reviewed, for example, in W. Lucha, F. F. Schöberl, and D. Gromes, *Phys. Rep.* **200**, 127 (1991).
- [5] Particle Data Group, *Phys. Rev. D* **45**, S1 (1992).
- [6] Heavy-quark symmetry predicts that the center of gravity of the $1S$ B_c states lies $34.5 \text{ MeV}/c^2$ above the pseudoscalar mass, as in the B system. We take $M(B_c) = 5368.5 \text{ MeV}/c^2$, an informal average of the observed values. F. Abe, et al. (CDF Collaboration), *Phys. Rev. Lett.* **71**, 1685 (1993), report the mass of the B_c meson as $5383.3 \pm 4.5 \text{ (stat.)} \pm 5.0 \text{ (sys.) MeV}$; D. Buskulic, et al. (ALEPH Collaboration), *Phys. Lett. B* **311**, 425 (1993), *ibid.* **B316**, 631E (1993), report $5368.6 \pm 5.6 \text{ (stat.)} \pm 1.5 \text{ (sys.) MeV}/c^2$. P. Abreu, et al. (DELPHI Collaboration), *Phys. Lett. B* **324**, 500 (1994), report $5374 \pm 16 \text{ (stat.)} \pm 2 \text{ (sys.) MeV}/c^2$. See also P. D. Acton, et al. (OPAL Collaboration), *Phys. Lett. B* **295**, 357 (1992). A preliminary value from CDF, $M(B_c) = 5367.7 \pm 2.4 \text{ (stat.)} \pm 4.8 \text{ (sys.) MeV}/c^2$, is reported in J. D. Lewis, "Mass and Lifetime Measurements with Exclusive B Reconstruction from CDF," CDF/PUB/BOTTOM/PUBLIC/2603, FERMILAB-CONF-94/128-E, to appear in the Proceedings of the 1994 Rencontre de Physique de la Vallée d'Aoste.
- [7] S. Godfrey and N. Isgur, *Phys. Rev. D* **32**, 189 (1985).
- [8] The validity of the quark model with a relativistic form for the kinetic energy has been investigated on the lattice by A. Duncan, E. Eichten, and H. Thacker, *Phys. Lett.* **303**, 109 (1993).

- [9] The D_{s2}^* has been reported for the first time by Y. Kubota, et al. (CLEO Collaboration), Cornell preprint CLNS 94/1266 (unpublished), with a mass of $2573.2 \pm 1.9 \text{ MeV}/c^2$.

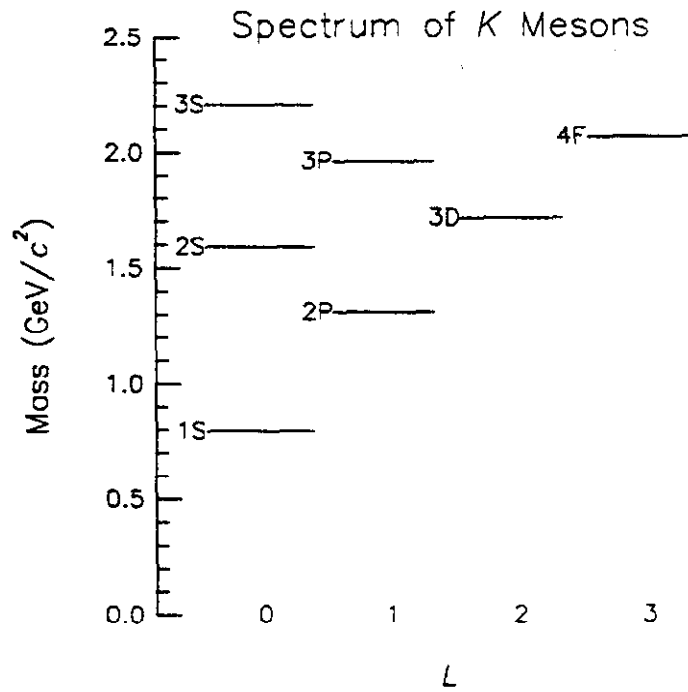


Figure 1: Spectrum of strange mesons in the Buchmüller-Tye potential.

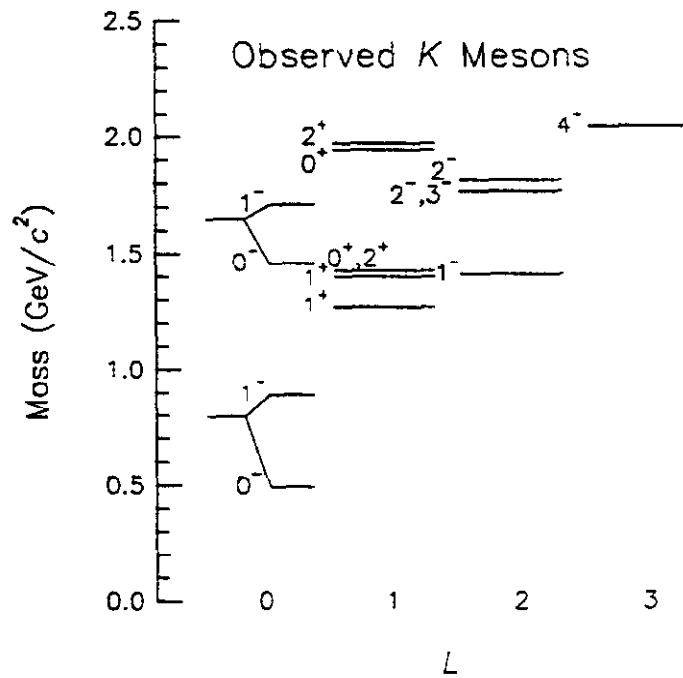


Figure 2: Spectrum of observed strange mesons.

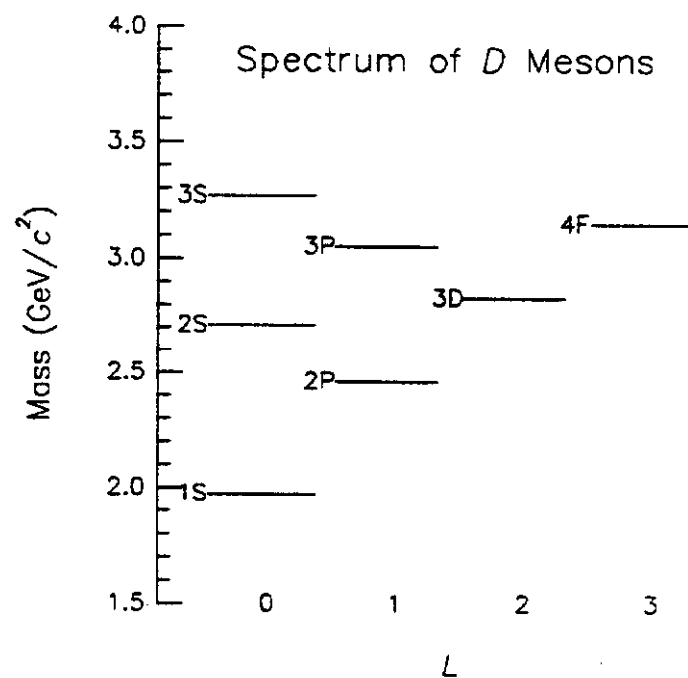


Figure 3: Spectrum of charmed mesons in the Buchmüller-Tye potential.

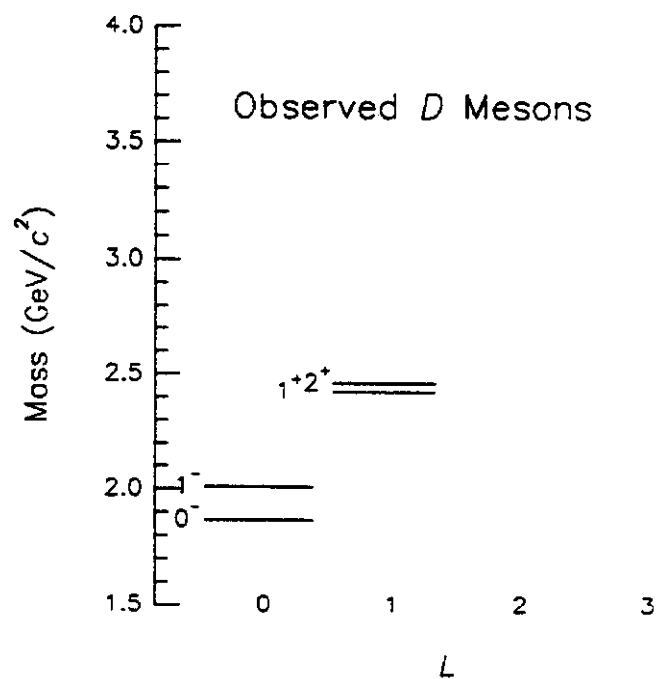


Figure 4: Spectrum of observed charmed mesons.

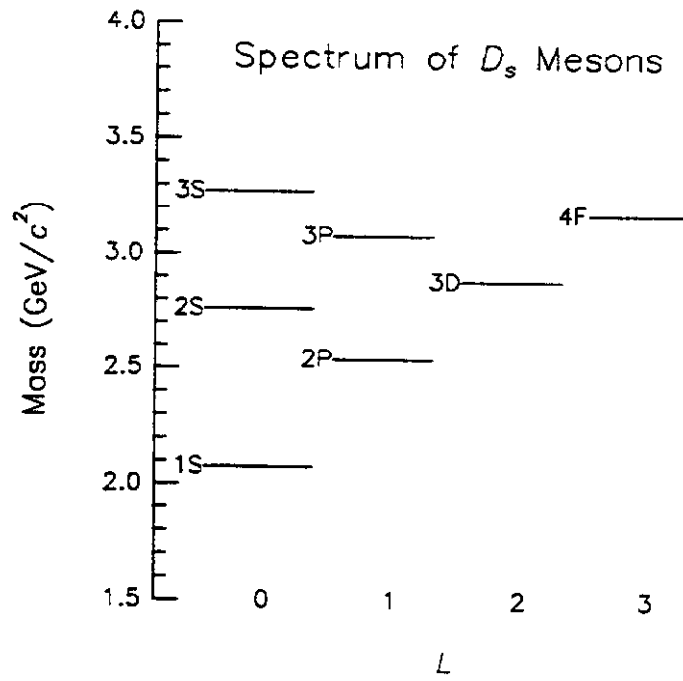


Figure 5: Spectrum of charmed-strange mesons in the Buchmüller-Tye potential.

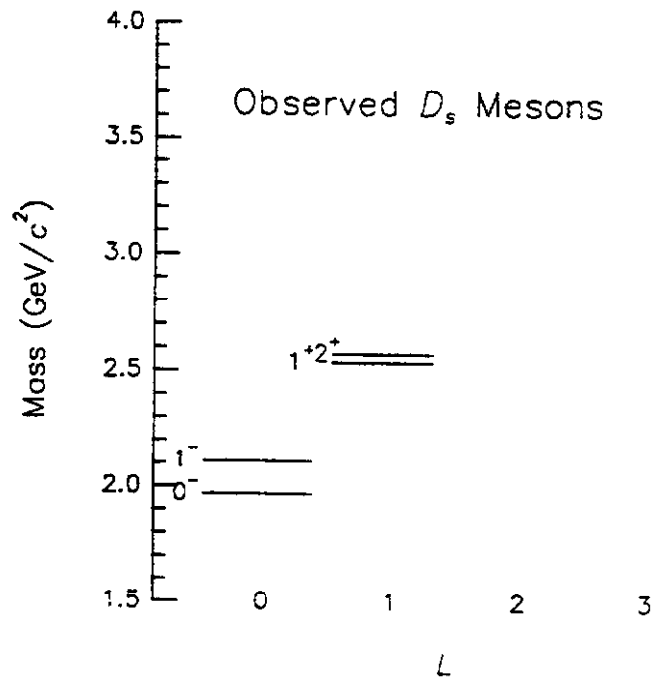


Figure 6: Spectrum of observed charmed-strange mesons.

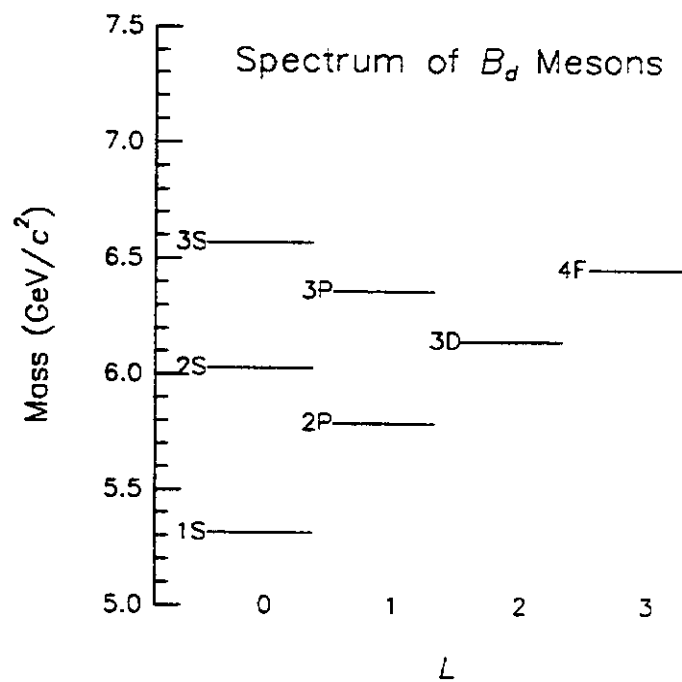


Figure 7: Spectrum of B mesons in the Buchmüller-Tye potential.

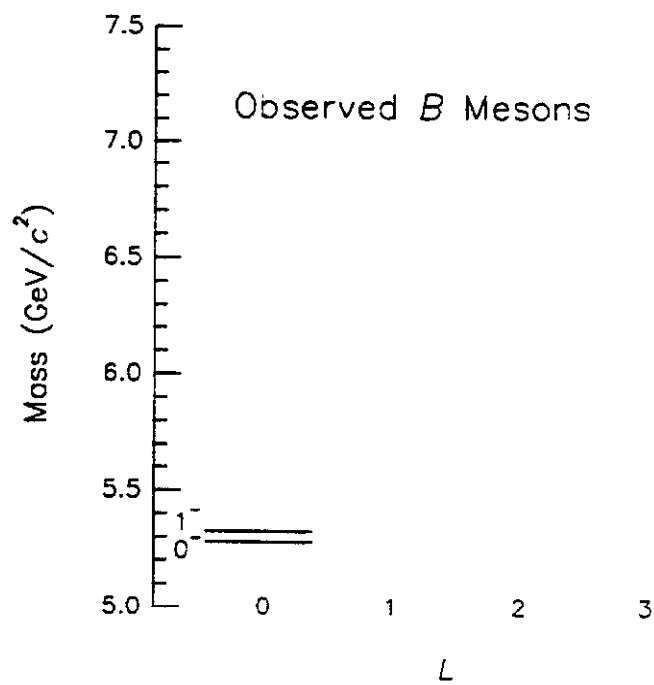


Figure 8: Spectrum of observed B mesons.

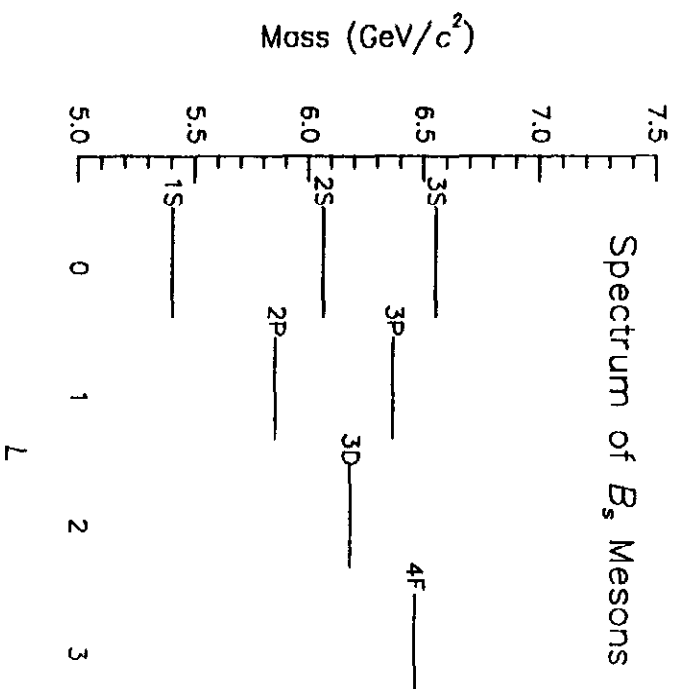


Figure 9: Spectrum of B_s mesons in the Buchmüller-Tye potential.

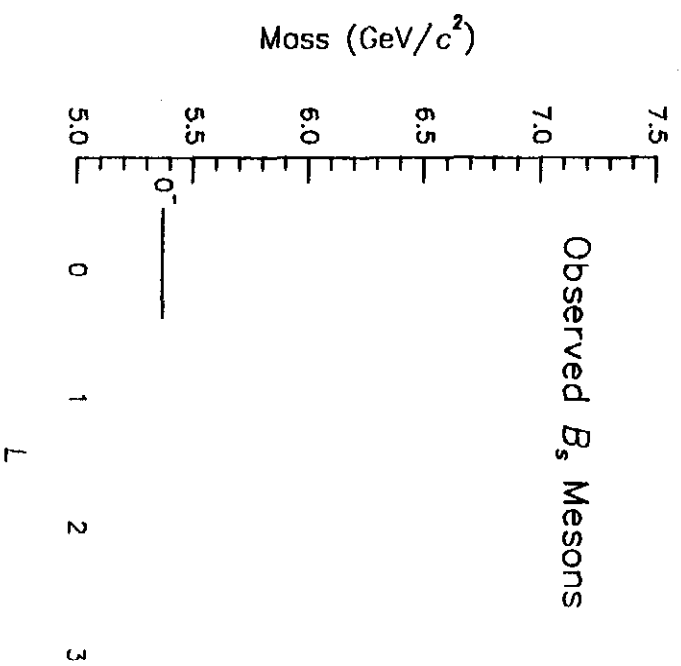


Figure 10: Spectrum of observed B_s mesons.

Orbitally Excited Heavy-Light Mesons Revisited

Estia J. Eichten, * Christopher T. Hill, † and Chris Quigg ‡

Fermi National Accelerator Laboratory

P.O. Box 500, Batavia, Illinois 60510

(May 25, 1994)

Abstract

We refine heavy-quark-symmetry estimates of masses and widths of orbitally excited B , B_s , and D_s mesons given in [1]. We present additional details of the predictions for d -wave states.

Incisive study of particle-antiparticle mixing and CP -violation for neutral B mesons requires that the quantum numbers of the meson be identified at the time of production. That identification can be made by observing the decay of a B^0 or \bar{B}^0 produced in association with a particle of opposite b -number whose decay signals the flavor of the neutral B of interest. The efficiency of flavor identification might be dramatically enhanced if the neutral B under study were self-tagging [2].

Charmed mesons have been observed as (strong) decay products of orbitally excited ($c\bar{q}$) states, through the decays $D^{**} \rightarrow \pi D$ and $D^{**} \rightarrow \pi D^*$ [3]. The charge of the pion emitted in the strong decay signals the flavor content of the charmed meson. If significant numbers of B mesons are produced through one or more narrow excited ($\bar{b}q$) states, the strong decay $B^{**\pm} \rightarrow B^{(*)0}\pi^\pm$ tags the neutral meson as $(\bar{b}d)$ or $(b\bar{d})$, respectively.

The ultimate application of B^{**} -tagging would be in the search for the expected large CP -violating asymmetry in $(B^0 \text{ or } \bar{B}^0) \rightarrow J/\psi K_S$ decay [4]. The study of time-dependent B^0 - \bar{B}^0 oscillations would also benefit from efficient tagging. B^{**} -tagging may also resolve

*Internet address: eichten@fnal.gov

†Internet address: hill@fnal.gov

‡Internet address: quigg@fnal.gov

kinematical ambiguities in semileptonic decays of charged and neutral B mesons by choosing between two solutions for the momentum of an undetected neutrino. In hadron colliders and Z^0 -factories, kinematic tagging may make practical high-statistics determinations of the form factors in semileptonic weak decay, and enable precise measurements of V_{cb} and V_{ub} [5,6]. The study of B_s - \bar{B}_s mixing would be made easier if the kaon charge in the decay $B^{***} \rightarrow K^\pm(B_s \text{ or } \bar{B}_s)$ served as a flavor tag. Overall, efficient B^{**} -tagging would dramatically enhance the prospects for studying CP -violation and B_s - \bar{B}_s mixing.

In Ref. [1], we estimated the masses, widths, and branching fractions of orbitally excited B , D_s , and B_s states from the properties of corresponding K and D levels. Our results showed that one requirement for the utility of B^{**} -tagging, narrow resonances, is likely to be met by the B_2^* and B_1 . Experiment must rule on the strength of these lines and the ratio of signal to background.

For hadrons containing a heavy quark Q , quantum chromodynamics displays additional symmetries in the limit as the heavy-quark mass m_Q becomes large compared with a typical QCD scale [7]. These heavy-quark symmetries are powerful aids to understanding the spectrum and decays of heavy-light $(Q\bar{q})$ mesons. Because $m_b \gg \Lambda_{\text{QCD}}$, heavy-quark symmetry should provide an excellent description of the B and B_s mesons. It is plausible that properties of D mesons, and even K mesons, should also reflect approximate heavy-quark symmetry.

One essential idea of the heavy-quark limit is that the spin \vec{s}_Q of the heavy quark and the total (spin + orbital) angular momentum $\vec{j}_q = \vec{s}_q + \vec{L}$ of the light degrees of freedom are separately conserved [8]. Accordingly, each energy level in the excitation spectrum of $(Q\bar{q})$ mesons is composed of a degenerate pair of states characterized by j_q and the total spin $\vec{J} = \vec{j}_q + \vec{s}_Q$, i.e., by $J = j_q \pm \frac{1}{2}$. The ground-state pseudoscalar and vector mesons, which are degenerate in the heavy-quark limit, correspond to $j_q = \frac{1}{2}$, with $J = 0$ and 1. Orbital excitations lead to two distinct doublets associated with $j_q = L \pm \frac{1}{2}$.

Masses. The leading corrections to the spectrum prescribed by heavy-quark symmetry are inversely proportional to the heavy-quark mass. We may write the mass of a heavy-light meson as

$$M(nL_J(j_q)) = M(1S) + E(nL(j_q)) + \frac{C(nL_J(j_q))}{m_Q}, \quad (1)$$

where n is the principal quantum number and $M(1S) = [3M(1S_1) + M(1S_0)]/4$ is the mass of the ground state. In the heavy-quark limit, the excitation energy $E(nL(j_q))$ is independent of the heavy-quark mass [9].

Let us focus first upon the $j_q = \frac{3}{2}$ states observed as narrow $D\pi$ or $D^*\pi$ resonances. We will show below that their counterparts in other heavy-light systems should also be narrow. Our overall strategy is to use the observed properties of the K and D mesons to predict the properties of the orbitally excited B , D_s , and B_s mesons. The charmed mesons alone would suffice to predict the 2^+-1^+ splitting. Further information, involving a different heavy quark, is needed to estimate the $2P$ excitation energy. Since no excited B or B_s levels are yet known, we provisionally use the strange resonances. According to Eq. (1), the masses of the strange and charmed mesons with $j_q = \frac{3}{2}$ are given by

$$\begin{aligned} M(2P_2)_K - M(1S)_K &= E(2P) + \frac{C(2P_2)}{m_s} \quad , \\ M(2P_1)_K - M(1S)_K &= E(2P) + \frac{C(2P_1)}{m_s} \quad , \\ M(2P_2)_D - M(1S)_D &= E(2P) + \frac{C(2P_2)}{m_c} \quad , \\ M(2P_1)_D - M(1S)_D &= E(2P) + \frac{C(2P_1)}{m_c} \quad , \end{aligned} \tag{2}$$

where we have suppressed the j_q label for brevity. We are left with four linear equations in the five unknowns $E(2P)$, $C(2P_2)$, $C(2P_1)$, m_s^{-1} , and m_c^{-1} .

The K - and D -meson masses we use as experimental inputs are displayed in Table I. There is no ambiguity about the $2^+(\frac{3}{2})$ levels. We identify $D_1(2424)$ as a $j_q = \frac{3}{2}$ level because it is narrow, as predicted [12,13] by heavy-quark symmetry. We follow Ito et al. [14] in identifying $K_1(1270)$ as the $1^+(\frac{3}{2})$ level, because that assignment gives a consistent picture of masses and widths.

To proceed, we choose a value for the charmed-quark mass, m_c . After solving Eqs. (2), we verify the reasonableness of m_s and predict the $j_q = \frac{3}{2}$ masses for the B , D_s , and B_s families. We consider two sets of parameters inspired by J/ψ and Υ spectroscopy: $m_c = 1.48 \text{ GeV}/c^2$, $m_b = 4.8 \text{ GeV}/c^2$ [15]; and $m_c = 1.84 \text{ GeV}/c^2$, $m_b = 5.18 \text{ GeV}/c^2$ [16]. Both solutions [$C(2P_2) = (0.0629, 0.0783) \text{ (GeV}/c^2)^2$, $C(2P_1) = (0.0105, 0.0132) \text{ (GeV}/c^2)^2$, $E(2P) = (0.4437, 0.4437) \text{ GeV}/c^2$, $m_s = (0.3295, 0.4097) \text{ GeV}/c^2$] yield reasonable values for

the strange-quark mass. Their implications for the B , D_s , and B_s levels are consistent within 2 MeV. The average values are presented in Table I.

The heavy-quark-symmetry prediction for the $1^+ D_s$ meson lies 10 MeV below the level observed [10,17] at 2536.5 ± 0.8 MeV/ c^2 . The prediction for the $2^+ D_{s2}^*$ meson lies 12 MeV below the level observed [18] at 2573.2 ± 1.9 MeV/ c^2 . We take the discrepancy between calculated and observed masses as a measure of the limitations of our method.

The $2P(\frac{1}{2})$ D mesons have not yet been observed, so we cannot predict the masses of other heavy-light states by this technique. Splitting within the multiplet can be estimated using Eq. (1) from the kaon spectrum alone. The small splitting between $K_0^*(1429)$ and $K_1(1402)$ implies that the $1^+(\frac{1}{2})$ and $0^+(\frac{1}{2})$ levels should be nearly degenerate in all the heavy-light systems. Chiral symmetry and heavy-quark symmetry combined suggest that, like their counterparts in the strange-meson spectrum, the heavy-light $j_q = \frac{1}{2}$ p -wave states should have large widths for pionic decay to the ground states [19]. This will make the discovery and study of these states challenging, and will limit their utility for B^{**} -tagging.

Decay widths. Consider the decay of an excited heavy-light meson H , characterized by $L_J(j_q)$, to a heavy-light meson $H'(L_{J'}(j'_q))$, and a light hadron h with spin s_h . The amplitude for the emission of h with orbital angular momentum ℓ relative to H' satisfies certain symmetry relations because the decay dynamics become independent of the heavy-quark spin in the $m_Q \rightarrow \infty$ limit of QCD [12]. The decay amplitude can be factored [13] into a reduced amplitude \mathcal{A}_R times a normalized 6- j symbol,

$$\mathcal{A}(H \rightarrow H' h) = (-1)^{s_Q + j_h + J' + j_q} C_{j_h, J, j_q}^{s_Q, j'_q, J'} \mathcal{A}_R(j_h, \ell, j_q, j'_q),$$

where $C_{j_h, J, j_q}^{s_Q, j'_q, J'} = \sqrt{(2J' + 1)(2j_q + 1)} \begin{Bmatrix} s_Q & j'_q & J' \\ j_h & J & j_q \end{Bmatrix}$ and $\vec{j}_h \equiv \vec{s}_h + \vec{\ell}$. The coefficients C depend only upon the total angular momentum j_h of the light hadron, and not separately on its spin s_h and the orbital angular momentum wave ℓ of the decay. The two-body decay rate may be written as

$$\Gamma_{j_h, \ell}^{H \rightarrow H' h} = (C_{j_h, J, j_q}^{s_Q, j'_q, J'})^2 p^{2\ell+1} F_{j_h, \ell}^{j_q, j'_q}(p^2), \quad (3)$$

where p is the three-momentum of the decay products in the rest frame of H . Heavy-quark symmetry does not predict the reduced amplitude \mathcal{A}_R or the related $F_{j_h, \ell}^{j_q, j'_q}(p^2)$ for a particular

decay. Once determined from the charmed or strange mesons, these dynamical quantities may be used to predict related decays, including those of orbitally excited B mesons. For each independent decay process, we assume a modified Gaussian form

$$F_{j_h, \ell}^{j_q, j'_q}(p^2) = F_{j_h, \ell}^{j_q, j'_q}(0) \exp(-p^2/\kappa^2) \left[\frac{M_\rho^2}{M_\rho^2 + p^2} \right]^\ell, \quad (4)$$

and determine the overall strength of the decay and the momentum scale κ by fitting existing data. The final factor moderates the p^ℓ threshold behavior of the decay amplitude at high momenta [20]. Our ability to predict decay rates depends on the quality of the information used to set these parameters.

In writing (3) we have ignored $1/m_Q$ corrections to heavy-quark symmetry predictions for decay rates, except as they modify the momentum p of the decay products. We assume that the momentum scale κ of the form factor in (4) is typical of hadronic processes (≈ 1 GeV) and that it varies little with decay angular momentum ℓ .

The decays $2P(\frac{3}{2}) \rightarrow 1S(\frac{1}{2}) + \pi$ are governed by a single $\ell = 2$ amplitude. To evaluate the transition strength $F_{2,2}^{\frac{3}{2}, \frac{1}{2}}(0)$, we fix $\Gamma(D_2^* \rightarrow D\pi) + \Gamma(D_2^* \rightarrow D^*\pi) = 25$ MeV, as suggested by recent experiments [3]. This determines all pionic transitions between the $2P(\frac{3}{2})$ and $1S(\frac{1}{2})$ multiplets. The results are shown in Table II, where we have used experimentally observed masses of the D , D_s , and K levels and our calculated masses for the B and B_s states. The predicted rates are stable as the momentum scale κ ranges from 0.8 to 1.2 GeV. $SU(3)$ determines the strengths of K and η transitions [21]. The predictions agree well with what is known about the $L = 1$ D and D_s states [22]. The ratio $\Gamma(D_2^* \rightarrow D\pi)/\Gamma(D_2^* \rightarrow D^*\pi) = 1.8$ is consistent with the 1992 Particle Data Group average, 2.4 ± 0.7 [10], and with a recent CLEO measurement, $2.1 \pm 0.6 \pm 0.6$ [23].

The narrow width observed for D_{s1} is consistent with the prediction from heavy-quark symmetry. This suggests that mixing of the narrow $2P(\frac{3}{2})$ level with the broader $2P(\frac{1}{2})$ state [12,13] is negligible [24]. This pattern should hold for B and B_s as well. We have also applied heavy-quark dynamics to the decays of the $2P(\frac{3}{2})$ strange mesons. The pionic transition rates given in Table II for the strange resonances are somewhat lower than the experimental values, but the ratios agree well with experiment.

The low-mass tail of $\rho(770)$ is kinematically accessible in decays $2P(\frac{3}{2}) \rightarrow \text{vector meson} + 1S(\frac{1}{2})$. These decays are governed by three independent decay amplitudes characterized by

$(j_h, \ell) = (2, 2)$, $(1, 2)$, and $(1, 0)$. $SU(6)$ symmetry identifies the $(2, 2)$ transition strength with the $F_{2,2}^{\frac{3}{2}, \frac{1}{2}}(0)$ for pion emission. The two new amplitudes occur in a fixed combination that should be dominated by the $\ell = 0$ amplitude. We have to evaluate one new transition strength, $F_{1,0}^{\frac{3}{2}, \frac{1}{2}}(0)$. Lacking measurements of partial widths for vector meson emission in the charmed states, and encouraged by the pattern of pionic decay widths for the strange resonances, we use the decay rate $\Gamma(K_1(1270) \rightarrow \rho + K) = 37.8 \text{ MeV}$ to fix $F_{1,0}^{\frac{3}{2}, \frac{1}{2}}(0)$. We smear the expression (3) for the partial width over a Breit-Wigner form to take account of the 150-MeV width of the ρ resonance. The resulting estimates for the ρ transitions are also shown in Table II. We predict that the $D\rho$ channel contributes about one-third of the total width of D_1 . Rates for $K^{**} \rightarrow K\omega$ decays follow by $SU(3)$ symmetry.

The results collected in Table II show that both the B_2^* and the B_1 states should be narrow, with large branching fractions to a ground-state B or B^* plus a pion. These states should also have significant two-pion transitions that we have modeled by the low-mass tail of the ρ resonance. The strange states, B_{s2}^* and B_{s1} , are very narrow ($\Gamma \lesssim 10 \text{ MeV}$); their dominant decays are by kaon emission to the ground-state B and B^* . The consistent picture of K_1 and K_2^* decay rates supports the identification [14] of $K_1(1270)$ as the $2P_1(\frac{3}{2})$ level.

To assess the prospects for tagging B_s , we consider briefly the $L = 2$ heavy-light mesons with $j_q = \frac{5}{2}$. Only the strange resonances have been observed. The identification of the $K_3^*(1770)$ as a $3D_3(\frac{5}{2})$ level is clear. Two $J^P = 2^-$ levels, $K_2(1773)$ and $K_2(1816)$, are candidates for its partner [25]. We use the Buchmüller-Tye potential [15] to estimate the masses of the $L = 2$ heavy-light states shown in Table III [26]. Whatever the assignment for the $3D_2(\frac{5}{2})$ level, the splitting within the $j_q = \frac{5}{2}$ doublet will be very small for the $D^{***}(2830)$, $B^{***}(6148)$, $D_s^{***}(2880)$, and $B_s^{***}(6198)$ systems.

To evaluate the transition strength $F_{3,3}^{\frac{5}{2}, \frac{1}{2}}(0)$ for pseudoscalar emission, we fix $\Gamma(K_3^* \rightarrow K^*\pi) = 45 \text{ MeV}$. As before, $SU(6)$ symmetry determines the strength $F_{3,3}^{\frac{5}{2}, \frac{1}{2}}(0)$ for vector meson emission. In the absence of measurements that would allow us to fix the other important decay amplitude, we have set $F_{2,1}^{\frac{5}{2}, \frac{1}{2}}(0) = 0$. Our projections for vector-meson emission will therefore be underestimates. We summarize our expectations for the total widths of the $3D(\frac{5}{2})$ states in Table III. The $3D(\frac{5}{2})$ B mesons will be broad ($\approx 175 \text{ MeV}$), but decay with about twenty percent probability to B_s and B_s^* by emitting a kaon. The

favorable branching fraction means that it might be possible to use B_3^* and B_2 decays to tag the B_s , in spite of the large total widths.

The investigation of orbitally excited heavy-light mesons is important for the insights it can provide into strong-interaction dynamics and for engineering purposes as well. Heavy-quark symmetry provides a network that links the decay rates and masses of all the heavy-light families. It is even possible that heavy-quark symmetry may offer a new perspective on the spectrum of strange mesons. If the narrow B_2^* and B_1 are copiously produced with little background, efficient tagging of flavor and momentum may be at hand. Prospects for incisive studies of B^0 - \bar{B}^0 mixing and CP violation at high energies would then be dramatically enhanced. We conclude this note with two “shopping lists” that summarize some of the urgent experimental issues in the spectroscopy of $c\bar{q}$ and $b\bar{q}$ mesons.

This work was performed at the Fermi National Accelerator Laboratory, which is operated by Universities Research Association, Inc., under contract DE-AC02-76CHO3000 with the U.S. Department of Energy.

REFERENCES

- [1] E. J. Eichten, C. T. Hill, and C. Quigg, Phys. Rev. Lett. **71**, 4116 (1993).
- [2] M. Gronau, A. Nippe, and J. L. Rosner, Phys. Rev. D **47**, 1988 (1993); M. Gronau, in *Proceedings of the Workshop on B Physics at Hadron Colliders*, Snowmass, Colorado, edited by P. McBride and C. S. Mishra, SSCL-SR-1225 / FERMILAB-CONF-93/267, p. 1; M. Gronau and J. L. Rosner, Phys. Rev. Lett. **72**, 195 (1994), Phys. Rev. D **49**, 254 (1994).
- [3] Observations of the $L = 1$ charmed (and charmed-strange) mesons are reported in H. Albrecht et al. (ARGUS Collaboration), Phys. Lett. B **221**, 422 (1989), ibid. **230**, 162 (1989), ibid. **231**, 208 (1989), ibid. **232**, 398 (1989), ibid. **297**, 425 (1992); J. C. Anjos et al. (Tagged Photon Spectrometer Collaboration), Phys. Rev. Lett. **62**, 1717 (1989); P. Avery et al. (CLEO Collaboration), Phys. Rev. D **41**, 774 (1990), Phys. Lett. B **303**, 377 (1993). P.L. Frabetti et al. (E687 Collaboration), Phys. Rev. Lett. **72**, 324 (1994), determine $\Gamma(D_2^*) = 24 \pm 7 \pm 5$ MeV, $\Gamma(D_1) = 15 \pm 8 \pm 5$ MeV, $\Gamma(D_{s1}) < 3.2$ MeV; P. Avery, et al. (CLEO Collaboration), Cornell preprint CLNS-94-1280 (unpublished), find $\Gamma(D_2^*) = 28^{+8+6}_{-7-6}$ MeV, $\Gamma(D_1) = 20^{+6+3}_{-5-3}$ MeV, $\Gamma(D_{s1}) < 2.3$ MeV.
- [4] C. Kim, J. L. Rosner, and C.-P. Yuan, Phys. Rev. D **42**, 96 (1990), D **45**, 389(E), (1992); C. Dib, I. Dunietz, F. J. Gilman, and Y. Nir, Phys. Rev. D **41**, 1522 (1990).
- [5] M. Neubert, Phys. Lett. B **264**, 455 (1991); P. Cho and B. Grinstein, ibid. **285**, 153 (1992).
- [6] C. T. Hill, in *Proceedings of the Workshop on B Physics at Hadron Colliders*, Snowmass, Colorado, edited by P. McBride and C. S. Mishra, SSCL-SR-1225 / FERMILAB-CONF-93/267, p. 127.
- [7] N. Isgur and M. B. Wise, Phys. Lett. B **232**, 113 (1989). For a review, see M. Neubert, SLAC-PUB-6263, Phys. Rep. (to be published).
- [8] E. Eichten and F. Feinberg, Phys. Rev. D **23**, 2724 (1981); W. E. Caswell and G. P. Lepage, Phys. Lett. B **167**, 437 (1986); E. Eichten, in *Proc. 1987 International*

Symposium on Field Theory on the Lattice, ed. A. Billoire et al. [Nucl. Phys. B (Proc. Suppl.) **4**, 170 (1988)]; G. P. Lepage and B. A. Thacker, *ibid.*, p. 199.

- [9] In Ref. [1], we used a potential model to estimate the weak dependence of the excitation energy on quark masses. The resulting variation of excitation energy lowered the predicted masses by about $25 \text{ MeV}/c^2$ for the D_s states, which significantly worsens the agreement between the heavy-quark-symmetry prediction and experiment. We accept the hint that nature is simpler than we expected.
- [10] Particle Data Group, Phys. Rev. D **45**, S1 (1992).
- [11] Heavy-quark symmetry predicts that the center of gravity of the $1S$ B_s states lies $34.5 \text{ MeV}/c^2$ above the pseudoscalar mass, as in the B system. We take $M(B_s) = 5368.5 \text{ MeV}/c^2$, an informal average of the observed values. F. Abe, et al. (CDF Collaboration), Phys. Rev. Lett. **71**, 1685 (1993), report the mass of the B_s meson as 5383.3 ± 4.5 (stat.) ± 5.0 (sys.) MeV; D. Buskulic, et al. (ALEPH Collaboration), Phys. Lett. B **311**, 425 (1993), *ibid.* **316**, 631E (1993), report 5368.6 ± 5.6 (stat.) ± 1.5 (sys.) MeV/c^2 . P. Abreu, et al. (DELPHI Collaboration), Phys. Lett. B **324**, 500 (1994), report 5374 ± 16 (stat.) ± 2 (sys.) MeV/c^2 . See also P. D. Acton, et al. (OPAL Collaboration), Phys. Lett. B **295**, 357 (1992). A preliminary value from CDF, $M(B_s) = 5367.7 \pm 2.4$ (stat.) ± 4.8 (sys.) MeV/c^2 , is reported in J. D. Lewis, "Mass and Lifetime Measurements with Exclusive B Reconstruction from CDF," CDF/PUB/BOTTOM/PUBLIC/2603, FERMILAB-CONF-94/128-E, to appear in the Proceedings of the 1994 Rencontre de Physique de la Vallée d'Aoste.
- [12] N. Isgur and M. Wise, Phys. Rev. Lett. **66**, 1130 (1991).
- [13] A. F. Falk and M. Luke, Phys. Lett. B **292**, 119 (1992).
- [14] T. Ito, T. Morii, and M. Tanimoto, Prog. Theor. Phys. **90**, 419 (1993).
- [15] W. Buchmüller and S.-H. H. Tye, Phys. Rev. D **24**, 132 (1981). To calculate excitation energies in heavy-light systems, We take constituent-quark masses $m_q = 0.3 \text{ GeV}/c^2$, $m_s = 0.45 \text{ GeV}/c^2$, $m_c = 1.48 \text{ GeV}/c^2$, and $m_b = 4.8 \text{ GeV}/c^2$.

- [16] E. J. Eichten, K. Gottfried, T. Kinoshita, K. D. Lane, and T.-M. Yan, Phys. Rev. D **21**, 203 (1980).
- [17] J. Alexander et al. (CLEO Collaboration), Phys. Lett. B **303**, 377 (1993), confirm the 1^+ assignment.
- [18] The D_{s2}^* has been reported for the first time by Y. Kubota, et al. (CLEO Collaboration), Cornell preprint CLNS 94/1266 (unpublished).
- [19] W. A. Bardeen and C. T. Hill, Phys. Rev. D **49**, 409 (1994).
- [20] This damping factor chiefly affects the f -wave contributions to the $3D(\frac{5}{2})$ decay rates discussed below.
- [21] We take the η wave function to be $(u\bar{u} + d\bar{d} - s\bar{s})/\sqrt{3}$.
- [22] Dynamical models for these decays were explored by S. Godfrey and R. Kokoski, Phys. Rev. D **43**, 1679 (1991). The possibility of a significant s -wave contribution (at order $1/m_Q$) to the decay $D_1 \rightarrow D^*\pi$ was raised by Ming-Lu, M. B. Wise, and N. Isgur, *ibid.* **45**, 1553 (1992).
- [23] Avery et al., Ref. [3].
- [24] For a quantitative exploration of $2P_1(\frac{3}{2})$ - $2P_1(\frac{1}{2})$ mixing in the D_s system, see P. Cho and S. Trivedi, "Strong Decays of Strange Charmed P-Wave Mesons," Caltech preprint CALT-68-1902 (unpublished).
- [25] D. Aston et al. (LASS Collaboration), Phys. Lett. **B308**, 186 (1993).
- [26] Estia J. Eichten, Christopher T. Hill, and Chris Quigg, "Spectra of Heavy-Light Mesons" FERMILAB-CONF-94/117-T.

TABLES

TABLE I. Masses (in MeV/c^2) predicted for the $2P(\frac{3}{2})$ levels of the B , D_s , and B_s systems.

Underlined entries are Particle Data Group averages [10] used as inputs.

Meson Family	K	D	B	D_s	B_s
$M(1S)$	<u>794.3</u>	<u>1973.2</u>	<u>5313.1</u>	<u>2074.9</u>	5403.0 ^a
$M(2^+(\frac{3}{2}))$	<u>1429 ± 6</u>	<u>2459.4 ± 2.2</u>	5771	2561	5861
$M(1^+(\frac{3}{2}))$	<u>1270 ± 10</u>	<u>2424 ± 6</u>	5759	2526	5849
$M(2^+(\frac{3}{2})) - M(1^+(\frac{3}{2}))$	159	35	12	35	12

^aAssuming that $M(1S) = M(1S_0) + 34.5 \text{ MeV}/c^2$, as in the B system. The pseudoscalar mass, $M(B_s) = 5368.5 \text{ MeV}/c^2$, is an average of the reported values [11].

TABLE II. Heavy-quark-symmetry predictions for decays of $2P(\frac{3}{2})$ heavy-light mesons.

Transition	Calculated	Width (MeV)		
		PDG 1992 ^a	CLEO 1993 ^b	E687 1993 ^c
$D_2^*(2459) \rightarrow D^*\pi$	9 ^d			
$D_2^*(2459) \rightarrow D\pi$	16 ^d			
$D_2^*(2459) \rightarrow D\eta$	~ 0.1			
$D_2^*(2459) \rightarrow D^*\rho$	3			
$D_2^*(2459) \rightarrow D\rho$	< 1			
$D_2^*(2459) \rightarrow \text{all}$	28	19 ± 7	28^{+8+6}_{-7-6}	$24 \pm 7 \pm 5$
$D_1(2424) \rightarrow D^*\pi$	11			
$D_1(2424) \rightarrow D^*\rho$	< 1			
$D_1(2424) \rightarrow D\rho$	6			
$D_1(2424) \rightarrow \text{all}$	18	20^{+9}_{-5}	20^{+6+3}_{-5-3}	$15 \pm 8 \pm 5$
$D_{s2}^*(2573) \rightarrow D^*K$	1.2			
$D_{s2}^*(2573) \rightarrow DK$	9.4			
$D_{s2}^*(2573) \rightarrow D_s\eta$	~ 0.1			
$D_{s2}^*(2573) \rightarrow \text{all}$	11	16^{+5+3e}_{-4-3}		
$D_{s1}(2536) \rightarrow D^*K$	< 1	< 4.6	< 2.3	< 3.2
$B_2^*(5771) \rightarrow B^*\pi$	11			
$B_2^*(5771) \rightarrow B\pi$	11			
$B_2^*(5771) \rightarrow B^*\rho$	3			
$B_2^*(5771) \rightarrow B\rho$	< 1			
$B_2^*(5771) \rightarrow \text{all}$	25			
$B_1(5759) \rightarrow B^*\pi$	17			
$B_1(5759) \rightarrow B^*\rho$	1			
$B_1(5759) \rightarrow B\rho$	3			
$B_1(5759) \rightarrow \text{all}$	21			
$B_{s2}^*(5861) \rightarrow B^*K$	~ 1			
$B_{s2}^*(5861) \rightarrow BK$	2.6			
$B_{s2}^*(5861) \rightarrow \text{all}$	4			
$B_{s1}(5849) \rightarrow B^*K$	~ 1			
$K_2^*(1429) \rightarrow K^*\pi$	12	25		
$K_2^*(1429) \rightarrow K\pi$	27	50		
$K_2^*(1429) \rightarrow K\rho$	12	9		
$K_2^*(1429) \rightarrow K\omega$	3	3		
$K_2^*(1429) \rightarrow \text{all}$	55	~ 103		
$K_1(1270) \rightarrow K^*\pi$	6	14		
$K_1(1270) \rightarrow K\rho$	38 ^f	38		
$K_1(1270) \rightarrow K\omega$	7	10		
$K_1(1270) \rightarrow \text{all}$	51	(90 ± 20)		

^aParticle Data Group, Ref. [10].

^bP. Avery, et al. (CLEO Collaboration), Ref. [3].

^cP.L. Frabetti et al. (E687 Collaboration), Ref. [3].

^dSum fixed at 25 MeV.

^eY. Kubota et al. (CLEO Collaboration), Ref. [18].

^fInput value.

TABLE III. Heavy Quark Symmetry predictions for decays of $3D(\frac{5}{2})$ heavy-light mesons.

Transition	Width (MeV)	
	Calculated	Observed ^a
$K_3^*(1770) \rightarrow K^*\pi$	45 ^b	45
$K_3^*(1770) \rightarrow K\pi$	62	32
$K_3^*(1770) \rightarrow K^*\rho$	13	
$K_3^*(1770) \rightarrow K\rho$	73	74
$K_3^*(1770) \rightarrow \text{all}$	193	(164 ± 17)
$K_2(1768) \rightarrow K^*\pi$	78	
$K_2(1768) \rightarrow K^*\rho$	21	
$K_2(1768) \rightarrow K\rho$	0 ^c	
$K_2(1768) \rightarrow \text{all}$	99	(136 ± 18)
$D_3^*(2830) \rightarrow D^*\pi$	54	
$D_3^*(2830) \rightarrow D\pi$	58	
$D_3^*(2830) \rightarrow D_s^*K$	14	
$D_3^*(2830) \rightarrow D_sK$	39	
$D_3^*(2830) \rightarrow D^*\rho$	18	
$D_3^*(2830) \rightarrow D\rho$	41	
$D_3^*(2830) \rightarrow D_s^*K^*$	< 1	
$D_3^*(2830) \rightarrow D_sK^*$	14	
$D_3^*(2830) \rightarrow \text{all}$	238	
$D_2(2830) \rightarrow D^*\pi$	95	
$D_2(2830) \rightarrow D_s^*K$	20	
$D_2(2830) \rightarrow D^*\rho$	23	
$D_2(2830) \rightarrow D\rho$	0 ^c	
$D_2(2830) \rightarrow D_s^*K^*$	< 1	
$D_2(2830) \rightarrow D_sK^*$	0 ^c	
$D_2(2830) \rightarrow \text{all}$	138	
$D_{s3}^*(2880) \rightarrow D^*K$	34	
$D_{s3}^*(2880) \rightarrow DK$	47	
$D_{s3}^*(2880) \rightarrow D^*K^*$	2	
$D_{s3}^*(2880) \rightarrow DK^*$	15	
$D_{s3}^*(2880) \rightarrow \text{all}$	98	
$D_{s2}(2880) \rightarrow D^*K$	60	
$D_{s2}(2880) \rightarrow D^*K^*$	3	
$D_{s2}(2880) \rightarrow DK^*$	0 ^c	
$D_{s2}(2880) \rightarrow \text{all}$	63	
$B_3^*(6148) \rightarrow B^*\pi$	70	
$B_3^*(6148) \rightarrow B\pi$	60	
$B_3^*(6148) \rightarrow B_s^*K$	18	
$B_3^*(6148) \rightarrow B_sK$	20	
$B_3^*(6148) \rightarrow B^*\rho$	7	
$B_3^*(6148) \rightarrow B\rho$	8	
$B_3^*(6148) \rightarrow B_s^*K^*$	< 1	
$B_3^*(6148) \rightarrow B_sK^*$	< 1	
$B_3^*(6148) \rightarrow \text{all}$	183	

$B_2(6148) \rightarrow B^* \pi$	122
$B_2(6148) \rightarrow B_s^* K$	32
$B_2(6148) \rightarrow B^* \rho$	12
$B_2(6148) \rightarrow B \rho$	0 ^c
$B_2(6148) \rightarrow B_s^* K^*$	< 1
$B_2(6148) \rightarrow B_s K^*$	0 ^c
$B_2(6148) \rightarrow \text{all}$	167
$B_{s3}^*(6198) \rightarrow B^* K$	49
$B_{s3}^*(6198) \rightarrow BK$	45
$B_{s3}^*(6198) \rightarrow B^* K^*$	2
$B_{s3}^*(6198) \rightarrow BK^*$	2
$B_{s3}^*(6198) \rightarrow \text{all}$	98
$B_{s2}(6198) \rightarrow B^* K$	85
$B_{s2}(6198) \rightarrow B^* K^*$	3
$B_{s2}(6198) \rightarrow BK^*$	0 ^c
$B_{s2}(6198) \rightarrow \text{all}$	88

^aParticle Data Group values, Ref. [10].

^bInput value.

^cSet to zero in the absence of experimental information.

D^{**} Shopping List

✓ Observe $D_{s2}^* \rightarrow DK$.

$$M(D_{s2}^*) = M(D_{s1}) + 35 \text{ MeV}/c^2 = 2572 \text{ MeV}/c^2 .$$

- Determine branching ratios for D_2^* , D_1 , D_{s2}^* .
- How narrow is D_{s1} ? (This probes mixing between the $j_q = \frac{1}{2}$ and $j_q = \frac{3}{2}$ p -wave states.)
- Determine strength of the transitions

$$\begin{aligned} D_2^* &\rightarrow D^* \rho \ (D\rho) \\ D_1 &\rightarrow (D^* \rho) \ D\rho \ . \end{aligned}$$

- Observe (or infer from total widths and observed partial widths) transitions between $D^{**}(j_q = \frac{3}{2}^+)$ and $D^{**}(j_q = \frac{1}{2}^+)$ levels. Can the broad 0^+ and 1^+ charm states be detected through

$$\begin{aligned} D_2^* &\rightarrow \pi(D_0^*, D_1') \\ D_1 &\rightarrow \pi D_0^* \text{ transitions?} \end{aligned}$$

Will the charm-strange 0^+ and 1^+ states be narrow because of the limited phase space for kaon emission?

- Discover

$$\begin{aligned} D_3^*(2830) &\rightarrow D^* \pi, \ D\pi, \ D_s K, \ D\rho \\ D_2(2830) &\rightarrow D^* \pi, \ D_s K, \ D^* \rho, \ \underline{D\rho}, \ \underline{D_s K^*} \\ D_{s3}^*(2880) &\rightarrow D^* K, \ D^* \bar{K}, \ DK^* \\ D_{s2}(2880) &\rightarrow D^* K, \ \underline{DK^*} \ . \end{aligned}$$

The underlined channels would provide a direct measure of the strength of the amplitude that we have been forced, by ignorance, to set to zero.

- Observe the cascade transitions

$$\begin{aligned} D_3^*(2830) &\rightarrow D_2^* \pi, \ D_1 \pi \\ D_2(2830) &\rightarrow D_2^* \pi \ . \end{aligned}$$

Given one partial width, we can use heavy-quark symmetry to predict all other $3D(\frac{5}{2}) \rightarrow 2P(\frac{3}{2}) +$ pseudoscalar transitions.

B^{**} Shopping List

- Observe $B_2^*(5767) \rightarrow B^{(*)}\pi$ and $B_1(5755) \rightarrow B^*\pi$. If these states are important channels for the production of B , they may make possible highly efficient flavor tagging for the study of CP violation and B^0 - \bar{B}^0 mixing.
- Observe $B_{s2}^*(5846) \rightarrow B^{(*)}K$ and $B_{s1}(5834) \rightarrow B^*K$.
- Determine branching ratios for B_2^* , B_1 , B_{s2}^* .
- How narrow is B_{s1} ? (This probes mixing between the $j_q = \frac{1}{2}$ and $j_q = \frac{3}{2}$ p -wave states.) Will the $j_q = \frac{1}{2}$ levels B_{s0}^* and B_{s1} be narrow because of the limited phase space for kaon emission?
- Search for

$$\begin{aligned} B_3^*(6148) &\rightarrow B^{(*)}\pi, B_s K, B^{(*)}\rho \\ B_2(6148) &\rightarrow B^*\pi, B_s^* K, B^*\rho, \underline{B\rho}, \underline{B_s K^*} \end{aligned}$$

If these states are narrow and prominent, they may be useful for tagging the flavor of B_s and \bar{B}_s .

$$\begin{aligned} B_{s3}^*(6198) &\rightarrow B^* K, B K, B K^* \\ B_{s2}(6198) &\rightarrow B^* K, \underline{B K^*} . \end{aligned}$$

These narrow states may be especially easy to identify.

The underlined channels would provide a direct measure of the strength of the amplitude that we have been forced, by ignorance, to set to zero.

- Do the B^{***} states (B_3^* , B_2) cascade through the B^{**} levels? Observe the cascade transitions

$$\begin{aligned} B_3^*(6148) &\rightarrow B_2^*\pi, B_1\pi \\ B_2(6148) &\rightarrow B_2^*\pi . \end{aligned}$$

The E781 Trigger and Data Acquisition System

Jürgen Engelfried*
Fermi National Accelerator Laboratory
Batavia, IL 60510

Abstract

The trigger and data acquisition system of Fermilab Experiment 781 (SELEX), a high statistics charm baryon experiment scheduled to run in the next Fermilab fixed target run in 1996, is briefly described. The first and second level hardware triggers are expected to reduce the trigger rate by at least a factor of 10 compared to the interaction rate. A third level software trigger searching for secondary vertices is expected to cut by another factor of 40.

1 Experiment Description

E781 [1] expects to collect several 10^5 reconstructed charm baryons. The experiment is described in more detail in [2]. Here we will only point out important parts used to trigger on charm particles.

Charm particles will be produced in a segmented target (4 % of an interaction length) by a 650 GeV, 2 MHz negative beam, mostly containing Σ^- and π^- . Twenty planes of 20 μm and 25 μm pitch silicon microstrip detectors immediately follow the target and are used to reconstruct tracks from the primary and secondary vertices with high precision. Three magnets surrounded by proportional wire and drift chambers are used to measure the momenta of charged particles. A TRD and a RICH are used for particle identification. The setup is completed by a three-stage electromagnetic leadglass calorimeter and a hadron calorimeter. The overall length of the experiment is about 50 meters. Scintillator hodoscopes are placed behind the second magnet to be used in the trigger.

2 Level One and Two Hardware Triggers

The first level trigger requires at least 3 positive particles in the hodoscopes behind the second magnet, which has an implicit momentum cut of $\approx 15 \text{ GeV}/c$. This, together with a signal from an interaction counter directly after the second microstrip plane and an (optional) beam particle tag obtained from the beam TRD, will form the first level trigger within $\leq 150 \text{ nsec}$ after the interaction. We will use this signal to gate the front end electronics.

*for the E781 Collaboration

In the second level trigger we may use the hit correlation in the hodoscopes to select at least one positive track of $> 25 \text{ GeV}/c$, but the second level is mostly needed for other physics triggers. After this signal we will start the front end readout, otherwise we will clear the front end electronics.

3 Trigger Rates and Readout Speed

We expect the hardware trigger (level one and two together) to reduce the interaction rate by at least a factor of ten. This was checked with data from E653 and with Monte Carlo. We expect a raw trigger rate of 10 KHz. With an online deadtime of $\leq 30 \mu\text{sec}$ and an event size of $\approx 5 \text{ KBytes}$ we have to read out 35 MBytes/sec.

4 The Data Acquisition System

The data acquisition system was developed in close collaboration with other experiments and the FNAL OLS group as part of the Fermilab DART project [3]. The data will be collected in ten independent streams and stored in VME dual ported memories. We expect to collect 140,000 events with 700 MBytes of data over the twenty second spill. A schematic layout of the system is shown in figure 1.

During the whole 1 minute cycle time of the Tevatron we will transfer the data of two of the streams containing the silicon microstrip, the PWC, and the RICH data (about 25 % of the event size) via a fast VME to VME crate interconnect to an SGI Challenge L with twelve processors, with a total computing power of 1300 MIPs. The data will be distributed to twelve filter jobs using the DART Data Flow Manager (DFM) [4]. After a positive decision of the level three filter job the total event will be logged from the VME crate to 8 mm tape at a rate of about 300 KByte/sec.

5 The Level Three Software Filter

To select charm particles we make use of the long lifetime (several 100 femtoseconds) which produces typical laboratory flight paths of several millimeters. This secondary vertex can be separated from the primary vertex by a high-resolution vertex detector consisting of silicon microstrips. We will not reconstruct the full secondary vertex in the filter code. Instead we ask only that one of the tracks seen in the downstream spectrometer has a sizeable miss-distance (impact parameter) from the beam particle at the center of the thin ($< 1.5 \text{ mm}$) production target.

First the tracks in the second spectrometer will be reconstructed, using only the information from the proportional wire chambers. The tracks will be extrapolated back to the silicon microstrip detector to select hits. The impact parameter of these tracks to the primary vertex reconstructed from the beam track is then calculated.

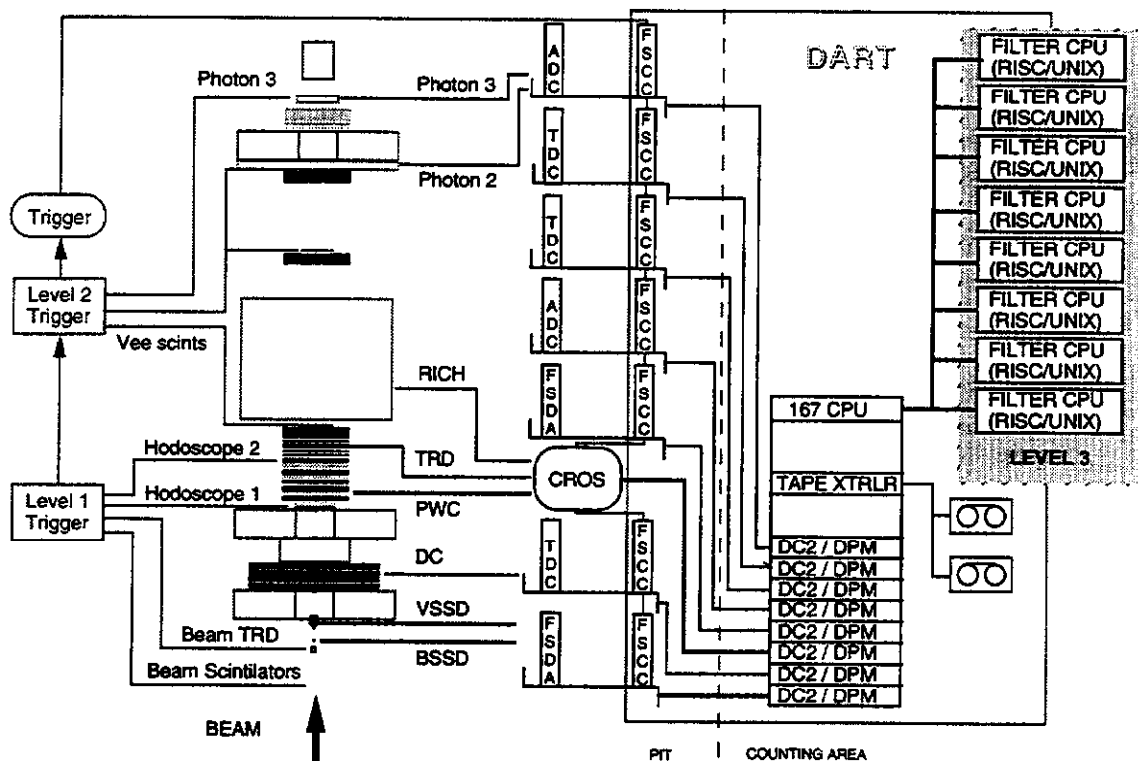


Figure 1: Schematic layout of the E781 data acquisition system

In Figure 2 we show the distribution of the maximum miss distance in each event for downstream 3-track events from the E781T data [5]. A cut at a miss distance of $30\text{ }\mu\text{m}$ gives a rejection factor of 10; extrapolating to the full E781 vertex detector, which will have 20 plans in 4 views instead of 8 planes in 2 views, we project gaining at least a factor of 2 in additional rejection.

With this algorithm we will select most of the charmed baryons with high efficiency. For states with extremely short lifetimes [6] we plan to use additional information from the RICH detector to select final states with a simultaneous K^- and proton, indicative of a Ξ_c^0 or Ω_c^0 decay, as well as to trigger on exotic strong-interaction states which have baryons in their decays.

To measure the speed of the algorithm, we used code developed for E781T and timed it on a SGI Challenge L. At the current time, we need about 7msec/event for the miss-distance algorithm, which will translate to about 1700 MIPs of computing power to process 140000 events/minute. However, we are confident that we can reduce the time by optimizing

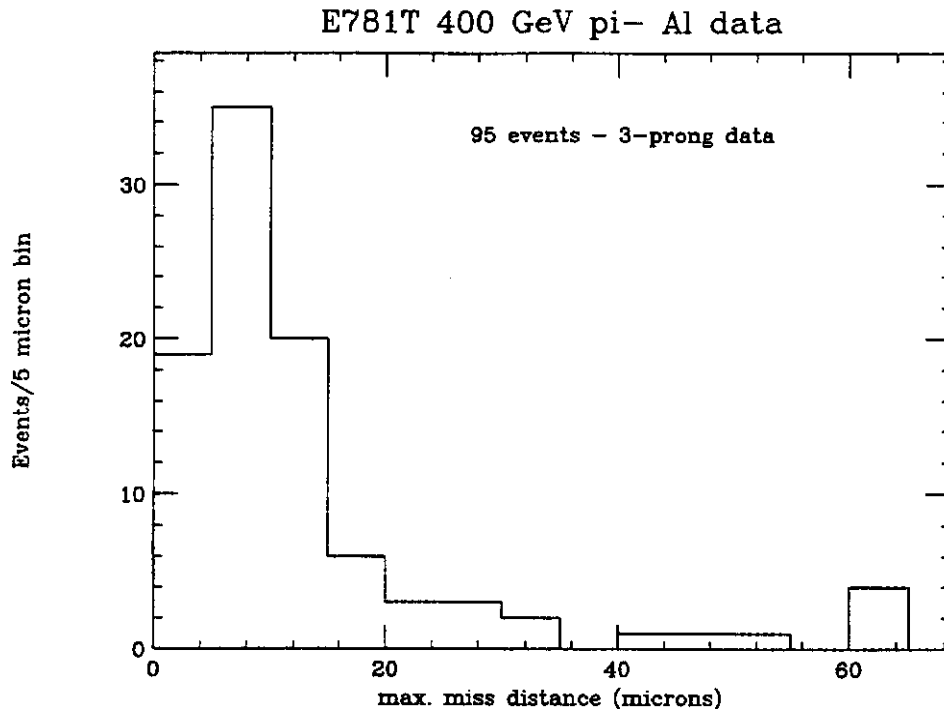


Figure 2: Maximum miss-distance for downstream 3-track events from E781T.

the code. The RICH part will only add a few hundred μsec per event, since most of the information needed for the RICH algorithm, especially the track information from the second spectrometer, is already calculated for the miss distance algorithm.

References

- [1] E781 Collaboration: Carnegie Mellon University, Fermilab, University of Iowa, University of Rochester, University of Washington, Petersburg Nuclear Physics Institute, ITEP (Moscow), IHEP (Protvino), Moscow State University, University of São Paulo, Centro Brasileiro de Pesquisas Físicas, Universidade Federal de Paraíba, IHEP (Beijing), University of Bristol, Tel Aviv University, Max-Planck-Institut für Kernphysik (Heidelberg), Universidad Autonoma de San Luis Potosi.
- [2] J. Russ, these proceedings.
- [3] R. Pordes et al., "Fermilab's DART DA System", FERMILAB-CONF-94-103.
- [4] D. Berg et al., "Data Flow Manager for DART", FERMILAB-CONF-94-104.
- [5] J. Russ et al, in DPF 92, C.H. Albright, P.H. Kasper, R. Raja, J. Yoh, eds., (World Scientific) 1746 (1992).
- [6] J. Butler (E687), private communication.

The $D^0\bar{D}^0$ Mixing Search — Current Status and Future Prospects

Tiehui (Ted) Liu

Harvard University, Cambridge, MA 02138

Abstract

The search for $D^0\bar{D}^0$ mixing carries a large discovery potential for new physics since the $D^0\bar{D}^0$ mixing rate is expected to be very small in the Standard Model. The past decade has seen significant experimental progress in sensitivity, from 20% down to 0.37%. This paper discusses the techniques (including some new ideas), current experimental status, and future prospects for the mixing search. The conclusion is that while it is possible that the mixing sensitivity may decrease to 10^{-5} around the year 2000, reaching the 10^{-6} level will certainly be quite difficult.

1 Introduction

Following the discovery of the D^0 meson at SPEAR in 1976, experimenters began to search for $D^0\bar{D}^0$ mixing, using a variety of techniques. The past decade has seen significant experimental progress in sensitivity (from 20% down to 0.37% [1] to [13]), as can be seen in Figure 1. Much of the enthusiasm for searching for $D^0\bar{D}^0$ mixing comes from the belief that the search for $D^0\bar{D}^0$ mixing carries a large discovery potential for New Physics, since the mixing rate $R_{\text{mixing}} \equiv \mathcal{B}(D^0 \rightarrow \bar{D}^0 \rightarrow \bar{f}) / \mathcal{B}(D^0 \rightarrow f)$ is expected to be very small in the Standard Model. Theoretical calculations of $D^0\bar{D}^0$ mixing in the Standard Model are plagued by large uncertainties. While short distance effects from box diagrams are known [14] to give a negligible contribution ($\sim 10^{-10}$), the long distance effects from second-order weak interactions with mesonic intermediate states may give a much larger contribution. Estimates of R_{mixing} from long distance effects range from 10^{-7} to 10^{-3} [15]. However, it has recently been argued by Georgi and others that the long distance contributions are smaller than previously estimated, implying that cancellations occur between contributions from different classes of intermediate mesonic states [16], and the prevailing conclusion within the Standard Model seems to be that $R_{\text{mixing}} < 10^{-7}$. A measurement of such a small mixing rate is impossible with present experimental sensitivity. However, the observation of a larger value for R_{mixing} in the $D^0\bar{D}^0$ system would imply the existence of new physics beyond the Standard Model [17]. Examples includes flavor-changing neutral currents mediated by the exchange of a non-standard Higgs scalar with a mass of a few TeV/ c^2 , which could lead to R_{mixing} as large as 0.5%.

Recently, CLEO has observed a signal for $D^0 \rightarrow K^+\pi^-$ [18], and found $R = \mathcal{B}(D^0 \rightarrow K^+\pi^-) / \mathcal{B}(D^0 \rightarrow K^-\pi^+) \sim 0.8\%$ [19]. Normally, D^0 decays by Cabibbo favored decay $D^0 \rightarrow K^-\pi^+$ and $\bar{D}^0 \rightarrow K^+\pi^-$. A signal for $D^0 \rightarrow K^+\pi^-$ could indicate mixing of $D^0 \rightarrow \bar{D}^0$. But it could also indicate a different decay channel, namely, Doubly Cabibbo Suppressed

Decay(DCSD) $D^0 \rightarrow K^+\pi^-$, which is suppressed with respect to the Cabibbo favored decay by a factor of $\tan^4\theta_C \sim 0.3\%$ where θ_C is the Cabibbo angle. Unfortunately, without a precision vertex detector, CLEO is unable to distinguish a potential mixing signal from DCSD. As Purohit pointed out [20]: “The CLEO II result makes the entire subject of $D^0\bar{D}^0$ mixing very interesting. It really calls for a fixed-target experiment to use its decay time resolution to decide whether the signal is due to DCSD or mixing”. If the number of reconstructed charm decays can reach 10^8 around the year 2000, that would allow one to reach a new threshold of sensitivity to $D^0\bar{D}^0$ mixing, and perhaps actually observe it. This is why charm mixing has been singled out for its own working group at this workshop.

This paper is organized as follows: Section 2 discusses the techniques which can be used to search for mixing, including two new ideas. One of them is to use $D^0 \rightarrow K^+K^-, \pi^+\pi^-$ etc. to study mixing (see 2.1.1), and the other is to use the difference in the resonant substructure in $D^0 \rightarrow K^+\pi^-\pi^0, D^0 \rightarrow K^+\pi^-\pi^+\pi^-$ etc. to distinguish mixing and DCSD (see 2.1.2). In each case, the relevant phenomenology will be briefly presented. Section 3 discusses the present status and future prospects of searching for mixing at different experiments. In section 4, a comparison of the future prospects of the different experiments with different techniques will be given. A brief summary is in Section 5.

2 The Techniques

The techniques which can be used to search for mixing can be roughly divided into two classes: hadronic and semi-leptonic. Each method has advantages and limitations, which are described below.

2.1 Hadronic method

The hadronic method is to search for the D^0 decays $D^0 \rightarrow K^+\pi^-(X)$. These decays can occur either through $D^0\bar{D}^0$ mixing followed by Cabibbo favored decay $D^0 \rightarrow \bar{D}^0 \rightarrow K^+\pi^-(X)$, or through DCSD $D^0 \rightarrow K^+\pi^-(X)$. This means that the major complication for this method is the need to distinguish between DCSD and mixing [21]. The hadronic method can therefore be classified according to how DCSD and mixing are distinguished. In principle, there are at least three different ways to distinguish between DCSD and mixing candidates experimentally: (A) use the difference in the decay time-dependence; (B) use the possible difference in the resonant substructure in $D^0 \rightarrow K^+\pi^-\pi^0, K^+\pi^-\pi^+\pi^-$, etc. modes; (C) use the quantum statistics of the production and the decay processes.

Method (A) requires that the D^0 be highly boosted and so that the decay time information can be measured. Method (B) requires knowledge of the resonant substructure of the DCSD decays, which is unfortunately something about which we have no idea at this time. Finally, method (C) requires that one use e^+e^- annihilation in the charm threshold region. In the following, we will discuss these three methods in some detail.

2.1.1 Method A –use the difference in the time-dependence of the decay

This method [22] is to measure the decay time of the $D^0 \rightarrow K^+\pi^-$ decay. Here the D^0 tagging is usually done by using the decay chain $D^{*+} \rightarrow D^0\pi_s^+$ followed by $D^0 \rightarrow K^+\pi^-$. The π_s^+ from D^{*+} has a soft momentum spectrum and is referred to as the slow pion. The idea is to search for the wrong sign D^{*+} decays, where the slow pion has the same charge as the kaon arising from the D^0 decay. This technique utilizes the following facts: (1) DCSD and mixing have different decay time-dependence, which will be described below. (2) The charge of the slow pion is correlated with the charm quantum number of the D^0 meson and thus can be used to tag whether a D^0 or \bar{D}^0 meson was produced in the decay $D^{*+} \rightarrow D^0\pi_s^+$ or $D^{*-} \rightarrow \bar{D}^0\pi_s^-$. (3) The small Q value of the D^{*+} decay results in a very good mass resolution in the mass difference $\Delta M \equiv M(D^{*+}) - M(D^0) - M(\pi_s^+)$ and allows a D^{*+} signal to be obtained with very low background. (4) The right sign signal $D^{*+} \rightarrow D^0\pi_s^+$ followed by $D^0 \rightarrow K^-\pi^+$ can be used to provide a model-independent normalization for the mixing measurement.

A pure D^0 state generated at $t = 0$ decays to the $K^+\pi^-$ state either by $D^0\bar{D}^0$ mixing or by DCSD, and the two amplitudes may interfere. The amplitude for a D^0 decays to $K^+\pi^-$ relative to the amplitude for a D^0 decays to $K^-\pi^+$ is given by

$$A = \sqrt{R_{\text{mixing}}/2} t + \sqrt{R_{\text{DCSD}}} e^{i\phi} \quad (1)$$

where ϕ is an unknown phase, t is measured in units of average D^0 lifetime. Here $R_{\text{mixing}} = (x^2 + y^2)/2$ where $x = \delta m/\gamma_+$, $y = \gamma_-/\gamma_+$. The quantities γ_{\pm} and δm are defined by $\gamma_{\pm} = (\gamma_1 \pm \gamma_2)/2$ and $\delta m = m_2 - m_1$ with m_i, γ_i ($i = 1, 2$) being the masses and decay rates of the two CP eigen states. Besides, $R_{\text{DCSD}} = |\rho|^2$ (assuming CP conservation), where ρ is defined as $\rho = \text{Amp}(D^0 \rightarrow K^+\pi^-)/\text{Amp}(\bar{D}^0 \rightarrow K^+\pi^-)$. Here we have also assumed a small mixing; namely, $\delta m, \gamma_- \ll \gamma_+$ or $x, y \ll 1$.

The first term, which is proportional to t , is due to mixing and the second term is due to DCSD. It is this unique attribute of the decay time-dependence of mixing which can be used to distinguish between DCSD and mixing. Now we have:

$$R(t) = (R_{\text{DCSD}} + \sqrt{2R_{\text{mixing}}R_{\text{DCSD}}} t \cos\phi + 1/2 R_{\text{mixing}} t^2) e^{-t} \quad (2)$$

Define $\alpha = R_{\text{mixing}}/R_{\text{DCSD}}$, which describes the strength of mixing relative to DCSD. Then equation (2) can then be rewritten as:

$$R(t) = R_{\text{DCSD}}(1 + \sqrt{2\alpha} t \cos\phi + 1/2 \alpha t^2) e^{-t} \quad (3)$$

From this equation, one may read off the following properties: (1) The mixing term peaks at $t = 2$. (2) The interference term peaks at $t = 1$. (3) A small mixing signature can be greatly enhanced by DCSD through interference (with $\cos\phi \neq 0$) at lower decay times. The ratio between the interference term and the mixing term, denoted $\xi(t)$, is given by $\xi(t) = \sqrt{8/\alpha} \cos\phi/t \propto \sqrt{1/\alpha}$. So when $\alpha \rightarrow 0$, $\xi \rightarrow \infty$. For example, with $\cos\phi=1$, at $t = 1$ for $\alpha = 10\%, 1\%, 0.1\%, 0.01\%, 0.001\%$ (corresponding to $R_{\text{mixing}} = 10^{-3}, 10^{-4}, 10^{-5}, 10^{-6}, 10^{-7}$) one

has $\xi(t) = 9, 28, 90, 280, 900$ respectively. (4) Only for $t > \sqrt{8/\alpha} |\cos\phi|$ does the interference term become smaller than the mixing term. (5) $R(t_0) = 0$ happens and only happens when $\cos\phi = -1$, and only at location $t_0 = \sqrt{2/\alpha}$. For $\alpha = 10\%, 1\%, 0.1\%$, one has $t_0 = 4.5, 14.1, 44.7$. (6) One can obtain a very pure DCSD sample by cutting at low decay time: $t < \zeta \sim 0.1$. At such low t , the mixing term drops out and leaving only the interference term. Let's define the purity of DCSD to be $\mathcal{P}_{DCSD} = 1 - \int_0^\zeta \sqrt{2\alpha} \cos\phi (te^{-t}) / \int_0^\zeta e^{-t}$. For $\zeta \sim 0.1$ one get $\mathcal{P}_{DCSD} = \sqrt{2\alpha} \cos\phi \zeta / (2 + \zeta)$. Let's take $\zeta = 0.2$, for $\alpha = 10\%, 1\%$, we can get $\mathcal{P}_{DCSD} = 96\%, 99\%$ pure DCSD respectively. (7) The cut $t \leq \zeta$ cuts off only $1 - (1 + \zeta)e^{-\zeta} \sim \zeta^2/2 = 2\%$ from the whole interference term.

While Property (1) tells us that the mixing term does live at longer decay time, Property (3) tells us clearly that we should not ignore the interference term. In fact, that's the last thing one wants to ignore! (unless we know for sure $\cos\phi = 0$). It is the commonly believed "annoying background", namely DCSD, that could greatly enhance the chance of seeing a very small mixing signal. (In semi-leptonic method, one does not have this advantage). For a very small mixing rate, almost all the mixing signature could show up in the interference term, not in the mixing term, as long as $\cos\phi \neq 0$. Property (2) tells us at which location one expect to find the most rich signature of a potential small mixing, which is where the interference term peaks: $t \sim 1$ (why should one keep worrying about long lived DCSD tails? let's hope for $\cos\phi \neq 0$ first.) Property (5) shows that destructive interference is not necessarily a bad thing. In fact, it could provide extra information. For example, if $\cos\phi = -1$, then one should find $R(t_0) = 0$ at $t_0 = \sqrt{2/\alpha}$, see Figure 5. For the general case, interference will lead to very characteristic time distribution, as can be clearly seen in Figure 6. Properties (6) and (7) show that we can study DCSD well without being confused by the possible mixing component. This will become important when we discuss method B.

Figure 5 shows that the signature of mixing is a deviation from a perfect exponential time distribution with the slope of γ_+^{-1} . Our ability to observe this signature depends on the number of $D^0 \rightarrow K^+\pi^-(X)$ events we will have. Right now this is limited by the rather poor statistics. Figures 3 and 4 show each term with $\alpha = 10\%$ and $\cos\phi = \pm 1$ (with $R_{DCSD} = 1$).

It is interesting to point out here that, in principle, the Singly Cabibbo Suppressed Decays (SCSD), such as $D^0 \rightarrow K^+K^-, \pi^+\pi^-$ can be used to study mixing. This is because (assuming CP conservation) those decays occur only through the CP even eigenstate, which means the decay time distribution is a perfect exponential time distribution with the slope of γ_1 . Therefore, one can use those modes to measure γ_1 . The mixing signature is not a deviation from a perfect exponential (again assuming CP conservation), but rather a deviation of the slope from $(\gamma_1 + \gamma_2)/2$. Since $\gamma_+ = (\gamma_1 + \gamma_2)/2$ can be measured by using the $D^0 \rightarrow K^-\pi^+$ decay time distribution, one can then measure $y = \gamma_-/\gamma_+ = (\gamma_1 - \gamma_2)/(\gamma_1 + \gamma_2)$. Observation of a non-zero y would demonstrate mixing caused by the decay rate difference ($R_{\text{mixing}} = (x^2 + y^2)/2$). It is worth pointing out that in this case other CP even (odd) final states such as $D^0 \rightarrow K^+K^-K^+K^-, \pi^+\pi^-\pi^+\pi^-$ ($\pi^+\pi^-\pi^0, K^+K^-\pi^0$) can be used to measure $\gamma_1(\gamma_2)$. In addition, there is no need to tag the D^0 nor know the primary vertex location,

¹One can use $D^0 \rightarrow K^-\pi^-$ to study the acceptance function versus decay time.

since we only need to determine the slope. I should point out also that this method is only sensitive to mixing caused by the decay rate difference between the two eigen states, not to mixing caused by the mass difference $x = \delta m / \gamma_+$ ($\delta m = m_2 - m_1$). The sensitivity of this method is discussed in section 4.1.

2.1.2 Method B – use difference in resonant substructure

The idea of this new method is to use the wrong sign decay $D^{*+} \rightarrow D^0 \pi_s^+$ followed by $D^0 \rightarrow K^+ \pi^- \pi^0$, $K^+ \pi^- \pi^+ \pi^-$, etc., and use the possible differences of the resonant substructure between mixing and DCSD to study mixing. There are good reasons to believe that the resonant substructure of DCSD decay is different from that of mixing (Cabibbo favored decay, CFD). We can use the $D^0 \rightarrow K^+ \pi^- \pi^0$ decay as an example. For CFD and DCSD, the true yield density $n(p)$ at a point p in the Dalitz plot can be written as:

$$n(p) \propto |f_1 e^{i\phi_1} A_{3b} + f_2 e^{i\phi_2} BW_{\rho^+}(p) + f_3 e^{i\phi_3} BW_{K^{*0}}(p) + f_4 e^{i\phi_4} BW_{K^{*0}}(p)|^2 \quad (4)$$

where f_i are the relative amplitudes for each component and ϕ_i are the interference phases between each submode. A_{3b} is the S-wave three-body decay amplitude, which is flat across the Dalitz plot. The various $BW(p)$ terms are Breit-Wigner amplitudes for the $K^* \pi$ and $K \rho$ sub-reactions. Note that in general ²,

$$f_i^{DCSD} / f_i^{CFD} \neq f_j^{DCSD} / f_j^{CFD} \quad (i \neq j) \quad (5)$$

$$\phi_i^{DCSD} \neq \phi_i^{CFD} \quad (6)$$

This means that the resonant substructure (the true yield density $n(p)$) for DCSD is different from that of mixing ³. As both DCSD and mixing contribute to the wrong sign decay, the yield density for the wrong sign events $n_w(p)$ will have a complicated form, due to the fact that for each submode DCSD and mixing may interfere with each other. Just like in method A, for very small mixing, the interference term between DCSD and mixing will be the most important one.

In principle, one can use the difference between the resonant substructure for DCSD and mixing events to distinguish mixing from DCSD. For instance, combined with method A, one can perform a multi-dimensional fit to the data by using the information on ΔM , $M(D^0)$, proper decay time t and the yield density on Dalitz plot $n_w(p, t)$. The extra information

²It has been pointed out [23, 33] that it is unlikely that just one universal suppression factor will affect the individual DCSD. For example, SU(3) breaking can introduce a significant enhancement for D^0 DCSD decays $D^0 \rightarrow K^+ \pi^-$, $K^{*+} \pi^-$, while SU(6) breaking can introduce a sizeable suppression relative to the naive expectation for D^0 DCSD decay $D^0 \rightarrow K^+ \rho^-$.

³The sign of the interference between each submode changes whenever $\cos\theta_R$ (θ_R is the helicity angle of the resonance) changes sign. This is the same for both the Cabibbo favored decay and the DCSD. This can be easily seen from the Breit-Wigner amplitude which describes the strong resonances and decay angular momentum conservation: $BW_R \propto \frac{\cos\theta_R}{M_{ij} - M_R - i\Gamma_R/2}$ where M_R and Γ_R are the mass and width of the M_{ij} resonance (the K^* or ρ). The difference between Cabibbo favored decay and DCSD comes from the relative amplitude f_i for each submode and the interference phase term $e^{i\phi_i}$.

on the resonant substructure will, in principle, put a much better constraint on the amount of mixing. Of course, precise knowledge of the resonant substructure for DCSD is needed here and so far we do not know anything about it. Because of this, for current experiments this method is more likely to be a complication rather than a better method when one tries to apply method A to $D^0 \rightarrow K^+\pi^-\pi^0$ (see section 3.2 and [24]) or $D^0 \rightarrow K^+\pi^-\pi^+\pi^-$. In principle, however, one can use wrong sign samples at low decay time (which is almost pure DCSD, see section 2.1.1.) to study the resonant substructure of the DCSD decays. In the near future, we should have a good understanding of DCSD decays and this method could become a feasible way to search for mixing.

2.1.3 Method C —use quantum statistics of the production and decay processes

This method is to search for dual identical two-body hadronic decays in $e^+e^- \rightarrow \Psi'' \rightarrow D^0\bar{D}^0$, such as $(K^-\pi^+)(K^-\pi^+)$, as was first suggested by Yamamoto in his Ph.D thesis [25]. The idea is that when $D^0\bar{D}^0$ pairs are generated in a state of odd orbital angular momentum (such as Ψ''), the DCSD contribution to identical two-body pseudo-scalar-vector ($D \rightarrow PV$) and pseudo-scalar-pseudo-scalar ($D \rightarrow PP$) hadronic decays (such as $(K^-\pi^+)(K^-\pi^+)$) cancels out, leaving only the contribution of mixing [25, 23, 26]. As many people have asked about this, I would like to show here the essence of Yamamoto's original calculation for the $(K^-\pi^+)(K^-\pi^+)$ case. Let's define $e_i(t) = e^{-im_it - \gamma_i t/2}$ ($i = 1, 2$) and $e_{\pm}(t) = (e_1(t) \pm e_2(t))/2$. A state that is purely $|D^0\rangle$ or $|\bar{D}^0\rangle$ at time $t = 0$ will evolve to $|D(t)\rangle$ or $|\bar{D}(t)\rangle$ at time t , with $|D(t)\rangle = e_+(t)|D^0\rangle + e_-(t)|\bar{D}^0\rangle$ and $|\bar{D}(t)\rangle = e_-(t)|D^0\rangle + e_+(t)|\bar{D}^0\rangle$. In $e^+e^- \rightarrow \Psi'' \rightarrow D^0\bar{D}^0$, the $D^0\bar{D}^0$ pair is generated in the state $D^0\bar{D}^0 - \bar{D}^0D^0$ as the relative orbital angular momentum of the pair $\mathcal{L} = 1$. Therefore, the time evolution of this state is given by $|D(t)\bar{D}(t')\rangle - |\bar{D}(t)D(t')\rangle$, where t (t') is the time of decay of the D (\bar{D}). Now the double-time amplitude $\mathcal{A}_w(t, t')$ that the left side decays to $K^-\pi^+$ at t and the right side decays to $K^-\pi^+$ at t' , giving a wrong sign event $(K^-\pi^+)(K^-\pi^+)$, is given by:

$$\mathcal{A}_w(t, t') = (e_+(t)e_-(t') - e_-(t)e_+(t'))(a^2 - b^2) \quad (7)$$

where $a = \langle K^-\pi^+ | D^0 \rangle$ is the amplitude of the Cabibbo favored decay $D^0 \rightarrow K^-\pi^+$, while $b = \langle K^-\pi^+ | \bar{D}^0 \rangle$ is the amplitude of DCSD $\bar{D}^0 \rightarrow K^-\pi^+$. Similarly, the double-time amplitude $\mathcal{A}_r(t, t')$ for the right sign event $(K^-\pi^+)(K^+\pi^-)$ is given by:

$$\mathcal{A}_r(t, t') = (e_+(t)e_+(t') - e_-(t)e_-(t'))(a^2 - b^2) \quad (8)$$

One measures the wrong sign versus right sign ratio R , which is:

$$R = \frac{N(K^-\pi^+, K^-\pi^+) + N(K^+\pi^-, K^+\pi^-)}{N(K^-\pi^+, K^+\pi^-) + N(K^+\pi^-, K^-\pi^+)} = \frac{\iint \mathcal{A}_w(t, t') dt dt'}{\iint \mathcal{A}_r(t, t') dt dt'} \quad (9)$$

Note in taking the ratio, the amplitude term $(a^2 - b^2)$ in Equations (7) and (8) drop out. Thus, clearly R does not depend on whether b is zero (no DCSD) or finite (with DCSD). Integrating over all times, one then obtains $R = (x^2 + y^2)/2 = R_{\text{mixing}}$, where x and y are defined as before.

This is probably the best way to separate DCSD and mixing. The exclusive nature of the production guarantees both low combinatoric backgrounds and production kinematics essential for background rejection. This method requires one use e^+e^- annihilation in the charm threshold region (where one cannot observe the D decay vertex). Here the best final state is $(K^-\pi^+)(K^-\pi^+)$. In principle, one can also use final states like $(K^-\rho^+)(K^-\rho^+)$ or $(K^{*-}\pi^+)(K^{*-}\pi^+)$, etc., although again there are complications. For example, it is hard to differentiate experimentally $(K^-\rho^+)(K^-\rho^+)$ from $(K^-\rho^+)(K^-\pi^+\pi^0)$, where DCSD can contribute. With high statistics, in principle, this method could be combined with method B.

It is worth pointing out that quantum statistics yield different correlations for the $D^0\bar{D}^0$ decays from $e^+e^- \rightarrow D^0\bar{D}^0, D^0\bar{D}^0\gamma, D^0\bar{D}^0\pi^0$. The well-defined coherent quantum states of the $D^0\bar{D}^0$ can be, in principle, used to provide valuable cross checks on systematic uncertainties and, more importantly, to extract $x = \delta m/\gamma_+$ and $y = \gamma_-/\gamma_+$ if mixing is observed [32].

2.2 Semi-leptonic method

The semi-leptonic method is to search for $D^0 \rightarrow \bar{D}^0 \rightarrow Xl^-\nu$ decays, where there is no DCSD involved. However, it usually (not always!) suffers from a large background due to the missing neutrino, in addition, the need to understand the large background often introduces model dependence. In the early days, the small size of fully reconstructed samples of exclusive D^0 hadronic decays and the lack of the decay time information made it difficult to constrain the $D^0\bar{D}^0$ mixing rate using the hadronic method, many experiments used semi-leptonic decays. The techniques that were used were similar—searching for like-sign $\mu^+\mu^+$ or $\mu^-\mu^-$ pairs in $\mu^+N \rightarrow \mu^+(\mu^+\mu^+)X$ [4, 7] and $\pi^-Fe \rightarrow \mu^+\mu^+$ [5], $\pi^-W \rightarrow \mu^+\mu^+$ [10]. These techniques rely on the assumptions on production mechanisms, and the accuracy of Monte Carlo simulations to determine the large conventional sources of background.

There are other ways of using the semi-leptonic method. The best place to use the semi-leptonic method is probably in e^+e^- annihilation near the charm threshold region. The idea is to search for $e^+e^- \rightarrow \Psi'' \rightarrow D^0\bar{D}^0 \rightarrow (K^-l^+\nu)(K^-l^+\nu)$ or $e^+e^- \rightarrow D^-D^{*+} \rightarrow (K^+\pi^-\pi^-)(K^+l^-\nu)\pi_s^+$ [27, 28]. The latter is probably the only place where the semi-leptonic method does not suffer from a large background. It should have a low background, as there is only one neutrino missing in the entire event, and therefore threshold kinematics constraints should provide clean signal.

It is worth pointing out that one can not claim a $D^0\bar{D}^0$ mixing signal based on the semi-leptonic method alone (unless with the information on decay time of D^0)⁴. Nevertheless, one can always use this method to set upper limit for mixing.

⁴Bigi [32] has pointed out that an observation of a signal on $D^0 \rightarrow l^+X$ establishes only that a certain selection rule is violated in processes where the charm quantum number is changed, namely the rule $\Delta\text{Charm} = -\Delta Q_l$ where Q_l denotes leptonic charge. This violation can occur either through $D^0\bar{D}^0$ mixing (with the unique attribute of the decay time-dependence of mixing), or through new physics beyond the Standard Model (which could be independent of time).

3 Mixing Searches at Different Experiments

3.1 e^+e^- running on $\Psi''(3770)$ – MARK III, BES, Tau-charm factory

The MARK III collaboration was the first (though hopefully not the last) to use the $e^+e^- \rightarrow \Psi'' \rightarrow D^0 \bar{D}^0$ technique. They reported preliminary results for two “wrong-sign” D^0 decay events (unpublished) [30], one was consistent with $K^-\rho^+$ vs. $K^-\rho^+$, while the other one was consistent with $K^{*0}\pi^0$ vs. $K^{*0}\pi^0$. This was a very interesting result at that time, and had a strong influence on the subject. However, one cannot draw a firm conclusion about the existence of $D^0 \bar{D}^0$ mixing based on these events. There are at least two reasons: (1) The background study has to rely on Monte Carlo simulation of the PID (particle identification – Time-of-Flight). As Gladding has pointed out: “These results must be considered preliminary because the calculation of the confidence level is sensitive to the tails of PID distribution for the background” [31]; (2) Assuming that the Monte Carlo background study is correct, and that the events are real, one still cannot claim the two events are due to mixing, for example, the non-resonant decays $D^0 \rightarrow K\pi\pi^0$ may contribute to one side of the pair in each of the events, in which DCSD can contribute.

The MARK III puzzle can be completely solved at a τ -charm factory, which is a high luminosity ($10^{33} \text{ cm}^{-2} \text{ s}^{-1}$) e^+e^- storage ring operating at center-of-mass energies in the range 3-5 GeV. The perspectives for a $D^0 \bar{D}^0$ mixing search at a τ -charm factory have been studied in detail [27, 28]. I will outline here the most important parts. The best way to search for mixing is probably to use $e^+e^- \rightarrow \Psi'' \rightarrow D^0 \bar{D}^0 \rightarrow (K^-\pi^+)(K^-\pi^+)$. The sensitivity is not hard to estimate. Assuming a one year run with a luminosity of $10^{33} \text{ cm}^{-2} \text{ s}^{-1}$, 5.8×10^7 D^0 s would be produced from Ψ'' . Therefore about 9×10^4 $(K^-\pi^+)(K^+\pi^-)$ events would be produced. About 40% of them (3.6×10^4) could be fully reconstructed. A detailed study has shown that the potential dominant background comes from doubly misidentified $(K^-\pi^+)(K^+\pi^-)$, and if TOF resolution is 120 ps, this background can be kept to the level of one event or less. This means one can set an upper limit at the 10^{-4} level.

As mentioned above, the best place to use the semi-leptonic method is probably at a τ -charm factory. One good example is to search for $e^+e^- \rightarrow D^- D^{*+} \rightarrow (K^+\pi^-\pi^+)(K^+l^-\nu)\pi_s^+$. It is expected that this method can also have a sensitivity at the 10^{-4} level. There are many other independent techniques that one can use for a mixing search at a τ -charm factory. By combining several independent techniques (which require running at different energies), it was claimed that $D^0 \bar{D}^0$ mixing at the 10^{-5} level could be observable.

There have been several schemes around the world for building a τ -charm factory. If such a machine is built, it could be a good place to study mixing. At the workshop, Walter Toki told us the history of the τ -charm factory: one was proposed at SLAC in 1989 and at Spain in 1993. It was discussed at Dubna in 1991, at IHEP (China), and at Argonne (this workshop). It will be discussed again at IHEP (China) soon. Let us hope that we will have one in the not too distant future.

3.2 e^+e^- running near $\Upsilon(4S)$ – ARGUS, CLEO II, CLEO III, B factory

Using the CLEO II data sample, with an integrated luminosity of 1.8 fb^{-1} at and near the $\Upsilon(4S)$ resonance, CLEO has observed a signal for $D^0 \rightarrow K^+\pi^-$ [19] from the decay chain $D^{*+} \rightarrow D^0\pi_s^+ \rightarrow (K^+\pi^-)\pi_s^+$, as can be seen in Figure 2.

Without a precision vertex detector, CLEO II can only in effect measure the rate $\mathcal{B}(D^0 \rightarrow K\pi)$ integrated over all times of a pure D^0 decaying to a final state $K\pi$. The ratio $R = \mathcal{B}(D^0 \rightarrow K^+\pi^-) / \mathcal{B}(D^0 \rightarrow K^-\pi^+)$ is given by integrating equation (2) over all times:

$$R = R_{\text{mixing}} + R_{\text{DCSD}} + \sqrt{2R_{\text{mixing}}R_{\text{DCSD}}\cos\phi} \quad (10)$$

CLEO II finds $R = (0.77 \pm 0.25 \text{ (stat.)} \pm 0.25 \text{ (sys.)})\%$. This signal could mean one of two things: (1) mixing could be quite large, which would imply that mixing can be observed in the near future; (2) the signal is dominated by DCSD. The theoretical prediction for R_{DCSD} is about $2 \tan^4\theta_C \sim 0.6\%$ [23, 34], which is quite consistent with the measured value. It is, therefore, believed by many that the signal is mostly due to DCSD, although it remains consistent with the current best experimental upper limits on mixing, which are $(0.37 - 0.7)\%$ [12] and 0.56% [10].

CLEO has also tried to use hadronic method B, by searching for $D^0 \rightarrow K^+\pi^-\pi^0$. This mode has never been studied before due to the need to detect the π^0 . The excellent photon detection at CLEO II allows one to study this mode with a sensitivity close to $D^0 \rightarrow K^+\pi^-$ mode. The main complication faced here is that (as discussed in section 2.1.2) the resonant substructure is not necessarily the same for wrong sign and right sign decays. Because of this, the interpretation of R as R_{mixing} or R_{DCSD} will be complicated by the lack of knowledge of the details of the interference between submodes (and also the decay time information). Moreover, one has to worry about the detection efficiency across the Dalitz plot. Setting an upper limit for each submode is clearly very difficult. CLEO has thus set an upper limit on the inclusive rate for $D^0 \rightarrow K^+\pi^-\pi^0$ as $R = \mathcal{B}(D^0 \rightarrow K^+\pi^-\pi^0) / \mathcal{B}(D^0 \rightarrow K^-\pi^+\pi^0) < 0.68\%$ [24]. Note this upper limit includes the possible effects of the interference between the DCSD and mixing for each submode as well as the interference between submodes.

This summer, CLEO will install a silicon vertex detector (SVX) with a longitudinal resolution on vertex separation around $75 \mu\text{m}$. This will enable CLEO to measure the decay time of the D^0 , and reduce the random slow pion background (as the resolution of the $D^{*+} - D^0$ mass difference is dominated by the angular resolution on the slow pion, this should be greatly improved by the use of the SVX). By the year 2000, with CLEO III (a symmetric B factory) and asymmetric B factories at SLAC and KEK, each should have about thousands $D^0 \rightarrow K^+K^-(X), \pi^+\pi^-(X)$ and a few hundred $D^0 \rightarrow K^+\pi^-$ (and perhaps $D^0 \rightarrow K^+\pi^-\pi^0, K^+\pi^-\pi^+\pi^-$ too) signal events with decay time information for one year of running. The typical decay length of D^0 (\mathcal{L}) is about a few hundred μm , and the resolution of the decay length ($\sigma_{\mathcal{L}}$) is about $80 \mu\text{m}$ ($\mathcal{L}/\sigma_{\mathcal{L}} \sim 3$). The sensitivity to mixing at CLEO III and asymmetric B factory has not been carefully studied yet. A reasonable guess is that it could be as low as 10^{-4} . If mixing is indeed as large as DCSD, it should be observed by

then.

3.3 Fixed target experiments—E615, E691, E791, E687

A significant amount of our knowledge has been gained from Fermilab fixed target experiments, and in fact the current best upper limits on mixing have emerged from these experiments (E615, E691), and will come from their successors E687 and E791 very soon.

The best upper limit using the semi-leptonic method comes from the Fermilab experiment E615, which used a 255 GeV pion beam on a tungsten target. The technique is to search for the reaction $\pi N \rightarrow D^0 \bar{D}^0 \rightarrow (K^- \mu^+ \nu) D^0 \rightarrow (K^- \mu^+ \nu)(K^- \mu^+ \nu)$, where only the final state muons are detected (like sign $\mu^+ \mu^+$ or $\mu^- \mu^-$ pairs). Assuming $\sigma(c\bar{c}) \sim A^1$ nuclear dependence, they obtained $R_{\text{mixing}} < 0.56\%$ [10].

The best upper limit using the hadronic method by measuring the decay time information comes from E691, which is the first high statistics fixed target (photoproduction) experiment. In fact, E691 was the first experiment which used the decay time information (obtained from the excellent decay time resolution of their silicon detectors) to distinguish DCSD and mixing. The decay chains $D^{*+} \rightarrow D^0 \pi_s^+$ followed by $D^0 \rightarrow K^+ \pi^-$, $K^+ \pi^- \pi^+ \pi^-$ were used. The upper limits from the $D^0 \rightarrow K^+ \pi^-$ mode are $R_{\text{mixing}} < (0.5 - 0.9)\%$ and $R_{\text{DCSD}} < (1.5 - 4.9)\%$, while the upper limits from $D^0 \rightarrow K^+ \pi^- \pi^+ \pi^-$ are $R_{\text{mixing}} < (0.4 - 0.7)\%$ and $R_{\text{DCSD}} < (1.8 - 3.3)\%$. The combined result gives $R_{\text{mixing}} < (0.37 - 0.7)\%$. The ranges above reflect the possible effects of interference between DCSD and mixing with an unknown phase(ϕ). Note that for $D^0 \rightarrow K^+ \pi^- \pi^+ \pi^-$, the resonant substructure in the Cabibbo favored and DCSD decays has been ignored.

At this workshop, both E687 and E791 have reported their preliminary result from part of their data. One can find the details in Jim Wiss's talk. The best upper limits on mixing should come from these two experiments soon. It is worth pointing out here that both the E687 and E791 results reported in the workshop are based on the assumption that there is no interference between DCSD and mixing. Future analysis should include the interference term for the reasons discussed in section 2.1.1.

4 Comparison of Different Experiments

4.1 Hadronic method A

This measurement requires: (1) excellent vertexing capabilities, at least good enough to see the interference structure; (2) low background around the primary vertex. The background level around the primary vertex is an important issue as the interference term in equation (2) does peak at $t = 1$. In addition, low background around primary vertex means that one does not suffer much from random slow pion background and also one can measure the DCSD (or direct SCSD) component at low decay time well. This is important for understanding DCSD (or direct SCSD) at large decay times. The vertexing capabilities at

e^+e^- experiments ($\mathcal{L}/\sigma \sim 3$) for CLEO III and asymmetric B factories at SLAC and KEK should be sufficient for a mixing search. The extra path-length due to the Lorentz boost, together with the use of silicon detectors for high resolution position measurements, have given the fixed target experiments an advantage over e^+e^- experiments ($\mathcal{L}/\sigma \sim 8 - 10$). The low background around the primary vertex at e^+e^- experiments and photoproduction experiments is a certain advantage. It is worth pointing out here that at the e^+e^- experiments (esp. at asymmetric B factory or Z factory) it maybe possible to use $B^0 \rightarrow D^{*+}l^-\nu$, where the primary (D^{*+} decay) vertex can be determined by the l^- together with the slow pion coming from the D^{*+} . In this case, the background level around the primary vertex is intrinsically very low.

However, in the case of $D^0 \rightarrow K^+K^-, \pi^+\pi^-$, etc., the requirement on the background level around the primary vertex is not so important. In this case, the mixing signature is not a deviation from a perfect exponential (again assuming CP conservation), but rather a deviation of the slope from $(\gamma_1 + \gamma_2)/2$ (which can be measured by using $D^0 \rightarrow K^-\pi^+$). In addition, since we only need to determine the slope here, we do not need to tag the D^0 nor know the primary vertex location. The sensitivity of this method depends on how well we can determine the slope. Roughly speaking, the sensitivity to y would be $1/\sqrt{N}$, where N is the number of $D^0 \rightarrow K^+K^-, \pi^+\pi^-$, etc. events, which means that the sensitivity to mixing caused by the decay rate difference ($\sim y^2$) is $1/N$. For example, a fixed-target experiment capable of producing $\sim 10^8$ reconstructed charm events could lower the sensitivity ⁵ to $\sim 10^{-6}$ for the y^2 term in $R_{\text{mixing}} = (x^2 + y^2)/2$.

4.2 Hadronic method B

In the near future, we should be able to have a good understanding of DCSD ⁶ in $D^0 \rightarrow K^+\pi^-\pi^0, D^0 \rightarrow K^+\pi^-\pi^+\pi^-$, etc. modes, then method B will become a feasible way to study mixing and the sensitivity should be improved. Just like method A, this method requires very good vertexing capabilities and very low background around the primary vertex (this is even more important than in method A, since precise knowledge of DCSD is very important here). In addition, this method requires that the detection efficiency (for the mode being searched) across Dalitz plot be quite uniform (at least the detector should have good acceptance on the Dalitz plot at locations where DCSD and mixing resonant substructure are different). This is necessary so that detailed information on the resonant substructure can be obtained in every corner on the Dalitz plot.

The excellent photon detection capabilities will allow e^+e^- experiments to study the $D^0 \rightarrow K^+\pi^-\pi^0$ mode with very low background. From the CLEO II $D^0 \rightarrow K^+\pi^-\pi^0$ analysis, the detection efficiency across the Dalitz plot will have some variations due to cuts

⁵Since I came up with this idea the day before the deadline of this paper, the sensitivity has not been carefully estimated yet.

⁶It may be possible that good understanding of DCSD can be reached by measuring the pattern of D^+ DCSD decays where the signature is not confused by a mixing component. It is worth pointing out that the D^+ DCSD decays can be studied very well at future fixed target experiments.

needed to reduce background, however, it is still good enough to obtain detailed information on the resonant substructure [24]. Future fixed target experiments may have a good chance to study $D^0 \rightarrow K^+ \pi^- \pi^+ \pi^-$ mode, since the detection efficiency across Dalitz plot should be quite flat. The sensitivity that each experiment can reach by using this method depends on many things and need to be carefully studied in the future.

4.3 Hadronic method C

The sensitivity of this method depends crucially on the particle identification capabilities. Since the D^0 is at rest, the K and π mesons will have the same momentum, so a doubly misidentified Cabibbo favored decay $D^0 \rightarrow K^- \pi^+$ ($K^- \rightarrow \pi^-$, $\pi^+ \rightarrow K^+$) mimics a $D^0 \rightarrow K^+ \pi^-$ with almost the same D^0 mass. It is worth pointing out here that particle identification is not as crucial to method A as it is to this method, as far as this particular background is concerned. This is because in method A, the D^0 is highly boosted, and doubly misidentified $D^0 \rightarrow K^+ \pi^-$ decays will have a broad distribution in the D^0 mass spectrum around the D^0 mass peak; this background can be kinematically rejected with only a small reduction of the efficiency for the signal events ⁷.

Once the sensitivity reaches $\mathcal{O}(10^{-5})$, one may have to worry about other contributions. For instance, $e^+e^- \rightarrow 2\gamma \rightarrow D^0 \bar{D}^0$ may produce C-even states, where DCSD can contribute [26].

4.4 Semi-leptonic method

The semi-leptonic method usually suffers from large background (except at a τ charm factory), the traditional method of looking for like sign $\mu^+ \mu^+$ or $\mu^- \mu^-$ pairs is an example. New ideas are needed in order to improve the sensitivity significantly. Some promising techniques have been suggested by Rolly Morrison and others, and have been discussed in the working group [29].

5 Summary

The search for $D^0 \bar{D}^0$ mixing carries a large discovery potential for new physics since the $D^0 \bar{D}^0$ mixing rate is expected to be very small in the Standard Model. The past decade has seen significant experimental progress in sensitivity (from 20% down to 0.37%).

In light of the recent CLEO II signal in $D^0 \rightarrow K^+ \pi^-$, if the mixing rate is close to that of DCSD (above 10^{-4}), then it might be observed by the year 2000 with either the hadronic or the semi-leptonic method, either at fixed target experiments, CLEO III, asymmetric B

⁷The idea is for each $K^+ \pi^-$ candidates, one can invert the kaon and pion assignments and recalculate the D^0 mass, denoted M_{flip} . If M_{flip} lies close to the nominal D^0 mass, the combination is discarded. This veto works as long as the momentum measurement is correct. One can say that excellent tracking capabilities is crucial in order to get rid of this background here.

factories(at SLAC and KEK), or at a τ -charm factory. If the mixing rate is indeed much smaller than DCSD, then the hadronic method may have a better chance as the potentially very small mixing signature could be enhanced by the presence of the relatively large “annoying background” DCSD. The design of future experiments should focus on improving the vertexing capabilities and reducing the background level around the primary vertex, in order to fully take advantage of having the possible DCSD interference. In addition, since decays such as $D^0 \rightarrow K^+K^-, \pi^+\pi^-$, occur only through the CP eigenstate, the decay time distribution is a perfect exponential time distribution with the slope of γ_1 (the decay rate of the CP eigenstate, assuming CP conservation). This fact can be used to measure the decay rate difference $y = \gamma_-/\gamma_+ = (\gamma_1 - \gamma_2)/(\gamma_1 + \gamma_2)$ alone. Observation of a non-zero y would demonstrate mixing caused by the decay rate difference. Moreover, the possible differences between the resonant substructure in many DCSD and mixing decay modes could be used (method B) and the sensitivity could be improved significantly this way. This means that understanding DCSD in D decays could be a very important step on the way to observe mixing. Experimenters and theorists should work hard on this. In this sense, it is best to think of the quest to observe mixing as a program rather than a single effort.

Acknowledgement

Much of my knowledge on this subject has been gained by having worked closely with Hitoshi Yamamoto over the past three years, I would like to express my sincere gratitude to him. Besides, I would like to express special thanks to Rolly Morrison for many useful and stimulating discussions, to Richard Wilson for encouragement and careful reading of the draft, to Gary Gladding, Tom Browder and Milind Purohit for helping me to understand the details of MARK III, E691 and E791 analysis (respectively), to Dan Kim who made Figure 1. Finally, I would like to thank the organizers of the workshop for providing me the opportunity to write this paper.

References

- [1] G.J.Feldman *et al.*, *Phys. Rev. Lett.* **38**, 1313(1977).
- [2] G.Goldhaber *et al.*, *Phys. Lett. B* **69**, 503 (1977).
- [3] P.Avery *et al.*, *Phys. Rev. Lett.* **44**, 1309(1980).
- [4] J.J.Aubert *et al.*, *Phys. Lett. B* **106**, 419 (1981).
- [5] A.Bodek *et al.*, *Phys. Lett. B* **113**, 82 (1982).
- [6] R.Bailey *et al.*, *Phys. Lett. B* **132**, 237 (1983).
- [7] A.Benvenuti *et al.*, *Phys. Lett. B* **158**, 531 (1985).
- [8] H.Yamamoto *et al.*, *Phys. Rev. Lett.* **54**, 522 (1985).
- [9] S.Abachi *et al.*, *Phys. Lett. B* **182**, 101 (1986).
- [10] W.C.Louis *et al.*, *Phys. Rev. Lett.* **56**, 1027 (1986).

- [11] H. Albrecht *et al.*, *Phys. Lett.* **199**, 447 (1987).
- [12] J.C. Anjos *et al.*, (E691 Collaboration), *Phys. Rev. Lett.* **60**, 1239 (1988). For details of this study, see T. Browder, Ph.D. Thesis, UCSB-HEP-88-4, (1988).
- [13] R. Ammar *et al.*, (CLEO Collaboration), *Phys. Rev. D* **44**, 3383 (1991).
- [14] M.K. Gaillard and B.W. Lee, *Phys. Rev. D* **10**, 897 (1974); A. Datta, *Phys. Lett. B* **154**, 287 (1985).
- [15] L. Wolfenstein, *Phys. Lett. B* **164**, 170 (1985); J. Donoghue, E. Golowich, B.R. Holstein and J. Trampetic, *Phys. Rev. D* **33**, 179 (1986).
- [16] H. Georgi, *Phys. Lett. B* **297**, 353 (1992); T. Ohl, G. Ricciardi and E.H. Simmons, *Nucl. Phys. B* **403**, 603 (1993). Also see G. Burdman's talk in this workshop.
- [17] A. Datta, *Phys. Lett. B* **154**, 287 (1985); A.M. Hadeed and B. Holdom, *Phys. Lett. B* **159**, 379(1985); B. Mukhopadhyaya, A. Raychaudhuri and A. Ray, *Phys. Lett. B* **190**, 93(1987); K.S. Babu *et al.* *Phys. Lett. B* **205**, 540(1988); E. Ma *et al.* *Mod. Phys. Lett. A3*, 319(1988); L. Hall and S. Weinberg, *et al.* *Phys. Rev. D* **48**, 979 (1993).
- [18] We discuss D^0 decays explicitly in the text, its charge conjugate decays are also implied throughout the text unless otherwise stated.
- [19] D.Cinabro *et al.*, (CLEO Collaboration), *Phys. Rev. Lett.* **72**, 1406 (1994).
- [20] M. Purohit, "A $D^0 \bar{D}^0$ mixing and DCSD analysis of E791 data", E791 memo. March, 1994.
- [21] In the early days when people searched for $D^0 \bar{D}^0$ mixing using the hadronic method, the lack of knowledge on DCSD decays and the lack of statistics and decay time information have forced one to assume that DCSD is negligible in order to set upper limit for mixing [1, 2, 3, 6, 8, 9, 11, 13].
- [22] This idea was first suggested by J.D. Bjorken in 1985, private communication with Tom Browder and Mike Witherell.
- [23] I. Bigi and A.I. Sanda, *Phys. Lett. B* **171**, 320 (1986).
- [24] T.Liu, "Search for $D^0 \rightarrow K^+ \pi^- (\pi^0)$ ", to appear in the Proceedings of the Eighth Meeting of the Division of Particles and Fields of the American Physics Society (DPF'94), Albuquerque, New Mexico. (World Scientific).
- [25] H. Yamamoto, Ph.D. Thesis, CALT-68-1318 (1985).
- [26] D. Du and D. Wu, *Chinese Phys. Lett.* **3**, No. 9(1986).
- [27] G.E. Gladding, in Proceedings of the τ -charm factory workshop, SLAC-Report-343, June 1989.
- [28] R.H. Schindler, in Proceedings of the τ -charm factory workshop, SLAC-Report-343, June 1989.
- [29] T.Liu, "Charm mixing working group summary report", in this Proceedings.
- [30] G.E. Gladding, in Proceedings of the Fifth International Conference on Physics in Collision, Autun, France, 1985 (World Scientific).
- [31] G.E. Gladding, " $D^0 \bar{D}^0$ Mixing, The Experimental Situation" in Proceedings of International Symposium on Production and Decay of Heavy Flavors, Stanford, 1988.
- [32] I.Bigi, in Proceedings of the τ -charm factory workshop, SLAC-Report-343, June 1989.
- [33] I.Bigi, in SLAC summer institute on Particle Physics, Stanford, 1987; edited by E.C. Brennan (SLAC, 1988); Other predictions can be found in R.C. Verma and A.N. Kamal, *Phys.Rev. D***43**,829(1991).
- [34] L.L. Chau and H.Y.Cheng, ITP-SB-93-49, UCD-93-31 (HEP-PH-9404207).

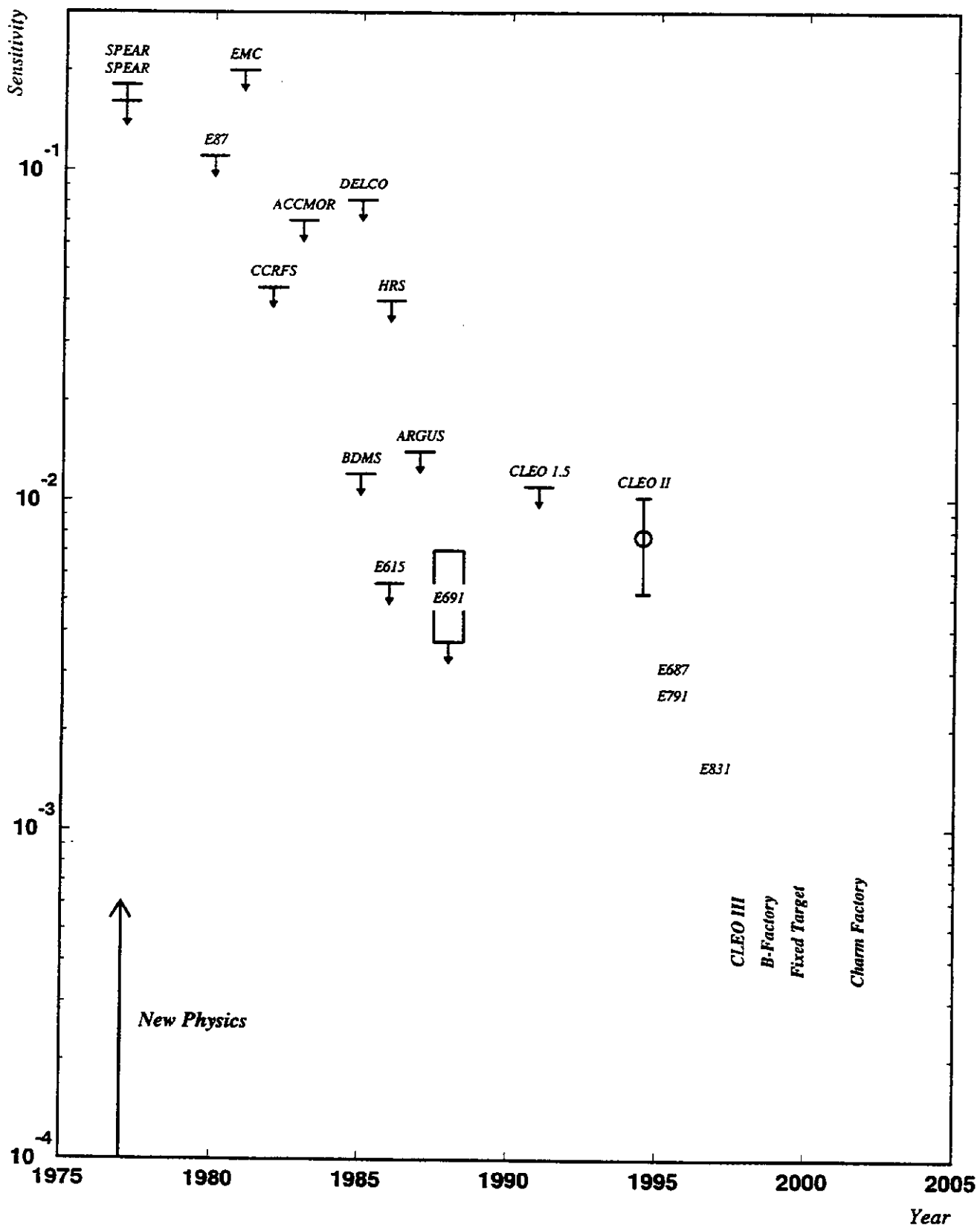


Figure 1: The quest for $D^0\bar{D}^0$ mixing. Note that the range in E691 result reflects the possible effects of interference between DCSD and mixing, and the CLEO II signal could be due to either mixing or DCSD, or a combination of the two.

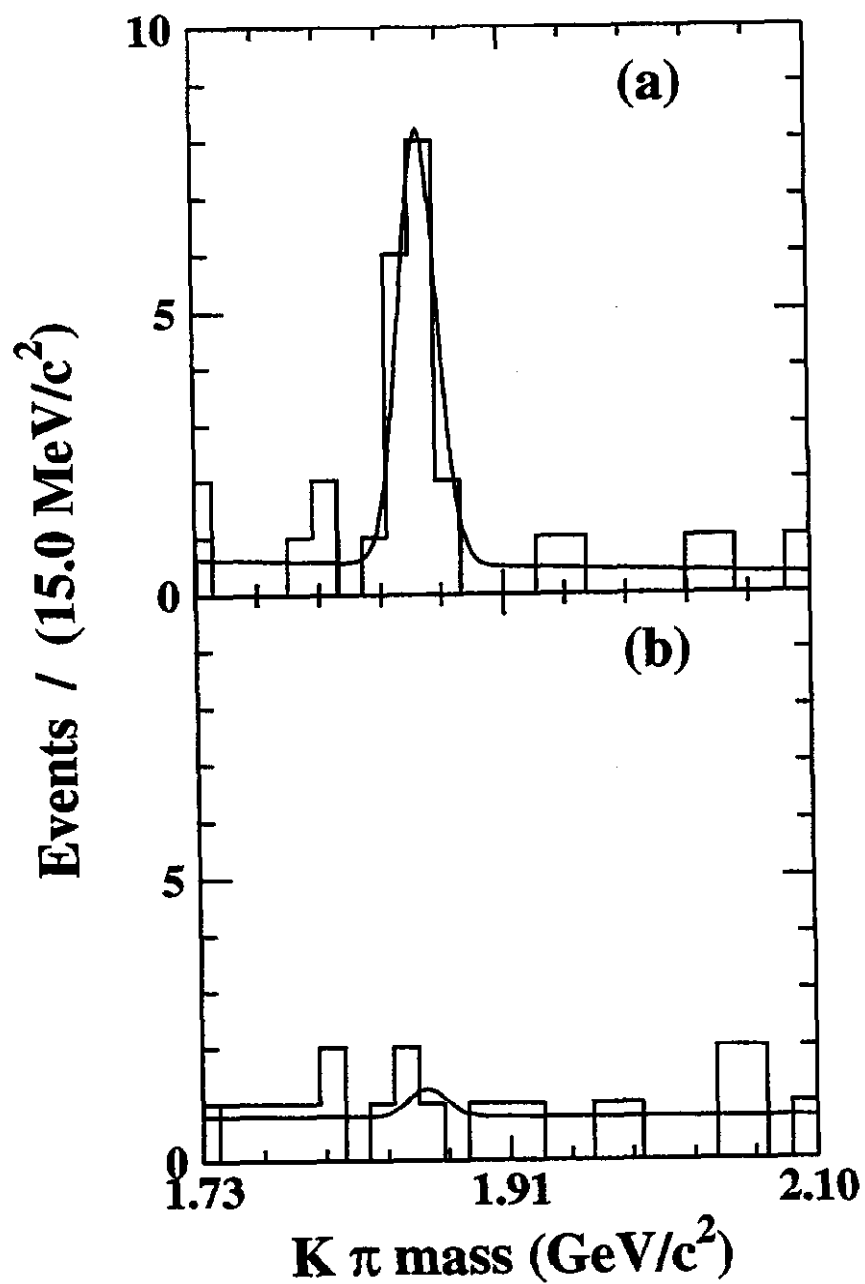


Figure 2: The CLEO II signal for $D^0 \rightarrow K^+\pi^-$. The D^0 mass for wrong sign events. (a) for events in the ΔM peak; (b) for events in the ΔM sidebands. The solid lines are the fits using the corresponding right sign mean and σ in data.

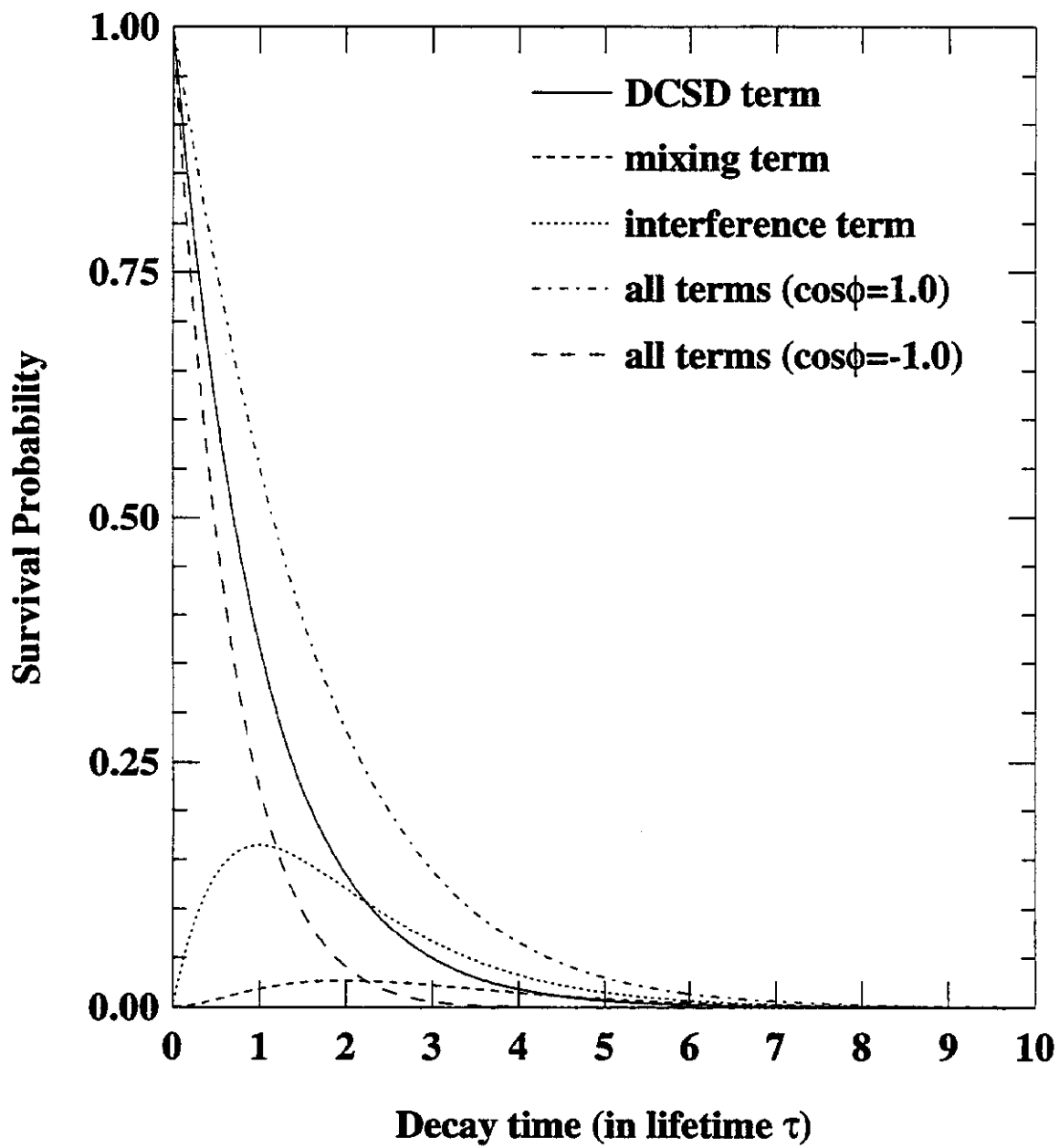


Figure 3: The decay time dependence of DCSD and mixing with $\alpha = R_{\text{mixing}}/R_{\text{DCSD}} = 10\%$.

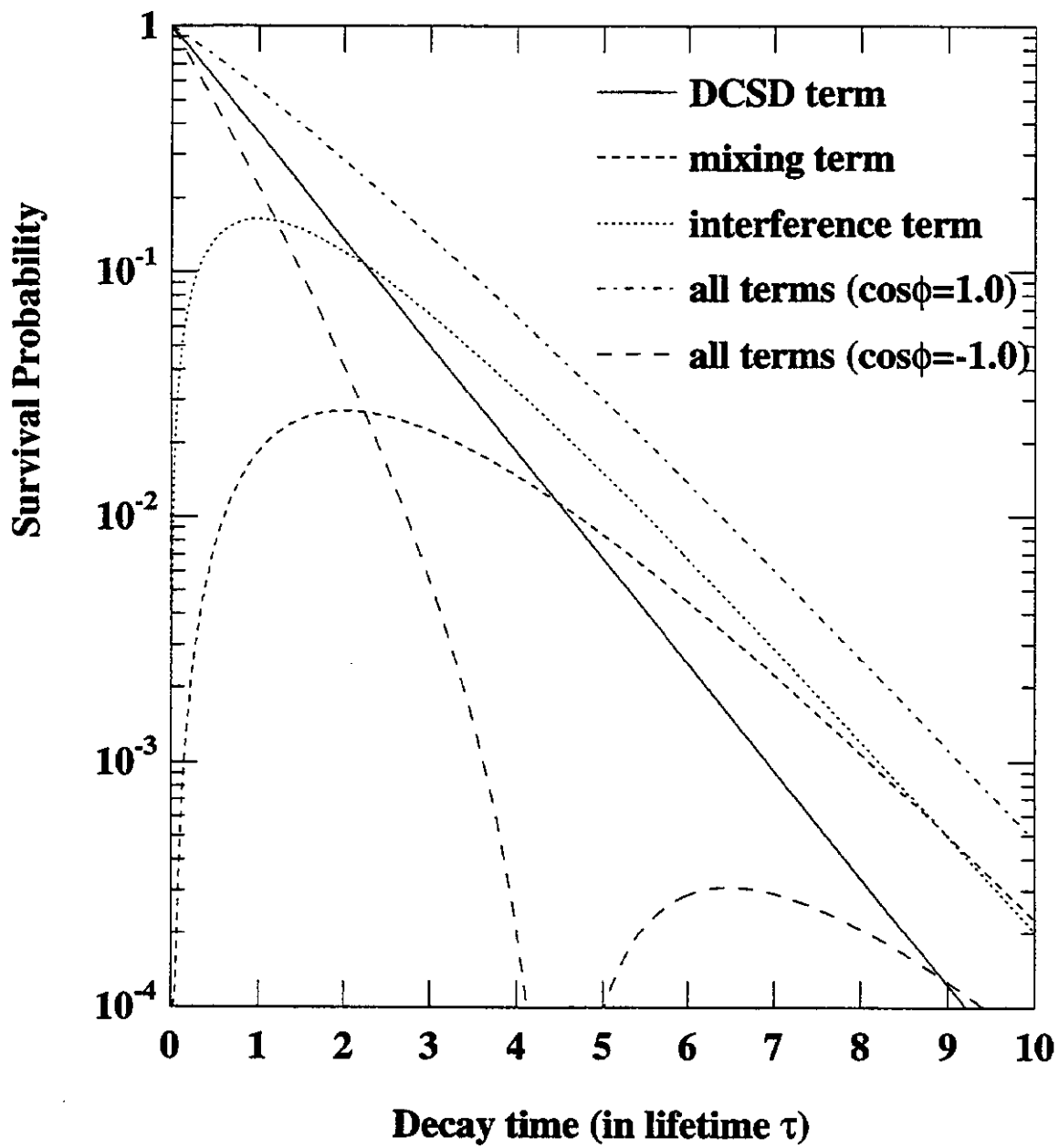


Figure 4: The decay time dependence of DCSD and mixing with $\alpha = R_{\text{mixing}}/R_{\text{DCSD}} = 10\%$, in log scale.

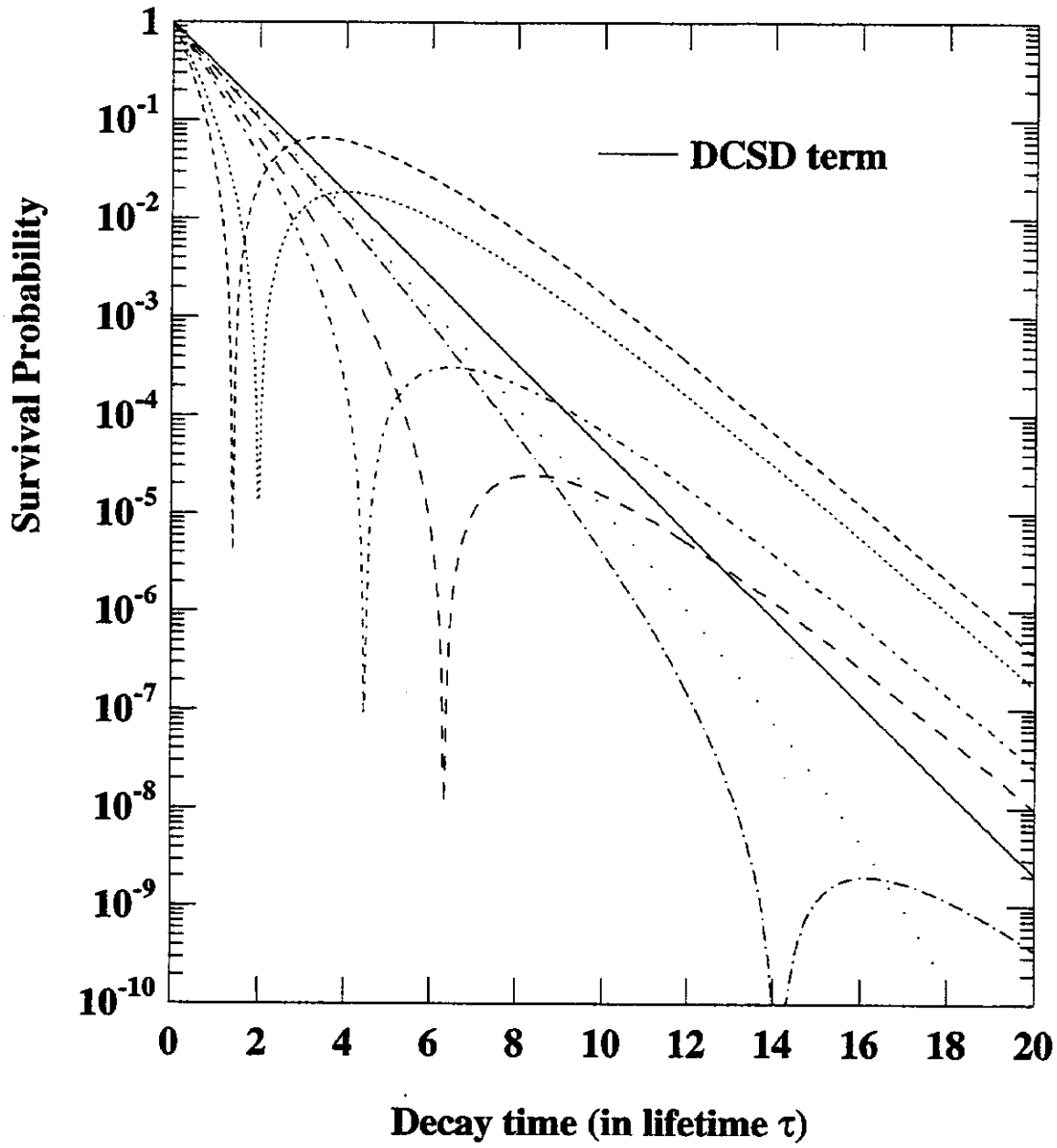


Figure 5: The decay time dependence of DCSD and mixing with maximal destructive interference $\cos\phi = -1.0$. For different $\alpha = R_{\text{mixing}}/R_{\text{DCSD}}$ values: from left to right, $\alpha = 100\%, 50\%, 10\%, 5\%, 1\%, 0.5\%$ (with $R_{\text{DCSD}} = 10^{-2}$, this corresponds to $R_{\text{mixing}} = 10^{-2}, 5 \times 10^{-3}, 10^{-3}, 5 \times 10^{-4}, 10^{-5}, 5 \times 10^{-6}$).

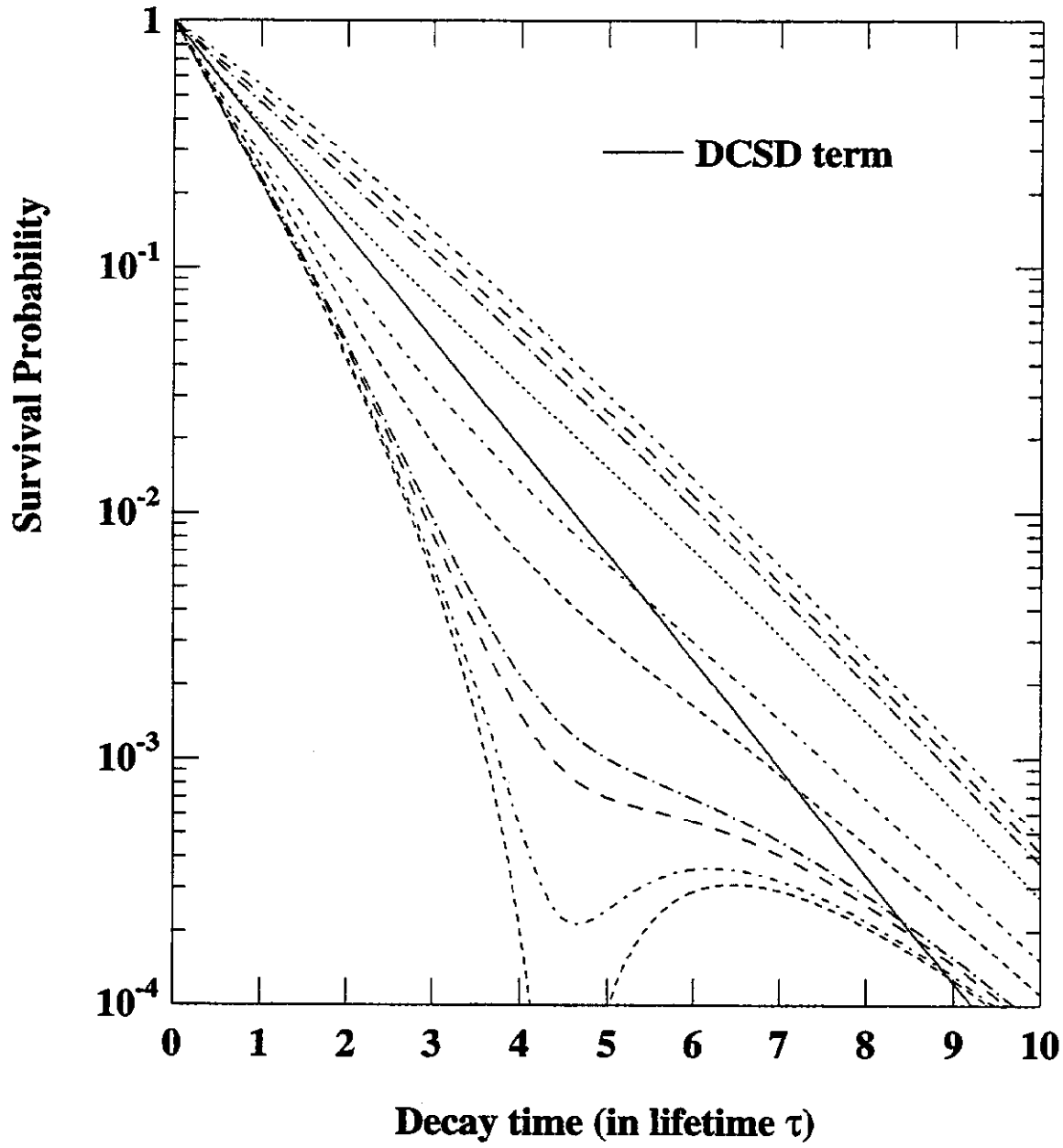


Figure 6: The decay time dependence of DCSD and mixing with $\alpha = R_{\text{mixing}}/R_{\text{DCSD}} = 10\%$. For different $\cos\phi$ values: from bottom to top, $\cos\phi = -1.0, -0.99, -0.96, -0.94, -0.80, -0.6, 0.0, 0.5, 0.7, 1.0$. The solid line is the DCSD term, as a reference line.

Upper Limits for Charm Hadron Decays to Two Muons plus a Hadron

Etsuko NIU

CERN

(for the Fermilab E653 Collaboration)

Abstract

A search for charm hadron decays into two muons plus a hadron has been carried out using a hybrid emulsion spectrometer. No evidence for such decays has been found, which allows upper limits ranging from 1.7×10^{-4} to 7.2×10^{-4} at 90 % confidence level to be placed on the branching fractions for charm-changing neutral-current and lepton-number violating decay modes. A possible new experiment aiming to lower the upper limits down to 10^{-7} is proposed as an extension of the present emulsion hybrid experiment.

1 Introduction

So far the standard model of electroweak and strong interactions is consistent with all known phenomena in particle physics [1], although it is not thought of as the ultimate theory. In this situation, searches for non-standard processes such as flavor-changing neutral-current (FCNC) decays, which are forbidden to first order in the standard model, are particularly interesting because they may provide evidence for “new physics” [2]. FCNC decays of strange particles, such as $K_L^0 \rightarrow e^+e^-$ and $K_L^0 \rightarrow \pi^0 e^+e^-$, have been studied to the level of 10^{-10} to 10^{-9} [1]. For the charm-decay sector, the existing experimental limits for FCNC decay modes are much less stringent [1]. The best limit at present [3] is $B(D^0 \rightarrow \mu^+\mu^-) < 1.1 \times 10^{-5}$. However, this decay mode is expected to be helicity suppressed [4] by a factor of $(m_\mu/m_D)^2$. Therefore the study of helicity-unsuppressed FCNC decays into two leptons plus a hadron is a more sensitive test for FCNC interactions of the charm quark.

In this paper, we describe a search for these decays in a hybrid emulsion experiment, Fermilab E653, and report resulting upper limits for FCNC charm decays such as $B(D^0 \rightarrow \pi^0 \mu^+ \mu^-)$ and $B(D^+ \rightarrow \pi^+ \mu^+ \mu^-)$ ¹. This search is sensitive to modes with missing neutral hadrons, as well as to constrained decays in which a signal would appear as a visible invariant mass equal to that of a charm state. In addition to these FCNC decay modes, we have also searched for lepton-number violating decays into same-sign muons plus a hadron, e.g. $D^+ \rightarrow \pi^- \mu^+ \mu^+$, by the same scanning procedure, and also report upper limits for such decays. In the last part of this paper, a proposal is made to get 10^3 times more stringent upper limits for both FCNC and lepton-number violating decays of charm particles.

¹Throughout this paper, charge-conjugate modes are implied unless otherwise stated.

2 Features of the Apparatus and the Recording of the Events

Fermilab experiment E653, as described in detail elsewhere [5], used a hybrid emulsion spectrometer which consisted of a nuclear emulsion target and an electronic spectrometer. The primary interaction and short-lived decay vertices were observed visually with high spatial resolution of $1\text{ }\mu\text{m}$ in the emulsion target. The electronic spectrometer provided the track and decay vertex reconstruction and muon identification downstream of the emulsion target, and identified the selection of events to be scanned.

The emulsion target, 1.47 cm thick, was composed of 20 plates placed perpendicular to the beam. The high-resolution decay volume was extended by the use of two precision emulsion analyzers: a thin analysis plate separated from the target by 1.0 cm of low-density plastic honeycomb, and a moving emulsion tape 1.2 cm further downstream. The electronic spectrometer consisted of an 18-plane silicon microstrip vertex detector which began 5.7 cm downstream of the emulsion target, a large-aperture dipole magnet, 55 drift chamber planes, and a liquid argon calorimeter. A second spectrometer for muon analysis, which began after 1700 g/cm^2 of absorber, comprised 12 drift chamber planes on either side of an iron toroidal magnet.

The data used in this analysis were obtained in a $600\text{ GeV}/c\text{ }\pi^-$ beam with a trigger which required both a beam particle to interact in the target and a muon to penetrate 3900 g/cm^2 of absorber. A total of 8.2×10^6 events, corresponding to 2.5×10^8 interactions, was collected.

3 Selection of Dimuon Events

Dimuon candidates to be scanned, selected from events reconstructed in the spectrometer, satisfied the following requirements:

- (1) Two muon tracks, with either opposite or same charges, were identified in the muon system.
- (2) The muon tracks must be cleanly reconstructed. In particular, the χ^2 's for matching the track segments upstream and downstream of the dipole magnet had to be smaller than 3.0. This reduced the number of accepted charged hadrons, especially kaons, which decayed in the magnet volume.
- (3) For both muons tracks, the momenta p_μ must satisfy $8 < p_\mu < 150\text{ GeV}/c$. The lower p_μ requirement was chosen to reduce the feedthrough of hadron decays in flight, and the upper limit to reduce hadron punchthrough.
- (4) For at least one muon, the transverse momentum with respect to the beam direction, $p_{T\mu}$, must be greater than $0.8\text{ GeV}/c$. This requirement was designed to have good efficiency for charm, but to discriminate against other sources of secondary vertices such as strange particle decay.

Thus, selection criteria (2) and (3) provided unambiguous matching of the muon tracks

in the upstream spectrometer, while the selection (4) reduced considerably the number of events to be scanned without serious loss of signal. At this stage, before scanning, there was no requirement that the muons originate from the same vertex. A total of 1158 events² passed these selection criteria.

4 Results of Scanning

After events with primary interaction vertices outside the target fiducial volume had been eliminated, 950 events remained. The primary vertex was looked for in this sample using the procedures described in refs. [6, 7], and was found for 946 (99.6%) of them.

The next step was to determine whether either muon originated from the primary vertex, since most of the muons in these events came from the decays of kaons or pions emitted from the primary interaction. To remove these primary muons, the slopes of the spectrometer muon tracks were compared visually with the emulsion track slopes at the primary vertex. If either muon matched with an emulsion track, no further scanning was done on the event. The matching criterion was that the difference in the slopes of the tracks be less than 2 mrad³.

This track-matching procedure at the primary vertex eliminated 897 of the 946 events. For the remaining 49 events with both muons unmatched at the primary vertex, scanning of the emulsion downstream of the primary vertex, and also interactive track-matching by physicists of spectrometer tracks downstream of the emulsion ("graphic scan") [7], continued until all emulsion-spectrometer track matches were found. As a result of this decay search, 33 of the 49 dimuons were identified as charm-anticharm pairs in which both charm particles decayed semimuonically. This number agrees well with the expected number of ~ 35 events from a Monte Carlo simulation based on the cross section measured [10] in this experiment.⁴ An additional 13 dimuons were attributed to events in which at least one muon was emitted from a secondary interaction with dark nuclear breakup tracks, or from a kaon decay.

Only three events had dimuon decay candidates (no evidence of nuclear breakup, and prong count consistent with charge conservation). There were no three-prong (C3) or five-prong (C5) charged decay candidates. Two events had neutral two-prong (N2) decay candidates found inside the emulsion target, and the third had a neutral four-prong (N4) candidate found outside the emulsion target by the graphic scan procedure. No partner decay was observed in any of these three events, although the overall finding probability for finding a partner charm decay was [6, 11] about 80 %.

²Of these 1158 events, 19 had three muons; each muon satisfied the selections (2) and (3), and at least one of three muons had $p_T > 0.8 \text{ GeV}/c$.

³A larger matching tolerance was used for tracks with production angle $\theta > 0.04 \text{ rad}$.

⁴This expected value includes feedthrough from hadronic decays in which a pion or kaon decayed into a muon.

5 Simulations and Detection Efficiencies

To estimate the detection efficiency and the expected values of possible backgrounds, a Monte Carlo simulation was carried out. Uncorrelated charm pairs with the production distributions measured in this experiment [10],

$$\frac{d^2\sigma}{dx_F dp_T^2} \propto (1 - |x_F|)^n \cdot \exp(-bp_T^2),$$

where $n = 4.25 \pm 0.24(\text{stat.}) \pm 0.23(\text{syst.})$ and $b = 0.76 \pm 0.03 \pm 0.03 (\text{GeV}/c)^{-2}$ for $x_F > 0$ were superimposed on primary interactions generated by the FRITIOF [12] routine. All experimental conditions, namely the experimental apparatus, the trigger conditions, the offline selections, the scanning procedure, and the analysis method, were taken into account. The detection efficiency ϵ can be decomposed into several parts and written as:

$$\epsilon = A_{\mu\mu} \cdot \epsilon_{\text{selection}} \cdot \epsilon_{\mu}^2 \cdot \epsilon_{\text{emulsion}},$$

where $A_{\mu\mu}$ is the geometrical acceptance of the apparatus for two muons from the decay, and $\epsilon_{\text{selection}}$ is the efficiency for the decay to pass the selection criteria discussed above. The efficiency ϵ_{μ} for finding and linking a prompt muon in the two spectrometers was 81.7 %. The detection efficiency in emulsion $\epsilon_{\text{emulsion}}$ (93 %) has contributions from incorrect matching in emulsion (94 %), and from scanning efficiency for a muonic decay vertex (99 %).

The net efficiency ϵ for the phase space decay of the mode $D^0 \rightarrow \pi^0 \mu^+ \mu^-$ was found to be 12.9% by the simulation⁵. The efficiencies for other modes are listed in Table 1. Although the scanning procedure and efficiency for finding a decay vertex are almost the same for various decay modes, the overall efficiencies vary due to the selection criterion (4) of $p_{T\mu} > 0.8 \text{ GeV}/c$.

6 Estimated Backgrounds

The largest source of background is due to the feedthrough from semi-muonic (hadronic) decay modes of charm hadrons in which a pion or kaon (pions or kaons) decayed into a muon (muons). The amount of the feedthrough background was estimated by the simulation to be 0.81 event for the two-prong N2 topology; 0.15 for N4; and 0.75 and 0.02 for the charged topologies C3 and C5. Another possible background source is the early decay of $K_S^0 \rightarrow \pi^+ \pi^-$, with $\pi^\pm \rightarrow \mu^\pm \nu$, which is expected to be 0.4 event in our N2 sample. The expected number of secondary interactions of neutral hadrons without evidence of nuclear breakup, in which two pions or kaons decayed into two muons, was estimated to be less than 0.1 event from the observed number of secondary interactions with nuclear breakup tracks.

⁵This number includes a small correction (9.6 %) for the contribution from detecting the decay in the region of Feynman $x_F < 0$.

Table 1. 90% confidence level (CL) upper limits on the branching fractions B for exclusive charm decays into dimuons plus a hadron. The last five decay modes are due to lepton-number violating processes.

Decay mode	Number of signal events N_s	Upper limit on N_s (90 % CL)	Efficiency ϵ (%)	Upper limit on B (90 % CL)
$D^0 \rightarrow \pi^0 \mu^+ \mu^-$	2	5.0	15.9	1.7×10^{-4}
$D^0 \rightarrow \bar{K}^0 \mu^+ \mu^-$	2	5.0	10.8	2.5×10^{-4}
$D^0 \rightarrow \rho^0 \mu^+ \mu^-, \rho^0 \rightarrow \pi^+ \pi^-$	0	2.5	5.8	2.4×10^{-4}
$D^+ \rightarrow \pi^+ \mu^+ \mu^-$	0	2.5	15.9	2.2×10^{-4}
$D^+ \rightarrow K^+ \mu^+ \mu^-$	0	2.5	10.7	3.3×10^{-4}
$D^+ \rightarrow \rho^+ \mu^+ \mu^-, \rho^+ \rightarrow \pi^+ \pi^0$	0	2.5	6.0	5.8×10^{-4}
$D_S^+ \rightarrow K^+ \mu^+ \mu^-$	0	2.9	12.6	6.0×10^{-4}
$\Lambda_C^+ \rightarrow p \mu^+ \mu^-$	0	3.0	9.9	3.3×10^{-4}
$D^+ \rightarrow \pi^- \mu^+ \mu^+$	0	2.5	15.9	2.2×10^{-4}
$D^+ \rightarrow K^- \mu^+ \mu^+$	0	2.5	10.7	3.3×10^{-4}
$D^+ \rightarrow \rho^- \mu^+ \mu^+$	0	2.5	6.0	5.8×10^{-4}
$D_S^+ \rightarrow K^- \mu^+ \mu^+$	0	2.9	12.6	6.0×10^{-4}
$\Lambda_C^+ \rightarrow \Sigma^- \mu^+ \mu^+$	0	3.0	4.6	7.2×10^{-4}

7 FCNC Limits

The 90 % confidence level upper limits on the decay branching fractions are calculated by (e.g. for $B(D^0 \rightarrow \pi^0 \mu^+ \mu^-)$) :

$$B(D^0 \rightarrow \pi^0 \mu^+ \mu^-) < \frac{N(\text{signal})}{N(D^0)} \cdot \epsilon^{-1},$$

where $N(\text{signal})$ is the upper limit on the number of signal candidates ($D^0 \rightarrow \pi^0 \mu^+ \mu^-$) and $N(D^0)$ is the number of D^0 produced in the region $x_F > 0$ (1.83×10^5). The numbers of D^0 , D^\pm (0.718×10^5), and D_S^\pm (0.38×10^5) were calculated from the cross sections measured in this experiment: $\sigma(D^0; x_F > 0) = 22.05 \pm 1.37 \pm 4.82 \mu\text{b/nucleon}$ [10], $\sigma(D^\pm; x_F > 0) = 8.66 \pm 0.46 \pm 1.96 \mu\text{b/nucleon}$ [10], and $\sigma(D_S^\pm; x_F > 0) = 4.6 \pm 1.2 \pm 1.5 \mu\text{b/nucleon}$ [14] while the number of Λ_C^+ baryons (0.91×10^5) was estimated by the cross section obtained from other experiments [15].

For a conservative estimate, the two N2 candidates described in Sec. 4 are treated as signal in the upper limit calculation, although they could be background. Also, the number of estimated N2 background events has conservatively been taken as only the charm feedthroughs, 0.81. Thus the 90% confidence level upper limit on the number of N2 decays, $N(\text{signal})$, is 5.0, based on 2 candidates and 0.81 events of estimated background. For all other decay topologies, $N(\text{signal})$ is 2.3 since there are no candidates. Effects due to

uncertainty in $N(D^0)$ and uncertainty (5 %) in the overall efficiency are taken into account by convoluting the Poisson distribution for $N(\text{signal})$ with Gaussian distributions of the uncertainties. Table 1 shows the 90% confidence level upper limits on the numbers of various dimuon decays and the resulting upper limit on the branching fractions for the decay modes, together with corresponding efficiencies.

The upper limit on the branching fraction for $D^0 \rightarrow \pi^0 \mu^+ \mu^-$, the first reported measurement for this mode, is 1.7×10^{-4} . The upper limit for $D^+ \rightarrow \pi^+ \mu^+ \mu^-$ is 2.2×10^{-4} , an order of magnitude lower than the present published result [1]. Most of the limits obtained for other FCNC and lepton-number violating decay branching fractions are either first reported measurements, or else an order of magnitude smaller than previous published results [1, 16, 17, 18].

8 Possible new experiment for the study of charm dimuon decays

Depending on the E653 results, a new experiment could be proposed for the study of charm dimuon decays which aims a goal of $B(D \rightarrow X \mu \mu)$ of the order of 10^{-7} .

The primary interaction and short-lived decay vertices were observed visually with high spatial resolution of $1 \mu\text{m}$ in the emulsion target. The electronic spectrometer provided the track and decay vertex reconstruction and muon identification downstream of the emulsion target, and selected the events to be scanned.

The strong point of the Emulsion Hybrid Experiment such as E653 is as follows. One can observe directly both of primary and secondary vertices under the high magnification microscope, and this enables us,

- 1) to reject almost backgrounds such as $\pi^\pm \rightarrow \mu^\pm \nu$ or $K^\pm \rightarrow \mu^\pm \nu$ at the primary vertex,
- 2) to discriminate the candidates clearly from backgrounds such as nuclear interactions etc. at the secondary vertex, retaining high signal-to-background ratio and also retaining high detection efficiency.

An expansion of the order of 10^3 of this type of experiment could reach an upper limit of the order of 10^{-7} with 90 % CL for the branching ratio of charm dimuon decay. Of course, a simple expansion of 10^3 is impossible, both because of high cost of emulsion plates, and because of heavy load of measurement and analysis.

Possible strategy to overcome these difficulties is to use a few emulsion plates separated by air gaps as an analyser of secondary tracks and vertices, and to use thin tungsten sheet as a target. Fig. 1 shows a proposed set up of this kind of experiment. The detector consists of a tungsten target, a hybrid vertex detector (emulsion + SSD), an em- and hadron-calorimeters, and a muon spectrometer. A detail of the hybrid vertex detector is shown in Fig. 2. An analyser which consists of 4 emulsion plates with the area of 1 m^2 coated each $60 \mu\text{m}$ on both surfaces of $300 \mu\text{m}$ thick Acrylic base separated each other by air gaps of 5 mm is

attached just downstream of the tungsten target of 2 mm thick. This part is followed by DSSD layers with different pitches. The emulsion-space analyser will be moved by the target mover during the exposure to the beam, in order to get uniform event distribution over the whole area of the analyser.

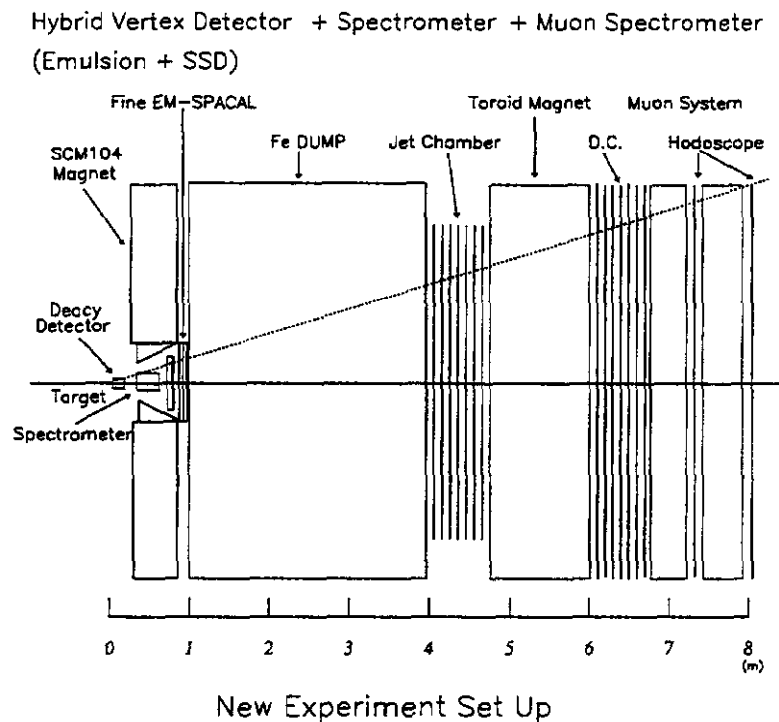


Figure 1: New experiment set up.

On one hand, this method enables us to reduce drastically the volume of emulsion needed, and to decrease the scanning load. On the other hand, this method throws away the direct observation of vertices. With the highest spatial resolution of sub-micron of the emulsion plates, however, the above type of analyser will retain points of advantages claimed only for nuclear emulsion.

- 1) One can reject muons from decays of pions by pointing them back to the primary vertex.
- 2) One can observe tracks of charged parent through the emulsion- space analyser.
- 3) One can measure the angle of charged parent with high accuracy of the order of 1 mrad.
- 4) One can resolve plural decay vertices, if they are separated more than $5 \mu\text{m}$ in x-y projection, and more than $100 \mu\text{m}$ in z projection.

Table 2 and Table 3 show the comparison of the proposed experiment and the experiment E653. Quantitatively, the relative gain of 10^3 of the new experiment against the E653

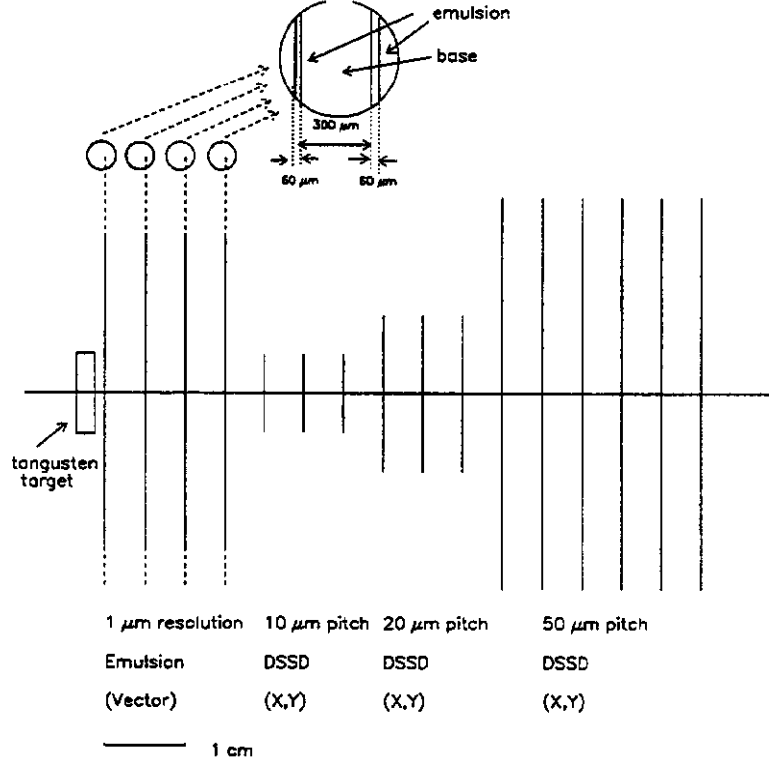


Figure 2: Schematic view of the decay vertex detector.

will be obtained by the ratio product of Target Thickness \times Total Target Area \times Beam Density on Target,

$$\frac{2.1\% \text{m.f.p.}}{3.7\% \text{m.f.p.}} \times \frac{1 \times 1 \text{m}^2 \times 300}{0.25 \times 0.25 \text{m}^2 \times 31} \times \frac{10^6 / \text{cm}^2}{10^5 / \text{cm}^2} = 880$$

Besides the above quantitative expansion, certain qualitative improvement will be expected.

- 1) Decreasing of the distance between the target and the dump (6 m for E653; 1 m for new experiment) will reduce the backgrounds down to 1/6, which come from $\pi^\pm \rightarrow \mu^\pm \nu$ and $K^\pm \rightarrow \mu^\pm \nu$, and this means the reduction of the fake dimuons of 1/36.
- 2) 2 times enlargement of the acceptance for muons (100 mrad for E653; 200 mrad for new experiment) will results the increase of factor 4 of the detection efficiency of the dimuon events as well as the acceptance of muons.

About the technical feasibility of the proposed experiment, following points could be mentioned.

- 1) We have an experience of handling large emulsion plates as large as $1.4 \times 1.4 \text{ m}^2$, and a big amount of emulsion as big as 200 liters, in the experiment CERN WA95.

Table 2. Comparison E653 run 2 and New Experiment (Apparatus).

	E653 run 2	New Experiment	comments
beam	600 GeV/c π^-	700 GeV/c π^-	
target	emulsion 1.5 cm $\sim 3.7\%$ m.f.p.	tangusten 2 mm $\sim 2.1\%$ m.f.p.	We cannot observe the decay in the target \rightarrow detection eff. $\times \frac{2}{3}$
emulsion	330 μm double side 20 layers $0.25 \times 0.25 \text{ m}^2$ 31 modules $\sim 26 \ell$	60 μm double side 4 layers $1 \times 1 \text{ m}^2$ 300 modules $\sim 150 \ell$	We have experience to make $1.4 \times 1.4 \text{ m}^2$ in CERN WA95. Total target area $\times 150$, while total emulsion volume $\times 6$.
SSD	single side 18 layer 12.5, 25, 50 μm pitch	double side ~ 10 layer 10, 20, 50 μm pitch	
beam density	$10^5 / \text{cm}^2$	$10^6 / \text{cm}^2$	The limit from emulsion measurement.
distance to DUMP	6 m	1 m	$\times \frac{1}{6}$ backgrounds : ($\pi^\pm \rightarrow \mu^\pm \nu, K^\pm \rightarrow \mu^\pm \nu$) $\times (\frac{1}{6})^2$, fake dimuon event $\times (\frac{1}{6})^2$
muon acceptance	100 mrad	200 mrad	$\times 2$ acceptance and detection efficiency $\times 4$

Table 3. Comparison E653 run 2 and New Experiment (Analysis).

	E653 run 2	New Experiment	comments
number of beam	2.8×10^9	3×10^{12}	$\times 10^3$
number of D^0 produced	1.8×10^5	1.8×10^8	
number of interaction	1.2×10^8	6.3×10^{10}	
number of triggered event	3.8×10^6	2.1×10^9	
number of selected event	950	$\sim 7 \times 10^4$	$\times 70$
scanning	semi-automatic	full-automatic	practically using in CERN WA95
backgrounds			
(1) both muons from primary int. $\rightarrow \pi \rightarrow \mu$		$\sim 1.4 \times 10^4$	checking first emulsion sheet, we can reject backgrounds both (1) and (2).
(2) one muon from primary int. $\rightarrow \pi \rightarrow \mu$	(1) and (2)	$\sim 2.4 \times 10^4$	
another muon from charm $\rightarrow \mu X$	total 901		
(3) both muons from charm $\rightarrow \mu X$	33	$\sim 3.3 \times 10^4$	

- 2) The beam density of $10^6/\text{cm}^2$ on the emulsion surface may be near the limit, but not unacceptable for the analysis.
- 3) Full automatic scanning and measuring system are already in practice in the experiment CERN WA95, in which 10^5 events will be treated per year.

As described before, the separating power of plural vertices in air gap in this method is $5 \mu\text{m}$ and $100 \mu\text{m}$ respectively in x-y and z projections. The number of background events falling in this region is, however, expected to be only 2.2 in the proposed experiment, and even in those cases, we can discriminate the true signal by the minimum parent mass method.

From the points mentioned above, this proposal depends on actuality, even though it being very preliminary one.

9 Conclusions

In conclusion, we have reported results of a search for charm hadron decays into two muons plus a hadron. Some of the upper limits on branching fractions for charm-changing neutral-current decays and lepton-number violating decays are obtained for the first time, and most of the other limits are an order of magnitude smaller than the previous results. As an extension of the present type of emulsion hybrid experiment, a possible new experiment aiming a goal to get upper limit of 10^{-7} is proposed.

References

- [1] Particle Data Group, K. Hikasa et al., Phys. Rev. D 45 (1992) 1.
- [2] B.A. Campbell et al., Int. J. Mod. Phys. A 2 (1987) 831;
W. Buchmüller and D. Wyler, Phys. Lett. B 177 (1986) 377.
- [3] E615 Collab., W.C. Louis et al., Phys. Rev. Lett. 56 (1986) 1027.
- [4] I.I. Bigi, Precious Rarities - On Rare Decays of K, D, and B Mesons, in: Proc. Sixteenth SLAC Summer Institute on Particle Physics, (Stanford, July 1988), ed. E.C. Brennan (SLAC Report No. 336, Stanford, 1989) p. 31.
- [5] E653 Collab., K. Kodama et al., Nucl. Instr. & Meth. A 289 (1990) 146.
- [6] E653 Collab., K.Kodama et al., Prog. Theor. Phys. 89 (1993) 679.
- [7] E653 Collab., K. Kodama et al., "New Techniques for Emulsion Analysis in a Hybrid Experiment", submitted to Nucl. Instr. & Meth. A.
- [8] E672 Collab., S. Kartik et al., Phys. Rev. D41 (1990) 1.
- [9] UA6 Collab., C. Morel et al., Phys. Lett. B 252 (1990) 505.
- [10] E653 Collab., K. Kodama et al., Phys. Lett. B 284 (1992) 461.
- [11] E653 Collab., K. Kodama et al., "Additional Lifetime Measurements of Charged and Neutral Beauty Hadrons," to be submitted to Phys. Rev. D.
- [12] B. Nilsson-Almqvist et al., Comp. Phys. Comm. 43 (1987) 387.
- [13] E653 Collab., K. Kodama et al., Phys. Lett. B 303 (1993) 359.
- [14] E653 Collab., K. Kodama et al., Phys. Lett. B 309 (1993) 483.
- [15] ACCMOR Collab., S. Barlag et al., Phys. Lett. B 247 (1990) 113;
CLEO Collab., P. Avery et al., Phys. Rev. D43 (1991) 3599; and
E653 Collab., K. Kodama et al., Phys. Lett. B 286 (1992) 187.
- [16] CLEO Collab., P. Haas, et al., Phys. Rev. Lett. 60 (1988) 1614.
- [17] Mark III Collab., J. Adler et al., Phys. Rev. D 40 (1989) 906.
- [18] Mark II Collab., A.J. Weir et al., Phys. Rev. D 41 (1990) 1384.
- [19] K.S. Babu et al., Phys. Lett. B 205 (1988) 540.

W-Emission for $\Delta S = 1$ and $\Delta C = 1$ Weak Decays

M. D. Scadron
Physics Department
University of Arizona
Tucson, AZ 85721, USA

The W-emission quark (i.e. hadron vacuum saturation VS) graphs depicted in Figs 1 and 2 for nonleptonic Cabibbo-angle-suppressed $K^+ \rightarrow \pi^+\pi^0$ and $D^+ \rightarrow \pi^+\pi^0$ weak decays agree very well with data for the vector form factor $f_+(0) \approx 1$. More specifically, for the standard weak hamiltonian

$$H_W = (G_F/2\sqrt{2})(J_\mu^+ J^\mu + J^\mu J_\mu^+), \quad (1)$$

the VS prescription predicts for $K^+ \rightarrow \pi^+\pi^0$ with $f_\pi \approx 93$ MeV,

$$\begin{aligned} |\langle \pi^+\pi^0 | H_W | K^+ \rangle|_{VS} &= (G_F s_1 c_1 / 2\sqrt{2}) | \langle \pi^+ | A_\mu | 0 \rangle \langle \pi^0 | V^\mu | K^+ \rangle | \\ &= (G_F s_1 c_1 / 2\sqrt{2}) f_\pi (m_K^2 - m_\pi^2) \\ &\approx 1.9 \times 10^{-8} \text{GeV}, \end{aligned} \quad (2)$$

and the PDG finds the nearby experimental amplitude [1]

$$|\langle \pi^+\pi^0 | H_W | K^+ \rangle|_{exp} = m_K [8\pi\Gamma/q]^{1/2} = (1.834 \pm 0.007) \times 10^{-8} \text{GeV}. \quad (3)$$

Likewise the W-emission VS amplitude for $D^+ \rightarrow \pi^+\pi^0$ with $f_+(0) = 1$ is

$$\begin{aligned} |\langle \pi^+\pi^0 | H_W | D^+ \rangle|_{VS} &= (G_F s_1 c_1 / 2\sqrt{2}) f_\pi (m_D^2 - m_\pi^2) \\ &\approx 0.29 \times 10^{-6} \text{GeV}, \end{aligned} \quad (3)$$

while the PDG total rate combined with the recently measured $D^+ \rightarrow \pi^+\pi^0$ branching ratio [2] 0.22 ± 0.05 finds

$$|\langle \pi^+\pi^0 | H_W | D^+ \rangle|_{exp} = m_D [8\pi\Gamma/q]^{1/2} \approx 0.36 \times 10^{-6} \text{GeV}. \quad (4)$$

On the other hand, the Cabibbo-angle-enhanced $D^+ \rightarrow \pi^+\bar{K}^0$ VS decay depicted in Fig 3 needs the usual [3] form factor suppression $f_+(0) \approx 0.76$

$$\begin{aligned} |\langle \pi^+\bar{K}^0 | H_W | D^+ \rangle|_{VS} &= (G_F c_1^2 / 2) f_\pi (m_D^2 - m_K^2) f_+(0) \\ &\approx 1.3 \times 10^{-6} \text{GeV}, \end{aligned} \quad (5)$$

in order to agree with the PDG value

$$|(\pi^+ \bar{K}^0 | H_W | D^+) |_{exp} = m_D [8\pi\Gamma/q]^{1/2} = (1.3 \pm 0.1) \times 10^{-6} \text{ GeV}. \quad (6)$$

The above W-emission at the quark level or vacuum saturation at the hadron level also works well for $\Delta S = 1$ nonleptonic weak baryon decays [4].

Contrast the above W-emission $\Delta I = 3/2$ amplitudes with the $\Delta I = 1/2$ transitions for both $K^0 \rightarrow \pi\pi$ and $D^0 \rightarrow \pi\pi$ weak decays. The charged W-emission quark graphs of Figs. 1 and 2 are then replaced by the (off-diagonal) quark self-energy plus spectator graphs of Figs. 4 and 5. In the $K^0 \rightarrow \pi\pi$ case, the GIM mechanism [5] converts the \bar{s} to \bar{c} or \bar{u} quarks in Fig. 4, leading to the observed $\Delta I = 1/2$ enhanced K^0 decay amplitudes [6]

$$|\langle \pi\pi | H_W | K^0 \rangle |_{GIM} = \frac{G_F s_1 c_1 f_K}{8\pi^2 f_\pi^2} (m_c^2 - m_u^2)(m_K^2 - m_\pi^2) \approx 24 \times 10^{-8} \text{ GeV}, \quad (7)$$

near data [1]

$$|\langle \pi\pi | H_W | K^0 \rangle |_{exp} = (26.26 \pm 0.12) \times 10^{-8} \text{ GeV}. \quad (8)$$

However for $D^0 \rightarrow \pi\pi$, the GIM mechanism turns the c to s or d quarks in Fig. 5, resulting in the observed $\Delta I = 1/2$ nonenhancement for D^0 decays [1]. It is interesting that the charmed quark mass controls both $\Delta S = 1$ K decays (via the m_c^2 factor in eq. (7)), and the $\Delta C = 1$ decays (via the m_D^2 factor in eqs. (3) and (5)).

References

1. Particle Data Group, Phys. Rev. D45, II, 1 (1992).
2. Cleo Collab., M. Selen et al., Phys. Rev. Lett. 71, 1973 (1993).
3. See e.g. M. Bauer, B. Stech and M. Wirbel, Zeit. Phys. C 34, 103 (1987).
4. R. E. Karlsen and M. D. Scadron, Phys. Rev. D44, 2192 (1991).
5. S. Glashow, J. Iliopoulos and L. Maiani, Phys. Rev. D2, 1285 (1970).
6. V. Elias, D. G. C. McKeon and M. D. Scadron, Can. J. Phys., 68, 1330 (1990);
R. E. Karlsen and M. D. Scadron, Mod. Phys. Lett. A in press (1994).

Figures

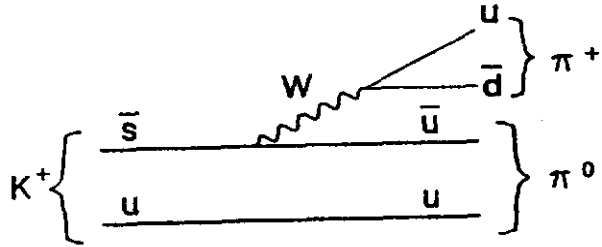


Fig. 1. W-emission quark graph for $K^+ \rightarrow \pi^+ \pi^0$

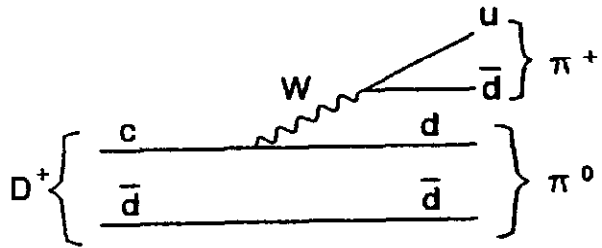


Fig. 2. W-emission quark graph for $D^+ \rightarrow \pi^+ \pi^0$

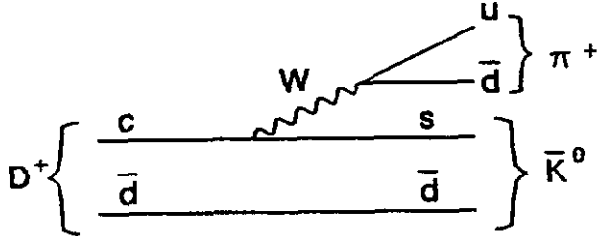


Fig. 3. W-emission quark graph for $D^+ \rightarrow \pi^+ \bar{K}^0$

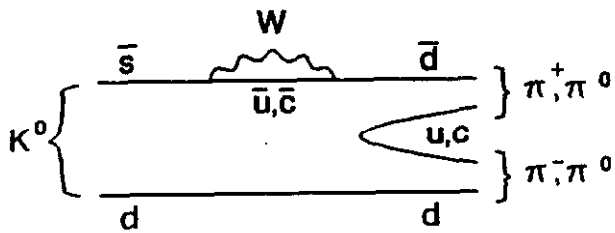


Fig. 4. Self-energy quark graph dominating $K^0 \rightarrow 2\pi$ decays

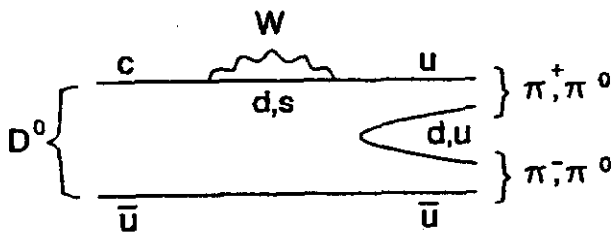


Fig. 5. Self-energy quark graph not dominating $D^0 \rightarrow 2\pi$ decays

CHARMONIUM HADROPRODUCTION AND CHARM2000

Leonard Spiegel
Fermi National Accelerator Laboratory
Batavia, IL 60510

ABSTRACT

FNAL experiment E-705 has recently published several results on the production of charmonium states in 300 GeV/c secondary hadron beams. This brief note summarizes results from proton-induced charmonium production. Theoretical motivations for the studies are described, with emphasis on those results which would benefit from further experimental probing. It is argued that charmonium hadroproduction should be viewed as a natural and important adjunct to the CHARM2000 program and that special considerations should be given to the spectrometer design so as to enhance sensitivity for charmonium χ states.

1. QCD Motivation

Charmonium hadroproduction is invariably studied within the framework of Quantum Chromodynamics. One wishes to relate observed differential distributions of charmonium states to parton level diagrams and, in the process, clarify some of the assumptions involved in QCD calculations. In addition to the mathematical difficulties presented by QCD expansions, detailed predictions are also necessarily complicated by convolutions with target and beam particle structure functions. Experimentally, one would like to focus on charmonium states that tend to isolate features of theoretical interest. For example, it has long been appreciated that 30-40% of fixed target J/ψ 's are the result of χ and ψ' decays.¹⁻⁶ This implies an additional set of production-level diagrams which must be taken into account in order to fully account for ψ production. In contrast, χ states are mostly directly produced and thus represent an interesting set for exploring QCD questions.⁷⁻¹²

Figures 1a and 1b illustrate two conceivable lowest-level diagrams for $c\bar{c}$ production by gluon fusion (appropriate for proton-nucleon reactions, especially at small x_F). Figure 1a assumes that color conservation is maintained at all levels of the production process. Along with the diagrams are predictions for the relative production cross sections for the χ_0 , χ_1 , and χ_2 states. The null prediction for the χ_1 state is easy to understand: two massless, spin 1 gluons will not couple to a spin 1 state.¹³ Figure 1b, on the other hand, allows for an intermediate colored state which subsequently "evaporates" a soft gluon to yield a colorless $c\bar{c}$ state. In lack of detailed understanding of the evaporation process, the model simply assumes the χ states are produced in proportion to their $2J + 1$ spin projections. This leads to a sharp contrast with the color

singlet model for the relative yields of χ_1 and χ_2 states. Unfortunately these states are separated by only $45 \text{ MeV}/c^2$, which makes their isolation experimentally challenging.

2. Experiment E-705

Experiment E-705 ran in the Proton West beamline of the Fermi National Accelerator Laboratory and was designed to trigger on high mass dimuons while at the same time maintaining good acceptance for charged hadrons, electrons, and photons. Beam to the experiment alternated at approximately monthly intervals between $300 \text{ GeV}/c$ positives (55% percent protons and 45% pions) and $300 \text{ GeV}/c$ negatives (98% pions and 2% antiprotons). The beam was targeted upon a 33 cm lithium target. Two beamline Cerenkov counters tagged on an event-by-event basis the beam particle composition. No distinction was made between pions and kaons.

Reconstruction of the dimuon data yielded a sample of approximately 23,000 J/ψ 's. Of these, approximately one half come from $\pi^- Li$ interactions, one quarter from $\pi^+ Li$, one quarter from protons, and a small percentage from antiprotons. E-705 also observed signals above background (in the combined data sample) of around 500 $\psi' \rightarrow \mu^+ \mu^-$ and 1,100 $\chi_{1,2} \rightarrow \psi \gamma \rightarrow \mu^+ \mu^- \gamma$ states. The dimuon spectrum for protons is shown in Fig. 2a.¹⁴ By observing J/ψ signals within specific Feynman- x bins and correcting them for the spectrometer acceptance, the J/ψ x_F distribution is obtained. This distribution is shown in Fig. 2b along with a structure function inspired parameterization.

3. Direct J/ψ Production

The main sources of non-direct J/ψ production include radiative χ decays and $\psi' \rightarrow \psi \pi \pi$ decays. The branching ratios for $\chi_{0,1,2} \rightarrow \psi \gamma$ are $(6.6 \pm 1.8) \cdot 10^{-3}\%$, $(27.3 \pm 1.6)\%$, and $(13.5 \pm 1.1)\%$ respectively.¹⁵ Thus the χ_0 state can be neglected as a source of indirect ψ 's. By comparing the number of χ_1 and χ_2 states above background with the number of J/ψ states above background and correcting for the γ acceptance, E-705 measures the fraction of J/ψ states that arise from χ decays. For this analysis, it is not necessary to resolve the χ_1 and χ_2 states. One does make the reasonable assumption that the spectrometer acceptance is identical for χ_1 and χ_2 photons.

In a similar fashion E-705 estimated the fraction of J/ψ 's arising from $\psi' \rightarrow \psi \pi \pi$ decays by using its own measurement for the ψ' cross section and the tabulated branching ratio.¹⁶ This result, along with χ state estimates, is shown in Table 1. By removing the known decay contributions to the observed dimuon spectrum, E-705 is able to estimate the cross section for direct J/ψ production. It should be noted that components of this determination were all measured within a single experiment, thus tending to minimize the systematic errors.

Table 1. E-705 production results for protons. σ in nanobarns/nucleon for $x_F > 0$.

$\sigma_{total}(\psi)$	$\sigma(\psi')/\sigma(\psi)$	ψ from $\chi_1 + \chi_2$	ψ from ψ'	$\sigma_{direct}(\psi)$
143 ± 17	0.14 ± 0.03	0.30 ± 0.04	0.08 ± 0.02	89 ± 12

4. χ Production

Figure 3 illustrates the mass difference, $M(\mu\mu\gamma) - M(\mu\mu)$, for proton-produced dimuons in the J/ψ range.¹⁷ The background curve was obtained by combining dimuons with γ 's from other events. Following a background subtraction, the resultant histogram is shown in the upper right hand corner of Fig. 3. Superimposed on the background-subtracted curve are fits for the individual contributions of the χ_1 and χ_2 . The shape of these response curves was obtained by measuring the energy resolution of conversion electrons, where one has accurately measured their momentum, and cross-checking the results with π^0 signals. The expected width (sigma) of the two χ signals is 30 ± 3 MeV/c².¹⁴ By centering the Gaussian fits at the known masses of the χ_1 and χ_2 and by allowing the normalizations to float so as to best fit the mass difference spectrum, the relative contributions of the χ_1 and χ_2 are measured. Removing the branching ratios yields a ratio,¹⁷ $\sigma_1/\sigma_2 = 0.08^{+0.25}_{-0.15}$, which can be contrasted with the analogous measurement for pions: $\sigma_1/\sigma_2 = 0.52^{+0.57}_{-0.27}$.

Although the errors are fairly large, the E-705 cross section ratio for protons suggests the dominance of the color singlet model diagram of Fig. 1. Only one other proton experiment⁵ has attempted to separately measure the individual χ state cross sections and their result, $\sigma_1/\sigma_2 = 0.24 \pm 0.28$, is again suggestive of strict color conservation.

5. Relevance to CHARM2000

There are many open questions with regards to charmonium hadroproduction that would benefit from fresh theoretical and experimental investigations. With a suitable dimuon trigger, the CHARM2000 program could easily amass a substantial charmonium data sample. Special consideration should be given to the photon calorimeter so that the resulting energy resolution is sharp enough to well resolve the χ_1 and χ_2 charmonium states. With unprecedented signals consisting of hundreds of thousands of J/ψ 's and tens of thousands of ψ' and χ states, and with hopefully a renewed theoretical interest, CHARM2000 should be able to offer deeper insights into QCD.

References

1. J.H. Cobb *et al.*, *Phys. Lett.* **72B** (1978) 497.
2. C. Kourkoumelis *et al.*, *Phys. Lett.* **81B** (1979) 405.
3. Y. Lemoigne *et al.*, *Phys. Lett.* **113B** (1982) 509.
4. F. Binon *et al.*, *Nucl. Phys.* **B239** (1984) 311.
5. S.R. Hahn *et al.*, *Phys. Rev.* **D30** (1984) 671.
6. D.A. Bauer, *et al.*, *Phys. Rev. Lett.* **54** (1985) 753.
7. C.E. Carlson and R. Suaya, *Phys. Rev.* **D15** (1977) 1416.
8. C.H. Chang, *Nucl. Phys.* **B172** (1980) 425.
9. R. Baier and R. Rückl, *Z. Phys.* **C19** (1983) 251.
10. J.H. Kühn, *Phys. Lett.* **89B** 385 (1980) 385.
11. H. Fritzsch, *Phys. Lett.* **67B** (1977) 217.
12. M. Glück *et al.*, *Phys. Rev.* **D17** (1978) 2324.
13. C.N. Yang, *Phys. Rev.* **77** (1950) 242.
14. L. Antoniazzi *et al.*, *Phys. Rev.* **D46** (1993) 4829.
15. D.M. Aguilar-Benitez Doe, *Phys. Rev.* **45D** (1992).
16. L. Antoniazzi *et al.*, *Phys. Rev. Lett.* **70** (1993) 383.
17. L. Antoniazzi *et al.*, *Phys. Rev.* **D49** (1994) 543.

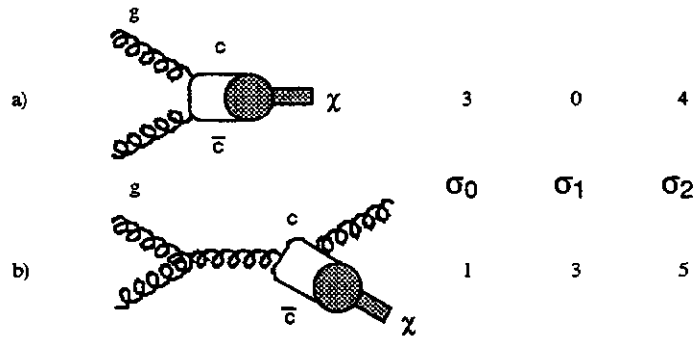


Fig. 1. Gluon fusion diagrams: a) color singlet model; b) color evaporation.

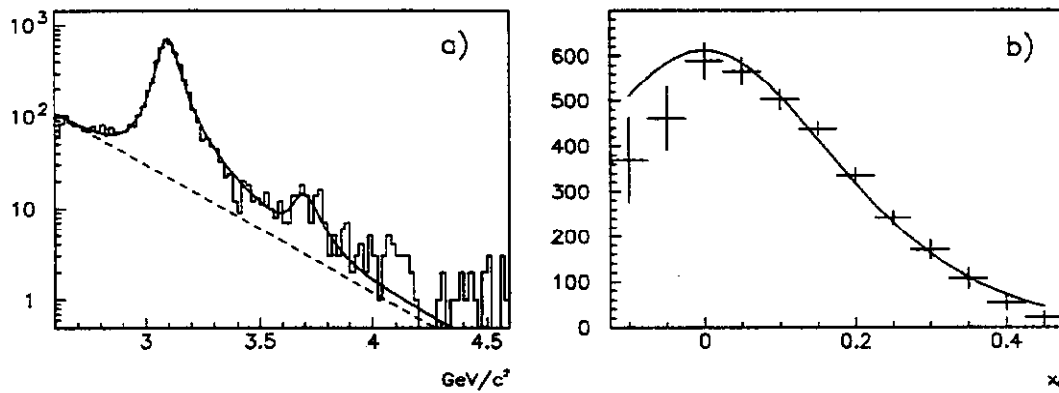


Fig. 2. a) E-705 dimuon spectrum for protons; b) Acceptance corrected J/ψ Feynman-x distribution.

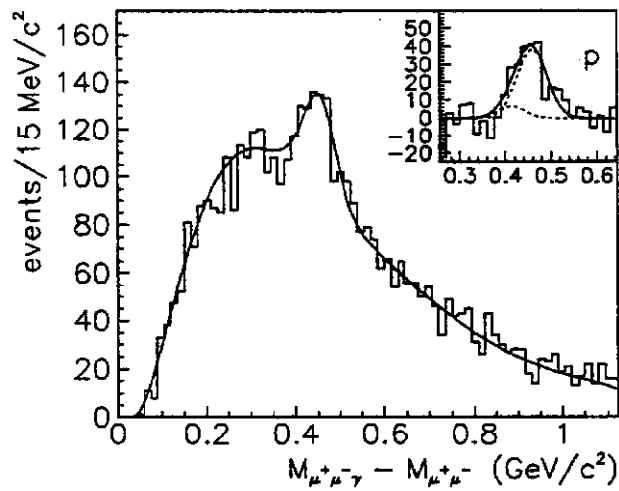


Fig. 3. Mass difference for protons. The insert shows the resultant spectrum after a background subtraction along with a simultaneous fit for χ_1 and χ_2 states.

Polarization as a Probe to the Production Mechanisms of Charmonium in πN Collisions¹

W.-K. Tang² and S. J. Brodsky²
Stanford Linear Accelerator Center
Stanford University, Stanford, CA 94309

M. Vanttinen and P. Hoyer
Department of Physics
University of Helsinki, Finland

Abstract

Measurements of the polarization of J/ψ produced in pion-nucleus collisions are in disagreement with leading twist QCD prediction where J/ψ is observed to have negligible polarization whereas theory predicts substantial polarization. We argue that this discrepancy cannot be due to poorly known structure functions nor the relative production rates of J/ψ and χ_J . The disagreement between theory and experiment suggests important higher twist corrections, as has earlier been surmised from the anomalous non-factorized nuclear A -dependence of the J/ψ cross section.

1 Introduction

One of the most sensitive tests of the QCD mechanisms for the production of heavy quarkonium is the polarization of the J/ψ in hadron collisions. In fact, there are serious disagreements between leading twist QCD prediction [2] and experimental data [3, 4, 5, 6, 7] on the production cross section of 'direct' J/ψ and χ_1 . We would like to advocate that polarization of J/ψ provides strong constraints on the production mechanisms of J/ψ and thus can pinpoint the origin of these disagreements.

In this paper we will present some preliminary results on the theoretical calculation of the polarization of J/ψ in πN collisions. The completed analysis will be published in a later paper[1]. We found that the polarization of J/ψ provides important constraints on the nature of the production mechanisms and urge that polarization measurement of J/ψ should be included in the design of future charm production experiment.

The paper is organized as follow. In section 2, we show that from the experimental data on the production cross sections and leptonic decay widths of direct J/ψ and ψ' , the long

¹Presented by W.-K. Tang at QCD Tests Working Group, Workshop on the Future of High Sensitivity Charm Experiments: Charm2000, Fermilab, Batavia, IL, June 7-9, 1994

²Work supported by the Department of Energy, contract DE-AC03-76SF00515

distance physics of formation of bound states of $c\bar{c}$ can be separated from the short distance physics of production of the $c\bar{c}$ pair. Thus, the perturbative analysis is under control in calculating J/ψ production even though the mass of charm quark is not much larger than Λ_{QCD} . Once the validity of perturbative method is established, we calculate the production cross sections of direct J/ψ , χ_1 and χ_2 in πN collisions in PQCD. These results are presented in section 3 and discrepancies are observed. We show that, in comparison with the recent E705 and E672 data [8, 10], the predicted ratio of direct J/ψ production compared to the χ_2 production is too low by a factor of about 3. In addition the production ratio of production cross sections of χ_1 to χ_2 is too low by a factor of 10 compared to data. A similar conclusion has been reached in [11]. The polarization data of J/ψ [12, 13, 14] allows us to make further conclusion of the origin of the disagreements. In section 4, we find that even if the relative production rates of the J/ψ , χ_1 and χ_2 are adjusted (using K -factors) to agree with the data, the J/ψ polarization data is still not reproduced. Therefore, the discrepancies do not arise from an incorrect relative normalization of the various channels and new production mechanisms are needed. We will present our conclusion in the last section.

2 Can direct J/ψ production be calculated in PQCD?

In leading twist QCD, the production of the J/ψ at low transverse momentum occurs both ‘directly’ from the gluon fusion subprocess $gg \rightarrow J/\psi + g$ [Fig. 1a] and indirectly via the production and decay of χ_1 and χ_2 states. These states have sizable decay branching fractions $\chi_{1,2} \rightarrow J/\psi + \gamma$ of 27% and 13%, respectively.

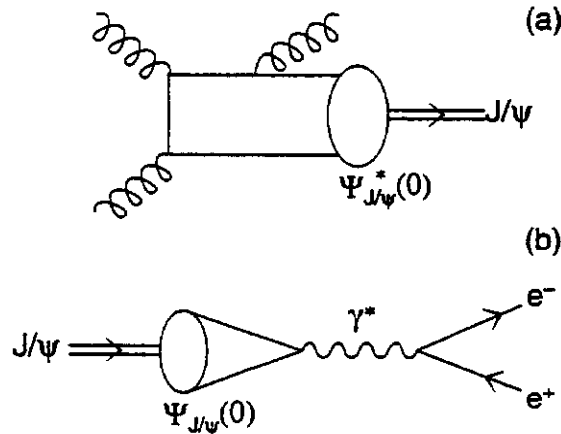


Figure 1: Fig. 1a shows direct J/ψ production through gg scattering. The formation of bound state is described by the wavefunction $\Psi_{J/\psi}^*(0)$ at the origin. Fig. 1b shows leptonic decay of J/ψ into e^+e^- pair. The probability of finding the $c\bar{c}$ pair is given by the wavefunction $\Psi_{J/\psi}(0)$.

In this model, we assume that the non-perturbative physics, which is described by the wave function at the origin in cases of production of J/ψ and ψ' , is separable from the

perturbative hard subprocess, *i.e.*, factorization holds. As the wave function at the origin can be related to the leptonic decay amplitude [Fig. 1b], the ratio of ψ' to direct J/ψ production can be expressed in terms of the ratio of their leptonic decay width. More precisely, taking into account of the phase space factor,

$$\frac{\sigma(\psi')}{\sigma_{dir}(J/\psi)} \simeq \frac{\Gamma(\psi' \rightarrow e^+e^-)}{\Gamma(J/\psi \rightarrow e^+e^-)} \frac{M_{J/\psi}^3}{M_{\psi'}^3} \simeq 0.24 \pm 0.03 \quad (1)$$

where $\sigma_{dir}(J/\psi)$ is the cross section for direct production of the J/ψ . The ratio (1) should hold for all beams and targets, independently of the size of the higher twist corrections in producing the point-like $c\bar{c}$ state. The energy should be large enough for the bound state to form outside the target. The available data is indeed compatible with (1). In particular, the E705 value [8] is 0.24. In Table 1, the ratio of ψ' to direct J/ψ production with different projectiles is presented. They are all consistent with the value 0.24.

	$\sigma(\psi')$ [nb]	$\sigma_{dir}(J/\psi)$	$\sigma(\psi')/\sigma_{dir}(J/\psi)$
π^+	22 ± 5	97 ± 14	0.23 ± 0.07
π^-	25 ± 4	102 ± 14	0.25 ± 0.05
p	20 ± 3	89 ± 12	0.23 ± 0.05

Table 1: Production cross sections for ψ' , direct J/ψ and their ratio in π^+N , π^-N and pN collisions. The data is from Ref. [8].

The anomalous nuclear target A -dependence observed for the J/ψ is also seen for the ψ' [15], so that the ratio (1) is indeed independent of A . Therefore, at high energies, the quarkonium bound state forms long after the production of the $c\bar{c}$ pair and the formation process is well described by the non-relativistic wavefunction at the origin.

3 Production rates of ψ and χ_J states at leading twist

In leading twist and to leading order in α_s , J/ψ production can be computed from the convolution of hard subprocess cross section $gg \rightarrow J/\psi g$, $gg \rightarrow \chi_j$, *etc.*, with the parton distribution functions in the beam and target. Higher order corrections in α_s , and relativistic corrections to the charmonium bound states, are unlikely to change our qualitative conclusions at moderate x_F . Contributions from direct J/ψ production, as well as from indirect production via χ_1 and χ_2 decays, will be included. Due to the small branching fraction $\chi_0 \rightarrow J/\psi + \gamma$ of 0.7%, the contribution from χ_0 to J/ψ production is expected (and observed) to be negligible. Decays from the radially excited 2^3S_1 state, $\psi' \rightarrow J/\psi + X$, contribute to the total J/ψ rate at the few per cent level and will be ignored here.

The $\pi N \rightarrow \chi_2 + X$ production cross section to lowest order is

$$\sigma(\pi N \rightarrow \chi_2 + X; x_F > 0) = \int_{\sqrt{\tau}}^1 \frac{dx_1}{x_1} F_{g/\pi}(x_1) F_{g/N}(\tau/x_1) \sigma_0(gg \rightarrow \chi_2) \quad (2)$$

where $\tau = M_{\chi_2}^2/s$ and the quantity $\sigma_0(gg \rightarrow \chi_2) = 16\pi^2\alpha_s^2|R'_P(0)|^2/M_{\chi_2}^7$ [18]. We restrict the χ_2 momentum range to the forward CM hemisphere ($x_F > 0$) in accordance with the available data, and use the structure functions of Ref. [16, 17] evaluated at $Q^2 = M_{\chi_2}^2$. We also take the renormalization scale to be $Q^2 = M_{\chi_2}^2$.

The direct $\pi N \rightarrow J/\psi + X$ cross section is similarly given by

$$\begin{aligned} \sigma(\pi N \rightarrow J/\psi + X; x_F > 0) &= \int_{\tau}^1 dx_1 \int_{\tau/x_1}^1 dx_2 \int_{\hat{t}_{\min}}^0 d\hat{t} F_{g/\pi}(x_1) F_{g/N}(x_2) \\ &\times \frac{d\sigma}{d\hat{t}}(gg \rightarrow J/\psi + g) \end{aligned} \quad (3)$$

where \hat{t} is the invariant momentum transfer in the subprocess, and

$$\hat{t}_{\min} = \max \left(\frac{x_2 M_{J/\psi}^2 - x_1 \hat{s}}{x_1 + x_2}, M_{J/\psi}^2 - \hat{s} \right). \quad (4)$$

Eq. (3) also applies to the $\pi N \rightarrow \chi_1 + X$ reaction, in which case a sum over the relevant subprocesses $gg \rightarrow \chi_1 g$, $gq \rightarrow \chi_1 q$, $g\bar{q} \rightarrow \chi_1 \bar{q}$ and $q\bar{q} \rightarrow \chi_1 g$ is necessary. The differential cross sections $d\sigma/d\hat{t}$ for all subprocesses are given in [18, 19].

In Table 2 we compare the χ_2 production cross section, and the relative rates of direct J/ψ and χ_1 production, with the data of E705 and WA11 on $\pi^- N$ collisions at $E_{lab} = 300$ GeV and 185 GeV [8].

	$\sigma(\chi_2)$ [nb]	$\sigma_{dir}(J/\psi)/\sigma(\chi_2)$	$\sigma(\chi_1)/\sigma(\chi_2)$
Experiment	$188 \pm 30 \pm 21$	$0.54 \pm 0.11 \pm 0.10$	$0.70 \pm 0.15 \pm 0.12$
Theory	72	0.19	0.069

Table 2: Production cross sections for χ_1 , χ_2 and directly produced J/ψ in $\pi^- N$ collisions. The data from Ref. [8, 9] include measurements at 185 and 300 GeV. The theoretical calculation is at 300 GeV.

The χ_2 production rate in QCD agrees with the data within a ‘ K -factor’ of order 2 to 3. This is within the theoretical uncertainties arising from the J/ψ and χ wavefunctions, higher order corrections, structure functions, and the renormalization scale. A similar factor is found between the lowest-order QCD calculation and the data on lepton pair production [20, 21]. On the other hand, Table 2 shows a considerable discrepancy between the calculated and measured relative production rates of direct J/ψ and χ_1 , compared to χ_2 production. *A priori* we would expect the K -factors to be roughly similar for all three processes. We conclude that leading twist QCD appears to be in conflict with the data on direct J/ψ and χ_1 production. Although in Table 2 we have only compared our calculation with the E705 and WA11 $\pi^- N$ data, this comparison is representative of the overall situation (for a recent comprehensive review see [11]).

4 Polarization of the J/ψ

The polarization of the J/ψ is determined by the angular distribution of its decay muons in the J/ψ rest frame. By rotational symmetry and parity, the angular distribution of massless muons, integrated over the azimuthal angle, has the form

$$\frac{d\sigma}{d\cos\theta} \propto 1 + \lambda \cos^2\theta \quad (5)$$

where we take θ to be the angle between the μ^+ and the projectile direction (*i.e.*, we use the Gottfried-Jackson frame). The parameter λ can be calculated from the $c\bar{c}$ production amplitude and the electric dipole approximation of radiative χ decays.

The electric dipole approximation of the radiative decay $\chi_J \rightarrow \psi\gamma$ is exact in the heavy quark limit; *i.e.*, when terms of $\mathcal{O}(E_\gamma/m_c)$ are neglected. As a consequence, the heavy quark spins are conserved in the decay, while the orbital angular momentum changes.

The lowest order subprocess $g(\mu_1)g(\mu_2) \rightarrow c\bar{c} \rightarrow \chi_2(J_z)$ only produces χ_2 with $J_z = \pm 2$ states assuming that the transverse momenta of the incoming gluons are neglected. In the $J_z = \pm 2$ polarization state the spin and orbital angular momenta of its constituent charm quarks are aligned, $S_z = L_z = \pm 1$. Since S_z is conserved in the radiative decay $\chi_2 \rightarrow J/\psi + \gamma$, it follows that $J_z(J/\psi) = S_z = \pm 1$ ($L = 0$ for the J/ψ). Thus the J/ψ 's produced via χ_2 decay are transversely polarized, *i.e.*, $\lambda = 1$ in (5). This result is exact if both the photon recoil and the intrinsic transverse momenta of the incoming partons are neglected. Smearing of the beam parton's transverse momentum distribution by a Gaussian function $\exp[-(k_\perp/500 \text{ MeV})^2]$ would bring λ down to $\lambda \simeq 0.85$.

From the $gg \rightarrow J/\psi + g$ amplitude we find for direct J/ψ production, $\pi N \rightarrow J/\psi + X \rightarrow \mu^+\mu^- + X$,

$$\begin{aligned} \frac{1}{B_{\mu\mu}} \frac{d\sigma}{dx_F d\cos\theta} &= \frac{3}{64\pi} \int \frac{dx_1 dx_2}{(x_1 + x_2)s} F_{g/\pi}(x_1) F_{g/N}(x_2) \\ &\times [\varrho_{11} + \varrho_{00} + (\varrho_{11} - \varrho_{00}) \cos^2\theta] \end{aligned} \quad (6)$$

where $B_{\mu\mu}$ is the $J/\psi \rightarrow \mu^+\mu^-$ branching fraction, $x_F = 2p_\psi^z/\sqrt{s}$ is the longitudinal-momentum fraction of the J/ψ , and θ is the muon decay angle of Eq. (5). The $\varrho_{11}, \varrho_{00}$ are the density matrix elements and can be found in [1].

For the $\pi N \rightarrow \chi_1 + X \rightarrow J/\psi + \gamma + X \rightarrow \mu^+\mu^- + \gamma + X$ production process we get similarly

$$\begin{aligned} \frac{1}{B_{\mu\mu}} \frac{d\sigma}{dx_F d\cos\theta} &= \frac{3}{128\pi} \text{Br}(\chi_1 \rightarrow \psi\gamma) \Sigma_{ij} \int \frac{dx_1 dx_2}{(x_1 + x_2)s} F_{i/\pi}(x_1) F_{j/N}(x_2) \\ &\times [\varrho_{00}^{ij} + 3\varrho_{11}^{ij} + (\varrho_{00}^{ij} - \varrho_{11}^{ij}) \cos^2\theta], \end{aligned} \quad (7)$$

where the density matrix elements for $ij = gg, gq, g\bar{q}$ and $q\bar{q}$ scattering are again given in [1].

In Fig. 2a we show the predicted value of the parameter λ of Eq. (5) in the GJ-frame as a function of x_F , separately for the direct J/ψ and the $\chi_{1,2} \rightarrow J/\psi + \gamma$ processes. Direct J/ψ production gives $\lambda \simeq 0.25$, whereas the production via χ_1 results in $\lambda \simeq -0.15$.

The $\lambda(x_F)$ -distribution obtained when both the direct and indirect J/ψ production processes are taken into account is shown in Fig. 2b and is compared with the Chicago-Iowa-Princeton [13] and E537 data [14] for 252 GeV πW collisions and 150 GeV $\pi^- W$ collisions respectively. Our QCD calculation gives $\lambda \simeq 0.5$ for $x_F \lesssim 0.6$, significantly different from the measured value $\lambda \simeq 0$.

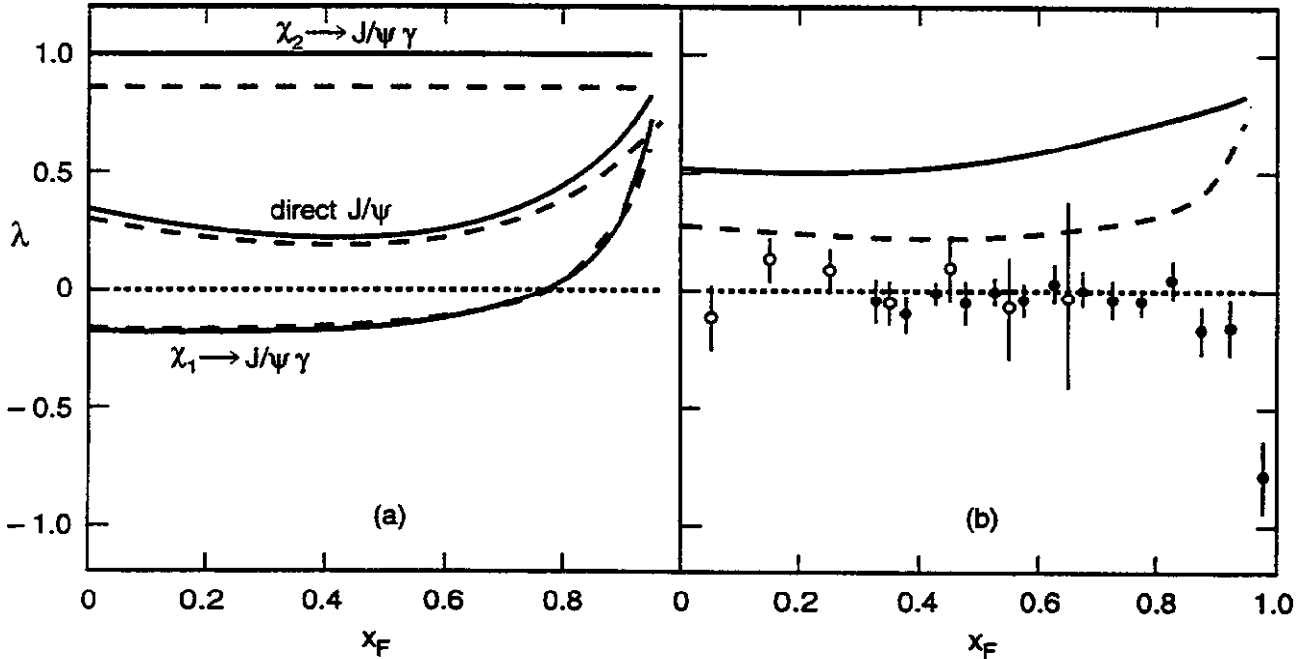


Figure 2: CIP (\bullet) and E537 (\circ) data compared with theoretical prediction. Fig. 2a shows the parameter λ from different contributions: direct J/ψ , $\chi_{1,2} \rightarrow J/\psi + \gamma$ processes. Solid curves show the results with the intrinsic transverse momentum of the incoming partons neglected while the dashed curves have the beam parton's transverse momentum modeled by a Gaussian function $\exp[-(k_\perp/500\text{MeV})^2]$. Fig. 2b takes into account both the direct and indirect J/ψ production: without K factors correction (solid curve), and with K factors correction (dashed curve).

The discrepancies between the calculated and measured values of λ is one further indication that the standard leading twist processes considered here are not adequate for explaining charmonium production. The J/ψ polarization is particularly sensitive to the production mechanisms and allows us to make further conclusions on the origin of the disagreements, including the above discrepancies in the relative production cross sections of J/ψ , χ_1 and χ_2 . If these discrepancies arise from an incorrect relative normalization of the various subprocess contributions (e.g., due to higher order effects), then we would expect the J/ψ polarization to agree with data when the relative rates of the subprocesses are adjusted according to the measured cross sections of direct J/ψ , χ_1 and χ_2 production³. The dashed curve in Fig. 2b

³In the case of Drell-Yan virtual photon production, it is known that higher-order corrections do not

shows the effect of multiplying the partial J/ψ cross sections with the required K -factors. The λ parameter is still predicted incorrectly over most of the x_F range.

A similar conclusion is reached (within somewhat larger experimental errors) if we compare our calculated value for the polarization of direct J/ψ production, shown in Fig. 2a, with the measured value of λ for ψ' production. In analogy to Eq. (1), the ψ' polarization data should agree with the polarization of directly produced J/ψ 's, regardless of the production mechanism. Based on the angular distribution of the muons from $\psi' \rightarrow \mu^+ \mu^-$ decays in 253 GeV $\pi^- W$ collisions, Ref. [23] quotes $\lambda_{\psi'} = 0.02 \pm 0.14$ for $x_F > 0.25$, appreciably smaller than our QCD values for direct J/ψ 's in Fig. 2a.

5 Discussion

We have seen that the J/ψ and χ_1 hadroproduction cross sections in leading twist QCD are at considerable variance with the data, whereas the χ_2 cross section agrees with measurements within a reasonable K -factor of 2 to 3. On the other hand, the inclusive decays of the charmonium states based on the minimal perturbative final states (gg and $q\bar{q}g$) have been studied in detail using perturbation theory [24, 25, 11], and appear to work fairly well. It is therefore improbable that the treatment of the $c\bar{c}$ binding should require large corrections. This conclusion is supported by the fact that the relative rate of ψ' and direct J/ψ production (Eq. 1), which at high energies should be independent of the production mechanism, is in agreement with experiment.

In a leading twist description, an incorrect normalization of the charmonium production cross sections can arise from large higher order corrections or uncertainties in the parton distributions[11]. Taking into account that the normalization may be wrong by as much as a factor of 10 and that even such a K -factor does not explain the polarization data of J/ψ , a more likely explanation may be that there are important higher-twist contributions to the production of the J/ψ and χ_1 as suggested in large x_F case [26, 27].

Further theoretical work is needed to establish that the data on direct J/ψ and χ_1 production indeed can be described from higher twist mechanisms. Experimentally, it is important to check whether the J/ψ 's produced indirectly via χ_2 decay are transversely polarized. This would show that χ_2 production is dominantly leading twist, as we have argued. Thus, the polarization of J/ψ production from different channels provides a very sensitive discriminant of different production mechanisms.

References

- [1] M. Vanttinen, P. Hoyer, S. J. Brodsky and W.-K. Tang, in preparation.
- [2] V. Barger and A. D. Martin, Phys. Rev. D **31**, 1051 (1985).

change the γ^* polarization significantly [22], which makes it plausible to represent these corrections by a simple multiplicative factor, which does not affect the polarization of the photon.

- [3] A. G. Clark, *et al.*, Nucl. Phys. **B142**, 29 (1978).
- [4] R806: C. Kourkouvelis *et al.*, Phys. Lett. **B81**, 405 (1979)
- [5] WA11: Y. Lemoigne, *et al.*, Phys. Lett. **B113**, 509 (1982).
- [6] E673: S. R. Hahn, *et al.*, Phys. Rev. **D30**, 671 (1984); D. A. Bauer, *et al.*, Phys. Rev. Lett. **54**, 753 (1985).
- [7] F. Binon, *et al.*, Nucl. Phys. **B239**, 311 (1984).
- [8] E705: L. Antoniazzi, *et al.*, Phys. Rev. Lett. **70**, 383 (1993)
- [9] E705: L. Antoniazzi, *et al.*, Phys. Rev. **D46**, 4828 (1992)
- [10] E672: A. Zieminski, *et al.*, Proc. XXVI Int. Conf. on High Energy Physics, Dallas, Texas, 1992, AIP Conf. Proc. No. 272, Ed. by J. R. Sanford, p. 1062.
- [11] G. A. Schuler, preprint CERN-TH.7170/94.
- [12] NA3: J. Badier, *et al.*, Z. Phys. **C20**, 101 (1983).
- [13] C. Biino, *et al.*, Phys. Rev. Lett. **58**, 2523 (1987).
- [14] E537: C. Akerlof, *et al.*, Phys. Rev. **D48**, 5067 (1993).
- [15] E772: D. M. Alde, *et al.*, Phys. Rev. Lett. **66**, 133 (1991).
- [16] J. F. Owens, Phys. Rev. **D30**, 943 (1984).
- [17] J. F. Owens, Phys. Lett. **B266**, 126 (1991).
- [18] R. Baier and R. Rückl, Z. Phys. **C19**, 251 (1983).
- [19] R. Gastmans and T. T. Wu, *The Ubiquitous Photon: Helicity Method for QED and QCD*, Clarendon Press, Oxford, 1990
- [20] J. Badier, *et al.*, Z. Phys. **C18**, 281 (1983).
- [21] J. S. Conway, *et al.*, Phys. Rev. **D39**, 92 (1989).
- [22] P. Chiappetta and M. Le Bellac, Z. Phys. **C32**, 521 (1986)
- [23] J. G. Heinrich, *et al.*, Phys. Rev. **D44**, 1909 (1991).
- [24] W. Kwong, J. L. Rosner and C. Quigg, Ann. Rev. Nucl. Part. Sci. **37**, 325 (1987).
- [25] L. Köpke and N. Wermes, Phys. Rep. **174**, 67 (1989).
- [26] S. J. Brodsky, P. Hoyer, A. H. Mueller and W.-K. Tang, Nucl. Phys. **B369**, 519 (1992).
- [27] P. Hoyer, M. Vanttinen and U. Sukhatme, Phys. Lett. **B246**, 217 (1990).

Warm Liquid Calorimetry Using TMP: An Update

WALIC Collaboration

B. Aubert,^a K. Abe,^f A. Ciocio,^b J. Colas,^a L. Dobrzynski,^d P. Ghez,^a M. Hoff,^b Y. Hoshi,^g H. Iso,^g J. Kadyk,^b R. Kikuchi,^c D. Kryn,^d J.C. Lacotte,^a P. Lavocat,^e M. Long,^b B. Mansoulie,^e D. Marchand,^d J.P. Mendiburu,^d K. Neichi,^f M. Pripstein,^b G. Przybylski,^b P. Salin,^d J. Teiger,^e W. Thur,^b T. Weber,^b W.A. Wenzel,^b and H. Yuta^f

^a LAPP, IN2P3-CNRS, Annecy, France

^b LBL, Berkeley, CA, USA

^c Kyoto University, Kyoto, Japan

^d College de France, IN2P3-CNRS, Paris, France

^e CEN, Saclay, France

^f Tohoku University, Sendai, Japan

^g Tohoku Gakuin University, Tagajo, Japan

Abstract

A summary is given of recent measurements of performance of warm-liquid calorimeters, using tetramethyl pentane (TMP) as the active medium. A comprehensive set of tests were performed using beams of electrons and pions to study the signal response ratio e/π , ie. compensation, over the energy range 5 - 150 GeV/c. Studies were made with iron and lead absorber, varying the ratio of absorber to TMP. It was found that compensation was not achievable using iron, but was nearly so using lead. The response ratio, e/π , is relatively insensitive to the ratio of thicknesses, absorber/TMP, but is very sensitive to electric field strength because of signal saturation for large ionization density. Thus, the e/π ratio can be tuned by adjusting the electric field strength. In another part of the investigation, a calorimeter was built with the lead absorber plates immersed in the TMP medium, a design not previously attempted. This calorimeter was successfully tested in the same beam, exhibiting good performance. Finally, this calorimeter and two other test cells were irradiated by a Co60 source to doses as high as 30 Mrad. A surprising result was found: the electron lifetime first improved by a large amount from an initially low value, and then decreased rather slowly. The predicted maximum dose for good calorimeter performance without cleaning or renewing the TMP is more than 150 Mrad. The two test cells were built to study further the lifetime degradation as well as possible space charge limitations under very intense irradiation. The results indicated that space charge is not a limitation with rates as high as 1.3 Mrad/day, and the projected electron lifetime limit was > 600 Mrad.

I. Compensation Studies

The warm-liquid calorimetry (WALIC) collaboration has performed a systematic study of the relative electron and pion signal response, e/π , as a function of the thickness ratio of TMP to absorber, and of the type of absorber material[1, 2]. These results were obtained in a series of beam tests at Fermilab, with tagged electrons or pions over the energy range 5 to 150 GeV. The absorbers used were: (1)iron, (2)lead, and (3) aluminum-

clad lead. The calorimeter was highly modularized[1], with the TMP in thin detector modules interleaved between absorber plates to facilitate changes of configuration. The total number of TMP detector modules was as large as 70, allowing for sampling intervals as small as 0.1 interaction lengths and 0.8 radiation lengths. The total calorimeter depth was seven to nine interaction lengths, depending upon the configuration. In the case of iron, the ratio of iron to TMP thickness was varied from 2.5 to 30, and the lead/TMP ratio was varied from 2.5 to more than 10. The study of composite aluminum-clad lead absorber plates was intended to test the effect on e/π of the "transition region effect", i.e. the effect on the electromagnetic shower of the atomic number of the cladding material at the surface boundary between the absorber and the sensing medium (TMP). A complete description of the apparatus and the beam setup is given in references [1] and [2].

The results of these beam tests clearly demonstrated that compensation could not be fully achieved using iron as the absorber, regardless of the iron/TMP ratio, while compensation can be achieved using lead absorber. Varying the ratio of absorber to TMP thickness had little effect on the e/π ratio either for iron or lead absorber. However, it is essential to take into account the effects of ion recombination and saturation [3] in the TMP, which strongly affect the signal response and cause a preferential suppression of the hadronic signal. Only a relatively low field, 6.7 keV/cm, was possible with the TMP modules used in this test, and at such a low field the response to the hadronic component was suppressed because of recombination. However, this effect has been measured [3], and full compensation in lead would occur at a field of about 20 keV/cm. This field is achievable since we have subsequently operated with fields in excess of 35 keV/cm in another TMP calorimeter, and over 50 keV/cm in other test devices using TMP. The aluminum clad lead absorber was shown to have a small ($\approx 1\%$) but definite effect in decreasing the e/π ratio.

The beam test results described above are generally quite well reproduced by Monte Carlo simulations using the GEANT program [4]. In particular, the dependence upon particle energy, the insensitivity to the absorber/TMP ratio, and the effect of aluminum cladding on lead absorber are all reproduced.

II. A 'Swimming Pool' Calorimeter: Beam and Irradiation Tests

A calorimeter module has been built and successfully tested in which the absorber plates are immersed directly in the TMP sensing liquid [5]: this is referred to as a "swimming pool" design. Materials in contact with the TMP were the lead absorber plates, the aluminum containment vessel, ceramic standoff insulators, and Kapton sheet insulators between plates. The calorimeter described here consisted of two towers, mounted side-by-side, each having nine lead plates 11.5cm x 11.5cm wide by 1cm thick, resulting in a total depth of 18 radiation lengths per tower. The TMP gap between plates was 2mm, and fields of 35kV/cm were achieved. The plates were connected in the "electrostatic transformer" mode to minimize the output capacitance and achieve maximum speed[6]. The shaping time used was 0.1 μ s, and the total drift time of electrons in each gap was about 0.2 μ s. Moreover, the leading edge of the signal is extremely fast and quite suitable as a first-level trigger at the LHC [7]. The electric field is in the range where full compensation can be achieved, as discussed above in section I. This module was tested briefly in the FNAL beam used for the tests described in section I.,

and performed well. In particular, the cross-talk between the two adjacent towers was measured to be only about 0.5%, i.e. when the beam impinged upon one tower and the signal was measured from the adjacent tower.

A major concern with use of warm-liquid calorimeters in experiments has been the possible degradation of the lifetime of the free electron carriers in the liquid due to attachment on impurities, especially those produced from the liquid itself by radiolysis resulting from exposure to the ambient particle flux. As an example, the most intense flux in the forward calorimeter of the SDC experiment was estimated to be $\approx 1\text{Mrad/day}$. According to some earlier measurements on small liquid samples [8,9], the lifetime would decrease to an unusable level in a short time. Therefore, sophisticated filtering schemes had been devised to produce very high purities of liquids, to achieve maximum use of the calorimeter before refilling or repurifying.

However, our tests showed a rather different effect. Starting with a rather poor lifetime, about $0.4\mu\text{s}$, we irradiated our calorimeter with gamma-rays from an intense Co60 source at a rate of about 0.16Mrad/day . Instead of the lifetime decreasing, it increased to over $2\mu\text{s}$, and then decreased, but more slowly than indicated by the previously published results [8,9], and had lifetimes generally one order of magnitude larger than would have been expected based upon those results. When extrapolated to the dose where the lifetime would preclude good calorimeter performance, at $0.1\mu\text{s}$, we obtained an estimate of 150Mrad before the TMP would need re-purification. At first we thought this unexpected performance was due to a "gettering" action of the electric field in sweeping out electronegative impurities which had attached electrons. However, measurements with and without the electric field showed that, although there is a measurable effect due to the field in the presence of radiation, the largest improvement of lifetime comes from the radiation alone.

In order to study the effect of the high density of ionization, i.e. "space charge", due to intense radiation flux, two small devices were built. These consisted of only one plate, made of aluminum and about 3" in diameter. This device, smaller than the calorimeter described above, could be placed much closer to the Co60 source, allowing dose rates as high as 1.5Mrad/day . Since the intensity was very high, individual signal pulses could not be monitored, but instead the total current was measured as a function of both the radiation intensity and the electric field. It was found that for a dose rate of 1.3Mrad/day there was only a 10% decrease in current when operating at 26kV/cm , and even smaller at the maximum field attainable with this device, 35kV/cm . These devices were also tested for electron lifetime up to a total exposure of over 30Mrad , and the extrapolation to maximum usable dose gave an estimated 600Mrad before replacement or repurification of the TMP would be necessary. Gas was found to be evolved from these cells, and was measured both in volume and in composition. The results can be compared with published estimates [8]: the volume of gas was ≈ 0.01 moles for ≈ 400 cc of TMP, about a factor of two less than the prediction, and consisted almost entirely of hydrogen and methane, in the ratio of $\approx 2:1$, in good agreement with predictions.

References

1. B. Aubert et al., Nucl. Instr. and Meth. A313 (1992) 357.
2. B. Aubert et al., Nucl. Instr. and Meth. A334 (1993) 383.
3. B. Aubert et al., Nucl. Instr. and Meth. A286 (1990) 147.
4. R. Brun et al., GEANT3 User's Guide, CERN-DD/EE 84-1, Geneva (1986).
5. B. Aubert et al., LBL-34551, Lawrence Berkely Laboraory, Sept. 1993. Presented at the IV International Conference on Calorimetry in HEP, La Biodola, Elba, Italy, Sept. 1993, and to appear in the Proceedings of the Conference.
6. J. Colas et al., Nucl. Instr. and Meth. A294 (1990) 583.
7. D. Gingrich et al., Nucl. Instr. and Meth. A344 (1994) 39. Here will be found additional references.
8. R. Holroyd, IEEE Trans. Nucl. Sci. NS-37 (1990) 513.
9. A. Givernaud, et al., Nucl. Instr. and Meth. A321 (1992) 551.

3 Working-Group Summaries

Charm Baryon Working Group Report

Harry W. K. Cheung and Peter Cooper
Fermi National Accelerator Laboratory, Wilson Road, Batavia, IL 60510

- *Working Group Co-chairmen:* Harry W. K. Cheung and Peter Cooper.
- *In attendance:* Nural Akchurin, Dave Besson, John Cumalat, Isi Dunietz, Lynn Garren, Catherine James, Jürgen Engelfried, Murray Moinester, Austin Napier, Charles Ray Newsom, Michael Procario, Jean-Marc Richard and Jim Russ.

Charm baryons has been singled out as a separate study group for a good reason. Most of what we have learned on charm physics comes from the study of charm mesons, because there are much more data for charm mesons than for charm baryons. The standard dogma is that this will continue to be true in the future. However, significant experimental progress has been made recently for charm baryons, and this has been slowly followed by more theoretical interest [1]. The charge of this working group was to determine how much the study of charm baryons can increase our knowledge of charm physics; what physics can be studied more easily with charm baryons than with charm mesons; and how to boost the production and reconstruction efficiency for charm baryons. We start our discussion with a list of physics topics.

1. **LIFETIMES.** A systematic study of the lifetimes of the weakly decaying charm baryons can give us information on the different roles of spectator decay, W-exchange, and interference. A number of circumstances make the study of charm baryon lifetimes extremely important in their own right and also complementary to what can be learned from charm meson lifetimes. The four weakly decaying (singly) charm baryons, when added to the three charm mesons, more than doubles the amount of possible lifetime measurements and makes a comparison of lifetime ratios with theory much more practical. Since W-exchange is not helicity suppressed in Cabibbo-favored charm baryon decays, and since there are more interference possibilities in charm baryon decays, charm baryon lifetimes are more sensitive to W-exchange and interference contributions. This neatly complements the study of charm meson decays.

Although there have been recent improvements in the lifetime measurements of a number of different charm particles, improvements in the reliability of theoretical predictions have not followed. It can be seen from some older work on charm baryon lifetimes [2], that the absolute lifetimes are difficult to predict reliably but the ratios of lifetimes can be more reliably calculated. It has even been said that the QCD-based ‘inclusive’ approach adopted in these calculations will never become fully quantitative [3], however,

measurements of the lifetimes will still be informative [4]. So on the theoretical side one needs to improve the reliability of calculations for the absolute lifetimes and also set out a procedure whereby one can extract useful information on the various decay contributions from the different lifetime measurements. On the experimental side, the precision of lifetime measurements of the D mesons are now at the 1% level. One may expect similar precision to be reached for the Λ_c^+ and Ξ_c^+ , but the short lifetimes of the Ξ_c^0 and Ω_c^0 are almost comparable to the current experimental resolution of 0.05–0.07 ps, which limits the precision of lifetime measurements. Improvements in the longitudinal vertex resolution are required in the future. This will also improve signal-to-noise and produce a more uniform acceptance with lifetime.

2. **HADRONIC DECAYS.** We can surely learn more about W-exchange from the study of charm baryons, since this is not helicity or color suppressed as in charm meson decays, but can we learn more about final state interactions and interference effects? Also, two-body decays appear quite dominant in charm meson decays; is this true for charm baryons? Maybe W-exchange can play a role in the resonant structure of charm decays? It is difficult to answer these questions at present due to both the lack of data on charm baryon exclusive hadronic decays and the corresponding lack of theoretical knowledge. There are several older and more recent theoretical analyses of charm baryon hadronic decays [5]. A desirable theoretical work would be a compilation of specific charm baryon decays from which one can extract useful information on W-exchange and Final State Interactions.

Traditional Dalitz plot analyses would be useful, but no Dalitz plot analysis on charm baryon decays has yet been done that correctly handles the spin effects. Some theoretical work on this would be helpful. Resonant analyses greatly benefit from large signal-to-noise, but in the past this has been difficult to achieve with large efficiency, mainly due to the short lifetime of charm baryons and background from the more abundant charm meson decays. Another area of charm baryons that could be greatly improved is the number of different fully reconstructed decay modes. Not many have so far been seen, and for a good reason: the decay baryon has to be reconstructed. These consist of: protons, which must be identified with good efficiency to eliminate abundant pions and kaons; neutrons, which are difficult to reconstruct and cannot be used in vertexing; Λ^0 , which normally cannot be used in vertexing and some are lost due to its relatively long lifetime; $\Sigma^{\pm,0}$, difficult to reconstruct due to neutral particles in their decay modes, and some are lost due to their relatively long lifetimes; and $\Xi^{-,0}$ and Ω^- , which require the reconstruction of a Λ^0 (and π^0 for the Ξ^0) and some of which are lost due to two relatively long-lived decays. To compete with charm meson decays, one has to increase the acceptance and efficiency for reconstruction of these baryons relative to what has been achieved so far.

3. **ABSOLUTE BRANCHING RATIOS.** To aid in comparisons with theory where (normally) absolute rates are calculated, one requires the absolute branching ratios, as well as lifetimes. We could not think of any particularly good methods of obtaining absolute branching ratios for the $\Xi_c^{+,0}$ and Ω_c^0 charm baryons. Methods already exist for extract-

ing the absolute branching ratio for Λ_c^+ [6, 7]. Using theoretical predictions of exclusive semileptonic decays one may be able to relate the Λ_c^+ decays to the $\Xi_c^{+,0}$ and Ω_c^0 decays, but one still needs more knowledge of their production. Probably a specialized experiment is needed for a measurement of the absolute branching ratio of the $\Xi_c^{+,0}$ and Ω_c^0 charm baryons.

4. SPECTROSCOPY. Recently there has been a lot of interest in excited D mesons (D^{**}). The spectroscopy of excited charm baryon states should be much "richer" just because there are more of them; these should complement our studies of excited D mesons although they are theoretically more difficult to handle [8]. The large number of mass splittings that can be studied should provide an excellent testing ground for theory, but an experimental analysis will require excellent photon and π^0 reconstruction efficiency, as well as very efficient reconstruction of the ground-state charm baryons. In order to measure narrow natural widths, it is anticipated that one would require better mass resolution than is typical of charm experiments so far. Since most resonances are expected to decay strongly, there would be an advantage to having a primary vertex which is relatively clean of pions, as in photoproduction.
5. SPIN DEPENDENT DECAYS. It is possible that charm baryons could be produced polarized in hadroproduction, as has been observed for strange baryons [9]. Charm baryons offer another experimental ground for this study and a spin analysis should be easily achievable as long as we have excellent signal-to-noise [10].
6. CHARM BARYON PRODUCTION. Almost all the experimental results on charm production have come from J/ψ and D studies. Charm baryon production will complement this study, and also enables investigation of other features of charm production like associated production. We know of no recent theoretical work on charm baryon production. A theoretical analysis may motivate more enthusiasm for future experimental studies [11]. We expect many new results from Fermilab experiment E791 and upcoming experiment E781 on charm baryon hadroproduction. Results on charm baryon photoproduction should come from the upcoming Fermilab E831 experiment.
7. DOUBLY CHARM BARYONS. The physics interest of the doubly charm baryons ccd , ccu and ccs is covered in an article by Jean-Marc Richard in these Proceedings. We did not come up with a method to calculate reliably the production of these baryons, but a back-of-the-envelope calculation shows that it is quite possible that a few could be seen in the next generation of charm experiments (Fermilab E831 and E781). These are expected to decay weakly with reasonably charm-like lifetimes into D mesons plus baryons or into charm baryons, mainly Ξ_c [12]. Reconstruction of these doubly charm states require excellent reconstruction efficiency for Ξ_c . It is not known how the production of these doubly charm baryons could be enhanced.
8. RARE/EXOTIC DECAYS. We cannot normally hope to compete with charm meson studies in the search for rare or exotic decays, and we could not think of any phenomena that would affect uniquely charm baryon decays but not charm mesons.

9. SEMILEPTONIC DECAYS. The inclusive semileptonic partial widths for D^0 and D^+ are observed to be the same. It would be interesting to study whether this is true for the charm baryons. This would not be true if interference effects are important for one charm baryon and not another. Information on the inclusive semileptonic partial widths may be helpful in determining the charm baryon lifetimes if one has a reliable theoretical model for what fraction of the total width is semileptonic. A determination of the inclusive semileptonic width is experimentally difficult due to large backgrounds unless one can produce a particular charm baryon cleanly or can find a clean tag. Exclusive semileptonic charm baryon decays should be easier to reconstruct. It would be interesting to study whether these decays are saturated by pure 3-body decays (one hadron and the lepton and neutrino) as in the case of the D mesons. These studies would also complement our studies using charm mesons of form factors and CKM matrix elements. Measurement of the exclusive semileptonic charm baryon decays may be helpful in extracting absolute branching ratios for the charm baryons.

It is clear to this working group that the study of charm baryons can provide unique physics and also information complementary to that gained from a study of charm mesons. It is also clear that in the majority of past experiments, the focus of beam considerations, triggering conditions and detector elements have been on charm mesons. It was felt by this group that to gain significantly in our knowledge of charm physics through the study of charm baryons, one has to focus on the special requirements of charm baryons: enhancing their production and improving their reconstruction. The reconstruction needs improvement in vertex resolution, due to the short lifetimes of the charm baryons; in momentum/mass resolution to improve the signal-to-noise and measure natural widths; in acceptance of the relatively long lived hyperons that have to be reconstructed; and in particle identification to improve signal-to-noise. These considerations were taken into account for CERN experiment WA89 and the upcoming Fermilab experiment E781, which have been designed to study charm-strange baryons. The upcoming Fermilab experiment E831, which is a "normal charm meson" experiment, is expected to fully reconstruct 20,000 $\Lambda_c^+ \rightarrow pK^-\pi^+$ and one million charm mesons. A future CHARM 2000 "normal charm meson" experiment that reconstructs 100 million charm mesons may be expected to reconstruct one million $\Lambda_c^+ \rightarrow pK^-\pi^+$ and 10,000 each of Ξ_c^+ , Ξ_c^0 and Ω_c^0 . Obviously the impact of such an experiment will depend on whether E781 can achieve their goal of fully reconstructing 100,000 $\Lambda_c^+ \rightarrow pK^-\pi^+$, 150,000 each of Ξ_c^+ and Ξ_c^0 , and 5,000 Ω_c^0 [13]. If so, we believe a specialized charm baryon experiment will be required to significantly improve on that.

References

- [1] For a list of references of recent experimental results on charm baryons please refer to the reviews given in these proceedings. The main recent results on charm baryon physics have come from ARGUS, CLEO, Fermilab E687 and CERN WA89.
- [2] B. Guberina, R. Rückl and J. Trampetić, Z. Phys. C33, 297 (1986); M. B. Voloshin and M. A. Shifman, Sov. Phys. JETP 64, 698 (1986); V. Gupta and K. V. L. Sarma, Int. J. Mod. Phys. A5, 879 (1990); H. Y. Cheng, Phys. Lett. B289, 455 (1992).

- [3] B. Blok and M. Shifman, "*Lifetimes of Charm Hadrons Revisited. Facts and Fancy*", in proceedings of the 3rd Workshop on the Tau-Charm Factory, Marbella, Spain, June 1993, TPI-MINN-93/55-T.
- [4] I. I. Bigi and N. G. Uraltsev, "*D_s Lifetime, m_b , m_c and $|V_{cb}|$ in the Heavy Quark Expansion*", CERN Preprint CERN-TH.7063/93.
- [5] J. G. Körner and G. Krämer, Z. Phys. **C2**, 117 (1979) and Z. Phys. **C55**, 659 (1992); T. Uppal, R. C. Verma and M. P. Khanna, Phys. Rev. **D49**, 3417 (1994); J. G. Körner, M. Krämer and D. Pirjol, "*Heavy Baryons*", DESY Preprint DESY 94-095.
- [6] S. R. Klein, Int. J. Mod. Phys. **A5**, 1457 (1990) and references therein.
- [7] H. W. K. Cheung, "*Charm Baryon Production and Decays in E687*", in proceedings of the 28th Recontres de Moriond, QCD and High Energy Hadronic Interactions, Les Arcs, France, March 20-27 1993, p.473, FERMILAB-Conf-93/164-E.
- [8] L. A. Copley, N. Isgur and G. Karl, Phys. Rev. **D20**, 768 (1979); N. Isgur and M. B. Wise, Phys. Rev. Lett. **66**, 1130 (1991); T. Uppal and R. C. Verma, Phys. Rev. **D47**, 2858 (1993).
- [9] J. Lach, "*Hyperon Polarization: An Experimental Overview*", in proceedings of the Int. Workshop on Flavour and Spin in Hadronic and EM Interactions, Torino, Italy, September 21-23 1992, FERMILAB-Conf-92/378.
- [10] J. D. Bjorken, Phys. Rev. **D40**, 1513 (1989); M. Jezabek, K. Rybicki and R. Rylko, Phys. Lett. **B286**, 175 (1992).
- [11] M. Fontannaz, B. Pire and D. Schiff, Z. Phys. **C11**, 211 (1981); M. P. Alvarez *et al.*, Phys. Lett. **B246**, 256 (1990); M. P. Alvarez *et al.*, Z. Phys. **C60**, 53 (1993).
- [12] J.D. Bjorken, "*Estimates of Decay Branching Ratios for Hadrons Containing Charm and Bottom Quarks*", unpublished notes from the Heavy quark working group meeting 3, on July 17th 1985.
- [13] R. Edelstein *et al.*, Fermilab E781 (SELEX) Proposal.

CP Violation in the Charm Sector

K. Gounder, P.E. Karchin, S. Pakvasa,
K.C. Peng, M.D. Sokoloff, T. Takeuchi, W. Toki

Abstract

This is a summary of the CP Violation Working Group discussions. The minimal Standard Model predicts direct CP violation at the level of a few tenths of a percent, or less, in singly Cabibbo-suppressed decay modes. The statistical sensitivity of the experiments discussed at this workshop would be on the order of one percent. A signal at this level would provide evidence for new physics at the TeV scale.

CP violation may be observed experimentally through particle-antiparticle mixing, as is done in the $K^0\bar{K}^0$ system, or directly through the difference of particle and antiparticle partial decay rates to charge-conjugate final states (for charged or neutral D s). Standard Model predictions for mixing are generally very low[1], $r_{mix} \approx 10^{-7}$ or less, so the possibility of observing CP violation via mixing is negligible for the foreseeable future. Standard Model predictions for direct CP violation are somewhat more encouraging, but again, the prospects for observing a statistically significant signal in a foreseeable experiment are poor. Particle and antiparticle partial decay rates to charge conjugate final states can differ only if (at least) two amplitudes with different weak phases and different strong phases lead to the same final state. In the Standard Model this occurs only for singly Cabibbo-suppressed decays. For decay modes with branching ratios on the order of 0.1% the expected asymmetries are at most a few times 0.1%[2], assuming the Kobayashi-Maskawa phase is fairly large ($\sin \delta$ of order 0.5).

To observe an $m\sigma$ signal, one requires a parent charm meson sample of at least $m^2/(A^2 \cdot \text{BR})$ events, where A is the asymmetry between particle and antiparticle decay rates normalized to their sum. For a 5σ signal, we want a parent meson sample of at least 10^{10} events. While this is nominally within the reach of the experiments considered at this workshop, it is unlikely that measurements can really be made with this precision. The most interesting decay modes (those where one might anticipate that at least two amplitudes contribute to the same final state) are generally more difficult to pick out experimentally. For example, the $\bar{K}^0 K^0$ final state cannot be produced via spectator amplitudes (because these decays have no final state d -quarks at tree level), and the W -exchange amplitudes are GIM-suppressed[3]. Yet the branching ratio is around 0.1%, not that much less than the $K^- K^+$ final state. Unfortunately, to tag a decay as particle or antiparticle requires that the D be a D^* decay product (and only 20% to 25% of D^0 s come from D^* decays), and only 2/9 of $D^0 \rightarrow \bar{K}^0 K^0$ decay as $K_S^0 \rightarrow \pi^+ \pi^-$, $K_L^0 \rightarrow \pi^+ \pi^-$. Additionally, $\gamma\tau$ is typically one to several meters for these K_S^0 s,

so relatively few $K_S^0 \rightarrow \pi^+\pi^-$ decays will be picked up in a precision vertex detector. Self-tagging decays such as $D^+ \rightarrow K^0 K^+$, which has been predicted to have enhanced penguin amplitudes which can lead to enhanced CP violation[4], have similar problems.

We are not aware of any physics beyond the Standard Model which predicts direct CP violation greater than a fraction of a percent[5]. However, an ultra-high statistics experiment should have the statistical power to measure CP asymmetries of order 1% in singly Cabibbo-suppressed decay modes and of order 5% in doubly Cabibbo-suppressed decay modes, assuming backgrounds can be controlled and possible systematic errors minimized and measured well. A 5% asymmetry in a doubly Cabibbo-suppressed decay rate would correspond to an amplitude almost a factor of 100 less than the dominant spectator decay amplitudes of the Standard Model. Assuming that new physics produces amplitudes $\propto (g'/M_X)^2$, where g' is a conventional coupling strength and M_X is the mass scale of the new physics, a search for direct CP violation would be probing physics at the TeV scale.

References

- [1] J.F. Donoghue, E. Golowich, B.R. Holstein, and J. Trampetic, Phys. Rev. **D33**, 179 (1986);
Howard Georgi, Phys. Lett. **B297**, 353 (1993);
T. Ohl, G. Ricciardi, and E.H. Simmons, Nucl. Phys. **B403**, 605 (1993);
Gustavo Burdman, Proceedings of the CHARM-2000 Workshop and FERMILAB-Conf-94/200 (1994).
- [2] F. Buccella *et al.*, Physics Lett. **B302**, 319 (1993).
- [3] X.Y. Pham, Phys. Lett. **B193**, 331 (1987).
- [4] M. Golden and B. Grinstein, Phys. Lett. **B222**, 501 (1989).
- [5] A. Le Yaouanc, L. Oliver, and J.-C. Raynal, Phys. Lett. **B292**, 353 (1992).

Report by the CHARMED MESONS Working Group

Donald Isenhower, *Abilene Christian University*
Scott Radeztsky, *University of Wisconsin*, co-convenor
Jonathan L. Rosner, *University of Chicago*
Michael D. Scadron, *University of Arizona*
Shekhar Shukla, *Fermilab*, co-convenor

Abstract

The main topic of discussion was decays of excited charmed mesons. The group discussed the current status of knowledge about the excited states of charmed mesons, the problems encountered in the study of these states, and measurements on the excited states that would be desirable in the near future. The other topics discussed were charm production, and W-emission for $\Delta S=1$ and $\Delta C=1$ weak decays.

1 EXCITED CHARMED MESONS

Charmed mesons are useful for testing our ideas about the quark model and about QCD via the quark model. As pointed out by DeRujula, Georgi and Glashow [1] in 1976, for a meson containing a heavy and a light quark, as the mass of the heavy quark increases, the properties of the meson are determined increasingly by the dynamics of the light quark, and approach a universal limit. There is some recent theoretical work, for example that by Eichten, Hill and Quigg [2] and that by Godfrey and Kokoski [3], that analyzes data on charm mesons using this Heavy Quark Symmetry. Experimental information on the properties of charmed mesons is useful for developing and testing these models.

A better knowledge of the characteristics of charmed mesons also helps the understanding of B-mesons [4]. The models using Heavy Quark Symmetry use the observations on charmed mesons to predict the properties of the B-mesons [2]. Experimental measurements on B-mesons require a knowledge of the properties of the charmed mesons because B-mesons usually decay to charmed mesons.

1.1 Difficulties in Observing Excited States

While the properties of the $L=0$ charmed mesons (1S states) are fairly well understood, the spectroscopy of the $L=1$ mesons (2P states) is in its beginning stages, and none of the higher excited states (the 2S, 3D, etc.) has been observed. The excited charm states are expected to decay strongly, either directly or through other excited D-mesons, to one $L=0$ D-meson and one or more lighter mesons. They are more difficult to observe and analyze

than the $L=0$ mesons because they are not produced as copiously, and are wider. The combinatoric background under the peak is also worse, partly due to the larger width of the states, and partly because they have a larger number of particles at the end of their decay chains.

In fixed target experiments, there is an additional reason for a higher combinatoric background in case of the excited D-mesons. Unlike the case of weak charm decays, the decay vertex cannot be distinguished from the production vertex. Hence, the mass combination hypotheses will include tracks other than those actually associated with the decay. As a result, there is a higher combinatoric background, which gets worse with increasing multiplicity in the primary vertex (the vertex associated with the production of charm). Since multiplicity in the primary vertex generally is higher when the charm is produced by hadroproduction as opposed to photoproduction, a photoproduction experiment is likely to have smaller combinatoric background.

There are other difficulties associated with the larger width of the excited D-mesons than just a larger statistical uncertainty resulting from a higher combinatoric background under the peak. One of them is the systematic error in the determination of the magnitude and shape of the background. The standard method to observe a new state is to look for a peak over a smooth background in a mass plot. The background under the peak is obtained by interpolating between two regions on either side of the peak with the assumption that the background varies in a smooth simple fashion (usually parametrizable with up to four or five parameters). For a reliable determination of the background one needs a wide enough window around the peak (≈ 6 times the full width of the state if the width is much larger than the resolution of the mass measurement, and ≈ 10 times the resolution if the width is narrow).

If the state being investigated is wide, it is difficult sometimes to find such a window, because of structures near the peak due to other states (partially or fully reconstructed), or from the state being investigated, if it is only partially reconstructed. For example, when looking for the decay $D_2^{*0}(2460)$ to $D^+\pi^-$ in the difference mass distribution $\Delta M = M(D^+\pi^-) - M(D^+)$, one sees a peak at $\Delta M \approx 590 \text{ MeV}/c^2$ arising from the decay of $D_2^{*0}(2460)$ to $D^+\pi^-$, and an additional bump at $\Delta M \approx 420 \text{ MeV}/c^2$ due to the decays $D_2^{*0}(2460)$ and $D_1^0(2420)$ to $D^{*+}\pi^-$, with the D^{*+} decaying to $D^+\pi^0$ [5]. If all such structures were caused by known states, they could be dealt with. Unfortunately, many of them are due to heavier states which have not yet been observed or are not very well understood. These structures are more likely to be a problem if they are of a width comparable to that of the state being investigated. A very wide structure would provide a smooth background under the peak. A very narrow structure usually does not affect the determination of the characteristics of the peak, unless it is very close to the peak (within \approx one full width of the center of the peak). If the narrow structure was tall enough to affect the background determination it would be easy to identify and deal with.

Sometimes peaks due to two states can overlap. The analysis in that case becomes more complicated, especially if one does not have any a priori knowledge about any of the states. An example is the peaks due to the $D_1^0(2420)$ and $D_2^{*0}(2460)$ in the $D^{*+}\pi^-$ mass distribution.

In such cases, one attempts to find another decay mode in which the peak is more isolated. In the particular case of $D_2^{*0}(2460)$, one looks for the state in the decay $D_2 \rightarrow D^+\pi^-$. Additional information about the decay (for example, the helicity information in the above case [5]) can also be used to disentangle the overlapping states.

1.2 Current Status

For a given pair of quarks, $c\bar{u}$, $c\bar{d}$, or $c\bar{s}$ with orbital angular momentum $L=1$, there are three total angular momentum states, $J^P=0^+$, 1^+ , and 2^+ , corresponding to the value $S=1$ for the sum of the quark spins. There is one state, $J^P=1^+$, corresponding to $S=0$. The 2^+ states have been observed for all three quark pairs $c\bar{u}$, $c\bar{d}$, and $c\bar{s}$. The two $J=1$ states are expected to mix. One of the two observable states after the mixing is expected to be narrow and the other is expected to be relatively wide ($\Gamma > 200$ MeV) [3]. The narrow state has been observed for $c\bar{u}$ and $c\bar{s}$. The full reconstruction of the $J=1$ $c\bar{d}$ state, which decays to $D^{*+}\pi^0$ or $D^{*0}\pi^+$, but not to $D^+\pi^0$ or $D^0\pi^+$, requires efficient detection of a π^0 . In a fixed target experiment, a decay to a π^0 has a higher background than a decay to a π^+ because the direction of a potential π^0 track is not as well known as that of a π^+ track. The rest of the $L=1$ states have yet to be observed. Most of them are expected to be fairly broad [2][3]. The $2S$ states or states with higher radial excitations have not been observed either.

1.3 Measurements to be made

1.3.1 Branching Fractions

More decay modes of the known states have to be observed and the branching fractions for the various decays measured. One decay mode that seems to be especially important for measurements on B-decays is the decay of the $L=1$ D-mesons to $D\rho$. Even though the central value of the ρ mass is too high to allow a decay of an $L=1$ D-meson to $D\rho$, the large width of the ρ is expected to result in a significant branching fraction to $D\rho$ [6]. Full reconstruction of this decay might require some special attention during the design of a detector.

The information on branching fractions, for example, $\Gamma(D_2 \rightarrow D^+\pi^-) / \Gamma(D_2 \rightarrow D^{*+}\pi^-)$, has large uncertainties and many theoretical predictions remain plausible. A better measurement of these fractions is needed to help develop the details in the theoretical models and increase the reliability and accuracy of their predictions. A better knowledge of the branching fractions also helps measurements on B-mesons, due to the decay of B-mesons to excited D-mesons.

1.3.2 Widths

The widths of the observed $L=1$ states have a large uncertainty. The uncertainty in the width due to a systematic uncertainty in the background under the peak is, in all cases, comparable to the statistical error. With higher statistics available, more excited states are

expected to be observed and understood. This should lead to a better understanding of the reflections they cause in the various mass plots used to observe the $L=1$ mesons. A better understanding of the background would in turn enable a better measurement of the widths of these states.

When obtaining the ratio of the number of events, a large part of the error in the ratio comes from the uncertainty in the shape of the peak. Thus a better measurement of the width of the peak would result in a better measurement of the number of events in the various decay modes and hence of the branching fractions.

1.3.3 Observation of New States

Most of this discussion centered around the items in the D^{**} Shopping List of Eichten, Hill and Quigg [6]. The radially excited states in the list are wider than the $L=1$ states observed so far. The $3D$ and $2P$ states are 400 MeV heavier than the $2P$ states. They are probably too heavy to observe at CLEO. One might be able to observe them at the Fermilab experiments E687 and E791, depending on how well the background can be handled. If one intends to observe them in a future experiment through decays to other excited states one should make sure that the apparatus has a satisfactory acceptance for capturing the decay products of these excited state. For example, if one intends using decays through D^* , it should be noted that a soft pion from a D^* can be swept out by a magnetic field quite easily, and the apparatus might have a bad acceptance for D^* while being efficient at reconstructing ground state D -mesons.

2 Charm Production

Study of charm production provides a means to test QCD via production models. The mass of the charm quark places it in a unique position, where it can provide a link between perturbative and nonperturbative QCD. Charm production data is starting to reach new kinematic regions where it can distinguish between the various theoretical predictions.

J/ψ hadroproduction at large x_f by Fermilab experiment E789 [7] was discussed. J/ψ production at large x_f is especially interesting because the production cross section at large x_f has appreciable contribution from quark-antiquark annihilation (gluon-gluon fusion dominates the total cross section elsewhere). The results from E789 indicate a negligible contribution to the cross section from intrinsic charm [7]. FNAL experiment E791 [9] will have a sample of high x_f open charm mesons which will allow further investigation of hadroproduction. It is important to have a high statistics experiment in the near future that can probe these newly explored regimes more effectively.

3 Weak Decays

Michael Scadron talked about W-emission for $\Delta S=1$ and $\Delta C=1$ weak decays. The talk is written in a report in these proceedings [8].

4 Summary

The group concentrated most of its efforts on discussing the existing and intended measurements on the excited charmed mesons. Many of the problems associated with these measurements were identified as a first step towards planning future measurements on these excited states.

References

- [1] A. DeRujula, H. Georgi and S. L. Glashow, Phys.Rev.Lett. 37 (1976) 785.
- [2] E. J. Eichten, T. Hill and C. Quigg Phys.Rev.Lett. 71 (1994) 4116.
- [3] S. Godfrey and R. Kokoski, Phys.Rev.D 43, 1679 (1991).
- [4] J. L. Rosner, *What Charm Can Tell Us About Beauty*, these proceedings.
- [5] H. Albrecht et al (ARGUS Collab.) Phys.Lett.B 232 (1989) 398, P. Avery et al (CLEO Collab.) Phys.Rev.D 41 (1990) 774, P. L. Frabetti et al (E687 Collab.), Phys.Rev.Lett. 72, 324 (1994).
- [6] E. J. Eichten, T. Hill and C. Quigg, *Orbitally Excited Heavy-Light Mesons Revisited*, FERMILAB-CONF-94/118-T.
- [7] M. S. Kowitt et al (E789 Collab.) Phys.Rev.Lett. 72 (1994) 1318.
- [8] M. D. Scadron, *W-emission for $\Delta S=1$ and $\Delta C=1$ Weak Decays*, these proceedings
- [9] T. Carter, et al., presented at the Washington APS meeting, April 1994.

Summary Report of the mixing working group

Tiehui (Ted) Liu
Harvard University, Cambridge, MA 02138

1 Introduction

The agenda for the mixing group is to consider the details of the following experimental situations: (A) Fixed-target experiments, including E687, E791, E781, E831 and next generation. (B) e^+e^- machines, including the τ -charm factory, CLEO II, III, Asymmetric B factories (SLAC and KEK) and a possible Z factory. We should evaluate these options in terms of: (a) the advantages and limitations of each approach; (b) techniques: hadronic modes vs. semileptonic modes; (c) how to improve the sensitivity: implications for the design of detectors. This includes how to improve the total yield of D^0 and D^{*+} events, the mass resolution of the D^0 and D^{*+} , the background (from other D^0 decays) rejection and the resolution on the decay length measurement; (d) the sensitivity to mixing each might have.

Due to the limited time for the working group discussion, we could not cover all the topics mentioned above (some of them are discussed in Liu's talk, see mixing review paper in this proceedings). At the working group, we rather focused on the question: are semileptonic decays ever going to be a feasible way to get a mixing limit? This summary will briefly summarize two interesting ideas (both are the semileptonic methods) discussed at the working group.

2 Morrison's idea

The idea is very similar to the hadronic method: one uses the decay chain $D^{*+} \rightarrow D^0\pi^+$, instead of looking for $D^0 \rightarrow K^+\pi^-$, one can search for $D^0 \rightarrow K^+l^-\nu$ where there is no DCSD involved. Of course, due to the missing neutrino, this mode usually suffers from large background. However, for events in which the neutrino is very soft in D^0 rest frame, $D^0 \rightarrow K^+l^-\nu$ is quite similar to $D^0 \rightarrow K^+\pi^-$ kinematically. In this case, one has the same advantages as $D^{*+} \rightarrow D^0\pi^+$ followed by $D^0 \rightarrow K^+\pi^-$ has. In addition, as the neutrino is soft, the proper decay time of the D^0 can be reasonably estimated from K^+l^- . The potential mixing signal therefore should show up as a t^2 term in the proper decay time distribution. To select the events with soft neutrino, one can require the K^+l^- mass above 1.4 GeV. This requirement will keep about 50% of the total signal. One major background here is the random slow pion background, as the effective mass difference width is still much larger

(a factor of 10) than $D^{*+} \rightarrow D^0 \pi^+$ followed by $D^0 \rightarrow K^+ \pi^-$. In order to reduce this background, Rolly Morrison suggested to look for a lepton with the correct charge sign in the other side of the charm decay. Another background is DCSD decay $D^0 \rightarrow K^+ \pi^-$ when the π^- fakes a l^- , however, this background will only populates at the higher end of the $K^+ l^-$ mass spectrum where the neutrino energy is almost zero. This can be eliminated by cutting off that high end of the $K^+ l^-$ mass. In principle, this idea can be used in a fixed target experiment as well as in a $e^+ e^-$ experiment. The sensitivity of this method depends on the lepton fake rate (meson fakes as a lepton). One can find some detail discussions in Rolly Morrison's workshop summary paper.

3 CLEO way

This idea, suggested by Arne Freyberger of CLEO, is based on the technique which has been used by ALEPH, HRS and CLEO to extract the number of $D^{*+} \rightarrow D^0 \pi_s^+$ events. The technique utilizes the following facts: (1) Continuum production of $c\bar{c}$ events are jet like. (2) The jet axis, calculated by maximizing the observed momentum projected onto an axis, approximates the D^{*+} direction. (3) The $D^{*+} \rightarrow D^0 \pi_s^+$ decay is a two-body process, and the small amount of energy available means that the π_s^+ is very soft, having a transverse momentum p_\perp relative to the D^{*+} direction which cannot exceed 40 MeV/c. This low transverse momentum provides the $D^{*+} \rightarrow D^0 \pi_s^+$ signature.

The facts are used in the following way. The maximum momentum in the lab that the π_s^+ can have perpendicular to the line of flight of the D^{*+} is 40 MeV. One can define this quantity as $p_\perp = |p_\pi| \sin \theta_\pi$, where $\sin \theta_\pi$ is the angle between the D^{*+} and the π_s^+ in the lab frame, and p_π is the magnitude of the π_s^+ momentum. Hence, the π_s^+ from D^{*+} will populate the low p_\perp (or $\sin \theta_\pi$) region. The signal is enhanced if one plots p_\perp^2 (or $\sin^2 \theta_\pi$) instead of p_\perp . One then looks for an lepton in the jet with the correct sign, namely, $\pi_s^+ l^+$ right sign combination and $\pi_s^+ l^-$ wrong sign combination. The signal $D^{*+} \rightarrow D^0 \pi_s^+$ followed by $D^0 \rightarrow K^- l^+ \nu$ will peak in the low p_\perp^2 (or $\sin^2 \theta_\pi$) region for the right sign events; while the potential mixing signal $D^{*+} \rightarrow D^0 \pi^+$ followed by $D^0 \rightarrow K^+ l^- \nu$ will peak in the low p_\perp^2 (or $\sin^2 \theta_\pi$) region for the wrong sign events. It is worth pointing out that one can look for a lepton in the other side of the event to reduce background.

There are many kinds of background to this method one has to worry about. One of the major backgrounds is fake lepton background. For example, the decay chain $D^{*+} \rightarrow D^0 \pi_s^+ \rightarrow (K^- X) \pi_s^+$ will also peak at the low p_\perp^2 (or $\sin^2 \theta_\pi$) if the K^- is misidentified as a l^- . Another major background is probably the π^0 dalitz and γ conversions in $D^0 \rightarrow X \pi^0$ followed by $\pi^0 \rightarrow \gamma e^+ e^-$ or $D^0 \rightarrow X \pi^0$ followed by $\pi^0 \rightarrow \gamma \gamma$ and then $\gamma \rightarrow e^+ e^-$. These two major backgrounds are at about 0.3% level in the current CLEO II data. Understanding these backgrounds is the major difficulty faced by this method. Although for CLEO III, things should improve, it is not clear what kind of sensitivity one can expect from this method for future experiments. Nevertheless, it is an interesting idea and worth investigating.

SUMMARY OF THE WORKING GROUP ON TESTS OF QCD*

Vassili Papavassiliou[†]
Argonne National Laboratory, Argonne, IL 60439

Abstract

The working group discussed several topics related to charm production that can provide important input for our understanding of QCD. It was recognized that studies of both open and hidden charm in a high-statistics experiment will be essential in order to understand the production mechanisms. Nuclear effects were also discussed and a connection was made to similar effects observed in other reactions.

1 INTRODUCTION

It has been recognized for some time that charm production is a very important tool for studying QCD. The reason for that is obvious. The charm quark is the lightest of the heavy quarks, heavy enough for perturbative methods to be meaningful and on the other hand light enough that it is readily accessible in fixed-target experiments in large numbers. Charmonium and open-charm states have been studied in hadron-hadron and hadron-nucleus interactions, in real and virtual photon-nucleon processes on free and bound nuclei, in neutrino interactions, and in electron-positron collisions. The wealth of data has lead to significant progress in understanding the fundamental processes that are responsible for charm production and the strong interaction that is behind them. It is equally evident that much more can be learned from an improved study of charm production with much higher statistics. The working group discussed several topics in which the considered high-statistics charm experiment could have an impact in our understanding of QCD. This paper summarizes the subjects that were discussed and a few additional relevant topics. More information can be found in the contributions of the members of the working group and in the references.

In QCD, charm hadroproduction is understood as a hard scattering process between the elementary constituents of the participating hadrons, quarks and gluons, followed by fragmentation and hadronization of the produced charm quarks. The hard process provides the opportunity to test perturbative QCD mechanisms, while the hadronization allows studies of longer-range aspects of the strong interaction. Once the production mechanism is well understood, the process can then provide a measurement of the parton distributions of the

*Present: T. Carter, K. Cheung, R. Gardner H. Goldberg, G. Herrera, B. Kopeliovich, V. Papavassiliou, L. Spiegel, W.-K. Tang, S. Watanabe

[†]Work supported in part by the U.S. Department of Energy, Nuclear Physics Division, under Contract No. W-31-109-ENG-38

interacting hadrons. This is of particular interest since the process is dominated, at present energies, by gluon interactions and therefore can provide direct information on the gluon distribution, which is poorly constrained by other types of experiments.

2 TOTAL CHARM HADROPRODUCTION CROSS SECTION

The QCD prediction for the charm hadroproduction cross section is given by an expression of the form

$$\sigma = \sum_{ij} \int dx_1 dx_2 f_i(x_1, \mu^2) f_j(x_2, \mu^2) \hat{\sigma}(x_1 x_2 s, \mu^2) \quad (1)$$

where $f_i(x_1, \mu)$, $f_j(x_2, \mu)$ are the distributions of the partons i, j participating in the interaction, in the beam and target, respectively, evaluated at some appropriate scale μ , x_1 and x_2 are the momentum fractions carried by the partons, and $\hat{\sigma}$ is the elementary cross section between the partons. Here, s is the hadron-hadron center-of-mass energy, while $x_1 x_2 s$ is the CMS energy for the parton-parton subprocess, which to leading order can be gluon-gluon fusion ($gg \rightarrow c\bar{c}$) or quark-antiquark annihilation ($q\bar{q} \rightarrow c\bar{c}$). The cross section $\hat{\sigma}$ can be calculated in perturbative QCD, while the parton distribution functions are taken from measurements in other experiments, usually deep inelastic lepton scattering.

Earlier calculations, to leading order in QCD, underestimated the observed cross section, unless a very light (1.2 GeV) charm quark mass was used (see Ref. [1] for a review). Recent, next-to-leading order, calculations reproduce the data both in magnitude and in shape (energy dependence), using a mass of 1.5 GeV; however, the theoretical uncertainties are still substantial. The situation was summarized in the plenary talk by Ridolfi[2].

Recent results from E769[3], at 250 GeV beam energy, provide a much more accurate measurement of the cross section than has been available until now. A precise measurement at 800 GeV can be used as an even more stringent test of the QCD calculations, using the lower-energy data to constrain the absolute normalization, since the shape is less sensitive to uncertainties such as the charm quark mass and the renormalization scale. It may therefore help to discriminate between different sets of parton distributions, especially different gluon densities.

3 HADROPRODUCTION OF OPEN-CHARM STATES

Additional tests of QCD are possible by studying the differential distributions $d\sigma/dx_F$ and $d\sigma/dp_T^2$ in semi-inclusive production of various charm states, as well as correlations in associated charm-anticharm production. A detailed comparison of theoretical predictions with experimental data was presented by Ridolfi[2]. In general, the distributions agree qualitatively with the theoretical calculations, except that a "leading-particle effect" is seen by several experiments[4][5][6] in D -meson production by pion beams: the distribution of

the D that shares a valence quark with the incoming beam pion (D^- for a π^- beam) is harder in x_F . This asymmetry between leading and non-leading particles is not predicted by the perturbative QCD mechanism $gg \rightarrow c\bar{c}$, where the c and the \bar{c} have equal probabilities to be produced at high x_F . It can be understood as a “color-drag” effect, where a valence quark from the beam recombines with the produced c or \bar{c} and pulls it along the beam direction. Fragmentation models that include the effect, such as the PYTHIA Monte Carlo, can reproduce the observed asymmetry.

Alternatively, the asymmetry can be explained in terms of an intrinsic-charm component in the beam[7]: a π^- fluctuating into a $|d\bar{u}c\bar{c}\rangle$ state can break up into a D^- or a D^0 ($|d\bar{c}\rangle$ or $|\bar{u}c\rangle$) carrying a substantial fraction of the beam momentum, while no such mechanism exists for the charge-conjugate states D^+ and \bar{D}^0 . A similar picture arises in the context of the valon model[8] with a significant component of c and \bar{c} quarks in the sea. The upcoming results from the full data sample of the high-statistics experiment E791[6] will allow a detailed comparison of the asymmetry as a function of x_F and p_T with the theoretical predictions of these models. In particular, the intrinsic-charm model predicts that the asymmetry will be predominantly at low p_T , where the heavy and valence quarks are aligned. It will be extremely interesting to search for a similar asymmetry in a future experiment with a proton beam, not only for D production, but also for Λ_c and $\bar{\Lambda}_c$, for which a similar effect would be expected.

An intrinsic-charm component in the proton wavefunction would give rise to diffractive production of charm in proton-nucleon interactions. A search for such diffractive production by E653[9] produced an upper limit of 1.8% of the total cross section for D^+ production in p-Si interactions. This does not rule out the intrinsic-charm model of Ref. [7], which predicts a value of about 1.1%. This number should be well within reach of the future charm experiment, if diffractive events can be identified efficiently.

3.1 Fragmentation in Perturbative QCD

The hadronization of a produced charm quark into a bound state is in general a non-perturbative process, due to the small masses of the light quark-antiquark pairs produced in the fragmentation. Several phenomenological models exist that attempt to describe the process. However, it has been recently realized that fragmentation of heavy quarks or gluons into bound states containing two heavy quarks, such as η_c , J/ψ , χ_c , and (the yet unobserved) B_c , can be substantial and in the kinematic region of large p_T , perhaps the dominant mechanism. Because of the large masses involved, this processes should be calculable in PQCD. In fact, there has been a significant amount of work in the last two years in calculating fragmentation functions into heavy-heavy quark systems. This has been motivated in part by the apparent excess of J/ψ production at the Tevatron[10], compared to the expectations from the lowest-order production mechanism.

In this workshop, Cheung presented a model[11], in which the derived expressions for the perturbative fragmentation functions are treated as phenomenological functions with two free parameters that can be fitted to describe the non-perturbative fragmentation of a heavy

quark to a heavy-light system. The free parameters are the mass ratio $r = m_{\text{light}}/m_{\text{meson}}$ of the light quark to the meson, and an overall normalization. The model makes specific predictions about the relative production of different spin states. In the limit $r \rightarrow 0$, the treatment is similar to the methods of the Heavy Quark Effective Theory.

As an example, the fragmentation functions $c \rightarrow D$ and $c \rightarrow D^*$ were presented. The observables $P_V = D^*/(D + D^*)$ (the ratio of vector mesons to total), $\langle z \rangle$ (average fractional energy carried by a meson), and $\alpha = (2L - T)/L$ (the spin asymmetry parameter) as a function of z , were calculated and compared with data. Good agreement was obtained with $r = 0.167$ ($m_{\text{light}} = 0.3$ GeV) for P_V and $\langle z \rangle$, less good for $\alpha(z)$. The model can be further tested with more data, especially on production rates of P-wave states, and more precise measurements of the spin asymmetry parameter.

4 HADROPRODUCTION OF CHARMONIUM STATES

Even though production of charmonium states is not the main purpose of the experiment considered here, the possibility of a dimuon trigger presents the opportunity to accumulate a very substantial sample of hidden-charm states decaying into two muons. With reasonable assumptions on trigger and reconstruction efficiencies, an experiment with 10^8 fully reconstructed charm decays should also expect to have between 0.5 and 1 million $J/\psi \rightarrow \mu^+\mu^-$ events[12]. Furthermore, the open geometry of this experiment will also allow it to see charmonium states decaying to additional particles, such as photons and pions, also with high statistics. The importance of charmonium production in testing perturbative QCD processes was stressed by several speakers in the working group.

4.1 Production of χ_c States

Production of the different 1P charmonium states offers a good tool for discriminating among different perturbative production mechanisms. In the color-evaporation model[13], the fundamental hard process, either gluon-gluon fusion or quark-antiquark annihilation, involves a color-octet intermediate state (a single gluon) which decays into a $c\bar{c}$ pair; the color is “evaporated” from the final state through emission of soft gluons that are neglected in the calculation (see Fig. 1, left). The prediction for the relative rates of the three spin states, χ_{c0} , χ_{c1} , and χ_{c2} is simply given by $2J + 1$ (1:3:5). In the color-singlet model[14], on the other hand, the intermediate state is a colorless object, as two gluons couple directly to $c\bar{c}$, or a quark and an antiquark annihilate into two gluons (Fig. 1, right). The predicted relative rates are 3:0:4 for the gluon-fusion subprocess and 0:4:1 for the annihilation subprocess.

During the workshop, Spiegel presented[15] preliminary results from E672 on production of χ_{c1} and χ_{c2} by a 515-GeV π^- beam, detected in the decay channel $\chi_c \rightarrow \gamma J/\psi$. The ratio of χ_{c1} to χ_{c2} production cross section was 0.6 ± 0.2 , consistent with, but more accurate than, earlier results with similar beams. This is what would be expected from the color-evaporation model, either from gluon fusion or quark annihilation. However, the result can

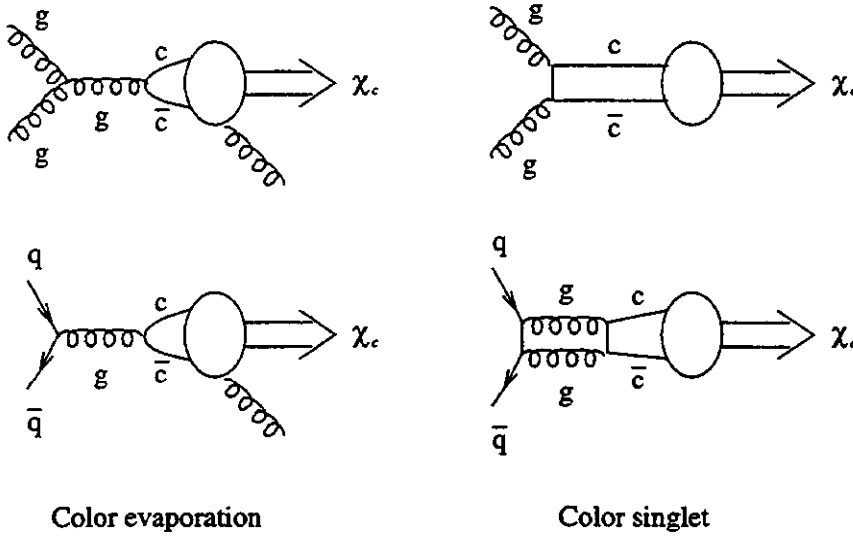


Figure 1: Diagrams for χ_c production in perturbative QCD, in the color-evaporation model (left) and the color-singlet model (right). The top graphs are for gluon-gluon fusion, the bottom ones for quark-antiquark annihilation.

also be understood in the color-singlet model, with the contributions from the two diagrams combining to produce the same ratio.

On the other hand, results from E705[16] with a 300-GeV p beam give a ratio consistent with zero, which seems to exclude the evaporation model and to favor the color-singlet model, dominated by the fusion diagram. However, the evaporation model is ruled out by only 2σ . In addition, it is not clear why both graphs should contribute in the pion experiment, while the gluon-fusion graph dominates in the lower-energy proton experiment. Furthermore, this particular mechanism predicts very little direct J/ψ production, while the experiments see a substantial direct J/ψ component, about 90 nb/nucleon with protons[15]. Clearly, the issue is still far from settled.

A high-statistics charm experiment that combines muon identification and good photon detection will undoubtedly provide important new information, at an energy more than twice that of previous experiments. In addition, higher statistics should allow studies of angular correlations, which can further help discriminate among different mechanisms.

4.2 J/ψ and ψ' Production

As mentioned in the previous section, in addition to the directly produced J/ψ and ψ' states, a substantial fraction of the observed rates is due to the radiative decays of the χ_c states. The fraction of directly produced J/ψ 's can provide additional tests of the production mechanism. In the workshop, it was shown by Tang[17] that measurement of the polarization of the produced states provides such a test.

The polarization λ of the J/ψ is determined by the angular distribution of its decay muons in the J/ψ rest frame. This has the form, in the Gottfried-Jackson frame,

$$\frac{d\sigma}{d\cos\theta} \propto 1 + \lambda \cos^2\theta, \quad (2)$$

where θ is the angle between the μ^+ and the projectile direction.

The polarization of the J/ψ was calculated[17], both for the direct component and the contributions from χ_{c1} and χ_{c2} radiative decays (the contribution from χ_{c0} is negligible). Direct production gives $\lambda \simeq 0.25$, while the two χ_c states produce $\lambda \simeq -0.15$ and 0.85 , respectively. The result was also shown as a function of x_F and was compared with data from πN interactions. Discrepancies were found between the calculated and the measured values. These discrepancies could not be removed by adjusting the individual subprocess normalizations (K factors) according to the observed cross sections of direct and radiative J/ψ 's. It was further argued that the polarization of ψ' should be the same as that of the direct J/ψ . However, the measured value is $\lambda_{\psi'} = 0.02 \pm 0.14$, significantly lower than the expected 0.25 . From this discussion, it appears likely that higher-twist contributions, such as those due to an intrinsic charm component in the beam, may be important in the production of the ψ and χ states. More precise data on the production rates and polarizations would be helpful in deciding the merit of the different theoretical arguments.

5 NUCLEAR DEPENDENCE OF CHARM PRODUCTION

One of the outstanding puzzles of charm hadroproduction is the observation of a significant reduction in the per-nucleon production cross section for J/ψ and ψ' on heavy targets[18][19], while no nuclear dependence was seen by several experiments on open-charm production[20][21], consistent with a hard scattering process. If the A -dependence of the cross section is parameterized as A^α , then $\alpha = 1$ implies no nuclear effects, while $\alpha < 1$ ($\alpha > 1$) means nuclear suppression (enhancement). A hard, pointlike process is characterized by $\alpha \simeq 1$, while typical hadronic total cross sections show a dependence close to $\alpha \simeq 2/3$, implying that the interaction takes place mostly on the surface of the nucleus. The two ψ states show a similar nuclear dependence, $\alpha \simeq 0.9$. Understanding the origin of the nuclear effects is very important, not only in order to disentangle the aspects of charm production that are due to the hard process, rather than a medium influence, but also for the additional information they provide on the strong interaction. In particular, studies of nuclear effects provide the opportunity to investigate longer-range aspects of QCD, using relatively well understood short-range processes.

A tempting explanation for the depletion seen in the ψ cross section in nuclear targets would be a suppression of the gluon sea in a bound, compared to a free, nucleon. Indeed, the ψ data correspond to smaller values of x_2 (see Eq. (1)) than the open-charm production data, obtained at lower beam energies (results from E789[21] with 800-GeV protons were at small x_F and therefore also at larger x_2 than the ψ data). This would imply a nuclear "shadowing" effect for the gluon sea significantly larger than the corresponding effect for the quark-antiquark sea, as seen in Drell-Yan production. However, this explanation probably fails considering the fact that the effect does not appear to scale with x_2 , when the results

are compared with ones at lower energies[22]. Instead, the effect scales with x_F and is larger at higher x_F .

An alternative explanation is higher-twist terms, due to intrinsic charm, present in the beam, dissociating diffractively in the presence of a nucleus[23]. Since diffraction occurs primarily on the surface, it is characterized by an exponent $\alpha \simeq 2/3$, and the diffractive component reduces the A-dependence of the total cross section from $\alpha = 1$ to a smaller number. In addition, the intrinsic charm component becomes more significant at high x_F , due to the high mass of the charm quark. However, E789 sees no need for such a component in their J/ψ differential cross section as a function of x_F , which can be described in terms of gluon-fusion and quark-annihilation processes exclusively. This can be used to set very stringent upper limits in the contribution from intrinsic charm[18], which not consistent with this model.

In this workshop, Kopeliovich presented a calculation based on final-state interactions of the $c\bar{c}$ state propagating through the nucleus[24]. Naively, this appears to be an unlikely explanation: the ψ' has a radius 4 times larger than J/ψ and the rescattering effects should be more important. Also, one might expect less suppression of the cross section at high x_F , since the faster $c\bar{c}$ pair remains longer, due to time dilation, in its presumably small-sized, color-singlet state, before it evolves into a full-size vector meson and therefore has fewer interactions propagating through nuclear matter, according to the ideas of color transparency. Nevertheless, a detailed calculation of the space-time evolution of the state reveals a much more complicated picture.

In this approach, the effect is closely related to nuclear effects seen in other processes, such as photoproduction of vector mesons and deep inelastic scattering at low x , which can be described as fluctuation of the virtual photon into a $q\bar{q}$ pair, followed by propagation of the pair through the nucleus. Rather than assume a monotonic increase of the quark-antiquark separation with time, the strength of the final state interactions is calculated quantum-mechanically, by expanding the matrix element in a series of all the appropriate intermediate states, including off-diagonal elements (a detailed presentation can be found in a recent review on color transparency presented by Nikolaev[25] and in references therein). The interplay of coherence and formation lengths can lead to an increase or decrease of the cross section, depending on energy and mass scale (corresponding to shadowing and antishadowing in inelastic scattering). The overlap of the initial and final states is also affected by the nodal structure of the first radially excited state, in this case ψ' . The calculation reproduces the observed x_F dependence of the nuclear suppression of the charmonium states fairly well and it also provides a unified description of a large number of similar effects in other processes.

In this model, the similarity in the nuclear dependences of the J/ψ and ψ' hadroproduction cross sections is accidental and is only approximate (in photoproduction, a significant variation is predicted with Q^2). Furthermore, a similar x_F dependence is expected[24] for the nuclear effects in hadroproduction of open charm; however, the overall level of $\alpha(x_F)$ is shifted upwards, so that $\alpha(0) \simeq 1$. This is consistent with all measurements, where no nuclear suppression is seen in the central region. The additional suppression in the production of the charmonium states is due to the total absorption of these states in nuclear

matter, while no such channel is available for open charm. This of course can be tested in an experiment with enough statistics at high x_F , if at least two targets with different A are used. Indeed, it is imperative to study any possible nuclear effects in charm production at high x_F where no such data exist, before results from production on heavy targets can be interpreted properly.

References

- [1] J.A. Appel, *Annu. Rev. Nucl. Part. Sci.* **42** (1992) 367.
- [2] G. Ridolfi *et al.*, these Proceedings.
- [3] E769 Coll., A. Wallace *et al.*, to appear in the Proceedings of the 1994 APS Meeting, Crystal City, VA, April 18–22, 1994.
- [4] WA82 Coll., M.I. Adamovich *et al.*, *Nucl. Phys.* **B27** (1992) 212.
- [5] E769 Coll., G.A. Alves *et al.*, *Phys. Rev. Lett.* **72** (1994) 812.
- [6] E791 Coll., S. Banerjee *et al.*, to appear in the Proceedings of the XXIX Rencontres de Moriond, March 19–26, 1994.
- [7] R. Vogt, S.J. Brodsky, and P. Hoyer, *Nucl. Phys.* **B383** (1992) 643;
R. Vogt and S.J. Brodsky, LBL Preprint LBL-35380 (1994).
- [8] R.C. Hwa, *Phys. Rev.* **D22** (1980) 1593;
R.C. Hwa, Univ. of Oregon Preprint OITS-539 (1994).
- [9] E653 Coll., K. Kodama *et al.*, *Phys. Lett.* **B316** (1993) 188.
- [10] CDF Coll., V. Papadimitriou *et al.*, to appear in the Proceedings of the Rencontres de la Vallée d'Aoste, La Thuille, March 1994.
- [11] K. Cheung, these Proceedings.
- [12] D.M. Kaplan, these Proceedings and private communication.
- [13] H. Fritzsch, *Phys. Lett.* **67B** (1977) 217;
M. Glück, J.F. Owens, and E. Reya, *Phys. Rev.* **D17** (1978) 2324.
- [14] J. Kühn, *Phys. Lett.* **89B** (1980) 385.
- [15] L. Spiegel, presented at the meeting of the Working Group on Tests of QCD.
- [16] E705 Coll., L. Antoniazzi *et al.*, *Phys. Rev.* **D49** (1994) 543.
- [17] W.-K. Tang, these Proceedings.
- [18] E789 Coll., M.S. Kowit *et al.*, *Phys. Rev. Lett.* **72** (1994) 1318.
- [19] E772 Coll., D.M. Alde *et al.*, *Phys. Rev. Lett.* **66** (1991) 133.
- [20] E769 Coll., G.A. Alves *et al.*, *Phys. Rev.* **D49** (1994) 4317; *Phys. Rev. Lett.* **70** (1993) 722.
- [21] E789 Coll., M.J. Leitch *et al.*, Preprint FERMILAB-Pub-94/012-E.
- [22] E537 Coll., S. Katsanevas *et al.*, *Phys. Rev. Lett.* **60** (1988) 2121.
- [23] P. Hoyer, M. Vanttinen, and U. Sukhatme, *Phys. Lett.* **246B** (1990) 217.
- [24] B.Z. Kopeliovich, presented at the meeting of the Working Group on Tests of QCD.
- [25] J. Nemchik, N.N. Nikolaev and B.G. Zakharov, Preprint KFA-IKP(Th)-1994-20 presented at the Workshop on CEBAF at Higher Energies, CEBAF, April 14–16, 1994.

Summary of the Rare Decay Working Group, Charm 2000 Workshop

Ai Nguyen
Kansas State University

Paul Sheldon
Vanderbilt University

1 Introduction

This working group concentrated primarily on searches for Flavor Changing Neutral Current (FCNC), Lepton Family Number Violating (LFNV), and Lepton Number Violating (LNV) charm decays. In the standard model, FCNC charm decay is expected to be extremely rare, LFNV and LNV charm decays are forbidden. (Just how rare FCNC decays are expected to be was the subject of some discussion, see below.)

Searches for the above decays provide an important opportunity to search for new physics, beyond the Standard Model. While sensitive searches have been carried out in kaon decay, it is still important to look in charm decay because the “new physics” may only couple to “up”-type quarks.

In this summary we list the contributed talks and briefly summarize the ensuing discussions. Where available we include documents provided by the speakers on their results. Where such documents are not available we attempt to describe results in more detail.

2 Contributed talks

The rare decay working group received contributions from E. Niu, K. Lau, S. Pakvasa, and A. Schwartz. Pakvasa expanded on his plenary talk on mechanisms leading to rare decays, followed by a brief discussion of the uncertainties in theoretical estimates of branching ratios. Schwartz compared rare K and rare D decays. Niu and Lau gave results from rare D decay searches in Fermilab E653 and E771, respectively. Niu also sketched a next-generation experiment which would be 100 times more sensitive to rare D decays than E653.

3 Summary of discussions

The present round of Fermilab fixed-target charm experiments has pushed the limit on the branching ratio of several rare D decays to a few $\times 10^{-5}$. It seemed clear that CLEO II will at best equal this sensitivity. However with secondary-vertex detection and improved statistics CLEO III will perhaps surpass the current fixed-target results. Possibilities at the Fermilab-collider experiments were brought up but not discussed in detail. Advantages (and drawbacks) of closed versus open geometries were also discussed but the working group did not achieve any conclusions. A dedicated (closed-geometry) design would benefit from a limited focus on rare decays.

4 Sandip Pakvasa

There was further discussion of Pakvasa's plenary talk, to which the interested reader is referred.

5 Alan Schwartz

A calculation of the rate for $c \rightarrow ul^+l^-$ in the Standard Model has been made. This calculation was reviewed at the working group and compared to the analogous strange-quark rate. Nonperturbative (di-gamma) contributions which plague the kaon measurements are expected to be negligible in rare D decays. D mesons are the only available system where lepton-flavor-violating processes involving "up-like" quarks (e.g. $c \rightarrow u\mu^+e^-$) can be searched for.

6 Etsuko Niu

Results from rare D -decay searches in Fermilab E653 were presented and a next-generation experiment which would be 100 times more sensitive to rare D decays than E653 was sketched. We refer to the plenary talk by Paul Sheldon and to Niu's transparencies and paper for details.

7 Kwong Lau

Based on 25% of E771 data a limit of $B(D^0 \rightarrow \mu^+\mu^-) \leq 1.1 \times 10^{-5}$ was set at the 90% confidence level. Details of this analysis are described in an E771 draft, appended below.

Semi- and Fully-Leptonic Decays of Charm
Report of CHARM2000 Working Group, 7-9 June 94

Dario Barberis, *Genoa and INFN*
Tim Bolton, *Columbia University*
Arne Freyberger, *University of Florida*, co-convenor
Peter H. Garbincius, *Fermilab*, co-convenor
Michael Luke, *University of Toronto*
Jim Wiss, *University of Illinois*
Chong Zhang, *Kansas State University*

Abstract

Some of the interesting semileptonic and fully-leptonic charm decay physics topics that we anticipate investigating over the next few years are discussed.

1 Introduction

This small working group discussed some important and exciting topics that still can and should be addressed regarding semileptonic and fully-leptonic decays of charm particles. Earlier in the plenary sessions, Jim Wiss summarized the current general experimental situation, Arne Freyberger discussed pertinent CLEO results, and Michael Luke motivated the usefulness of inclusive studies of semileptonic decays. Many of the topics for semi- and fully-leptonic are currently limited by statistical precision. Much progress can be expected in many of these areas from the higher statistics experiments Fermilab E-831, Fermilab E-781, CLEO 2.5, CLEO 3, BES, $\tau - charm$, and the b -factories. We concentrated on near-term leads, without waiting for the machines and the experiments of the next millenium. This report summarizes our discussions.

2 Form Factors, CKM Elements, and Absolute Branching Fractions

The semileptonic decay rates are proportional to the product of the square of the CKM matrix element and the square of the form factor, the latter being a function of q^2 , the mass-squared of the virtual W^\pm emitted, $\Gamma \approx |V_{cq}|^2 f^2(q^2)$.

The form factors $f(q^2)$ are important in their own right and our imperfect knowledge of their magnitude and q^2 dependence limits our capability of measuring the CKM matrix elements accurately. As examples, we can only measure $|V_{cs}|$ to about 20% using $D \rightarrow K\ell\nu$, and we really haven't studied $f_{\pi^0}^2(q^2)$ which is needed to extract $|V_{cd}|^2/|V_{cs}|^2$ from the relative rates

$$\frac{\Gamma(D^+ \rightarrow \pi^0 \ell \nu)}{\Gamma(D^+ \rightarrow \bar{K}^0 \ell \nu)} = \frac{|V_{cd}|^2 f_{\pi^0}^2(q^2)}{|V_{cs}|^2 f_{\bar{K}^0}^2(q^2)}.$$

Thus it is important to get the q^2 dependence of both the decays into π and into K , in a model independent way, with good $\pi - K$ separation over the entire acceptance and q^2 range.

Just what is the functional form of these form factors for semileptonic decays into pseudoscalars and into vector particles? Are they best represented by exponentials, $f(q^2) = e^{\alpha q^2}$ as suggested by ISGW, or by the pole formalism, $f(q^2) = \frac{1}{1 - q^2/M_{pole}^2}$? Both forms are basically *ad hoc*. How are the studies of form factors affected by q^2 -resolution, particle identification, acceptances, and backgrounds? For $K\ell\nu$ decays, there is not sufficient q^2 range to fully study the dependence on functional form and pole mass. The $\pi\ell\nu$ decays, although Cabibbo suppressed, can have a larger q^2 range and possibly better sensitivity by more closely approaching the pole mass.

The form factors for $\pi\ell\nu$ and $\rho\ell\nu$ should be related to those for $K\ell\nu$ and $K^*\ell\nu$ by HQET symmetries.

Although in this working group we have concentrated on the form factors for semileptonic decays of charm into pseudoscalar mesons, it was pointed out that no experiment has yet had the sensitivity to study the R_3 form factor ratio in decays into vector mesons, such as $K^*\ell\nu$.

The study of many of these topics is related to and often requires the measurement of absolute decay rates or absolute branching fractions. For example, Tim Bolton described that the lack of absolute branching fractions is a limitation in determining the CKM matrix elements using ν and $\bar{\nu}$ production of same sign dileptons.

In the Fixed Target environment, which is the preferable method: hadroproduction or photoproduction? Using 500 GeV π^- , the average reconstructed charm particle momentum is about 70 GeV, while for E-687 using an average interacting photon of 200 GeV, the average charm momentum is about 90 GeV. So acceptances, vertex separation/Lorentz boosts, particle identifications, *etc.* all are about the same for the two approaches. Hadroproduction is likely to result in higher multiplicities than photoproduction, which difference might be important in certain physics, such as absolute branching ratio work and semileptonic decays requiring a soft pion tag, *etc.*

3 Inclusive vs. Exclusive Semileptonic Decays

Although HQET is not expected to be very applicable in *exclusive* $c \rightarrow sW^+$ transitions, it may be useful in similar *inclusive* decays where one integrates over all the messy, perturbative, low-energy hadronic physics complications.

The question was raised whether one can measure the kinematics of the W^+ well enough by measuring only the charged lepton and integrating over or ignoring the remaining hadronic fragments. Could you use vertexing and the direction of the parent charm particle to measure (or infer) the neutrino momentum? Would any of this be better studied at an $e^+e^- \rightarrow \psi'' \rightarrow c\bar{c}$ machine?

In studying inclusive semileptonic decays, one is often left only with the laboratory momentum of the charged lepton, possibly relative to a *thrust* axis. Typically there is a lower energy cut off for the acceptance or identification of the lepton, typically about 0.7 GeV at CLEO. How could this lepton threshold be lowered to increase the q^2 range available for study?

Inclusive semileptonic decays (easily calculated, but measured with difficulty) are used in measuring absolute branching ratios, such as for $D_s^+ \rightarrow \phi\pi^+$. This is accomplished by summing up all the *exclusive* semileptonic modes and relating to the *inclusive* semileptonic rates. If one has included *all* the exclusive semileptonic modes, then one may find the CKM matrix element squared, and by relying on symmetry arguments such as $\Gamma(D^0 \rightarrow K^*\ell\nu) = \Gamma(D_s^+ \rightarrow \phi\ell\nu)$, one can infer $\Gamma(D_s^+ \rightarrow \phi\pi^+)$ from the relative $D_s^+ \rightarrow \phi\ell\nu, \eta\ell\nu, \eta'\ell\nu$, and $f_0\ell\nu$ decay rates.

A basic expectation, requiring experimental verification, is the equality of all such charm meson semileptonic decay widths to about 3%.

The inclusive semileptonic decay rates of D^0 and D^+ have been measured to about 5% accuracy, that of the Λ_c^+ to about 25%, and the D_s^+ not at all.

Are there differences in the decays into *electrons* or into *muons*? The fully leptonic decay of D_s^+ is expected to be dominated by decays into τ , but for semileptonic decays, the $e - \mu$ differences are expected to be on the order of 4% due to the different phase space available. Are there any surprises for the form factors? As Jim Wiss noted in his plenary talk, an $e - \mu$ difference would show up in the $f_-(q^2)$ part of the form factor.

Semileptonic decays also show promise in the search for $D^0 - \bar{D}^0$ mixing, for which there is no background due to double Cabibbo-suppressed decay processes.

4 Decay Constants

Although there was not much discussion of the fully-leptonic decays, measurements of the decay constants f_{D^+} and $f_{D_s^+}$ were both considered important and could be used to bootstrap your way up to understanding the similar decays of b -mesons.

There have recently been observations of the fully-leptonic decay $D_s^+ \rightarrow \mu^+ \nu_\mu$ by WA-75, CLEO, and E-653. CLEO and WA-75 have preliminary measurements of $f_{D_s^+}$. E-653 also has three candidate $D_s^+ \rightarrow \tau^+ \nu_\tau$ with $\tau^+ \rightarrow \mu^+ \nu_\mu \bar{\nu}_\tau$, with all particles tracked in the emulsion target.

The emulsion techniques rely heavily on the observation of the D_s^+ track *before* decay. Can the emulsion technique be pushed another factor of 100 in processing capacity, or must there be new totally electronic approaches. Can the CLEO techniques of tagging $D_s^{*+} \rightarrow \gamma D_s^+$ and of using the *electron* samples to estimate backgrounds in the μ sample be extended to fixed target or hadron collider applications?

Can we study the Cabibbo suppressed leptonic decay $D^+ \rightarrow \mu \nu$? What about backgrounds from $D_s^+ \rightarrow \mu \nu$? Can we get enough $D_s^+ \rightarrow \tau \nu$ to test $\mu - \tau$ lepton universality?

5 Semileptonic Decays of Charm Baryons

This topic was also heavily discussed in the Charm Baryon Working Group.

Not much is now known about the semileptonic decays of charm baryons. ARGUS had previously observed semileptonic decays of Ξ_c^0 and Ξ_c^+ . Now CLEO is beginning to observe $\Xi_c^0 \rightarrow \Xi^- \ell^+ \nu$ and $\Xi_c^+ \rightarrow \Xi^0 \ell^+ \nu$.

Theoretically, we might expect that there would be about a 20% difference in the inclusive semileptonic decay rates $\Gamma(\Lambda_c \rightarrow X \ell \nu)$ and $\Gamma(D \rightarrow X \ell \nu)$. Such a quantitative measurement might be very difficult in a Fixed Target experiment, but might be conceivable at a threshold e^+e^- machine.

Other than for providing the impact parameter of the lepton, conventional vertex detectors don't seem that useful unless they can track the parent charged charm baryon, such as Λ_c^+ or Ξ_c^+ , or unless they can verticize the ℓ^+ and the Ξ^- from the decay of the Ξ_c^0 . Does even a single space point (or pixel) at the downstream end of the target help much in this application?

6 Vertex Tracking

Dario Barberis then described the vertex tracker of WA-92 (previously WA-82). This system has the capability of tracking the parent D_s^+ or charm baryon before it decays and therefore of producing a vertex between the parent charm and the decay lepton. This is needed to find the angle and p_\perp of the decay.

The vertex tracker system consists of an upstream incident π^- beam spectrometer and a 2 mm Cu target, followed by 13 planes of silicon strips, 10 μm pitch, each separated by 1.2 mm. This very close tracking is done in one projection only and forms the basis of an on-line impact parameter trigger which Dario described in the plenary session. This vertex tracker is then followed by a more conventional 3-dimensional silicon tracker. The first 6 planes of the vertex tracker are 150 μm thick, while the last 7 planes are 300 μm thick. Dario noted the tradeoffs between amount of material for signal to noise ratio and for multiple scattering and secondary interactions. Pulse height analysis is done on these vertex strips for rejecting secondary nuclear interactions within the silicon. Nuclear breakup typically deposits energy over many adjacent strips, while large pulse heights due to Landau fluctuations in dE/dx typically involve only one strip.

Dario noted that even 10 μm pitch detectors aren't that great considering the angular resolution at such closeness to the primary vertex. He also noted that 2-dimensions would be much better for identification of the kink, and are probably required for decay angle determination in these fully-leptonic decays or in any 1-prong decay topology.

Dario showed an event with two B -particle candidates, corresponding to one charged B and one neutral B , decaying within this tiny 5 mm x 5 mm x 1.75 cm (target through 13 detector planes) 8500 channel vertex decay detector.

7 Backgrounds

Some of the troublesome backgrounds experienced include understanding the lepton fake rates, particularly at CLEO, and hadron misidentification. For example, E-653 did not have $\pi - K$ identification capability and relied on the minimum parent mass technique. Therefore much effort was put into insuring the dominant $D^+ \rightarrow \bar{K}^{*0} \ell \nu$ was not confused with the Cabibbo-suppressed mode $D^+ \rightarrow \rho \ell \nu$.

An interesting Cabibbo-suppressed decay with a different background problem is $D_s^+ \rightarrow K^0 \ell \nu$, which has identical, and not fully reconstructed final state particles as $D^+ \rightarrow K^0 \ell \nu$. Due to the similar masses of the D^+ and the D_s^+ , the form factors are expected to be almost equal, leading to a fairly unbiased measurement of $|V_{cd}|^2/|V_{cs}|^2$. Since there is a missing neutrino for both processes, a mass constraint will not work, and the only discrimination between signal and background might be on the basis of lifetimes.

A final background complication related to radiative corrections where an additional photon is radiated, such as $D \rightarrow K^* \ell \nu + \gamma$. These corrections are often added late in the analysis using the CERN PHOTOS program and are expected to be of the level of a 1-3% X_0 equivalent (external) radiator for charm meson semileptonic decays. With its CsI calorimeter with good efficiency and resolution for low energy photons, CLEO has observed the radiative decays $\tau \rightarrow e \nu \bar{\nu} + \gamma$ and $K_s^0 \rightarrow \pi^+ \pi^- + \gamma$, finding agreement with the PHOTOS prediction. CLEO has not observed $D \rightarrow K \ell \nu + \gamma$, however.

8 A Dedicated Experiment?

If you really wanted to study leptonic decays - fully leptonic, inclusive semileptonic, and exclusive semileptonic - how would you optimize your experiment? These experiments, always involving the detection of and often triggering on leptons, concentrate on many of the most pressing issues in charm particle physics, such as CKM matrix elements and form factors, and the search for rare phenomena such as $D^0 - \bar{D}^0$ mixing. Could other than open geometry experiments be more optimal? Are open or restrictive triggers more optimal? Experimentally, should one concentrate on muons or electrons (or both simultaneously)? Do you really need particle (charged hadron) identification capability? Can one adequately identify the charm states topologically or by minimum parent mass, as done by Fermilab E-653 for $K^* \ell \nu$ and $\rho \ell \nu$? Can you forgo hadron identification in order to increase overall acceptance, at the loss of capability of studying hadronic decays and Cabibbo suppressed modes?

A large acceptance approach would surely help, by catching both charm particle decays. Even if you trigger on one semileptonic decay, the other charm decay is unbiased and often tagged, maybe sufficiently for $D^0 - \bar{D}^0$ mixing searches. Single lepton triggers are required. Triggering on at least one lepton that came from a decay vertex not associated with the primary vertex, would also be helpful. Similarly, large acceptance helps in picking up the slow pion in $D^{*+} \rightarrow \pi^+ D^0$ decays to tag the D^0 for studies of its decays. A short, wide spectrometer, sounding a lot like E-771 with a WA-92 vertex tracker, seems to be optimal.

Could one sell a proposal for such a dedicated, ultra high rate experiment, concentrating solely on leptonic triggers and tags?

9 Summary

We concentrated on discussing near term leads for physics we could do with our existing detectors, we shot the breeze on future fantasies, and we did some wishful thinking on future prospects and possible programs. A lot of interesting technical questions that deserve more extensive follow-up study were generated.

Report of the Working Group on Beams and Architectures

Charles N. Brown

Fermi National Accelerator Laboratory, Batavia, IL 60510

Daniel M. Kaplan

Northern Illinois University, DeKalb, IL 60115

Donald J. Summers

University of Mississippi, Oxford, MS 38677

The working group first considered the pros and cons of possible fixed target beams (see Table 1). Note that the nuclear enhancement of charm production ($\propto A^1$) relative to the total cross section ($\propto A^{2/3}$) has not been included in the Table and can increase charm yields by a factor of almost 5 for heavy targets, however at the expense of worsened mass resolution for D^{*+} 's, since the soft pion from e.g. $D^{*+} \rightarrow D^0 \pi^+$ can be significantly scattered while emerging from the target. (A 1-mm Pt target, for example, represents 16% X_0 on average, contributing 6 MeV rms p_t kick, which is a significant fraction of the 40 MeV imparted to the soft pion by the decay.) Don Summers suggested ^{13}C -diamond as a target combining high density, long radiation length, good heat conductivity, and a modest ($\times 2$) nuclear enhancement factor. The motive for a dense target is to be able to require charm decays in air to minimize background.

If one assumes (see talk by Jeff Appel) that one reaches for the highest "equivalent" number of charm decays by restricting the trigger and geometry to the decay topologies of interest, then proton beams can probably reach the highest effective charm luminosities. Proton beams have the added advantage of very small spot sizes, which can allow simple impact-parameter trigger strategies. Overall, it appears that a proton beam would be a good choice for a Charm 2000 experiment (see talk by Dan Kaplan). However, it may be possible to increase the intensity of photon beams using crystals. Hard bremsstrahlung is enhanced

Table 1: Estimated yields of produced charm (antiparticles included) neglecting A -dependence enhancement

Beam	$\sigma_{c\bar{c}}$ (cm^2)	Intensity Limit/spill	Charm/spill
Protons (800 GeV)	2×10^{-29}	10^{11} (1 int./RF bucket)	1×10^6
π^- (500 GeV)	2×10^{-29}	10^8 (Proton economics)	3×10^3
Photons (200 GeV)	1×10^{-30}	10^8 (Proton economics)	2×10^2

as an electron passes through the electric field of a crystal lattice. For now though, protons appear to be favored.

The working group looked at architecture issues. The architecture of an experiment is closely tied to the choice of the beam. For a pion or photon beam, large acceptance is crucial since the maximum beam intensity achievable is limited. The large spot sizes of these beams also tend to drive the design to a large-angular-acceptance detector. For a fixed acceptance, large spot size requires larger silicon-detector area and thus (for fixed resolution) more channels.

The possible classes of detector configurations can be reduced to three generic types, as shown in Fig. 1 [1]. Clearly the choice of particle identification directly influences the details of the layout. A single-magnet design is probably more consistent with RICH particle-ID while a two-magnet design allows multiple threshold-Cherenkov detectors. The three-magnet approach taken by E781 is clearly driven by the need to reconstruct hyperons in decays of charmed baryons with high efficiency but is not necessarily optimal for an experiment concentrating on mesons. A longer spectrometer does increase the fraction of kaons and pions decaying in flight.

With modern tracking detectors, silicon, scintillating fibers, straw tubes, microstrip chambers, etc., the multiple-scattering resolution limit can probably be reached with a modest magnetic field of about 0.5 GeV kick. The channel count may need to be in the 100K to 1M range to achieve this limit, and care must be taken to minimize the amount of material traversed by the detected particles. Recent work with helium based drift chamber gases and aluminum field wires may prove useful.

Using a 500 GeV π^- beam, E791 achieved a ratio of reconstructed charm per interaction of $\approx 10^{-5}$. If this ratio can be maintained in future experiments, then a proton-beam experiment running at 1 interaction/RF-bucket (53 MHz) should be able to reconstruct $\sim 10^9$ charm in a run of $2 - 3 \times 10^6$ live beam seconds, while a pion-beam experiment is limited by proton economics to perhaps 10^7 (assuming it is not permitted to monopolize the accelerator!) for 800 GeV primary energy. Since the charm cross sections are about the same in the two cases while the total pion inelastic cross section is only $\approx 2/3$ that for protons, achieving this ratio with a high-intensity primary proton beam will be nontrivial. The future experiment will have to feature much higher trigger rejection and hotter DA than E791 (which essentially wrote all inelastic interactions to tape). D. Christian's paper and the Triggering Working-Group Summary (these Proceedings) address the prospects for on-line vertex triggering. E789 has run with a 1-view vertex trigger processor taking $\approx 10 \mu\text{s}/\text{event}$ that rejected 9 out of 10 events. It enhanced the two-body decay, $D^0 \rightarrow K^- \pi^+$, by a factor of 5 to 7. The spectrometer arrangement imposed momentum cuts on the K^- and π^+ , as well as a minimum opening angle cut of 40 mr. Extending the E789 technology by an order of magnitude or perhaps a bit more seems workable. Beyond this only lepton triggers may be feasible without a technological breakthrough.

A better spectrometer may compensate for a low trigger efficiency and slow DA, within limits. Possibilities include increased solid angle acceptance, increased detector element

efficiency, lower channel occupancy, less mass for multiple scattering, higher magnetic field, and higher resolution. New detector elements might include a RICH and a muon system that measures momentum.

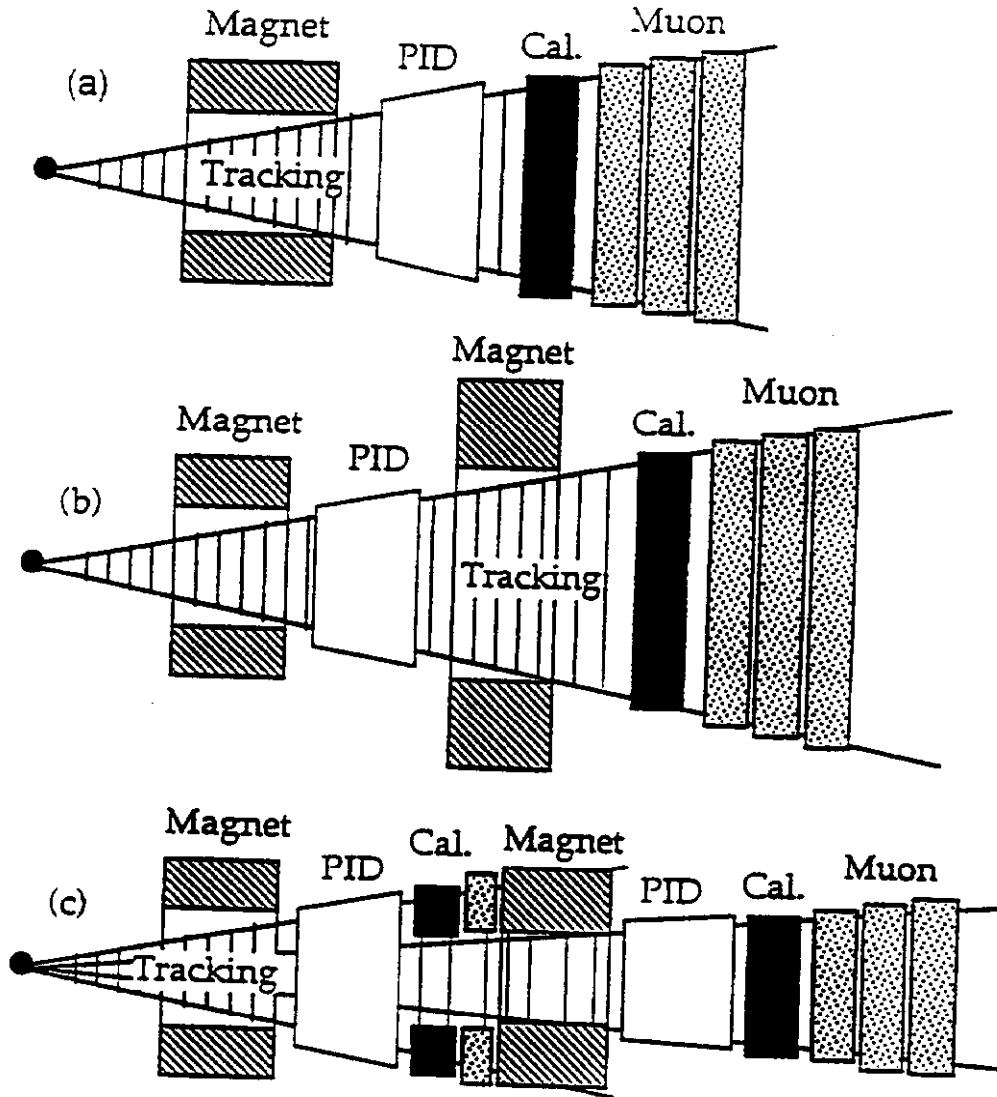


Figure 1: Three alternative configurations for a heavy-quark spectrometer (from Ref. [1]).

References

- [1] H. Albrecht *et al.*, "An Experiment to Study CP Violation in the B System Using an Internal Target at the HERA Proton Ring," (HERA- B Letter of Intent), DESY-PRC 92/04, October 1992.

Summary of the Triggering, DAQ, and Analysis Working Group

Catherine C. James and Mike Halling
Fermilab, Batavia, IL 60510

Fixed target charm experiments have dramatically increased their charm yields over the last 15 years. As described in Jeff Appel's introductory talk, the increase is primarily due to better secondary vertex resolution using silicon detectors, and due to high data taking/analysis capacities. Certainly, DAQ and analysis capabilities must be matched in any future experiment; there is little use in recording more data than can be examined in a reasonable length of time. So far, the most successful high statistics charm experiments have run with fairly open triggers. Most participants believe, however, that significantly higher charm statistics will not be achieved by simply recording more interactions.

As an illustration of the problem consider the "strawman" experiment proposed for the workshop with a 5 MHz interaction rate. One proven trigger technology is the E_t trigger, which can reject at most about $\times 5$ of the interactions and still remain reasonably efficient for charm. If one used an E_t or similar trigger and recorded "all" triggered events the DAQ system would accept a 1 MHz trigger rate. For an event size of 3kb (typical for FNAL E687 and E791), there would be a 3 Gb/s rate from the front ends during the spill cycle, and a 1 Gb/s continuous rate to tape. After a 3×10^6 second run, which is only a couple of months at 50% percent on-time, one would have a 3000 Tb data set, consisting of 3×10^{12} events. An offline fast filter might be used, for example, to pick out events with secondary vertices. A filter code that takes 2 MIPS-sec per event (optimistic compared to current experiments) requires 200,000 MIPS-years of computing just to complete this fast filter. Computing costs may come down in the year 2000 to \$50 per MIPS; even so, this scenario presents an expensive and long-term analysis problem.

After this exercise it is clear why many participants in the Workshop agreed that an increase to 10^8 reconstructed charm requires a technological innovation, and the most likely breakthrough must come in better triggering on charm events. In the Working Group there was general agreement that a DAQ that could log data at 100 Mb/s or so could be built for the Charm2000 experiment. This is a factor of 20 below the rate described in the above scenario. So Charm2000 needs a trigger that can give an additional $\times 20$ in conjunction with an E_t trigger, or $\times 100$ reduction from the interaction rate. This additional trigger device must work at input rates of 1MHz.

Most of the discussion in the Working Group revolved around the various types of triggers and triggering devices that might be developed to solve this problem. The discussion began with a description of the triggers to be used in the two charm experiments approved for the 1996 FNAL fixed target run, E781 and E831. E831 is a follow-on to the photoproduction

experiment E687. That experiment will use much the same trigger as before, selecting hadronic events seen in the calorimeter with a total energy threshold. E781 will use a sigma-hyperon beam to produce charm. The 1st stage of the trigger is topological, looking for more than 2 positive tracks above 15 GeV, and perhaps also a selection based upon track multiplicity. Events passing the 1st stage of the trigger will be passed to a Unix processor farm that will select events based upon the impact parameters of a subset of the tracks. At the expected event rate to the Unix processor the code must execute in 4.5 msec/event or less.

The rest of the discussion in the Working Group concentrated on new trigger developments that might be used for a Charm2000 experiment. Dave Christian's contribution to these proceedings covers all the topics in the discussion very well, and it will not be repeated here. There was agreement that if one wanted to concentrate on semileptonic charm decays a lepton trigger could be devised that would operate at Charm2000 rates. But, if one wanted to be open to all types of charm events triggering becomes difficult. The general impression was that hardware devices such as a multiplicity jump detector, or the optical impact parameter device, could probably work as beauty triggers, but may have intrinsic difficulties as charm triggers. The best hope for fast and efficient charm triggers appears to be data-driven "hardware" processors discussed at length in Dave Christian's contribution.

The implementation of processor triggers has matured over the last few years, as experiments using them learn from earlier experiences. It was noted that such hard-wired tracking and vertexing processors can never do a better job than offline reconstruction programs, but several techniques for making them perform at a level closer to the full offline analysis were brought up. Placing the entire vertexing detector system in a magnetic field to sweep out low momentum tracks would allow a processor to make a quick momentum selection, allowing it to find only high momentum tracks with large impact parameters. In addition, inchworm motors could be used to position the SMDs, eliminating the need for a large set of offline fiducial constants. Pure offsets are easy for hardware trackers to deal with, but rotations are not. It is generally agreed that event selection based on vertexing can achieve the necessary factor of $\times 10$ to $\times 20$ in trigger rate needed to make the Charm2000 experiment possible, and there are at least two examples of experiments with working hardware trackers capable of track reconstruction in the 10 to 20 μ s range. If the data flow is pipelined these devices could be used in the Charm2000 experiment.

The working group ended with mild optimism that a trigger/DAQ for such an experiment could be created with the technology of the year 2000, if money were no constraint. Improvements in one of the two optical triggers could help significantly in making such an experiment practical.

Vertexing Working Group Summary

Charles Ray Newsom
University of Iowa

Abstract

The working group conducted an informal discussion of the various aspects involved in improving vertexing beyond the present limits. The discussions are briefly summarized in the following sections, followed by comments and conclusions.

1 Beam Considerations

(a) Higher energy beams will help move BOTH secondary vertices away from the target and will reduce multiple scattering problems.

(b) A higher beam intensity will benefit both collider and fixed target programs.

2 Target Considerations

(a) Thin, dense targets will be needed, as usual.

(b) Vacuum should reduce secondary interactions to a minimum.

(c) An active target can ID secondary interactions and possibly remove them at the trigger level.

3 Detectors

(a) Single sided silicon detectors

These detectors are a mature technology. Pitch size will remain about 10-20 microns, limited by the thickness of the detector, which is in turn limited by electronic noise. No large resolution improvements are foreseen for this type of detector.

(b) Double sided silicon detectors

These detectors are severely limited on the back side at the moment. There is a technical solution to improving the back-side resolution by adding an additional layer. This could be a significant improvement in the resolution. Since fewer silicon planes would be needed multiple scattering effects would be reduced and better vertex resolution would result.

(c) Pixel detectors

—The minimum pixel size will not shrink much below $50\mu\text{m}\times 50\mu\text{m}$.

—There will be problems with scaling these to full detector sizes.

—It is possible to read out pixel detectors in "strip mode" where one rapidly reads the logical "or" of all pixels within a single column and/or row. When used in a front-end trigger processor, one might obtain a significant additional rejection factor.

—They are very important in reducing track confusion, and will be an integral part of future experiments.

(d) Diamond detectors show great promise for very high rate experiments. They won't be required (but they may be useful) in the next round of experiments.

4 Readout

(a) Massive on-detector parallelism and pipelining show the main promise of speed improvements in the near future.

(b) Pixel readout is now becoming viable (e.g. at reasonable speeds).

5 Computing

The biggest gain in vertexing is thought to be in this category. Industry driven improvements are sufficient to move one forward rapidly. No major HEP effort is needed, other than as a major user of new high-end systems. Since this subject is the topic of another working group, no further discussion was required by this working group.

6 General Comments by Individuals

(a) A 2x improvement in detector readout noise will allow a 2x thickness reduction in thickness (mechanical problems aside), which will allow small pitches. $10\mu\text{m}$ pitches will become more usable.

(b) Pixels are very useful to clarify confusion (x-y correlations) but will not compete in resolution with strips. Vertex detectors will remain mostly strips with a few pixel planes.

(c) We need to commercially manufacture pixels to overcome present size (scaling up and down!) and yield problems.

(d) It is time to build pixel detectors for real experiments.

(e) SSC funding losses have severely affected R and D efforts in the USA. Additional sources of funding are needed and desirable.

7 Conclusions

The main charge given to the members of the working groups was to examine the feasibility of increasing the number of fully reconstructed charm events in a next generation experiment by a factor of roughly 100. The working group divided this factor into two separate categories as summarized below.

(a) A single factor of ten improvement seems achievable within the next few years using existing technologies. This would be achieved by many different improvements as discussed above, with the biggest factor coming from improvements in computer hardware.

(b) An improvement factor of 100 is not possible with present day silicon detectors. For this reason, no member of the working group was prepared to make such a large step at this time. No one felt that it would be possible to incrementally achieve this type of improvement with existing detector technology. Diamond detectors are clearly felt to be one promising solution to explore for use after the forthcoming generation of experiments are completed.

AUTHOR INDEX

Abe, K.	423	Landsberg, L. G.	275
Anderson, D. F.	171	Lavocat, P.	423
Appel, J. A.	1	Lipkin, H. J.	275
Ashery, D.	275	Liu, T.	375, 441
Atiya, M.	143	Long, M.	423
Aubert, B.	423	Luke, M.	67, 453
Barberis, D.	213, 453	Kaplan, D. M.	229, 459
Besson, D. Z.	35	Kwan, S.	171
Bigi, I.	323	Mangano, M. L.	237
Bolton, T.	267, 453	Mansoulie, B.	423
Brodsky, S. J.	415	Marchand, D.	423
Brown, C. N.	459	Marx, M.	143
Burdman, G.	75	Mendiburu, J. P.	423
Carrigan, R. A., Jr.	123	Moinester, M. A.	275
Cheung, H. W. K.	427	Moroni, L.	153
Cheung, K.	335	Morrison, R. J.	313
Christian, D. C.	221	Nason, P.	237
Ciocio, A.	423	Neichi, K.	423
Colas, J.	423	Newsom, C. R.	465
Cooper, P.	427	Nguyen, A.	451
Cumalat, J. P.	103	Niu, E.	395
Dobrzynski, L.	423	Norem, J.	135
Eichten, E. J.	345, 355	Pakvasa, S.	85, 433
Engelfried, J.	371	Papavassilion, V.	443
Freyburger, A.	35, 453	Peng, K. C.	433
Fixione, S.	237	Pripstein, M.	423
Garbincius, P. H.	453	Przybylski, G.	423
Ghez, P.	423	Quigg, C.	345, 355
Gounder, K.	287, 433	Radeztsky, S.	435
Halling, A. M.	463	Repond, J.	135
Hill, C. T.	345, 355	Richard, J.-M.	95
Hoff, M.	423	Ridolfi, G.	237
Hoshi, Y.	423	Rosenberg, E. I.	193
Hoyer, P.	415	Rosner, J. L.	297, 435
Isenhower, L. D.	435	Ruchti, R.	173
Iso, H.	423	Russ, J.	111
James, C. C.	463	Salin, P.	423
Kadyk, J.	423	Scadron, M. D.	407, 435
Karchin, P. E.	433	Sheaff, M.	201
Kikuchi, R.	423	Sheldon, P. D.	25, 451
Kryn, D.	423	Shukla, S.	435
Lacotte, J. C.	423	Smith, V. J.	123

Sokoloff, M. D.	433
Spiegel, L.	411
Summers, D. J.	287, 459
Takeuchi, T.	433
Tang, W.-K.	251, 415
Teiger, J.	423
Tesarek, R. J.	163
Thur, W.	423
Toki, W.	57, 433
Vänttinen, M.	415
Weber, T.	423
Wenzel, W. A.	423
White, S.	143
Wiss, J.	11, 453
Yuta, H.	423
Zhang, C.	453